UNIVERSITY OF CALIFORNIA SAN DIEGO

Theoretical development of framed space curve and its applications to higher-order geometrically-exact rod theory, shape sensing, path estimation, and computer graphics

A dissertation submitted in partial satisfaction of the
requirements for the degree
Doctor of Philosophy

in

Structural Engineering

by

Mayank Chadha

Committee in charge:

Professor Michael D. Todd, Chair
Professor Jiun-Shyan Chen
Professor Joel P. Conte
Professor Charles R. Farrar
Professor Elham Izadi

2019

The dissertation of Mayank Chadha is approved, and it is acceptable in quality and form for publication on microfilm and electronically:

_____

_____

_____

_____

_____

Chair

University of California San Diego

2019

DEDICATION

To my parents, Manjula and Munishwer Chander Chadda

For their incredible teachings, unfathomable sacrifices, and boundless faith.

EPIGRAPH

Mathematics reveals its secrets only to those
who approach it with pure love, for its own beauty.
–Archimedes

Truth can be stated in a thousand different ways,
yet each one can be true.
–Swami Vivekananda

TABLE OF CONTENTS

LIST OF FIGURES

LIST OF TABLES

ACKNOWLEDGEMENTS

I have been immensely fortunate to be surrounded and influenced by my wonderful family, friends, teachers, and most importantly, my mentors. It is their constant support, teachings, and guidance that have facilitated the growth in my career thus far.

My time in Port Blair from 2006-2010 has influenced my interest in physics and mathematics immensely. I was blessed with high school teachers who rooted for me from the get-go and helped me exercise my potential to the fullest. I am thankful to the faculty of Civil Engineering at PSG College of Technology for their constant backing and motivation, especially Dr. J. V. Ramasamy, Dr. G. Sankarasubramanian, Dr. M. Palanikumar, Mr. C. G. Shivakumar, and Mr. G. Venkatraman. I cherish and apply to this day the numerous personal and scientific discussions, primarily on classical and quantum Mechanics with Dr. C. K. Shashidharan Nair, former Head of the Applied Sciences department.

My Ph. D. could not have been possible without my thesis committee. I express my deepest gratitude to my advisor, Professor Michael D. Todd for his mentorship. From trusting me with your graduate classes to encouraging me to participate in many conferences and seminars, for always having an open door for me, for supporting all my ideas no matter how crazy they seemed, and for providing me with a favorable environment to carry on with my research, I thank you. I really could not have asked for more.

Many thanks to Professor Joel P. Conte, for being a wonderful teacher and for encouraging my research. I appreciate your valuable pieces of advice now and then, and many other discussions that we have had. These discussions have provided me with interesting outlooks towards my research. Thank you, Professor Chuck Farrar, for supporting me, for introducing me to the topic of complexity, and for referring me to the fascinating work of Arien Ben-Neim on information and entropy. Thank you, Professor J. S. Chen, for sharing your insightful feedback and appreciation of my work, as well as for your lessons on Meshfree and Finite Element Analysis. Also thanks to Professor Elham Izadi for being patient with me during your differential geometry course and for

all the helpful discussions about applying the knowledge in my research.

I am tremendously thankful to my late grandparents Mr. Madan Mohan Chadda and Mrs. Kailash Rani Chadda, my Bauji and Bibi, for the value they placed on family, and for the influence they had in connecting me with nature during my early childhood, that eventually propelled my interest in physics growing up. Thank you, Daddy, for fostering in me the passion for physics and the skill to reason with things. Thank you, Mummy, for your incredible life lessons and immeasurable sacrifices that led me to achieve all that I have. Thank you, Shiva, my little brother, for always believing in me. I also thank my wife, Drishti, who has been by my side consistently supporting me throughout the journey.

I must also extend my thanks to my American family: Mrs. Ruth Newmark, Katya Newmark, and Matthew Costello along with their family for making me feel at home, for celebrating my accomplishments, and for their continual faith in my potentials. This journey would have been incomplete without everyday morning coffee and discussions with my friend Dr. See Yenn Chong (Andy). Thanks to Mukesh Ramancha for sitting patiently through my many trial presentations and for his feedback and discussions. I also value numerous scientific conversations with my friend Dr. Vishaal Krishnan, and Angshuman Deb.

The research presented in this dissertation was funded by Department of Structural Engineering, United States Army Corps of Engineers through the U.S. Army Engineer Research and Development Center, and Friends of International Center fellowship (FIC). This content of this dissertation has been published in numerous journals that are listed in the following Vita and Publication section, authored by the dissertation author, and Dr. Michael D. Todd.

The discussion carried out in chapters 1 and 2 has been published in Computers & Structures Journal, Mayank Chadha and Michael D. Todd, 2019. The title of this paper is “On the material and material-adapted approaches to curve framing with applications in path estimation, shape reconstruction, and computer graphics”. The dissertation author is the primary investigator and author of this paper.

Chapter 3 has been published in Applied Mathematics Letters Journal, Mayank Chadha and Michael D. Todd, 2019. The title of this paper is "On the derivatives of curvature of framed space curve and their time-updating scheme". An extended version of the same paper, with MATLAB code, is published in arXiv of Mathematics (Differential Geometry). The dissertation author is the primary investigator and author of these papers.

The discussion carried out in chapters 4, 5, and the early portion of chapter 6 has been published in the International Journal of Solids and Structures, Mayank Chadha and Michael D. Todd, 2019. The title of this paper is: "A comprehensive kinematic model of single-manifold Cosserat beam structures with application to a finite strain measurement model for strain gauges". The dissertation author is the primary investigator and author of this paper.

The shape reconstruction methodology developed in chapter 6, has been published in the Journal of Applied Mechanics (ASME), Mayank Chadha and Michael D. Todd, 2017. The title of this paper is: "A generalized approach for reconstructing the three-dimensional shape of slender structures including the effects of curvature, shear, torsion, and elongation". The dissertation author is the primary investigator and author of these papers.

A portion of the content in chapter 7 is part of a publication in the International Journal of Solids and Structures authored by Mayank Chadha and Michael D. Todd, titled: "An introductory treatise on reduced balance laws of Cosserat beams". The remaining discussion carried out in chapter 7 and the chapters 8, 9, and 10 is currently being prepared to be published in a journal titled: "Mathematical theory of a higher-order geometrically-exact beam with a deforming cross-section". The dissertation author is the primary investigator and author of this paper.

VITA

2014	B. E. in Civil Engineering (Gold Medalist), P. S. G. College of Technology, Anna University, Coimbatore, India
2016	M. S. in Structural Engineering, University of California San Diego
2019	Ph. D. in Structural Engineering, University of California San Diego

PUBLICATIONS

Peer Reviewed Published Journal Articles

Chadha, M., and Todd, M.D., 2017, "A generalized approach for reconstructing the three-dimensional shape of slender structures including the effects of curvature, shear, torsion, and elongation," Journal of Applied Mechanics, 84(4), p.041003.

Chadha, M., and Todd, M.D., 2017, "An introductory treatise on reduced balance laws of Cosserat beams," International Journal of Solids and Structures, 126, pp.54-73.

Chadha, M., and Todd, M.D., 2019, "A comprehensive kinematic model of single-manifold Cosserat beam structures with application to a finite strain measurement model for strain gauges," International Journal of Solids and Structures, 159, pp.58-76.

Chadha, M., and Todd, M.D., 2019, "On the material and material-adapted approaches to curve framing with applications in path estimation, shape reconstruction, and computer graphics," Computers & Structures, 218, pp.60-81.

Chadha, M., and Todd, M.D., 2020, "On the derivatives of curvature of framed space curve and their time-updating scheme," Applied Mathematics Letters, 99, pp.105989.

Peer Reviewed Journal Articles in Progress

Chadha, M., and Todd, M.D., 2020 (expected), "Mathematical theory of a higher-order geometrically-exact beam with a deforming cross-section".

Conference Publications

Chadha, M., and Todd, M.D., 2017, July, "A displacement reconstruction strategy for long, slender structures from limited strain measurements and its application to underground pipeline monitoring," In International Conference on Experimental Vibration Analysis for Civil Engineering Structures (pp. 317-327). Springer, Cham.

Chadha, M., and Todd, M.D., 2018, "Comprehensive kinematics and kinetics of Cosserat beams and their application for developing a measurement model for strain gauges," In European Conference on Computational Mechanics ECCM 6.

Chadha, M., and Todd, M.D., 2019, "An Improved Shape Reconstruction Methodology for Long Rod Like Structures Using Cosserat Kinematics-Including the Poisson's Effect," In Nonlinear Dynamics, Volume 1 (pp. 237-246). Springer, Cham.

arXiv Articles

Chadda, M., C., and **Chadha, M.**, 2018, "On the structure of tree: A conceptual article," arXiv of Popular Physics, arXiv:1807.00033.

Chadha, M., and Todd, M.D., 2019, "On the derivatives of curvature of framed space curve and their time-updating scheme: Extended version with MATLAB code," arXiv of Differential Geometry, arXiv:1907.11271.

FIELD OF STUDY

Major field: Structural Engineering
Specialization: Applied Mechanics and Mathematics

ABSTRACT OF THE DISSERTATION

Theoretical development of framed space curve and its applications to higher-order geometrically-exact rod theory, shape sensing, path estimation, and computer graphics

by

Mayank Chadha

Doctor of Philosophy in Structural Engineering

University of California San Diego, 2019

Professor Michael D. Todd, Chair

There are many systems such as beams, pipelines, coordinated drones swarm, DNA, etc., for which the configuration may be described by a framed space curve characterized by a single parameter. This research, therefore, utilizes the application of differential geometry and mechanics to investigate such systems. This work leads to the development of kinematically enhanced geometrically-exact beam theory, shape reconstruction of slender structures, path-estimation of a moving object, and computational geometry and graphics method.

The evolution of the system can be mathematically defined by a state space. An approach to approximate the state space of a single-manifold characteristic system using discrete material linear

and angular velocity data is proposed. The methodology of path-estimation can be successfully applied to reconstruct the shape of deformed slender structures that captures the effect of curvature, shear, torsion, Poisson's deformation, warping, and axial deformation. The relationships are applied to generate some complicated structures like a double helix intertwined about a space curve, a leaf, and an entire plant.

Room for further improvisation of geometrically-exact beam theory was realized. A comprehensive kinematics of geometrically-exact beam subjected to a large deformation and finite strain is obtained. Among other deformation effects, the proposed kinematics also capture a fully coupled Poisson's and warping effects. The developed kinematics are ultimately used to establish a measurement model of discrete and finite length strain gauges attached to the beam.

The weak and strong form, Hamiltonian form, and Poisson bracket form of balance laws considering the enhanced kinematics of the beam are derived. The finite element model of the geometrically-exact beam with linear material properties is developed. Modal analysis is performed for a small deformation case.

The geometrically exact formulation discussed can be used to develop a reduced finite element model for DNA and bio-polymers. The shape sensing method has the potential to serve in the medical industry by helping in the location of surgical tubing, developing smart tethers that would help in the study of ocean surfaces, etc. Finally, the state-space estimation technique can be further extended to higher-order manifold problems like shape reconstruction of composite panels, membranes, distortion in space-time fabric, etc.

Chapter 1

Framed Space Curves

1.1 Introduction to various curve framing techniques

The space curves are the simplest structures in the theory of differential geometry because they are manifolds of dimension one. The interest in space curves dates back to the 17^{th} century. The idea of a tangent to the curve is attributed to Pierre De Fermat that was first mentioned in 1629 in a letter to M. Despagnet. It seemingly was invented as a side product of Fermat's investigation on maxima and minima (refer to [1]). In 1637, Descartes was the first to define the algebraic curve in his famous work [2]. In 1748, Euler used the parametric representation of curves in his renowned work [3]. The idea of curve framing using tangent, normal, and binormal vectors are attributed to Frenet [4] and Serret [5]. Darboux [6] exploited the moving frame technique to study surfaces, which was further generalized by Cartan (refer to: for example, [7] and [8]) and it was used to develop tetrad theory of general relativity [9]. Under the Frenet-Serret curve framing technique, the curve is geometrically characterized by means of coordinate system invariant quantities: *curvature* $\overline{\kappa}$ and *torsion* $\overline{\tau}$. A unique Frenet frame exists for a regular, at least C^3 continuous and non-degenerate curve.

Despite the fact that a Frenet–Serret formulation is at the heart of curve framing, it has

limitations for certain practical problems and applications including, but not limited to, graphics generation, shape reconstruction from finite strain measurements, modeling the trajectory and motion of certain classes of moving objects, defining the configuration of object swarms, modeling the continuum mechanics of Cosserat beams, and so forth. These applications demand the existence of a continuously varying frame along the curve, even if the curvature vanishes at a certain point on the curve. The principal normal of the curve is discontinuous at the point where the curvature is 0 (point of inflection or when the curve straightens momentarily), rendering a limitation to the use of the Frenet frame for these applications.

Bishop [10] proposed an alternative framing methodology called *Relatively Parallel Adapted Frame* (RPAF). RPAF can be used to frame a regular, minimally C^2 continuous curve using two invariants, say $(\overline{\kappa}_1, \overline{\kappa}_2)$, that can be uniquely defined if we specify the orthogonal vectors spanning the normal plane of such a curve at a particular point on it. Bishop called the invariants $(\overline{\kappa}_1, \overline{\kappa}_2)$ as the *normal development* of the curve. Like the Frenet frame, we only have two invariants in RPAF that define the curve. The curve still needs to be regular, but the requirements of continuity and the non-degeneracy condition of the curve are relaxed.

The benefit of RPAF has been proven since its proposal in 1975. The application of RPAF in computer graphics to create ribbons, tubes from 3D space curves, and the generation of forward-facing camera orientation was investigated by Hanson and Ma [11]. The RPAF has successfully been used to develop trajectory tracking and auto-pilot control system for UAVs (refer to figure 1 in Xargay et al. [12] and references therein). The work by Zahradová [13] used RPAF to construct waveguides for curves that did not possess unique Frenet frames.

The Frenet frames and RPAF are intrinsic to the curve itself. Therefore, the curvature terms $(\overline{\kappa}, \overline{\tau})$ in case of Frenet frame and the terms $(\overline{\kappa}_1, \overline{\kappa}_2)$ in case of a unique RPAF are frame invariants and depend solely on the properties of the curve. However, in multiple practical applications where a physical system can be modeled through a framed curve, it is convenient to frame the curve using the *material frame* (MF). The evolution of the MF along the curve depends

on the configuration-dependent parameters. When MF includes the tangent vector of the curve, it is called a *material-adapted frame* (MAF). The curvatures related to such frames usually have a physical meaning associated with the change of state of the system.

In this chapter, we discuss various framing techniques spanning from intrinsic frames to system-dependent material frames. We systematically elucidate the construction of the MAF and establish the relationship between MAF, Frenet frame, and RPAF. We finally detail the general material frame.

Note on Notations: The n dimensional Euclidean space is represented by $\mathbb{R}^n$, with $\mathbb{R}^1 \equiv \mathbb{R}$. The dot product, ordinary vector product and tensor product of two Euclidean vectors $\boldsymbol{v}_1$ and $\boldsymbol{v}_2$ are defined as $\boldsymbol{v}_1 \cdot \boldsymbol{v}_2$, $\boldsymbol{v}_1 \times \boldsymbol{v}_2$, and $\boldsymbol{v}_1 \otimes \boldsymbol{v}_2$ respectively. The Euclidean norm is represented by $\|.\|$ or the un-bolded version of the symbol (for example, $\|\boldsymbol{v}\| \equiv v$). Secondly, n^{th} (with $n \geq 0$) order partial derivative with respect to a scalar quantity, ξ for instance, is given by the operator $\frac{\partial^n}{\partial \xi^n} = \partial^n_\xi$. For $n = 1$, we define $\partial^1_\xi \equiv \partial_\xi$ and note that for $n = 0$, ∂^0_ξ is an identity operator. A vector, tensor or a matrix is represented by bold symbol and their components are given by indexed un-bolded symbols. The action of a tensor $\boldsymbol{A}$ onto the vector $\boldsymbol{v}$ is represented by $\boldsymbol{A}\boldsymbol{v} \equiv \boldsymbol{A}.\boldsymbol{v}$. We note that the centered dot "$\cdot$" is meant for dot product between two vectors, whereas the action of a tensor onto the vector, the matrix multiplication or product of two scalars, a scalar to a matrix (or a vector) is denoted by a lower dot ".".

1.2 Frenet-Serret and Relatively Parallel Adaptive Frames

1.2.1 Frenet-Serret Frame

Consider a fixed orthonormal Cartesian frame $\{\boldsymbol{E}_i\}$ in Euclidean space $\mathbb{R}^3$. Consider a *non-degenerate* and at least C^3 continuous space curve $\boldsymbol{\varphi} : [0, L] \longrightarrow \mathbb{R}^3$, such that, $\boldsymbol{\varphi}(\xi) = \varphi_i(\xi)\boldsymbol{E}_i$, with the arclength $\xi \in [0, L]$. Uniquely framing a curve using Frenet frame requires a continuously

varying Frenet triad consisting of tangent $\boldsymbol{T}(\xi)$, principal normal $\boldsymbol{N}(\xi)$, and binormal vectors $\boldsymbol{B}(\xi)$ defined as:

$$\begin{aligned} \boldsymbol{T}(\xi) &= \partial_\xi \boldsymbol{\varphi}; \\ \boldsymbol{N}(\xi) &= \frac{\partial_\xi^2 \boldsymbol{\varphi}}{\|\partial_\xi^2 \boldsymbol{\varphi}\|}; \\ \boldsymbol{B}(\xi) &= \boldsymbol{T}(\xi) \times \boldsymbol{N}(\xi). \end{aligned} \tag{1.1}$$

The vector triad $\{\boldsymbol{T}(\xi), \boldsymbol{N}(\xi), \boldsymbol{B}(\xi)\}$ as given in Eq. (1.1) defines the Frenet frame. Before we mention the Frenet formula that governs the evolution of the Frenet triad, we make the following remarks that are required to understand the unique existence and continuity requirement of the frame.

Remarks:

Remark 1.1: A parametrized C^1 continuous curve $\boldsymbol{\varphi}(\xi)$ is called a *regular curve* if it has a non-vanishing derivative. This guarantees the existence of non-zero and continuous tangent vector field $\boldsymbol{T}(\xi)$. A regular curve parametrized by the arc-length ξ gives a unit tangent vector, i.e. $\|\partial_\xi \boldsymbol{\varphi}\| = 1$.

Remark 1.2: For a parametrized C^2 continuous curve $\boldsymbol{\varphi}(\xi)$, we define the scalar curvature $\overline{\kappa}(\xi) = \|\partial_\xi^2 \boldsymbol{\varphi}\|$. The point on the curve at which the curvature vanishes $\overline{\kappa} = 0$, is called as the *inflection point*. The point with $\overline{\kappa} \neq 0$ on a regular curve is called as a *strongly regular* point. At the point of inflection, the curve is momentarily straight and the normal vector is not uniquely defined. Thus, the Frenet frame consisting of unique principal normal does not exist at the *point of inflection*.

Remark 1.3: At a *strongly regular* point of C^2 continuous curve with $\overline{\kappa}(\xi) \neq 0$, the tangent $\boldsymbol{T}$ and the principal normal vector $\boldsymbol{N}$ are linearly independent (orthonormal) and spans the *osculating plane*. This condition is called as *non-degeneracy*. The normal vector points towards the *center of*

curvature. The circle on the osculating plane centered at the *center of curvature* with the radius $\frac{1}{\overline{\kappa}}$ is called as the *osculating circle*. A regular C^2 curve with $\overline{\kappa}(\xi) \neq 0$ (implying linear independence of $\boldsymbol{T}$ and $\boldsymbol{N}$) is called as *non-degenerate* curve. The curvature $\overline{\kappa}(\xi)$ measures the rate of change of the tangent when moving along the curve. It represents the deviation of the curve at a point from a straight line (along the tangent at a point) in the neighborhood of the point in consideration.

Remark 1.4: The binormal vector $\boldsymbol{B}$ as defined in Eq. (1.1) is perpendicular to the *osculating plane*. The plane spanned by the vectors $\boldsymbol{T}$ and $\boldsymbol{B}$ is called as the *rectifying plane*. For the Frenet frame to be continuous along the curve, the osculating plane must change continuously along the curve. This brings us to the definition of *torsion* $\overline{\tau}(\xi)$. The deviation of the osculating plane is obtained from the derivative of the binormal vector, which can be obtained as $\partial_\xi \boldsymbol{B} = -\overline{\tau}\boldsymbol{N}$ (refer Chapter II of Kreyszig [14]). The continuity of the Frenet frame along the curve requires the vector $\partial_\xi \boldsymbol{B}$ to be at least C^0 continuous, implying the curve $\boldsymbol{\varphi}(\xi)$ to be at least C^3 continuous. The C^2 continuity of a non-degenerate curve implies the existence of osculating circle (curvature continuity) and the C^3 continuity of such curve implies that osculating circle or osculating plane changes smoothly (torsion continuity).

The Frenet-Serret formulas represent the first derivatives of vectors $\partial_\xi \boldsymbol{T}$, $\partial_\xi \boldsymbol{N}$ and $\partial_\xi \boldsymbol{B}$ as a linear combination of the Frenet triad as is shown below

$$\begin{bmatrix} \boldsymbol{T}_{,\xi} \\ \boldsymbol{N}_{,\xi} \\ \boldsymbol{B}_{,\xi} \end{bmatrix} = \begin{bmatrix} 0 & \overline{\kappa} & 0 \\ -\overline{\kappa} & 0 & \overline{\tau} \\ 0 & -\overline{\tau} & 0 \end{bmatrix} \begin{bmatrix} \boldsymbol{T} \\ \boldsymbol{N} \\ \boldsymbol{B} \end{bmatrix}. \tag{1.2}$$

The Frenet triad continuously moves along the curve. If the Frenet triad is obtained by finite rotation of the fixed triad $\{\boldsymbol{E}_i\}$, we have,

$$\boldsymbol{Q}_{\mathrm{f}} = \boldsymbol{T} \otimes \boldsymbol{E}_1 + \boldsymbol{N} \otimes \boldsymbol{E}_2 + \boldsymbol{B} \otimes \boldsymbol{E}_3. \tag{1.3}$$

The tensor $\boldsymbol{Q}_{\mathrm{f}}(\xi)$ represents the family of orthogonal tensors belonging to the $SO(3)$ rotational

Lie group (discussed later in section 1.3.2.1). From Eq. (1.3), the following holds

$$\begin{aligned}\partial_\xi \boldsymbol{T} &= \partial_\xi \boldsymbol{Q}_\mathrm{f}.\boldsymbol{Q}_\mathrm{f}^T\boldsymbol{T} = \boldsymbol{\kappa}_\mathrm{f}\times\boldsymbol{T};\\ \partial_\xi \boldsymbol{N} &= \partial_\xi \boldsymbol{Q}_\mathrm{f}.\boldsymbol{Q}_\mathrm{f}^T\boldsymbol{N} = \boldsymbol{\kappa}_\mathrm{f}\times\boldsymbol{N};\\ \partial_\xi \boldsymbol{B} &= \partial_\xi \boldsymbol{Q}_\mathrm{f}.\boldsymbol{Q}_\mathrm{f}^T\boldsymbol{B} = \boldsymbol{\kappa}_\mathrm{f}\times\boldsymbol{B}.\end{aligned} \tag{1.4}$$

For an orthogonal matrix $\boldsymbol{Q}_\mathrm{f}$, it can be proven that $\boldsymbol{Q}_{\mathrm{f},\xi}\boldsymbol{Q}_\mathrm{f}^T$ is an anti-symmetric matrix. Therefore, there exists a corresponding axial vector $\boldsymbol{\kappa}_\mathrm{f}$ such that Eq. (1.4) holds. The vector $\boldsymbol{\kappa}_\mathrm{f} = \overline{\tau}\boldsymbol{T} + \overline{\kappa}\boldsymbol{B}$ is called as the *Darboux vector* (refer Chapter II of Kreyszig [14]). It can also be interpreted as a rotation vector of the Frenet triad for a non-degenerate C^3 continuous curve $\boldsymbol{\varphi}(\xi)$ causing infinitesimal rotation of the triad as we move along the curve. Finally, we present the formula for the frame invariants $(\overline{\kappa}, \overline{\tau})$ as,

$$\begin{aligned}\overline{\kappa}(\xi) &= \frac{\|\partial_\xi\boldsymbol{\varphi}\times\partial_\xi^2\boldsymbol{\varphi}\|}{\|\partial_\xi\boldsymbol{\varphi}\|^3};\\ \overline{\tau}(\xi) &= \frac{\left(\partial_\xi\boldsymbol{\varphi}\times\partial_\xi^2\boldsymbol{\varphi}\right)\cdot\left(\partial_\xi^3\boldsymbol{\varphi}\right)}{\|\partial_\xi\boldsymbol{\varphi}\times\partial_\xi^2\boldsymbol{\varphi}\|^2}.\end{aligned} \tag{1.5}$$

Figure 1.1 illustrates the construction discussed above.

1.2.2 Relatively Parallel Adapted Frame (RPAF): Bishop's frame

As explained in the last section, a curve may be uniquely framed by Frenet triad if it is non-degenerate and at least C^3 continuous. Richard L. Bishop [10] proposed an alternative curve framing approach that relaxes the continuity requirement among others. For a curve to be framed by RPAF, it needs to be at least C^2 continuous and regular. We present an argument that justifies the construction of RPAF.

Let us consider a regular and at least C^2 continuous curve. Such a curve guarantees a non-zero tangent vector. The idea is to device a method to span the plane perpendicular to the tangent vector (*normal plane*) such that the two vector fields spanning the normal plane and the

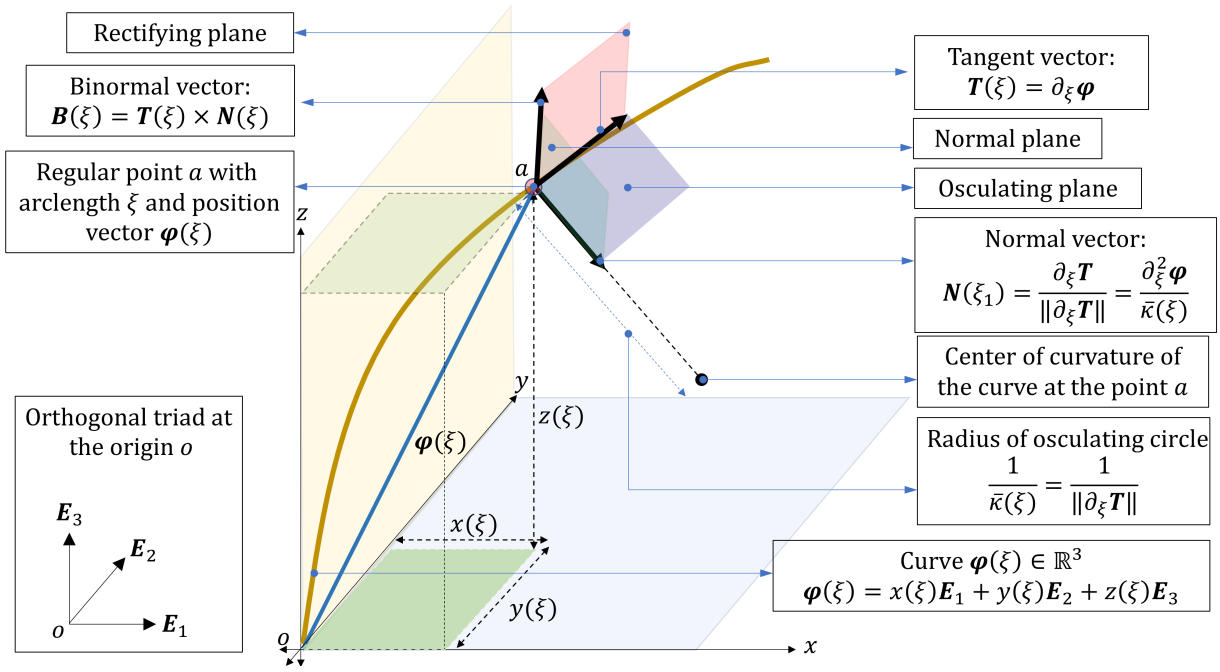

Figure 1.1: Frenet-Serret frame.

tangent vector forms an orthonormal triad that is continuously varying along the curve. Therefore, we first define a *normal vector field* as the vector field that is perpendicular to the tangent vector $\boldsymbol{T}(\xi)$ of the curve $\boldsymbol{\varphi}(\xi)$. Let χ represent set of all the continuous normal vector field. The aim is to obtain a *unique* pair of *orthonormal vector fields* $\boldsymbol{N}_1(\xi), \boldsymbol{N}_2(\xi) \in \chi$ spanning the normal plane. For the construction of the triad, we assume that the normal vector fields $\boldsymbol{N}_1(\xi)$ and $\boldsymbol{N}_2(\xi)$ are perpendicular to each other. Bishop proposed that the normal vector fields $\boldsymbol{N}_i(\xi)$ can be obtained if the total derivative $\frac{\mathrm{d}\boldsymbol{N}_i}{\mathrm{d}\xi} = \partial_\xi \boldsymbol{N}_i$ is parallel to the tangent vector field $\boldsymbol{T}(\xi)$ for $i = 1, 2$. Here we assume that $\boldsymbol{N}_i$ is function of the arc-length ξ only. The uniqueness of this field can be guaranteed by fixing the normal vectors at a fixed arclength ξ_{10} such that $\boldsymbol{N}_i(\xi_{10}) = \boldsymbol{N}_{i0}$ (called as *generators*). Let us call this as the *uniqueness criterion* and the vector $\boldsymbol{N}_{i0}$ as the *generator*.

The vector field $\boldsymbol{N}_i(\xi) \in \chi$ is called as *relatively parallel normal field* if $\partial_\xi \boldsymbol{N}_i$ is parallel to the tangent vector $\boldsymbol{T}(\xi)$. Theorem 1 in Bishop [10] gives continuity and uniqueness requirement of relatively parallel normal fields. The frame consisting of the tangent vector $\boldsymbol{T}(\xi)$ and two unique

relatively parallel orthonormal fields $\boldsymbol{N}_1(\xi), \boldsymbol{N}_2(\xi) \in \chi$ is called as *relatively parallel adapted frame* (RPAF). Theorem 2 in Bishop [10] defines the family of RPAF (we can obtain a unique frame by invoking the *uniqueness criterion*). If $\{\boldsymbol{T}, \boldsymbol{N}_1, \boldsymbol{N_2}\}$ is a RPAF, we have,

$$\begin{bmatrix} \partial_\xi \boldsymbol{T} \\ \partial_\xi \boldsymbol{N}_1 \\ \partial_\xi \boldsymbol{N}_2 \end{bmatrix} = \begin{bmatrix} 0 & \overline{\kappa}_1 & \overline{\kappa}_2 \\ -\overline{\kappa}_1 & 0 & 0 \\ -\overline{\kappa}_2 & 0 & 0 \end{bmatrix} \begin{bmatrix} \boldsymbol{T} \\ \boldsymbol{N}_1 \\ \boldsymbol{N}_2 \end{bmatrix}. \tag{1.6}$$

It is thus clear that if the regular curve $\boldsymbol{\varphi}$ is C^r continuous with $r \geq 2$, the tangent vector is C^{r-1} continuous. Using Eq. (1.6), this fact implies that the normal fields are C^{r-1} continuous (refer Theorem 1 in Bishop [10]). The parameters $(\overline{\kappa}_1, \overline{\kappa}_2)$ governs the evolution of the RPAF and are determined uniquely up to rotation (for *properly oriented* frame). These parameters can be determined uniquely by invoking the *uniqueness criterion* defined above and are called as the *normal development* of the curve $\boldsymbol{\varphi}$. The *Darboux vector* corresponding to RPAF is $\boldsymbol{\kappa}_\mathrm{b} = \overline{\kappa}_1 \boldsymbol{N}_2 - \overline{\kappa}_2 \boldsymbol{N}_1$.

For a regular non-degenerate and at least C^3 curve, the relationship between Frenet frame and the RPAF can be summarized as (refer Bishop [10]),

$$\overline{\kappa}^2 = \overline{\kappa}_1^2 + \overline{\kappa}_2^2; \tag{1.7a}$$

$$\overline{\tau} = \partial_\xi \eta; \tag{1.7b}$$

$$\eta = \arctan \frac{\overline{\kappa}_2}{\overline{\kappa}_1}. \tag{1.7c}$$

Here, η represents the angular deviation of the vectors $\boldsymbol{N}$ and $\boldsymbol{B}$ from the vectors $\boldsymbol{N}_1$ and $\boldsymbol{N}_2$ respectively measured in clockwise direction (refer Fig. 1.2).

Remarks:

Remark 1.5: An arbitrary vector field is relatively parallel if its tangential component is a constant multiple of the unit tangent field $\boldsymbol{T}(\xi)$ and its normal component is relatively parallel in

the sense discussed above.

Remark 1.6: In differential geometry, there is a notion of *parallel-transport*, in which, a geometric object (say a vector) is said to be parallel transported along a curve in a manifold if its covariant derivative vanishes (refer chapter 2 of Do Carmo [15]). Two parallel-transported vector fields do preserve length and relative orientation in Riemannian manifold. However, it must be noted that the relatively parallel vector field, say $\boldsymbol{M}(\xi)$, is not obtained by *parallel-transport* of the normal vector $\boldsymbol{M}(\xi_{10}) = \boldsymbol{M}_{10}$ along the curve. Therefore, in the author's opinion, it is inappropriate and misleading to call RPAF as *parallel-transport frame*.

1.3 Material frames and finite rotations

1.3.1 Motivation

In numerous practical applications, the idea of curve framing is very useful to model the geometry of the system. Many times, the frame is required to be attached to the system, thus justifying the word *material* in *Material frames* (MF). The configuration of such a system is defined by a curve and the frame attached to it. If the frame consists of the tangent vector of the curve as one of three orthogonal vectors, it is called as an *adapted* frame. We shall see in a while that there are systems that require a more general frame that is attached to the curve but do not contain a tangent vector as a part of the triad (for example, a general director triad). Those are still *material* frames, but not *material-adapted* frames. Unlike the Frenet frame or the RPAF, the orientation of these frames depends on the parameters defining the configuration of the system under consideration. Let us explain the idea of the *material-adapted* frame with some examples.

Consider the non-linear large deformation of a cantilever beam subjected to pure bending (no shear deformation) and elongation. Such a structure may be modeled by a curve (called the mid-curve, obtained by joining the cross-sectional centroidal loci along the rod) and the family of

rigid cross-sections. Euler-Bernoulli beam theory assumes bending as the predominant cause of deformation and ignores shear and other in-plane and out-of-plane deformations. For such a case, bending guarantees that the cross-sections of the rod are perpendicular to the tangent vector of the mid-curve, or in other words, the cross-sections lie on the normal plane of the curve at any deformed configuration. This is also valid for non-linear Kirchhoff-Love beams that constraints the cross-section to be perpendicular to the mid-curve. Thus, we need a material-adapted frame to model such a rod (as we shall see later, this frame will be called as *special material adapted frame* SMAF). Todd et al. [16] in their first work on shape reconstruction used SMAF because bending curvatures and elongation dominate the overall contributions to deformation in case of slender rods.

Consider a similar rod subjected to torsion along with the bending and elongation. The cross-sections still lie on the normal plane but they are subjected to rotation about the tangent vector. Consider another example of a fixed-wing airplane that has three degrees of freedom in rotation. The configuration of an airplane can be modeled by a curve parametrized with time. The normalized tangent vector of such curve is along the *roll axis*, whereas the *pitch axis* and *yaw axis* span the normal plane. We call these kinds of frames as *general material adapted frame* (GMAF). If the roll angle in case of an airplane and the torsion deformation in case of rods vanish, the GMAF reduces to SMAF. In other words, GMAF can be obtained from SMAF by orthogonal rotation about the tangent vector.

Finally, consider a general example of rod deformation. Let us subject the rod to shear deformation along with all the other effects discussed before. The inclusion of shear deformation relaxes the constraint of the cross-section to lie on the normal plane. Therefore, to model such a structure, we need a frame that contains a vector perpendicular to the cross-section (need not be along the tangent vector of the curve) and a pair of orthogonal vectors to span the cross-section (that need not lie on the normal plane but still is subjected to rigid cross-section assumption). Chadha and Todd [17] and [18] (discussed later in chapter 4) used this framing technique (in

this case we used *Cosserat frame*) to generalize the theory of shape sensing to include shear deformations and Poisson's in-plane cross-sectional deformation among other effects. In general, we call this frame as *material frame* (MF) and not MAF because the tangent vector is not a part of the triad anymore.

Another interesting application of MF can be realized in the design of a spiral staircase. If the central column is straight (which is usually the case in practical designs), the tread falls on the normal plane of the column and the handrail is perfectly spiral, thus MAF is apt to describe such geometry. However, if the central column is slightly deviated or inclined due to construction requirements, the tread may no longer be on the normal plane and secondly, the handrail will not be a perfect spiral anymore. We would need MF to address such geometries.

1.3.2 Finite rotations

In practical applications, the material frames are obtained by finite rotation of the triad $\{\boldsymbol{E}_i\}$. For instance, the Inertial Measurement Unit (IMU) of a dynamic system is always initially calibrated with respect to some fixed triad, say $\{\boldsymbol{E}_i\}$. Before we construct various material frames, we briefly describe the finite rotation of a vector and an orthonormal triad.

1.3.2.1 Rotation of a vector: Rotation tensor

Finite rotations are represented by an element of a proper orthogonal rotation group $SO(3)$. The $SO(3)$ manifold is a non-linear compact Lie group that has a linear skew-symmetric matrix as its Lie algebra, $so(3)$. The Lie algebra to $SO(3)$ represents its tangent plane at the identity $\boldsymbol{I}_3 \in SO(3)$. The $SO(3)$ manifold and its Lie algebra $so(3)$ are defined as

$$SO(3) := \{\boldsymbol{Q} : \mathbb{R}^3 \longrightarrow \mathbb{R}^3 |\ \boldsymbol{Q}^T\boldsymbol{Q} = \boldsymbol{I}_3, \text{ and } \det \boldsymbol{Q} = 1\}; \tag{1.8a}$$

$$so(3) := \{\hat{\boldsymbol{\theta}} : \mathbb{R}^3 \longrightarrow \mathbb{R}^3 |\ \hat{\boldsymbol{\theta}} \text{ is linear, and } \hat{\boldsymbol{\theta}} + \hat{\boldsymbol{\theta}}^T = \boldsymbol{0}_3\}. \tag{1.8b}$$

In the equation above, $\mathbf{0}_3$ represents 3×3 zero matrix, whereas $\boldsymbol{I}_3 = \boldsymbol{E}_i \otimes \boldsymbol{E}_i$ is the identity tensor with respect to which the director frame field is calibrated. The anti-symmetric tensor $\hat{\boldsymbol{\theta}} \in so(3)$ is equivalent to the associated axial vector $\boldsymbol{\theta} \in \mathbb{R}^3$ in the sense that for any vector $\boldsymbol{v} \in \mathbb{R}^3$, we have $\hat{\boldsymbol{\theta}}.\boldsymbol{v} = \boldsymbol{\theta} \times \boldsymbol{v}$. Therefore, there exist an isomorphism between $\mathbb{R}^3$ and $so(3)$. The action of $\hat{\boldsymbol{\theta}}$ onto the vector $\boldsymbol{v}$ (yielding $\hat{\boldsymbol{\theta}}.\boldsymbol{v}$) results into an infinitesimal rotation of the vector $\boldsymbol{v}$ about the unit vector $\frac{\boldsymbol{\theta}}{\|\boldsymbol{\theta}\|}$ by an amount $\|\boldsymbol{\theta}\|$ (referred to as rotation about $\boldsymbol{\theta}$ vector; hence, $\boldsymbol{\theta}$ is called an *axial vector*). From here on, any matrix quantity with a hat on it ($\hat{\cdot}$) represents an anti-symmetric matrix. For later use, we define zero vector as $\mathbf{0}_1 = [0,0,0]^T$. At this point, we define the Lie-bracket of two anti-symmetric matrix as $[.,.] : so(3) \times so(3) \longrightarrow \mathbb{R}^3$, such that for any $\hat{\boldsymbol{a}}, \hat{\boldsymbol{b}} \in so(3)$ with corresponding axial vectors $\boldsymbol{a}, \boldsymbol{b} \in \mathbb{R}^3$ respectively and any vector $\boldsymbol{v} \in \mathbb{R}^3$, we have,

$$\left[\hat{\boldsymbol{a}}, \hat{\boldsymbol{b}}\right] = (\hat{\boldsymbol{a}}.\hat{\boldsymbol{b}} - \hat{\boldsymbol{b}}.\hat{\boldsymbol{a}}); \tag{1.9a}$$

$$\left[\hat{\boldsymbol{a}}, \hat{\boldsymbol{b}}\right].\boldsymbol{v} = (\boldsymbol{a} \times \boldsymbol{b}) \times \boldsymbol{v}. \tag{1.9b}$$

We note two important properties of Lie-bracket:

$$[\hat{\boldsymbol{a}}, \hat{\boldsymbol{a}}] = \mathbf{0}_3; \tag{1.10a}$$

$$\left[\hat{\boldsymbol{a}}, \hat{\boldsymbol{b}}\right] = -\left[\hat{\boldsymbol{b}}, \hat{\boldsymbol{a}}\right]. \tag{1.10b}$$

Consider a vector $\boldsymbol{V}_\mathrm{i}$ that is to be rotated to $\boldsymbol{V}_\mathrm{f}$ by a proper orthogonal tensor $\boldsymbol{Q} \in SO(3)$ such that, $\boldsymbol{V}_\mathrm{f} = \boldsymbol{Q}.\boldsymbol{V}_\mathrm{i}$. The component of the tensor $\boldsymbol{Q}$ represented by the matrix $[\boldsymbol{Q}]_{\boldsymbol{E}_i \otimes \boldsymbol{E}_j} = Q_{ij}(\boldsymbol{E}_i \otimes \boldsymbol{E}_j)$ has three independent entries because of the orthogonality constraint: $\boldsymbol{Q}^T.\boldsymbol{Q} = \boldsymbol{I}_3$. Therefore, $\boldsymbol{Q}$ can be parametrized by three parameters or a vector in $\mathbb{R}^3$. There are multiple ways for the parametrization of the rotation tensor. We focus on three of them: the Euler Angles, the quaternions and the Rodrigues rotation formula. We omit the description of Euler angles (that deals with sequential rotations) for they are straight forward and common. However, we briefly describe the quaternion approach and Rodrigues rotation formula.

Rodrigues rotation formula: We first describe Rodrigues rotation approach for finite rotations. The vector $\boldsymbol{V}_{\mathrm{f}}$ can be obtained by rotation of the vector $\boldsymbol{V}_{\mathrm{i}}$ about the unit vector $\boldsymbol{n}_\theta = n_{\theta i}\boldsymbol{E}_i$ by an angle θ. This enables us to parametrize the rotation tensor $\boldsymbol{Q}$ by means of a vector $\boldsymbol{\theta} = \theta \boldsymbol{n}_\theta$, such that $\theta = \|\boldsymbol{\theta}\|$ and $\boldsymbol{V}_{\mathrm{f}} = \boldsymbol{Q}(\boldsymbol{\theta}).\boldsymbol{V}_{\mathrm{i}}$. By Rodrigues formula,

$$\boldsymbol{V}_{\mathrm{f}} = (\boldsymbol{V}_{\mathrm{i}} + \boldsymbol{n}_\theta \times \boldsymbol{n}_\theta \times \boldsymbol{V}_{\mathrm{i}}) + \sin\theta\,(\boldsymbol{n}_\theta \times \boldsymbol{V}_{\mathrm{i}}) - \cos\theta\,(\boldsymbol{n}_\theta \times \boldsymbol{n}_\theta \times \boldsymbol{V}_{\mathrm{i}})\,. \tag{1.11}$$

If $\hat{\boldsymbol{\theta}} \in so(3)$ represents the spin matrix with the corresponding axial vector $\boldsymbol{\theta} = \theta(n_{\theta i}\boldsymbol{E}_i) = \theta_i \boldsymbol{E}_i$, we have,

$$\hat{\boldsymbol{\theta}} = \theta \begin{bmatrix} 0 & -n_{\theta 3} & n_{\theta 2} \\ n_{\theta 3} & 0 & -n_{\theta 1} \\ -n_{\theta 2} & n_{\theta 1} & 0 \end{bmatrix}. \tag{1.12}$$

We state a useful property associated with Eq.(1.12) as

$$\theta^2 = \boldsymbol{\theta}\cdot\boldsymbol{\theta} = \frac{1}{2}\hat{\boldsymbol{\theta}} : \hat{\boldsymbol{\theta}} = \frac{1}{2}\mathrm{Tr}\left(\hat{\boldsymbol{\theta}}^2\right). \tag{1.13}$$

The definition of $SO(3)$ in Eq. (1.8a) allows rotation tensor to be parameterized by a rotation vector $\boldsymbol{\theta} \in \mathbb{R}^3$ (with corresponding anti-symmetric matrix $\hat{\boldsymbol{\theta}} \in so(3)$). The rotation tensor can be derived using Rodrigues formula (1.11) using the fact that $\boldsymbol{V}_{\mathrm{f}} = \boldsymbol{Q}(\boldsymbol{\theta}).\boldsymbol{V}_{\mathrm{i}}$, $\boldsymbol{n}_\theta \times \boldsymbol{V}_i = \left(\frac{1}{\theta}\right)\hat{\boldsymbol{\theta}}.\boldsymbol{V}_i$ and using the MacLaurin expansion of $\sin\theta$ and $\cos\theta$ (refer Eq. (29) in Argyris [19]). This brings us to the definition of exponential map $\exp : so(3) \longrightarrow SO(3)$ such that,

$$\boldsymbol{Q}(\boldsymbol{\theta}) = \boldsymbol{I}_3 + \frac{\sin\theta}{\theta}\,\hat{\boldsymbol{\theta}} + \frac{(1-\cos\theta)}{\theta^2}\hat{\boldsymbol{\theta}}^2 = \sum_{i\geq 0}\frac{\hat{\boldsymbol{\theta}}^i}{i!} = \exp\left(\hat{\boldsymbol{\theta}}\right); \tag{1.14a}$$

$$\boldsymbol{Q}^T(\boldsymbol{\theta}) = \boldsymbol{Q}^{-1}(\boldsymbol{\theta}) = \boldsymbol{I}_3 - \frac{\sin\theta}{\theta}\,\hat{\boldsymbol{\theta}} + \frac{(1-\cos\theta)}{\theta^2}\hat{\boldsymbol{\theta}}^2 = \exp\left(-\hat{\boldsymbol{\theta}}\right). \tag{1.14b}$$

Here $\hat{\boldsymbol{\theta}}^0 = \boldsymbol{I}_3$. Subtracting Eq. (1.14b) from (1.14a), we obtain the associated anti-symmetric matrix $\hat{\boldsymbol{\theta}}$ as,

$$\hat{\boldsymbol{\theta}} = \frac{\theta}{2\sin\theta}\left(\boldsymbol{Q} - \boldsymbol{Q}^T\right). \tag{1.15}$$

Taking trace of $\boldsymbol{Q}$ in Eq. (1.14a) and using the result in Eq. (1.13), we get another important relation:

$$\cos\theta = \frac{\text{trace}(\boldsymbol{Q}) - 1}{2}. \tag{1.16}$$

The exponential map is a local homeomorphism in the neighborhood of identity $\boldsymbol{I}_3 \in SO(3)$ for $\theta \in [0, \pi)$. The local homeomorphism of exp map guarantees the existence of a unique inverse of exponential map in the neighborhood of $\boldsymbol{I}_3 \in SO(3)$, called the logarithm map $\log : SO(3) \longrightarrow so(3)$, such that

$$\log\left(\boldsymbol{Q}(\boldsymbol{\theta})\right) = \log(\exp(\hat{\boldsymbol{\theta}})) = \hat{\boldsymbol{\theta}} \in so(3). \tag{1.17}$$

The norm of logarithm map is defined as the Euclidean norm of the associated rotation vector as

$$\|\log\left(\boldsymbol{Q}(\boldsymbol{\theta})\right)\| = \theta = \sqrt{\frac{1}{2}\text{Tr}\left(\hat{\boldsymbol{\theta}}.\hat{\boldsymbol{\theta}}\right)}. \tag{1.18}$$

Equation 1.18 above defines a metric that is useful in measuring errors in the director triad. The rotation tensor can also be represented by means of unit quaternion. For a detailed discussion on finite rotation, refer to Argyris [19], Ibrahimbegovic [20] and Diebel [21]. Section 1.3.2.2 discusses local homeomorphism of exponential maps.

Unit quaternions Another approach to capture finite rotations is by using unit quaternions. In general, a quaternion is a 4-tuple $q = q_0 + q_1 i + q_2 j + q_3 k$, where $q_i \in \mathbb{R}$, such that,

$$\begin{aligned} i^2 = j^2 = k^2 = ijk = -1; \\ ij = k, ji = -k; \\ jk = i, kj = -i; \\ ki = j, ik = -j. \end{aligned} \tag{1.19}$$

The first of the equations mentioned above has a special significance in the history of mathematics (refer to [22]). The relationship between a complex number and plane geometry inspired *William*

Rowan Hamilton to find a higher dimensional number that can be associated with 3D geometry. Hamilton realized need of 4-tuple (not a triplet) to establish a 4D algebra that can be related to 3D geometry, that he called *quaternions*.

The multiplication between two quaternion (called Hamilton product) can be carried in a way similar to the complex numbers using the properties in Eq. (1.19). Unlike complex numbers, the multiplication of quaternion is non-commutative. The conjugate, norm and inverse of a quaternion are defined as:

$$\begin{aligned} \text{conjugate}: \ & q^* = q_0 - q_1 i - q_2 j - q_3 k; \\ \text{norm}: \ & \|q\| = \sqrt{qq^*} = \sqrt{q_0^2 + q_1^2 + q_2^2 + q_3^2}; \\ \text{inverse}: \ & q^{-1} = \frac{q^*}{\|q\|^2}. \end{aligned} \tag{1.20}$$

To establish the relationship between a quaternion and 3D geometry, Hamilton suggested considering quaternion to be consisting of a *scalar* and a *vector* (the terms that he proposed), such that $q = (q_0, \boldsymbol{q})$. For two quaternion $q = (q_0, \boldsymbol{q})$ and $a = (a_0, \boldsymbol{a})$, the quaternion sum, Hamilton product, conjugate and norm are then given by:

$$\begin{aligned} & q + a = (q_0 + a_0, \boldsymbol{q} + \boldsymbol{a}); \\ & qa = (q_0 a_0 - \boldsymbol{q} \cdot \boldsymbol{a}, q_0 \boldsymbol{a} + a_0 \boldsymbol{q} + \boldsymbol{q} \times \boldsymbol{a}); \\ & q^* = (q_0, -\boldsymbol{q}); \\ & \|q\| = \sqrt{q_0^2 + \boldsymbol{q} \cdot \boldsymbol{q}}. \end{aligned} \tag{1.21}$$

We can consider a vector $\boldsymbol{V}_\mathrm{i}$ as a pure quaternion $V_\mathrm{initial} = (0, \boldsymbol{V}_\mathrm{i})$. A unit quaternion $q_\mathrm{u} = (q_0, \boldsymbol{q})$ with $\|q_\mathrm{u}\| = 1$ can be used to rotate vector $\boldsymbol{V}_\mathrm{i}$ to $\boldsymbol{V}_\mathrm{f}$ (with the associated pure quaternion $V_\mathrm{final} = (0, \boldsymbol{V}_\mathrm{f})$), such that,

$$\begin{aligned} V_\mathrm{final} = q_\mathrm{u}.V_\mathrm{initial}.q_\mathrm{u}^* = (0, \boldsymbol{Q}(q_\mathrm{u}).\boldsymbol{V}_\mathrm{i}); \\ \boldsymbol{V}_\mathrm{f} = \boldsymbol{Q}(q_\mathrm{u}).\boldsymbol{V}_\mathrm{i}. \end{aligned} \tag{1.22}$$

The rotation tensor $\boldsymbol{Q}$ can be parametrized by a unit quaternion q_{u}. If $\boldsymbol{V}_{\mathrm{i}} = V_{\mathrm{i}j}\boldsymbol{E}_j$ and $\boldsymbol{q} = q_i\boldsymbol{E}_i$, then using Eq. (1.22), we get

$$[\boldsymbol{Q}(q_{\mathrm{u}})]_{\boldsymbol{E}_i\otimes\boldsymbol{E}_j} = 2\begin{bmatrix} q_0^2+q_1^2-0.5 & q_1q_2-q_0q_3 & q_0q_2+q_1q_3 \\ q_0q_3+q_1q_2 & q_0^2+q_2^2-0.5 & q_2q_3-q_0q_1 \\ q_1q_3-q_0q_2 & q_0q_1+q_2q_3 & q_0^2+q_3^2-0.5 \end{bmatrix}. \tag{1.23}$$

We can parametrize the unit quaternion using the rotation vector $\boldsymbol{\theta}$. Notice from Eq. (1.23) that the trace $(\boldsymbol{Q}(q_{\mathrm{u}})) = 4q_0^2 - 1$. A trace being an invariant of a tensor implies (from Eq.(1.16)) that

$$\begin{aligned} 4q_0^2 - 1 &= 2\cos\theta + 1; \\ q_0 &= \sqrt{\frac{\cos\theta+1}{2}}. \end{aligned} \tag{1.24}$$

Thus, there exist two possible and equivalent q_{u} leading towards same rotation. The q_{u} with $q_0 > 0$ implies $0 < \theta \leq \pi$ about the axis $\boldsymbol{n}_\theta$ and the one with $q_0 < 0$ represents rotation about the axis $-\boldsymbol{n}_\theta$ with the magnitude $2\pi - \theta$, representing same rotation. We call this property as the *equivalence of the unit quaternion and its negative* or *double cover*.

Lets consider $q_0 = \cos\left(\frac{\theta}{2}\right)$. The unity quaternion constraint implies

$$q_{\mathrm{u}}(\boldsymbol{\theta}) = \left(\cos\left(\frac{\theta}{2}\right), \sin\left(\frac{\theta}{2}\right)\boldsymbol{n}_\theta\right). \tag{1.25}$$

This representation, sometimes called as rotation vector representation, satisfies the unit quaternion constraint and is same as the Rodrigues rotation.

The *equivalence of the unit quaternion and its negative* in representing rotation was exploited by Klumpp [23] to extract the quaternion from the component of rotation tensor without any singularity. Spurrier [24] recognized the Klumpp's algorithm to be sensitive to numerical imprecision and proposed a modified algorithm, now popularly known as *Spurrier's algorithm*.

The primary disadvantage of representing the rotation using Euler angle formulation is its dependence on the sequence of angles considered and singularities arising due to gimbal

lock. Unit quaternion approach completely gets rid of this singularity but is subjected to the unit quaternion constraint. There is plenty of excellent literature to which one may refer for further understanding of rotations (for example, [19], [20], [25] and [21]). The work by Diebel [21] serves as an excellent resource that describes all these approaches and establishes relationships to obtain one form from the other.

1.3.2.2 On many-to-one nature and local homeomorphism of exponential map

As discussed in section 1.3.2.1, the exponential map is a mapping from Lie algebra $so(3)$ to Lie group $SO(3)$. However, the exponential map is not bijective. For a given $\hat{\boldsymbol{\theta}} \in so(3)$, there is a unique $\boldsymbol{Q}(\boldsymbol{\theta}) = \exp(\hat{\boldsymbol{\theta}}) \in SO(3)$ (thus surjective), however, for a given $\boldsymbol{Q}(\boldsymbol{\theta}) = \exp(\hat{\boldsymbol{\theta}}) \in SO(3)$, there are many possible $\hat{\boldsymbol{\theta}} \in so(3)$ (hence not injective). For example, for $\boldsymbol{\theta}_1 = \theta \boldsymbol{n}_\theta$ and $\boldsymbol{\theta}_2 = (\theta + 2n\pi)\boldsymbol{n}_\theta$ with n being an integer, $\boldsymbol{Q}(\boldsymbol{\theta}_1) = \boldsymbol{Q}(\boldsymbol{\theta}_2)$. However, if we restrict $\theta \in [0, \pi)$, we obtain a local homeomorphism in the exponential map as explained below.

Let us start our discussion by restricting $\theta \in [-\pi, \pi)$. For this case every rotation tensor identifies a unit vector as $\pm\boldsymbol{n}_\theta$ (unique up to a multiple of ± 1) except at $\theta = -\pi$, in which case $\boldsymbol{n}_\theta$ is unique. Thus, the rotation angle and unit vector combination $(\theta, \boldsymbol{n}_\theta)$ and $(-\theta, -\boldsymbol{n}_\theta)$ defines same rotation vector. This fact looks trivial because $\boldsymbol{\theta} = \theta \boldsymbol{n}_\theta$, however, it forbids us to uniquely define a unit rotation vector $\boldsymbol{n}_\theta$.

To uniquely define the unit rotation vector $\boldsymbol{n}_\theta$, we restrict θ to positive value $\theta \in [0, \pi)$. At $\theta = 0$, the unit vector $\boldsymbol{n}_\theta$ can be any arbitrary vector but $\boldsymbol{\theta} = \boldsymbol{0}$ and the corresponding rotation tensor is $\boldsymbol{Q} = \boldsymbol{I}_3$. At $\theta = \pi$, there are two possible unit vectors $\pm\boldsymbol{n}_\theta$ (thus, the map is not homeomorphic for $\theta = \pi$). Thus the exponential map is local homeomorphism in the neighborhood of $\boldsymbol{I}_3$ such that $\theta \in [0, \pi)$.

From equation (1.16), $\mathrm{Tr}(\boldsymbol{Q}) = -1$ at $\theta = \pi$. Therefore, the logarithm map is a well-defined continuous map if $\mathrm{Tr}(\boldsymbol{Q}) \neq -1$ and $\theta \in [0, \pi)$. Equation (1.15) can be used to obtain logarithm of rotation tensor (the associates spin matrix), however, as θ approaches 0 and π radians, Eq

(1.15) becomes unstable as $\sin\theta$ vanishes. Spurrier's algorithm [24] can be used to extract the quaternions and the associated rotation vector. Spurrier's algorithm gives $\theta \in [0, \pi]$ and restricts quaternion component $q_0 \geq 0$. However, at $q_0 = 0$ or equivalently $\theta = \pi$, there are two possible unit vectors. The quaternions are related to the rotation vector $\boldsymbol{\theta} = \theta \boldsymbol{n}_\theta$ by the following relationships:

$$\begin{aligned} \theta &= 2\arcsin\left(\sqrt{q_1^2 + q_2^2 + q_3^2}\right) = 2\arccos(q_0); \\ n_{\theta i} &= \frac{q_i}{\sqrt{q_1^2 + q_2^2 + q_3^2}}. \end{aligned} \tag{1.26}$$

1.3.2.3 Rotation of a triad: rotation matrix

The entity $\boldsymbol{Q}$ discussed in previous section, transforms one vector to another. Therefore, it is a tensor. However, consider a properly orthonormal triad $\{\boldsymbol{d}_i\}$ such that $\boldsymbol{d}_i = \boldsymbol{Q}.\boldsymbol{E}_i$. We can then obtain *direction cosine matrix* $\mathfrak{R}$ such that, $[\boldsymbol{d}_1, \boldsymbol{d}_2, \boldsymbol{d}_3]^T = \mathfrak{R}.[\boldsymbol{E}_1, \boldsymbol{E}_2, \boldsymbol{E}_3]^T$. The component of matrix $\mathfrak{R}_{ij} = \boldsymbol{d}_i \cdot \boldsymbol{E}_j = Q_{ji}$. Here, Q_{ji} represents $\boldsymbol{E}_j \otimes \boldsymbol{E}_i$ component of the rotation tensor $\boldsymbol{Q}$. It can be observed that $\mathfrak{R} = [\boldsymbol{Q}]^T_{\boldsymbol{E}_i \otimes \boldsymbol{E}_j}$. Notice that $\mathfrak{R}$ is a matrix whereas $\boldsymbol{Q}$ is a tensor.

1.3.3 Construction of material-adapted and material frames

In this section, we construct these frames by carrying finite rotations of the fixed orthogonal triad $\{\boldsymbol{E}_i\}$ using Euler angle approach. We use the following notations: $\cos\theta = c_\theta$ and $\sin\theta = s_\theta$, for any angle θ.

1.3.3.1 Special material adapted frame: SMAF

Consider a regular and at least C^2 continuous curve $\boldsymbol{\varphi}(\xi)$. Let $\boldsymbol{Q}_\mathrm{s} \in SO(3)$ be the rotation tensor that generates SMAF consisting of orthonormal triad $\{\boldsymbol{T}, \boldsymbol{Y}_\mathrm{s}, \boldsymbol{P}_\mathrm{s}\}$, such that $\boldsymbol{P}_\mathrm{s} \cdot \boldsymbol{E}_2 = 0$. This can be obtained by first rotating the frame $\{\boldsymbol{E}_i\}$ about $\boldsymbol{E}_2$ by an angle ϕ_y (yaw angle) and then rotating about the updated $\boldsymbol{E}_3$ by an angle ϕ_p (pitch angle). Thus, if,

$\boldsymbol{Q}_{\mathrm{s}} = \boldsymbol{T} \otimes \boldsymbol{E}_1 + \boldsymbol{Y}_{\mathrm{s}} \otimes \boldsymbol{E}_2 + \boldsymbol{P}_{\mathrm{s}} \otimes \boldsymbol{E}_3$, then,

$$\begin{bmatrix} \boldsymbol{T} \\ \boldsymbol{Y}_{\mathrm{s}} \\ \boldsymbol{P}_{\mathrm{s}} \end{bmatrix} = \overbrace{\begin{bmatrix} c_{\phi_p} c_{\phi_y} & s_{\phi_p} & -c_{\phi_p} s_{\phi_y} \\ -s_{\phi_p} c_{\phi_y} & c_{\phi_p} & s_{\phi_p} s_{\phi_y} \\ s_{\phi_y} & 0 & c_{\phi_y} \end{bmatrix}}^{[\boldsymbol{Q}_{\mathrm{s}}]^T_{\boldsymbol{E}_i \otimes \boldsymbol{E}_j}} \begin{bmatrix} \boldsymbol{E}_1 \\ \boldsymbol{E}_2 \\ \boldsymbol{E}_3 \end{bmatrix}. \tag{1.27}$$

Here, $\boldsymbol{Y}_{\mathrm{s}}$ and $\boldsymbol{P}_{\mathrm{s}}$ represent the yaw and pitch axis respectively.

The fact that $\boldsymbol{P}_{\mathrm{s}}(\xi) \cdot \boldsymbol{E}_2 = 0$ or $\boldsymbol{P}_{\mathrm{s}}(\xi)$ lies in $\boldsymbol{E}_1 - \boldsymbol{E}_3$ plane is advantageous in practical standpoint. This is because $\boldsymbol{P}_{\mathrm{s}}(\xi)$ acts as a reference vector in the normal plane with respect to which, the torsion angle or the roll angle and the shear angles can be defined to obtain GMAF and MF. Note that we can define another special case in which only one angle is non-zero (either pitch or yaw angle). However, that would define a curve in the 2D plane, hence it is not desirable for spatial curves.

1.3.3.2 General material adapted frame: GMAF

Rotating SMAF about the tangent vector by an angle ϕ_r (roll angle) gives us GMAF consisting of orthonormal triad $\{\boldsymbol{T}, \boldsymbol{Y}_{\mathrm{g}}, \boldsymbol{P}_{\mathrm{g}}\}$, obtained by finite rotation of $\{\boldsymbol{E}_i\}$ by the rotation tensor $\boldsymbol{Q}_{\mathrm{g}}$, such that $\boldsymbol{Q}_{\mathrm{g}} = \boldsymbol{T} \otimes \boldsymbol{E}_1 + \boldsymbol{Y}_{\mathrm{g}} \otimes \boldsymbol{E}_2 + \boldsymbol{P}_{\mathrm{g}} \otimes \boldsymbol{E}_3$. Thus,

$$\begin{bmatrix} \boldsymbol{T} \\ \boldsymbol{Y}_{\mathrm{g}} \\ \boldsymbol{P}_{\mathrm{g}} \end{bmatrix} = \overbrace{\begin{bmatrix} c_{\phi_p} c_{\phi_y} & s_{\phi_p} & -c_{\phi_p} s_{\phi_y} \\ -c_{\phi_r} c_{\phi_y} s_{\phi_p} + s_{\phi_r} s_{\phi_y} & c_{\phi_p} c_{\phi_r} & c_{\phi_y} s_{\phi_r} + c_{\phi_r} s_{\phi_p} s_{\phi_y} \\ c_{\phi_y} s_{\phi_p} s_{\phi_r} + c_{\phi_r} s_{\phi_y} & -c_{\phi_p} s_{\phi_r} & c_{\phi_r} c_{\phi_y} - s_{\phi_p} s_{\phi_r} s_{\phi_y} \end{bmatrix}}^{[\boldsymbol{Q}_{\mathrm{g}}]^T_{\boldsymbol{E}_i \otimes \boldsymbol{E}_j}} \begin{bmatrix} \boldsymbol{E}_1 \\ \boldsymbol{E}_2 \\ \boldsymbol{E}_3 \end{bmatrix}. \tag{1.28}$$

This sequence of rotations falls under Tiat-Bryan intrinsic rotation with the sequence yaw first, pitch second, and roll third.

1.3.3.3 Material frames: MF

As discussed in section 1.3.1, we might encounter a situation in which the plane of interest need not be normal to the curve. Consider a general orthogonal triad $\{\boldsymbol{d}_i\}$ such that the vector $\boldsymbol{d}_1$ is not along the tangent vector of the curve $\boldsymbol{T}$ and the vectors $\{\boldsymbol{d}_2, \boldsymbol{d}_3\}$ spans a plane normal to $\boldsymbol{d}_1$. For instance, a cross-section of a beam subjected to shear is not normal to the tangent vector or a rigid swarm of drones need not be perpendicular to the direction of motion. In such instances, MF are desirable.

Consider a general orthonormal frame $\{\boldsymbol{d}_i\}$ with its origin at some point on the curve. It can be obtained from finite rotation of the frame $\{\boldsymbol{E}_i\}$ such that $\boldsymbol{d}_i = \boldsymbol{Q}_{\mathrm{m}}.\boldsymbol{E}_i$ or from any other triad, say SMAF using the rotation tensor $\boldsymbol{Q}_{\mathrm{ms}}$ (the subscript"ms" implies *material-frame* relative to *special material adapted frame*) such that,

$$\begin{aligned} \boldsymbol{Q}_{\mathrm{m}} &= \sum_{i=1}^{3} \boldsymbol{d}_i \otimes \boldsymbol{E}_i; \\ \boldsymbol{Q}_{\mathrm{ms}} &= \boldsymbol{d}_1 \otimes \boldsymbol{T} + \boldsymbol{d}_2 \otimes \boldsymbol{Y}_{\mathrm{s}} + \boldsymbol{d}_3 \otimes \boldsymbol{P}_{\mathrm{s}}; \\ \boldsymbol{Q}_{\mathrm{m}} &= \boldsymbol{Q}_{\mathrm{ms}}.\boldsymbol{Q}_{\mathrm{s}}. \end{aligned} \tag{1.29}$$

1.4 Curvature of an evolving frame

1.4.1 Curvatures of a general material frame

Let us consider the material frame $\{\boldsymbol{d}_i\}$. The frame is a function of the quantity parameterizing the curve under consideration. The choice of parameter is problem-dependent. For instance, the frame attached to a UAV is evolving with *time*. Similarly, a frame representing the orientation of a cross-section of a beam varies along the *arclength* of the deformed beam or the frame attached at a fixed cross-section of a cable changes with *time* when the cable undergoes dynamic deformation. The change of directors relative to the parameter gives local information

about the deviation of the configuration of the system at a point. For instance, the curvature $\overline{\kappa}$ of the Frenet frame gives the deviation of the curve from its tangent vector at the given arclength.

The derivative of the director triad $\{\boldsymbol{d}_i\}$ with respect to the arclength parameter ξ is obtained using the Eq. (1.29) as,

$$\partial_\xi \boldsymbol{d} = \partial_\xi \boldsymbol{Q}_\mathrm{m}.\boldsymbol{E}_i = \partial_\xi \boldsymbol{Q}_\mathrm{m}.\boldsymbol{Q}_\mathrm{m}^T.\boldsymbol{d}_i = \hat{\boldsymbol{\kappa}}.\boldsymbol{d}_i = \boldsymbol{\kappa} \times \boldsymbol{d}_i. \tag{1.30}$$

Since $\boldsymbol{Q}_\mathrm{m}^T.\boldsymbol{Q}_\mathrm{m} = \boldsymbol{I}_3$, it can be proved that $\hat{\boldsymbol{\kappa}} = \partial_\xi \boldsymbol{Q}_\mathrm{m}.\boldsymbol{Q}_\mathrm{m}^T$ is anti-symmetric with corresponding axial vector $\boldsymbol{\kappa}$. Here, $\boldsymbol{\kappa} = \kappa_i \boldsymbol{E}_i = \overline{\kappa}_i \boldsymbol{d}_i$, represents the Darboux vector of the frame when parameterized by the arclength ξ. Note that the overline on the components $\overline{\kappa}_i$ represents the component of the Darboux vector in the MF. In matrix form,

$$\begin{bmatrix} \partial_\xi \boldsymbol{d}_1 \\ \partial_\xi \boldsymbol{d}_2 \\ \partial_\xi \boldsymbol{d}_3 \end{bmatrix} = \overbrace{\begin{bmatrix} 0 & \overline{\kappa}_3 & -\overline{\kappa}_2 \\ -\overline{\kappa}_3 & 0 & \overline{\kappa}_1 \\ \overline{\kappa}_2 & -\overline{\kappa}_1 & 0 \end{bmatrix}}^{\hat{\boldsymbol{\kappa}}^T} \begin{bmatrix} \boldsymbol{d}_1 \\ \boldsymbol{d}_2 \\ \boldsymbol{d}_3 \end{bmatrix}. \tag{1.31}$$

1.4.1.1 Curvature terms of Frenet frame

The fact that the tangent vector $\boldsymbol{T}(\xi)$ depends on the pitch ϕ_p and yaw angle ϕ_y, enables us to represent the Frenet frame in terms of these functions. With the rotation about $\boldsymbol{E}_2$ first followed by the rotation about the updated $\boldsymbol{E}_3$, and using the results discussed in section 1.2.1, the following results can be obtained:

$$\boldsymbol{\varphi}(\xi) = \boldsymbol{\varphi}(0) + \int_0^\xi \boldsymbol{T}(s)\, \mathrm{d}s; \tag{1.32a}$$

$$\overline{\kappa}^2 = (\partial_\xi \phi_p)^2 + (\partial_\xi \phi_y)^2 c_{\phi_p}^2; \tag{1.32b}$$

$$\overline{\tau} = \left(\frac{1}{\overline{\kappa}^2}\right)\left(\partial_\xi \phi_y.\left(2 s_{\phi_p}(\partial_\xi \phi_p)^2 + c_{\phi_p}\left(c_{\phi_p} s_{\phi_p}(\partial_\xi \phi_y)^2 + \partial_\xi^2 \phi_p\right)\right) - c_{\phi_p}.\partial_\xi \phi_p.\partial_\xi^2 \phi_y\right); \tag{1.32c}$$

$$[\boldsymbol{Q}_{\mathrm{f}}]^{T}_{\boldsymbol{E}_i\otimes\boldsymbol{E}_j} = \left(\frac{1}{\overline{\kappa}}\right)\begin{bmatrix} \overline{\kappa}c_{\phi_p}c_{\phi_y} & \overline{\kappa}s_{\phi_p} & -\overline{\kappa}c_{\phi_p}s_{\phi_y} \\ -c_{\phi_y}s_{\phi_p}.\partial_\xi\phi_p - c_{\phi_p}s_{\phi_y}.\partial_\xi\phi_y & c_{\phi_p}.\partial_\xi\phi_p & s_{\phi_p}s_{\phi_y}.\partial_\xi\phi_p - c_{\phi_p}c_{\phi_y}.\partial_\xi\phi_y \\ s_{\phi_y}.\partial_\xi\phi_p - c_{\phi_p}c_{\phi_y}s_{\phi_p}.\partial_\xi\phi_y & c^2_{\phi_p}.\partial_\xi\phi_y & c_{\phi_y}.\partial_\xi\phi_p + c_{\phi_p}s_{\phi_p}s_{\phi_y}.\partial_\xi\phi_y \end{bmatrix}. \tag{1.32d}$$

1.4.1.2 Curvature terms of SMAF and GMAF

From Eqs. (1.27) and (1.30), we arrive at the Darboux vector for the SMAF $\boldsymbol{\kappa}_{\mathrm{s}} = \overline{\kappa}_{\mathrm{s}1}\boldsymbol{T} + \overline{\kappa}_{\mathrm{s}2}\boldsymbol{Y}_{\mathrm{s}} + \overline{\kappa}_{\mathrm{s}3}\boldsymbol{P}_{\mathrm{s}}$ such that,

$$\overline{\kappa}_{\mathrm{s}1} = s_{\phi_p}.\partial_\xi\phi_y;\ \ \overline{\kappa}_{\mathrm{s}2} = c_{\phi_p}.\partial_\xi\phi_y;\ \ \overline{\kappa}_{\mathrm{s}3} = \partial_\xi\phi_p. \tag{1.33a}$$

$$\|\boldsymbol{\kappa}_{\mathrm{s}}\|^2 = (\partial_\xi\phi_p)^2 + (\partial_\xi\phi_y)^2; \tag{1.33b}$$

$$\overline{\kappa}^2 = \overline{\kappa}^2_{\mathrm{s}2} + \overline{\kappa}^2_{\mathrm{s}3}. \tag{1.33c}$$

Similarly, from Eqs. (1.28) and (1.31), we arrive at the Darboux vector for the GMAF, $\boldsymbol{\kappa}_{\mathrm{g}} = \overline{\kappa}_{\mathrm{g}1}\boldsymbol{T} + \overline{\kappa}_{\mathrm{g}2}\boldsymbol{Y}_{\mathrm{g}} + \overline{\kappa}_{\mathrm{g}3}\boldsymbol{P}_{\mathrm{g}}$ such that,

$$\overline{\kappa}_{\mathrm{g}1} = \partial_\xi\phi_r + s_{\phi_p}.\partial_\xi\phi_y = \partial_\xi\phi_r + \overline{\kappa}_{\mathrm{s}1}; \tag{1.34a}$$

$$\overline{\kappa}_{\mathrm{g}2} = c_{\phi_p}c_{\phi_r}.\partial_\xi\phi_y + s_{\phi_r}.\partial_\xi\phi_p = \overline{\kappa}_{\mathrm{s}2}c_{\phi_r} + \overline{\kappa}_{\mathrm{s}3}s_{\phi_r}; \tag{1.34b}$$

$$\overline{\kappa}_{\mathrm{g}3} = c_{\phi_r}\phi_{p,\xi} - c_{\phi_p}s_{\phi_r}\phi_{y,\xi} = -\overline{\kappa}_{\mathrm{s}2}s_{\phi_r} + \overline{\kappa}_{\mathrm{s}3}c_{\phi_r}; \tag{1.34c}$$

$$\|\boldsymbol{\kappa}_{\mathrm{g}}\|^2 = (\partial_\xi\phi_p^2 + \partial_\xi\phi_y^2 + \partial_\xi\phi_r^2) + 2s_{\phi_p}.\partial_\xi\phi_r.\partial_\xi\phi_y. \tag{1.34d}$$

It is interesting to note from above relations that

$$\begin{bmatrix} \overline{\kappa}_{\mathrm{g}1} \\ \overline{\kappa}_{\mathrm{g}2} \\ \overline{\kappa}_{\mathrm{g}3} \end{bmatrix} = \begin{bmatrix} 1 & 0 & 0 \\ 0 & c_{\phi_r} & s_{\phi_r} \\ 0 & -s_{\phi_r} & c_{\phi_r} \end{bmatrix}\begin{bmatrix} \overline{\kappa}_{\mathrm{s}1} \\ \overline{\kappa}_{\mathrm{s}2} \\ \overline{\kappa}_{\mathrm{s}3} \end{bmatrix} + \begin{bmatrix} \partial_\xi\phi_r \\ 0 \\ 0 \end{bmatrix}. \tag{1.35}$$

The expression for the curvature can be obtained in terms of unit quaternion using Eq. (1.23).

$$\overline{\kappa}_{\mathrm{g}1} = 2\left(-q_1.\partial_\xi q_0 + q_0.\partial_\xi q_1 + q_3.\partial_\xi q_2 - q_2.\partial_\xi q_3\right); \tag{1.36a}$$

$$\overline{\kappa}_{\mathrm{g}2} = 2\left(-q_2.\partial_\xi q_0 - q_3.\partial_\xi q_1 + q_0.\partial_\xi q_2 + q_1.\partial_\xi q_3\right); \tag{1.36b}$$

$$\overline{\kappa}_{\mathrm{g}3} = 2\left(-q_3.\partial_\xi q_0 + q_2.\partial_\xi q_1 - q_1.\partial_\xi q_2 + q_0.\partial_\xi q_3\right). \tag{1.36c}$$

Similarly, the expression of curvature vector can be expressed in terms of Rodriguez parameters by using Eqs. (1.12) and (1.14a) or alternatively by substituting $q_0 = c_{(\theta/2)}, q_i = s_{(\theta/2)}n_{\theta i}$ where $i = 1-3$, in equations (1.36a), (1.36b) and (1.36c).

$$\overline{\kappa}_{\mathrm{g}1} = s_\theta.\partial_\xi n_{\theta 1} + (1-c_\theta)(n_{\theta 3}.\partial_\xi n_{\theta 2} - n_{\theta 2}.\partial_\xi n_{\theta 3}) + n_{\theta 1}.\partial_\xi \theta; \tag{1.37a}$$

$$\overline{\kappa}_{\mathrm{g}2} = s_\theta.\partial_\xi n_{\theta 2} + (1-c_\theta)(n_{\theta 1}.\partial_\xi n_{\theta 3} - n_{\theta 3}.\partial_\xi n_{\theta 1}) + n_{\theta 2}.\partial_\xi \theta; \tag{1.37b}$$

$$\overline{\kappa}_{\mathrm{g}3} = s_\theta.\partial_\xi n_{\theta 3} + (1-c_\theta)(n_{\theta 2}.\partial_\xi n_{\theta 1} - n_{\theta 1}.\partial_\xi n_{\theta 2}) + n_{\theta 3}.\partial_\xi \theta. \tag{1.37c}$$

1.4.2 RPAF and Frenet frame as GMAF

The RPAF can be considered as GMAF with $\phi_r = \rho_{\mathrm{b}}$ representing the rotation of the normal vectors $\boldsymbol{N}_1$ and $\boldsymbol{N}_2$ from the vector $\boldsymbol{Y}_{\mathrm{s}}$ and $\boldsymbol{P}_{\mathrm{s}}$ respectively, in a constrained fashion. It is clear from Eqs. (1.6) and (1.31) that the constraint over RPAF is $\overline{\kappa}_{\mathrm{g}3} = 0$. With this constraint in mind, we can obtain the roll angle field $\rho_{\mathrm{b}}(\xi)$ for the RPAF by using Eq. (1.34a). We have

$$\rho_{\mathrm{b}}(\xi) = \rho_{\mathrm{b}}(0) - \int_0^\xi \overline{\kappa}_{\mathrm{s}1}(k)\mathrm{d}k. \tag{1.38}$$

Fixing the value of $\rho_{\mathrm{b}}(0)$ provides uniqueness to the RPAF. From Eqs. (1.34b) and (1.34c), we can arrive at the expression of the normal development (or curvatures) of RPAF in terms of the Euler angles associated with the GMAF as

$$\overline{\kappa}_1 = -\overline{\kappa}_{\mathrm{g}2}|_{(\phi_r=\rho_{\mathrm{b}})} = -\overline{\kappa}_{\mathrm{s}3}s_{\rho_{\mathrm{b}}} - \overline{\kappa}_{\mathrm{s}2}c_{\rho_{\mathrm{b}}}; \tag{1.39a}$$

$$\overline{\kappa}_2 = \overline{\kappa}_{\mathrm{g}3}|_{(\phi_r=\rho_{\mathrm{b}})} = \overline{\kappa}_{\mathrm{s}3}c_{\rho_{\mathrm{b}}} + \overline{\kappa}_{\mathrm{s}2}s_{\rho_{\mathrm{b}}}. \tag{1.39b}$$

Substituting for $\overline{\kappa}_1$ and $\overline{\kappa}_2$ from the results obtained in Eqs. (1.39a) and (1.39b) into the Eq. (1.7a) yields the result in Eq. (1.33c). Using equations (1.39a) and (1.39b) along with the result in (1.7c), we arrive at an important relationship between the angle ρ_b and η, thus enabling us to express Frenet frame as a GMAF (refer Fig. 1.2).

$$\tan\rho_\mathrm{b} = -\left(\frac{\overline{\kappa}_{\mathrm{s}2} + \overline{\kappa}_{\mathrm{s}3}\tan\eta}{\overline{\kappa}_{\mathrm{s}3} + \overline{\kappa}_{\mathrm{s}2}\tan\eta}\right). \tag{1.40}$$

We can independently arrive at the angle ($\phi_r = \rho_\mathrm{f}$) subtended by the vectors $\boldsymbol{N}$ and $\boldsymbol{B}$ with $\boldsymbol{Y}_\mathrm{s}$ and $\boldsymbol{P}_\mathrm{s}$ respectively by imposing a constraint $\overline{\kappa}_{\mathrm{g}2} = 0$ on GMAF such that,

$$\tan\rho_\mathrm{f} = -\frac{\overline{\kappa}_{\mathrm{s}2}}{\overline{\kappa}_{\mathrm{s}3}} = \tan(\eta + \rho_\mathrm{b}). \tag{1.41}$$

We note that the results obtained in Eqs. (1.40) and (1.41) are consistent. Figure 1.3 shows a curve

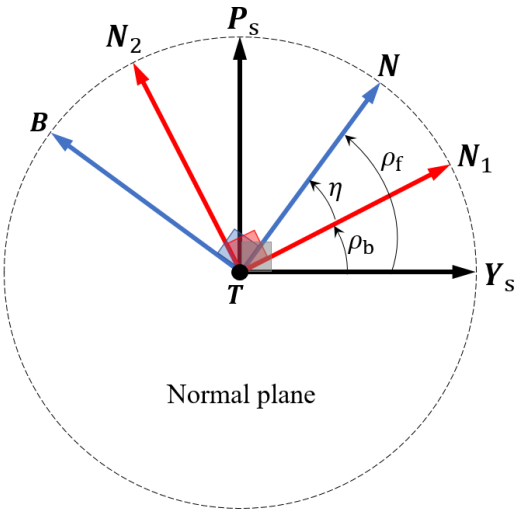

Figure 1.2: The orientation of various adapted frames in the normal plane.

with the point of inflection marked by a dot, the red vectors representing the tangent vector field and the circles representing the normal plane to the curve. In Fig. 1.3a, the solid green and blue arrows represent $\boldsymbol{Y}_\mathrm{s}$ and $\boldsymbol{P}_\mathrm{s}$ field, whereas the dotted green and blue vectors stand for $\boldsymbol{N}_1$ and $\boldsymbol{N}_2$ respectively. Similarly, the green and blue vectors in Fig. 1.3b show $\boldsymbol{N}$ and $\boldsymbol{B}$ respectively. Figure 1.3a and 1.3b shows that the SMAF and RPAF (obtained using Eq. (1.38) and setting $\rho_\mathrm{b}(0) = 0$)

are continuous whereas the Frenet frame is not uniquely defined at the point of inflection and the normal vector (binormal vector as well) abruptly changes its orientations at the inflection point.

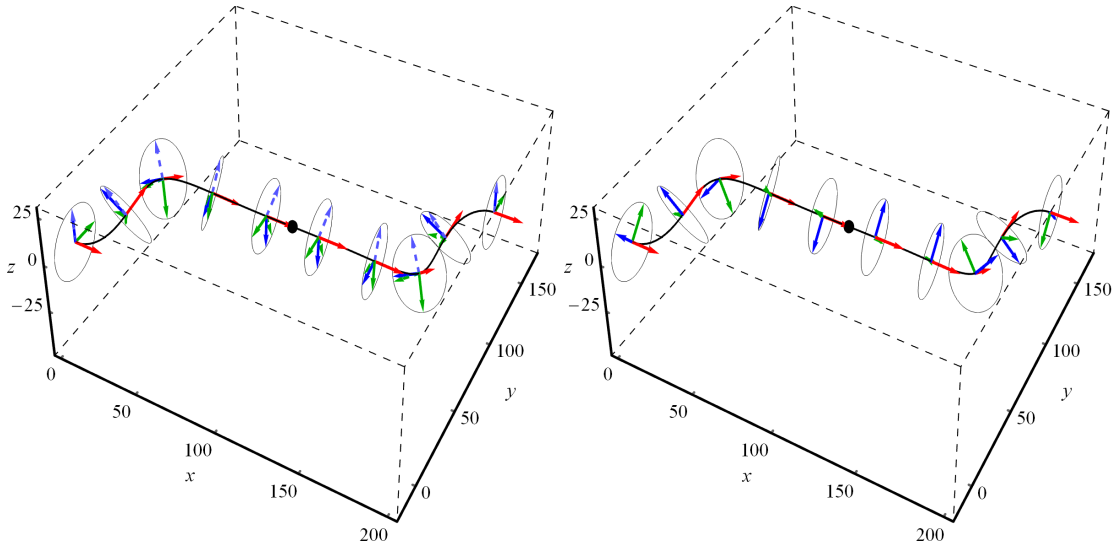

(a) SMAF and RPAF (dashed arrows) (b) Frenet frame

Figure 1.3: Example of a curve with the point of inflection (marked by a black dot), SMAF, RPAF, and Frenet frames.

1.5 Summary

This chapter details various approaches to curve framing. After a brief discussion on Frenet and RPAF frame and their continuity requirements, the construction of general material frame MF is delineated. Three approaches to parameterize finite rotations: Euler angle approach, unit quaternion, and Rodrigues rotation formula are discussed. The relationship between the curvature tensor of various frames is obtained.

This chapter is fundamental to the forthcoming chapters. The curve framing techniques discussed here are directly used in chapter 2 to develop path estimation methodology and to investigate applications of framed space curves in computer graphics. Chapter 3 is the theoretical extension of the current chapter, dealing with higher-order derivatives of curvature of material frames. We exploit the material frames discussed in this chapter to develop generalized kinematics

of geometrically-exact beams in chapters 4 and 5. The shape reconstruction technique detailed in chapter 6 uses the results presented in this chapter and chapter 4. Chapters 7–10 establishes the mechanics of geometrically-exact beams modeled using a material-framed space curve.

The discussion carried out in this chapter has been published in Computers & Structures Journal, Mayank Chadha and Michael D. Todd [26], 2019. The title of this paper is "On the material and material-adapted approaches to curve framing with applications in path estimation, shape reconstruction, and computer graphics". The dissertation author is the primary investigator and the author of this paper.

Chapter 2

Path Estimation and Computer Graphics

2.1 Introduction

In this chapter, we investigate the configuration and state space of a single-manifold characterized system, that can be modeled using framed space curves. We derive the evolution equations of the material frames and illustrate an algorithm to estimate a smooth framed curve using a limited set of curvature data. This estimation technique is very useful for structural monitoring of slender structures like pipelines (discussed in chapter 6) or for path estimation of underwater drones, where the data is scarce due to challenges associated with underwater communication. We illustrate various interpolation approaches here. One of the approaches that have a closed-form solution is *smooth patch estimation and gluing technique* (SPEG) that involves C^{-1} estimation of the material linear and angular velocity data (or equivalently cross-sectional strain and curvature in case of a beam). We develop curvature-dependent local shape functions (for a given segment or patch of the curve) and "glue" these patches together such that the global solution obtained is smooth. Another higher-order interpolation of the input curvature data to numerically obtain the configuration space is also discussed. The accuracy of the estimated curve depends on the quality of the curvatures data set and the interpolation method that was

used to estimate the path. We illustrate the application of this algorithm to estimate the path of a moving object or swarm of drones using a limited set of data obtained from the sensors (like Inertial Measurement Units (IMU), strain gauges, etc.). We illustrate the application of the frames discussed in chapter 1 towards the generation of certain structures: double helix intertwining a space curve (like DNA), a leaf and a plant.

2.2 Configuration and state space of single-manifold characterized systems

2.2.1 Tangent space and tangent bundle of the configuration space

Consider a rigid body, the configuration of which is defined by a space curve $\boldsymbol{\varphi}$ and the vector triad field $\{\boldsymbol{d}_i\}$ that defines the orientation of the rigid body under motion. Thus, the configuration space $\mathbb{C} := \mathbb{R}^3 \times SO(3) \equiv SE(3)$ defines such systems and is parameterized by a single-parameter (time in case of rigid body motion). Here $SE(3)$ is the *special Euclidean group*, that defines rigid body motion. Thus,

$$\boldsymbol{\Phi}(t) := \left\{(\boldsymbol{\varphi}(t), \boldsymbol{Q}(t)) \mid \ \boldsymbol{\varphi} : \mathbb{R}^+ \longrightarrow \mathbb{R}^3, \ \ \boldsymbol{Q} : \mathbb{R}^+ \longrightarrow SO(3)\right\} \subset \mathbb{C}. \tag{2.1}$$

In the equation above, $\mathbb{R}^+$ represents set of non-negative real number. If $\xi(t) \in \mathbb{R}^+$ represents the total distance travel at time $t \in \mathbb{R}^+$, the linear velocity is defined as $\partial_t \xi = v(t)$.

Consider the curve parameterized by the arc length ξ. For any $\boldsymbol{\Phi}(\xi) \in \mathbb{C}$, we define the tangent space $T_{\boldsymbol{\Phi}}\mathbb{C}$ as,

$$T_{\boldsymbol{\Phi}}\mathbb{C} := \left\{\left(\partial_\xi \boldsymbol{\varphi}, \partial_\xi \boldsymbol{Q}\right) \mid \ \partial_\xi \boldsymbol{\varphi} : \mathbb{R}^+ \longrightarrow \mathbb{R}^3, \ \ \partial_\xi \boldsymbol{Q} = \hat{\boldsymbol{\kappa}}.\boldsymbol{Q} : \mathbb{R}^+ \longrightarrow T_{\boldsymbol{Q}}SO(3)\right\}. \tag{2.2}$$

Here, $T_{\boldsymbol{Q}}SO(3)$ refers to the tangent plane of the non-linear manifold $SO(3)$ at $\boldsymbol{Q}$ such that $\partial_\xi \boldsymbol{Q} \in T_{\boldsymbol{Q}}SO(3)$. We recall that $\hat{\boldsymbol{\kappa}} = \partial_\xi \boldsymbol{Q}.\boldsymbol{Q}^T$ is an anti-symmetric matrix with the axial vector

$\boldsymbol{\kappa}(\xi)$. If the rotation tensor $\boldsymbol{Q}$ is parameterized by the rotation vector $\boldsymbol{\theta} = \theta \boldsymbol{n}_\theta$ as shown in the section 1.3.2, then using Eq.(1.14b) the following relationship can be obtained,

$$\hat{\boldsymbol{\kappa}} = \partial_\xi \exp(\hat{\boldsymbol{\theta}}).\exp(-\hat{\boldsymbol{\theta}}) = \left(\frac{\sin\theta}{\theta}\right)\partial_\xi\hat{\boldsymbol{\theta}} + \left(\frac{1-\cos\theta}{\theta^2}\right)\left[\hat{\boldsymbol{\theta}}, \partial_\xi\hat{\boldsymbol{\theta}}\right] + (\boldsymbol{\theta}.\partial_\xi\boldsymbol{\theta})\left(\frac{\theta-\sin\theta}{\theta^3}\right)\hat{\boldsymbol{\theta}}. \tag{2.3}$$

Using Eq. (2.3) and the definition of Lie bracket in Eq. (1.9), we obtain the corresponding axial vector (the curvature vector) as:

$$\begin{aligned} \boldsymbol{\kappa} &= \boldsymbol{T}_\theta.\partial_\xi\boldsymbol{\theta}; \\ \boldsymbol{T}_\theta &= \left(\frac{\sin\theta}{\theta}\right)\boldsymbol{I}_3 + \left(\frac{1-\cos\theta}{\theta^2}\right)\hat{\boldsymbol{\theta}} + \left(\frac{\theta-\sin\theta}{\theta^3}\right)\boldsymbol{\theta}\otimes\boldsymbol{\theta}. \end{aligned} \tag{2.4}$$

similarly, we have,

$$\begin{aligned} \partial_\xi\boldsymbol{\theta} &= \boldsymbol{T}_\theta^{-1}.\boldsymbol{\kappa}; \\ \boldsymbol{T}_\theta^{-1} &= \left(\frac{1}{2}\frac{\theta}{\tan\frac{\theta}{2}}\right)\boldsymbol{I}_3 - \frac{\hat{\boldsymbol{\theta}}}{2} + \frac{1}{\theta^2}\left(1 - \frac{1}{2}\frac{\theta}{\tan\frac{\theta}{2}}\right)\boldsymbol{\theta}\otimes\boldsymbol{\theta}. \end{aligned} \tag{2.5}$$

Readers can refer to Ibrahimbegovic et al. [20] for the derivation of $\boldsymbol{T}_\theta^{-1}$. In the above equations $\hat{\boldsymbol{\theta}}$ and $\hat{\boldsymbol{\theta}}$ represents the spin matrix associated with the vector $\partial_\xi\boldsymbol{\theta}$ and $\boldsymbol{\theta}$ respectively.

Therefore, with slight abuse of notation, we define an abused but equivalent tangent space as,

$$T_{\boldsymbol{\Phi}}\mathbb{C} \equiv \left\{\tilde{\boldsymbol{\Phi}} = \left(\partial_\xi\boldsymbol{\varphi}, \boldsymbol{\kappa}\right) \mid \ \partial_\xi\boldsymbol{\varphi} : \mathbb{R}^+ \longrightarrow \mathbb{R}^3, \ \ \boldsymbol{\kappa} : \mathbb{R}^+ \longrightarrow \mathbb{R}^3\right\} \subset \mathbb{R}^3 \times \mathbb{R}^3. \tag{2.6}$$

A one-to-one correspondence between $\mathbb{R}^3$ and $so(3)$ justifies this abuse of notation. The state space of the problem is defined by the tangent bundle $T\mathbb{C}$ of the configuration space $\mathbb{C}$ defined as,

$$T\mathbb{C} := \left\{\left(\boldsymbol{\Phi}, \tilde{\boldsymbol{\Phi}}\right) \mid \ \boldsymbol{\Phi} \in \mathbb{C}, \ \ \tilde{\boldsymbol{\Phi}} \in T_{\boldsymbol{\Phi}}\mathbb{C}\right\}. \tag{2.7}$$

From Eqs. (2.6) and (2.7) it is clear that the state space is defined by the set $\left(\boldsymbol{\varphi}, \{\boldsymbol{d}_i\}, \partial_\xi\boldsymbol{\varphi}, \boldsymbol{\kappa}\right)$.

It is interesting to interpret the curvature vector $\boldsymbol{\kappa}$ and the derivative of the rotation vector $\partial_\xi\boldsymbol{\theta}$ from a physical viewpoint. At an arc-length ξ, the director triad $\{\boldsymbol{d}_i(\xi)\}$ rotates about the

vector $\boldsymbol{\kappa}(\xi).\mathrm{d}\xi$ to yield the triad at $\{\boldsymbol{d}_i(\xi+\mathrm{d}\xi)\}$. The triad $\{\boldsymbol{d}_i(\xi)\}$ and $\{\boldsymbol{d}_i(\xi+\mathrm{d}\xi)\}$ are obtained by finite rotation of the frame $\{\boldsymbol{E}_i\}$ about the rotation vector $\boldsymbol{\theta}(\xi)$ and $\boldsymbol{\theta}(\xi+\mathrm{d}\xi) = \boldsymbol{\theta}(\xi) + \partial_\xi\theta(\xi).\mathrm{d}\xi$ respectively. In terms of the exponential map,

$$\begin{gathered}\boldsymbol{Q}(\xi+\mathrm{d}\xi) = \exp(\hat{\boldsymbol{\kappa}}(\xi).\mathrm{d}\xi).\boldsymbol{Q}(\xi) = \exp(\hat{\boldsymbol{\kappa}}(\xi).\mathrm{d}\xi).\exp(\hat{\boldsymbol{\theta}}(\xi));\\ \boldsymbol{Q}(\xi+\mathrm{d}\xi) = \boldsymbol{Q}(\boldsymbol{\theta}(\xi+\mathrm{d}\xi)) = \exp(\hat{\boldsymbol{\theta}}(\xi) + \partial_\xi\hat{\boldsymbol{\theta}}(\xi).\mathrm{d}\xi).\end{gathered} \tag{2.8}$$

2.2.2 Material and spatial representation of curvature (or equivalently angular velocity and the associated spin tensor)

We define the quantity $\hat{\overline{\boldsymbol{\kappa}}} = \boldsymbol{Q}^T.\hat{\boldsymbol{\kappa}}.\boldsymbol{Q} \in T_{\boldsymbol{I}_3}SO(3) := so(3)$ obtained by parallel transport of $\hat{\boldsymbol{\kappa}}.\boldsymbol{Q}$ from $T_{\boldsymbol{Q}}SO(3) \longrightarrow so(3)$. Thus, if $\boldsymbol{Q} = \boldsymbol{d}_i \otimes \boldsymbol{d}_i$, such that $\boldsymbol{d}_i = \boldsymbol{Q}.\boldsymbol{E}_i$, then $\boldsymbol{Q}$ represents the finite rotation, whereas $\hat{\overline{\boldsymbol{\kappa}}}$ represents an infinitesimal rotation with respect to the calibrating frame of reference $\{\boldsymbol{E}_i\}$. Whereas, $\boldsymbol{Q}.\hat{\overline{\boldsymbol{\kappa}}} = \hat{\boldsymbol{\kappa}}.\boldsymbol{Q}$ represents infinitesimal rotation with respect to $\{\boldsymbol{d}_i\}$ frame. In the physical context of rotation, the tangent vector $\boldsymbol{Q}.\hat{\overline{\boldsymbol{\kappa}}}$ and $\hat{\boldsymbol{\kappa}}.\boldsymbol{Q}$ performs an infinitesimal rotation with respect to $\{\boldsymbol{d}_i\}$ frame but the quantity $\boldsymbol{Q}.\hat{\overline{\boldsymbol{\kappa}}}$ is obtained by left translation of the quantity $\hat{\overline{\boldsymbol{\kappa}}} \in so(3)$ to $\boldsymbol{Q}.\hat{\overline{\boldsymbol{\kappa}}} \in T_{\boldsymbol{Q}}SO(3)$, whereas, $\hat{\boldsymbol{\kappa}}.\boldsymbol{Q}$ represents the superimposition of infinitesimal rotation contributed by $\boldsymbol{K}$ onto the finite rotation contributed by $\boldsymbol{Q}$ (this is also called as right translation of $\hat{\boldsymbol{\kappa}} \in so(3)$ to the tangent vector $\hat{\boldsymbol{\kappa}}.\boldsymbol{Q} \in T_{\boldsymbol{Q}}SO(3)$). The former kind of tangent vector fields are known as *left-invariant* and the later as *right-invariant* fields. We also observe that,

$$[\hat{\boldsymbol{\kappa}}]_{\boldsymbol{d}_i\otimes\boldsymbol{d}_j} = \left[\hat{\overline{\boldsymbol{\kappa}}}\right]_{\boldsymbol{E}_i\otimes\boldsymbol{E}_j} = \begin{bmatrix} 0 & -\overline{\kappa}_3 & \overline{\kappa}_2 \\ \overline{\kappa}_3 & 0 & -\overline{\kappa}_1 \\ -\overline{\kappa}_2 & \overline{\kappa}_1 & 0 \end{bmatrix}. \tag{2.9}$$

Let $\boldsymbol{\kappa}$ and $\overline{\boldsymbol{\kappa}}$ represent the axial vector corresponding to the anti-symmetric matrix $\hat{\boldsymbol{\kappa}}$ and $\hat{\overline{\boldsymbol{\kappa}}}$ respectively. It can then be proved that $\overline{\boldsymbol{\kappa}} = \boldsymbol{Q}^T.\boldsymbol{\kappa}$ such that if $\boldsymbol{\kappa} = \overline{\kappa}_i\boldsymbol{d}_i$, then $\overline{\boldsymbol{\kappa}} = \overline{\kappa}_i\boldsymbol{E}_i$. As in continuum mechanics, we call the quantities $\hat{\overline{\boldsymbol{\kappa}}}$ and $\overline{\boldsymbol{\kappa}}$ as *material representation*; and $\hat{\boldsymbol{\kappa}}$ and $\boldsymbol{\kappa}$ are

the *spatial representation* of the *curvature tensor* and the *curvature vector* respectively. Figures 2.1 and 2.2 provide a physical and geometric interpretation of the discussions carried out in this section.

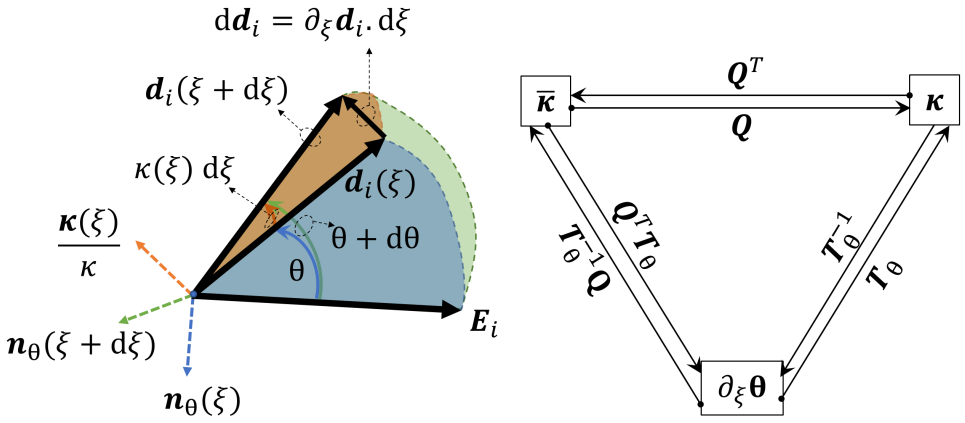

Figure 2.1: Finite and infinitesimal rotations and the flowchart of various transformations.

2.2.3 Linear and angular velocity of rigid body

A regular C^r continuous curve $\boldsymbol{\varphi}(\xi)$ parametrized by the arclength ξ can be re-parametrized by another variable t (say time) such that $\xi = \xi(t)$ is at least C^1 continuous and $\frac{\mathrm{d}\xi}{\mathrm{d}t} \neq 0$. We define linear velocity of the curve as,

$$\partial_t \boldsymbol{\varphi} = \frac{\partial \boldsymbol{\varphi}}{\partial \xi}\frac{\mathrm{d}\xi}{\mathrm{d}t} = \frac{\mathrm{d}\xi}{\mathrm{d}t}\boldsymbol{T} = v(t)\boldsymbol{T} = \bar{v}_i \boldsymbol{d}_i. \tag{2.10}$$

The scalar $v(t) = \frac{\mathrm{d}\xi}{\mathrm{d}t} = \sqrt{\bar{v}_1^2 + \bar{v}_2^2 + \bar{v}_3^2}$ gives the magnitude of linear velocity vector at time t.

The angular velocity vector $\boldsymbol{\omega}$ is related to the evolution of the frame when the curve is parameterized by time. Let us consider the derivative of the director triad $\{\boldsymbol{d}_i(t)\}$ with respect to time t. From Eq. (1.29), we have,

$$\partial_t \boldsymbol{d}_i = \partial_t \boldsymbol{Q}.\boldsymbol{E}_i = \partial_t \boldsymbol{Q}.\boldsymbol{Q}^T.\boldsymbol{d}_i = \hat{\omega}(t).\boldsymbol{d}_i = \boldsymbol{\omega}(t) \times \boldsymbol{d}_i(t). \tag{2.11}$$

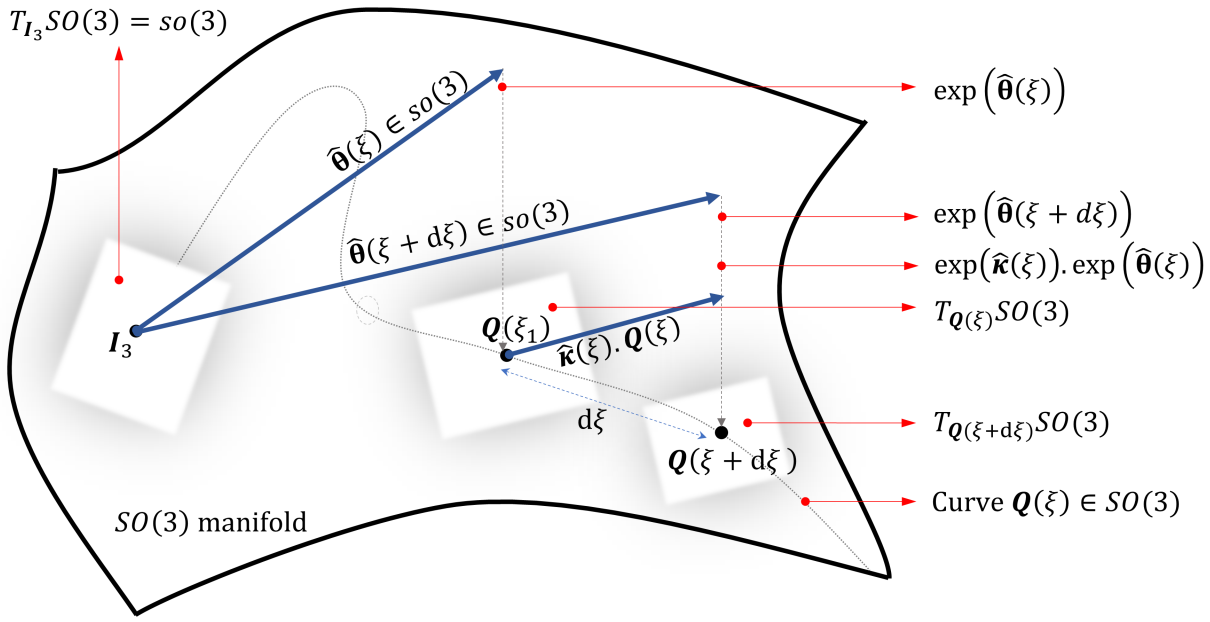

Figure 2.2: Geometric representation of the finite and infinitesimal rotations, curvature tensor $\hat{\boldsymbol{\kappa}}$, and the projection from the tangent plane $T_{\boldsymbol{Q}}SO(3)$ to the manifold $SO(3)$ using the exponential map.

The fact that $\hat{\boldsymbol{\kappa}} = \partial_t \boldsymbol{Q}.\boldsymbol{Q}^T$ implies that $\hat{\boldsymbol{\omega}}(t) = v(t)\hat{\boldsymbol{\kappa}}(\xi(t))$ or $\boldsymbol{\omega}(t) = v(t)\boldsymbol{\kappa}(\xi(t))$. Thus,

$$\begin{bmatrix} \partial_t \boldsymbol{d}_1 \\ \partial_t \boldsymbol{d}_2 \\ \partial_t \boldsymbol{d}_3 \end{bmatrix} = v(t) \begin{bmatrix} 0 & \overline{\kappa}_3(\xi(t)) & -\overline{\kappa}_2(\xi(t)) \\ -\overline{\kappa}_3(\xi(t)) & 0 & \overline{\kappa}_1(\xi(t)) \\ \overline{\kappa}_2(\xi(t)) & -\overline{\kappa}_1(\xi(t)) & 0 \end{bmatrix} \begin{bmatrix} \boldsymbol{d}_1 \\ \boldsymbol{d}_2 \\ \boldsymbol{d}_3 \end{bmatrix} = \begin{bmatrix} 0 & \overline{\omega}_3(t) & -\overline{\omega}_2(t) \\ -\overline{\omega}_3(t) & 0 & \overline{\omega}_1(t) \\ \overline{\omega}_2(t) & -\overline{\omega}_1(t) & 0 \end{bmatrix} \begin{bmatrix} \boldsymbol{d}_1 \\ \boldsymbol{d}_2 \\ \boldsymbol{d}_3 \end{bmatrix}. \tag{2.12}$$

Note that $\boldsymbol{\omega} = \overline{\omega}_i \boldsymbol{d}_i = \omega_i \boldsymbol{E}_i$, we have $[\omega_1, \omega_2, \omega_3]^T = [\boldsymbol{Q}]_{\boldsymbol{E}_i \otimes \boldsymbol{E}_j}.[\overline{\omega}_1, \overline{\omega}_2, \overline{\omega}_3]^T$. Similar to the curvature tensor discussed in section 2.2.2, we summarize following relationship associated with the angular velocity vector $\boldsymbol{\omega}$ and the tensor $\hat{\boldsymbol{\omega}}$:

$$\begin{gathered} \hat{\boldsymbol{\omega}} = -\epsilon_{ijk}\overline{\omega}_k(\boldsymbol{d}_i \otimes \boldsymbol{d}_j); \\ \hat{\overline{\boldsymbol{\omega}}} = \boldsymbol{Q}^T.\hat{\boldsymbol{\omega}}.\boldsymbol{Q} = -\epsilon_{ijk}\overline{\omega}_k(\boldsymbol{E}_i \otimes \boldsymbol{E}_j); \quad \overline{\boldsymbol{\omega}} = \boldsymbol{Q}^T.\boldsymbol{\omega} \\ \boldsymbol{\omega}.\boldsymbol{Q} \in T_{\boldsymbol{Q}}SO(3) \text{ and } \hat{\overline{\boldsymbol{\omega}}} \in so(3). \end{gathered} \tag{2.13}$$

2.3 Estimating global framed curve from limited material curvature and velocity data

We motivate the problem statement by a real-life example. Consider a moving rigid body with mid-curve and director triad parametrized with time. From section 2.2.3, the system is governed by the following set of differential equations

$$\begin{bmatrix} \partial_t \boldsymbol{\varphi} \\ \partial_t \boldsymbol{d}_1 \\ \partial_t \boldsymbol{d}_2 \\ \partial_t \boldsymbol{d}_3 \end{bmatrix} = v(t) \begin{bmatrix} 0 & \boldsymbol{T}\cdot\boldsymbol{d}_1 & \boldsymbol{T}\cdot\boldsymbol{d}_2 & \boldsymbol{T}\cdot\boldsymbol{d}_3 \\ 0 & 0 & \overline{\kappa}_3 & -\overline{\kappa}_2 \\ 0 & -\overline{\kappa}_3 & 0 & \overline{\kappa}_1 \\ 0 & \overline{\kappa}_2 & -\overline{\kappa}_1 & 0 \end{bmatrix} \begin{bmatrix} \boldsymbol{\varphi} \\ \boldsymbol{d}_1 \\ \boldsymbol{d}_2 \\ \boldsymbol{d}_3 \end{bmatrix} = \begin{bmatrix} 0 & \overline{v}_1 & \overline{v}_2 & \overline{v}_3 \\ 0 & 0 & \overline{\omega}_3 & -\overline{\omega}_2 \\ 0 & -\overline{\omega}_3 & 0 & \overline{\omega}_1 \\ 0 & \overline{\omega}_2 & -\overline{\omega}_1 & 0 \end{bmatrix} \begin{bmatrix} \boldsymbol{\varphi} \\ \boldsymbol{d}_1 \\ \boldsymbol{d}_2 \\ \boldsymbol{d}_3 \end{bmatrix}. \tag{2.14}$$

In this section, we attempt to obtain estimated state space from discrete linear velocity (equivalently axial strain in case of beams) and angular velocity (or equivalently Darboux or curvature vector in case of beams). This would involve integrating equation 2.14. We assume the initial condition at $t = 0$ as $\boldsymbol{\varphi}(0) = \mathbf{0}$ and $\boldsymbol{d}_i(0) = \boldsymbol{d}_{i0} = \boldsymbol{E}_i$. There is no loss of generality in considering the initial condition $\boldsymbol{d}_{i0}$ as our reference frame. We assume that we have the data for linear and angular velocity expressed in $\{\boldsymbol{d}_i\}$ frame at time steps t_n such that $\overline{\boldsymbol{v}}(t_n) = \overline{\boldsymbol{v}}_n$, $\overline{\boldsymbol{\omega}}(t_n) = \overline{\boldsymbol{\omega}}_n$ (with $\hat{\overline{\boldsymbol{\omega}}}_n$ being corresponding material spin matrix) and $n = 1, 2, 3, ..., N$. The frame $\{\boldsymbol{d}_i\}$ is to be approximated using Eq. (2.14). However, knowing the component of spatial quantity in current frame $\{\boldsymbol{d}_i\}$ naturally gives the associated material quantity as is clear in Eqs. (2.9) and (2.13). This is the key observation that is exploited to develop the estimation algorithm discussed in the upcoming section.

The idea is to approximate the material linear and angular velocity (recall $\mathbb{R}^3$ and $so(3)$ are linear spaces). We use these interpolated quantities to estimate our state space. From here on, the component of any material quantity will be expressed in $\{\boldsymbol{E}_i\}$ frame. Thus, for simplicity, we write $\left[\hat{\overline{\boldsymbol{\omega}}}\right]_{\boldsymbol{E}_i\otimes\boldsymbol{E}_j} = \hat{\overline{\boldsymbol{\omega}}}$.

2.3.1 Smooth Patch Estimation and Gluing technique (SPEG)

In this approach, we discretized the total time span into N patches ($\overline{n} = 1, 2, ..., N$) or segments with center of the segment $\overline{n}$ being at t_n (except for the first and last segment). We consider the co-rotated derivatives of linear velocity and the angular velocity to vanish for each patch. Equivalently, we truncate the Taylor series expansion of the velocity fields about t_n to zeroth order, thereby reducing the system of differential equations (2.14) into a constant-coefficient system such that the solution of the differential equation gives an approximated configuration $\mathbf{\Phi}^h_{\overline{n}} = (\boldsymbol{\varphi}^h_{\overline{n}}, \boldsymbol{Q}^h_{\overline{n}}) \equiv (\boldsymbol{\varphi}^h_{\overline{n}}, \{\boldsymbol{d}^h_{i\overline{n}}\}) \in \mathbb{C}$ valid in the patch $\overline{n}$. Therefore, N segments would involve solving for $12N$ constants of integration. Imposing continuity in the $(\boldsymbol{\varphi}, \{\boldsymbol{d}_i\})$ fields at the boundary between the segments gives $12(N-1)$ constraints, and an appropriate boundary condition gives the additional 12 conditions. We obtain a solution for $\overline{n}^{\text{th}}$ segment as

$$\begin{aligned} \boldsymbol{\varphi}^h_{\overline{n}}(t) &= \boldsymbol{A}_{\overline{n}1} + \boldsymbol{A}_{\overline{n}2}t + \boldsymbol{A}_{\overline{n}3}\sin\omega_n t + \boldsymbol{A}_{\overline{n}4}\cos\omega_n t; \\ \boldsymbol{d}^h_{i\overline{n}}(t) &= \boldsymbol{B}_{\overline{n}i1} + \boldsymbol{B}_{\overline{n}i2}t + \boldsymbol{B}_{\overline{n}i3}\sin\omega_n t + \boldsymbol{B}_{\overline{n}i4}\cos\omega_n t. \end{aligned} \tag{2.15}$$

In the above equation $\omega_n = \|\overline{\boldsymbol{\omega}}_n\|$. We represent the vector coefficients in Eq. (2.19) in a more desirable form given below,

$$\left[[\boldsymbol{A}_{\overline{n}1}]_{\{\boldsymbol{E}_i\}}, [\boldsymbol{A}_{\overline{n}2}]_{\{\boldsymbol{E}_i\}}, [\boldsymbol{A}_{\overline{n}3}]_{\{\boldsymbol{E}_i\}}, [\boldsymbol{A}_{\overline{n}4}]_{\{\boldsymbol{E}_i\}}\right]_{3\times4} = [\boldsymbol{C}_{\overline{n}}]_{3\times4}[\boldsymbol{A}_{\overline{n}}]_{4\times4}; \tag{2.16a}$$

$$\left[[\boldsymbol{B}_{\overline{n}i1}]_{\{\boldsymbol{E}_i\}}, [\boldsymbol{B}_{\overline{n}i2}]_{\{\boldsymbol{E}_i\}}, [\boldsymbol{B}_{\overline{n}i3}]_{\{\boldsymbol{E}_i\}}, [\boldsymbol{B}_{\overline{n}i4}]_{\{\boldsymbol{E}_i\}}\right]_{3\times4} = [\boldsymbol{C}_{\overline{n}}]_{3\times4}[\boldsymbol{B}_{i\overline{n}}]_{4\times4}. \tag{2.16b}$$

In the equation above, the notation $[\boldsymbol{A}_{\overline{n}j}]_{\{\boldsymbol{E}_i\}} = [\boldsymbol{A}_{\overline{n}j}\cdot\boldsymbol{E}_1, \boldsymbol{A}_{\overline{n}j}\cdot\boldsymbol{E}_2, \boldsymbol{A}_{\overline{n}j}\cdot\boldsymbol{E}_3]^T$, represents the component of the coefficient vector $[\boldsymbol{A}_{\overline{n}j}]_{\{\boldsymbol{E}_i\}}$ in $\{\boldsymbol{E}_i\}$ frame. Therefore, the approximated solution is expressed in $\{\boldsymbol{E}_i\}$ frame (note that the boundary conditions were expressed in $\{\boldsymbol{E}_i\}$ frame). The matrix $[\boldsymbol{C}_{\overline{n}}]$ represents the 12 constants of integration corresponding to $\overline{n}^{\text{th}}$ patch and is determined using continuity conditions or the boundary conditions. The matrices $[\boldsymbol{A}_{\overline{n}}]$ and $[B_{i\overline{n}}]$ (for $i = 1, 2, 3$) contains coefficients that are function of the discrete velocity data $\overline{\boldsymbol{v}}_n$ and $\overline{\boldsymbol{\omega}}_n$ and

are given as,

$$[\boldsymbol{A}_{\overline{n}}] = \begin{bmatrix} \frac{(\overline{\boldsymbol{\omega}}_n \times \overline{\boldsymbol{v}}_n)\cdot \boldsymbol{E}_1}{\omega_n^2} & \frac{(\overline{\boldsymbol{v}}_n \cdot \overline{\boldsymbol{\omega}}_n).(\overline{\boldsymbol{\omega}}_n \cdot \boldsymbol{E}_1)}{\omega_n^2} & -\frac{(\overline{\boldsymbol{\omega}}_n \times \overline{\boldsymbol{\omega}}_n \times \overline{\boldsymbol{v}}_n)\cdot \boldsymbol{E}_1}{\omega_n^3} & -\frac{(\overline{\boldsymbol{\omega}}_n \times \overline{\boldsymbol{v}}_n)\cdot \boldsymbol{E}_1}{\omega_n^2} \\ \frac{(\overline{\boldsymbol{\omega}}_n \times \overline{\boldsymbol{v}}_n)\cdot \boldsymbol{E}_2}{\omega_n^2} & \frac{(\overline{\boldsymbol{v}}_n \cdot \overline{\boldsymbol{\omega}}_n).(\overline{\boldsymbol{\omega}}_n \cdot \boldsymbol{E}_2)}{\omega_n^2} & -\frac{(\overline{\boldsymbol{\omega}}_n \times \overline{\boldsymbol{\omega}}_n \times \overline{\boldsymbol{v}}_n)\cdot \boldsymbol{E}_2}{\omega_n^3} & -\frac{(\overline{\boldsymbol{\omega}}_n \times \overline{\boldsymbol{v}}_n)\cdot \boldsymbol{E}_2}{\omega_n^2} \\ \frac{(\overline{\boldsymbol{\omega}}_n \times \overline{\boldsymbol{v}}_n)\cdot \boldsymbol{E}_3}{\omega_n^2} & \frac{(\overline{\boldsymbol{v}}_n \cdot \overline{\boldsymbol{\omega}}_n).(\overline{\boldsymbol{\omega}}_n \cdot \boldsymbol{E}_3)}{\omega_n^2} & -\frac{(\overline{\boldsymbol{\omega}}_n \times \overline{\boldsymbol{\omega}}_n \times \overline{\boldsymbol{v}}_n)\cdot \boldsymbol{E}_3}{\omega_n^3} & -\frac{(\overline{\boldsymbol{\omega}}_n \times \overline{\boldsymbol{v}}_n)\cdot \boldsymbol{E}_3}{\omega_n^2} \\ 1 & 0 & 0 & 0 \end{bmatrix}; \tag{2.17}$$

$$[\boldsymbol{B}_{i\overline{n}}] = \begin{bmatrix} \frac{(\boldsymbol{d}_{i0}+\overline{\boldsymbol{\omega}}_n \times \overline{\boldsymbol{\omega}}_n \times \boldsymbol{d}_{i0})\cdot \boldsymbol{E}_1}{\omega_n^2} & 0 & \frac{(\boldsymbol{d}_{i0} \times \overline{\boldsymbol{\omega}}_n)\cdot \boldsymbol{E}_1}{\omega_n} & -\frac{(\overline{\boldsymbol{\omega}}_n \times \overline{\boldsymbol{\omega}}_n \times \boldsymbol{d}_{i0})\cdot \boldsymbol{E}_1}{\omega_n^2} \\ \frac{(\boldsymbol{d}_{i0}+\overline{\boldsymbol{\omega}}_n \times \overline{\boldsymbol{\omega}}_n \times \boldsymbol{d}_{i0})\cdot \boldsymbol{E}_2}{\omega_n^2} & 0 & \frac{(\boldsymbol{d}_{i0} \times \overline{\boldsymbol{\omega}}_n)\cdot \boldsymbol{E}_2}{\omega_n} & -\frac{(\overline{\boldsymbol{\omega}}_n \times \overline{\boldsymbol{\omega}}_n \times \boldsymbol{d}_{i0})\cdot \boldsymbol{E}_2}{\omega_n^2} \\ \frac{(\boldsymbol{d}_{i0}+\overline{\boldsymbol{\omega}}_n \times \overline{\boldsymbol{\omega}}_n \times \boldsymbol{d}_{i0})\cdot \boldsymbol{E}_3}{\omega_n^3} & 0 & \frac{(\boldsymbol{d}_{i0} \times \overline{\boldsymbol{\omega}}_n)\cdot \boldsymbol{E}_3}{\omega_n} & -\frac{(\overline{\boldsymbol{\omega}}_n \times \overline{\boldsymbol{\omega}}_n \times \boldsymbol{d}_{i0})\cdot \boldsymbol{E}_3}{\omega_n^2} \\ 0 & 0 & 0 & 0 \end{bmatrix}. \tag{2.18}$$

Equation (2.15) yields a helix (which is smooth). This is commensurate with *Mozzi–Chasles's theorem*, the equivalent statement of which for this case would be: '*the motion of a rigid body with the co-rotational derivative of linear and angular velocity vanishing, is a screw (or helix) motion*'.

We glue the solution of each patch using heavy side function (as shown in (2.19)) such that the global approximated configuration $\boldsymbol{\Phi}^h = (\boldsymbol{\varphi}^h, \{\boldsymbol{d}_i^h\}) \in \mathbb{C}$ is continuous at the point of gluing, thus justifying the name *smooth patch estimation and gluing technique* (SPEG).

$$\begin{aligned} \boldsymbol{\varphi}^h(t) &= \sum_{\overline{n}=1}^{N} \boldsymbol{\varphi}_{\overline{n}}^h(t) \left[H(t-\hat{t}_{\overline{n}-1}) - H(t-\hat{t}_{\overline{n}})\right]; \\ \boldsymbol{d}_i^h(t) &= \sum_{\overline{n}=1}^{N} \boldsymbol{d}_{i\overline{n}}^h(t) \left[H(t-\hat{t}_{\overline{n}-1}) - H(t-\hat{t}_{\overline{n}})\right]. \end{aligned} \tag{2.19}$$

In the equation above $H(.)$ represents Heaviside function and $\hat{t}_{\overline{n}}$ represents the right boundary of $\overline{n}^{\text{th}}$ segment (such that $\hat{t}_{\overline{n}-1} < \hat{t}_{\overline{n}}$), with $\hat{t}_0 = 0$.

Interestingly, a closed-form solution of the director triads can be arrived without solving the differential Eq. (2.14), by using our understanding of $SO(3)$ manifold as discussed in section 1.3.2.

To carry out the discussion further, let $\boldsymbol{Q}^h(t) \in SO(3)$ represent the approximated rotation tensor with respect to $\boldsymbol{I}_3 = \boldsymbol{E}_i \otimes \boldsymbol{E}_i = \boldsymbol{d}_{0i} \otimes \boldsymbol{d}_{0i}$. For the first segment $\overline{n} = 1$, the approximated director $\boldsymbol{d}^h_{i(\overline{n}=1)} = \boldsymbol{d}^h_{i1}$ is obtained by rotating the prescribed boundary $\boldsymbol{d}_{i0} = \boldsymbol{E}_i$ by an angle $\int_0^t \omega_1 dt = \omega_1 t$ (with $\hat{t}_0 \leq t \leq \hat{t}_1$) about the unit vector $\frac{\overline{\omega}_1}{\omega_1}$ such that,

$$\boldsymbol{d}^h_{i1}(t) = \exp\left(\hat{\overline{\boldsymbol{\omega}}}_1 t\right).\boldsymbol{d}_{i0} = \boldsymbol{Q}^h_1(t).\boldsymbol{d}_{i0} \;\text{ with }\; \hat{t}_0 \leq t < \hat{t}_1. \tag{2.20}$$

The director triad at the right end of patch 1 becomes the boundary for the patch $\overline{n} = 2$. For patch 2 with $\hat{t}_1 \leq t \leq \hat{t}_2$ the approximate director triad $\boldsymbol{d}^h_{i2}(t)$ can be obtained by rotating $\boldsymbol{d}^h_{i1}(\hat{t}_1)$ (obtained in Eq. (2.20)). However, $\hat{\overline{\boldsymbol{\omega}}}_2 \in T_{\boldsymbol{I}_3}SO(3)$ is a material tensor whose corresponding spatial counterpart associated with $T_{\boldsymbol{Q}^h_1(\hat{t}_1)}SO(3)$ is given by $\hat{\boldsymbol{\omega}}^h_2 = \boldsymbol{Q}^h_1(\hat{t}_1).\hat{\overline{\boldsymbol{\omega}}}_2.\boldsymbol{Q}^{h^T}_1(\hat{t}_1)$ such that $\hat{\boldsymbol{\omega}}^h_2.\boldsymbol{Q}^h_1(\hat{t}_1) \in T_{\boldsymbol{Q}^h_1(\hat{t}_1)}SO(3)$. We observe that $\hat{\boldsymbol{\omega}}^h_2.\boldsymbol{Q}^h_1(\hat{t}_1)$ is a *right translated* vector field. Similarly, we can obtain *left translated* vector field as $\boldsymbol{Q}^h_1(\hat{t}_1).\hat{\overline{\boldsymbol{\omega}}}_2 \in T_{\boldsymbol{Q}^h_1(\hat{t}_1)}SO(3)$. Equation (2.21a) and (2.21b) gives the approximated director field for patch 2 by using *right invariant* and *left invariant* vector fields, respectively as,

$$\begin{aligned}\boldsymbol{d}^h_{i2}(t) &= \exp\left(\hat{\boldsymbol{\omega}}^h_2.(t-\hat{t}_1)\right)\boldsymbol{d}^h_{i1}(\hat{t}_1) = \exp\left(\hat{\boldsymbol{\omega}}^h_2.(t-\hat{t}_1)\right).\boldsymbol{Q}^h_1(\hat{t}_1).\boldsymbol{d}_{i0} \\ &= \boldsymbol{Q}^h_2(t).\boldsymbol{d}_{i0} \;\text{ with }\; \hat{t}_1 \leq t \leq \hat{t}_2;\end{aligned} \tag{2.21a}$$

$$\boldsymbol{d}^h_{i2}(t) = \boldsymbol{Q}^h_1(\hat{t}_1).\exp\left(\hat{\boldsymbol{\omega}}_2.(t-\hat{t}_1)\right).\boldsymbol{d}_{i0} \;\text{ with }\; \hat{t}_1 \leq t \leq \hat{t}_2. \tag{2.21b}$$

Similarly, for the third patch with $\hat{\boldsymbol{\omega}}^h_3 = \boldsymbol{Q}^h_2(\hat{t}_2).\hat{\overline{\boldsymbol{\omega}}}_3.\boldsymbol{Q}^{h^T}_2(\hat{t}_2)$, we have,

$$\boldsymbol{d}^h_{i3}(t) = \exp\left(\hat{\boldsymbol{\omega}}^h_3.(t-\hat{t}_2)\right).\boldsymbol{Q}^h_2(\hat{t}_2).\boldsymbol{d}_{i0} = \boldsymbol{Q}^h_3(t).\boldsymbol{d}_{i0} \;\text{ with }\; \hat{t}_2 \leq t \leq \hat{t}_3; \tag{2.22a}$$

$$\boldsymbol{d}^h_{i3}(t) = \boldsymbol{Q}^h_2(\hat{t}_2).\exp\left(\hat{\overline{\boldsymbol{\omega}}}_3.(t-\hat{t}_2)\right).\boldsymbol{d}_{i0} \;\text{ with }\; \hat{t}_2 \leq t \leq \hat{t}_3. \tag{2.22b}$$

Along similar lines of reasoning, the solution for $\overline{n}^{\text{th}}$ patch is given by

$$\boldsymbol{d}^h_{i\overline{n}}(t) = \boldsymbol{Q}^h_{\overline{n}}(t).\boldsymbol{d}_{i0}. \tag{2.23}$$

where,

$$\text{Using } \textit{right invariant} \text{ vector field : } \boldsymbol{Q}_{\overline{n}}^{h}(t) = \exp\left(\hat{\omega}_{n}^{h}.(t-\hat{t}_{\overline{n}-1})\right).\boldsymbol{Q}_{\overline{n}-1}^{h}(\hat{t}_{\overline{n}-1}) \text{ with } \hat{t}_{\overline{n}-1} \leq t \leq \hat{t}_{\overline{n}}; \tag{2.24a}$$

$$\text{Using } \textit{left invariant} \text{ vector field : } \boldsymbol{Q}_{\overline{n}}^{h}(t) = \boldsymbol{Q}_{\overline{n}-1}^{h}(\hat{t}_{\overline{n}-1}).\exp.\left(\hat{\overline{\omega}}_{n}.(t-\hat{t}_{\overline{n}-1})\right) \text{ with } \hat{t}_{\overline{n}-1} \leq t \leq \hat{t}_{\overline{n}}. \tag{2.24b}$$

The spatial curvature tensor $\hat{\omega}_{n}^{h}$ in Eq. (2.24a) is given as,

$$\hat{\omega}_{n}^{h} = \boldsymbol{Q}_{\overline{n}-1}^{h}(\hat{t}_{\overline{n}-1}).\hat{\overline{\omega}}_{n}.\boldsymbol{Q}_{\overline{n}-1}^{h^{T}}(\hat{t}_{\overline{n}-1}). \tag{2.25}$$

Note that $\hat{\omega}_{n}^{h}$ is not a function of time for a given patch $\overline{n}$ and unlike the material tensor $\hat{\overline{\omega}}_{n}$, the spatial curvature tensor is an approximated quantity. The global approximated rotation tensor is then given by,

$$\boldsymbol{Q}^{h}(t) = \sum_{\overline{n}=1}^{N} \boldsymbol{Q}_{\overline{n}}^{h}(t)\left(H(t-\hat{t}_{\overline{n}-1}) - H(t-\hat{t}_{\overline{n}})\right). \tag{2.26}$$

From Eqs. (2.14) and (2.24b), the approximated position vector for patch $\overline{n}$ is obtained as,

$$\boldsymbol{\varphi}_{\overline{n}}^{h}(t) = \left(\int_{\hat{t}_{\overline{n}-1}}^{t} \exp\left(\hat{\overline{\omega}}_{n}t\right)\mathrm{d}t\right).\overline{\boldsymbol{v}}_{n} + \sum_{k=1}^{\overline{n}-1}\left(\int_{\hat{t}_{k-1}}^{\hat{t}_{k}} \exp\left(\hat{\overline{\omega}}_{k}t\right)\mathrm{d}t\right).\overline{\boldsymbol{v}}_{k}. \tag{2.27}$$

Figure 2.3 gives geometric interpretation of the discussion so far. The following remarks details few noteworthy geometric interpretations on the interpretation approach discussed above:

Remark 2.1: Consider the $\overline{n}^{\text{th}}$ patch where the approximated configuration $\boldsymbol{\Phi}_{\overline{n}}^{h}$ is parametrized by $t \in [t_{\overline{n}-1}, t_{\overline{n}}]$. The co-rotated derivative of angular velocity being zero implies that the angular velocity is parallel-transported along a curve $\boldsymbol{Q}_{\overline{n}}^{h}(t)$ on the manifold $SO(3)$ such that the approximated angular velocity $\boldsymbol{\omega}_{\overline{n}}^{h}$ at time t is given as,

$$\boldsymbol{\omega}_{\overline{n}}^{h}(t) = \boldsymbol{Q}_{\overline{n}}^{h}(t)\overline{\boldsymbol{\omega}}_{n} = \boldsymbol{Q}_{\overline{n}}^{h}(t).\boldsymbol{Q}_{\overline{n}}^{h^{T}}(\hat{t}_{n}).\boldsymbol{\omega}_{n}^{h}. \tag{2.28}$$

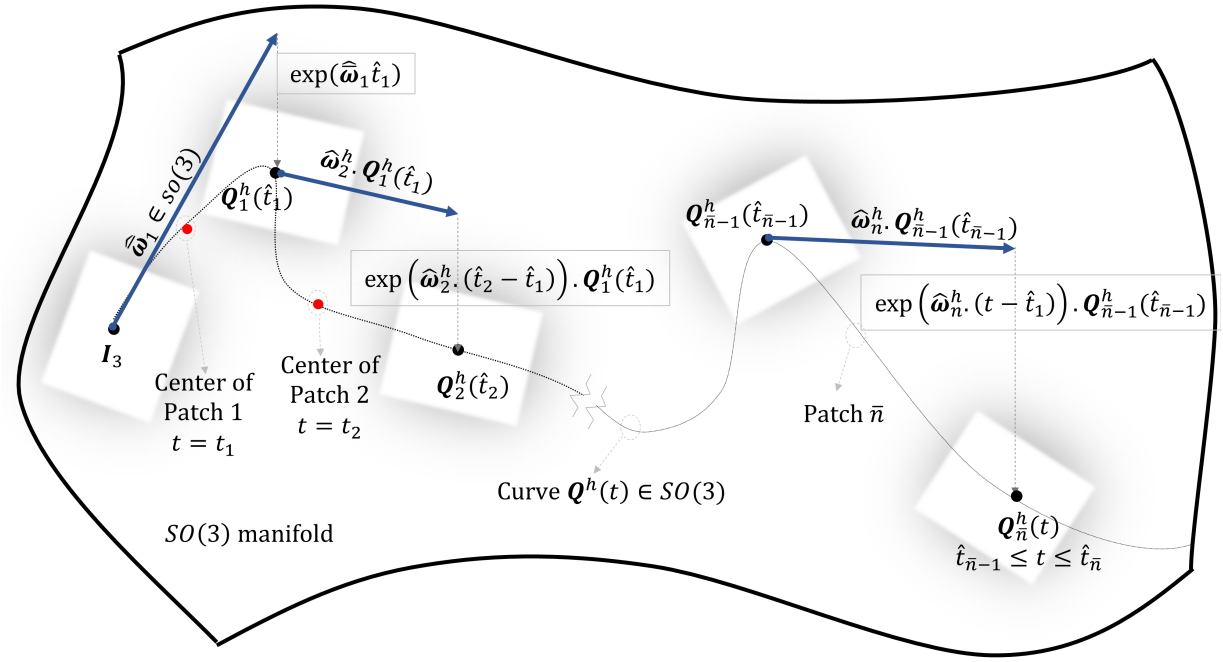

Figure 2.3: Geometric representation of SPEG.

The vector $\boldsymbol{\omega}_n^h$ is the associated axial vector for the spatial tensor $\hat{\boldsymbol{\omega}}_n^h$. From the equation above and Eq. (2.25), we observe that the spatial angular velocity $\boldsymbol{\omega}_n^h = \boldsymbol{Q}_{\bar{n}}^h(t_n).\overline{\boldsymbol{\omega}}_n$ and the associated spin tensor $\hat{\boldsymbol{\omega}}_n^h$ are approximate quantities. It is interesting to observe that $\|\boldsymbol{\omega}_n^h\| = \|\overline{\boldsymbol{\omega}}_n\| = \omega_n$.

Remark 2.2: The solution obtained above is free of singularity (unlike Frenet frame). If the angular velocity measurement for the $\overline{n}^{\text{th}}$ patch is zero (implying point of inflection), we have the solution of the form,

$$\lim_{\omega_n \to \mathbf{0}} \boldsymbol{\varphi}_{\bar{n}}^h(t) = \left(C_{\bar{n}i4} + t(C_{\bar{n}ij}\overline{v}_{nj})\right)\boldsymbol{E}_i; \tag{2.29a}$$

$$\lim_{\omega_n \to \mathbf{0}} \boldsymbol{d}_{i\bar{n}}^h(t) = C_{\bar{n}ji}\boldsymbol{E}_j = \boldsymbol{d}_{i(\bar{n}-1)}^h(\hat{t}_{\bar{n}-1}). \tag{2.29b}$$

Solution of the form above suggests a local linear solution for the approximated position vector and a constant solution for the approximated director triads. However, if $\overline{\boldsymbol{v}}_n = \mathbf{0}$ and $\overline{\boldsymbol{\omega}}_n = \mathbf{0}$, the approximated local solution is a point (the object is stationary) with a fixed director triad given by

Eq. (2.29b) and the position vector reduces to,

$$\lim_{\substack{\boldsymbol{v}_n \to \mathbf{0} \\ \boldsymbol{\omega}_n \to \mathbf{0}}} \boldsymbol{\varphi}^h_{\overline{n}}(t) = C_{\overline{n}i4}\boldsymbol{E}_i = \boldsymbol{\varphi}^h_{\overline{n}-1}(\hat{t}_{\overline{n}-1}). \tag{2.30}$$

Similarly, the limiting case of solution with $\overline{\boldsymbol{v}}_n = \mathbf{0}$ represents a rotating rigid body with no translation. In case where $\overline{\boldsymbol{v}}_n \neq \mathbf{0}$ and $\overline{\boldsymbol{\omega}}_n \neq \mathbf{0}$, the solution represented by Eq. (2.15) is a helix. Thus, if the moving object follows a helix exactly with constant speed, we need only one data point along with the prescribed boundary condition to give exact state space (provided there is no noise in the data). Lastly, the accuracy of global solution depends on the nature of data. If the data is representative of the local configuration of a patch, a good approximation is obtained.

2.3.2 Higher order approximation techniques

In the SPEG technique discussed above, the approximated linear and angular velocity fields were C^{-1} continuous. The advantage of the SPEG technique lies in the existence of a closed-form solution, making it a desirable approach provided the linear and angular velocity data (or equivalently, strain and curvature data in case of shape sensing of rods) does not vary too much along with the patch. Todd et al. [16] and Chadha and Todd [17], [18] used SPEG to develop shape reconstruction (refer to chapter 5) of rods and observed that a fairly accurate solution is obtained in such case. However, if the system is more dynamic (like a UAV), a higher-order approximation of linear and angular velocity field is desirable. We can approximate these fields using Lagrangian polynomial, cubic splines, Hermite polynomial interpolation, and moving least square (MLS), to name a few.

Note that the data for linear and angular velocity are obtained in $\{\boldsymbol{d}_i\}$ frame, which is time dependent. However, to numerically integrate Eq. (2.14), we utilize the approximated fields of the components $\overline{v}^h_i$ and $\overline{\omega}^h_i$ (we do not approximate the spatial linear velocity and the angular velocity vectors). Equivalently, we are interpolating the material linear velocity $\overline{\boldsymbol{v}}(t) = \overline{v}_i\boldsymbol{E}_i$ and the material angular velocity $\overline{\boldsymbol{\omega}}(t) = \overline{\omega}_i\boldsymbol{E}_i$. Let $\overline{\boldsymbol{v}}^h(t)$ and $\overline{\boldsymbol{\omega}}^h(t)$ (with $\hat{\overline{\boldsymbol{\omega}}}^h(t)$ being the corresponding

spin tensor) represent the approximated material linear and angular velocity. The estimated configuration is obtained as

$$\begin{aligned} \boldsymbol{Q}^h(t) &= \exp\left(\int_0^t \hat{\overline{\boldsymbol{\omega}}}^h(t)\,\mathrm{d}t\right); \\ \boldsymbol{\varphi}^h(t) &= \int_0^t \boldsymbol{Q}^h(t).\overline{\boldsymbol{v}}^h(t)\,\mathrm{d}t, \end{aligned} \tag{2.31}$$

with,

$$\int_0^t \hat{\overline{\boldsymbol{\omega}}}^h(t)\,\mathrm{d}t \in so(3). \tag{2.32}$$

2.3.3 Error quantification

We quantify the error $e_{\boldsymbol{\varphi}}(t)$ in the position vector by the usual Euclidean norm of difference in the exact and estimated position vector,

$$e_{\boldsymbol{\varphi}}(t) = \|\boldsymbol{\varphi}(t) - \boldsymbol{\varphi}^h(t)\|; \tag{2.33a}$$

$$\mathrm{RMS}_{\boldsymbol{\varphi}} = \sqrt{\frac{\sum_{k=1}^{M} e_{\boldsymbol{\varphi}}^2(t_k)}{M}}. \tag{2.33b}$$

Similarly, we define error in each director as,

$$e_{\boldsymbol{d}_i}(t) = \|\boldsymbol{d}_i(t) - \boldsymbol{d}_i^h(t)\|; \tag{2.34a}$$

$$\mathrm{RMS}_{\boldsymbol{d}_i} = \sqrt{\frac{\sum_{k=1}^{M} e_{\boldsymbol{d}_i}^2(t_k)}{M}}. \tag{2.34b}$$

Local homeomorphism (refer to section 1.3.2.2) of exponential map allows us to define *Reimannian metric* on $SO(3)$ that evaluates the deviation between the approximated rotation tensor $\boldsymbol{Q}^h(t)$ and the exact rotation tensor $\boldsymbol{Q}(t)$ by measuring the length of geodesic between them. The error is associated with the amount of rotation $\boldsymbol{Q}_{\mathrm{error}}(t)$ required to align $\boldsymbol{Q}^h(t)$ with $\boldsymbol{Q}(t)$ such that,

$$\boldsymbol{Q}(t) = \boldsymbol{Q}_{\mathrm{error}}(t).\boldsymbol{Q}^h(t). \tag{2.35}$$

Let $\boldsymbol{Q}_{\text{error}}(t)$ be parametrized by $\boldsymbol{\theta}_e = \theta_e \boldsymbol{n}_{\theta_e}$ such that $\theta_e \in [0, \pi)$. We define the error $e_{\boldsymbol{Q}}$ as,

$$e_{\boldsymbol{Q}}(t) = \left\langle \boldsymbol{Q}, \boldsymbol{Q}^h \right\rangle = \theta_e(t) = \|\log(\boldsymbol{Q}_{\text{error}}(t))\| \in [0, \pi); \tag{2.36a}$$

$$\text{RMS}_{\boldsymbol{Q}} = \sqrt{\frac{\sum_{k=1}^{M} e_{\boldsymbol{Q}}(t_k)^2}{M}}. \tag{2.36b}$$

In the equation above, $\langle ., . \rangle : SO(3) \times SO(3) \longrightarrow [0, \pi)$ defines a bi-invariant (refer to Eqs. 2.38e and 2.38f below) Reimannian metric such that for any $\boldsymbol{Q}_1, \boldsymbol{Q}_2 \in SO(3)$,

$$\langle \boldsymbol{Q}_1, \boldsymbol{Q}_2 \rangle = \|\log(\boldsymbol{Q}_1 . \boldsymbol{Q}_2^T)\|. \tag{2.37}$$

For any $\boldsymbol{Q}_1, \boldsymbol{Q}_2, \boldsymbol{Q}_3 \in SO(3)$ the metric defined above has following properties:

Non-negativity :	$\langle \boldsymbol{Q}_1, \boldsymbol{Q}_2 \rangle \in [0, \pi)$	(2.38a)
Identity of indiscernibles :	$\langle \boldsymbol{Q}_1, \boldsymbol{Q}_2 \rangle = 0 \Leftrightarrow \boldsymbol{Q}_1 = \boldsymbol{Q}_2$	(2.38b)
Symmetry :	$\langle \boldsymbol{Q}_1, \boldsymbol{Q}_2 \rangle = \langle \boldsymbol{Q}_2, \boldsymbol{Q}_1 \rangle$	(2.38c)
Triangle inequality :	$\langle \boldsymbol{Q}_1, \boldsymbol{Q}_2 \rangle \leq \left\langle \boldsymbol{Q}_1, \boldsymbol{Q}_3 \right\rangle + \left\langle \boldsymbol{Q}_3, \boldsymbol{Q}_2 \right\rangle$	(2.38d)
Right invariant :	$\left\langle \boldsymbol{Q}_1 . \boldsymbol{Q}_3, \boldsymbol{Q}_2 . \boldsymbol{Q}_3 \right\rangle = \langle \boldsymbol{Q}_1, \boldsymbol{Q}_2 \rangle$	(2.38e)
Left invariant :	$\left\langle \boldsymbol{Q}_3 . \boldsymbol{Q}_1, \boldsymbol{Q}_3 . \boldsymbol{Q}_2 \right\rangle = \langle \boldsymbol{Q}_1, \boldsymbol{Q}_2 \rangle$	(2.38f)

Refer to Park [27] for more details on this metric. The paper by Huynh [28] serves as a great reference to understand various kinds of metric on $SO(3)$. Huynh [28] also provides proof for the properties stated above.

2.3.4 Illustration and simulation

We simulate the path of a moving rigid body like UAV. We consider the pitch, yaw and roll angle fields parametrized by $t \in [0, \bar{t}]$ calibrated with respect to $\{\boldsymbol{E}_i\}$ frame,

$$\begin{aligned}
\phi_p(t) &= 0.5\sin(0.7\bar{t}) + \frac{\pi}{2}\left[\cos\left(\frac{\pi t}{\bar{t}}\right) + \sin\left(\frac{\pi t}{\bar{t}}\right).\left(1 - \sin\left(\frac{3.5\pi t}{\bar{t}}\right)\right)\right];\\
\phi_y(t) &= 4 + \frac{1}{25}(t - \bar{t}) + \sin(t) + \pi\sin\left(\frac{4\pi t}{\bar{t}}\right);\\
\phi_r(t) &= 0.1\left(\pi\sin\left(\frac{4\pi t}{\bar{t}}\right) + \sin(t)\right);\\
\overline{v}_1(t) &= 1 + 0.15\sin(0.3t) + 0.2\cos\left(\frac{4\pi t}{2\bar{t}}\right);\\
\overline{v}_2(t) &= \overline{v}_3 = 0.
\end{aligned} \tag{2.39}$$

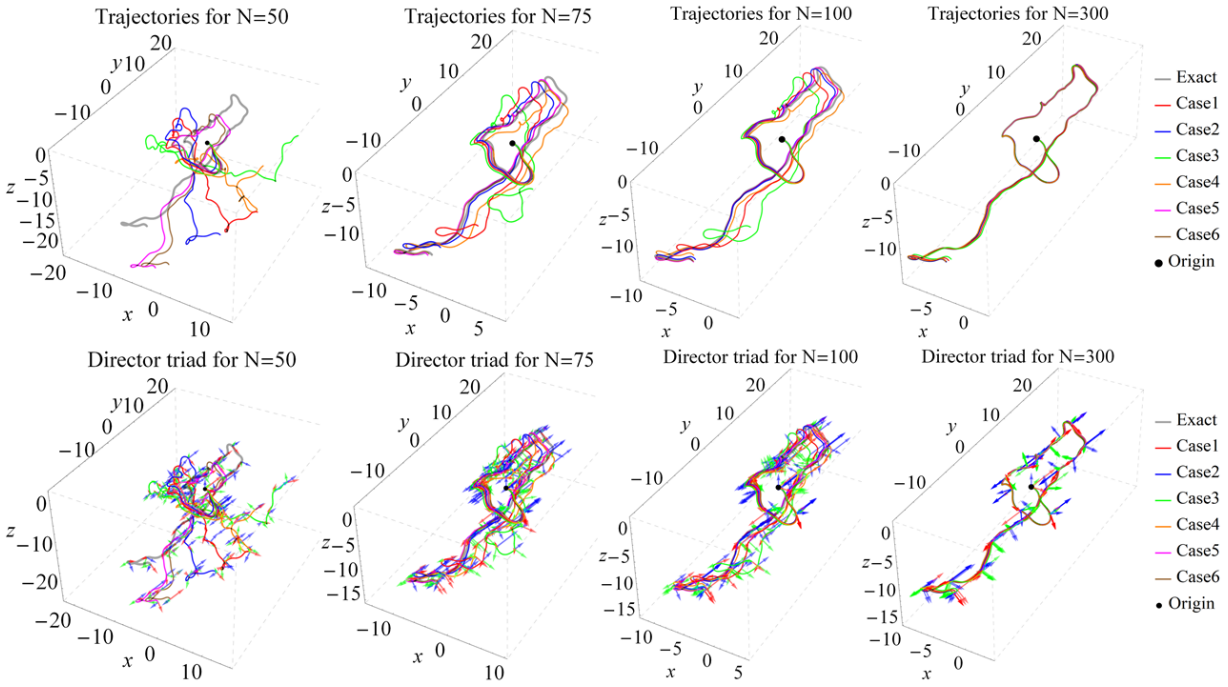

Figure 2.4: Estimated trajectory and the orientation of the rigid body.

The rigid-body motion defined by (2.39) is similar to Kirchhoff beam kinematics. A GMAF is sufficient to frame this path because $\overline{v}_2(t) = \overline{v}_3(t) = 0$. Thus, we obtain the angular

Table 2.1: Various approach to interpolate the material linear and angular velocity data

Cases	Interpolation method
Case 1	C^{-1} approximation (constant over the patch $\overline{n}$ of SPEG)
Case 2	Cubic Hermite
Case 3	C^0 approximation
Case 4	Moving least square approximation (MLS)
Case 5	Cubic B-Spline
Case 6	Quadratic B-Spline

velocity components $\overline{\omega}_i$ from the assumed Euler angles in Eq. (2.39) using the results obtained in section 1.4.1.2 (except that the independent parameter here is time t). We can equivalently consider unit quaternion field and obtained the angular velocity using equations (1.36a), (1.36b) and (1.36c). The exact rotation tensor is obtained by using Eq. (1.28). Note that for this example $\{\boldsymbol{d}_1, \boldsymbol{d}_2, \boldsymbol{d}_3\} \equiv \{\boldsymbol{T}, \boldsymbol{Y}_g, \boldsymbol{P}_g\}$. At $t = 0$, the initial conditions are $\boldsymbol{d}_i(0) = \boldsymbol{d}_{i0} = \boldsymbol{E}_i$. The exact position vector is then obtained as,

$$\boldsymbol{\varphi}(t) = \int_0^t \overline{v}_1(k)\boldsymbol{d}_1(k)\,\mathrm{d}k. \tag{2.40}$$

We consider $t_0 = 100$s and number of discrete data points as N with t_n representing the time corresponding to n^{th} data point. We assume $t_1 = 0.25$s and $t_N = (\bar{t} - 0.25)$s. The time steps in between t_1 and t_n are uniformly spaced. We use 6 different interpolation techniques listed in table 2.1 to approximate the material linear and angular velocity.

Consider the following points:

1. In case 1, the data $\overline{\boldsymbol{v}}_n$ and $\overline{\boldsymbol{\omega}}_n$ are assumed constant over the patch $\overline{n}$ as described in section 2.3.1. The estimated configuration space using SPEG is the same as the configuration space obtained using equation (2.31) with $\overline{\boldsymbol{v}}_n^h$ and $\overline{\boldsymbol{\omega}}_n^h$ being C^{-1} approximation of the data over the patch $\overline{n}$. This technique will be deployed in later chapter to develop shape sensing algorithm for beams.

2. Readers can refer to chapter 3 of Bartels et al. [29] for more information on Cubic Hermite and B-Spline interpolation. Case 3 represents the data being linearly interpolated between

two time steps t_n and t_{n+1}.

3. We briefly describe the MLS approach here. Let $\boldsymbol{P}(t) = \{1, t, t^2, ..., t^m\}^T$ represent set of m^{th} order polynomial set and $W(t - t_n)$ represent the moving weight function, then the approximate linear velocity component $\overline{v}_i^h(t)$ is given as,

$$\begin{aligned} \overline{v}_i^h(t) &= \boldsymbol{P}^T(t_n).\boldsymbol{M}^{-1}.\sum_{n=1}^{N}\boldsymbol{P}(t_n).\overline{v}_{ni}.W(t-t_n); \\ M := \text{Moment matrix} &= \sum_{n=1}^{N}\boldsymbol{P}(t_n).\boldsymbol{P}^T(t_n).W(t-t_n). \end{aligned} \tag{2.41}$$

We have used cubic B-spline weight function, such that,

$$W(t-t_n) = W(z_n) = \begin{cases} \frac{2}{3} - 4z_n^2 + 4z_n^3, & \text{for } 0 \le z_n \le 0.5 \\ \frac{4}{3} - 4z_n + 4z_n^2 - \frac{4}{3}4z_n^3, & \text{for } 0.5 \le z_n \le 1 \\ 0 & \text{otherwise} \end{cases}; \tag{2.42}$$
$$z_n = \frac{|t-t_n|}{a}.$$

The term a in the equation above is the support size. For m^{th} order basis set, the weight function must be spread enough to cover at least $(m + 1)$ data points. This fact is used to evaluate the support size. The accuracy of MLS approach depends on the choice of support size and the order of polynomial. In a similar fashion, the approximate angular velocity fields $\overline{\omega}_i^h(t)$ is obtained. Interested readers can refer to the landmark paper on interpolation of surface using MLS approach by Lancaster and Salkauskas [30]. A paper by Levin [31] discusses how MLS is the near-best approach towards interpolation. MLS approximation became popular in the field of applied mechanics after it was used to develop Meshfree finite element analysis (refer Belytschko et al. [32] and Chen et al. [33]).

We consider N=20, 50, 75, 100, 300 and 500 to compare various approaches. The idea is to estimate the configuration space $(\boldsymbol{\varphi}^h(t), \boldsymbol{Q}^h(t))$ using Eq. (2.31) (for all cases except Case 1)

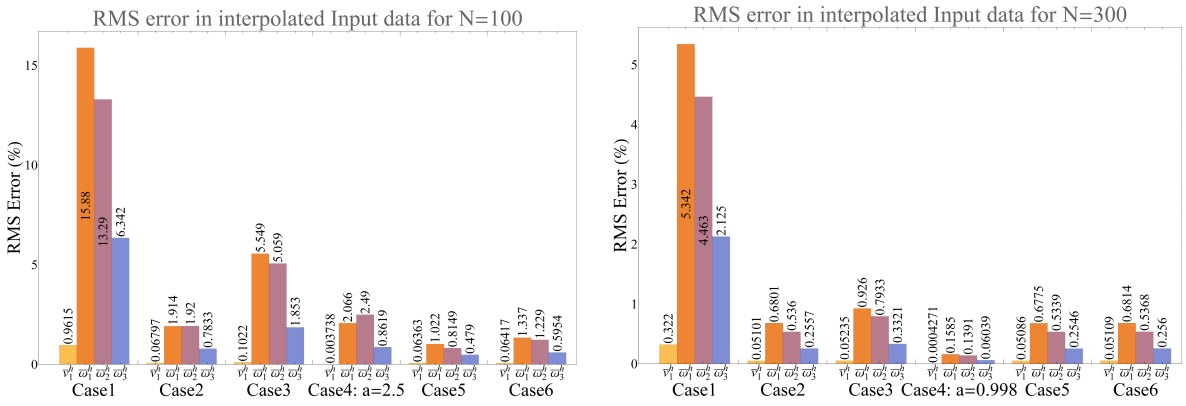

(a) N=100 (b) N=300

Figure 2.5: RMS error in the estimated material linear and angular velocity fields approximated by various approaches.

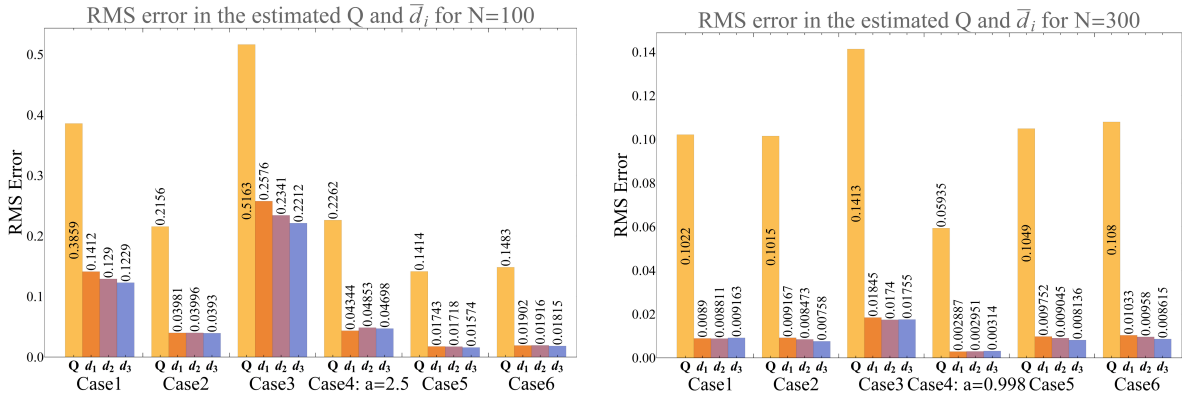

(a) N=100 (b) N=300

Figure 2.6: RMS error in the estimated $\boldsymbol{Q}$ and $\boldsymbol{d}_i$ approximated by various approaches.

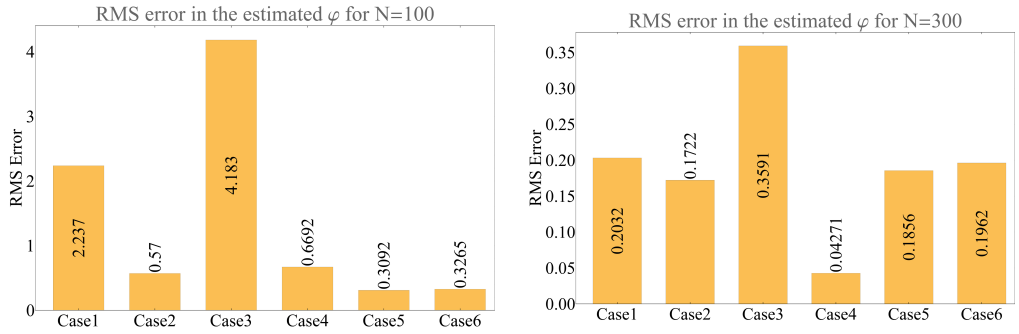

(a) N=100 (b) N=300

Figure 2.7: RMS error in the estimated $\boldsymbol{\varphi}$ approximated by various approaches.

and (2.19) (for Case 1). The spatial linear and angular velocity is estimated by left translating approximated material linear and angular velocity as,

$$\begin{aligned} \boldsymbol{v}^h(t) &= \boldsymbol{Q}^h.\overline{\boldsymbol{v}}^h(t); \\ \boldsymbol{\omega}^h(t) &= \boldsymbol{Q}^h.\overline{\boldsymbol{\omega}}^h(t). \end{aligned} \tag{2.43}$$

Figure 2.4 demonstrates the estimated configuration (the trajectory and the orientation of object at 20 uniformly spaces time steps) for N=50, 75, 100 and 300 obtained using interpolation methods mentioned in Table 2.1. The estimated shape converges with the increase of data points as expected. Figure 2.5 shows RMS errors in the approximated material linear and angular velocity $(\overline{\boldsymbol{v}}^h, \overline{\boldsymbol{\omega}}^h)$ and the estimated position vector, director triads and rotation tensor for N=100 and 300, calculated using M=500 in equations (2.33b), (2.34b) and (2.36b). Excellent estimates are obtained for N=100 with the error: $\text{RMS}_{\boldsymbol{Q}} = \{0.386, 0.216, 0.516, 0.226, 0.141, 0.148\}$ radian and $\text{RMS}_{\boldsymbol{\varphi}} = \{2.237, 0.570, 4.193, 0.669, 0.309, 0.326\}$ m for case 1 to 6 respectively. The RMS error further reduces with increase of data points, as observed in Fig. 2.6. Figure 2.6 and 2.7 show the error fields $e_{\boldsymbol{\varphi}}(t)$, $e_{\boldsymbol{Q}}(t)$ and $e_{\boldsymbol{d}_i}(t)$ obtained using the error definition in equations (2.33a), (2.34a) and (2.36a). Figure 2.8 shows comparison of RMS error in the configuration space for different interpolation approaches with increasing number of sensors.

Here are the important observations:

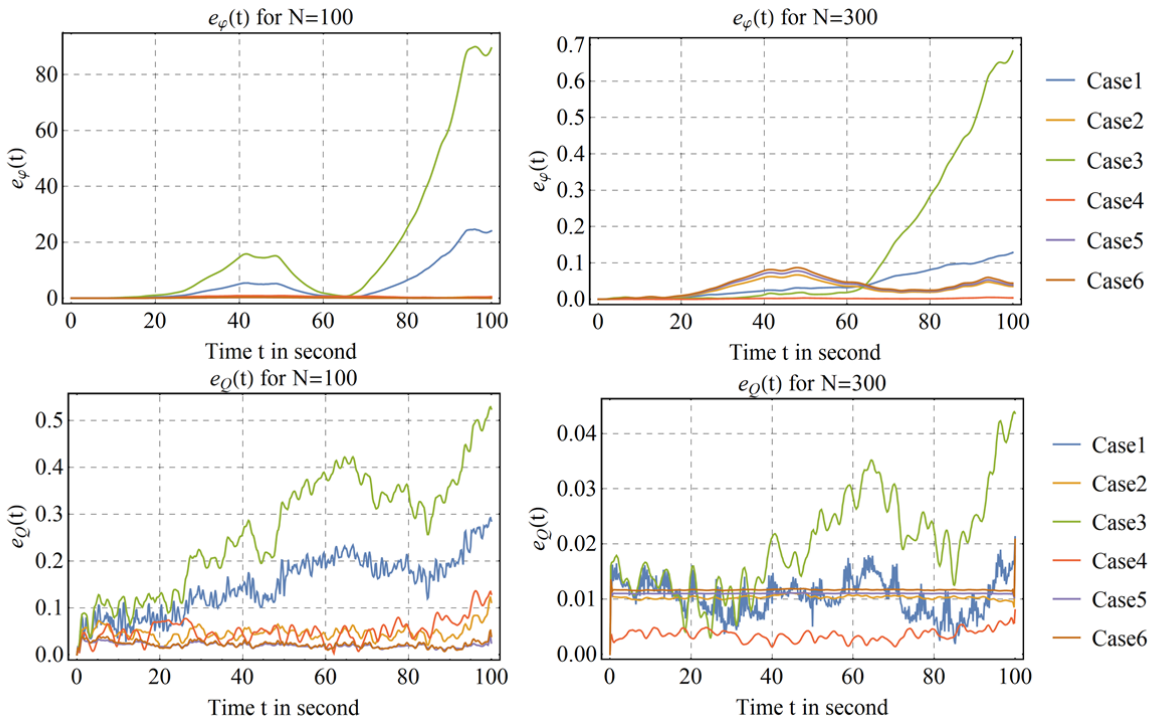

Figure 2.8: Error e_{φ} and e_{Q} for $N = 100$ and $N = 300$.

1. As is clear from figure 2.10, the algorithm is convergent.

2. The MLS (case 4) and Cubic spline interpolation (case 5 and 6) are amongst the best approaches to estimate the state space. This is because Case 4 and 5 (and 6) interpolated the input data better than other approaches.

3. Proper choice of support size and polynomial order in MLS method can drastically reduce the error. In this case, we have used polynomial of 2^{nd} order with support size of a=15.7, 5.08, 3.09, 2.5 and 0.998; for N=20, 50, 75, 100 and 300 respectively.

4. Linear interpolation of input data (case 3) is the worst performer in terms of the configuration space estimate.

5. Despite having highest RMS error in estimating the input data, SPEG technique (case 1) performs fairly well (better than case 3 that gives highest error) at the estimation of configuration. The advantage of SPEG is existence of a closed form solution as discussed

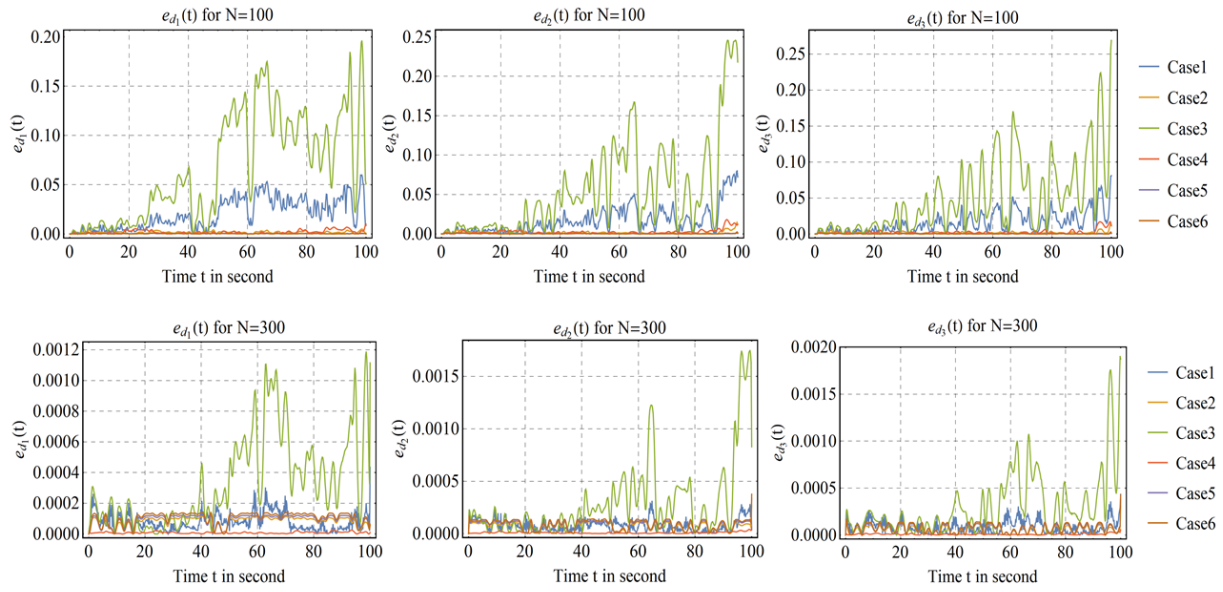

Figure 2.9: Error $e_{\boldsymbol{d}_i}$ for $N = 100$ and $N = 300$.

in section 2.3.1 whereas other higher order approaches (case 2-5) includes numerical integration (equation (2.31)) to obtain the configuration space. We also observe that the error propagates along the trajectory of object attaining maximum value at the farthest end from the point of initial condition.

6. Cubic and quadratic B-splines gives nearly same result. With increase in number of data, B-spline approximation and Cubic Hermite approximations converges.

7. The error discussed here is purely due to the numerical algorithm used to estimate the configuration space. However, in real time, the noise in the measurement must be considered. Another source of error might be in the uncertainty of initial condition (especially in shape sensing of beams: refer to Chadha and Todd[17]).

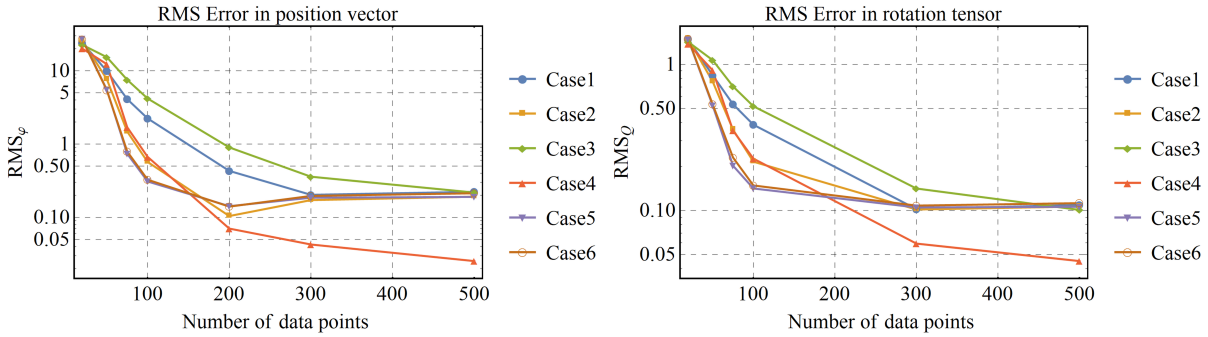

(a) RMS error in the position vector

(b) RMS error in the rotation tensor

Figure 2.10: RMS error in the approximated configuration space considering no noise in the data obtained from the sensors.

2.4 Applications in computer graphics

Theory of curves and moving frames have found a dominant place in generating computer graphics, including but not limited to ribbons, orientation of camera frames and quantum waveguide construction, CAD-CAM modeling and animations (refer [11], [13] and [29]). Extruding a cross-section along a straight center line has long been used in CAD modeling. In this section, we present a few applications of various types of framed space curves discussed so far in computer graphics.

2.4.1 Double helix intertwining a space curve

We elucidate the construction of double helix using GMAF. Consider the pitch $\phi_p(\xi)$ and yaw angle $\phi_y(\xi)$ field corresponding to the space curve $\boldsymbol{\varphi}(\xi)$ with total length L, parameterized by the arc-length $\xi \in [0, L]$ such that,

$$\boldsymbol{\varphi}(\xi) = \int_0^{\xi} \boldsymbol{T}(k)\, \mathrm{d}k. \tag{2.44}$$

In the above equation, $\boldsymbol{T}(\xi)$ represents the tangent vector field of the curve, the component of which can be obtained from either Eq. (1.27) or (1.28) (note than $\boldsymbol{T}(\xi)$ is sufficient to define

the mid-curve). Let r and c represent the radius and the total number of windings (that can be fractional) of double helix respectively. We can obtain the position vectors of two curves constituting the double helix as $\boldsymbol{\varphi}_1(\xi)$ and $\boldsymbol{\varphi}_2(\xi)$ as,

$$\begin{aligned} \boldsymbol{\varphi}_1(\xi) &= \boldsymbol{\varphi}(\xi) + r\boldsymbol{Y}_g(\xi); \\ \boldsymbol{\varphi}_2(\xi) &= \boldsymbol{\varphi}(\xi) - r\boldsymbol{Y}_g(\xi). \end{aligned} \tag{2.45}$$

In the equation above, $\boldsymbol{Y}_g(\xi)$ represents the constituent vector of GMAF as defined in (1.28), with the roll angle field given by,

$$\phi_r(\xi) = 2\pi c \left(\frac{\xi}{L}\right). \tag{2.46}$$

This formulation can be used to generate graphics and defining the reduced geometry of DNA molecule with the curves $\boldsymbol{\varphi}_1(\xi)$ and $\boldsymbol{\varphi}_2(\xi)$ representing the *sugar-phosphate backbone* and the vector $r\boldsymbol{Y}_g(\xi)$ and $-r\boldsymbol{Y}_g(\xi)$ showing the *nitrogenous base* pairs.

Figure 2.11 shows two examples of double helix intertwining a space curve $\boldsymbol{\varphi}(\xi)$. The dotted black curve represents the curve $\boldsymbol{\varphi}(\xi)$, the green and red strand (with n being number of strands per cycle) represents the vectors $r\boldsymbol{Y}_g(\xi)$ and $-r\boldsymbol{Y}_g(\xi)$ respectively. The blue curves shows the curves $\boldsymbol{\varphi}_1(\xi)$ (connected to green strands) and $\boldsymbol{\varphi}_2(\xi)$ (connected to red strands). Following are the parameters required to obtain the structures in Fig 2.11a,

$$\begin{gathered} L = 500, \;\; r = 40, \;\; c = 6, \;\; n = 16; \\ \phi_p(\xi) = \frac{\pi}{2} \sin\left(\frac{\pi\xi}{L}\right).\left(1 - 0.5\sin\left(\frac{3.5\pi}{L}\right)\right); \\ \phi_y(\xi) = \pi \sin\left(\frac{\pi\xi}{L}\right). \end{gathered} \tag{2.47}$$

Following are the parameters required to obtain Fig 2.11b,

$$\begin{gathered} L = 500, \;\; r = 35, \;\; c = 3, \;\; n = 12; \\ \phi_p(\xi) = \frac{\pi}{8} \sin\left(\frac{2\pi\xi}{L}\right); \\ \phi_y(\xi) = \frac{\pi}{8} \sin\left(\frac{2\pi\xi}{L}\right). \end{gathered} \tag{2.48}$$

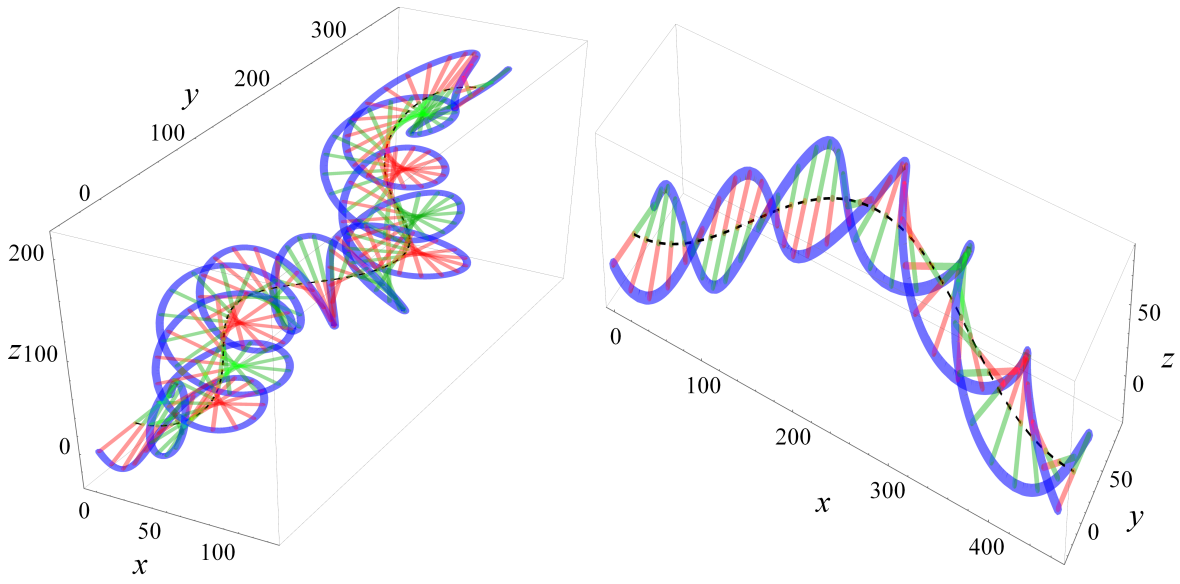

(a) Example 1

(b) Example 2

Figure 2.11: Double helix intertwining a space curve.

The winding and unwinding effects can be obtained by making $\phi_r(\xi)$ dynamic. Figure 2.12 shows a 3D printed model of double helix. The beads in the left figure mark the center curve $\boldsymbol{\varphi}(\xi)$ (absent in 3D printed model).

2.4.2 Leaf like structure using RPAF

To obtain a leaf like structure that bears a single manifold character, we first consider a leaf with *node* at origin (node is the point of contact of stem and leaf). The *midrib* of leaf (vein running from the *node* to the leaf *tip*) is given by the curve $\boldsymbol{\varphi}(\xi)$, obtained using the pitch and yaw angle fields $\phi_p(\xi)$ and $\phi_y(\xi)$ with $\xi \in [0, L]$. Here, L gives the length of *midrib*.

We generate the *lamina* of leaf as a mesh obtained using *relatively parallel normal vector field* and the inner and outer *margins* of the leaf. We divide the leaf surface into two parts: *lamina* 1 and *lamina* 2. The *relatively parallel normal vector field* $\boldsymbol{M}_1(\xi)$ and $\boldsymbol{M}_2(\xi)$ with the *generators*

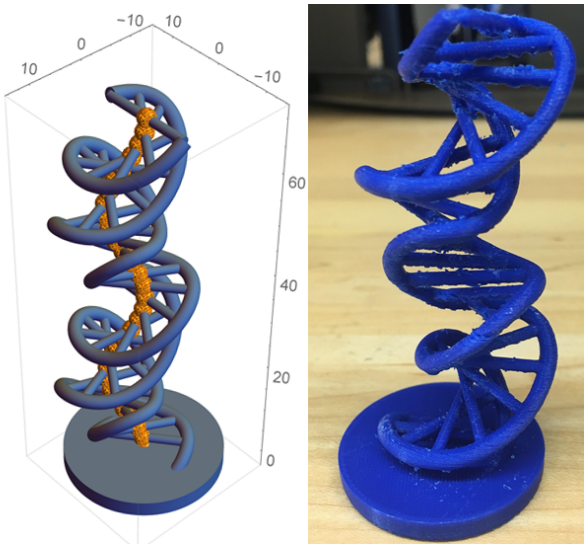

Figure 2.12: 3D printed model of double helix.

$\boldsymbol{M}_{10}$ and $\boldsymbol{M}_{20}$, used to define *lamina* 1 and 2 respectively, are given as

$$\boldsymbol{M}_i(\xi) = \boldsymbol{M}_{i0} + \left[\boldsymbol{Y}_g\right]_{\phi_r(\xi)=\rho_{\text{bi}}(\xi)}; \tag{2.49a}$$

$$\rho_{\text{bi}}(\xi) = \rho_{\text{bi}}(0) - \int_0^{\xi} \overline{\kappa}_{\text{s1}}(k)\,\mathrm{d}k = \rho_{\text{bi}}(0) - \int_0^{\xi} \partial_k \phi_y \sin\left(\phi_p(k)\right)\mathrm{d}k; \tag{2.49b}$$

$$\boldsymbol{M}_{i0} = \boldsymbol{Q}_g(0)\Big|_{(\phi_r(0)=\rho_{\text{bi}}(0))}.\boldsymbol{E}_2, \quad \text{with } i = 1, 2. \tag{2.49c}$$

In Eq. 2.49b, $\rho_{\text{bi}}(\xi)$ is obtained using the results (1.33a) and (1.38). It represents the roll angle field required to obtain a *relatively normal vector field* (refer section 1.4.2). The predefined angle $\rho_{\text{bi}}(0)$ are used to obtain the *generator* $\boldsymbol{M}_{i0}$ using Eq. (2.49c).

Leaf *margin* essentially represents the outer boundary of the *lamina*. We call that as an outer *margin*, with Γ^1_{outer} and Γ^2_{outer} representing outer *margin* for *lamina* 1 and 2 respectively. In order to mesh the *lamina*, we define inner *margins* with $\Gamma^1_{\text{inner}I}$ and $\Gamma^2_{\text{inner}I}$ representing I^{th} inner *margin* for *lamina* 1 and 2 respectively. The position vectors representing these curves are given by,

$$\boldsymbol{\varphi}_{\Gamma^{\text{i}}_{\text{outer}}} = \boldsymbol{\varphi} + rW(\xi)\boldsymbol{M}_i \quad \text{for outer margin of lamina } i; \tag{2.50a}$$

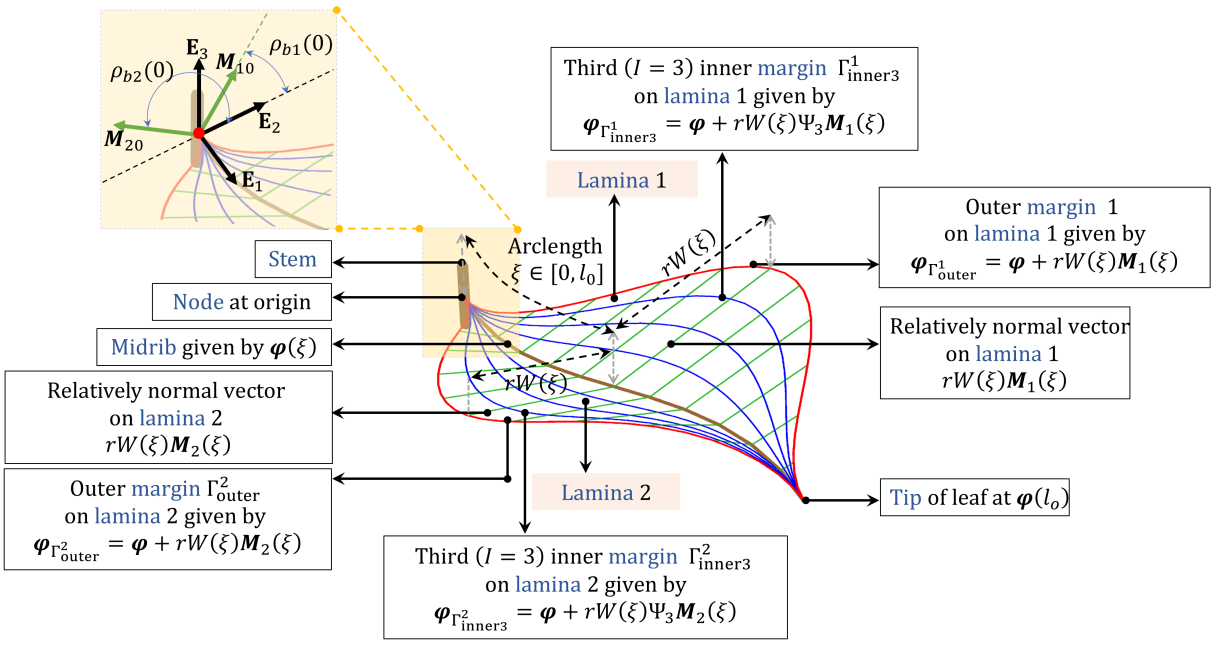

Figure 2.13: Geometry of leaf obtained using RPAF.

$$\boldsymbol{\varphi}_{\Gamma^i_{\text{inner}I}} = \boldsymbol{\varphi} + rW(\xi)\Psi_I\boldsymbol{M}_i \quad \text{for } I^{\text{th}} \text{ inner margin of lamina } i. \tag{2.50b}$$

In the equation above, r represents the width parameter of the *lamina*, $W(\xi)$ represents the weight function for the outer margin and $\Psi_I \in (0, 1)$ is additional weight for the I^{th} inner *margin*. Note that if $\max(W(\xi)) = 1$, then r represents the maximum width of *lamina*, similarly, if $W(\xi) =$ constant, then all the inner and outer *margins* transforms to *relatively parallel curves* to the *midrib*. Therefore, the width of *lamina* at the arclength ξ is given by $rW(\xi)$. Figure 2.13 demonstrates the construction discussed so far.

Any other orientation of the leaf defined by L, $\phi_p(\xi)$, $\phi_y(\xi)$, $\rho_{\text{bi}}(0)$, can be obtained by rotating the leaf pivoted at the origin and then translating it as required. The stem of the leaf can be obtained by extruding the cross-sections along a space curve.

Figure 2.14 shows three different leaves constructed using same L, $\phi_p(\xi)$, $\phi_y(\xi)$, $\rho_{\text{bi}}(0)$

but different weights $W_1(\xi)$, $W_2(\xi)$ and $W_3(\xi)$ and widths r as,

$$\begin{gathered} L = 6, \;\; \rho_{\mathrm{b}1}(0) = 0.7, \;\; \rho_{\mathrm{b}2}(0) = 0.7 + \frac{5\pi}{9}; \\ r_1 = r_2 = \frac{L}{3.5}, \;\; r_3 = 0.4; \\ \phi_p(\xi) = \phi_y(\xi) = \frac{\pi}{8} \sin\left(\frac{\pi\xi}{L}\right) \end{gathered} \tag{2.51}$$

$$\begin{gathered} W_1(\xi) = 0.5\left(1 + \sin\left(\frac{2\pi\xi}{L} - \frac{\pi}{2}\right)\right); \\ W_2(\xi) = W_1(\xi) + \frac{2}{75}\sin^2\left(\frac{4\pi\xi}{L} - \pi\right); \\ W_3(\xi) = f(\xi) + \begin{cases} \frac{14\xi}{3} & 0 \le \xi \le 0.75 \\ \frac{-4\xi}{3} + 4.5 & 0.75 \le \xi \le 1.5 \\ \frac{5\xi}{6} + 1.25 & 1.5 \le \xi \le 3 \\ \frac{-3\xi}{5} + 3.6 & 3.5 \le \xi \le L \end{cases} . \end{gathered} \tag{2.52}$$

In the equation for the weight, W_3 of leaf 3, the function $f(\xi)$ represents the triangular wave with a period of 0.16 and an amplitude of 0.084. This is used to generate corrugation and irregularity in the outer margin of the leaf 3 (Figure 2.14).

An entire plant can be generated as shown in figure 2.15. The stems are obtained by extruding circular cross-section varying smoothly along the curves. Leaves of different sizes and orientations are obtained as discussed before.

The dynamic motion in the leaf (say due to wind load) can be graphically obtained by making $\phi_p(\xi)$, $\phi_y(\xi)$, $\rho_{\mathrm{bi}}(0)$ dynamic.

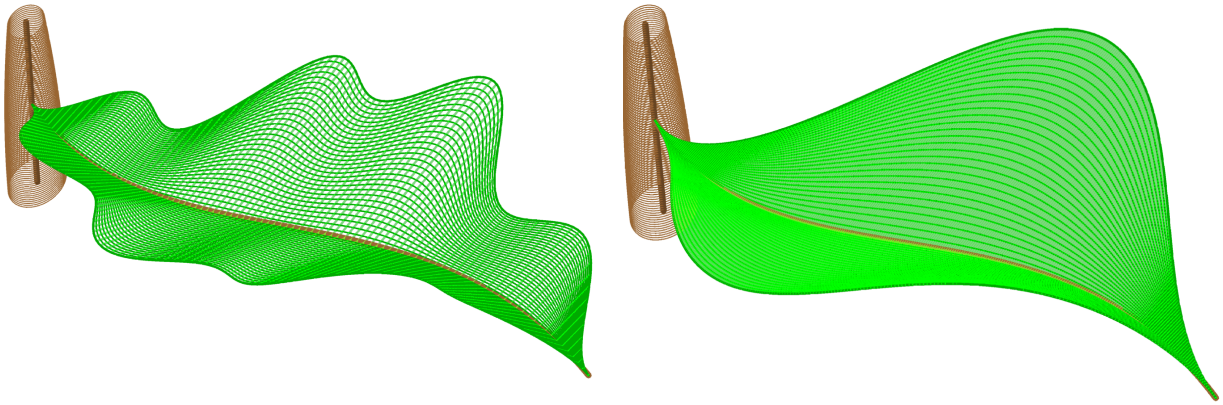

(a) Leaf 1

(b) Leaf 2

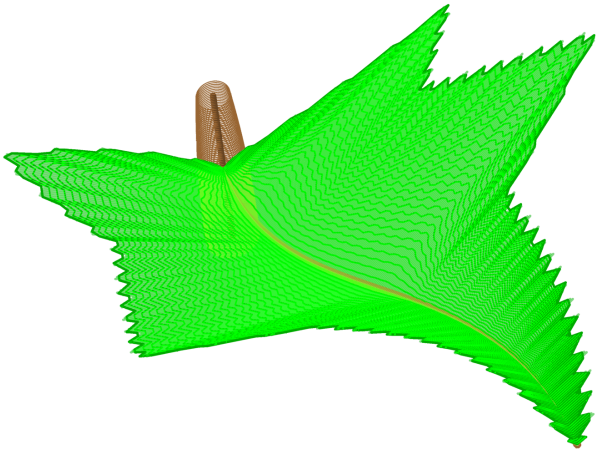

(c) Leaf 3

Figure 2.14: Leaves obtained using same midrib but different weight functions.

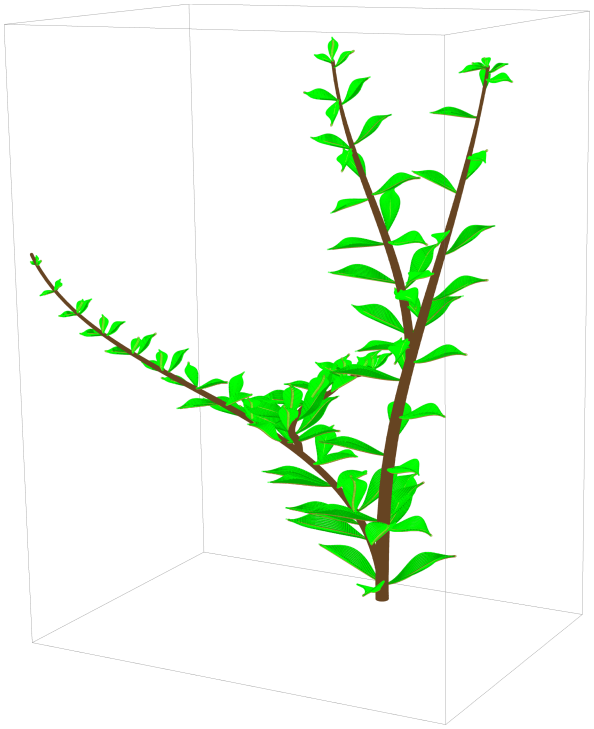

(a) View 1

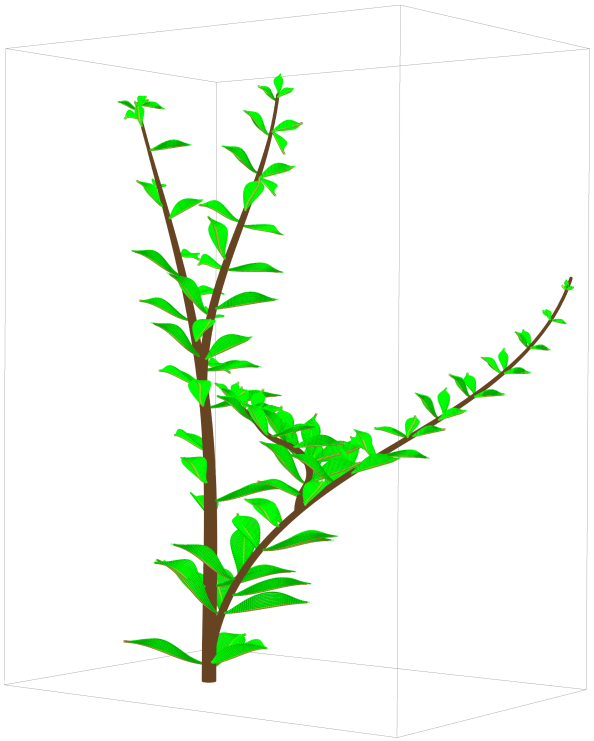

(b) View 2

Figure 2.15: Computer generated plant with varying sizes and orientation of leaves.

2.5 Summary

This chapter is essentially the application of concepts discussed in chapter 1 in the area of path-estimation and computer graphics. An algorithm to estimate the state space of a single manifold characterized system using a limited set of material curvature and velocity data is elucidated. The idea is to estimate the material linear and angular velocity data using various consistent interpolation approaches. The approximated fields $(\overline{\boldsymbol{v}}^h(\xi_1), \overline{\boldsymbol{\omega}}^h(\xi_1))$ are first used to estimate the configuration space $(\boldsymbol{\varphi}^h(\xi_1), \boldsymbol{Q}^h(\xi_1))$ and then the tangent space $(\boldsymbol{v}^h, \boldsymbol{\omega}^h)$ is approximated. Among all the interpolation approaches suggested, the C^{-1} interpolation of material data is special because it results in a closed-form solution to the estimated configuration, and because it leads to the development of curvature dependent shape functions that may be glued together to obtain a smooth global configuration. We call this approach *Smooth Patch Estimation and Gluing technique* (SPEG). An interesting method to obtain the solution of SPEG merely by using the idea of parallel-transport is presented. The estimation methods discussed are convergent and free of singularity. An illustration that compares all the approaches and demonstrates the error analysis is presented. The SPEG and other higher-order interpolation techniques of framed space curves discussed here are used in developing the shape-reconstruction technique detailed in chapter 6.

The applications of framed space curves are numerous. Finally, the ability of the framed space curve to develop computer graphics is demonstrated. This is done by presenting the construction of double helix intertwining a space curve using GMAF. A second example demonstrating the construction of leaves and plants using RPAF is illustrated.

The discussion carried out in this chapter has been published in Computers & Structures, Mayank Chadha and Michael D. Todd [26], 2019. The title is "On the material and material-adapted approaches to curve framing with applications in path estimation, shape reconstruction, and computer graphics". The dissertation author is the primary author of this paper.

Chapter 3

On the Derivatives of Curvature and their Linearized Updating Scheme

3.1 Introduction:

This chapter is an extension of the theory of the rotational Lie group discussed in chapter 1. In this chapter, we discuss the higher-order derivatives, variations, and co-rotational derivatives of the curvature tensor. We realize that parameterizing rotation tensor using the Gibbs vector is effective in deriving a closed-form formula to obtain any order derivative of the curvature tensor as the summation of functions of the parameterizing quantity and its derivatives. We use these results for formulating a linearized updating algorithm for curvature and its derivatives when the configuration of the curve acquires a small increment.

We have presented the need for obtaining higher-order derivatives of curvature while investigating higher-order geometrically-exact beam/rod theory. The kinematics of beam/rods under arbitrarily-large deformations defined in Chadha and Todd [34] (and later discussed in chapter 4) renders the deformation map not only to be a function of curvature but also a function of its higher-order derivatives. The numerical solution of such problems using Finite Element

Analysis needs updating of these kinematic quantities. In such problems, derivatives of the curvature tensor gain importance. Apart from a practical viewpoint, the fact that the Lie proper orthogonal rotational group $SO(3)$ and its Lie Algebra $so(3)$ constitute a central role in the area of Lie group theory makes it worthwhile to investigate the higher-order partial and co-rotational derivatives of curvature and the associated quantities.

Note on Notations: We conclude this introductory section with a note on notation and definitions. The n dimensional Euclidean space is represented by $\mathbb{R}^n$, with $\mathbb{R}^1 \equiv \mathbb{R}$. The space of real numbers and integers is denoted by $\mathbb{R}$ and $\mathbb{Z}$, with $\mathbb{R}^+$ and $\mathbb{Z}^+$ giving the set of positive real numbers and integers (including 0) respectively. The dot product, ordinary vector product and tensor product of two Euclidean vectors $\boldsymbol{v}_1$ and $\boldsymbol{v}_2$ are defined as $\boldsymbol{v}_1 \cdot \boldsymbol{v}_2$, $\boldsymbol{v}_1 \times \boldsymbol{v}_2$, and $\boldsymbol{v}_1 \otimes \boldsymbol{v}_2$ respectively. The Euclidean norm is represented by $\|\cdot\|$ or the un-bolded version of the symbol (for example, $\|\boldsymbol{v}\| \equiv v$). Secondly, n^{th} (with $n \in \mathbb{Z}^+$) order partial derivative with respect to a scalar quantity, ξ for instance, is given by the operator $\frac{\partial^n}{\partial \xi^n} = \partial^n_\xi$. For $n = 1$, we define $\partial^1_\xi \equiv \partial_\xi$ and note that for $n = 0$, ∂^0_ξ is an identity operator. A vector, tensor or a matrix is represented by bold symbol and their components are given by indexed un-bolded symbols. For $i, j \in \mathbb{Z}^+$, the Kronecker delta function is defined as $\delta_{ij} = \begin{cases} 0 & \text{if } i \neq j \\ 1 & \text{if } i = j \end{cases}$. The action of a tensor $\boldsymbol{A}$ onto the vector $\boldsymbol{v}$ is represented by $\boldsymbol{A}\boldsymbol{v} \equiv \boldsymbol{A}.\boldsymbol{v}$. We note that the centered dot "$\cdot$" is meant for dot product between two vectors, whereas the action of a tensor onto the vector, the matrix multiplication or product of a scalar to a matrix (or a vector) is denoted by a lower dot ".". For $n, i \in \mathbb{Z}^+$ and $n \geq i \geq 0$, the binomial coefficient is defined as $C^n_i = \frac{n!}{i!(n-i)!}$. We note two useful properties of binomial coefficient in *Theorem 3.0*.

Theorem 3.0: For $i, n \in \mathbb{Z}^+$ and $i \leq n$, the following holds

$$C^n_i = C^n_{(n-i)}; \tag{3.1a}$$

$$C_i^n = \begin{cases} 1 & \text{if } i = 0 \text{ or } i = n; \\ C_{(i-1)}^{(n-1)} + C_i^{(n-1)} & \text{otherwise.} \end{cases} \tag{3.1b}$$

Proof: Result (3.1a) follows from the definition of binomial coefficient. The recurrence-formula (3.1b) is obtained from the result $C_{(i+1)}^{(n+1)} = C_i^n + C_{(i+1)}^n$, that is easily provable using the definition of binomial coefficient. □

3.2 Material and spatial quantities and their derivatives

To begin with, consider a framed space curve, parameterized by the arc-length $\xi \in [0, L]$, is defined by the position vector $\boldsymbol{\varphi}(\xi) \in \mathbb{R}^3$ and the orthonormal material frame field $\{\boldsymbol{d}_i(\xi)\}$. Let $\{\boldsymbol{E}_i\}$ define a fixed orthonormal reference frame such that we may define the orthogonal rotation tensor $\boldsymbol{Q}(\xi)$ as:

$$\begin{aligned} \boldsymbol{d}_i(\xi) = \boldsymbol{Q}(\xi).\boldsymbol{E}_i; \quad \boldsymbol{Q}(\xi) = \sum_{i=1}^{3} \boldsymbol{d}_i(\xi) \otimes \boldsymbol{E}_i; \\ [\boldsymbol{Q}]_{\boldsymbol{E}_i \otimes \boldsymbol{E}_j} = \sum_{i,j=1}^{3} Q_{ij} \boldsymbol{E}_i \otimes \boldsymbol{E}_j; \quad Q_{ij} = \boldsymbol{E}_i \cdot \boldsymbol{d}_j. \end{aligned} \tag{3.2}$$

As we have defined the material and spatial forms of the curvature vector (and tensor) in section (2.2.2), it is rather useful to define a vector $\boldsymbol{v} \in \mathbb{R}^3$ in its material and spatial form. Consider a spatial and material vector $\boldsymbol{v} = \overline{v}_i \boldsymbol{d}_i$ and $\overline{\boldsymbol{v}} = \overline{v}_i \boldsymbol{E}_i$, respectively, such that $\boldsymbol{v} = \boldsymbol{Q}.\overline{\boldsymbol{v}}$. Figure 3.1 illustrates the idea of material and spatial form of a vector. The derivative of these vectors are obtained as:

$$\begin{aligned} \partial_\xi \boldsymbol{v} = \partial_\xi \overline{v}_i.\boldsymbol{d}_i + \overline{v}_i.\partial_\xi \boldsymbol{d}_i = \tilde{\partial}_\xi \boldsymbol{v} + \boldsymbol{\kappa} \times \boldsymbol{v}; \\ \partial_\xi \overline{\boldsymbol{v}} = \partial_\xi \overline{v}_i.\boldsymbol{E}_i = \boldsymbol{Q}^T.\tilde{\partial}_\xi \boldsymbol{v}. \end{aligned} \tag{3.3}$$

In the equation above, $\tilde{\partial}_\xi \boldsymbol{v}$ defines co-rotational derivative of spatial vector $\boldsymbol{v}$. It essentially gives the change in components of the vector $\boldsymbol{v}$, provided the frame of reference is assumed to be fixed. Geometrically, it is obtained by parallel-transport (left translation) of the vector $\partial_\xi \overline{\boldsymbol{v}}$.

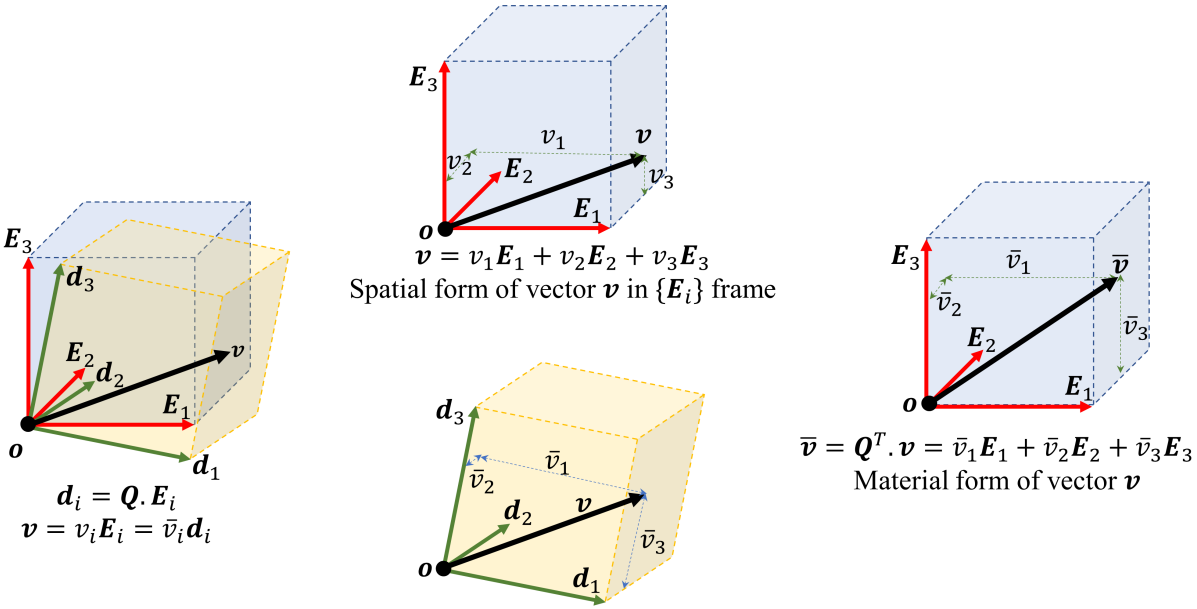

Figure 3.1: Illustration of the material and spatial form of a vector.

Along similar lines, consider a spatial and material tensor $\boldsymbol{A} = \sum_{i,j=1}^{3} \overline{A}_{ij} \boldsymbol{d}_i \otimes \boldsymbol{d}_j$ and $\overline{\boldsymbol{A}} = \sum_{i,j=1}^{3} \overline{A}_{ij} \boldsymbol{E}_i \otimes \boldsymbol{E}_j$ respectively, such that $\boldsymbol{A} = \boldsymbol{Q}.\overline{\boldsymbol{A}}.\boldsymbol{Q}^T$ (or equivalently, $\overline{\boldsymbol{A}} = \boldsymbol{Q}^T.\boldsymbol{A}.\boldsymbol{Q}$). Realizing $\partial_\xi \boldsymbol{Q} = \hat{\boldsymbol{\kappa}}.\boldsymbol{Q}$ and $\partial_\xi \boldsymbol{Q}^T = -\boldsymbol{Q}^T.\hat{\boldsymbol{\kappa}}$, we have the following:

$$\begin{aligned} \partial_\xi \boldsymbol{A} &= \boldsymbol{Q}.\partial_\xi \overline{\boldsymbol{A}}.\boldsymbol{Q}^T + \partial_\xi \boldsymbol{Q}.\overline{\boldsymbol{A}}.\boldsymbol{Q}^T + \boldsymbol{Q}.\overline{\boldsymbol{A}}.\partial_\xi \boldsymbol{Q}^T \\ &= \boldsymbol{Q}.\partial_\xi \overline{\boldsymbol{A}}.\boldsymbol{Q}^T + \hat{\boldsymbol{\kappa}}.(\boldsymbol{Q}.\overline{\boldsymbol{A}}.\boldsymbol{Q}^T) - (\boldsymbol{Q}.\overline{\boldsymbol{A}}.\boldsymbol{Q}^T).\hat{\boldsymbol{\kappa}} \\ &= \tilde{\partial}_\xi \boldsymbol{A} + \hat{\boldsymbol{\kappa}}.\boldsymbol{A} - \boldsymbol{A}.\hat{\boldsymbol{\kappa}}. \end{aligned} \tag{3.4}$$

In the equation above, we define the co-rotational derivative of the tensor $\boldsymbol{A}$ as $\tilde{\partial}_\xi \boldsymbol{A} = \boldsymbol{Q}.\partial_\xi \overline{\boldsymbol{A}}.\boldsymbol{Q}^T$. Physically, it gives the change in components of tensor $\boldsymbol{A}$ setting the reference frame constant. From here on, $\tilde{\partial}_x(.)$ represents the co-rotational derivative of some quantity $(.)$ with respect to the variable x. We now present some propositions describing higher order co-rotational derivatives.

Proposition 3.1: For any vector $\boldsymbol{v} \in \mathbb{R}^3$, define the operator $\hat{\partial}_\xi$ such that $\hat{\partial}_\xi^n \boldsymbol{v} = \hat{\boldsymbol{\kappa}}^n.\boldsymbol{v}$, where, for example $\hat{\boldsymbol{\kappa}}^3 = \hat{\boldsymbol{\kappa}}.\hat{\boldsymbol{\kappa}}.\hat{\boldsymbol{\kappa}}$. The n^{th} order co-rotational derivative $\tilde{\partial}_\xi^n$ is then given by $(\partial_\xi - \hat{\partial}_\xi)^n$ such

that the order of operations are not commutative (for example, $\partial_\xi \hat{\partial}_\xi \neq \hat{\partial}_\xi \partial_\xi$) and $\tilde{\partial}^0_\xi = (\partial_\xi - \hat{\partial}_\xi)^0$ is an identity operator.

Proof: We prove the above proposition by using the principle of mathematical induction. Consider a vector $\boldsymbol{v} \in \mathbb{R}^3$, assuming that $\tilde{\partial}^n_\xi \boldsymbol{v} = (\partial_\xi - \hat{\partial}_\xi)^n \boldsymbol{v}$, for $n = 1, 2$ and 3, we have

$$\begin{aligned}
&\tilde{\partial}^1_\xi \equiv \tilde{\partial}_\xi = (\partial_\xi - \hat{\partial}_\xi);\\
&\tilde{\partial}^2_\xi = (\partial_\xi - \hat{\partial}_\xi)^2 = \partial^2_\xi - \partial_\xi \hat{\partial}_\xi - \hat{\partial}_\xi \partial_\xi + \hat{\partial}^2_\xi;\\
&\tilde{\partial}^3_\xi = (\partial_\xi - \hat{\partial}_\xi)^3 = \partial^3_\xi - \partial^2_\xi \hat{\partial}_\xi - \partial_\xi \hat{\partial}_\xi \partial_\xi + \partial_\xi \hat{\partial}^2_\xi - \hat{\partial}_\xi \partial^2_\xi + \hat{\partial}^2_\xi \partial_\xi + \hat{\partial}_\xi \partial_\xi \hat{\partial}_\xi - \hat{\partial}^3_\xi;
\end{aligned} \tag{3.5}$$

such that

$$\tilde{\partial}_\xi \boldsymbol{v} = \partial_\xi \boldsymbol{v} - \hat{\partial}_\xi \boldsymbol{v} = \partial_\xi \boldsymbol{v} - \hat{\boldsymbol{\kappa}}.\boldsymbol{v}; \tag{3.6a}$$

$$\begin{aligned}
\tilde{\partial}^2_\xi \boldsymbol{v} &= \partial^2_\xi \boldsymbol{v} - \partial_\xi \hat{\partial}_\xi \boldsymbol{v} - \hat{\partial}_\xi \partial_\xi \boldsymbol{v} + \hat{\partial}^2_\xi \boldsymbol{v} = \partial^2_\xi \boldsymbol{v} - \partial_\xi(\hat{\boldsymbol{\kappa}}.\boldsymbol{v}) - \hat{\boldsymbol{\kappa}}.\partial_\xi \boldsymbol{v} + \hat{\boldsymbol{\kappa}}.\hat{\boldsymbol{\kappa}}.\boldsymbol{v}\\
&= \partial^2_\xi \boldsymbol{v} + (\hat{\boldsymbol{\kappa}}.\hat{\boldsymbol{\kappa}} - \partial_\xi \hat{\boldsymbol{\kappa}}).\boldsymbol{v} - 2\hat{\boldsymbol{\kappa}}.\partial_\xi \boldsymbol{v};
\end{aligned} \tag{3.6b}$$

$$\begin{aligned}
\tilde{\partial}^3_\xi \boldsymbol{v} &= \partial^3_\xi \boldsymbol{v} - \partial^2_\xi(\hat{\boldsymbol{\kappa}}.\boldsymbol{v}) - \partial_\xi(\hat{\boldsymbol{\kappa}}.\partial_\xi \boldsymbol{v}) + \partial_\xi(\hat{\boldsymbol{\kappa}}.\hat{\boldsymbol{\kappa}}.\boldsymbol{v}) - \hat{\boldsymbol{\kappa}}.\partial^2_\xi \boldsymbol{v} + \hat{\boldsymbol{\kappa}}.\hat{\boldsymbol{\kappa}}.\partial_\xi \boldsymbol{v} + \hat{\partial}_\xi \partial_\xi(\hat{\boldsymbol{\kappa}}.\boldsymbol{v})\\
&\quad - \hat{\boldsymbol{\kappa}}.\hat{\boldsymbol{\kappa}}.\hat{\boldsymbol{\kappa}}.\boldsymbol{v} = \partial^3_\xi \boldsymbol{v} - 3\hat{\boldsymbol{\kappa}}.\partial^2_\xi \boldsymbol{v} + (\partial_\xi \hat{\boldsymbol{\kappa}}.\hat{\boldsymbol{\kappa}} + 2\hat{\boldsymbol{\kappa}}.\partial_\xi \hat{\boldsymbol{\kappa}} - \partial^2_\xi \hat{\boldsymbol{\kappa}} - \hat{\boldsymbol{\kappa}}.\hat{\boldsymbol{\kappa}}.\hat{\boldsymbol{\kappa}}).\boldsymbol{v}\\
&\quad + (3\hat{\boldsymbol{\kappa}}.\hat{\boldsymbol{\kappa}} - 3\partial_\xi \hat{\boldsymbol{\kappa}}).\partial_\xi \boldsymbol{v}.
\end{aligned} \tag{3.6c}$$

We now prove that the equation set (3.6) may be derived using the definition of co-rotational derivatives in Eq. (3.3). Equation (3.6a) is true by definition (refer to Eq. (3.3)). Taking the derivative of Eq. (3.6a) yields

$$\partial_\xi \tilde{\partial}_\xi \boldsymbol{v} = \partial^2_\xi \boldsymbol{v} - \partial_\xi \hat{\boldsymbol{\kappa}}.\boldsymbol{v} - \hat{\boldsymbol{\kappa}}.\partial_\xi \boldsymbol{v}. \tag{3.7}$$

We note from the definition of co-rotational derivative in Eq. (3.3) that

$$\partial_\xi \tilde{\partial}_\xi \boldsymbol{v} = \tilde{\partial}^2_\xi \boldsymbol{v} + \hat{\boldsymbol{\kappa}}.\tilde{\partial}_\xi \boldsymbol{v} = \tilde{\partial}^2_\xi \boldsymbol{v} + \hat{\boldsymbol{\kappa}}.(\partial_\xi \boldsymbol{v} - \hat{\boldsymbol{\kappa}}.\boldsymbol{v}) = \tilde{\partial}^2_\xi \boldsymbol{v} + \hat{\boldsymbol{\kappa}}.\partial_\xi \boldsymbol{v} - \hat{\boldsymbol{\kappa}}.\hat{\boldsymbol{\kappa}}.\boldsymbol{v}. \tag{3.8}$$

From Eq. (3.7) and (3.8), we have,

$$\tilde{\partial}_\xi^2 \boldsymbol{v} = \partial_\xi \tilde{\partial}_\xi \boldsymbol{v} - \hat{\boldsymbol{\kappa}}.\partial_\xi \boldsymbol{v} + \hat{\boldsymbol{\kappa}}.\hat{\boldsymbol{\kappa}}.\boldsymbol{v} = \partial_\xi^2 \boldsymbol{v} + (\hat{\boldsymbol{\kappa}}.\hat{\boldsymbol{\kappa}} - \partial_\xi \hat{\boldsymbol{\kappa}}).\boldsymbol{v} - 2\hat{\boldsymbol{\kappa}}.\partial_\xi \boldsymbol{v}. \tag{3.9}$$

Expression obtained in (3.9) is same as (3.6b). Similarly, to derive the expression for $\tilde{\partial}_\xi^3 \boldsymbol{v}$, we consider

$$\partial_\xi \tilde{\partial}_\xi^2 \boldsymbol{v} = \partial_\xi^3 \boldsymbol{v} - 2\hat{\boldsymbol{\kappa}}.\partial_\xi^2 \boldsymbol{v} + (\hat{\boldsymbol{\kappa}}.\hat{\boldsymbol{\kappa}} - 3\partial_\xi \hat{\boldsymbol{\kappa}}).\partial_\xi \boldsymbol{v} + (\partial_\xi \hat{\boldsymbol{\kappa}}.\hat{\boldsymbol{\kappa}} + \hat{\boldsymbol{\kappa}}.\partial_\xi \hat{\boldsymbol{\kappa}} - \partial_\xi^2 \hat{\boldsymbol{\kappa}}).\boldsymbol{v}. \tag{3.10}$$

From (3.3), we have,

$$\tilde{\partial}_\xi^3 \boldsymbol{v} = \partial_\xi \tilde{\partial}_\xi^2 \boldsymbol{v} - \hat{\boldsymbol{\kappa}}.(\partial_\xi \tilde{\partial}_\xi^2 \boldsymbol{v}). \tag{3.11}$$

Using the results in Eq. (3.10) and (3.11), we arrive at the expression of $\tilde{\partial}_\xi^3 \boldsymbol{v}$ as obtained in (3.6c). We can continue the process explained above and realize that for any n, $\tilde{\partial}_\xi^n = (\partial_\xi - \hat{\partial}_\xi)(\partial_\xi - \hat{\partial}_\xi)^{(n-1)} = (\partial_\xi - \hat{\partial}_\xi)^n$. Using binomial theorem, we can also write

$$(\partial_\xi - \hat{\partial}_\xi)^n = \sum_{i=0}^{n} (-1)^{(n-i)} C_i^n \partial_\xi^n \hat{\partial}_\xi^{(n-i)}. \tag{3.12}$$

This completes the proof. □

Proposition 3.2: For any $\hat{\boldsymbol{A}} \in so(3)$ with the corresponding axial vector $\boldsymbol{A} \in \mathbb{R}^3$, the recurrence formula for the n^{th} order co-rotational derivative $\tilde{\partial}_\xi^n \hat{\boldsymbol{A}} \in so(3)$ and $\tilde{\partial}_\xi^n \boldsymbol{A} \in \mathbb{R}^3$ is given as

$$\tilde{\partial}_\xi^n \hat{\boldsymbol{A}} = \partial_\xi^n \hat{\boldsymbol{A}} - (1 - \delta_{n0}) \sum_{i=1}^{n} \partial_\xi^{(i-1)} \left[\hat{\boldsymbol{\kappa}}, \tilde{\partial}_\xi^{(n-i)} \hat{\boldsymbol{A}} \right]; \tag{3.13a}$$

$$\tilde{\partial}_\xi^n \boldsymbol{A} = \partial_\xi^n \boldsymbol{A} - (1 - \delta_{n0}) \sum_{i=1}^{n} \partial_\xi^{(i-1)} (\boldsymbol{\kappa} \times \tilde{\partial}_\xi^{(n-i)} \boldsymbol{A}). \tag{3.13b}$$

Proof: From definition of co-rotational derivatives and Lie-bracket in Eq. (3.4) and (1.9a) respectively, we have,

$$\tilde{\partial}_\xi \hat{\boldsymbol{A}} = \partial_\xi \hat{\boldsymbol{A}} - \hat{\boldsymbol{\kappa}}.\hat{\boldsymbol{A}} + \hat{\boldsymbol{A}}.\hat{\boldsymbol{\kappa}} = \partial_\xi \hat{\boldsymbol{A}} - \left[\hat{\boldsymbol{\kappa}}, \hat{\boldsymbol{A}} \right]. \tag{3.14}$$

Since, $\partial_\xi^m \hat{\boldsymbol{A}} \in so(3)$ for any $m \in \mathbb{Z}^+$, the result above can be used to obtain the recurrence-relation for n^{th} order co-rotational derivative. For $n \in \mathbb{Z}^+ - \{0\}$, we have,

$$\begin{aligned}
\tilde{\partial}_\xi^n \hat{\boldsymbol{A}} =& \partial_\xi \left(\tilde{\partial}_\xi^{(n-1)} \hat{\boldsymbol{A}} \right) - \left[\hat{\boldsymbol{\kappa}}, \tilde{\partial}_\xi^{(n-1)} \hat{\boldsymbol{A}} \right] \\
=& \partial_\xi \left(\partial_\xi \left(\tilde{\partial}_\xi^{(n-2)} \hat{\boldsymbol{A}} \right) - \left[\hat{\boldsymbol{\kappa}}, \tilde{\partial}_\xi^{(n-2)} \hat{\boldsymbol{A}} \right] \right) - \left[\hat{\boldsymbol{\kappa}}, \tilde{\partial}_\xi^{(n-1)} \hat{\boldsymbol{A}} \right] \\
=& \partial_\xi^2 \left(\partial_\xi \left(\tilde{\partial}_\xi^{(n-3)} \hat{\boldsymbol{A}} \right) - \left[\hat{\boldsymbol{\kappa}}, \tilde{\partial}_\xi^{(n-3)} \hat{\boldsymbol{A}} \right] \right) - \partial_\xi \left[\hat{\boldsymbol{\kappa}}, \tilde{\partial}_\xi^{(n-2)} \hat{\boldsymbol{A}} \right] - \left[\hat{\boldsymbol{\kappa}}, \tilde{\partial}_\xi^{(n-1)} \hat{\boldsymbol{A}} \right] \\
=& \partial_\xi^n \hat{\boldsymbol{A}} - \left[\hat{\boldsymbol{\kappa}}, \tilde{\partial}_\xi^{(n-1)} \hat{\boldsymbol{A}} \right] - \partial_\xi \left[\hat{\boldsymbol{\kappa}}, \tilde{\partial}_\xi^{(n-2)} \hat{\boldsymbol{A}} \right] - \ldots - \partial_\xi^{(n-1)} \left[\hat{\boldsymbol{\kappa}}, \hat{\boldsymbol{A}} \right] \\
=& \partial_\xi^n \hat{\boldsymbol{A}} - \sum_{i=1}^{n} \partial_\xi^{(i-1)} \left[\hat{\boldsymbol{\kappa}}, \tilde{\partial}_\xi^{(n-i)} \hat{\boldsymbol{A}} \right].
\end{aligned} \tag{3.15}$$

We note that for $n = 0$, we have $\tilde{\partial}_\xi^0 \hat{\boldsymbol{A}} = \partial_\xi^0 \hat{\boldsymbol{A}} = \hat{\boldsymbol{A}}$. Thus, the sum part in the equation above vanish for $n = 0$, justifying the use of $(1 - \delta_{n0})$ factor in Eq. (3.13a). Result (3.13b) follows from above derivation using Eq. (1.9b). This completes the proof. □

Corollary 3.1: The *Proposition 3.2* can be extended for any tensor $\boldsymbol{B}$ (not necessarily an element of $so(3)$) as:

$$\tilde{\partial}_\xi^n \boldsymbol{B} = \partial_\xi^n \boldsymbol{B} - (1 - \delta_{n0}) \sum_{i=1}^{n} \partial_\xi^{(i-1)} \left(\hat{\boldsymbol{\kappa}} . \tilde{\partial}_\xi^{(n-i)} \boldsymbol{B} - \tilde{\partial}_\xi^{(n-i)} \boldsymbol{B} . \hat{\boldsymbol{\kappa}} \right) \tag{3.16}$$

Proof: This extension is possible because Lie-brackets follow chain-rule just like product of two scalar or dot product except for the fact that Lie-brackets are non-commutative (which is a stronger condition) as observed in Eq. (3.26). □

Proposition 3.3: For spatial vector and tensor $\boldsymbol{v}$ and $\boldsymbol{A}$ respectively, with corresponding material quantities $\overline{\boldsymbol{v}}$ and $\overline{\boldsymbol{A}}$, the n^{th} order co-rotational derivative $\tilde{\partial}_\xi^n \boldsymbol{v}$ and $\tilde{\partial}_\xi^n \boldsymbol{A}$ can be obtained by left-translation of the n^{th} order derivative of the respective material quantities such that,

$$\tilde{\partial}_\xi^n \boldsymbol{v} = \boldsymbol{Q} . \partial_\xi^n \overline{\boldsymbol{v}}; \tag{3.17a}$$

$$\tilde{\partial}_\xi^n \boldsymbol{A} = \boldsymbol{Q} . \partial_\xi^n \overline{\boldsymbol{A}} . \boldsymbol{Q}^T. \tag{3.17b}$$

Proof: This proposition can be easily proved using product rule on $\overline{\boldsymbol{v}} = \boldsymbol{Q}^T.\boldsymbol{v}$ and $\overline{\boldsymbol{A}} = \boldsymbol{Q}^T.\boldsymbol{A}.\boldsymbol{Q}$ and substituting for $\partial_\xi \boldsymbol{Q}^T = -\boldsymbol{Q}^T.\hat{\boldsymbol{\kappa}}$. The result obtained after such computations (say for $n = 1, 2, 3$) when compared with the results obtained *Proposition 3.1* and *Corollary 3.1*, proves the intended result. □

3.3 Variation and linearization of rotation tensor

We obtain the virtual rotation tensor field by superimposing an admissible variation field $\delta\boldsymbol{Q}$ to the rotation field $\boldsymbol{Q}$. The varied configuration is then defined by $\boldsymbol{Q}_\epsilon$ such that for $\epsilon > 0$, we have

$$\begin{gathered}\boldsymbol{Q}_\epsilon = \boldsymbol{Q}(\boldsymbol{\theta} + \epsilon\delta\boldsymbol{\theta}) = \boldsymbol{Q}(\epsilon\delta\boldsymbol{\alpha}).\boldsymbol{Q}(\boldsymbol{\theta});\\ \delta\boldsymbol{Q} = \partial_\epsilon \boldsymbol{Q}_\epsilon|_{\epsilon=0}.\end{gathered} \tag{3.18}$$

The fact that $SO(3)$ is a non-linear manifold makes it difficult to geometrically understand and obtain the variation of rotation tensor. We also note that it is advantageous to express the virtual rotation tensor by means of *virtual rotation vector in current state* $\delta\boldsymbol{\alpha}$ (that is saying $\delta\hat{\boldsymbol{\alpha}}.\boldsymbol{Q} \in T_{\boldsymbol{Q}}SO(3)$) contrary to the *variation of total rotation vector* $\delta\boldsymbol{\theta}$ ($\delta\hat{\boldsymbol{\theta}} \in so(3)$). The varied director field is then given by

$$\boldsymbol{d}_{i\epsilon} = \boldsymbol{Q}_\epsilon.\boldsymbol{E}_i = \boldsymbol{Q}(\epsilon\delta\boldsymbol{\alpha}).\boldsymbol{d}_i \tag{3.19}$$

The rotation tensor $\boldsymbol{Q}_\epsilon = \boldsymbol{Q}(\boldsymbol{\theta} + \epsilon\delta\boldsymbol{\theta})$ transforms the vector $\boldsymbol{E}_i$ to $\boldsymbol{d}_{i\epsilon}$ in a single step, whereas, the tensor $\boldsymbol{Q}_\epsilon = \boldsymbol{Q}(\epsilon\delta\boldsymbol{\alpha}).\boldsymbol{Q}(\boldsymbol{\theta})$ performs the same transformation in two steps: $\boldsymbol{E}_i \xrightarrow{\boldsymbol{Q}(\boldsymbol{\theta})} \boldsymbol{d}_i \xrightarrow{\boldsymbol{Q}(\epsilon\delta\boldsymbol{\alpha})} \boldsymbol{d}_{i\epsilon}$. From Eq. (7.26b), we arrive at the expression of varied rotation tensor and director field:

$$\delta\boldsymbol{Q} = \partial_\epsilon \left(\exp(\epsilon\delta\hat{\boldsymbol{\alpha}}).\exp(\hat{\boldsymbol{\theta}})\right)|_{\epsilon=0} = \left(\delta\hat{\boldsymbol{\alpha}}.\exp(\epsilon\delta\hat{\boldsymbol{\alpha}}).\exp(\hat{\boldsymbol{\theta}})\right)|_{\epsilon=0} = \delta\hat{\boldsymbol{\alpha}}.\boldsymbol{Q}(\boldsymbol{\theta}); \tag{3.20a}$$

$$\delta\boldsymbol{d}_i = \delta\boldsymbol{Q}.\boldsymbol{E}_i = \delta\hat{\boldsymbol{\alpha}}.\boldsymbol{d}_i. \tag{3.20b}$$

Here, $\delta\hat{\boldsymbol{\alpha}}$ represents the anti-symmetric matrix associated with the vector $\delta\boldsymbol{\alpha}$. We define the material form of incremental rotation $\delta\hat{\overline{\boldsymbol{\alpha}}}$ (with $\delta\overline{\boldsymbol{\alpha}}$ being the associated axial vector) as,

$$\delta\hat{\overline{\boldsymbol{\alpha}}} = \boldsymbol{Q}^T.\delta\hat{\boldsymbol{\alpha}} = \boldsymbol{Q}^T.\delta\boldsymbol{Q};\ \delta\overline{\boldsymbol{\alpha}} = \boldsymbol{Q}^T.\delta\boldsymbol{\alpha}. \tag{3.21}$$

Like the variation, we define the linearized part of rotation tensor $\boldsymbol{Q}$, linearized at $\exp(\hat{\boldsymbol{\theta}})$ in the direction of $\Delta\hat{\boldsymbol{\alpha}}.\boldsymbol{Q} \in T_{\boldsymbol{Q}}SO(3)$ as,

$$\Delta\boldsymbol{Q} = \partial_\epsilon \boldsymbol{Q}_\epsilon|_{\epsilon=0} \text{ with } \boldsymbol{Q}_\epsilon = \boldsymbol{Q}(\epsilon\Delta\boldsymbol{\alpha}).\boldsymbol{Q}(\boldsymbol{\theta}). \tag{3.22}$$

It follows from the discussion above that $\partial_\xi\boldsymbol{Q}, \delta\boldsymbol{Q}, \Delta\boldsymbol{Q} \in T_{\boldsymbol{Q}}SO(3)$, and $\delta\hat{\overline{\boldsymbol{\alpha}}}, \delta\hat{\boldsymbol{\theta}}, \Delta\hat{\boldsymbol{\theta}} \in so(3)$. Like the relationship between $\boldsymbol{\kappa}$ and $\partial_\xi\boldsymbol{\theta}$, we arrive at the relation between $\delta\boldsymbol{\alpha}$ (or $\Delta\boldsymbol{\alpha}$) and $\delta\boldsymbol{\theta}$ (or $\Delta\boldsymbol{\theta}$). We utilize the results in Eq. (7.26b) and obtain

$$\partial_\epsilon \exp(\epsilon\delta\hat{\boldsymbol{\alpha}})|_{\epsilon=0} = \partial_\epsilon \left(\exp(\hat{\boldsymbol{\theta}} + \epsilon\delta\hat{\boldsymbol{\theta}}).\exp(-\hat{\boldsymbol{\theta}})\right)|_{\epsilon=0}. \tag{3.23}$$

Simplifying Eq. (3.23), we get,

$$\delta\boldsymbol{\alpha} = \boldsymbol{T}_{\boldsymbol{\theta}}.\delta\boldsymbol{\theta};\ \delta\boldsymbol{\theta} = \boldsymbol{T}_{\boldsymbol{\theta}}^{-1}.\delta\boldsymbol{\alpha}. \tag{3.24}$$

Proposition 3.3 also holds for the variation and mix of derivatives and variation, for example: $\delta^n\overline{\boldsymbol{v}} = \boldsymbol{Q}^T.\tilde{\delta}^n\boldsymbol{v}$ and $\delta^k(\partial_\xi^n\overline{\boldsymbol{v}}) = \boldsymbol{Q}^T.\tilde{\delta}^k(\tilde{\partial}_\xi^n\boldsymbol{v})$, where $\tilde{\delta}^k = (\delta - \hat{\delta})^k$ such that $\hat{\delta} = \delta\hat{\boldsymbol{\alpha}}$.

In figure 3.2, we originate three vectors (the reference vector $\boldsymbol{E}_i$, the vector $\boldsymbol{d}_i(\xi)$ obtained by finite rotation of $\boldsymbol{E}_i$, and the vector $\boldsymbol{d}_i(\xi + \mathrm{d}\xi)$) at a point to illustrates the concept of curvature and the incremental (or variation) current rotation vector.

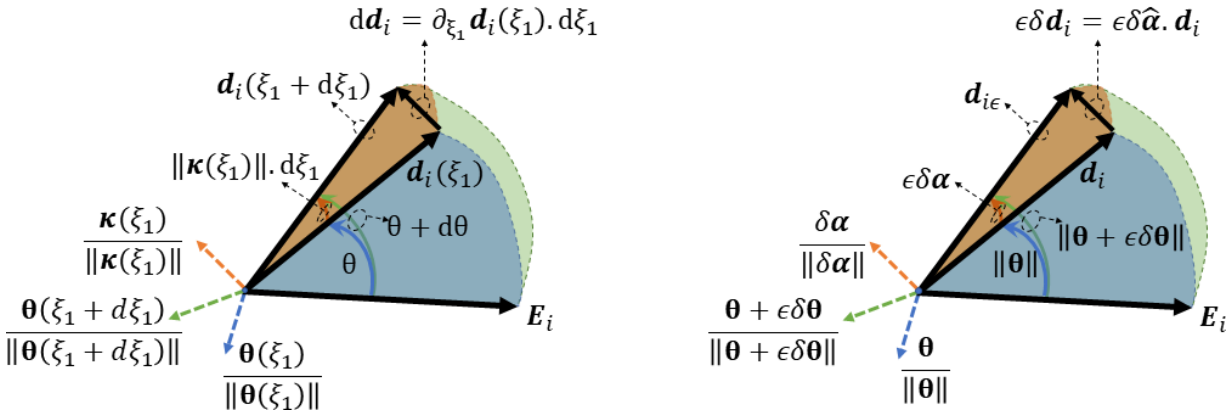

Figure 3.2: The physical interpretation of the curvature $\boldsymbol{\kappa}$ (left figure) and the variation of rotation vector $\delta\boldsymbol{\alpha}$ (right figure) resulting in an infinitesimal rotation.

3.4 On derivatives

3.4.1 Useful results on derivatives of Lie-bracket and higher-order product rule

Proposition 3.4: For any $\hat{\boldsymbol{a}}, \hat{\boldsymbol{b}} \in so(3)$ with corresponding axial vectors $\boldsymbol{a}, \boldsymbol{b} \in \mathbb{R}^3$ respectively, the following formula for derivatives hold:

$$\partial_\xi^n \left[\hat{\boldsymbol{a}}, \hat{\boldsymbol{b}}\right] = \sum_{i=0}^{n} C_i^n \left[\partial_\xi^{(n-i)}\hat{\boldsymbol{a}}, \partial_\xi^{(i)}\hat{\boldsymbol{b}}\right] = \sum_{i=0}^{n} C_i^n \left[\partial_\xi^{(i)}\hat{\boldsymbol{a}}, \partial_\xi^{(n-i)}\hat{\boldsymbol{b}}\right]; \tag{3.25a}$$

$$\partial_\xi^n(\boldsymbol{a} \times \boldsymbol{b}) = \sum_{i=0}^{n} C_i^n(\partial_\xi^{(n-i)}\boldsymbol{a} \times \partial_\xi^{(i)}\boldsymbol{b}) = \sum_{i=0}^{n} C_i^n(\partial_\xi^{(i)}\boldsymbol{a} \times \partial_\xi^{(n-i)}\boldsymbol{b}). \tag{3.25b}$$

Proof: Using the definition of Lie-bracket in Eq. (1.9a), we have,

$$\partial_\xi \left[\hat{\boldsymbol{a}}, \hat{\boldsymbol{b}}\right] = (\partial_\xi\hat{\boldsymbol{a}}.\hat{\boldsymbol{b}} + \hat{\boldsymbol{a}}.\partial_\xi\hat{\boldsymbol{b}}) - (\partial_\xi\hat{\boldsymbol{b}}.\hat{\boldsymbol{a}} + \hat{\boldsymbol{b}}.\partial_\xi\hat{\boldsymbol{a}}) = \left[\partial_\xi\hat{\boldsymbol{a}}, \hat{\boldsymbol{b}}\right] + \left[\hat{\boldsymbol{a}}, \partial_\xi\hat{\boldsymbol{b}}\right]. \tag{3.26}$$

Higher-order derivatives of the Lie-bracket derived using the above result yields an expression given by Eq. (3.25a). Using the definition of axial vector corresponding to the Lie-bracket in Eq. (1.9b), Eq. (3.25b) follows from Eq. (3.25a). The first and second equality in

(3.25a) and (3.25b) holds by virtue of result (3.1a) in *Theorem 3.0.* This completes the proof. □

Corollary 3.2: For scalars functions $f(\xi), g(\xi)$; vectors $\boldsymbol{u}(\xi), \boldsymbol{v}(\xi)$; and a second order tensors $\boldsymbol{A}(\xi), \boldsymbol{B}(\xi)$, the n^{th} order product rule is given by the following:

$$\partial_\xi^n(fg) = \sum_{i=0}^{n} C_i^n \partial_\xi^{(n-i)} f . \partial_\xi^{(i)} g = \sum_{i=0}^{n} C_i^n \partial_\xi^{(i)} f . \partial_\xi^{(n-i)} g; \tag{3.27a}$$

$$\partial_\xi^n(f\boldsymbol{u}) = \sum_{i=0}^{n} C_i^n \partial_\xi^{(n-i)} f . \partial_\xi^{(i)} \boldsymbol{u} = \sum_{i=0}^{n} C_i^n \partial_\xi^{(i)} f . \partial_\xi^{(n-i)} \boldsymbol{u}; \tag{3.27b}$$

$$\partial_\xi^n(f\boldsymbol{A}) = \sum_{i=0}^{n} C_i^n \partial_\xi^{(n-i)} f . \partial_\xi^{(i)} \boldsymbol{A} = \sum_{i=0}^{n} C_i^n \partial_\xi^{(i)} f . \partial_\xi^{(n-i)} \boldsymbol{A}; \tag{3.27c}$$

$$\partial_\xi^n(\boldsymbol{v} \cdot \boldsymbol{u}) = \sum_{i=0}^{n} C_i^n \partial_\xi^{(n-i)} \boldsymbol{v} \cdot \partial_\xi^{(i)} \boldsymbol{u} = \sum_{i=0}^{n} C_i^n \partial_\xi^{(i)} \boldsymbol{v} \cdot \partial_\xi^{(n-i)} \boldsymbol{u}; \tag{3.27d}$$

$$\partial_\xi^n(\boldsymbol{A}.\boldsymbol{u}) = \sum_{i=0}^{n} C_i^n \partial_\xi^{(n-i)} \boldsymbol{A} . \partial_\xi^{(i)} \boldsymbol{u} = \sum_{i=0}^{n} C_i^n \partial_\xi^{(i)} \boldsymbol{A} . \partial_\xi^{(n-i)} \boldsymbol{u}. \tag{3.27e}$$

$$\partial_\xi^n(\boldsymbol{A}.\boldsymbol{B}) = \sum_{i=0}^{n} C_i^n \partial_\xi^{(n-i)} \boldsymbol{A} . \partial_\xi^{(i)} \boldsymbol{B} = \sum_{i=0}^{n} C_i^n \partial_\xi^{(i)} \boldsymbol{A} . \partial_\xi^{(n-i)} \boldsymbol{B}. \tag{3.27f}$$

Proof: The result above follows directly from *proposition 3.4.* This is because, from Eq. (3.26), we see that Lie-brackets follow the chain rule just like the product of two scalars or a dot product except for the fact that Lie-brackets are non-commutative (which is a stronger condition). □

Proposition 3.5: For any $\hat{\boldsymbol{a}}(\xi) \in so(3)$, the following holds:

$$\partial_\xi^m \left[\hat{\boldsymbol{a}}, \partial_\xi \hat{\boldsymbol{a}}\right] = \sum_{j=0}^{j_m^{\max}} b_{mj} \left[\partial_\xi^{(j)} \hat{\boldsymbol{a}}, \partial_\xi^{(m-j+1)} \hat{\boldsymbol{a}}\right]. \tag{3.28}$$

where $m, j, j_m^{\max}, b_{mj} \in \mathbb{Z}^+$, such that the coefficient $j_m^{\max}$, and b_{mj} are given as

$$j_m^{\max} = \begin{cases} \text{floor}\left(\frac{m+1}{2}\right), & \text{if } \frac{m+1}{2} \notin \mathbb{Z}^+; \\ \frac{m+1}{2} - 1, & \text{if } \frac{m+1}{2} \in \mathbb{Z}^+. \end{cases} \tag{3.29a}$$

$$b_{mj} = C_j^m - C_{(m-j+1)}^m = C_j^m \left(\frac{m-2j+1}{m-j+1}\right). \tag{3.29b}$$

Proof: Using the result (3.25a) of *Proposition 3.4*, we get,

$$\begin{aligned}\partial_\xi^m[\hat{\boldsymbol{a}}, \partial_\xi \hat{\boldsymbol{a}}] &= \sum_{j=0}^{m} C_j^m \left[\partial_\xi^{(j)} \hat{\boldsymbol{a}}, \partial_\xi^{(m-j+1)} \hat{\boldsymbol{a}}\right] \\ &= \underbrace{C_0^m \left[\hat{\boldsymbol{a}}, \partial_\xi^{(m+1)} \hat{\boldsymbol{a}}\right]}_{\text{Term 0}} + \underbrace{\sum_{j=1}^{m} C_j^m \left[\partial_\xi^{(j)} \hat{\boldsymbol{a}}, \partial_\xi^{(m-j+1)} \hat{\boldsymbol{a}}\right]}_{\text{Term 1}}.\end{aligned} \tag{3.30}$$

The terms in the expansion of *Term 1* with $j = \frac{m+1}{2}$ vanishes (refer to Eq. (1.10a)). Keeping that in mind, we note that the expansion of *Term 1* can be written in two correct possible ways: the first possibility is when $j > \frac{m+1}{2}$, and the second option is considering $j < \frac{m+1}{2}$. In the first option, the coefficient of all the terms in the sum will be negative, whereas, for second case, the coefficients will be positive. This owes to the anti-commutative property of Lie-brackets mentioned in Eq. (1.10b). We consider the second case in our derivation.

We can further simplify *Term 1*. The total number of terms present in the expanded form of *Term 1* is less than m. This is because the terms with interchanged order of derivatives in Lie-bracket can be reduced to one term. For instance:

$$c_1 \left[\partial_\xi^x \hat{\boldsymbol{a}}, \partial_\xi^y \hat{\boldsymbol{a}}\right] + c_2 \left[\partial_\xi^y \hat{\boldsymbol{a}}, \partial_\xi^x \hat{\boldsymbol{a}}\right] = (c_1 - c_2) \left[\partial_\xi^x \hat{\boldsymbol{a}}, \partial_\xi^y \hat{\boldsymbol{a}}\right].$$

Thus, the maximum value of j is restricted by the fact that $j < \frac{m+1}{2}$ and $j \in \mathbb{Z}^+ - \{0\}$. Combining these two constraints yields $\max(j) = j_m^{\max}$ given by Eq. (3.29a). However, such a reduction or simplification of *Term 1* changes the coefficient by which each term in the sum is weighed. The discussion presented so far may be demonstrated, for example, for $m = 4$ as:

$$\begin{aligned}\text{Term 1}|_{m=4} &= \sum_{j=1}^{4} C_j^4 \left[\partial_\xi^{(j)} \hat{\boldsymbol{a}}, \partial_\xi^{(5-j)} \hat{\boldsymbol{a}}\right] \\ &= 3\left[\partial_\xi \hat{\boldsymbol{a}}, \partial_\xi^4 \hat{\boldsymbol{a}}\right] + 2\left[\partial_\xi^2 \hat{\boldsymbol{a}}, \partial_\xi^3 \hat{\boldsymbol{a}}\right] = -3\left[\partial_\xi^4 \hat{\boldsymbol{a}}, \partial_\xi \hat{\boldsymbol{a}}\right] - 2\left[\partial_\xi^3 \hat{\boldsymbol{a}}, \partial_\xi^2 \hat{\boldsymbol{a}}\right] \\ &= \|C_1^4 - C_4^4\| \left[\partial_\xi \hat{\boldsymbol{a}}, \partial_\xi^4 \hat{\boldsymbol{a}}\right] + \|C_2^4 - C_3^4\| \left[\partial_\xi^2 \hat{\boldsymbol{a}}, \partial_\xi^3 \hat{\boldsymbol{a}}\right]\end{aligned} \tag{3.31}$$

$$= \sum_{j=1}^{j_4^{max}=2} (C_j^4 - C_{(4-j+1)}^4) \left[\partial_\xi^{(j)} \hat{\boldsymbol{a}}, \partial_\xi^{(5-j)} \hat{\boldsymbol{a}} \right].$$

For a general case, if $j_m^{\max} \geq 1$, *Term 1* can be written as:

$$\text{Term 1} = \sum_{j=1}^{j_m^{\max}} b_{mj} \left[\partial_\xi^{(j)} \hat{\boldsymbol{a}}, \partial_\xi^{(m-j+1)} \hat{\boldsymbol{a}} \right]. \tag{3.32}$$

The modified coefficient $b_{mj} = (C_j^m - C_{(m-j+1)}^m)$ is defined in Eq. (3.29b). From the second equality in Eq. (3.29b), we also note that $b_{m0} = C_0^m = 1$. Therefore, combining *Term 0* and *Term 1* proves the proposition. Table 3.1 gives the value of coefficient $j_m^{\max}$ for $1 \leq m \leq 6$. □

Table 3.1: $j_m^{\max}$ for $0 \leq m \leq 6$

	$i=0$	$i=1$	$i=2$	$i=3$	$i=4$	$i=5$	$i=6$
$m=0$	0	-	-	-	-	-	-
$m=1$	0	0	-	-	-	-	-
$m=2$	1	0	0	-	-	-	-
$m=3$	1	1	0	0	-	-	-
$m=4$	2	1	1	0	0	-	-
$m=5$	2	2	1	1	0	0	-
$m=6$	3	2	2	1	1	0	0

3.4.2 Derivatives of curvature tensor

The derivative of the curvature tensor may be obtained using Eq. (2.3) deploying a straightforward application of the chain rule. However, deriving the expression of higher-order derivatives using Eq. (2.3) is cumbersome because of the involvement of trigonometric functions. Instead, we realize that the reparametrization of the rotation tensor by the *Gibbs vector* (the components of which are called as *Gibbs* or *Rodriguez parameters* in the literature) yields the formula of curvature tensor that is beneficial in obtaining the derivative of curvature tensor in the form of a single summation-formula. Consider a rotation tensor $\boldsymbol{Q}(\boldsymbol{\theta}) = \exp(\hat{\boldsymbol{\theta}}) \in SO(3)$. We

define the Gibbs vector $\boldsymbol{\phi}$ and the associated quantities as:

$$\hat{\boldsymbol{\phi}} = \frac{\tan\left(\frac{\theta}{2}\right)}{\theta}\hat{\boldsymbol{\theta}}; \quad \boldsymbol{\phi} = \frac{\tan\left(\frac{\theta}{2}\right)}{\theta}\boldsymbol{\theta}; \quad \phi = \|\boldsymbol{\phi}\| = \tan\left(\frac{\theta}{2}\right); \quad \overline{\phi} = 2\cos^2\left(\frac{\theta}{2}\right) = \frac{2}{\phi^2+1}. \tag{3.33}$$

The result defined in Eq. 1.14a may be manipulated using the definition given above as:

$$\begin{aligned} &\boldsymbol{Q}(\hat{\boldsymbol{\phi}}) = \boldsymbol{I}_3 + 2\cos^2\left(\frac{\theta}{2}\right).\left(\frac{1}{\theta}\tan\left(\frac{\theta}{2}\right)\hat{\boldsymbol{\theta}} + \left(\frac{1}{\theta}\tan\left(\frac{\theta}{2}\right)\right)^2\hat{\boldsymbol{\theta}}^2\right) = \boldsymbol{I}_3 + \overline{\phi}(\hat{\boldsymbol{\phi}} + \hat{\boldsymbol{\phi}}^2); \\ &\boldsymbol{Q}(\hat{\boldsymbol{\phi}})^T = \boldsymbol{Q}(-\boldsymbol{\theta}) = \boldsymbol{I}_3 + \overline{\phi}(-\hat{\boldsymbol{\phi}} + \hat{\boldsymbol{\phi}}^2). \end{aligned} \tag{3.34}$$

Proposition 3.6: $\hat{\boldsymbol{\phi}} \in so(3)$ and $n \in \mathbb{Z}^+ - \{0\}$, the following formulae hold true:

$$\hat{\boldsymbol{\phi}}^{2n-1} = (-1)^{n-1}\phi^{2(n-1)}\hat{\boldsymbol{\phi}}; \quad \hat{\boldsymbol{\phi}}^{2n} = (-1)^{n-1}\phi^{2(n-1)}\hat{\boldsymbol{\phi}}^2; \tag{3.35a}$$

$$\hat{\boldsymbol{\phi}}.\partial_\xi\hat{\boldsymbol{\phi}}.\hat{\boldsymbol{\phi}} = -(\boldsymbol{\phi}\cdot\partial_\xi\boldsymbol{\phi})\hat{\boldsymbol{\phi}}; \quad \hat{\boldsymbol{\phi}}.\partial_\xi\hat{\boldsymbol{\phi}}.\hat{\boldsymbol{\phi}}^2 = -(\boldsymbol{\phi}\cdot\partial_\xi\boldsymbol{\phi})\hat{\boldsymbol{\phi}}^2. \tag{3.35b}$$

Proof: Refer to Eq. [30] of Argyris [19] for identity (3.35a) that describes the recurrence formula for the power of anti-symmetric matrix. The identity (3.35b) can be proved by considering the action of tensor on left hand side of equation on to a vector, say $\boldsymbol{v} \in \mathbb{R}^3$ and using the vector triple product identity, such that

$$(\hat{\boldsymbol{\phi}}.\partial_\xi\hat{\boldsymbol{\phi}}.\hat{\boldsymbol{\phi}}).\boldsymbol{v} = \boldsymbol{\phi}\times(\partial_\xi\boldsymbol{\phi}\times(\hat{\boldsymbol{\phi}}.\boldsymbol{v})) = (\boldsymbol{\phi}\cdot(\hat{\boldsymbol{\phi}}.\boldsymbol{v}))\partial_\xi\boldsymbol{\phi} - (\boldsymbol{\phi}\cdot\partial_\xi\boldsymbol{\phi})\hat{\boldsymbol{\phi}}.\boldsymbol{v}. \tag{3.36}$$

Noting that $(\boldsymbol{\phi}\cdot(\hat{\boldsymbol{\phi}}.\boldsymbol{v})) = \boldsymbol{\phi}\cdot(\boldsymbol{\phi}\times\boldsymbol{v}) = \boldsymbol{0}$, we prove the first part of identity (3.35b). Along the similar lines, the second part can be proven. □

The curvature tensor can then be obtained using Eq. (3.34) and *proposition 3.6* as:

$$\hat{\boldsymbol{\kappa}} = \partial_\xi\boldsymbol{Q}.\boldsymbol{Q}^T = \overline{\phi}\left(\partial_\xi\hat{\boldsymbol{\phi}} + [\hat{\boldsymbol{\phi}}, \partial_\xi\hat{\boldsymbol{\phi}}]\right). \tag{3.37}$$

This expression is much simpler than the one presented in Eq. (2.3).

Proposition 3.7: The following holds:

$$\partial_\xi^n \hat{\boldsymbol{\kappa}} = \sum_{i=0}^{n} C_i^n \partial_\xi^{(i)} \overline{\phi} \left(\partial_\xi^{(n-i+1)} \hat{\boldsymbol{\phi}} + \sum_{j=0}^{j_{(n-i)}^{\max}} b_{(n-i)j} \left[\partial_\xi^{(j)} \hat{\boldsymbol{\phi}}, \partial_\xi^{(n-i+1-j)} \hat{\boldsymbol{\phi}} \right] \right); \tag{3.38a}$$

$$\partial_\xi^n \boldsymbol{\kappa} = \sum_{i=0}^{i=n} C_i^n \partial_\xi^{(i)} \overline{\phi} \left(\partial_\xi^{(n-i+1)} \boldsymbol{\phi} + \sum_{j=0}^{j_{(n-i)}^{\max}} b_{(n-i)j} \left(\partial_\xi^{(j)} \boldsymbol{\phi} \times \partial_\xi^{(n-i+1-j)} \boldsymbol{\phi} \right) \right). \tag{3.38b}$$

where, $n, i, j, j_{(n-i)}^{\max}, C_i^n, b_{(n-i)j} \in \mathbb{Z}^+$. Replacing $m \longrightarrow (n-i)$ in (3.29a) and (3.29b) yields $j_{(n-i)}^{\max}$, and $b_{(n-i)j}$.

Proof: We utilize Eq.(3.27c) of *Corollary 3.2* and the expression of curvature tensor in Eq. (3.37) and obtain

$$\begin{aligned} \partial_\xi^n \hat{\boldsymbol{\kappa}} &= \sum_{i=0}^{n} C_i^n \partial_\xi^{(i)} \overline{\phi}. \left(\partial_\xi^{(n-i)} \left(\partial_\xi \hat{\boldsymbol{\phi}} + \left[\hat{\boldsymbol{\phi}}, \partial_\xi \hat{\boldsymbol{\phi}} \right] \right) \right) \\ &= \sum_{i=0}^{n} C_i^n \partial_\xi^{(i)} \overline{\phi}. \left(\partial_\xi^{(n-i+1)} \hat{\boldsymbol{\phi}} + \partial_\xi^{(n-i)} \left[\hat{\boldsymbol{\phi}}, \partial_\xi \hat{\boldsymbol{\phi}} \right] \right) \end{aligned} \tag{3.39}$$

Using *Proposition 3.5* and replacing $m \longrightarrow (n-i)$, we get,

$$\partial_\xi^{(n-i)} \left[\hat{\boldsymbol{\phi}}, \partial_\xi \hat{\boldsymbol{\phi}} \right] = \sum_{j=0}^{j_{(n-i)}^{\max}} b_{(n-i)j} \left[\partial_\xi^{(j)} \hat{\boldsymbol{\phi}}, \partial_\xi^{((n-i)-j+1)} \hat{\boldsymbol{\phi}} \right]. \tag{3.40}$$

The equation above when substituted into Eq. (3.39) proves the result (3.38a). The axial vector corresponding to $\partial_\xi^n \hat{\boldsymbol{\kappa}}$, given by Eq. (3.38b), is obtained using the formula (1.9b). □

Note: Define $\frac{\boldsymbol{\theta}}{\theta} = \boldsymbol{e}$. We can use Eq. (3.34) and (3.38) to obtain $\boldsymbol{Q}$ and $\partial_\xi^n \hat{\boldsymbol{\kappa}}$ for small rotations (when $\|\boldsymbol{\theta}\| \to 0$), by setting $\partial_\xi^n \phi = \lim_{\theta \to 0} \partial_\xi^n \tan\left(\frac{\theta}{2}\right)$, $\partial_\xi^n \hat{\boldsymbol{\phi}} = \left(\lim_{\theta \to 0} \partial_\xi^n \tan\left(\frac{\theta}{2}\right) \right) . \hat{\boldsymbol{e}}$ and $\partial_\xi^n \overline{\phi} = 2 \lim_{\theta \to 0} \partial_\xi^n \cos^2\left(\frac{\theta}{2}\right)$. Here, $\boldsymbol{e}$ is the fixed unit vector about which the rotation occurs.

Corollary 3.3: The following holds:

$$\begin{aligned}\tilde{\partial}_\xi^n \hat{\boldsymbol{\kappa}} &= \partial_\xi^n \hat{\boldsymbol{\kappa}} - (1-\delta_{n0}) \sum_{i=1}^{n-1} \partial_\xi^{(i-1)} \left[\hat{\boldsymbol{\kappa}}, \tilde{\partial}_\xi^{(n-i)} \hat{\boldsymbol{\kappa}}\right] \\ &= \partial_\xi^n \hat{\boldsymbol{\kappa}} - (1-\delta_{n0}) \sum_{i=1}^{n-1} \sum_{j=0}^{i-1} C_j^{(i-1)} \left[\partial_\xi^{(j)} \hat{\boldsymbol{\kappa}}, \partial_\xi^{(n-i-j)} \tilde{\partial}_\xi^{(n-i)} \hat{\boldsymbol{\kappa}}\right];\end{aligned} \tag{3.41a}$$

$$\begin{aligned}\tilde{\partial}_\xi^n \boldsymbol{\kappa} = (\partial_\xi - \hat{\partial})^n \boldsymbol{\kappa} &= \partial_\xi^n \boldsymbol{\kappa} - (1-\delta_{n0}) \sum_{i=1}^{n-1} \partial_\xi^{(i-1)} (\boldsymbol{\kappa} \times \tilde{\partial}_\xi^{(n-i)} \boldsymbol{\kappa}) \\ &= \partial_\xi^n \boldsymbol{\kappa} - (1-\delta_{n0}) \sum_{i=1}^{n-1} \sum_{j=0}^{i-1} C_j^{(i-1)} (\partial_\xi^{(j)} \boldsymbol{\kappa} \times \partial_\xi^{(n-i-j)} \tilde{\partial}_\xi^{(n-i)} \boldsymbol{\kappa}).\end{aligned} \tag{3.41b}$$

$$\partial_\xi^n \hat{\overline{\boldsymbol{\kappa}}} = \boldsymbol{Q}^T . \tilde{\partial}_\xi^n \hat{\boldsymbol{\kappa}} . \boldsymbol{Q}. \tag{3.41c}$$

Proof: This corollary follows from the *Proposition 3.1, 3.2, 3.3* and *3.4*. We also note that in the sums presented above, $\max(i) = (n-1)$, because $\left[\hat{\boldsymbol{\kappa}}, \tilde{\partial}_\xi^{(n-i)} \hat{\boldsymbol{\kappa}}\right]\Big|_{(n=i)} = \boldsymbol{0}_3$. □

The n$^{\text{th}}$ order derivative of rotation tensor $\boldsymbol{Q}$ can be derived as a function of Gibbs vector and the associated parameters using Eq. (3.34). However, computationally, a much simpler approach would be to derive a recurrence formula for $\partial_\xi^n \boldsymbol{Q}$ using the fact that $\partial_\xi \boldsymbol{Q} = \hat{\boldsymbol{\kappa}} . \boldsymbol{Q}$ and *Proposition 3.7*. The recurrence formula for $\partial_\xi^n \boldsymbol{Q}$ yields the formula to obtain n$^{\text{th}}$ order derivative of director vectors $\boldsymbol{d}_m(\xi)$ with $m \in \{1,2,3\}$.

Proposition 3.8: For $n \geq 0$, the following holds:

$$\partial_\xi^n \boldsymbol{Q} = \delta_{n0} \boldsymbol{Q} + (1-\delta_{n0}) \sum_{i=0}^{n-1} C_i^{(n-1)} \partial_\xi^i \hat{\boldsymbol{\kappa}} . \partial_\xi^{(n-1-i)} \boldsymbol{Q}; \tag{3.42a}$$

$$\partial_\xi^n \boldsymbol{d}_m = \delta_{n0} \boldsymbol{d}_m + (1-\delta_{n0}) \sum_{i=0}^{n-1} C_i^{(n-1)} \partial_\xi^i \hat{\boldsymbol{\kappa}} . \partial_\xi^{(n-1-i)} \boldsymbol{d}_m. \tag{3.42b}$$

Proof: From the definition of curvature tensor, we have $\partial_\xi \boldsymbol{Q} = \hat{\boldsymbol{\kappa}} . \boldsymbol{Q}$. Therefore, for $n > 0$, we have $\partial_\xi^n \boldsymbol{Q} = \partial_\xi^{(n-1)} (\hat{\boldsymbol{\kappa}} . \boldsymbol{Q})$, which when simplified using Eq. (3.27f) yields the result (3.42a). The result (3.42b) follows from Eq. (3.42a) and the fact that $\partial_\xi^n \boldsymbol{d}_m = \partial_\xi^n \left(\boldsymbol{Q} . \boldsymbol{E}_m = \partial_\xi^n \boldsymbol{Q} . \boldsymbol{E}_m\right)$. □

Corollary 3.4: Alternate to *Proposition 3.1* and *Corollary 3.3*, the quantities $\partial_\xi^n \overline{\boldsymbol{\kappa}}$ and $\tilde{\partial}_\xi^n \overline{\boldsymbol{\kappa}}$ can be obtained using the relationship $\overline{\boldsymbol{\kappa}} = \boldsymbol{Q}^T.\boldsymbol{\kappa}$ as:

$$\partial_\xi^n \overline{\boldsymbol{\kappa}} = \sum_{i=0}^{n} C_i^n \partial_\xi^i \boldsymbol{Q}^T.\partial_\xi^{(n-i)} \boldsymbol{\kappa} \qquad \text{for } n \geq 0; \tag{3.43a}$$

$$\tilde{\partial}_\xi^n \boldsymbol{\kappa} = \boldsymbol{Q}.\partial_\xi^n \overline{\boldsymbol{\kappa}} \qquad \text{for } n > 0. \tag{3.43b}$$

Corollary 3.4 can be used to obtain co-rotational derivatives, material curvature and its derivatives, provided $\partial_\xi^n \boldsymbol{\kappa}$ and $\partial_\xi^n \boldsymbol{Q}$ are known.

3.5 Updating the curvature and its derivatives

In this section, we shall address the situation where the space curve is evolving with time in steps, such that the transformed curve is also parameterized spatially by ξ. At time t, let the *initial* rotation tensor field be $\boldsymbol{Q}(\xi, t) = \boldsymbol{Q}_{\mathrm{i}}(\xi) \in SO(3)$ and in the next time step $(t+1)$, the *updated* (or *final*) rotation tensor field is $\boldsymbol{Q}(\xi, t+1) = \boldsymbol{Q}_{\mathrm{f}}(\xi) \in SO(3)$. We assume *Eulerian updating* of rotation tensor field, i.e. the change in rotation tensor field from discrete time step t to $(t+1)$ is given by an *incremental current rotation vector field* $\Delta\boldsymbol{\alpha}$, such that $\Delta\hat{\boldsymbol{\alpha}}.\boldsymbol{Q}_{\mathrm{i}} \in T_{\boldsymbol{Q}_{\mathrm{i}}} SO(3)$. We are given the derivative fields $\partial_\xi^n \Delta\boldsymbol{\alpha}$ (or $\partial_\xi^n \Delta\hat{\boldsymbol{\alpha}}$) and $\partial_\xi^n \boldsymbol{Q}_{\mathrm{i}}$ up to order n (or equivalently, $\partial_\xi^{(n-1)} \hat{\boldsymbol{\kappa}}_{\mathrm{i}}$, where $\hat{\boldsymbol{\kappa}}_{\mathrm{i}} = \partial_\xi \boldsymbol{Q}_{\mathrm{i}}.\boldsymbol{Q}_{\mathrm{i}}^T$). The question posed is thus: "How do we obtain the updated curvature tensor, its spatial, material and co-rotational derivatives up to order $(n-1)$?" It is clear from (3.38) that the n^{th}-order derivative of the curvature tensor requires up to the $(n+1)^{\text{th}}$ derivative of the corresponding rotation vector. To proceed, we first present the updated rotation tensor as

$$\boldsymbol{Q}_{\mathrm{f}} = \exp(\Delta\hat{\boldsymbol{\alpha}}).\boldsymbol{Q}_{\mathrm{i}} = \boldsymbol{Q}_{+}.\boldsymbol{Q}_{\mathrm{i}} \text{ where, } \boldsymbol{Q}_{+} = \exp(\Delta\hat{\boldsymbol{\alpha}}). \tag{3.44}$$

We define the curvature corresponding to *incremental current rotation vector* $\Delta\boldsymbol{\alpha}$ and the *transport operator* $\mathbb{T}_{\boldsymbol{Q}}$ as:

$$\begin{aligned}\hat{\boldsymbol{\kappa}}_+ &= \partial_\xi \exp(\Delta\hat{\boldsymbol{\alpha}}).\exp(-\Delta\hat{\boldsymbol{\alpha}}) = \partial_\xi \boldsymbol{Q}_+.\boldsymbol{Q}_+^T; \\ \mathbb{T}_{\boldsymbol{Q}}[\hat{\boldsymbol{A}}] &= \boldsymbol{Q}.\hat{\boldsymbol{A}}.\boldsymbol{Q}^T \in so(3), \quad \forall \quad \boldsymbol{Q} \in SO(3), \hat{\boldsymbol{A}} \in so(3).\end{aligned} \tag{3.45}$$

We observe that $\mathbb{T}_{\boldsymbol{Q}}[\hat{\overline{\boldsymbol{\kappa}}}] = \hat{\boldsymbol{\kappa}}$ and $\mathbb{T}_{\boldsymbol{Q}^T}[\hat{\boldsymbol{\kappa}}] = \hat{\overline{\boldsymbol{\kappa}}}$.

Proposition 3.9: The n^{th} order derivative of the transport operator $\mathbb{T}_{\boldsymbol{Q}}[\hat{\boldsymbol{A}}]$ is given by

$$\partial_\xi^n \mathbb{T}_{\boldsymbol{Q}}[\hat{\boldsymbol{A}}] = \mathbb{T}_{\boldsymbol{Q}}[\partial_\xi^n \hat{\boldsymbol{A}}] + (1-\delta_{n0}) \sum_{k=1}^{n} \sum_{i=0}^{n-k} C_i^{(n-k)} \left[\partial_\xi^{(i)} \hat{\boldsymbol{\kappa}}, \partial_\xi^{(n-k-i)} \mathbb{T}_{\boldsymbol{Q}}[\partial_\xi^{(k-1)} \hat{\boldsymbol{A}}]\right]. \tag{3.46}$$

Proof: Consider

$$\partial_\xi \mathbb{T}_{\boldsymbol{Q}}[\hat{\boldsymbol{A}}] = \boldsymbol{Q}.\partial_\xi \hat{\boldsymbol{A}}.\boldsymbol{Q}^T + \hat{\boldsymbol{\kappa}}.\mathbb{T}_{\boldsymbol{Q}}[\hat{\boldsymbol{A}}] - \mathbb{T}_{\boldsymbol{Q}}[\hat{\boldsymbol{A}}].\hat{\boldsymbol{\kappa}} = \mathbb{T}_{\boldsymbol{Q}}[\partial_\xi \hat{\boldsymbol{A}}] + [\hat{\boldsymbol{\kappa}}, \mathbb{T}_{\boldsymbol{Q}}[\hat{\boldsymbol{A}}]]. \tag{3.47}$$

Using the above result along with *Proposition 3.4*, for $n \geq 1$, we have

$$\begin{aligned}\partial_\xi^n \mathbb{T}_{\boldsymbol{Q}}[\hat{\boldsymbol{A}}] =& \partial_\xi^{(n-1)}.(\partial_\xi \mathbb{T}_{\boldsymbol{Q}}[\hat{\boldsymbol{A}}]) = \partial_\xi^{(n-1)}.\left(\mathbb{T}_{\boldsymbol{Q}}[\partial_\xi \hat{\boldsymbol{A}}] + [\hat{\boldsymbol{\kappa}}, \mathbb{T}_{\boldsymbol{Q}}[\hat{\boldsymbol{A}}]]\right) \\ =& \partial_\xi^{(n-1)} \mathbb{T}_{\boldsymbol{Q}}[\partial_\xi \hat{\boldsymbol{A}}] + \sum_{i=0}^{(n-1)} C_i^{(n-1)} \left[\partial_\xi^{(i)} \hat{\boldsymbol{\kappa}}, \partial_\xi^{(n-1-i)} \mathbb{T}_{\boldsymbol{Q}}[\hat{\boldsymbol{A}}]\right] \\ =& \partial_\xi^{(n-2)} (\partial_\xi \mathbb{T}_{\boldsymbol{Q}}[\partial_\xi \hat{\boldsymbol{A}}]) + \sum_{i=0}^{(n-1)} C_i^{(n-1)} \left[\partial_\xi^{(i)} \hat{\boldsymbol{\kappa}}, \partial_\xi^{(n-1-i)} \mathbb{T}_{\boldsymbol{Q}}[\hat{\boldsymbol{A}}]\right] \\ =& \partial_\xi^{(n-2)} \mathbb{T}_{\boldsymbol{Q}}[\partial_\xi^2 \hat{\boldsymbol{A}}] + \sum_{i=0}^{(n-2)} C_i^{(n-2)} \left[\partial_\xi^{(i)} \hat{\boldsymbol{\kappa}}, \partial_\xi^{(n-2-i)} \mathbb{T}_{\boldsymbol{Q}}[\partial_\xi \hat{\boldsymbol{A}}]\right] \\ &+ \sum_{i=0}^{(n-1)} C_i^{(n-1)} \left[\partial_\xi^{(i)} \hat{\boldsymbol{\kappa}}, \partial_\xi^{(n-1-i)} \mathbb{T}_{\boldsymbol{Q}}[\hat{\boldsymbol{A}}]\right] \\ =& \mathbb{T}_{\boldsymbol{Q}}[\partial_\xi^n \hat{\boldsymbol{A}}] + \Bigg(\sum_{i=0}^{(n-1)} C_i^{(n-1)} \left[\partial_\xi^{(i)} \hat{\boldsymbol{\kappa}}, \partial_\xi^{(n-1-i)} \mathbb{T}_{\boldsymbol{Q}}[\hat{\boldsymbol{A}}]\right] \\ & \sum_{i=0}^{(n-2)} C_i^{(n-2)} \left[\partial_\xi^{(i)} \hat{\boldsymbol{\kappa}}, \partial_\xi^{(n-2-i)} \mathbb{T}_{\boldsymbol{Q}}[\partial_\xi \hat{\boldsymbol{A}}]\right] + \ldots + \sum_{i=0}^{0} C_i^{0} \left[\partial_\xi^{(i)} \hat{\boldsymbol{\kappa}}, \partial_\xi^{(n-i)} \mathbb{T}_{\boldsymbol{Q}}[\partial_\xi^{(n-1)} \hat{\boldsymbol{A}}]\right] \Bigg)\end{aligned}$$

$$= \mathbb{T}_{\boldsymbol{Q}}[\partial_\xi^n \hat{\boldsymbol{A}}] + \sum_{k=1}^{n} \sum_{i=0}^{n-k} C_i^{(n-k)} \left[\partial_\xi^{(i)} \hat{\boldsymbol{\kappa}}, \partial_\xi^{(n-k-i)} \mathbb{T}_{\boldsymbol{Q}}[\partial_\xi^{(k-1)} \hat{\boldsymbol{A}}] \right]. \tag{3.48}$$

Noting that at $n = 0$, the sum in equation (3.46) vanishes justifies the factor $(1 - \delta_{n0})$. □

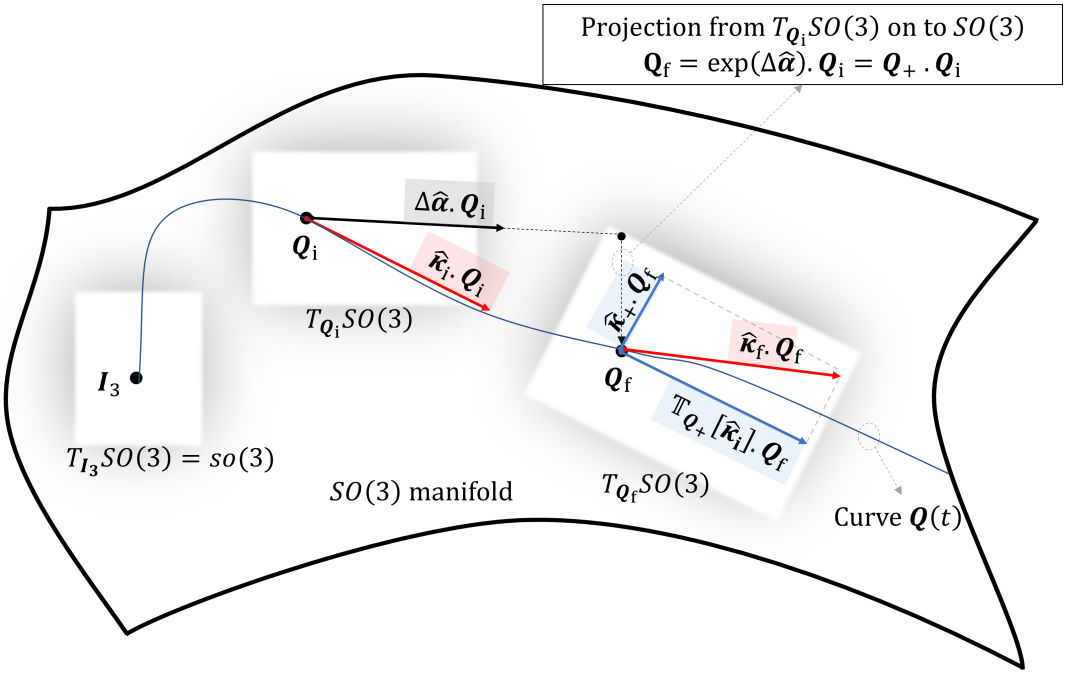

Figure 3.3: Geometric interpretation of the curvature updating: $\hat{\boldsymbol{\kappa}}_\mathrm{f} = \hat{\boldsymbol{\kappa}}_+ + \mathbb{T}_{\boldsymbol{Q}_+}[\hat{\boldsymbol{\kappa}}_\mathrm{i}]$.

Proposition 3.10: Let $\hat{\boldsymbol{\kappa}}_\mathrm{i} = \partial_\xi \boldsymbol{Q}_\mathrm{i}.\boldsymbol{Q}_\mathrm{i}^T$ and $\hat{\boldsymbol{\kappa}}_\mathrm{f} = \partial_\xi \boldsymbol{Q}_\mathrm{f}.\boldsymbol{Q}_\mathrm{f}^T$ denote the curvature field corresponding to the initial and final configurations respectively. The updated curvature tensor and its derivatives are given by the recurrence-formula,

$$\partial_\xi^n \hat{\boldsymbol{\kappa}}_\mathrm{f} = \partial_\xi^n \hat{\boldsymbol{\kappa}}_+ + \mathbb{T}_{\boldsymbol{Q}_+}[\partial_\xi^n \hat{\boldsymbol{\kappa}}_\mathrm{i}] + (1 - \delta_{n0}) \sum_{k=1}^{n} \sum_{i=0}^{n-k} C_i^{(n-k)} \left[\partial_\xi^{(i)} \hat{\boldsymbol{\kappa}}_+, \partial_\xi^{(n-k-i)} \mathbb{T}_{\boldsymbol{Q}_+}[\partial_\xi^{(k-1)} \hat{\boldsymbol{\kappa}}_\mathrm{i}] \right]. \tag{3.49}$$

Proof: Using the Eq. (3.44) and (3.45), we obtain updated curvature as:

$$\hat{\boldsymbol{\kappa}}_\mathrm{f} = \partial_\xi (\boldsymbol{Q}_+.\boldsymbol{Q}_i).(\boldsymbol{Q}_+.\boldsymbol{Q}_i)^T = \partial_\xi (\boldsymbol{Q}_+).\boldsymbol{Q}_+^T + \boldsymbol{Q}_+.\hat{\boldsymbol{\kappa}}_\mathrm{i}.\boldsymbol{Q}_+^T = \hat{\boldsymbol{\kappa}}_+ + \mathbb{T}_{\boldsymbol{Q}_+}[\hat{\boldsymbol{\kappa}}_\mathrm{i}]. \tag{3.50}$$

Therefore,

$$\partial_\xi^n \hat{\boldsymbol{\kappa}}_\mathrm{f} = \partial_\xi^n \hat{\boldsymbol{\kappa}}_+ + \partial_\xi^n \mathbb{T}_{\boldsymbol{Q}_+}[\hat{\boldsymbol{\kappa}}_\mathrm{i}]. \tag{3.51}$$

Substituting Eq. (3.46) obtained in *Proposition 3.9* in the above result proves this proposition. □

The curvatures $\hat{\boldsymbol{\kappa}}_+$ and their derivatives may be obtained using *Proposition 3.7*. Once the spatial curvature and its derivatives are obtained, the derivative of material curvature and co-rotational derivative can be obtained using *Proposition 3.1* or *Corollary 3.3* or *Corollary 3.4*. The reader should refer to Fig. 3.3 for a geometric interpretation of curvature updating.

3.6 Summary

The current chapter is a theoretical extension of chapter 1. Despite this fact, the current chapter is placed third because chapter 2 presents an immediate application of chapter 1. The curvature tensor and its derivatives associated with any space curve framed by a general *material frame* are dealt with. Therefore, the results presented here are valid for any frame, including the Frenet-Serret and Bishop frames. In addition to discussing the spatial and material forms of the curvature tensor, the higher-order derivatives and co-rotation derivatives of these quantities are investigated. A closed-form formula for all higher-order derivative of the spatial curvature tensor is presented. Finally, a time-updating algorithm for curvature (both spatial and material) and its derivatives (partial and co-rotational) was presented, which is particularly useful in practical problems like finite element formulation of geometrically-exact beams, among many other applications. The results presented in this chapter are used to develop finite element code for geometrically exact beams in chapter 10 (refer to section 10.4).

The chapter has been published in Applied Mathematics Letters Journal, Mayank Chadha and Michael D. Todd [35], 2019. The title of this paper is "On the derivatives of curvature of framed space curve and their time-updating scheme". An extended version of the same paper [36], with MATLAB code, is published in arXiv of Mathematics (Differential Geometry). The dissertation author is the primary investigator and author of these papers.

Chapter 4

Enhanced Kinematics of Geometrically-Exact Cosserat beam

4.1 Introduction to generalized kinematics

This chapter deals with the development of a geometrically-exact non-linear kinematic model to capture warping (out-of-plane deformation), fully coupled Poisson's transformation (in-plane deformation) along with axial deformation of the mid-curve, multiple curvatures, torsion and finite shear deformations in a Cosserat beam subjected to finite deformation and finite strain. This approach does not make the usual Euler-Bernoulli rigid cross-section assumption (plane cross-section remains plane after deformation). Instead, we propose a refined approach to capture various cross-sectional deformation (in-plane and out-of-plane) and coupling between them. We discuss the challenges associated with coupling Poisson's effect and warping. The proposed fully-coupled Poisson's effect captures the in-plane deformation of the cross-section. However, the fully-coupled Poisson's transformation presented in this work does not model the in-plane deformation due to local buckling, which is a prominent phenomenon in the case of thin-walled beam cross-sections. The work by Fang Yiu [37] describes the in-plane cross-sectional

distortion of thin-walled beam theory. Apart from this buckling limitation, the kinematics and the measurement model developed in this chapter is completely general.

For a Cosserat beam subjected to the Euler-Bernoulli rigid cross-section assumption, the configuration of the beam is defined by the mid-curve and the orthogonal body-centered director triad attached to the cross-section. The rigid cross-section assumption restricts the inclusion of Poisson's and warping effects. The problem of warping for various levels of complexities, from a simple Saint Venant problem (refer [38]) to a complicated non-uniform asymmetric case (refer to [39], [40], [41], [42], [43], [44], [45], [46] and [47]), has been previously explored.

Per our survey of the literature, an investigation on the geometric coupling between the Poisson's effect and warping has not been attempted before. We believe that fully-coupled Poisson's and warping effect for a single-manifold beam problem will capture the in and out of the cross-sectional deformation with enhanced accuracy which is beneficial for both forward modeling analyses and solving inverse problems like shape sensing. The first step of this investigation aims at obtaining a simplified governing differential equation of warping from an assumed small displacement field. This step attempts to extend the theory of warping proposed by Brown et al. [42] to incorporate the contribution of axial deformation and Poisson's effect on warping. We define a small displacement field including axial, bending, torsion and Poisson's effects for an asymmetric cross-section. We include the contribution due to bending because, in a general asymmetric cross-section, the bending also contributes to warping. In general, the proposed warping function captures the non-linear bending-induced shear strain distribution across the cross-section, unlike Timoshenko's theory which assumes a constant shear distribution thereby preventing any out-of-plane deformation. The effect of warping due to non-linear shear induced by bending is quite significant in deep beams.

The governing differential equations for warping are obtained. However, the governing equation and the boundary condition at the periphery of the cross-section reflect an inconsistency if the axial strain is included in the deformation field. We propose a solution to this inconsistency.

Elimination of the observed inconsistency suggests a solution that does not include the effect of axial strain on warping explicitly, but we obtain a consistently modified differential equation for warping. We suggest two different solution approaches that have a separable variable form.

The solution for the warping functions is assumed to be known to develop the fully-coupled Poisson's effect and establish the beam kinematics. Prior knowledge of the warping function guarantees the single manifold nature of the problem and allows us to obtain important parameters such as deformation gradient tensor and *Cauchy Green tensor* (or *Pull-back Riemannian metric*) for the beam. Assuming that we know the solution to these differential equations, we propose a *fully-coupled Poisson's effect* that incorporates the effects of axial strain across the cross-section due to axial deformation, bending curvatures and warping. Henceforth, we call the effect attributed to the cross-sectional deformation (including in- and out-of-plane) a *fully-coupled Poisson's and warping effect*.

The strain vectors and the deformation gradient tensor of the deformed configuration referenced to both an initially straight beam configuration and an initially curved reference beam configuration are obtained. The contribution to each of these strain vectors due to different deformation effects are discussed in great detail. The kinematics of various restraint cases is obtained. In the view of the author, the kinematics developed herein establishes the most comprehensive geometry of the Cosserat beam that still preserves the simplicity of the single-manifold nature of the problem. The notations mentioned at the end of section 3.1 are valid for this chapter.

4.2 Geometric description of various beam configurations

In the wake of proposing the fully-coupled Poisson's and warping effect within our presentation of the kinematics, we define the following configurations of the beam:

1. Ω_c: Curved reference beam configuration.

2. Ω_0: Mathematically straight beam configuration.

3. Ω_1: Deformed configuration of the beam assuming Euler-Bernoulli's rigid cross-section.

4. Ω_2: Deformed configuration of the beam allowing the cross-section to undergo out-of-plane warping only (no in-plane deformation).

5. Ω_3: Deformed configuration of the beam including fully-coupled Poisson's and warping effect.

These configurations will be described in the subsequent sections.

4.2.1 Description of the director frame and the mid-curve of beam

Let an open set $\Omega_0 \subset \mathbb{R}^3$ and $\Omega_3 \subset \mathbb{R}^3$ with at least piecewise smooth boundaries $\mathfrak{S}_0$ and $\mathfrak{S}_3$ represent the undeformed and deformed configuration of the beam respectively. The beam configuration is described by the mid-curve and a family of cross-sections. To start with the kinematic description of the beam, we assume the *straight* undeformed configuration Ω_0.

Let the fixed orthonormal reference basis (material basis) be represented by $\{\boldsymbol{E}_i\}$ with origin at $(0,0,0)$. We choose to have coincidental material and spatial reference axes to avoid unnecessary definition of additional fixed spatial frame. The regular curve $\boldsymbol{\varphi}_0 : [0, L] \longrightarrow \mathbb{R}^3$ represents the mid-curve associated with Ω_0. It is parameterized by the arc-length (curvilinear coordinate along the mid-curve) $\xi_1 \in [0, L]$. We assume that the undeformed configuration is made up of continuously varying plane family of cross-sections $\mathfrak{B}_0(\xi_1)$, such that $\boldsymbol{\varphi}_0 = \xi_1 \boldsymbol{E}_1$ is the locus of geometric centroid of the family of cross-sections $\mathfrak{B}_0(\xi_1)$. The cross-section $\mathfrak{B}_0(\xi_1)$ is spanned by the vectors $\boldsymbol{E}_2 - \boldsymbol{E}_3$ originating at $\boldsymbol{\varphi}_0(\xi_1)$ such that $(\xi_2, \xi_3) \in \mathfrak{B}_0(\xi_1)$. Let $\Gamma_0(\xi_1)$ represent the peripheral boundary of $\mathfrak{B}_0(\xi_1)$, such that $\mathfrak{S}_0 = \mathfrak{B}_0(0) \cup \mathfrak{B}_0(L) \cup_{\forall \xi_1} \Gamma_0(\xi_1)$. Any material point in the beam is defined by its material coordinate (ξ_1, ξ_2, ξ_3) with a position vector $\boldsymbol{R}_0 = \xi_i \boldsymbol{E}_i$.

In order to proceed further, we first define the deformed configuration Ω_1 of the beam

restrained by *rigid cross-section* constraint. Numerous seminal works addressing geometrically exact Cosserat beam with rigid cross-section exist (refer to [48], [49], [50], [51], [52], and [53]). The configuration Ω_1 is defined by a regular mid-curve $\boldsymbol{\varphi}(\xi_1)$ and a family of plane cross-sections $\mathfrak{B}_1(\xi_1)$, parameterized by the undeformed arc-length ξ_1. Equivalently, the mid-curve $\boldsymbol{\varphi}(s(\xi_1))$ and a family of plane cross-sections $\mathfrak{B}_1(s(\xi_1))$ are reparametrized by the deformed arc-length s (curvilinear coordinate along the mid-curve of deformed configuration) such that $\xi_1 = \xi_1(s)$ is at least C^1 continuous and $\frac{\mathrm{d}\xi_1}{\mathrm{d}s} \neq 0$. The director frame field $\{\boldsymbol{d}_i\}$ (also known as moving frame, body frame or material frame) defines the orientation of family of cross-section $\mathfrak{B}_1(s(\xi_1))$. We have, $\mathfrak{B}_1(\xi_1) = \{(\xi_2, \xi_3) \in \mathbb{R}^2_{\xi_1}\}$, where $\mathbb{R}^2_{\xi_1}$ is 2D Euclidean space spanned by the directors $\boldsymbol{d}_2(\xi_1) - \boldsymbol{d}_3(\xi_1)$, with origin at $\boldsymbol{\varphi}(\xi_1)$. We define the deformation map $\boldsymbol{\phi}_1 : \boldsymbol{R}_0 \in \Omega_0 \longmapsto \boldsymbol{R}_1 \in \Omega_1$, such that,

$$\boldsymbol{\phi}_1(\boldsymbol{R}_0) = \boldsymbol{R}_1 = \boldsymbol{\varphi}(\xi_1) + \boldsymbol{r}_1; \tag{4.1a}$$

$$\boldsymbol{r}_1 = \xi_2 \boldsymbol{d}_2 + \xi_3 \boldsymbol{d}_3; \tag{4.1b}$$

$$\boldsymbol{\varphi}(\xi_1) = \varphi_i \boldsymbol{E}_i; \tag{4.1c}$$

$$\boldsymbol{d}_i(\xi_1) = d_{ij} \boldsymbol{E}_j. \tag{4.1d}$$

The initially curved reference beam Ω_c is defined by the director triad $\boldsymbol{d}_{c_i}(\xi_1) = d_{c_{ij}} \boldsymbol{E}_j$ and the mid-curve position vector $\boldsymbol{\varphi}_c(\xi_1)$. Any point in Ω_c is defined by the vector $\boldsymbol{R}_c = \boldsymbol{\varphi}_c + \xi_2 \boldsymbol{d}_{c_2} + \xi_3 \boldsymbol{d}_{c_3}$.

The triad $\{\boldsymbol{E}_i\}, \{\boldsymbol{d}_{c_i}\}$ and $\{\boldsymbol{d}_i\}$ are related to each other by means of the orthogonal rotation tensor,

$$\boldsymbol{d}_i = \boldsymbol{Q}.\boldsymbol{E}_i;\ \boldsymbol{d}_{c_i} = \boldsymbol{Q}_c.\boldsymbol{E}_i;\ \boldsymbol{d}_i = \boldsymbol{Q}_r.\boldsymbol{d}_{c_i}, \tag{4.2}$$

such that the following relationships hold,

$$\begin{gathered} \boldsymbol{Q} = \boldsymbol{Q}_r.\boldsymbol{Q}_c, \\ \boldsymbol{Q} = \boldsymbol{d}_i \otimes \boldsymbol{E}_i;\ \boldsymbol{Q}_r = \boldsymbol{d}_i \otimes \boldsymbol{d}_{c_i};\ \boldsymbol{Q}_c = \boldsymbol{d}_{c_i} \otimes \boldsymbol{E}_i. \end{gathered} \tag{4.3}$$

4.2.2 Finite strain parameters defining the configuration Ω_1

The deformed configuration Ω_1 is subjected to axial deformation of the mid-curve, shear deformations of the cross-section, torsion, and the bending curvatures. We define the deformed arc-length as s, the axial strain as $e(\xi_1)$, and the three shear angles as $\gamma_{11}(\xi_1)$, $\frac{\pi}{2} - \gamma_{12}(\xi_1)$ and $\frac{\pi}{2} - \gamma_{13}(\xi_1)$ subtended by the directors $\boldsymbol{d}_1$, $\boldsymbol{d}_2$ and $\boldsymbol{d}_3$ with the tangent vector $\partial_s\boldsymbol{\varphi}$ respectively, such that,

$$\begin{aligned} e = \frac{\mathrm{d}s - \mathrm{d}\xi_1}{\mathrm{d}\xi_1} \Rightarrow \frac{\mathrm{d}\xi_1}{\mathrm{d}s} = \frac{1}{1+e}; \\ \partial_s\boldsymbol{\varphi} \cdot \boldsymbol{d}_i = \left\{ \begin{array}{ll} \cos\gamma_{1i}, & \text{for } i = 1 \\ \sin\gamma_{1i}, & \text{for } i = 2,3 \end{array} \right\}. \end{aligned} \tag{4.4}$$

Therefore,

$$\partial_{\xi_1}\boldsymbol{\varphi} = (1+e)(\cos\gamma_{11}\boldsymbol{d}_1 + \sin\gamma_{12}\boldsymbol{d}_2 + \sin\gamma_{13}\boldsymbol{d}_3). \tag{4.5}$$

The shear angles defined above are not unique and require construction of another moving frame to establish their uniqueness. However, by themselves, the shear angles are not of much use to us. The components of axial strain vector are rather more meaningful. We define the *axial strain vector* $\boldsymbol{\varepsilon}$ and its material form $\overline{\boldsymbol{\varepsilon}}$ representing the strain due to shear and mid-curve strain such that

$$\begin{aligned} \boldsymbol{\varepsilon} = \partial_{\xi_1}\boldsymbol{\varphi} - \boldsymbol{d}_1 = \overline{\varepsilon}_i\boldsymbol{d}_i; \\ \overline{\boldsymbol{\varepsilon}} = \boldsymbol{Q}^T.\boldsymbol{\varepsilon} = \boldsymbol{Q}^T.\partial_{\xi_1}\boldsymbol{\varphi} - \boldsymbol{E}_1 = \overline{\varepsilon}_i\boldsymbol{E}_i. \end{aligned} \tag{4.6}$$

Mathematically, the curvatures in the beam are captured by the derivative of the director with respect to the arc-length, such that

$$\partial_{\xi_1}\boldsymbol{d}_i = \partial_{\xi_1}\boldsymbol{Q}.\boldsymbol{Q}^T.\boldsymbol{d}_i = \hat{\boldsymbol{\kappa}}.\boldsymbol{d}_i = \boldsymbol{\kappa} \times \boldsymbol{d}_i. \tag{4.7}$$

The component $\overline{\kappa}_1$ represents the torsional curvature about the director $\boldsymbol{d}_1$. The curvature terms $\overline{\kappa}_2$ and $\overline{\kappa}_3$ represent the curvature due to bending about the director $\boldsymbol{d}_2$ and $\boldsymbol{d}_3$, respectively. As defined in section 2.2.2, $\overline{\boldsymbol{\kappa}} = \boldsymbol{Q}^T.\boldsymbol{\kappa}$ and $\hat{\overline{\boldsymbol{\kappa}}} = \boldsymbol{Q}^T.\hat{\boldsymbol{\kappa}}.\boldsymbol{Q}$ represents the material form of the curvature

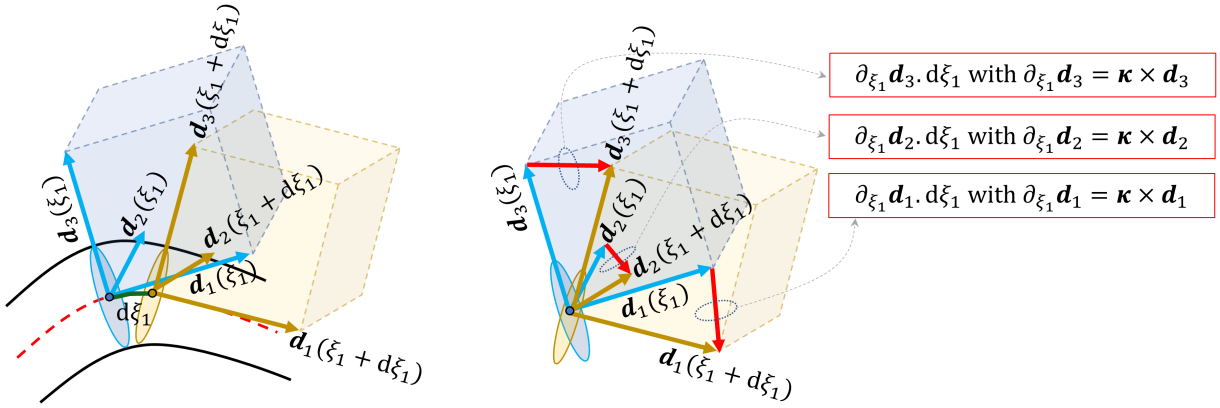

Figure 4.1: Geometric interpretation of derivative of director triad and curvature.

vector and tensor respectively. For the configuration Ω_1, $\boldsymbol{\varphi}(\xi_1) \in \mathbb{R}^3$ is sufficient to define the mid-curve, whereas the orientation of the cross-section is fully described by the director triad. Therefore, $\mathbb{R}^3 \times SO(3)$ is the configuration space for Ω_1.

Assume that the left end of the beam is fixed, implying $\boldsymbol{d}_i(0) = \boldsymbol{E}_i$ and $\boldsymbol{\theta}(\xi_1) = \boldsymbol{0}$. These also serve as the three vector boundary conditions to solve Eq. (4.7). The curvature vector, $\boldsymbol{\kappa} = \overline{\kappa}_i \boldsymbol{d}_i$, may be interpreted as the rotation of the director frame per unit arc length at ξ_1 by an angle $\|\boldsymbol{\kappa}\| = \sqrt{\overline{\kappa}_1^2 + \overline{\kappa}_2^2 + \overline{\kappa}_3^2}$. Since the left end of the beam is fixed, the director frame $\{\boldsymbol{d}_i(\xi_1)\}$ can be obtained by rotating the vectors $\boldsymbol{E}_i$ about the rotation vector $\boldsymbol{\theta}(\xi_1) = \int_0^{\xi_1} \overline{\boldsymbol{\kappa}}(\xi_1)\, \mathrm{d}\xi_1$.

Figure (4.2) geometrically explains the concept described above using a simplified 2D beam fixed at left end. The director $\boldsymbol{d}_3(\xi_1) = \boldsymbol{E}_3$ remains same throughout the mid-curve for the problem being planar in nature. Since the torsion is assumed to be zero, $\boldsymbol{\kappa}(\xi_1) = \overline{\kappa}_3 \boldsymbol{d}_3$. This scenario simplifies the unit vector about which rotation occurs at any arc-length as $\boldsymbol{n}_\theta(\xi_1) = \boldsymbol{E}_3$ and the angle of rotation of directors $\boldsymbol{d}_1(\xi_1)$ and $\boldsymbol{d}_2(\xi_1)$ with respect to the vectors $\boldsymbol{E}_1$ and $\boldsymbol{E}_2$ respectively as, $\theta(\xi_1) = \int_0^{\xi_1} \overline{\kappa}_3(\xi_1) d\xi_1$. Note that this is a special case where the vector $\boldsymbol{n}_\theta(\xi_1) = \boldsymbol{E}_3$ is constant for all ξ_1. Therefore, a general rotation tensor $\boldsymbol{Q}$, such that $\boldsymbol{d}_i(\xi_1) = \boldsymbol{Q}(\xi_1).\boldsymbol{E}_i$, for a beam fixed at left end, is then expressed in terms of the curvatures as,

$$\boldsymbol{Q}(\xi_1) = \exp\left(\int_0^{\xi_1} \hat{\overline{\boldsymbol{\kappa}}}(\xi_1)\, \mathrm{d}\xi_1\right). \tag{4.8}$$

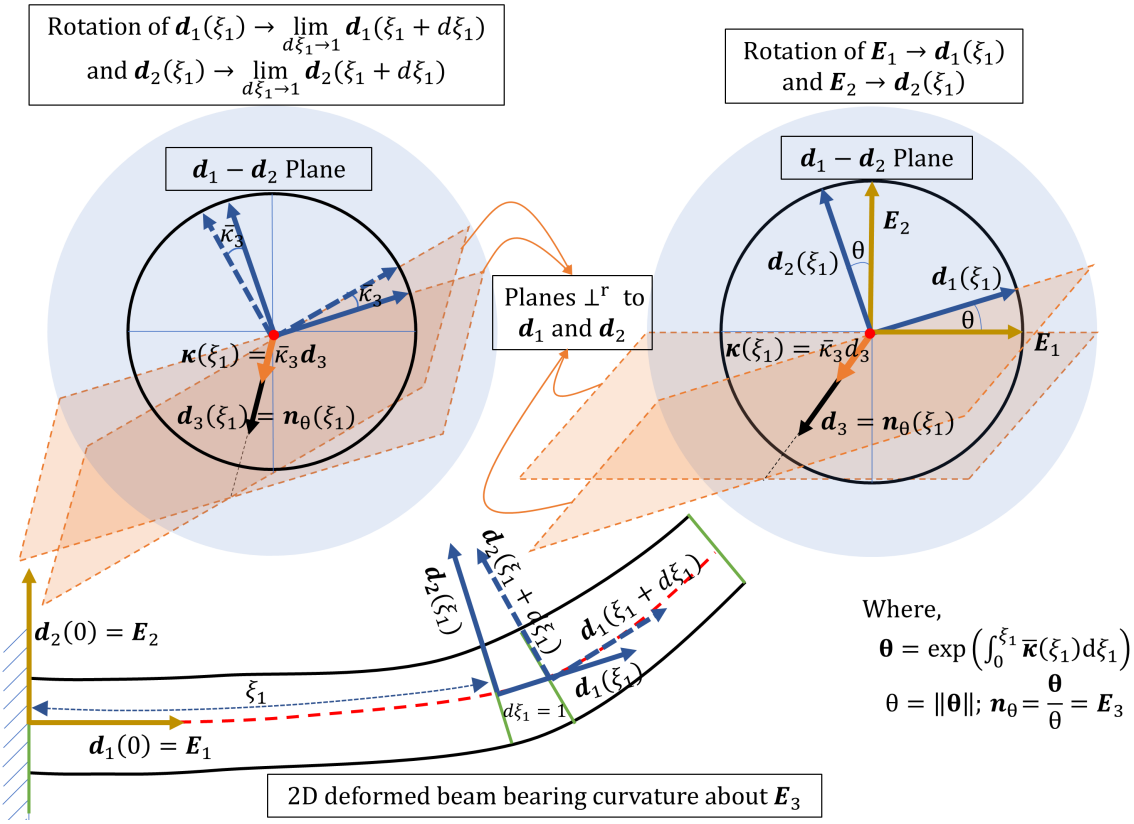

Figure 4.2: Geometric interpretation of curvature for a 2D plane beam.

The geometric description of more general configurations $\Omega_2 - \Omega_3$ comprises of different families of cross-sections obtained by further transformation of the cross-section $\mathfrak{B}_1$. Therefore, before we continue to describe the configurations $\Omega_2 - \Omega_3$, we will first obtain the *fully-coupled Poisson's and warping effect* in the next few sections.

4.2.3 An introductory remark on warping

The simplest non-trivial case of warping is Saint-Venant's uniform torsion problem (refer p. 113 of Sokolnikoff [38]) on a doubly symmetric prismatic bar subjected to a constant curvature $\bar{\kappa}_1(\xi_1) = \bar{\kappa}_1$. If the cross-section is not doubly symmetric, the torsion and bending are uncoupled by using the idea of shear-center. Elter [40] describes two formulations of shear-center, the first obtained using Saint-Venant's principle and the second attributed to Trefftz [39]. In Saint-Venant's

principle, the distributed forces at the end-section (say $\mathfrak{B}(L)$) are replaced by a statically equivalent concentrated force and couple. Trefftz [39] proposed that the work done by the distributed forces at the end-section is equal to the work done by statically equivalent concentrated force and couple, thereby proposing equivalence in energy. Note that both the approaches are meant for uniform torsion.

Let the straight asymmetric beam be subjected to uniform torsion with constant curvature $\overline{\kappa}_1$. Let $\boldsymbol{n} = n_2\boldsymbol{E}_2 + n_3\boldsymbol{E}_3$ be the normal vector to the boundary $\Gamma(\xi_1)$ of the deformed cross-section $\mathfrak{B}(\xi_1)$. Due to linear and small deformation nature of the problem, we express the displacement field in $\{\boldsymbol{E}_i\}$ frame. Let the position vector of the shear center from the centroid be $S_2\boldsymbol{E}_2 + S_3\boldsymbol{E}_3$. The corresponding linear displacement field $\boldsymbol{u}_s$ measured about the shear center can be obtained as:

$$\boldsymbol{u}_s = \overline{\kappa}_1\xi_1\left(\boldsymbol{E}_1 \times ((\xi_2 - S_2)\boldsymbol{E}_2 + (\xi_3 - S_3)\boldsymbol{E}_3)\right) + \overline{\kappa}_1\Psi_s(\xi_2, \xi_3)\boldsymbol{E}_1. \tag{4.9}$$

The warping function may then be obtained by solving the following Neumann boundary value problem,

$$\begin{aligned} \nabla^2\Psi_s = \partial^2_{\xi_2}\Psi_s + \partial^2_{\xi_3}\Psi_s = 0 \quad \text{on } \mathfrak{B}(\xi_1); \\ \partial_{\boldsymbol{n}}\Psi_s = \partial_{\xi_2}\Psi_s n_2 + \partial_{\xi_3}\Psi_s n_3 = -(((\xi_2 - S_2)\boldsymbol{E}_2 + (\xi_3 - S_3)\boldsymbol{E}_3) \times \boldsymbol{n}) \cdot \boldsymbol{E}_1 \quad \text{on } \Gamma(\xi_1). \end{aligned} \tag{4.10}$$

The second last equation in Elter [40] gives formula for the shear center, when the displacement field is expressed at any arbitrary point A other than the centroid. Considering the arbitrary point A to be the shear center S of the beam, we arrive at the following two conditions:

$$\int_{\mathfrak{B}} \xi_2\Psi_s \, \mathrm{d}\xi_2\mathrm{d}\xi_3 = \int_{\mathfrak{B}} \xi_3\Psi_s \, \mathrm{d}\xi_2\mathrm{d}\xi_3 = 0. \tag{4.11}$$

Equations (4.10) and (4.11) can be solved to obtain S_2, S_3 and Ψ_s, unique to a constant. Therefore, an additional normalization condition (that is also required for the axial force to vanish) can be invoked to solve for the constant,

$$\int_{\mathfrak{B}} \Psi_s \, \mathrm{d}\xi_2\mathrm{d}\xi_3 = 0. \tag{4.12}$$

Equations (4.10)-(4.12) gives a unique solution to the warping function Ψ_s for uniform torsion. Simo and Vu-Quoc [43] use the warping function Ψ_s weighted by the warping amplitude $p(\xi_1)$ to consider non-uniform torsion in finite deformation problem. This adds an additional finite strain parameter $p(\xi_1)$, introducing the idea of *bi-shear* and *bi-moment*.

As indicated in Elter [40], it is interesting to note that the warping function depends on the choice of origin. Consider the displacement field $\boldsymbol{u}$ defined with respect to the centroid, which may be written as $\boldsymbol{u} = \overline{\kappa}_1 \xi_1 \left(\boldsymbol{E}_1 \times (\xi_2 \boldsymbol{E}_2 + \xi_3 \boldsymbol{E}_3)\right) + \overline{\kappa}_1 \Psi(\xi_2, \xi_3) \boldsymbol{E}_1$. The warping function $\Psi(\xi_2, \xi_3)$ is then obtained by solving the following differential equation

$$\begin{aligned} \nabla^2 \Psi &= 0 \ \text{ on } \ \mathfrak{B}(\xi_1); \\ \partial_{\boldsymbol{n}} \Psi &= -t \quad \text{ on } \ \Gamma(\xi_1); \\ t &= ((\xi_2 \boldsymbol{E}_2 + \xi_3 \boldsymbol{E}_3) \times \boldsymbol{n}) \cdot \boldsymbol{E}_1. \end{aligned} \tag{4.13}$$

The location of the shear center can be obtained using a general Eq. (29) or Eq. (2) (for single and multi-connected regions), in Elter [40].

Burgoyne et al. [41] presents a detailed theory of warping for non-uniform torsion considering symmetric cross-section. The assumed displacement field, where $W(\xi_1, \xi_2, \xi_3)$ represents the warping deformation, is written as:

$$\begin{aligned} \boldsymbol{u} &= \theta(\xi_1) \left(\boldsymbol{E}_1 \times (\xi_2 \boldsymbol{E}_2 + \xi_3 \boldsymbol{E}_3)\right) + W(\xi_1, \xi_2, \xi_3) \boldsymbol{E}_1, \\ \theta(\xi_1) &= \theta(0) + \int_0^{\xi_1} \overline{\kappa}_1(\xi_1) \, \mathrm{d}\xi_1. \end{aligned} \tag{4.14}$$

Here, θ represents the total twist angle. The governing differential equations for linear elasticity

with Poisson's ratio $\nu = 0$ then become,

$$\begin{gathered}\nabla^2 W + \frac{E}{G}.\partial_{\xi_1}^2 W = 0 \ \text{ on } \ \mathfrak{B}(\xi_1); \\ \partial_{\boldsymbol{n}} W = -\partial_{\xi_1}\theta t \ \text{ on } \ \Gamma(\xi_1), \ \text{ such that,} \\ \partial_{\xi_1} W = 0 \ \text{ or } \ \partial_{\xi_1}^r \theta = 0 \ \text{ if the end is unrestrained in warping, where } \ r = 0, 2, 4, 6, \ldots \\ W = 0 \ \text{ or } \ \partial_{\xi_1}^r \theta = 0 \ \text{ if the end is restrained in warping, where } \ r = 1, 3, 5, \ldots\end{gathered} \tag{4.15}$$

The parameters E and G are the Young's modulus and shear modulus, respectively. One of the two solution approaches proposed by Burgoyne et al. [41] is to use infinite series sum of the form

$$W(\xi_1, \xi_2, \xi_3) = \sum_{r=0}^{\infty} \partial_{\xi_1}^r \theta(\xi_1).\Psi_r(\xi_2, \xi_3). \tag{4.16}$$

The idea is to solve for the functions Ψ_r, provided the twist angle $\theta(\xi_1)$ is known. This involves solving for Ψ_r that satisfies the following set of equations:

$$\begin{gathered}\Psi_r = 0 \ \text{ if } r \text{ is even or zero;} \\ \nabla^2 \Psi_1 = 0 \ \text{ on } \ \mathfrak{B}(\xi_1) \ \text{ and } \ \partial_{\boldsymbol{n}} \Psi_1 = -t \ \text{ on } \ \Gamma(\xi_1); \\ \nabla^2 \Psi_r + \frac{E}{G}\Psi_{r-2} = 0 \ \text{ on } \ \mathfrak{B}(\xi_1) \ \text{ and } \ \partial_{\boldsymbol{n}} \Psi_1 = 0 \ \text{ on } \ \Gamma(\xi_1) \ \text{ for } \ r \geq 3.\end{gathered} \tag{4.17}$$

Knowing the functions $\Psi_r(\xi_2, \xi_3)$, we can estimate the warping deformation for large deformation beam problem as a finite sum

$$W(\xi_1, \xi_2, \xi_3) = \sum_{r=1}^{n} \partial_{\xi_1}^{(r-1)} p(\xi_1).\Psi_r(\xi_2, \xi_3), \ \ r \text{ is odd.} \tag{4.18}$$

The weighting parameter $p(\xi_1)$, is an additional unknown finite strain parameter known as the warping amplitude.

Particularly notable work on the warping of a thin-walled open section for pure (non-uniform) torsion was presented by Vlasov [44]. Vlasov's theory considers the primary warping (or contour warping) but ignores the secondary warping (or thickness warping) of the cross-section. In Vlasov's theory, the line perpendicular to the contour remains perpendicular to the contour

and undeformed in the deformed state (assuming Kirchhoff's thin plate assumption). Goodier [45] and Gjelsvik [46] incorporated the warping of walls of the beam relative to the contour. The contour is defined as the intersection of the mid surface of the wall with the cross-section (refer to Gjelsvik [46]). Lin et al. [47] serves as an insightful reference to a complete derivation of torsional warping that includes both primary and secondary warping for a thin-walled open section beam subjected to pure torsion.

The idea of shear-center, the center of twist, and their synonymic nature is debatable. The work by Brown et al. [42] ignores the concept of shear-center and develops the coupled linear theory for torsion and flexure. They propose a trigonometric series solution for the governing equations to obtain the warping functions. As mentioned in Brown et al. [42], the wide adaptation of the idea of the shear center by engineers can probably be attributed to its convenience. Their work critically reviews the idea of shear center and center of twist.

We now present our approach to model the coupling between the Poisson's effect and warping deformation. In section 4.2.4 we attempt to extend the warping theory proposed by Burgoyne and Brown [41] and [42] to incorporate the effect of axial strain and Poisson's deformation into the warping. Therefore, section 4.2.4 along with chapter 5 elucidates the first stage of this coupling. In section 4.2.5, we further refine the coupling by defining the fully-coupled Poisson's transformation.

4.2.4 Coupling between axial strain, Poisson's effect and warping

As discussed before, the warping function is obtained for the linear elastic case and suitably modified to capture non-linear cases. Motivated from the work of Brown and Burgoyne [42], we assume a linear small deformation field including non-uniform torsion, bending, axial deformation and Poisson's effect for an asymmetric problem. For a general asymmetric cross-section, bending induces warping, causing a coupling between bending and torsion. The incorporation of axial deformation helps us to investigate the influence of Poisson's effect and axial strain on warping

(but not vice-versa, that is taken care of by the second stage of coupling, as we shall see later). We consider an asymmetric cross-section subjected to bending, axial deformation of mid-curve, torsion, and warping in the sense of small deformation. Consider a displacement field:

$$
\begin{aligned}
u_1 &= W(\xi_1,\xi_2,\xi_3) - \xi_2\left(\int \overline{\kappa}_3(\xi_1)\,\mathrm{d}\xi_1 + C_1\right) + \xi_3\left(\int \overline{\kappa}_2(\xi_1)\,\mathrm{d}\xi_1 + C_2\right) + \left(\int e(\xi_1)d\xi_1 + C_3\right);\\
u_2 &= \left(\int\int \overline{\kappa}_3(\xi_1)\,\mathrm{d}\xi_1\mathrm{d}\xi_1 + C_1\xi_1 + C_4\right) - \xi_3\left(\int \overline{\kappa}_1(\xi_1)\,\mathrm{d}\xi_1 + C_5\right) - \nu e(\xi_1)\xi_2;\\
u_3 &= -\left(\int\int \overline{\kappa}_2(\xi_1)\,\mathrm{d}\xi_1\mathrm{d}\xi_1 + C_2\xi_1 + C_6\right) + \xi_2\left(\int \overline{\kappa}_1(\xi_1)\,\mathrm{d}\xi_1 + C_5\right) - \nu e(\xi_1)\xi_3.
\end{aligned}
\tag{4.19}
$$

Here, $C_1 - C_6$ are the constants that depend on the boundary conditions and the initial undeformed state of the beam. The non-zero components of isotropic elastic stress tensor including the Poisson's effect can be obtained from Eq. (4.19) as,

$$
\begin{aligned}
\sigma_{11} &= \tilde{\lambda}(\partial_{\xi_1}W + \xi_3\overline{\kappa}_2 - \xi_2\overline{\kappa}_3) + (\tilde{\lambda} - 2\lambda\nu)e;\\
\sigma_{12} &= \sigma_{21} = G\left(\partial_{\xi_2}W - \xi_3\overline{\kappa}_1 - \nu\xi_2.\partial_{\xi_1}e\right);\\
\sigma_{13} &= \sigma_{31} = G\left(\partial_{\xi_3}W + \xi_2\overline{\kappa}_1 - \nu\xi_3.\partial_{\xi_1}e\right);\\
\sigma_{22} &= \lambda(\partial_{\xi_1}W + \xi_3\overline{\kappa}_2 - \xi_2\overline{\kappa}_3) - (\nu\tilde{\lambda} + \lambda(\nu-1))e;\\
\sigma_{33} &= \lambda(\partial_{\xi_1}W + \xi_3\overline{\kappa}_2 - \xi_2\overline{\kappa}_3) - (\nu\tilde{\lambda} + \lambda(\nu-1))e.
\end{aligned}
\tag{4.20}
$$

Here, $\lambda = \frac{\nu E}{(1+\nu)(1-2\nu)}$ and $\tilde{\lambda} = 2G + \lambda$. The parameters E, G and ν are Young's modulus, shear modulus and Poisson's ratio respectively. Note that $\lim_{\substack{\nu\to 0\\ e\to 0}} \sigma_{22} = 0$ and $\lim_{\substack{\nu\to 0\\ e\to 0}} \sigma_{33} = 0$. We restrict ourselves to stress-equilibrium in the $\boldsymbol{E}_1$ direction, as we are interested in solving for the warping function. Therefore, the governing differential equations are

$$
\partial_{\xi_j}\sigma_{1j} = 0 \Rightarrow \nabla^2 W + \frac{\tilde{\lambda}}{G}\left(\partial^2_{\xi_1}W - \xi_2.\partial_{\xi_1}\overline{\kappa}_3 + \xi_3.\partial_{\xi_1}\overline{\kappa}_2\right) + \overline{\lambda}.\partial_{\xi_1}e = 0 \ \text{ on } \ \mathfrak{B}(\xi_1); \tag{4.21a}
$$

$$
\partial_{\boldsymbol{n}}W = \overline{\kappa}_1\overbrace{\left((\boldsymbol{n}\times(\xi_2\boldsymbol{E}_2 + \xi_3\boldsymbol{E}_3))\cdot\boldsymbol{E}_1\right)}^{-t} + \nu.\partial_{\xi_1}e\overbrace{\left(\boldsymbol{n}\cdot(\xi_2\boldsymbol{E}_2 + \xi_3\boldsymbol{E}_3)\right)}^{\tilde{t}} \ \text{ on } \ \Gamma(\xi_1). \tag{4.21b}
$$

Here, $\overline{\lambda} = \frac{\tilde{\lambda}+2\nu(G-\tilde{\lambda})}{G}$. As Eq. (1) in Brown et. al. [42], we define the stress resultants for axial force, bending moment and torsion at the centroid as follows:

$$
\begin{aligned}
P_1(\xi_1) &= \int_{\mathfrak{B}(\xi_1)} \sigma_{11}\, \mathrm{d}\xi_2\mathrm{d}\xi_3 = (\tilde{\lambda} - 2\lambda\nu)Ae + \tilde{\lambda}\int_{\mathfrak{B}(\xi_1)} \partial_{\xi_1} W\, \mathrm{d}\xi_2\mathrm{d}\xi_3 \\
T(\xi_1) &= \int_{\mathfrak{B}(\xi_1)} (\xi_2\sigma_{13} - \xi_3\sigma_{12})\, \mathrm{d}\xi_2\mathrm{d}\xi_3 = GI_{11}\overline{\kappa}_1 + G\int_{\mathfrak{B}(\xi_1)} \left(\xi_2.\partial_{\xi_3} W - \xi_3.\partial_{\xi_2} W\right)\, \mathrm{d}\xi_2\mathrm{d}\xi_3; \\
M_2(\xi_1) &= \int_{\mathfrak{B}(\xi_1)} \xi_3\sigma_{11}\, \mathrm{d}\xi_2\mathrm{d}\xi_3 = \tilde{\lambda}\left(\int_{\mathfrak{B}(\xi_1)} \xi_3.\partial_{\xi_1} W\, \mathrm{d}\xi_2\mathrm{d}\xi_3 + I_{22}\overline{\kappa}_2 - I_{23}\overline{\kappa}_3\right); \\
M_3(\xi_1) &= \int_{\mathfrak{B}(\xi_1)} \xi_2\sigma_{11}\, \mathrm{d}\xi_2\mathrm{d}\xi_3 = \tilde{\lambda}\left(-\int_{\mathfrak{B}(\xi_1)} \xi_2.\partial_{\xi_1} W\, \mathrm{d}\xi_2\mathrm{d}\xi_3 + I_{33}\overline{\kappa}_3 - I_{23}\overline{\kappa}_2\right),
\end{aligned}
\tag{4.22}
$$

where $A(\xi_1) = \int_{\mathfrak{B}} \mathrm{d}\xi_2\mathrm{d}\xi_3$, $I_{ij} = \int_{\mathfrak{B}} \xi_i\xi_j\mathrm{d}\xi_2\mathrm{d}\xi_3$ for $i = 2, 3$ and $I_{11} = I_{22} + I_{33}$.

The warping differential equation (4.21a) across the cross-section $\mathfrak{B}(\xi_1)$ is inconsistent with the peripheral boundary condition (4.21b). To avoid a sharp deviation in the primary focus pf this chapter ("comprehensive kinematics of Cosserat beams"), we dedicate chapter 5 to discuss these inconsistency, solution procedure, and challenges associated with solving for the function $W(\xi_1, \xi_2, \xi_3)$.

To complete the description of the configurations Ω_2 and Ω_3, we assume that the warping function $W(\xi_1, \xi_2, \xi_3)$ can be expressed in a variable separable form (for instance, of form $p(\xi_1)\Psi(\xi_2, \xi_3)$) and the cross-sectional dependence of warping function (the function $\Psi(\xi_2, \xi_3)$) is known. Prior knowledge of $\Psi(\xi_2, \xi_3)$ guarantees the single manifold nature of the kinematics. In section 5.3.2.2 of chapter 5, we propose a simplified form of the warping function $W(\xi_1, \xi_2, \xi_3)$ that can be used to capture bending-induced shear warping and torsion warping in the beams subjected to large deformations. To understand the second stage of coupling, we need to define the deformed cross-sections Ω_2 and Ω_3.

4.2.5 Description of the configuration Ω_2 and Ω_3

We describe the deformed configuration Ω_2 of the beam allowing cross-sections to undergo out of plane warping only (no in-plane deformation). It is defined by the mid-curve $\boldsymbol{\varphi}(\xi_1)$ and non-planar family of warped cross-section $\mathfrak{B}_2(\xi_1) \subset \mathbb{R}^3_{\xi_1}$, where $\mathbb{R}^3_{\xi_1}$ is the 3D Euclidean space spanned by the director triad $\{\boldsymbol{d}_i(\xi_1)\}$ originating at $\boldsymbol{\varphi}(\xi_1)$. The deformation map $\boldsymbol{\phi}_2 : \boldsymbol{R}_0 \in \Omega_0 \longmapsto \boldsymbol{R}_2 \in \Omega_2$ is then defined as,

$$\boldsymbol{\phi}_2(\boldsymbol{R}_0) = \boldsymbol{R}_2 = \boldsymbol{\varphi}(\xi_1) + \xi_2\boldsymbol{d}_2(\xi_1) + \xi_3\boldsymbol{d}_3(\xi_1) + W(\xi_1,\xi_2,\xi_3)\boldsymbol{d}_1(\xi_1). \tag{4.23}$$

This brings us to the description of final deformed state $\Omega_3 \equiv \Omega$ defined by the mid-curve $\boldsymbol{\varphi}$ and a family of cross-section $\mathfrak{B}(\xi_1) = \left\{\left(W(\xi_1,\xi_2,\xi_3),\hat{\xi}_2,\hat{\xi}_3\right) \in \mathbb{R}^3_{\xi_1}\right\}$. It incorporates a fully coupled Poisson's and warping effect. The deformation map for Ω is given by $\boldsymbol{\phi}_3 : \boldsymbol{R}_0 \in \Omega_0 \longmapsto \boldsymbol{R_3} \in \Omega$ such that,

$$\begin{aligned} \boldsymbol{\phi}_3(\boldsymbol{R}_0) = \boldsymbol{R}_3 &= \boldsymbol{\varphi}(\xi_1) + \boldsymbol{r}; \\ \boldsymbol{r} &= \hat{\xi}_2\boldsymbol{d}_2(\xi_1) + \hat{\xi}_3\boldsymbol{d}_3(\xi_1) + W\boldsymbol{d}_1(\xi_1). \end{aligned} \tag{4.24}$$

Here, the vector $\boldsymbol{r}$ gives the position vector of a material point (ξ_2,ξ_3) in the deformed cross-section $\mathfrak{B}_3(\xi_1)$ with respect to the point $\boldsymbol{\varphi}(\xi_1)$. Let $\Gamma_3(\xi_1)$ represent the boundary of cross-section $\mathfrak{B}_3(\xi_1)$, such that $\mathfrak{S}_3 = \mathfrak{B}_3(0) \cup \mathfrak{B}_3(L) \cup_{\forall\xi_1} \Gamma_3(\xi_1)$. We define the planar cross-section $\mathfrak{B}_4 = \left\{(\hat{\xi}_2,\hat{\xi}_3) \in \mathbb{R}^2_{\xi_1}\right\}$ subjected to only in-plane Poisson's deformation. The coordinates $(\hat{\xi}_2,\hat{\xi}_3)$ are obtained by Poisson's transformation $P_{\xi_1} : \mathfrak{B}_1(\xi_1) \longrightarrow \mathfrak{B}_4(\xi_1)$, such that,

$$\begin{aligned} P_{\xi_1} &: (\xi_2,\xi_3) \longmapsto (\hat{\xi}_2,\hat{\xi}_3); \\ \hat{\xi}_i &= (1 - \nu(\boldsymbol{\lambda}_1^2 \cdot \boldsymbol{d}_1))\xi_i \text{ for } i = 2,3. \end{aligned} \tag{4.25}$$

In the equation above, ν represents Poisson's ratio and is assumed to be a constant (homogeneous material). The quantity $\boldsymbol{\lambda}_1^2$ is the first strain vector of the deformed configuration Ω_2 defined in equation (4.42). Therefore, $\boldsymbol{\lambda}_1^2 \cdot \boldsymbol{d}_1$ essentially gives the longitudinal strain along $\boldsymbol{d}_1$ at the material point (ξ_1,ξ_2,ξ_3) in the deformed state Ω_2.

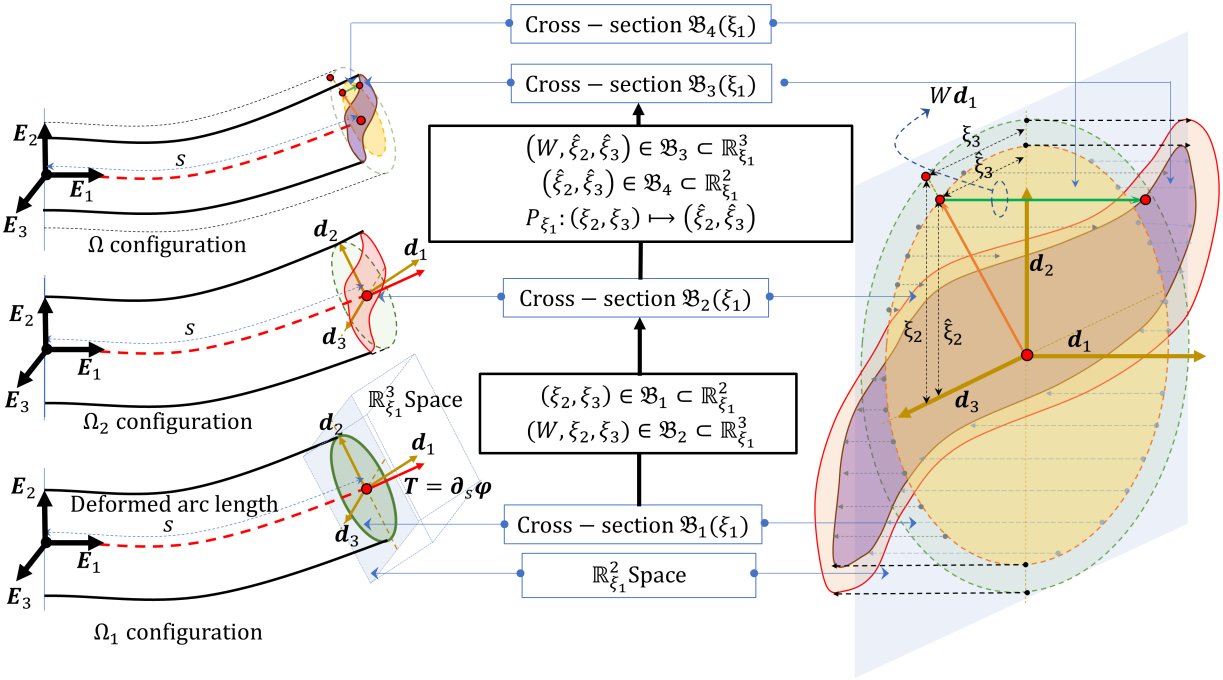

Figure 4.3: Schematic diagram illustrating the geometric description of various deformed configurations.

In general, the mid-curve need not necessarily be the locus of the geometric centroid of the beam. It can also be the locus of the center of mass or the shear-center. In this chapter, we assume locus of geometric centroid constituting the mid-curve. For homogeneous material with constant mass density, the geometric and mass centroid coincides, vanishing the first geometric and mass moment. This simplifies the computations. Figure 4.3 illustrates various configurations described so far.

4.3 Kinematics

4.3.1 Deformation gradient tensor and strain vectors

For a point $p \in \Omega_0$, and $\boldsymbol{\phi}_j(p) \in \Omega_j$, consider an infinitesimal tangent vectors $\mathrm{d}\boldsymbol{R}_0 = \mathrm{d}\xi_i.\boldsymbol{E}_i \in T_p\Omega_0$ and $\mathrm{d}\boldsymbol{R}_j \in T_{\boldsymbol{\phi}_j(p)}\Omega_j$. Since the configurations Ω_0 and Ω_j are subset of $\mathbb{R}^3$, their associated tangent space $T_p\Omega_0$ and $T_{\boldsymbol{\phi}(p)}\Omega_j$ are identical to $\mathbb{R}^3$. The two point deformation gradient

tensor $\boldsymbol{F}_j$ are given by the differential map $\mathrm{d}\boldsymbol{\phi}_j : \mathrm{d}\boldsymbol{R}_0 \longmapsto \mathrm{d}\boldsymbol{R}_j$, such that,

$$\mathrm{d}\boldsymbol{\phi}_j(\mathrm{d}\boldsymbol{R}_0) = \boldsymbol{F}_j.\mathrm{d}\boldsymbol{R}_0 = \mathrm{d}\boldsymbol{R}_j. \tag{4.26}$$

Using the result above,

$$\begin{aligned} &\mathrm{d}\boldsymbol{R}_j = \boldsymbol{F}_j.(\mathrm{d}\xi_i.\boldsymbol{E}_i) \implies \frac{\mathrm{d}\boldsymbol{R}_j}{\mathrm{d}\xi_i} = \boldsymbol{F}_j.\boldsymbol{E}_i; \\ &\boldsymbol{F}_j = \partial_{\xi_i}\boldsymbol{R}_j \otimes \boldsymbol{E}_i. \end{aligned} \tag{4.27}$$

The deformation gradient tensor consists of two parts: change in infinitesimal tangent vector by virtue of rotation (change in direction) and straining (change in magnitude). For $j = 1$, the first component of infinitesimal vector $\mathrm{d}\boldsymbol{R}_0$ strains, whereas the other two components just experience rotation because of Euler-Bernoulli's rigid cross-section assumption in the configuration Ω_1 (refer section 3.1.1 of Chadha and Todd [53]). For $j \neq 1$, the second and the third component of the infinitesimal vector $\mathrm{d}\boldsymbol{R}_0$ strains as well, owing to the coupled Poisson's and warping effect. Thus, we define,

$$\partial_{\xi_i}\boldsymbol{R}_j = \boldsymbol{\lambda}_i^j + \boldsymbol{d}_i. \tag{4.28}$$

Here, $\boldsymbol{\lambda}_i^j$ represents i^{th} strain vector in the Ω_j configuration. The deformation tensor in Eq. (4.27) referenced to the straight beam Ω_0 can be re-written as,

$$\boldsymbol{F}_j = \boldsymbol{\lambda}_i^j \otimes \boldsymbol{E}_i + \boldsymbol{d}_i \otimes \boldsymbol{E}_i = \boldsymbol{H}_j + \boldsymbol{Q}. \tag{4.29}$$

The material form of strain vectors $\boldsymbol{\lambda}_i$ and the deformation gradient tensor $\boldsymbol{F}$ are given by the following,

$$\overline{\boldsymbol{\lambda}}_i^j = \boldsymbol{Q}^T.\boldsymbol{\lambda}_i^j = \boldsymbol{Q}^T.\partial_{\xi_1}\boldsymbol{R}_j - \boldsymbol{E}_i; \tag{4.30a}$$

$$\overline{\boldsymbol{F}}_j = \overline{\boldsymbol{\lambda}}_i^j \otimes \boldsymbol{E}_i + \boldsymbol{I}_3 = \overline{\boldsymbol{H}}_j + \boldsymbol{I}_3 = \boldsymbol{Q}.\boldsymbol{F}_j.\boldsymbol{I}_3 = \boldsymbol{Q}.\boldsymbol{F}_j. \tag{4.30b}$$

Note that $\boldsymbol{H}_j = \boldsymbol{\lambda}_i^j \otimes \boldsymbol{E}_i$ and $\overline{\boldsymbol{H}} = \overline{\boldsymbol{\lambda}}_i^j \otimes \boldsymbol{E}_i$ in Eq. (4.29) and (4.30b) gives spatial and material form of *strain tensor* respectively. The deformation gradient tensor $\boldsymbol{F}_j$ can also be written as

$$\begin{aligned} \boldsymbol{F}_j &= \boldsymbol{V}_j.\boldsymbol{Q} = \boldsymbol{Q}.\boldsymbol{U}_j; \\ \boldsymbol{V}_j &= \boldsymbol{\lambda}_i^j \otimes \boldsymbol{d}_i + \boldsymbol{I}_3 = \boldsymbol{H}_j.\boldsymbol{Q}^T + \boldsymbol{I_3}; \\ \boldsymbol{U}_j &= \overline{\boldsymbol{\lambda}}_i^j \otimes \boldsymbol{E}_i + \boldsymbol{I}_3 = \overline{\boldsymbol{H}}_j. \end{aligned} \tag{4.31}$$

The vector $\boldsymbol{V}_j$ and $\boldsymbol{U}_j$ represent the *left stretch tensor* and *right stretch tensor*, respectively, for the deformed state Ω_j referenced to the configuration Ω_0. In component form, the deformation gradient tensor and the stretch tensors can be written as,

$$\begin{aligned} \left[\boldsymbol{F}_j\right]_{\boldsymbol{d}_p\otimes\boldsymbol{E}_q} = \left[\overline{\boldsymbol{F}}_j\right]_{\boldsymbol{E}_p\otimes\boldsymbol{E}_q} = \left[\boldsymbol{U}_j\right]_{\boldsymbol{E}_p\otimes\boldsymbol{E}_q} = \left[\boldsymbol{V}_j\right]_{\boldsymbol{d}_p\otimes\boldsymbol{E}_q} = \left[\nabla_{\Omega_0}\boldsymbol{u}_j\right]_{\boldsymbol{d}_p\otimes\boldsymbol{E}_q} + \boldsymbol{I_3}; \\ \left[F_{j_{pq}}\right]_{\boldsymbol{d}_p\otimes\boldsymbol{E}_q} = \boldsymbol{\lambda}_q^j \cdot \boldsymbol{d}_p + \delta_{pq}; \\ \left[\nabla_{\Omega_0}\boldsymbol{u}_j\right]_{\boldsymbol{d}_p\otimes\boldsymbol{E}_q} = \begin{bmatrix} \boldsymbol{\lambda}_1^j \cdot \boldsymbol{d}_1 & \boldsymbol{\lambda}_2^j \cdot \boldsymbol{d}_1 & \boldsymbol{\lambda}_3^j \cdot \boldsymbol{d}_1 \\ \boldsymbol{\lambda}_1^j \cdot \boldsymbol{d}_2 & \boldsymbol{\lambda}_2^j \cdot \boldsymbol{d}_2 & \boldsymbol{\lambda}_3^j \cdot \boldsymbol{d}_2 \\ \boldsymbol{\lambda}_1^j \cdot \boldsymbol{d}_3 & \boldsymbol{\lambda}_2^j \cdot \boldsymbol{d}_3 & \boldsymbol{\lambda}_3^j \cdot \boldsymbol{d}_3 \end{bmatrix}. \end{aligned} \tag{4.32}$$

The notation $[\boldsymbol{F}_j]_{\boldsymbol{d}_p\otimes\boldsymbol{E}_q}$ implies that in the operation $\boldsymbol{F}_j.\mathrm{d}\boldsymbol{R}_0 = \mathrm{d}\boldsymbol{R}_j$, the component of the vector $\mathrm{d}\boldsymbol{R}_0$ is expressed in $\{\boldsymbol{E}_i\}$ frame and the components of the vector $\mathrm{d}\boldsymbol{R}_j$ obtained after the operation is in $\{\boldsymbol{d}_i\}$ frame. The *displacement gradient tensor* for the configuration Ω_j referenced to Ω_0 is given by $\nabla_{\Omega_0}\boldsymbol{u}_j$, where $\boldsymbol{u}_j = \boldsymbol{R}_j - \boldsymbol{R}_0$.

We are now in the position to elaborate on the fully-coupled Poisson's effect. For the deformed configuration Ω_2, the strain vectors may be obtained using Eq. (4.23) and Eq. (4.28)

$$\boldsymbol{\lambda}_1^2 \cdot \boldsymbol{d}_1 = \left(\overline{\varepsilon}_1 + \xi_3\overline{\kappa}_2 - \xi_2\overline{\kappa}_3 + \partial_{\xi_1}W\right). \tag{4.33}$$

Intuitively, $\boldsymbol{\lambda}_1^2 \cdot \boldsymbol{d}_1$ is the axial strain field across the cross-section due to mid-curve axial strain, bending and warping. Therefore, we can write the Poisson's transformed coordinates defined in

Eq.(4.25) as,

$$\hat{\xi}_i = \left(1 - \nu\left(\overline{\varepsilon}_1 + \xi_3\overline{\kappa}_2 - \xi_2\overline{\kappa}_3 + \partial_{\xi_1}W\right)\right)\xi_i \quad \text{for } i\text{=2,3.} \tag{4.34}$$

The strain vectors for the final deformed state Ω_3 can be obtained by substituting Eq. (4.24) in Eq. (4.28), yielding

$$\begin{aligned}
\boldsymbol{\lambda}_1^3 &= \left(\boldsymbol{\varepsilon} + \hat{\xi}_3.\partial_{\xi_1}\boldsymbol{d}_3 + \hat{\xi}_2.\partial_{\xi_1}\boldsymbol{d}_2 + \partial_{\xi_1}\hat{\xi}_3.\boldsymbol{d}_3 + \partial_{\xi_1}\hat{\xi}_2.\boldsymbol{d}_2 + \partial_{\xi_1}W.\boldsymbol{d}_1 + W.\partial_{\xi_1}\boldsymbol{d}_1\right) \\
&= \left(\overbrace{((1+e)\cos\gamma_{11} - 1)}^{\overline{\varepsilon}_1=\boldsymbol{\varepsilon}.\boldsymbol{d}_1} + \hat{\xi}_3\overline{\kappa}_2 - \hat{\xi}_2\overline{\kappa}_3 + \partial_{\xi_1}W\right)\boldsymbol{d}_1 + \left(\overbrace{(1+e)\sin\gamma_{12}}^{\overline{\varepsilon}_2=\boldsymbol{\varepsilon}.\boldsymbol{d}_2} - \hat{\xi}_3\overline{\kappa}_1 + \partial_{\xi_1}\hat{\xi}_2 + W\overline{\kappa}_3\right)\boldsymbol{d}_2 \\
&\quad + \left(\overbrace{(1+e)\sin\gamma_{13}}^{\overline{\varepsilon}_3=\boldsymbol{\varepsilon}.\boldsymbol{d}_3} + \hat{\xi}_2\overline{\kappa}_1 + \partial_{\xi_1}\hat{\xi}_3 - W\overline{\kappa}_2\right)\boldsymbol{d}_3;
\end{aligned} \tag{4.35a}$$

$$\boldsymbol{\lambda}_2^3 = \partial_{\xi_2}W.\boldsymbol{d}_1 + \left(\partial_{\xi_2}\hat{\xi}_2 - 1\right)\boldsymbol{d}_2 + \partial_{\xi_2}\hat{\xi}_3.\boldsymbol{d}_3; \tag{4.35b}$$

$$\boldsymbol{\lambda}_3^3 = \partial_{\xi_3}W.\boldsymbol{d}_1 + \partial_{\xi_3}\hat{\xi}_2.\boldsymbol{d}_2 + \left(\partial_{\xi_3}\hat{\xi}_3 - 1\right)\boldsymbol{d}_3. \tag{4.35c}$$

Remark 4.1: It is interesting to note that the language that reads-"*The action of a tensor...onto the vector...*"- is acceptable in the field of engineering. However, it would not make much sense in differential geometry. This is because a tensor in differential geometry is defined as multi-linear function that take other tensors, vectors, one-forms etc. as its argument. However, as a matter of convenience, we have accepted this abuse of notations. For instance, in the language of differential geometry, a two-point deformation gradient tensor is defined as $\boldsymbol{F} : T^*_{\boldsymbol{\phi}(p)}\Omega \times T_p\Omega_0 \longrightarrow \mathbb{R}$. Here, $T^*_{\boldsymbol{\phi}(p)}\Omega$ is a cotangent space of the deformed configuration Ω, that is dual to the tangent space $T_{\boldsymbol{\phi}(p)}\Omega$. If the tangent space $T_{\boldsymbol{\phi}(p)}\Omega$ is spanned by the vector triad $\{\boldsymbol{E}_i\}$ (this is because $\Omega \subset \mathbb{R}^3$), then the cotangent space $T_{\boldsymbol{\phi}(p)}\Omega$ is spanned by the corresponding one-form $\{\boldsymbol{E}^*_i\}$ such that, $\boldsymbol{E}^*_j(\boldsymbol{E}_i) = \boldsymbol{E}_j \cdot \boldsymbol{E}_i = \delta_{ji}$. As such, the expression of deformation gradient tensor would then be

$\boldsymbol{F} = (\boldsymbol{\lambda}_i + \boldsymbol{d}_i) \otimes \boldsymbol{E}_i^*$, such that $F_{ij} = \boldsymbol{F}(\boldsymbol{\lambda}_j + \boldsymbol{d}_j, \boldsymbol{E}_i^*) = \boldsymbol{E}_i^*(\boldsymbol{\lambda}_j + \boldsymbol{d}_j) = (\boldsymbol{\lambda}_j + \boldsymbol{d}_j) \cdot \boldsymbol{E}_i$. We carefully note that in this chapter, we have conveniently gotten away with the idea of one-form by using dot product. This was possible because the Reimannian metric associated with $\mathbb{R}^3$ is identity matrix (refer section 3.5 of Schutz [54] to see how a metric acts as a mapping of vectors into one-form and vice-versa).

4.3.2 Physical interpretation of the strain vector $\boldsymbol{\lambda}_i^j$

Consider an infinitesimal vector $\mathrm{d}\xi_1 \boldsymbol{E}_1$ in the undeformed state Ω_0 joining two material points $(\xi_2, \xi_3) \in \mathfrak{B}_0(\xi_1)$ and $(\xi_2, \xi_3) \in \mathfrak{B}_0(\xi_1 + \mathrm{d}\xi_1)$. Similarly, consider an infinitesimal vector $\mathrm{d}\xi_2 \boldsymbol{E}_2$ connecting two material points $(\xi_2, \xi_3) \in \mathfrak{B}_0(\xi_1)$ and $(\xi_2 + \mathrm{d}\xi_2, \xi_3) \in \mathfrak{B}_0(\xi_1)$. Finally, consider an infinitesimal vector $\mathrm{d}\xi_3 \boldsymbol{E}_3$ connecting two material points $(\xi_2, \xi_3) \in \mathfrak{B}_0(\xi_1)$ and $(\xi_2, \xi_3 + \mathrm{d}\xi_3) \in \mathfrak{B}_0(\xi_1)$. These three vectors transform to the following in the deformed state Ω_j

$$\boldsymbol{F}_j.(\mathrm{d}\xi_i \boldsymbol{E}_i) = \mathrm{d}\xi_i(\boldsymbol{\lambda}_i^j + \boldsymbol{d}_i) \;\text{ for }\; i = 1-3 \;\text{ and }\; j = 1-3. \tag{4.36}$$

The Einstein summation is suppressed in the above equation. The index i represent the infinitesimal vectors. Therefore, for a unit arc length element

$$\boldsymbol{\lambda}_1^j = \boldsymbol{F}_j.\boldsymbol{E}_1 - \boldsymbol{d}_1. \tag{4.37}$$

For the unit vectors $\boldsymbol{E}_2$ and $\boldsymbol{E}_3$, (along the direction of $\mathrm{d}\xi_2 \boldsymbol{E}_2$ and $\mathrm{d}\xi_3 \boldsymbol{E}_3$, respectively), we see that

$$\boldsymbol{\lambda}_2^j = \boldsymbol{F}_j.\boldsymbol{E}_2 - \boldsymbol{d}_2; \;\; \boldsymbol{\lambda}_3^j = \boldsymbol{F}_j.\boldsymbol{E}_3 - \boldsymbol{d}_3. \tag{4.38}$$

Therefore, $\boldsymbol{\lambda}_i^j$ represents the strain vector in the deformed state Ω_j corresponding to the vector $\boldsymbol{E}_i$ in the undeformed state Ω_0. The action of deformation gradient tensor on an infinitesimal vector $\mathrm{d}\boldsymbol{R}_0$ can be understood from Eq. (4.29). The vector $\mathrm{d}\boldsymbol{R}_0$ is subjected to rigid body rotation (the contribution due to $\boldsymbol{Q}$ in Eq. (4.29)) and change in magnitude (the contribution due to $\boldsymbol{\lambda}_i^j \otimes \boldsymbol{E}_i$, sum implied over i). The outer product $\boldsymbol{\lambda}_i^j \otimes \boldsymbol{E}_i$ filters out the i^{th} component of the vector $\mathrm{d}\boldsymbol{R}_0$

(for each i) and strains it along the vector $\boldsymbol{\lambda}_i^j$.

4.3.3 Deformation of infinitesimal vector along the reference unit vectors $\boldsymbol{E}_i$

It is insightful to observe the deformation of vectors $\boldsymbol{E}_i$ (not necessarily at the centroid) with $i = 1 - 3$ in the deformed state Ω_3. Consider the infinitesimal vectors $\mathrm{d}\xi_1\boldsymbol{E}_1$, $\mathrm{d}\xi_2\boldsymbol{E}_2$ and $\mathrm{d}\xi_3\boldsymbol{E}_3$ as described in section 4.3.2. As explained before, the deformation gradient tensor $\boldsymbol{F}_3$ maps an infinitesimal vector $\mathrm{d}\boldsymbol{R}_0$ to $\mathrm{d}\boldsymbol{R}_3$. One might wonder as to what the deformation of a unit length vectors $\boldsymbol{E}_i$, which is not infinitesimally small, means. The idea is that if the deformation gradient tensor deforms the vector, say $\mathrm{d}\boldsymbol{R}_0 = \mathrm{d}\xi_i\boldsymbol{E}_i \in T_p\Omega_0$ (no sum on i) to some vector $\mathrm{d}\boldsymbol{R}_3 \in T_{\boldsymbol{\phi}_3(p)}\Omega_3$, then the vector $\boldsymbol{E}_i \in T_p\Omega_0$ deforms to $\frac{\mathrm{d}\boldsymbol{R}_3}{\mathrm{d}\xi_i} \in T_{\boldsymbol{\phi}_3(p)}\Omega_3$. Mathematically, for a point $p \in \Omega_0$ the fact $\boldsymbol{F}_j.(\mathrm{d}\xi_1\boldsymbol{E}_1) \in T_{\boldsymbol{\phi}_j(p)}\Omega_j$ implies $\boldsymbol{F}_j.\boldsymbol{E}_1 \in T_{\boldsymbol{\phi}_j(p)}\Omega_j$ and $\boldsymbol{F}_j.(\mathrm{d}\xi_1\boldsymbol{E}_1) \parallel \boldsymbol{F}_j\boldsymbol{E}_1$. One must understand that this deformation is different from the real deformed state of a finite length vector (which may be some curve!).

This idea of deformation of the unit vector or a unit arc length element is useful to understand the strain vectors and to interpret the contributions to the strain due to various finite strain parameters. Section [4.1] of Schutz [54] is an excellent read on the idea of *element* in continuum mechanics.

4.3.3.1 Deformation of the unit vector $\boldsymbol{E}_1$

It is clear from Eq. (4.35) and (4.37) that

$$\begin{aligned}\boldsymbol{F}_3.\boldsymbol{E}_1 &= \boldsymbol{\lambda}_1^3 + \boldsymbol{d}_1 \\ &= \left((1+e)\cos\gamma_{11} + \hat{\xi}_3\overline{\kappa}_2 - \hat{\xi}_2\overline{\kappa}_3 + \partial_{\xi_1}W\right)\boldsymbol{d}_1 + \left((1+e)\sin\gamma_{12} - \hat{\xi}_3\overline{\kappa}_1 + \partial_{\xi_1}\hat{\xi}_2 + W\overline{\kappa}_3\right)\boldsymbol{d}_2 \\ &+ \left((1+e)\sin\gamma_{13} + \hat{\xi}_2\overline{\kappa}_1 + \partial_{\xi_1}\hat{\xi}_3 - W\overline{\kappa}_2\right)\boldsymbol{d}_3.\end{aligned} \tag{4.39}$$

The Fig. 4.4 demonstrates straining of the vector $\boldsymbol{E}_1$ (not necessarily along the midcurve). Each subsequent step in the flowchart does not represent superimposition; rather, each step represents the inclusion of various deformation effects, as indicated.

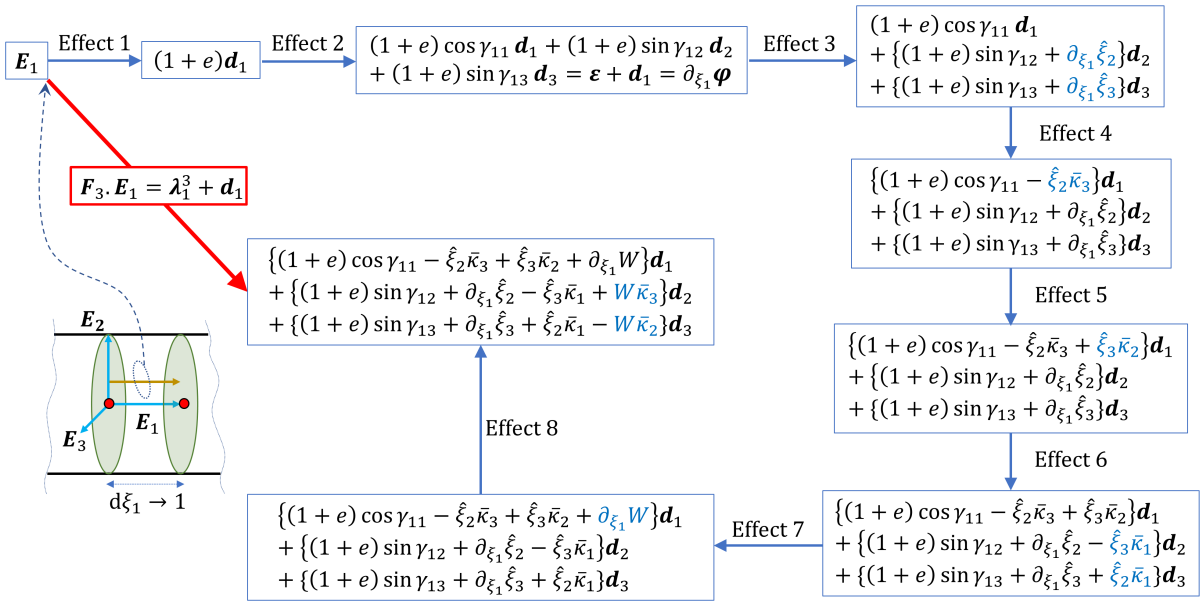

Figure 4.4: Flowchart showing the deformation of the unit vector $\boldsymbol{E}_1$ in the configuration Ω_3 referenced to the configuration Ω_0.

Certain points interpreting various deformation effects described in Fig. 4.4 are discussed below,

1. Fig. 4.4 is an improved version of Fig. 3 in Chadha and Todd [55] that considers the final deformed state to be Ω_1 (constraint by rigid cross-section assumption). The transformation of the vector $\boldsymbol{E}_1$ as showed in Fig. 4.4 considers the final deformed state as Ω_3 that incorporates fully-coupled Poisson's and warping effect.

2. Effects 1 and 2 represent the strain due to finite shear and midcurve axial deformation. Effect 1 is special case of effect 2, when there is no shear. The vector $\boldsymbol{E}_1$ transforms to the vector $\boldsymbol{\varepsilon} + \boldsymbol{d}_1$ if we consider effect 1 and 2 only. Figure 4.5 illustrates the effects 1 and 2.

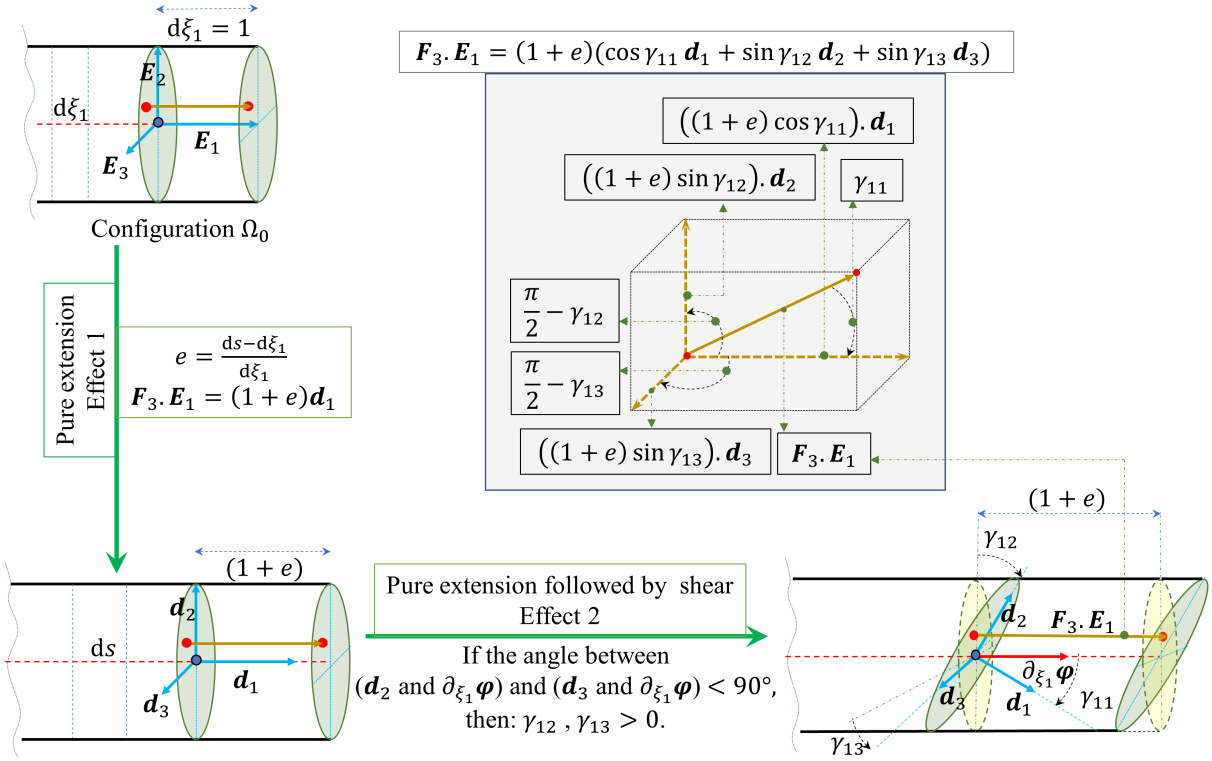

Figure 4.5: Geometric description of effects 1 and 2: deformation of the vector $\boldsymbol{E}_1$ considering elongation followed by shear.

3. Effect 3 addresses the strain in the vector $\boldsymbol{E}_1$ for a unit arc length element ($d\xi_1 = 1$) due to differential Poisson's deformation. Fig. 4.7 gives a geometric description of effect 1 and 3.

4. Effects 4, 5 and 6 represent the strain due to bending and torsion about the vectors $\boldsymbol{d}_3$, $\boldsymbol{d}_2$ and $\boldsymbol{d}_1$ respectively (refer Fig. 4.6). Unlike the description in Chadha and Todd [53] that utilizes the point (ξ_2, ξ_3) to define bending and torsion strains, we use $(\hat{\xi}_2, \hat{\xi}_3)$ to capture bending and torsion strains (notice the terms like $\hat{\xi}_2\overline{\kappa}_1, \hat{\xi}_2\overline{\kappa}_2, \hat{\xi}_2\overline{\kappa}_3$ etc.). This is direct consequence of the fully-coupled Poisson's effect.

5. Effect 7 represents axial strain in $\boldsymbol{E}_1$ due to differential warping deformation causing an additional axial strain of $\partial_{\xi_1} W$ along $\boldsymbol{d}_1$.

6. Effect 8 describes the strain $W.\partial_{\xi_1}\boldsymbol{d}_1 = W(\overline{\kappa}_3\boldsymbol{d}_2 - \overline{\kappa}_2\boldsymbol{d}_3)$. Note that effect 7 and 8 are obtained by realizing the strain contribution due to the quantity $\partial_{\xi_1}(W\boldsymbol{d}_1)$. In effect 7, the

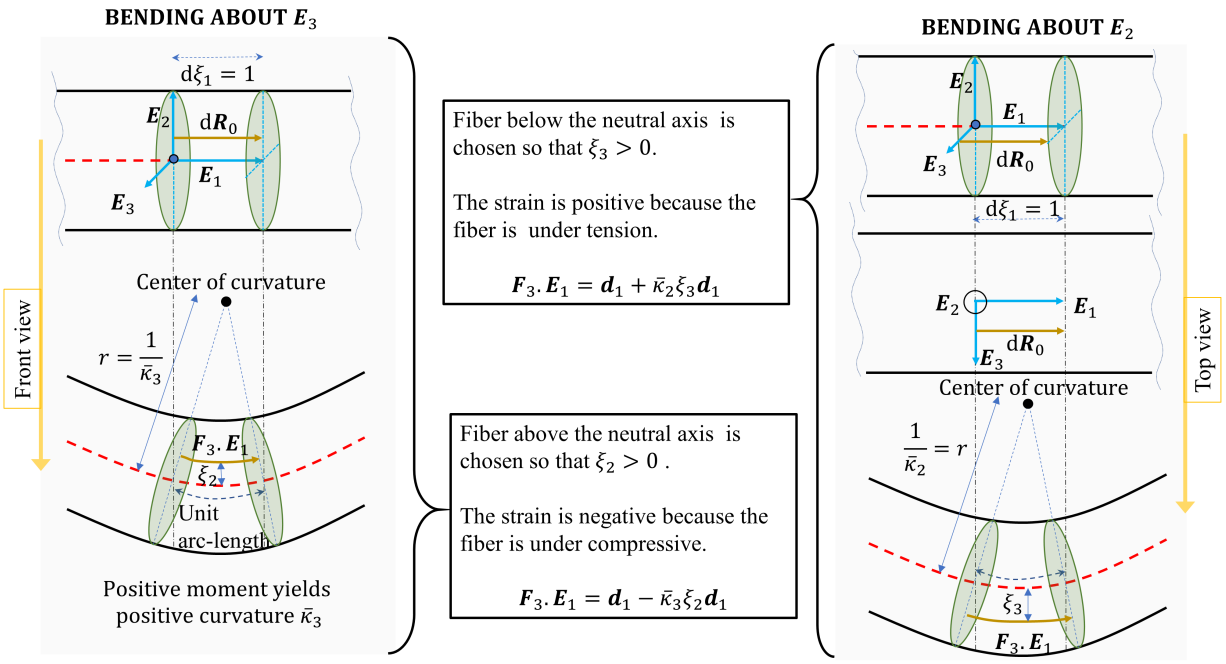

Figure 4.6: Geometric description of effects 4 and 5: deformation of the vector $\boldsymbol{E}_1$ under pure bending (no Poisson's deformation).

director $\boldsymbol{d}_1$ is kept constant but the change in the warping function is considered. Whereas, in effect 8, the warping deformation remains unchanged but the change in the orientation of director $\boldsymbol{d}_1$ is considered (attributed to bending about $\boldsymbol{d}_2$ and $\boldsymbol{d}_3$). Figure 4.9 describes effect 7 and 8.

4.3.3.2 Deformation of the unit vector $\boldsymbol{E}_2$ (or $\boldsymbol{E}_3$)

The deformation of the vector $\boldsymbol{E}_2$ is explored considering the deformation of the cross-section $\mathfrak{B}_0(\xi_1)$. Consider an infinitesimal vector $d\xi_2\boldsymbol{E}_2 \in \mathfrak{B}_0(\xi_1)$ that deforms to $d\xi_2(\boldsymbol{F}_3.\boldsymbol{E}_2)$ in the deformed configuration Ω_3. From Eq. (4.29) and (4.38),

$$\boldsymbol{F}_3.\boldsymbol{E}_2 = \overbrace{\partial_{\xi_2} W \boldsymbol{d}_1}^{\text{Effect b}} + \overbrace{\partial_{\xi_2}\hat{\xi}_2.\boldsymbol{d}_2 + \partial_{\xi_2}\hat{\xi}_3.\boldsymbol{d}_3}^{\text{Effect a}} \tag{4.40}$$

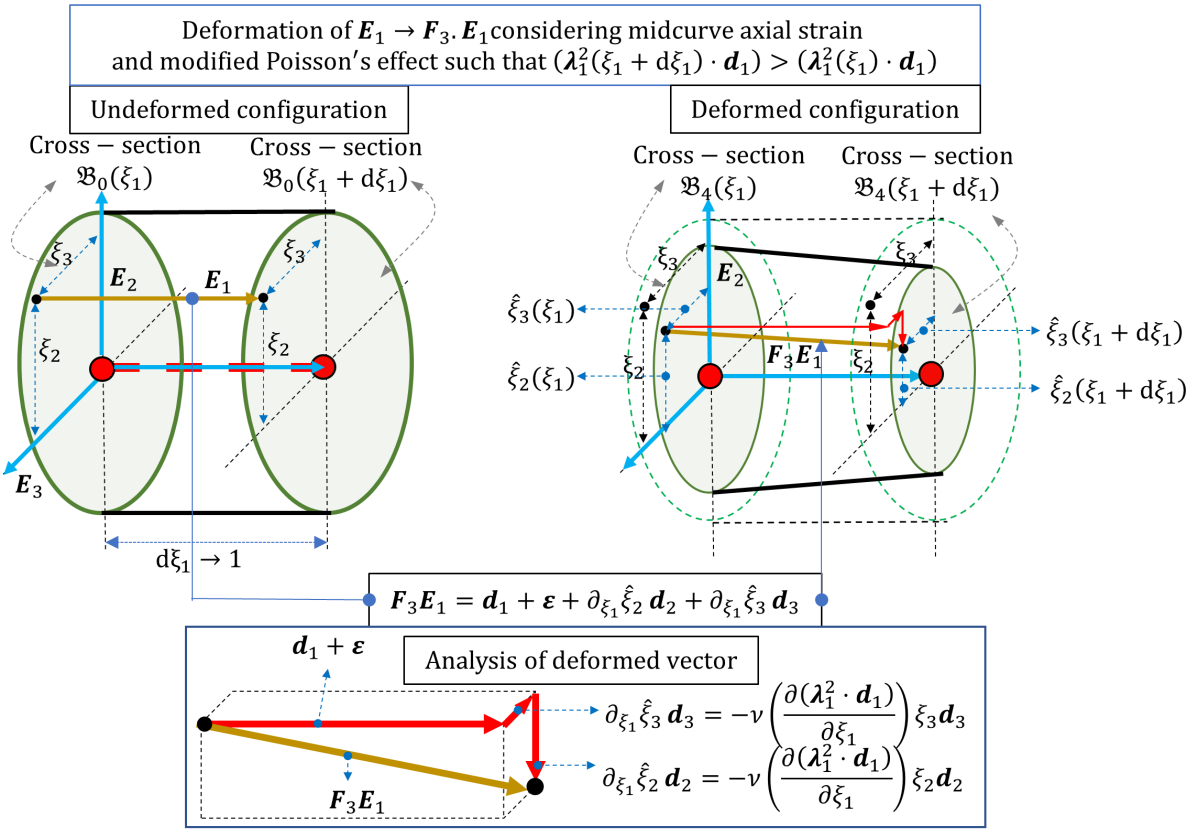

Figure 4.7: Geometric description of effects 1 and 3: deformation of the vector $\boldsymbol{E}_1$ considering differential Poisson's deformation.

It is observed that there are two effects that governs the deformation in this case. Effect *a* represents the straining in the vector $\mathrm{d}\xi_2\boldsymbol{E}_2$ due to in-plane deformation of the cross-section from $\mathfrak{B}_0(\xi_1) \rightarrow \mathfrak{B}_3(\xi_1)$ attributed to the fully-coupled Poisson's transformation P_{ξ_1}. Effect *b* represents the straining due to the out of plane deformation of the cross-section attributed to warping. Figure 4.10 illustrates the deformation of the vector $\boldsymbol{E}_2$.

It is clear from Eq. (4.29) that the deformation gradient tensor $\boldsymbol{F}_j$ in the configuration Ω_j referenced to the undeformed state Ω_0 can be obtained if the expression of $\boldsymbol{\lambda}_i^j$ is known (for $i = 1 - 3$). The expressions of $\boldsymbol{\lambda}_i^j$ for the deformed states Ω_2 and Ω_3 are described below:

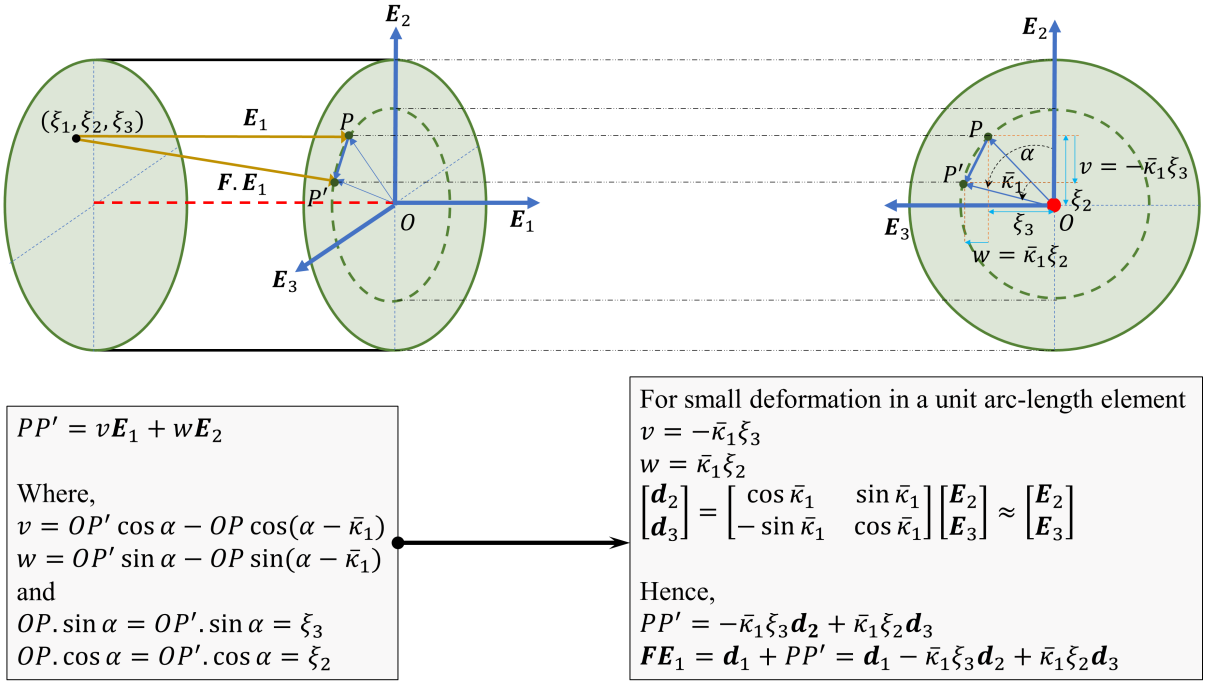

Figure 4.8: Geometric description of effect 6: deformation of the vector $\boldsymbol{E}_1$ under pure torsion (no out-of-plane warping).

For the deformed state Ω_1 :

$$\begin{aligned}\boldsymbol{\lambda}_1^1 &= (((1+e)\cos\gamma_{11} - 1) + \xi_3\bar{\kappa}_2 - \xi_2\bar{\kappa}_3)\,\boldsymbol{d}_1 + ((1+e)\sin\gamma_{12} - \xi_3\bar{\kappa}_1)\,\boldsymbol{d}_2 \\ &\quad + ((1+e)\sin\gamma_{13} + \xi_2\bar{\kappa}_1)\,\boldsymbol{d}_3; \\ \boldsymbol{\lambda}_2^1 &= \boldsymbol{\lambda}_3^1 = \boldsymbol{0}.\end{aligned} \tag{4.41}$$

For the deformed state Ω_2 :

$$\begin{aligned}\boldsymbol{\lambda}_1^2 &= \left(((1+e)\cos\gamma_{11} - 1) + \xi_3\bar{\kappa}_2 - \xi_2\bar{\kappa}_3 + \partial_{\xi_1}W\right)\boldsymbol{d}_1 + ((1+e)\sin\gamma_{12} - \xi_3\bar{\kappa}_1 + W\bar{\kappa}_3)\,\boldsymbol{d}_2 \\ &\quad + ((1+e)\sin\gamma_{13} + \xi_2\bar{\kappa}_1 - W\bar{\kappa}_2)\,\boldsymbol{d}_3; \\ \boldsymbol{\lambda}_2^2 &= \partial_{\xi_2}W.\boldsymbol{d}_1; \quad \boldsymbol{\lambda}_3^2 = \partial_{\xi_3}W.\boldsymbol{d}_1.\end{aligned} \tag{4.42}$$

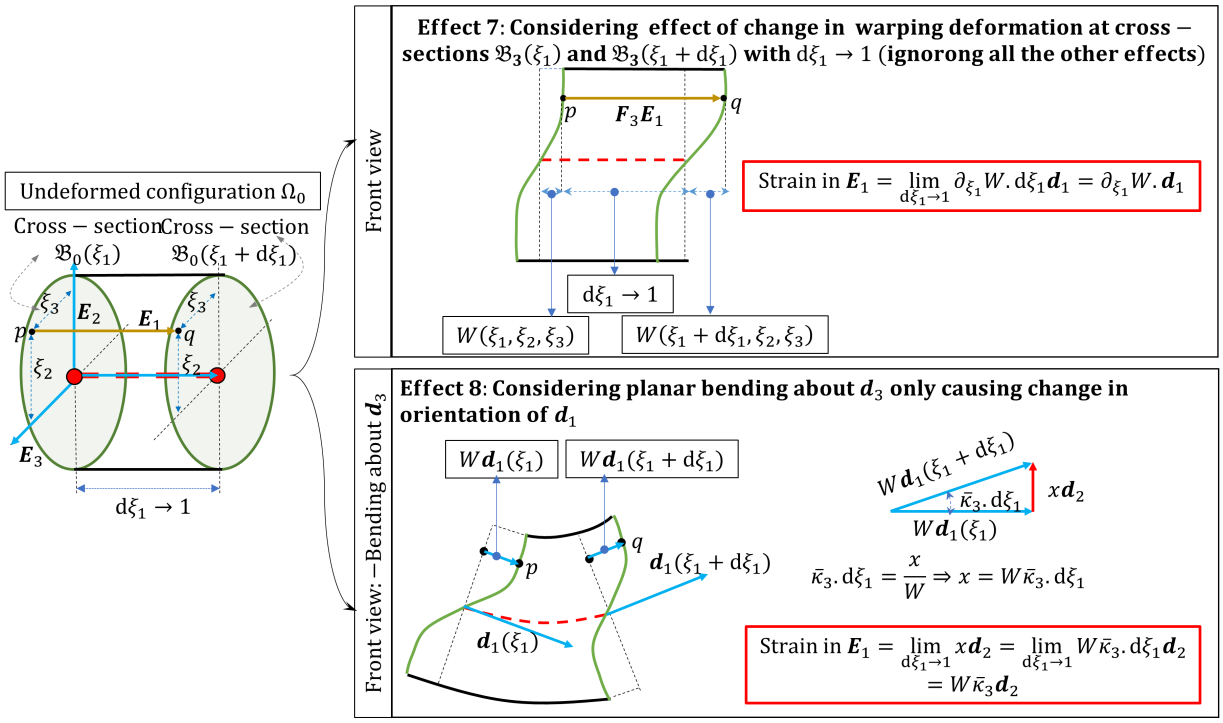

Figure 4.9: Geometric description of effects 7 and 8.

4.3.4 Deformation gradient tensor of the curved undeformed state referenced to the straight configuration

Consider that the curved reference beam configuration Ω_c is obtained by straining Ω_0 such that the total length of the mid-curve remains the same and there is no shear or torsion in the cross-sections. Consider an infinitesimal vector $\mathrm{d}\boldsymbol{R}_0$ in the straight configuration Ω_0 that transforms to $\mathrm{d}\boldsymbol{R}_c$ in the curved reference state Ω_c such that,

$$\boldsymbol{F}_c = \frac{\mathrm{d}\boldsymbol{R}_c}{\mathrm{d}\boldsymbol{R}_0} = (\xi_2.\partial_{\xi_1}\boldsymbol{d}_{c_2} + \xi_3.\partial_{\xi_1}\boldsymbol{d}_{c_3}) \otimes \boldsymbol{E}_1 + \boldsymbol{d}_{c_i} \otimes \boldsymbol{E}_i = \boldsymbol{\lambda}_c \otimes \boldsymbol{E}_1 + \boldsymbol{Q}_c;$$
$$\boldsymbol{\lambda}_c = \overbrace{(\xi_3\overline{\kappa}_{c_2} - \xi_2\overline{\kappa}_{c_3})}^{\overline{\lambda}_{c_1}}\boldsymbol{d}_{c_1}. \tag{4.43}$$

The vector $\boldsymbol{\lambda}_c$ represents the strain vector associated with the curved reference configuration. The parameters $\overline{\kappa}_{c_2}(\xi_1)$ and $\overline{\kappa}_{c_3}(\xi_1)$ represents the finite bending curvature field for the curved

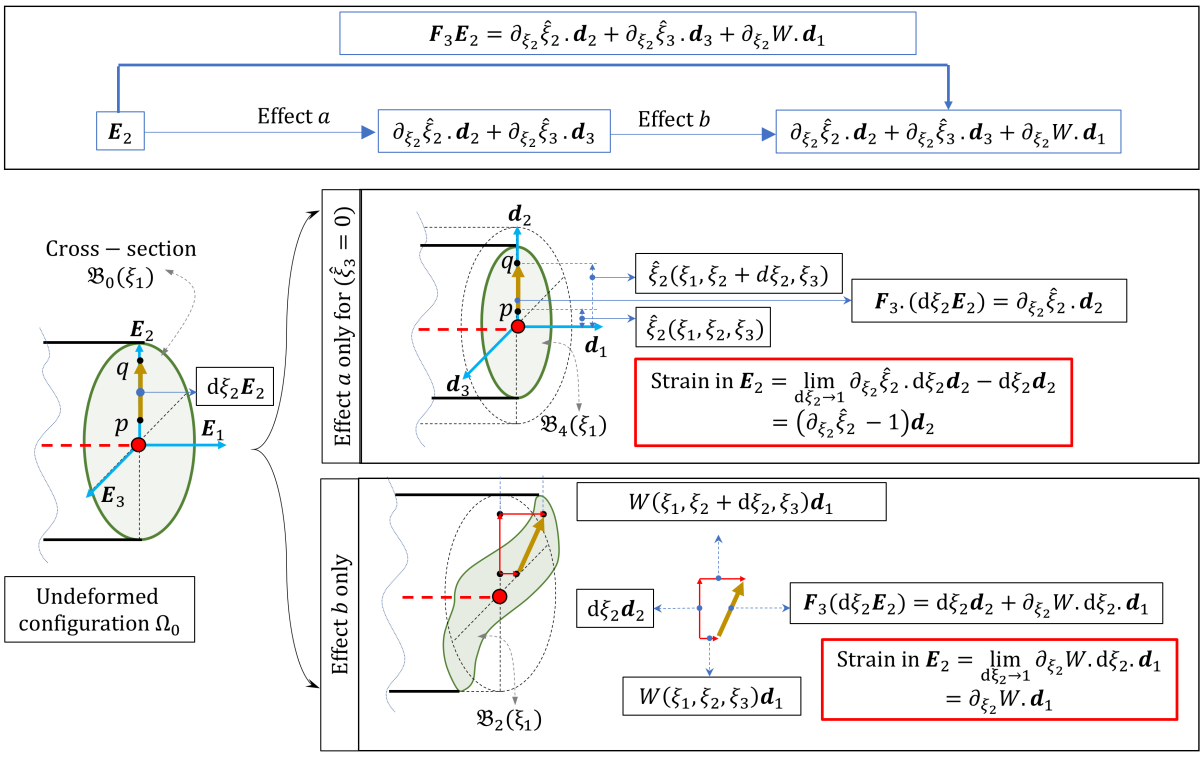

Figure 4.10: Deformation of the infinitesimal vector $\mathrm{d}\xi_2\boldsymbol{E}_2$.

reference state Ω_c. The corresponding material form $\overline{\boldsymbol{F}}_c$ and $\overline{\boldsymbol{\lambda}}_c$ is given as,

$$\begin{aligned} \overline{\boldsymbol{F}}_c &= \boldsymbol{Q}_c^T.\boldsymbol{F}_c.\boldsymbol{I}_3 = \overline{\boldsymbol{\lambda}}_c \otimes \boldsymbol{E}_1 + \boldsymbol{I}_3; \\ \overline{\boldsymbol{\lambda}}_c &= \boldsymbol{Q}_c^T.\boldsymbol{\lambda}_c. \end{aligned} \tag{4.44}$$

The strain vector $\boldsymbol{\lambda}_c$ comprises of strain due to curvatures only because there is no shear $\gamma_{1i} = 0$ and elongation $e(\xi_1) = 0$ in the curved reference configuration Ω_c. This ensures that the director $\boldsymbol{d}_{c_1}$ is tangent vector of the mid-curve such that $\partial_{\xi_1}\boldsymbol{\varphi} = \boldsymbol{d}_{c_1}$. Therefore, the axial strain vector $\boldsymbol{\varepsilon}_c = \partial_{\xi_1}\boldsymbol{\varphi} - \boldsymbol{d}_{c_1} = \boldsymbol{0}$. From Eq. (4.43) and (4.44), it is observed that

$$\begin{aligned} \boldsymbol{F}_c.\boldsymbol{E}_i &= \left\{ \begin{array}{ll} \boldsymbol{\lambda}_c + \boldsymbol{d}_1 = \overline{\lambda}_{c_i}\boldsymbol{d}_i + \boldsymbol{d}_1, & \text{for } i = 1 \\ \boldsymbol{d}_i, & \text{for } i = 2,3 \end{array} \right\}; \\ \overline{\boldsymbol{F}}_c.\boldsymbol{E}_i &= \left\{ \begin{array}{ll} \overline{\boldsymbol{\lambda}}_c + \boldsymbol{E}_1 = \overline{\lambda}_{c_i}\boldsymbol{E}_i + \boldsymbol{E}_1, & \text{for } i = 1 \\ \boldsymbol{E}_i, & \text{for } i = 2,3 \end{array} \right\}. \end{aligned} \tag{4.45}$$

From the above equation, $\det(\boldsymbol{F}_c)$ is obtained as

$$\det(\overline{\boldsymbol{F}}_c) = \det(\boldsymbol{Q}_c^T).\det(\overline{\boldsymbol{F}}_c).\det(\boldsymbol{I}_3) = \det(\boldsymbol{F}_c) = 1 + \overline{\lambda}_{c_1}. \tag{4.46}$$

Using equation (4.45), the first component of the vector $\mathrm{d}\boldsymbol{R}_0$ in the straight configuration $\mathrm{d}\xi_1\boldsymbol{E}_1$ gets strained to $\overline{\boldsymbol{F}}_c.(\mathrm{d}\xi_1\boldsymbol{E_1}) = \left(1 + \overline{\lambda}_1^c\right) d\xi_1\boldsymbol{d}_1^c$. This means that a fiber of unit length parallel to $\boldsymbol{E}_1$ in the configuration Ω_0 has length of $\det(\overline{\boldsymbol{F}}_c)$ in the configuration Ω_c along the director $\boldsymbol{d}_{c_1}$. In terms of classical continuum mechanics, $\det(\overline{\boldsymbol{F}}_c)$ is associated with volumetric strain

$$\det\left(\overline{\boldsymbol{F}}_c\right) = \frac{\mathrm{d}\Omega_c}{\mathrm{d}\Omega_0} = \frac{\rho_0}{\rho_c}. \tag{4.47}$$

where ρ_0 and ρ_c represents the density field in the configuration Ω_0 and Ω_c, respectively.

4.3.5 Deformation gradient tensor referenced to curved undeformed state

The deformation gradient tensor $\boldsymbol{F}_j^r$ of the deformed state Ω_j referenced to an initially curved (but unstrained) reference configuration Ω_c can be obtained using the expression $\boldsymbol{F}_j^r = \boldsymbol{F}_j.\boldsymbol{F}_c^{-1}$. However, the quantity $\boldsymbol{F}_c^{-1}$ is yet to be determined. It can be found by using the theorem for inverse of sum of matrices (refer to Miller [56]) as,

$$\begin{aligned}\overline{\boldsymbol{F}}_c^{-1} &= \left(\overline{\boldsymbol{\lambda}}_c \otimes \boldsymbol{E}_1 + \boldsymbol{I}_3\right)^{-1} = \boldsymbol{I}_3^{-1} - \frac{\boldsymbol{I}_3^{-1}.(\overline{\boldsymbol{\lambda}}_c \otimes \boldsymbol{E}_1).\boldsymbol{I}_3^{-1}}{1 + \mathrm{trace}(\overline{\boldsymbol{\lambda}}_c \otimes \boldsymbol{E}_1)} = \boldsymbol{I}_3 - \frac{(\overline{\boldsymbol{\lambda}}_c \otimes \boldsymbol{E}_1)}{1 + \overline{\lambda}_{c_1}} \\ &= -\frac{1}{\det(\boldsymbol{F}_c)}(\overline{\boldsymbol{\lambda}}_c \otimes \boldsymbol{E}_1) + \boldsymbol{I}_3.\end{aligned} \tag{4.48}$$

Note that the displacement gradient matrix $[\nabla_{\Omega_0}\boldsymbol{u}_c]_{\boldsymbol{d}_{c_l}\otimes\boldsymbol{E}_m}$, with $\boldsymbol{u}_c = \boldsymbol{R}_c - \boldsymbol{R}_0$, has rank 1 and is non-singular if $\boldsymbol{\lambda}_c \neq 0$ (it is zero along the mid-curve in the configuration Ω_c). This property allowed us to obtain Eq.(4.48) using the result Eq. (1) in Miller [56]. The tensor $\boldsymbol{F}_c^{-1}$ can be

found as,

$$\begin{aligned}\boldsymbol{F}_c^{-1} &= \left(-\frac{1}{\det(\boldsymbol{F}_c)}(\overline{\boldsymbol{\lambda}}_c \otimes \boldsymbol{E}_1) + \boldsymbol{I}_3\right).\boldsymbol{Q}_c^T = \left(-\frac{1}{\det(\boldsymbol{F}_c)}.\left((\boldsymbol{Q}_c^T.\boldsymbol{\lambda}_c) \otimes (\boldsymbol{Q}_c^T.\boldsymbol{d}_{c_1})\right) + \boldsymbol{I}_3\right).\boldsymbol{Q}_c^T \\ &= \boldsymbol{Q}_c^T.\left(\boldsymbol{I}_3 - \frac{1}{\det(\boldsymbol{F}_c)}(\boldsymbol{\lambda}_c \otimes \boldsymbol{d}_{c_1})\right).\end{aligned} \tag{4.49}$$

This brings us to the point of evaluating the deformation gradient tensor $\boldsymbol{F}_j^r$ of the deformed state Ω_j referenced to an initially curved (but unstrained) reference configuration Ω_c as,

$$\begin{aligned}\boldsymbol{F}_j^r = \boldsymbol{F}_j.\boldsymbol{F}_c^{-1} &= \left((\boldsymbol{\lambda}_i^j \otimes \boldsymbol{E}_i) + \boldsymbol{Q}\right).\boldsymbol{Q}_c^T.\left(\boldsymbol{I_3} - \frac{1}{\det(\boldsymbol{F}_c)}(\boldsymbol{\lambda}_c \otimes \boldsymbol{d}_{c_1})\right) \\ &= \left((\boldsymbol{\lambda}_i^j \otimes \boldsymbol{d}_{c_i}) + \boldsymbol{Q}_r\right) - \left(\frac{\boldsymbol{\lambda}_c \cdot \boldsymbol{d}_{c_1}}{\det(\boldsymbol{F}_c)}\left(\boldsymbol{\lambda}_1^j \otimes \boldsymbol{d}_{c_1}\right) + \frac{1}{\det(\boldsymbol{F}_c)}(\boldsymbol{Q}_r.\boldsymbol{\lambda}_c) \otimes \boldsymbol{d}_{c_1}\right) \\ &= (\boldsymbol{\lambda}_i^{r_j} \otimes \boldsymbol{d}_{c_i}) + \boldsymbol{Q}_r.\end{aligned} \tag{4.50}$$

In the above equation, the relative strain vectors $\boldsymbol{\lambda}_i^{r_j}$ are given as,

$$\begin{aligned}\boldsymbol{\lambda}_1^{r_j} &= \frac{1}{\det(\boldsymbol{F}_c)}\left(\boldsymbol{\lambda}_1^j - \boldsymbol{Q}_r.\boldsymbol{\lambda}_c\right); \\ \boldsymbol{\lambda}_2^{r_j} &= \boldsymbol{\lambda}_2^j; \;\; \boldsymbol{\lambda}_3^{r_j} = \boldsymbol{\lambda}_3^j.\end{aligned} \tag{4.51}$$

In component form,

$$[F_{j_{pq}}^r]_{\boldsymbol{d}_p \otimes \boldsymbol{d}_{c_q}} = \boldsymbol{\lambda}_q^{r_j} \cdot \boldsymbol{d}_p + \delta_{pq}. \tag{4.52}$$

Physically, $\boldsymbol{\lambda}_i^{r_j}$ represents the strain vector in the deformed state Ω_j corresponding to the vector $\boldsymbol{d}_{c_i}$ in the undeformed state Ω_c. The equation set below elaborates the vector $\boldsymbol{\lambda}_1^{r_j}$ for various deformed configurations Ω_j.

$$\begin{aligned}\boldsymbol{\lambda}_1^{r_1} &= \left(\frac{1}{\xi_3\overline{\kappa}_{c_2} - \xi_2\overline{\kappa}_{c_3}}\right)\left(((1+e)\cos\gamma_{11} - 1) + \xi_3(\overline{\kappa}_2 - \overline{\kappa}_{c_2}) - \xi_2(\overline{\kappa}_3 - \overline{\kappa}_{c_3})\right)\boldsymbol{d}_1 \\ &\quad + ((1+e)\sin\gamma_{12} - \xi_3\overline{\kappa}_1)\,\boldsymbol{d}_2 + ((1+e)\sin\gamma_{13} + \xi_2\overline{\kappa}_1)\,\boldsymbol{d}_3.\end{aligned} \tag{4.53a}$$

$$\begin{aligned}\boldsymbol{\lambda}_1^{r_2} &= \left(\frac{1}{\xi_3\overline{\kappa}_{c_2} - \xi_2\overline{\kappa}_{c_3}}\right)\left(((1+e)\cos\gamma_{11} - 1) + \xi_3(\overline{\kappa}_2 - \overline{\kappa}_{c_2}) - \xi_2(\overline{\kappa}_3 - \overline{\kappa}_{c_3}) + \partial_{\xi_1}W\right)\boldsymbol{d}_1 \\ &\quad + ((1+e)\sin\gamma_{12} - \xi_3\overline{\kappa}_1 + W\overline{\kappa}_3)\,\boldsymbol{d}_2 + ((1+e)\sin\gamma_{13} + \xi_2\overline{\kappa}_1 - W\overline{\kappa}_2)\,\boldsymbol{d}_3.\end{aligned} \tag{4.53b}$$

$$\boldsymbol{\lambda}_1^{r_3} = \left(\frac{1}{\xi_3\overline{\kappa}_{c_2} - \xi_2\overline{\kappa}_{c_3}}\right)\Big(((1+e)\cos\gamma_{11} - 1) + \hat{\xi}_3\overline{\kappa}_2 - \xi_3\overline{\kappa}_{c_2} - \hat{\xi}_2\overline{\kappa}_3 + \xi_2\overline{\kappa}_{c_3} + \partial_{\xi_1}W\Big)\,\boldsymbol{d}_1 \\ + \Big((1+e)\sin\gamma_{12} - \hat{\xi}_3\overline{\kappa}_1 + W\overline{\kappa}_3\Big)\,\boldsymbol{d}_2 + \Big((1+e)\sin\gamma_{13} + \hat{\xi}_2\overline{\kappa}_1 - W\overline{\kappa}_2\Big)\,\boldsymbol{d}_3. \tag{4.53c}$$

Figure 4.11 illustrates the relationship between the mathematically straight beam Ω_0, the curved

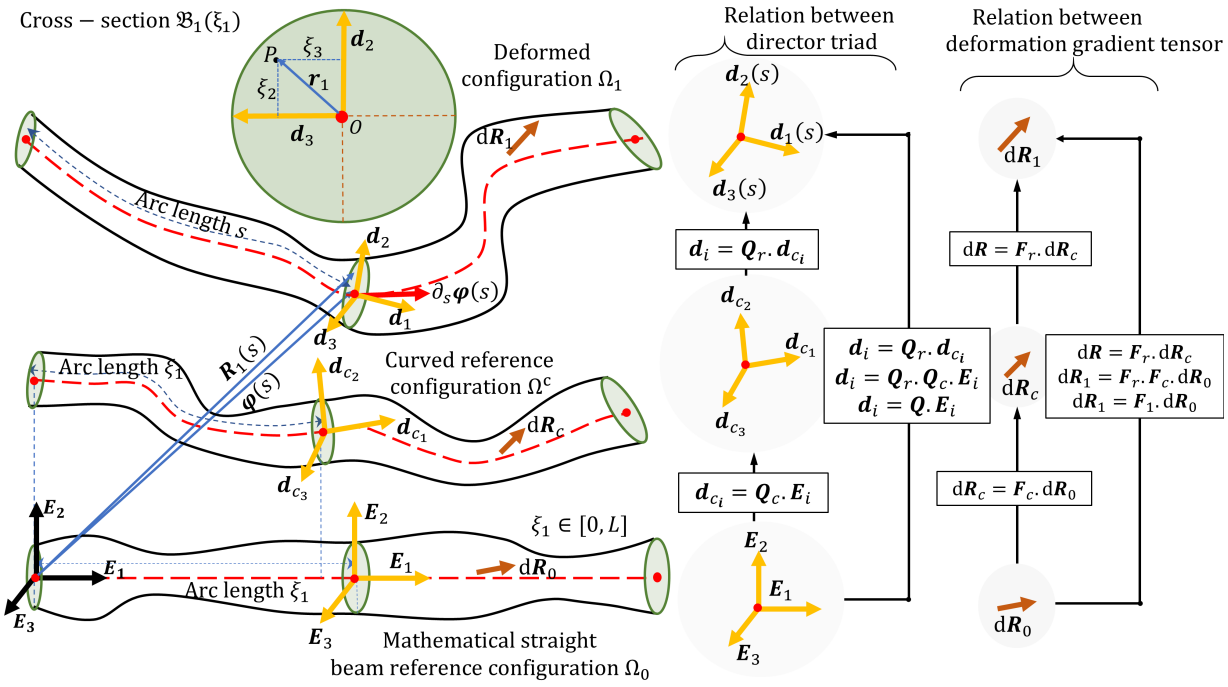

Figure 4.11: Deformed (Ω_1) and undeformed configurations (Ω_0, Ω_c) of Cosserat rod, material adapted frames, and deformation gradient tensors.

reference state Ω_c, and the deformed beam Ω_1. The next section 4.3.6 discusses the procedure to obtain deformation gradient tensor of a deformed configuration with respect to another deformed state.

4.3.6 Deformation gradient tensor referenced to another deformed state

We consider a deformation of class Ω_3. Suppose $\boldsymbol{F}_{3_p}$ and $\boldsymbol{F}_{3_q}$ represent the deformation gradient tensor of a deformed state Ω_{3_p} and Ω_{3_q} respectively, referenced to the undeformed state Ω_0. If $\{\boldsymbol{d}_{p_i}\}$ and $\{\boldsymbol{d}_{q_i}\}$ represent the director triad for the configurations Ω_{3_p} and Ω_{3_q}, we have, $\boldsymbol{Q}_p = \boldsymbol{d}_{p_i} \otimes \boldsymbol{E}_i$ and $\boldsymbol{Q}_q = \boldsymbol{d}_{q_i} \otimes \boldsymbol{E}_i$ (sum on i). We obtain the deformation gradient tensor $\boldsymbol{F}_{3_{qp}}$ of

the state Ω_{3_q} referenced to Ω_{3_p} as,

$$\boldsymbol{F}_{3_{qp}} = \boldsymbol{F}_{3_q}.\boldsymbol{F}_{3_p}^{-1} \tag{4.54}$$

where,

$$\begin{aligned} \boldsymbol{F}_{3_p} &= \boldsymbol{\lambda}_i^{3p} \otimes \boldsymbol{E}_i + \boldsymbol{Q}_p; \\ \boldsymbol{F}_{3_q} &= \boldsymbol{\lambda}_i^{3q} \otimes \boldsymbol{E}_i + \boldsymbol{Q}_q. \end{aligned} \tag{4.55}$$

In the equation above, $\boldsymbol{\lambda}_i^{3p}$ and $\boldsymbol{\lambda}_i^{3q}$ represent the strain vectors related to the configuration Ω_{3_p} and Ω_{3_q} respectively.

It is interesting to note that unlike the deformation gradient matrix $[\nabla_{\Omega_0}\boldsymbol{u}_0]_{\boldsymbol{d}_{p_l}\otimes\boldsymbol{E}_m}$, the matrix $[\nabla_{\Omega_0}\boldsymbol{u}_p]_{\boldsymbol{d}_{p_l}\otimes\boldsymbol{E}_m} = [\boldsymbol{\lambda}_1^{3p}\otimes\boldsymbol{E}_1]_{\boldsymbol{d}_{p_l}\otimes\boldsymbol{E}_m} + [\boldsymbol{\lambda}_2^{3p}\otimes\boldsymbol{E}_2]_{\boldsymbol{d}_{p_l}\otimes\boldsymbol{E}_m} + [\boldsymbol{\lambda}_3^{3p}\otimes\boldsymbol{E}_3]_{\boldsymbol{d}_{p_l}\otimes\boldsymbol{E}_m}$ has maximum rank 3. It has rank 3 and is non-singular if $\boldsymbol{\lambda}_1^{3p}\cdot\boldsymbol{d}_{p_1} \neq 0$, $\boldsymbol{\lambda}_2^{3p}\cdot\boldsymbol{d}_{p_2} \neq 0$ and $\boldsymbol{\lambda}_3^{3p}\cdot\boldsymbol{d}_{p_3} \neq 0$. Here the index l and m are used to represent the frames. Therefore, the expression for $\boldsymbol{F}_{3_p}^{-1}$ can not be obtained from Eq. [1] in Miller [56]. Consider the case where the matrix $[\nabla_{\Omega_0}\boldsymbol{u}_p]_{\boldsymbol{d}_{p_l}\otimes\boldsymbol{E}_m}$ has rank 3 and is non-singular. The fact that the matrix $[\boldsymbol{\lambda}_1^{3p}\otimes\boldsymbol{E}_1]_{\boldsymbol{d}_{p_l}\otimes\boldsymbol{E}_m}$, $[\boldsymbol{\lambda}_2^{3p}\otimes\boldsymbol{E}_2]_{\boldsymbol{d}_{p_l}\otimes\boldsymbol{E}_m}$ and $[\boldsymbol{\lambda}_3^{3p}\otimes\boldsymbol{E}_3]_{\boldsymbol{d}_{p_l}\otimes\boldsymbol{E}_m}$ are rank 1 and non-singular allows us to use the theorem in page 69 of Miller [56] to arrive at the expression for $\boldsymbol{F}_{3_p}^{-1}$.

4.4 Summary

This chapter details the development of an enhanced kinematics of geometrically-exact beams, that incorporates not only traditional deformation effects like curvature, shear and axial strains (as developed in Simo et al. [48]) and Saint Venant's uniform warping (refer to Simo et al. [43]), but also includes a fully-coupled warping and Poisson's deformation. This chapter addresses the coupling between Poisson's and warping effect and obtains a fully-coupled Poisson's transformation to develop comprehensive kinematics of Cosserat beams. The kinematics developed is not restricted to the Euler-Bernoulli rigid cross-section assumption, and it is simultaneously

maintaining the single manifold nature of the problem. The idea of having prior knowledge of the cross-sectional dependence of the warping function (a function of the form $\Psi(\xi_2, \xi_3)$) is certainly desirable for maintaining the single manifold nature of the kinematics, but it yields only an approximate solution. The primary reason to investigate the coupling between Poisson's and warping effect (along with the contribution to warping due to torsional and bending induced shear) and develop a fully-coupled Poisson's transformation, is to further refine the kinematics of the Cosserat beam model. This is beneficial for both forward modeling analyses and solving inverse problems like shape reconstruction from strain measurements.

Three different deformed configurations of the beam are detailed, with Ω_3 representing the most general configuration and $\Omega_1 - \Omega_2$ constituting more constrained cases. The coupled Poisson's and warping are developed in a two-stage process. The governing differential equations to capture warping in an asymmetric beam cross-section subjected to curvatures and axial strains for the linear elastic case are arrived at. The inclusion of axial strain and Poisson's effect on the small displacement field leads to an *inconsistent governing differential equation for warping*. Chapter 5 is dedicated to investigating the inconsistencies in the differential equation for warping and arriving at a simplified warping function. To proceed further with the investigation, the warping functions are assumed to be known. In stage two, the fully-coupled Poisson's transformation is proposed by considering the axial strain contributions due to mid-curve strain, finite shear, bending curvatures, and out of plane warping. This yields *fully coupled Poisson's and warping effect*.

The deformation gradient tensor and strain vector in a general deformed state Ω_j referenced to both a *mathematically straight beam configuration* Ω_0 and an *initially curved reference configuration* Ω_c are derived. The contribution to deformation due to various effects are carefully explored and explained.

The results in this chapter are used in developing a scalar strain gauge measurement model for finite length and discrete strain gauge attached to the beam, and in developing shape-

reconstruction technique as detailed in chapter 6. The kinematics developed in this chapter sets the basis to investigate the variational and finite element formulation of enhanced geometrically exact beam discussed in chapters 7–10.

The discussion carried out in this chapter has been published in the International Journal of Solids and Structures, Mayank Chadha and Michael D. Todd [34], 2019. The title of this paper is: "A comprehensive kinematic model of single-manifold Cosserat beam structures with application to a finite strain measurement model for strain gauges". The dissertation author is the primary investigator and author of this paper.

Chapter 5

Inconsistencies in the Governing Differential Equation of Warping

5.1 Introduction

In the last chapter, we presented generalized kinematics of Cosserat beams. One of the primary contributions was the inclusion of fully coupled Poisson's and warping effects. The coupled Poisson's and warping were developed in a two-stage process. We arrive at the governing differential equations to capture warping in an asymmetric beam cross-section subjected to curvatures and axial strains for the linear elastic case constituting the first stage of this coupling. Stage one represents the incorporation of the effects of axial strains and Poisson's transformation on warping. In stage two, we propose the fully-coupled Poisson's transformation by considering the axial strain contributions due to mid-curve strain, finite shear, bending curvatures, and out of plane warping. This yields *fully coupled Poisson's and warping effect*.

However, the inclusion of axial strain and Poisson's effect on the small displacement field leads to an *inconsistent governing differential equation for warping* (refer to Eq. (4.21a) and (4.21b)). In this chapter, we first explore the *inconsistency condition* and then obtain the *consistent*

differential equation by deliberately enforcing the *inconsistency condition* into the *inconsistent warping equation*. The consistent warping equation suggests a solution to the warping function W that is not explicitly dependent on the axial strain $e(\xi_1)$ and its derivatives. However, we carefully note that the elimination of *inconsistency* results in *consistent differential equations for warping* that could be solved, but the accuracy of the solution and their closeness to the exact 3D solution is open to further investigation. Motivated from the work of Burgoyne and Brown [41] and [42], we delineated two possible solution approaches to obtain the warping function in variable separable form. We also note that for the Poisson's ratio $\nu = 0$, the presented theory of warping reduces to the theory presented by Burgoyne and Brown in [41] and [42].

5.2 Inconsistency condition and the proposed Solution

5.2.1 Preliminary results

Before we present a deeper discussion, we note the following results. From the definition of t and $\tilde{t}$ as in Eq. (4.21b), we have

$$\begin{aligned}\oint t \, \mathrm{d}\Gamma &= \oint ((\xi_2 \boldsymbol{E}_2 + \xi_3 \boldsymbol{E}_3) \times \boldsymbol{n}) \cdot \boldsymbol{E}_1 \, \mathrm{d}\Gamma = \oint \boldsymbol{n} \cdot (-\xi_3 \boldsymbol{E}_2 + \xi_2 \boldsymbol{E}_3) \, \mathrm{d}\Gamma \\ &= \int_{\mathfrak{B}} \mathrm{Div}(-\xi_3 \boldsymbol{E}_2 + \xi_2 \boldsymbol{E}_3) \, \mathrm{d}\xi_2 \mathrm{d}\xi_3 = 0; \end{aligned} \tag{5.1a}$$

$$\oint \tilde{t} \, \mathrm{d}\Gamma = \oint \boldsymbol{n} \cdot (\xi_2 \boldsymbol{E}_2 + \xi_3 \boldsymbol{E}_3) \, \mathrm{d}\Gamma = \int_{\mathfrak{B}} \mathrm{Div}(\xi_2 \boldsymbol{E}_2 + \xi_3 \boldsymbol{E}_3) \, \mathrm{d}\xi_2 \mathrm{d}\xi_3 = 2\mathrm{A}(\xi_1); \tag{5.1b}$$

$$\int_{\mathfrak{B}} \nabla^2 W \mathrm{d}\xi_2 \mathrm{d}\xi_3 = \oint \partial_{\boldsymbol{n}} W \, \mathrm{d}\Gamma. \tag{5.1c}$$

From here on, we will represent the area of the cross-section $A(\xi_1)$ as A. Equation (5.1c) is obtained using the Gauss-divergence theorem. Recalling the governing differential equation for warping (4.21a) and (4.21b),

$$\nabla^2 W + \frac{\tilde{\lambda}}{G}\left(\partial^2_{\xi_1} W - \xi_2 . \partial_{\xi_1} \overline{\kappa}_3 + \xi_3 . \partial_{\xi_1} \overline{\kappa}_2\right) + \overline{\lambda} . \partial_{\xi_1} e = 0 \ \text{ on } \ \mathfrak{B}(\xi_1); \tag{5.2a}$$

$$\partial_{\boldsymbol{n}} W = -\overline{\kappa}_1 t + \nu.\partial_{\xi_1} e.\tilde{t} \;\text{ on }\; \Gamma(\xi_1). \tag{5.2b}$$

5.2.2 The inconsistency

Integrating Eq. (5.2b) along the boundary of the cross-section $\Gamma(\xi_1)$ and using the result (5.1a) and (5.1b), we have,

$$\oint \partial_{\boldsymbol{n}} W \, \mathrm{d}\Gamma = -\overline{\kappa}_1 \oint t \, \mathrm{d}\Gamma + \nu.\partial_{\xi_1} e. \oint \tilde{t} \, \mathrm{d}\Gamma = 2\nu A.\partial_{\xi_1} e. \tag{5.3}$$

Integrating Eq. (5.2a) across the cross-section $\mathfrak{B}(\xi_1)$ and realizing that $\int_{\mathfrak{B}} \xi_i \mathrm{d}\xi_2 \mathrm{d}\xi_3 = 0$ for $i = 2$ and 3, we have,

$$\int_{\mathfrak{B}} \nabla^2 W \, \mathrm{d}\xi_2 \mathrm{d}\xi_3 = -\frac{\tilde{\lambda}}{G} \int_{\mathfrak{B}} \partial^2_{\xi_1} W \, \mathrm{d}\xi_2 \mathrm{d}\xi_3 - \overline{\lambda} A.\partial_{\xi_1} e. \tag{5.4}$$

Using Eq. (5.1c) and (5.4), we get

$$\oint \partial_{\boldsymbol{n}} W \, \mathrm{d}\Gamma = -\frac{\tilde{\lambda}}{G} \int_{\mathfrak{B}} \partial^2_{\xi_1} W \, \mathrm{d}\xi_2 \mathrm{d}\xi_3 - \overline{\lambda} A.\partial_{\xi_1} e. \tag{5.5}$$

Comparing Eq. (5.3) and (5.5), we clearly observe an inconsistency which can be resolved only if

$$\int_{\mathfrak{B}} \partial^2_{\xi_1} W \, \mathrm{d}\xi_2 \mathrm{d}\xi_3 = -\left(\frac{GA(\xi_1)\left(\overline{\lambda} + 2\nu\right)}{\tilde{\lambda}} \right) \partial_{\xi_1} e = -\left(\frac{\tilde{\lambda} - 2\nu\lambda}{\tilde{\lambda}} \right) A(\xi_1).\partial_{\xi_1} e. \tag{5.6}$$

From the definition of the reduced axial force field $P_1(\xi_1)$ in Eq. (4.22), we obtain the following result

$$\partial_{\xi_1} P_1 = (\tilde{\lambda} - 2\nu\lambda) A.\partial_{\xi_1} e + \tilde{\lambda} \int_{\mathfrak{B}} \partial^2_{\xi_1} W \, \mathrm{d}\xi_2 \mathrm{d}\xi_3 \tag{5.7}$$

The inconsistency condition (5.6) and the Eq. (5.7) implies that the inconsistency can be resolved if

$$\partial_{\xi_1} P_1 = 0 \;\text{ or }\; P_1(\xi_1) = \text{constant}. \tag{5.8}$$

These kinds of inconsistencies or anomalies are commonly observed in simplified theories. For instance, the anomaly of the torque for the case of wholly-restrained end warping was observed by

Burgoyne et al. [41]. If the axial strain and the Poisson's effect is not included in the displacement field (4.19), it would require $\int_{\mathfrak{B}} \partial^2_{\xi_1} W \, \mathrm{d}\xi_2 \mathrm{d}\xi_3 = 0$. This condition is automatically satisfied if $P_1 = 0$ along the length of the beam, which is physically true if axial deformation and force are ignored as in Eq. (7) of Brown et al. [42]. At the most fundamental level, the reason for this inconsistency lies primarily in our objective to obtain a simplified warping function and our assumption of zero body force. In our opinion, the inconsistency indicates that the rigid body cross-sectional deformation due to constant axial strain field across the cross-section attributed to mid-curve axial strain $e(\xi_1)$ does not affect warping (essentially an out-of-plane deformation), which is observed later in equations (5.21) and (5.39).

5.2.3 The proposed consistent differential equation of warping

We attempt to resolve the inconsistency by enforcing the condition (5.6) in the inconsistent warping equation. Substituting for $\partial_{\xi_1} e$ (obtained using Eq. (5.6)) in Eq. (5.2a) and (5.2b), we obtain the modified consistent governing differential equation

$$\nabla^2 W + C_1 \left(\partial^2_{\xi_1} W - \xi_2 . \partial_{\xi_1} \overline{\kappa}_3 + \xi_3 . \partial_{\xi_1} \overline{\kappa}_2 \right) + C_2 \overline{\lambda} \int_{\mathfrak{B}} \partial^2_{\xi_1} W \, \mathrm{d}\xi_2 \mathrm{d}\xi_3 = 0 \ \text{ on } \ \mathfrak{B}(\xi_1), \tag{5.9a}$$

$$\partial_{\boldsymbol{n}} W = -\overline{\kappa}_1 t + \left\{ \nu C_2 \int_{\mathfrak{B}} \partial^2_{\xi_1} W \, \mathrm{d}\xi_2 \mathrm{d}\xi_3 \right\} \tilde{t} \ \text{ on } \ \Gamma(\xi_1), \tag{5.9b}$$

where,

$$C_1 = \frac{\tilde{\lambda}}{G} \ \text{ and } \ C_2 = -\frac{1}{A} \left(\frac{\tilde{\lambda}}{\tilde{\lambda} - 2\nu\lambda} \right). \tag{5.10}$$

5.3 Solution approach 1: Solution of warping function using series sum

5.3.1 Assumed solution and the governing differential equations

We assume a solution of the variable separable form

$$W(\xi_1,\xi_2,\xi_3) = \sum_{r=0}^{\infty}\left(\partial^r_{\xi_1}\overline{\kappa}_1.\Psi_{1r} + \partial^r_{\xi_1}\overline{\kappa}_2.\Psi_{2r} + \partial^r_{\xi_1}\overline{\kappa}_3.\Psi_{3r} + \partial^r_{\xi_1}e.\Psi_{4r}\right), \tag{5.11}$$

and aim at obtaining the functions Ψ_{ir}, where $i = 1-4$. Substituting Eq. (5.11) into the consistent differential equations (5.9a) and (5.9b), we can obtain the governing differential equations for the functions Ψ_{ir} with $i = 1-4$.

The governing differential equations for the functions Ψ_{1r}: We have,

for $r = 0$ and 1,

$$\begin{aligned}\nabla^2\Psi_{10} &= 0 \text{ on } \mathfrak{B}(\xi_1) \text{ with } \partial_{\boldsymbol{n}}\Psi_{10} = -t \text{ on } \Gamma(\xi_1);\\ \nabla^2\Psi_{11} &= 0 \text{ on } \mathfrak{B}(\xi_1) \text{ with } \partial_{\boldsymbol{n}}\Psi_{11} = 0 \text{ on } \Gamma(\xi_1);\end{aligned} \tag{5.12}$$

for $r \geq 2$,

$$\begin{aligned}\nabla^2\Psi_{1r} &= -\left(C_1\Psi_{1(r-2)} + \overline{\lambda}C_2\int_{\mathfrak{B}}\Psi_{1(r-2)}\,\mathrm{d}\xi_2\mathrm{d}\xi_3\right) \text{ on } \mathfrak{B}(\xi_1);\\ \partial_{\boldsymbol{n}}\Psi_{1r} &= \left(\nu C_2\int_{\mathfrak{B}}\Psi_{1(r-2)}\,\mathrm{d}\xi_2\mathrm{d}\xi_3\right)\tilde{t} \text{ on } \Gamma(\xi_1).\end{aligned} \tag{5.13}$$

From Eq. (5.12), we note that Ψ_{11} = constant. To avoid any rigid body motion of the cross-section due to warping, we take $\Psi_{11} = 0$. Eq. (5.13) then implies $\Psi_{1r} = 0$ for any odd r.

If the cross-section is symmetric, $\int_{\mathfrak{B}}\Psi_{10}\,\mathrm{d}\xi_2\mathrm{d}\xi_3 = 0$ as Ψ_{10} is anti-symmetric. This reduces the governing differential equation for Ψ_{1r} for any even $r = 2,4,6,\ldots$ to,

$$\nabla^2\Psi_{1r} = -C_1\Psi_{1(r-2)} \text{ on } \mathfrak{B}(\xi_1) \text{ with } \partial_{\boldsymbol{n}}\Psi_{1r} = 0 \text{ on } \Gamma(\xi_1); \tag{5.14}$$

It is easy to prove then that $\int_{\mathfrak{B}} \Psi_{1r}\, \mathrm{d}\mathfrak{B} = 0$ for any even $r = 2, 4, 6, \ldots$ implying that the non-trivial solution to the functions Ψ_{1r} is anti-symmetric. Thus, we observe that the anti-symmetric nature of the solution (contribution to warping due to torsion) for the symmetric cross-section is preserved.

The governing differential equations for the functions Ψ_{2r}: We have,

for $r = 0$ and 1,

$$\begin{aligned} \nabla^2 \Psi_{20} &= 0 \ \text{ on } \ \mathfrak{B}(\xi_1) \ \text{ with } \ \partial_{\boldsymbol{n}} \Psi_{20} = 0 \ \text{ on } \ \Gamma(\xi_1); \\ \nabla^2 \Psi_{21} &= -C_1 \xi_3 \ \text{ on } \ \mathfrak{B}(\xi_1) \ \text{ with } \ \partial_{\boldsymbol{n}} \Psi_{21} = 0 \ \text{ on } \ \Gamma(\xi_1); \end{aligned} \tag{5.15}$$

for $r \geq 2$,

$$\begin{aligned} \nabla^2 \Psi_{2r} &= -\left(C_1 \Psi_{2(r-2)} + \overline{\lambda} C_2 \int_{\mathfrak{B}} \Psi_{2(r-2)}\, \mathrm{d}\xi_2 \mathrm{d}\xi_3 \right) \ \text{ on } \ \mathfrak{B}(\xi_1); \\ \partial_{\boldsymbol{n}} \Psi_{2r} &= \left(\nu C_2 \int_{\mathfrak{B}} \Psi_{2(r-2)}\, \mathrm{d}\xi_2 \mathrm{d}\xi_3 \right) \tilde{t} \ \text{ on } \ \Gamma(\xi_1). \end{aligned} \tag{5.16}$$

The governing differential equations for the functions Ψ_{3r}: We have,

for $r = 0$ and 1,

$$\begin{aligned} \nabla^2 \Psi_{30} &= 0 \ \text{ on } \ \mathfrak{B}(\xi_1) \ \text{ with } \ \partial_{\boldsymbol{n}} \Psi_{30} = 0 \ \text{ on } \ \Gamma(\xi_1); \\ \nabla^2 \Psi_{31} &= C_1 \xi_2 \ \text{ on } \ \mathfrak{B}(\xi_1) \ \text{ with } \ \partial_{\boldsymbol{n}} \Psi_{31} = 0 \ \text{ on } \ \Gamma(\xi_1); \end{aligned} \tag{5.17}$$

for $r \geq 2$,

$$\begin{aligned} \nabla^2 \Psi_{3r} &= -\left(C_1 \Psi_{3(r-2)} + \overline{\lambda} C_2 \int_{\mathfrak{B}} \Psi_{3(r-2)}\, \mathrm{d}\xi_2 \mathrm{d}\xi_3 \right) \ \text{ on } \ \mathfrak{B}(\xi_1); \\ \partial_{\boldsymbol{n}} \Psi_{3r} &= \left(\nu C_2 \int_{\mathfrak{B}} \Psi_{3(r-2)}\, \mathrm{d}\xi_2 \mathrm{d}\xi_3 \right) \tilde{t} \ \text{ on } \ \Gamma(\xi_1). \end{aligned} \tag{5.18}$$

Following similar reasoning as before, we observe from Eq. (5.16) and (5.18) that $\Psi_{20} = 0$ and $\Psi_{30} = 0$. That implies, $\Psi_{2r} = 0$ and $\Psi_{3r} = 0$ for any even r. The inclusion of bending curvature in warping results in a non-linear strain profile across the cross-section.

The governing differential equations for the functions Ψ_{4r}: We have,

for $r = 0$ and 1,

$$\begin{aligned} \nabla^2\Psi_{40} &= 0 \ \text{ on } \ \mathfrak{B}(\xi_1) \ \text{ with } \ \partial_{\boldsymbol{n}}\Psi_{40} = 0 \ \text{ on } \ \Gamma(\xi_1); \\ \nabla^2\Psi_{41} &= 0 \ \text{ on } \ \mathfrak{B}(\xi_1) \ \text{ with } \ \partial_{\boldsymbol{n}}\Psi_{41} = 0 \ \text{ on } \ \Gamma(\xi_1). \end{aligned} \tag{5.19}$$

for $r \geq 2$,

$$\begin{aligned} \nabla^2\Psi_{4r} &= -\left(C_1\Psi_{4(r-2)} + \overline{\lambda}C_2\int_{\mathfrak{B}}\Psi_{4(r-2)}\,\mathrm{d}\xi_2\mathrm{d}\xi_3\right) \ \text{ on } \ \mathfrak{B}(\xi_1); \\ \partial_{\boldsymbol{n}}\Psi_{4r} &= \left(\nu C_2\int_{v}\Psi_{4(r-2)}\,\mathrm{d}\xi_2\mathrm{d}\xi_3\right)\tilde{t} \ \text{ on } \ \Gamma(\xi_1). \end{aligned} \tag{5.20}$$

Equation (5.19) implies $\Psi_{40} = 0$ and $\Psi_{41} = 0$. This result coupled with the Eq. (5.20) results in $\Psi_{4r} = 0$ for any r. This result eliminates the explicit contribution to warping due to axial strain. Hence, we are left with a solution of the form

$$\begin{aligned} W(\xi_1,\xi_2,\xi_3) = &\left(\overline{\kappa}_1\Psi_{10} + \partial^2_{\xi_1}\overline{\kappa}_1.\Psi_{12} + \partial^4_{\xi_1}\overline{\kappa}_1.\Psi_{14} + \ldots\right) + \left(\partial_{\xi_1}\overline{\kappa}_2.\Psi_{21} + \partial^3_{\xi_1}\overline{\kappa}_2.\Psi_{23} + \partial^5_{\xi_1}\overline{\kappa}_2.\Psi_{25} + \ldots\right) \\ &+ \left(\partial_{\xi_1}\overline{\kappa}_3.\Psi_{31} + \partial^3_{\xi_1}\overline{\kappa}_3.\Psi_{33} + \partial^5_{\xi_1}\overline{\kappa}_3.\Psi_{35} + \ldots\right). \end{aligned} \tag{5.21}$$

5.3.2 On the non-uniform shear based warping functions Ψ_{31} and Ψ_{21}

Proposition 5.1: The warping contribution $\partial_{\xi_1}\overline{\kappa}_3.\Psi_{31}$ (or $\partial_{\xi_1}\overline{\kappa}_2.\Psi_{21}$) in Eq. (5.21) represents the out-of-plane deformation of the cross-section due a non-uniform shear stress field induced by bending about $\boldsymbol{E}_3$ (or $\boldsymbol{E}_2$). This implies that the slope $\partial_{\xi_1}\overline{\kappa}_3.\partial_{\xi_2}\Psi_{31}$ (or $\partial_{\xi_1}\overline{\kappa}_2.\partial_{\xi_2}\Psi_{21}$) is the shear strain profile of the cross-section.

Proof: The warping is dependent on the geometry of the cross section. Therefore, let us consider a rectangular prismatic beam with the depth d and breadth b to proceed with further discussion. For the proof, we assume that the claim is true and arrive at the governing equation for Ψ_{31} as in Eq. (5.17). If $M(\xi_1)$ and $V(\xi_1)$ represent the cross-sectional bending moment (about $\boldsymbol{E}_3$) and shear respectively, then we know from the theory of bending that $V = \partial_{\xi_1}M$ and $M = \overline{\kappa}_3 EI_{33}$,

where $I_{33} = \frac{1}{12}bd^3$ is the moment of inertia about $\boldsymbol{E}_3$ axis. The expression for the shear strain profile of rectangular section is given as,

$$\gamma_{12} = \frac{6V}{Gbd^3}\left(\frac{d^2}{4} - \xi_2^2\right) = \frac{6EI_{33}.\partial_{\xi_1}\overline{\kappa}_3}{Gbd^3}\left(\frac{d^2}{4} - \xi_2^2\right) \tag{5.22}$$

Note that Poisson's effect is ignored in traditional beam theory limiting the constant $C_1 = \frac{E}{G}$ (in Eq. (5.10)). Substituting for I_{33} and C_1, the shear strain profile reduces to

$$\gamma_{12} = \frac{C_1.\partial_{\xi_1}\overline{\kappa}_3}{2}\left(\frac{d^2}{4} - \xi_2^2\right). \tag{5.23}$$

From our claim,

$$\begin{aligned} \partial_{\xi_1}\overline{\kappa}_3.\partial_{\xi_2}\Psi_{31} &= \gamma_{12}; \\ \partial_{\xi_2}\Psi_{31} &= \frac{C_1}{2}\left(\frac{d^2}{4} - \xi_2^2\right). \end{aligned} \tag{5.24}$$

Taking the derivative with ξ_2, and noting that γ_{12} is not a function of ξ_3 (implying $\partial^2_{\xi_3}\Psi_{31}$), we can write

$$\nabla^2\Psi_{31} = -C_1\xi_2 \ \text{ on } \ \mathfrak{B}(\xi_1). \tag{5.25}$$

We also note that for bending about $\boldsymbol{E}_3$, we have $\partial_{\xi_2}\Psi_{31}|_{\xi_2=\frac{d}{2}} = 0$ and $\partial_{\xi_3}\Psi_{31} = 0$ (because Ψ_{31} does not have ξ_3 dependence), implying

$$\partial_{\boldsymbol{n}}\Psi_{31} = 0 \ \text{ on } \ \Gamma(\xi_1). \tag{5.26}$$

This completes the proof. The results here can be extended to the warping function Ψ_{21}. □.

5.3.2.1 Non-uniform shear based warping function for rectangular section

Timoshenko's beam theory assumes plane cross-section remains plane after deformation but relaxes the restriction of cross-section remaining perpendicular to the neutral surface. Thus, assuming constant shear strain of $\gamma_{12} = \frac{1.5V}{Gbd} = 1.5\frac{E}{G}\left(\frac{d^2}{4}\right)$ for a rectangular section with a shear coefficient 1.5. This leads us to define an equivalent warping function that incorporates

Timoshenko shear deformation as

$$\begin{aligned}\Psi^t_{31} &= \frac{E}{2G}\left(\frac{d^2}{4}\xi_2\right);\\ \Psi^t_{21} &= \frac{E}{2G}\left(\frac{d^2}{4}\xi_3\right);\end{aligned} \tag{5.27}$$

such that if $v(\xi_1)$ and $w(\xi_1)$ represent total transverse displacement (including shear and bending) of the midcurve in $\boldsymbol{E}_2$ and $\boldsymbol{E}_3$ respectively and $\theta_2(\xi_1)$ and $\theta_3(\xi_1)$ represents bending rotations about the axes $\boldsymbol{E}_2$ and $\boldsymbol{E}_3$, respectively, then

$$\begin{aligned}\partial_{\xi_1} v - \theta_3 &= \partial_{\xi_1}\overline{\kappa}_3.\partial_{\xi_2}\Psi^t_{31};\\ \partial_{\xi_1} w + \theta_2 &= \overline{\kappa}_2.\partial_{\xi_3}\Psi^t_{21}.\end{aligned} \tag{5.28}$$

Using Eq.(5.24) and the fact that $\Psi_{31}(0,0) = \Psi_{21}(0,0) = 0$, the warping functions Ψ_{31} (or Ψ_{21}) are obtained as,

$$\begin{aligned}\Psi_{31} &= \frac{E}{2G}\left(\frac{d^2}{4}\xi_2 - \frac{\xi_2^3}{3}\right) = \Psi^t_{31} - \frac{E}{2G}\left(\frac{\xi_2^3}{3}\right);\\ \Psi_{21} &= \frac{E}{2G}\left(\frac{d^2}{4}\xi_3 - \frac{\xi_3^3}{3}\right) = \Psi^t_{21} - \frac{E}{2G}\left(\frac{\xi_3^3}{3}\right).\end{aligned} \tag{5.29}$$

Figure 5.1 illustrates the discussion here.

5.3.2.2 A practically useful warping function for large deformation

From the previous discussion, its clear that Ψ^t_{21} and Ψ^t_{31} are the linear part of the warping function Ψ_{21} and Ψ_{31} respectively. The displacement field assumed in (4.19) does not have shear deformation added explicitly. However, the inclusion of the warping component $\partial_{\xi_1}\overline{\kappa}_3.\Psi_{31}$ and $\partial_{\xi_1}\overline{\kappa}_2.\Psi_{21}$ generalizes the shear deformation assumed by Timoshenko to include out of plane bending-induced shear warping. Therefore, we should be careful in using this general warping solution if the shear deformations are explicitly added. Since the kinematics developed in this paper includes finite shear, we propose a simplified warping function for the large deformation

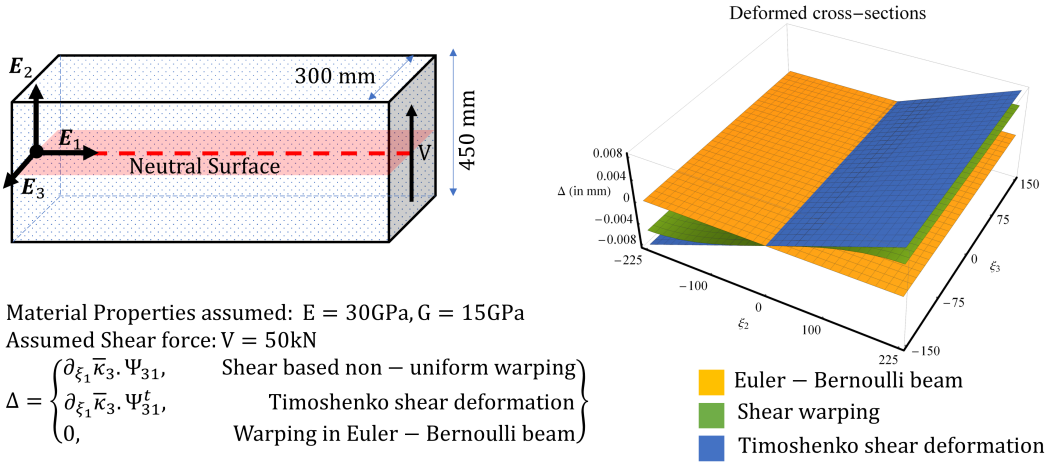

Figure 5.1: Example of non-uniform shear deformation of the rectangular cross-section in the beam subjected to plane bending.

problem as,

$$W(\xi_1,\xi_2,\xi_3) = \overline{\kappa}_1(\xi_1)\Psi_{10} + \partial_{\xi_1}\overline{\kappa}_2.(\Psi_{21} - \Psi^t_{21}) + \partial_{\xi_1}\overline{\kappa}_3.(\Psi_{31} - \Psi^t_{31}). \tag{5.30}$$

Secondly, an alternative warping function that can be defined as an improved version of warping used by Simo and Vu-Quoc [43] (as defined by equation (4.10)) as,

$$W(\xi_1,\xi_2,\xi_3) = p(\xi_1)\Psi_s + \partial_{\xi_1}\overline{\kappa}_2.(\Psi_{21} - \Psi^t_{21}) + \partial_{\xi_1}\overline{\kappa}_3.(\Psi_{31} - \Psi^t_{31}). \tag{5.31}$$

Here, $p(\xi_1)$ is the warping amplitude and an additional unknown finite strain parameter.

5.3.3 The end support conditions for warping

There are two possible end conditions for warping– *wholly restrained* and the *unrestrained*. Wholly restrained warping implies $W = 0$ at the end support. Unrestrained warping would eliminate a contribution of warping to the stress component σ_{11} at the end support resulting in

$\partial_{\xi_1} W = 0$. If a solution of form (5.21) is used, we can obtain the warping end conditions by imposing the following:

$$\text{Warping wholly restrained: } \partial^p_{\xi_1}\overline{\kappa}_1 = 0;\ \ \partial^q_{\xi_1}\overline{\kappa}_2 = 0 \ \text{ and } \ \partial^q_{\xi_1}\overline{\kappa}_3 = 0 \quad \text{for all even } \ p \geq 0 \ \text{ and for all odd } \ q \geq 1. \tag{5.32}$$

$$\text{Warping unrestrained: } \partial^p_{\xi_1}\overline{\kappa}_1 = 0;\ \ \partial^q_{\xi_1}\overline{\kappa}_2 = 0 \ \text{ and } \ \partial^q_{\xi_1}\overline{\kappa}_3 = 0 \quad \text{for all odd } \ p \geq 1 \ \text{ and for all even } \ q \geq 2. \tag{5.33}$$

5.3.3.1 An alternative way of arriving at the end support conditions for warping

Consider an end support condition with warping unrestrained. Such a warping function must satisfy $\partial_{\xi_1} W = 0$ for all the material points (ξ_2, ξ_3) across the cross-section of end support. Let us call this as *unrestrained warping condition*. Differentiating Eq. (5.9b), with respect to the arc-length ξ_1, we get,

$$\partial_{\xi_1}\partial_{\boldsymbol{n}} W = -\partial_{\xi_1}\overline{\kappa}_1.t + \left(\nu C_2 \int_{\mathfrak{B}} \partial^3_{\xi_1} W \, \mathrm{d}\xi_2 \mathrm{d}\xi_3\right)\tilde{t}. \tag{5.34}$$

As an implication of *unrestrained warping condition*, we have $\partial_{\xi_1}\partial_{\boldsymbol{n}} W = 0$. This can be guaranteed from Eq. (5.34) if following is satisfied at the end support:

$$\partial_{\xi_1}\overline{\kappa}_1 = 0 \ \text{ and } \ \int_{\mathfrak{B}} \partial^3_{\xi_1} W \, \mathrm{d}\xi_2 \mathrm{d}\xi_3 = 0. \tag{5.35}$$

Equation (5.35) is a part of much larger set of end conditions. To proceed further, we take the derivative of Eq. (5.9a) with respect to ξ_1 and use the previous result (5.35), obtaining

$$\partial^3_{\xi_1} W + \frac{1}{C_1}.\partial_{\xi_1}\nabla^2 W = \frac{1}{C_1}\left(\xi_2.\partial^2_{\xi_1}\overline{\kappa}_3 - \xi_3.\partial^2_{\xi_1}\overline{\kappa}_2\right). \tag{5.36}$$

Once again, as a result of *unrestrained warping condition*, we have $\partial_{\xi_1}\nabla^2 W = 0$. This result coupled with Eq. (5.36), implies $\partial^3_{\xi_1} W = \frac{1}{C_1}\left(\xi_2.\partial^2_{\xi_1}\overline{\kappa}_3 - \xi_3.\partial^2_{\xi_1}\overline{\kappa}_2\right)$, which is identically satisfied if

$$\partial^3_{\xi_1} W = 0, \ \ \partial^2_{\xi_1}\overline{\kappa}_2 = 0 \ \text{ and } \ \partial^2_{\xi_1}\overline{\kappa}_3 = 0. \tag{5.37}$$

We can continue the process of obtaining odd derivatives of Eq. (5.9a) and (5.9b) with respect to ξ_1 and proceed along the same reasoning used to obtain Eq. (5.35) and (5.37) to arrive at the end condition for the case of *unrestrained warping* as described in Eq. (5.32). In the very same way, we can obtain the set of end conditions for *warping wholly restrained*.

5.4 Solution approach 2: Solution of warping function using trigonometric series

5.4.1 The governing differential equations

The warping function W depends on the curvatures and the end support conditions. For a small (linear) deformation, we define the component of the displacement field $v_1(\xi_1)$, $v_2(\xi_1)$, $v_3(\xi_1)$ that represents the motion of the mid-curve due to axial deformation and bending. For small deformations, $\partial_{\xi_1} v_1 = e(\xi_1)$, $\partial^2_{\xi_1} v_2 = \overline{\kappa}_3$ and $\partial^2_{\xi_1} v_3 = -\overline{\kappa}_2$. Secondly if θ represents the angular rotation due to torsion, then $\partial_{\xi_1}\theta = \overline{\kappa}_1(\xi_1)$. To demonstrate the solution procedure of the modified consistent differential equation (5.9a) and (5.9b) using trigonometric series, we assume simple support at the end as in Brown et. al. [42]. The admissible end conditions for small deformation are

$$\begin{aligned} \theta = v_2 = v_3 = 0 \ \text{ at } \ \xi_1 = 0, L; \\ M_2 = M_3 = 0 \ \text{ at } \ \xi_1 = 0, L. \end{aligned} \tag{5.38}$$

Since, the consistent governing equation does not explicitly depend on the axial strain, we ignore the admissibility of the deformation field $v_1(\xi_1)$. We choose the strain parameters such that the

displacement and force boundary conditions are satisfied.

$$\begin{aligned}
\overline{\kappa}_1(\xi_1) &= \sum_{m=1}^{\infty} k_{1m} \cos\left(\frac{m\pi\xi_1}{L}\right); \\
\overline{\kappa}_2(\xi_1) &= \sum_{m=1}^{\infty} k_{2m} \sin\left(\frac{m\pi\xi_1}{L}\right); \\
\overline{\kappa}_3(\xi_1) &= \sum_{m=1}^{\infty} k_{3m} \sin\left(\frac{m\pi\xi_1}{L}\right); \\
W(\xi_1,\xi_2,\xi_3) &= \Psi_0(\xi_2,\xi_3) + \sum_{m=1}^{\infty} \Psi_m(\xi_2,\xi_3) \cos\left(\frac{m\pi\xi_1}{L}\right).
\end{aligned} \tag{5.39}$$

Substituting Eq. (5.39) into the equation set (5.9a) and (5.9b) and observing the orthogonality of trigonometric functions leads to the following,

Governing equation for Ψ_0: We have,

$$\nabla^2\Psi_0 = 0 \ \text{ on } \ \mathfrak{B}(\xi_1) \ \text{ with } \ \partial_{\boldsymbol{n}}\Psi_0 = 0 \ \text{ on } \ \Gamma(\xi_1). \tag{5.40}$$

Following similar reasoning as above, $\Psi_0 = 0$, to avoid any rigid body contribution due to warping.

Governing equation for Ψ_m with $m \geq 1$:

$$\nabla^2\Psi_m - C_1\left(\frac{m^2\pi^2}{L^2}\right)\Psi_m = C_1\left(\frac{m\pi}{L}\right)(k_{3m}\xi_2 - k_{2m}\xi_3) + C_2\overline{\lambda}\left(\frac{m^2\pi^2}{L^2}\right)\int_{\mathfrak{B}} \Psi_m \, \mathrm{d}\xi_2\mathrm{d}\xi_3 \ \text{ on } \ \mathfrak{B}(\xi_1); \tag{5.41a}$$

$$\partial_{\boldsymbol{n}}\Psi_m = -k_{1m}t - \left\{C_2\nu\left(\frac{m^2\pi^2}{L^2}\right)\int_{\mathfrak{B}} \Psi_m \, \mathrm{d}\xi_2\mathrm{d}\xi_3\right\}\tilde{t} \ \text{ on } \ \Gamma(\xi_1). \tag{5.41b}$$

The integral $\int_{\mathfrak{B}} \Psi_m \, \mathrm{d}\xi_2\mathrm{d}\xi_3$ can be obtained from the $\partial_{\xi_1} e$ field, by substituting the warping function as in Eq. (5.39) into the *inconsistency condition* (5.6) and utilizing the orthogonality relationship of trigonometric functions,

$$I_m(\xi_1) = \int_{\mathfrak{B}} \Psi_m \, \mathrm{d}\xi_2\mathrm{d}\xi_3 = \left(\frac{\tilde{\lambda} - 2\nu\lambda}{\tilde{\lambda}}\right)\left(\frac{L^2}{m^2\pi^2}\right) A(\xi_1) \sec\left(\frac{m\pi\xi_1}{L}\right)\int_0^L e_{,\xi_1}\left(\cos\frac{m\pi\xi_1}{L}\right) \mathrm{d}\xi_1. \tag{5.42}$$

Similarly, the Fourier coefficients k_{1m}, k_{2m} and k_{3m} can be obtained as,

$$k_{1m} = \frac{2}{L}\int_0^L \overline{\kappa}_1(\xi_1)\cos\left(\frac{m\pi\xi_1}{L}\right)\,\mathrm{d}\xi_1; \tag{5.43a}$$

$$k_{2m} = \frac{2}{L}\int_0^L \overline{\kappa}_2(\xi_1)\sin\left(\frac{m\pi\xi_1}{L}\right)\,\mathrm{d}\xi_1; \tag{5.43b}$$

$$k_{3m} = \frac{2}{L}\int_0^L \overline{\kappa}_3(\xi_1)\sin\left(\frac{m\pi\xi_1}{L}\right)\,\mathrm{d}\xi_1. \tag{5.43c}$$

Check for consistency of equation (5.41a) **and** (5.41b)**:** Using equation (5.41b), Gauss theorem and the results in equations (5.1a) and (5.1b), we have,

$$\begin{aligned}\int_{\mathfrak{B}} \nabla^2\Psi_m \mathrm{d}\xi_2\,\mathrm{d}\xi_3 = \oint \partial_{\boldsymbol{n}}\Psi_m\,\mathrm{d}\Gamma &= -k_{1t}\oint t\mathrm{d}\Gamma - \left\{C_2\nu\left(\frac{m^2\pi^2}{L^2}\right)\int_{\mathfrak{B}}\Psi_m\,\mathrm{d}\xi_2\mathrm{d}\xi_3\right\}\oint \tilde{t}\mathrm{d}\Gamma \\ &= -\left\{2\nu A C_2\left(\frac{m^2\pi^2}{L^2}\right)\int_{\mathfrak{B}}\Psi_m\,\mathrm{d}\xi_2\mathrm{d}\xi_3\right\}.\end{aligned} \tag{5.44}$$

Integrating equation (5.41a) across the cross-section $\mathfrak{B}(\xi_1)$, we have,

$$\begin{aligned}\int_{\mathfrak{B}} \nabla^2\Psi_m\,\mathrm{d}\xi_2\mathrm{d}\xi_3 = C_1\left(\frac{m^2\pi^2}{L^2}\right)\int_{\mathfrak{B}}\Psi_m\,\mathrm{d}\xi_2\mathrm{d}\xi_3 + C_1\left(\frac{m\pi}{L}\right)\Bigg(k_{3m}\overbrace{\int_{\mathfrak{B}}\xi_2\,\mathrm{d}\xi_2\mathrm{d}\xi_3}^{0} - k_{2m}\overbrace{\int_{\mathfrak{B}}\xi_3\,\mathrm{d}\xi_2\mathrm{d}\xi_3}^{0}\Bigg) \\ + C_2 A\overline{\lambda}\left(\frac{m^2\pi^2}{L^2}\right)\int_{\mathfrak{B}}\Psi_m\,\mathrm{d}\xi_2\mathrm{d}\xi_3 = \left(C_2 A\overline{\lambda} + C_1\right)\left(\frac{m^2\pi^2}{L^2}\right)\int_{\mathfrak{B}}\Psi_m\,\mathrm{d}\xi_2\mathrm{d}\xi_3.\end{aligned} \tag{5.45}$$

The consistency between equations (5.41a) and (5.41b) can be proved from equations (5.44) and (5.45), if we can show that $C_1 + C_2 A\overline{\lambda} = -2\nu A C_2$. Using the definitions of C_1, C_2, and $\overline{\lambda}$, we have

$$C_1 + C_2 A\overline{\lambda} = \frac{\tilde{\lambda}}{G} - \overbrace{\left(\frac{\tilde{\lambda} + 2\nu(G-\tilde{\lambda})}{G}\right)}^{\overline{\lambda}}\left(\frac{\tilde{\lambda}}{\tilde{\lambda}-2\nu\lambda}\right) = 2\left(\frac{\nu\tilde{\lambda}}{\tilde{\lambda}-2\nu\lambda}\right) = -2\nu A C_2. \tag{5.46}$$

Therefore, the governing differential equations for Ψ_m are consistent.

5.4.2 Solving for Ψ_m

Consider a solution of the form

$$\Psi_m = \Psi_{0m} + \sum_{i=1}^{3} \Psi_{im} k_{im}. \tag{5.47}$$

The functions Ψ_{jm} for $j = 0 - 3$ satisfies four set of differential equations. The governing differential equations for Ψ_{0m} are,

$$\nabla^2 \Psi_{0m} - C_1 \left(\frac{m^2\pi^2}{L^2}\right) \frac{\tilde{\lambda}}{G} \Psi_{0m} = C_2 \overline{\lambda} \left(\frac{m^2\pi^2}{L^2}\right) I_m(\xi_1) \text{ at } \mathfrak{B}(\xi_1); \tag{5.48a}$$

$$\partial_{\boldsymbol{n}} \Psi_{0m} = -C_2 \nu \left(\frac{m^2\pi^2}{L^2}\right) I_m(\xi_1) \tilde{t} \text{ at } \Gamma(\xi_1). \tag{5.48b}$$

The governing differential equations for Ψ_{1m} are,

$$\nabla^2 \Psi_{1m} - C_1 \left(\frac{m^2\pi^2}{L^2}\right) \frac{\tilde{\lambda}}{G} \Psi_{1m} = 0 \text{ at } \mathfrak{B}(\xi_1); \tag{5.49a}$$

$$\partial_{\boldsymbol{n}} \Psi_{1m} = -t \text{ at } \Gamma(\xi_1). \tag{5.49b}$$

The governing differential equations for Ψ_{2m} are,

$$\nabla^2 \Psi_{2m} - C_1 \left(\frac{m^2\pi^2}{L^2}\right) \frac{\tilde{\lambda}}{G} \Psi_{2m} = -C_1 \left(\frac{m\pi}{L}\right) \xi_3 \text{ at } \mathfrak{B}(\xi_1); \tag{5.50a}$$

$$\partial_{\boldsymbol{n}} \Psi_{2m} = 0 \text{ at } \Gamma(\xi_1). \tag{5.50b}$$

The governing differential equations for Ψ_{3m} are,

$$\nabla^2 \Psi_{3m} - C_1 \left(\frac{m^2\pi^2}{L^2}\right) \frac{\tilde{\lambda}}{G} \Psi_{3m} = C_1 \left(\frac{m\pi}{L}\right) \xi_2 \text{ at } \mathfrak{B}(\xi_1); \tag{5.51a}$$

$$\partial_{\boldsymbol{n}} \Psi_{3m} = 0 \text{ at } \Gamma(\xi_1). \tag{5.51b}$$

We can obtain the functions Ψ_{jm} with $j = 0 - 4$ by solving the equation set (5.48a)-(5.51b). Therefore, the warping function W can be obtained using equation (5.39), the Fourier coefficients as defined in equation set (5.43a)-(5.43c) and equation (5.47).

5.5 Summary

This chapter tackles the inconsistencies observed in the governing differential equations of warping. Two possible solution approaches to obtain the warping function in the variable separable form are explored. For the Poisson's ratio $\nu = 0$, the presented theory of warping reduces to the theory presented by Burgoyne and Brown in [41] and [42]. End support conditions for warping are explored. A practically useful warping function that includes the warping due to non-uniform torsion and bending induced shear is presented. Chapter 10 utilizes the simplified warping function defined in Eq. (5.31) to develop finite element code for the geometrically-exact beam.

The discussion carried out in this chapter has been published in the International Journal of Solids and Structures, Mayank Chadha and Michael D. Todd [34], 2019. The title of this paper is: "A comprehensive kinematic model of single-manifold Cosserat beam structures with application to a finite strain measurement model for strain gauges". The dissertation author is the primary investigator and author of this paper.

Chapter 6

Measurement Model for Strain Gauges and Shape Reconstruction of Slender Structures

6.1 Introduction

This chapter can be divided into two broader parts. In the first part, we delineate measurement model for *finite length* strain gauges, as well as *discrete* (or *point*) strain gauges attached to the surface or the beam or embedded into it. The measurement model constitutes a formula that relates the strain value measured by the strain gauge to the kinematic quantities of the beam. We then simplify the expression of the discrete strain gauge measurement model for small strain but large deformation and exploit it to develop a shape reconstruction methodology for slender structures. That constitutes the second part of this chapter.

Strain measurement devices ("strain gauges") are immensely important for a wide variety of measurement and monitoring applications ranging across civil structures, the energy sector, aerospace structures, and even biomedical systems, to name just a few. The development of

sensing mechanisms that measure strain has been a well-developed field for over a century; the solutions have spanned piezo-resistive gauges (arguably the most common and commercially-realized) to fiber optic systems to laser Doppler velocimetry (LDV). The sensing mechanism itself may require contact between the measuring device and structure (e.g., piezo-resistive gauges or fiber optics) or be non-contact (e.g., LDV). Realizations of these architectures can result in localized measurements (discrete measurement points with a fixed length scale) or distributed measurements (e.g., fiber optic Rayleigh backscatter sensing [57], where the length scale and location of measurement depending on the optical pulsing).

A significant number of these monitoring applications for which strain measurements are required involve, fundamentally, one-dimensional slender structures. In this chapter, we exploit the kinematics developed in chapter 5 to develop a measurement model for the scalar strain of *discrete* and *finite-length* strain gauges assumed affixed to the surface of the beam or embedded in the beam. The measurement gauge length of the measuring device must be small enough to classify it as a discrete sensor. A discrete strain gauge is treated like an infinitesimal (tangent) vector. We arrive at the *Pull-back Riemannian Metric* of the beam that is key in developing the expression of the strain that would be detected by a finite length strain gauge. We validate our result by demonstrating the applicability of the expression obtained on a simple case of deformation that includes constant torsion, axial strain, and Poisson's effect.

There are multiple instances where it is desirable to reconstruct the full-field deformed shape of a very long, slender object such as pipelines, suspension cables, tethers, surgical tubing, catheters, and others. For instance, the underground pipelines are prone to severe damage due to seismic activities like earthquake, liquefaction- induced lateral spreading, landslide, and others. These events have global effect on the pipeline configuration. Earthquakes causes transient ground deformation and permanent ground deformations. In the simplest sense, the primary cause of underground pipeline deformation is the movement of soil mass associated with the seismic activities. There is abrupt ground deformation at the margin of landslide. The schematic diagram

of the strike-slip fault effecting the underground pipeline is shown below. Hence, monitoring

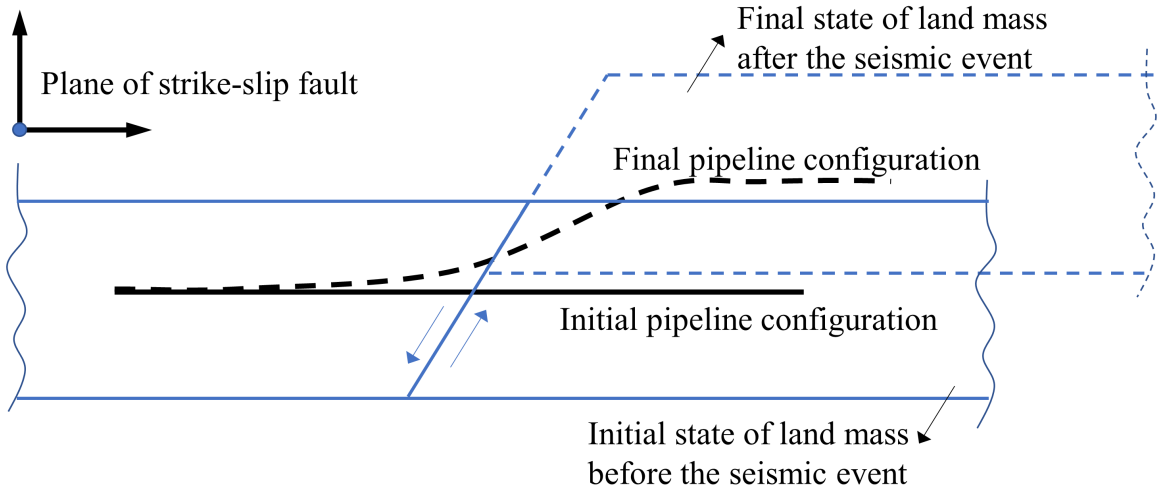

Figure 6.1: Schematic diagram of strike-slip fault.

the performance of underground pipelines during these seismic events and in real time is equally important as developing resilient design methodologies for the same.

We exploit the strain measurement model for discrete strain gauge to construct a shape-reconstruction methodology of slender structures from a limited set of scalar surface strain measurements. It is an exhaustive approach that captures the effect of curvature, shear, torsion, and elongation restricted to rigid cross-section assumption, such that the final deformed state is Ω_1. The inclusive consideration of shear effects extends the validity of the proposed approach to even more moderately-slender objects like beams or connecting rods while generally providing robustness in the predicted results. This theory mainly targets the single-manifold structures that are subjected to finite strains and large deformations.

The idea is to infer the global displacement (defined by the locus of the mid-curve) and the cross-sectional orientation (defined by shear and torsion) of such structures in their deformed state, using distributed sensing of some kind. As mentioned in Todd et al. [16], distributed sensing may be grouped into two types: non-contact (the sensing mechanism is remote, such as using Laser Doppler Vibrometry (LDV)), and contact (the sensing mechanism is affixed to the object

for in-situ measurement). Like [16], this theory focuses on the latter group of sensing methods, since a large number of applications do not lend themselves to the strict limitations of non-contact methods, such as line-of-sight or ranging restrictions. Conventional contact sensors typically involve measurement of kinematic/kinetic properties such as strain or acceleration (distributed or discrete) and then obtain the global displaced shape by means of some inverse model. This theory further considers the case of the measurement of a finite set of local, uniaxial, discrete strain readings that are obtained through any type of sensing approach, including Fiber Bragg Grating (FBG), Rayleigh back-scattering (refer to [57], [58] and [59]) or conventional resistive strain gauges. The aim is to develop a comprehensive inverse model that provides three-dimensional deformed shape and the kinematic generalized coordinates (like shear angles, curvatures, and elongations) from these limited sets of uniaxial strain values. This chapter extends the ideas presented in [16] and related works by including far more comprehensive mechanics in the model, allowing for applicability to a greater range of slender structures (such as non-negligible cross-sectional shear deformation).

6.2 On finite length strain gauge measurement

6.2.1 Geometric description of the deformation of finite strain gauge

Consider a strain gauge of finite length l_0 (not necessarily small) attached to the surface of beam $\mathfrak{S}_0$ in the undeformed state Ω_0. Let $a \in \mathfrak{S}_0$ and $b \in \mathfrak{S}_0$ represent two ends of the finite strain gauge. Let us consider the unstrained segment of FBG sensor as a space curve $\boldsymbol{\alpha} : [0, l_0] \longrightarrow \mathfrak{S}_0$, with $\boldsymbol{\alpha}(0) = a$ and $\boldsymbol{\alpha}(l_0) = b$, such that,

$$\boldsymbol{\alpha}(t) = \xi_i(t)\boldsymbol{E}_i, \;\; t \in [0, l_0], \;\; (\xi_1, \xi_2, \xi_3) \in \mathfrak{S}_0. \tag{6.1}$$

The curve $\boldsymbol{\alpha}(t)$ is parameterized by its arc-length t. Therefore, $\partial_t \boldsymbol{\alpha}(t) \in T_{\boldsymbol{\alpha}(t)}\mathfrak{S}_0$ is a unit tangent vector along the curve. Here, $T_{\boldsymbol{\alpha}(t)}\mathfrak{S}_0$ represents the tangent space of the manifold $\mathfrak{S}_0$

restricted to the curve $\boldsymbol{\alpha}(t)$. The curve $\boldsymbol{\alpha}(t)$ maps to the curve $\boldsymbol{\phi}_j(\boldsymbol{\alpha}(t)) = \boldsymbol{\beta}_j(t) : [0, l_0] \longrightarrow \mathfrak{S}_j$,

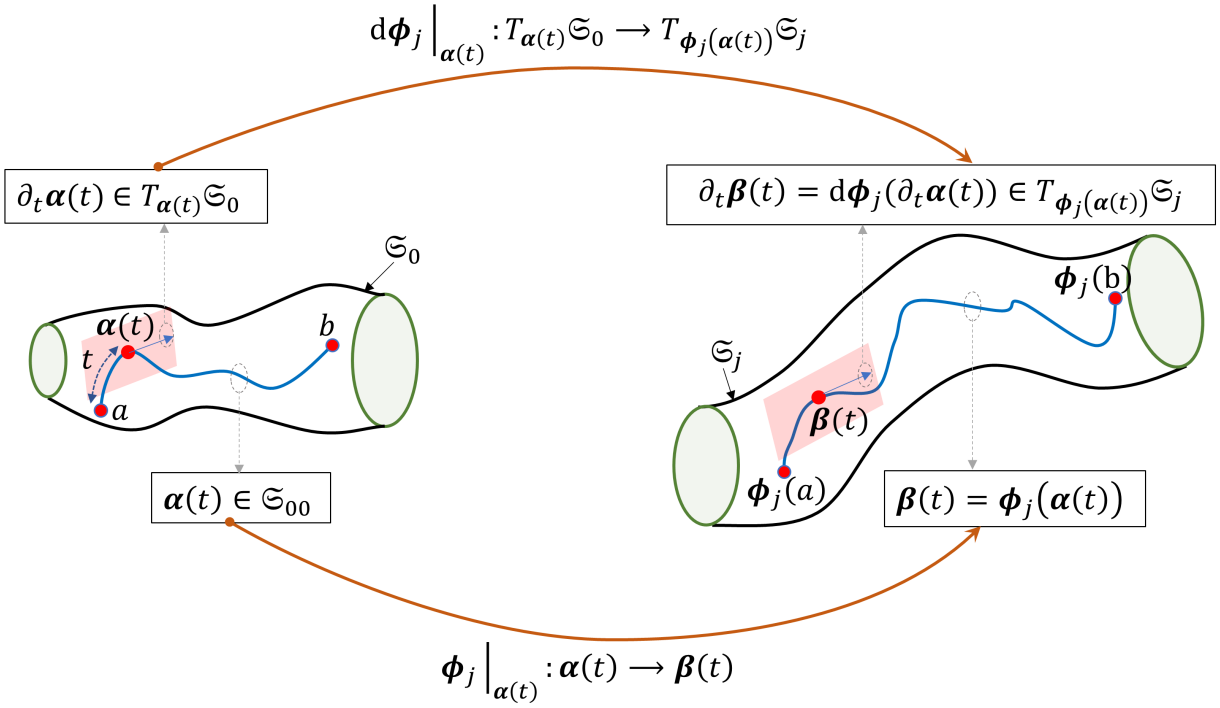

Figure 6.2: Deformation of a finite length curve on the beam surface.

such that $\boldsymbol{F}_j.\partial_t\boldsymbol{\alpha}(t) = \partial_t\boldsymbol{\beta}_j(t) \in T_{\boldsymbol{\phi}(\boldsymbol{\alpha}(t))}\mathfrak{S}_j$. The vector field $\partial_t\boldsymbol{\beta}_j(t)$ is not a unit vector as t is not the arc length of the curve $\boldsymbol{\beta}(t)$. The magnitude of the tangent vector $\partial_t\boldsymbol{\beta}_j(t)$ can be obtained as

$$\begin{aligned}\|\partial_t\boldsymbol{\beta}_j(t)\| &= \Big(\partial_t\boldsymbol{\beta}_j(t)\cdot\partial_t\boldsymbol{\beta}_j(t)\Big)^{\frac{1}{2}} = \big((\boldsymbol{F}_j.\partial_t\boldsymbol{\alpha}(t))\cdot(\boldsymbol{F}_j.\partial_t\boldsymbol{\alpha}(t))\big)^{\frac{1}{2}} = \Big(\partial_t\boldsymbol{\alpha}(t)\cdot(\boldsymbol{F}_j^T.\boldsymbol{F}_j.\partial_t\boldsymbol{\alpha}(t))\Big)^{\frac{1}{2}} \\ &= \big(\partial_t\boldsymbol{\alpha}(t)\cdot(\boldsymbol{C}_j.\partial_t\boldsymbol{\alpha}(t))\big)^{\frac{1}{2}}.\end{aligned} \tag{6.2}$$

Here, $\boldsymbol{C}_j = \boldsymbol{F}_j^T.\boldsymbol{F}_j = \boldsymbol{U}_j^T.\boldsymbol{U}_j$ represents the *right Cauchy Green deformation tensor*. In fact, the Cauchy Green deformation tensor can be thought as a *pull-back Riemannian Metric* (refer chapter 2 of Do Carmo [15] and Chapter 1 Marsden and Hughes [60]) in the deformed configuration Ω_j (and the surface $\mathfrak{S}_j$ as well). This is because for any pair of tangent vector $\boldsymbol{v}_1, \boldsymbol{v}_2 \in T_p\Omega_0$ (or $T_q\mathfrak{S}_0$), the tensor $\boldsymbol{C}_j$ associates an inner product $\big((\boldsymbol{F}_j.\boldsymbol{v}_1)\cdot(\boldsymbol{F}_j.\boldsymbol{v}_2)\big)$ on the tangent space $T_{\boldsymbol{\phi}(p)}\Omega_j$ (or $T_{\boldsymbol{\phi}(q)}\mathfrak{S}_j$) such that $\boldsymbol{F}_j.\boldsymbol{v}_1, \boldsymbol{F}_j.\boldsymbol{v}_2 \in T_{\boldsymbol{\phi}(p)}\Omega_j$ (or $T_{\boldsymbol{\phi}(q)}\mathfrak{S}_j$). The length of the curve $\boldsymbol{\beta}(t)$ as a function

of the parameter t is obtained as,

$$l_j(t) = \int_0^t \|\partial_t \boldsymbol{\beta}_j(k)\| \mathrm{d}k. \tag{6.3}$$

The scalar strain $\mathrm{e}_j^{\mathrm{f}}(t)$ (the super-script "f" stands for *finite length strain gauge* and the sub-script j indicates that the deformed configuration is Ω_j) at the material point $(\xi_1(t), \xi_2(t), \xi_3(t)) \in \Omega_j$ and the average scalar strain $\mathrm{e}_{j_{\mathrm{avg}}}^{\mathrm{f}}(t)$ in the strain gauge are obtained as,

$$\begin{aligned} \mathrm{e}_j^{\mathrm{f}}(t) &= \|\partial_t \boldsymbol{\beta}_j(t)\| - 1; \\ \mathrm{e}_{j_{\mathrm{avg}}}^{\mathrm{f}}(t) &= \frac{l_j(t = l_0)}{l_0} - 1. \end{aligned} \tag{6.4}$$

Figure 6.2 shows the construction discussed above.

6.2.2 Illustration

Consider a cantilever beam with circular cross-section of radius $r = 0.05$ m and length $l_0 = 1$ m. Let the finite length strain gauge join the material point $a = (0, 0, 0.05) \in \mathfrak{S}_0$ and $b = (1, 0, 0.05) \in \mathfrak{S}_0$ giving a straight curve $\boldsymbol{\alpha}(t) = \xi_1(t)\boldsymbol{E}_1 + 0.05\boldsymbol{E}_3$ with $t \equiv \xi_1 \in [0, 1]$. Note that in this case $\partial_t \xi_1(t) = 1$. Hence, $\partial_t \boldsymbol{\alpha}(t) = \boldsymbol{E}_1$. Let the beam be subjected to the following finite strain parameters,

$$\overline{\kappa}_1(\xi_1) = 2\pi, \;\; e(\xi_1) = 0.1, \;\; \text{with} \;\; \nu = 0.3. \tag{6.5}$$

The deformed state for this example is Ω_3 with vanishing $\overline{\kappa}_2, \overline{\kappa}_3$ and W. It is intuitive that the curve $\boldsymbol{\alpha}(t)$ deforms to $\boldsymbol{\beta}_3(t) \in \mathfrak{S}_3$ (hence j=3) which is a helix with pitch length $l_p = (1 + e) = 1.1\ m$, radius $r_1 = (1 - e\nu)r$ and number of turn $n_{\mathrm{turn}} = 1$. From the equation of length of helix, the length of the curve $\boldsymbol{\beta}_3(t)$ can be obtained as,

$$\begin{aligned} l_3 &= 2\pi n_{\mathrm{turn}} \sqrt{r_1^2 + \left(\frac{l_p}{2\pi}\right)^2} = 1.141m; \\ \mathrm{e}_{j_{\mathrm{avg}}}^{\mathrm{f}}(t) &= 14.1\%. \end{aligned} \tag{6.6}$$

Now we obtain the length of the curve $\boldsymbol{\beta}_3(t)$ using the discussion in chapter 4 and the result (4.29). We have,

$$\partial_t \boldsymbol{\beta}_3 = \boldsymbol{F}_3.\partial_t \boldsymbol{\alpha}(t) = \boldsymbol{\lambda}_1^3(t) + \boldsymbol{d}_1 = (1 + e(\xi_1(t)))\,.\boldsymbol{d}_1 - \hat{\xi}_3(t).\overline{\kappa}_1(\xi_1(t)).\boldsymbol{d}_2 + \hat{\xi}_2(t).\overline{\kappa}_1(\xi_1(t)).\boldsymbol{d}_3. \quad (6.7)$$

Since the undeformed curve (a mathematical equivalent of unstrained finite length strain gauge) is along $\boldsymbol{E}_1$ with $\xi_2 = 0$, we have $\hat{\xi}_2(t) = 0$ and $\hat{\xi}_3(t) = (1 - e\nu)r$. Hence,

$$l_3 = \int_0^1 \left(\partial_t \boldsymbol{\beta}_3 \cdot \partial_t \boldsymbol{\beta}_3\right)^{\frac{1}{2}} \mathrm{d}t = \int_0^1 \sqrt{\left((1+e)^2 + (1 - e\nu)r\overline{\kappa}_1\right)^2}\mathrm{d}t = 1.141m. \quad (6.8)$$

Thus, the results from Eq. (6.6) and (6.8) are exactly the same.

6.3 On discrete "point" strain measurements

In a strict sense, a discrete point strain gauge is an absurd idea because a point does not strain. In reality, a discrete strain gauge has a small but finite undeformed gauge length associated with it. The discrete strain gauge with small gauge length can be treated by considering it as an infinitesimal vector such that its orientation in the undeformed state is known and gauge length represents the length of the vector. This can help us estimate strain in an average sense, by assuming that the finite strain parameters along the length of discrete strain gauge are constant throughout its length. We consider the value of the deformation gradient tensor at the center point of the strain gauge. Since the gauge length of the discrete strain gauge is small and the finite strain parameters are continuous, this approach gives an excellent estimation of the scalar strain value.

6.3.1 Orientation of the surface strain gauge in the undeformed state Ω_0

Consider the undeformed configuration Ω_0 that consist of continuously varying family of planar cross-sections $\mathfrak{B}_0(\xi_1)$. Consider a strain gauge attached to the point $q_0 = \left(\xi_1^g, \xi_2^g, \xi_3^g\right) \in \mathfrak{S}_0$ such that the unit direction vector $\boldsymbol{n}_0 \in T_{q_0}\mathfrak{S}_0$. The strain gauge can be located from the point on

the mid-curve $p_0 = (0,0) \in \mathfrak{B}_0\left(\xi_1^g\right)$ by the vector $\boldsymbol{r}_0^g = \xi_2^g \boldsymbol{E}_2 + \xi_3^g \boldsymbol{E}_3$. The tangent plane $T_{q_0}\mathfrak{S}_0$ is spanned by the unit orthonormal vectors $\boldsymbol{t}_0\left(\xi_1^g, \xi_2^g, \xi_3^g\right) - \tilde{\boldsymbol{t}}_0\left(\xi_1^g, \xi_2^g, \xi_3^g\right)$. The vector $\tilde{\boldsymbol{t}}_0$ lies in the plane spanned by $\boldsymbol{E}_1 - \boldsymbol{r}_0^g$, such that,

$$\tilde{\boldsymbol{t}}_0 = \cos\tilde{\mu}\boldsymbol{E}_1 + \sin\tilde{\mu}\left(\frac{\boldsymbol{r}_0^g}{\|\boldsymbol{r}_0^g\|}\right) = \cos\tilde{\mu}\boldsymbol{E}_1 + \left(\frac{\xi_2^g \sin\tilde{\mu}}{\sqrt{\xi_2^{g^2} + \xi_3^{g^2}}}\right)\boldsymbol{E}_2 + \left(\frac{\xi_3^g \sin\tilde{\mu}}{\sqrt{\xi_2^{g^2} + \xi_3^{g^2}}}\right)\boldsymbol{E}_3. \tag{6.9}$$

The vector $\boldsymbol{t}_0$ represents the unit tangent vector to the periphery Γ_0 of the cross-section $\mathfrak{B}_0\left(\xi_1^g\right)$, such that

$$\boldsymbol{t}_0 = \boldsymbol{E}_1 \times \left(\frac{\boldsymbol{r}_0^g}{\|\boldsymbol{r}_0^g\|}\right) = -\left(\frac{\xi_3^g}{\sqrt{\xi_2^{g^2} + \xi_3^{g^2}}}\right)\boldsymbol{E}_2 + \left(\frac{\xi_2^g}{\sqrt{\xi_2^{g^2} + \xi_3^{g^2}}}\right)\boldsymbol{E}_3. \tag{6.10}$$

The vector $\boldsymbol{n}_0$ makes an angle μ with the vector $\tilde{\boldsymbol{t}}_0$ at the point q_0. Figure 6.3 describes the orientation of the strain gauge in the undeformed state. The expression for $\boldsymbol{n}_0$ is obtained as,

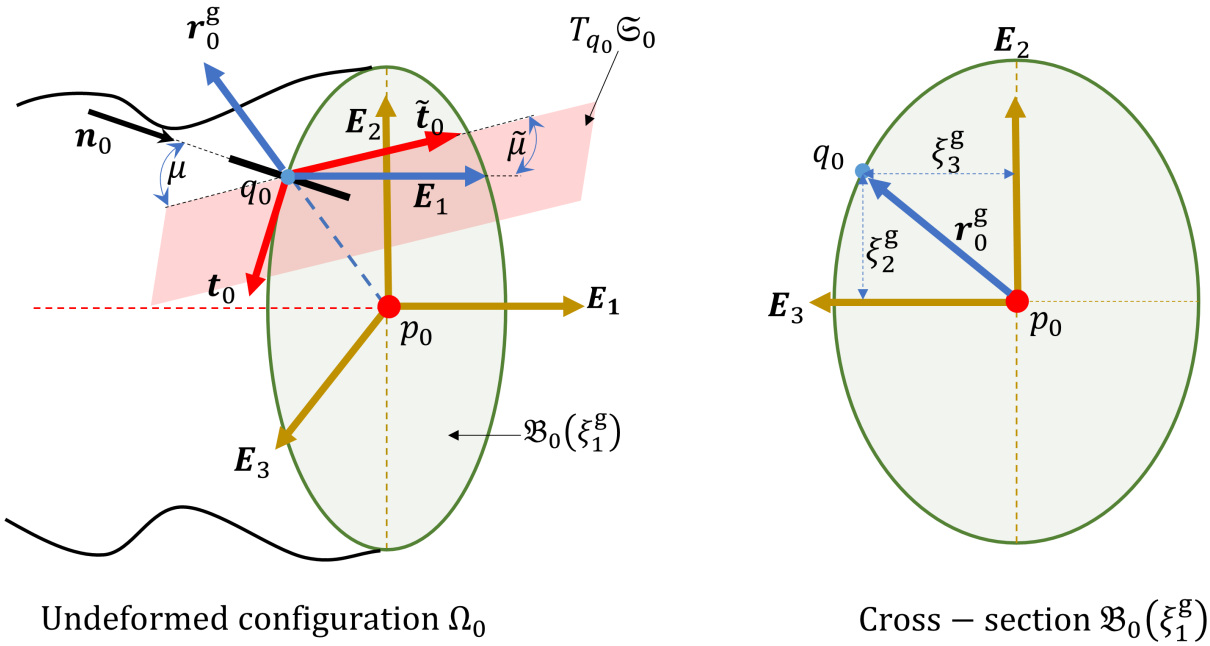

Figure 6.3: The orientation of the strain gauge in undeformed configuration Ω_0.

$$\boldsymbol{n}_0 = \cos\mu\tilde{\boldsymbol{t}}_0 + \sin\mu\boldsymbol{t}_0. \tag{6.11}$$

If the configuration Ω_0 consists of the same cross-sections (not varying along the beam), then $\tilde{\mu} = 0$.

As, $\mathrm{d}\boldsymbol{\phi} : T_{q_0}\mathfrak{S}_0 \longrightarrow T_{\boldsymbol{\phi}(q_0)}\mathfrak{S}_j$, the tangent space $T_{\boldsymbol{\phi}(q_0)}\mathfrak{S}_j$ is spanned by the normal basis vectors $\left(\frac{\boldsymbol{F}_j.\boldsymbol{t}_0}{\|\boldsymbol{F}_j.\boldsymbol{t}_0\|}, \frac{\boldsymbol{F}_j.\tilde{\boldsymbol{t}}_0}{\|\boldsymbol{F}_j.\tilde{\boldsymbol{t}}_0\|}\right)$. These basis vectors are not orthogonal unless $\boldsymbol{F}_j = \boldsymbol{Q}$ at the point q_0.

6.3.2 Expression of scalar strain value of discrete strain gauge

Consider a discrete strain gauge with the finite (but small) gauge length l_g with the orientation $\boldsymbol{n}_0$ in the undeformed state. Let the center point of the strain gauge be attached to the material point q_0. Considering the strain gauge as the vector $l_g\boldsymbol{n}_0$, the scalar strain $\mathrm{e}_j^{\mathrm{d}}$ (the super-script "d" stands for *discrete strain gauge*) in the deformed state Ω_j is,

$$\mathrm{e}_j^{\mathrm{d}} = \overbrace{\left((\boldsymbol{F}_j(q_0).\boldsymbol{n}_0)\cdot(\boldsymbol{F}_j(q_0).\boldsymbol{n}_0)\right)^{\frac{1}{2}}}^{\text{Stretch } \hat{\lambda}_j} - 1. \tag{6.12}$$

Equation (6.12) defines *nominal strain*. We can obtain natural strain, Lagrangian strain, Eulerian strain, and logarithmic strain fields using the expression of stretch $\hat{\lambda}_j$ (refer to section 4.2 of Asaro and Lubarda [61]). Note that a similar expression can be obtained by using Eq. (6.3) and (6.4) such that the deformation gradient tensor is assumed to be constant $\boldsymbol{F}_j(q_0)$ (considering its value at the center of the strain gauge) along the length of the discrete strain gauge.

6.3.3 Simplified discrete strain gauge measurement model for deformed case Ω_1 considering small strain case

As noted in section 6.4.1, the deformation gradient tensor considering the deformed configuration as Ω_1, is given by

$$\boldsymbol{F}_1 = \boldsymbol{\lambda}_1^1 \otimes \boldsymbol{E}_1 + \boldsymbol{d}_i \otimes \boldsymbol{E}_i = \boldsymbol{H}_1 + \boldsymbol{Q}. \tag{6.13}$$

Given $\boldsymbol{n}_0$ is the unit vector defining the direction of the strain gauge, the scalar strain for discrete gauge is simplified as follows:

$$\begin{aligned} \mathfrak{e}_1^d &= \|(\boldsymbol{F}_1.\boldsymbol{n}_0)\| - 1 = \|(\boldsymbol{H}_1.\boldsymbol{n}_0 + \boldsymbol{Q}.\boldsymbol{n}_0)\| - 1 \\ &= \sqrt{\|\boldsymbol{H}_1.\boldsymbol{n}_0\| + 2(\boldsymbol{H}_1.\boldsymbol{n}_0) \cdot (\boldsymbol{Q}.\boldsymbol{n}_0) + 1} - 1. \end{aligned} \tag{6.14}$$

For small strain, large deformation, $\|\boldsymbol{H}_1.\boldsymbol{n}_0\| << \boldsymbol{Q}.\boldsymbol{n}_0$. Therefore, expanding the expression for $\mathfrak{e}$ upto first order of $\boldsymbol{H}_1.\boldsymbol{n}_0$ yields,

$$\mathfrak{e}_1^d \approx (\boldsymbol{H}_1.\boldsymbol{n}_0) \cdot (\boldsymbol{Q}.\boldsymbol{n}_0) + O(\boldsymbol{H}_1.\boldsymbol{n}_0)^2. \tag{6.15}$$

6.4 Three dimensional shape reconstruction of slender structures

The theory of shape sensing developed in this chapter utilities the results discussed in chapters 1, 2 and 4. The following section represents the kinematic discussion and the solution algorithm.

6.4.1 Kinematic discussion

We consider that the deformed beam is subjected to multiple curvatures (bending and torsion), Poisson's deformation due to mid-curve axial strain only (in-plane cross-sectional deformation), shear deformation and warping due to torsion only. We exclude the warping due to bending induced shear and also exclude the effect of warping and bending on Poisson's deformation. We also assume that the warping function is known and the initial undeformed configuration is straight (not curved).

Let an open set $\Omega_0 \in \mathbb{R}^3$ and $\Omega \in \mathbb{R}^3$ represent the undeformed and deformed configuration of the rod. The inclusion of the aforementioned deformation effects has no impact on the definition

of mid-curve position vector $\boldsymbol{\varphi}(\xi_1)$, parameterized by the arc-length $\xi_1 \in [0, L] \subset \mathbb{R}^+$, and the cross-sectional orientation is defined by a *material frame* (MF) or director triad $\{\boldsymbol{d}_i\}$. Let $\{\boldsymbol{E}_i\}$ define a fixed orthonormal reference frame such that we define the orthogonal rotation tensor $\boldsymbol{Q}_{\mathrm{m}}$ (the sub-script "m" stands for material frame) and the curvature tensor $\hat{\boldsymbol{\kappa}}$ as,

$$\begin{aligned} \boldsymbol{Q}_{\mathrm{m}}(\xi_1) &= \boldsymbol{d}_i \otimes \boldsymbol{E}_i; \\ \hat{\boldsymbol{\kappa}} &= \partial_{\xi_1} \boldsymbol{Q}.\boldsymbol{Q}^T; \\ \partial_{\xi_1} \boldsymbol{d}_i &= \hat{\boldsymbol{\kappa}}.\boldsymbol{d}_i = \boldsymbol{\kappa} \times \boldsymbol{d}_i. \end{aligned} \tag{6.16}$$

The deformation map of such beam is defined as $\boldsymbol{\phi} : \boldsymbol{R}_0 \in \Omega_0 \longmapsto \boldsymbol{R} \in \Omega$ such that,

$$\boldsymbol{\phi}(\boldsymbol{R}_0) = \boldsymbol{R} = \boldsymbol{\varphi}(\xi_1) + \boldsymbol{r} + p\Psi \boldsymbol{d}_1; \tag{6.17a}$$

$$\boldsymbol{r} = (\hat{\xi}_2 \boldsymbol{d}_2 + \hat{\xi}_3 \boldsymbol{d}_3) = (1 - \nu\overline{\varepsilon}_1)\boldsymbol{r}_1; \tag{6.17b}$$

$$\boldsymbol{r}_1 = \xi_2 \boldsymbol{d}_2 + \xi_3 \boldsymbol{d}_3. \tag{6.17c}$$

In the equation set above, p, Ψ, and $\overline{\varepsilon}_1 = (\boldsymbol{Q}_{\mathrm{m}}^T.\partial_{\xi_1}\boldsymbol{\varphi} - \boldsymbol{E}_1) \cdot \boldsymbol{E}_1$ represents the warping amplitude, the known warping function, and the component of axial strain vector $\boldsymbol{\varepsilon}$ along $\boldsymbol{d}_1$. We realize that the deformation map is a special case of the map $\boldsymbol{\phi}_3$ discussed in chapter 4 described in equation set (4.24).

Let $\mathfrak{B}_0(\xi_1) = \{\xi_2, \xi_3\} \in \mathbb{R}^2_{\xi_1}$ and $\mathfrak{B}(\xi_1, \xi_2, \xi_3) = \{p\Psi, \hat{\xi}_2, \hat{\xi}_3\} \in \mathbb{R}^3_{\xi_1}$ represent the cross-section field for the configuration Ω_0 and Ω. Another deformed configuration of interest to us is Ω_1. It is a special case of Ω where we ignore warping and Poisson's deformation. We define another deformed configuration $\Omega_4 \in \mathbb{R}^3$ such that the associated cross-section field is given by $\mathfrak{B}_4(\xi_1, \xi_2, \xi_3) = \{\hat{\xi}_2, \hat{\xi}_3\} \in \mathbb{R}^2_{\xi_1}$. It is a special case of Ω when we ignore warping. The discussed shape sensing algorithm will be simulated for the deformation states Ω_1 and Ω_4. The configuration space for Ω_1, Ω_4, and Ω is given by:

$$\boldsymbol{\Phi}_1 := \left\{(\boldsymbol{\varphi}, \boldsymbol{Q}_{\mathrm{m}}) \mid \ \boldsymbol{\varphi} : \mathbb{R}^+ \to \mathbb{R}^3, \ \ \boldsymbol{Q}_{\mathrm{m}} : \mathbb{R}^+ \to SO(3)\right\} \subset \mathbb{C}_1; \tag{6.18}$$

$$\boldsymbol{\Phi}_4 := \left\{(\boldsymbol{\varphi}, \boldsymbol{Q}_{\mathrm{m}}, \overline{\varepsilon}_1) \mid \ \boldsymbol{\varphi} : \mathbb{R}^+ \to \mathbb{R}^3, \ \ \boldsymbol{Q}_{\mathrm{m}} : \mathbb{R}^+ \to SO(3), \ \ \overline{\varepsilon}_1 : \mathbb{R}^+ \to \mathbb{R}\right\} \subset \mathbb{C}_4; \tag{6.19}$$

$$\boldsymbol{\Phi} := \left\{(\boldsymbol{\varphi}, \boldsymbol{Q}_{\mathrm{m}}, \overline{\varepsilon}_1, p) \mid \ \boldsymbol{\varphi} : \mathbb{R}^+ \to \mathbb{R}^3, \ \ \boldsymbol{Q}_{\mathrm{m}} : \mathbb{R}^+ \to SO(3), \ \ \overline{\varepsilon}_1, p : \mathbb{R}^+ \to \mathbb{R}\right\} \subset \mathbb{C}. \tag{6.20}$$

Therefore, we note that $\mathbb{C}_1 = \mathbb{R}^3 \times SO(3)$, $\mathbb{C}_4 = \mathbb{R}^3 \times SO(3) \times \mathbb{R}$ and $\mathbb{C} = \mathbb{R}^3 \times SO(3) \times \mathbb{R} \times \mathbb{R}$. However, as noted in section 2.3.1, the quantities $(\boldsymbol{\varphi}, \boldsymbol{Q}_{\mathrm{m}})$ can be approximated to the least order by SPEG technique, where we use linearized shape functions (refer to Eq. (2.15)). However, since $\overline{\varepsilon}_1$ is functionally dependent on $\partial_{\xi_1}\boldsymbol{\varphi}$, it can separately be approximated using higher order techniques from the discrete values of the estimated $\boldsymbol{\varphi}$. In that case $\mathbb{C}_1 \equiv \mathbb{C}_4$.

The associated deformation gradient tensor is given by $\boldsymbol{F}_1 = \boldsymbol{H}_1 + \boldsymbol{Q}_{\mathrm{m}} = \boldsymbol{\lambda}_1^1 \otimes \boldsymbol{E}_1 + \boldsymbol{Q}_{\mathrm{m}}$, $\boldsymbol{F}_4 = \boldsymbol{H}_4 + \boldsymbol{Q}_{\mathrm{m}} = \boldsymbol{\lambda}_i^4 \otimes \boldsymbol{E}_i + \boldsymbol{Q}_{\mathrm{m}}$, and $\boldsymbol{F} = \boldsymbol{H} + \boldsymbol{Q}_{\mathrm{m}} = \boldsymbol{\lambda}_i \otimes \boldsymbol{E}_i + \boldsymbol{Q}_{\mathrm{m}}$. Here, the strain vector $\boldsymbol{\lambda}_1^1$ for the deformed configuration Ω_1 is given by Eq. (4.41). The strain vectors corresponding to the deformed configuration Ω_4 and Ω can be deduced from the expression of strain vectors of most general deformed case Ω_3 as defined in equation set (4.35) by neglecting the terms associated with the not-included deformation effects (i.e., bending induced shear warping and contribution to in-plane deformation due to warping). For the configuration Ω_4, we have,

$$\boldsymbol{\lambda}_1^4 = \left(\overline{\varepsilon}_1 + \hat{\xi}_3\overline{\kappa}_2 - \hat{\xi}_2\overline{\kappa}_3\right)\boldsymbol{d}_1 + \left(\overline{\varepsilon}_2 - \hat{\xi}_3\overline{\kappa}_1 + \partial_{\xi_1}\hat{\xi}_2\right)\boldsymbol{d}_2 + \left(\overline{\varepsilon}_3 + \hat{\xi}_2\overline{\kappa}_1 + \partial_{\xi_1}\hat{\xi}_3\right)\boldsymbol{d}_3; \tag{6.21a}$$

$$\boldsymbol{\lambda}_2^4 = \left(\partial_{\xi_2}\hat{\xi}_2 - 1\right)\boldsymbol{d}_2 + \partial_{\xi_2}\hat{\xi}_3.\boldsymbol{d}_3; \tag{6.21b}$$

$$\boldsymbol{\lambda}_3^4 = \partial_{\xi_3}\hat{\xi}_2.\boldsymbol{d}_2 + \left(\partial_{\xi_3}\hat{\xi}_3 - 1\right)\boldsymbol{d}_3. \tag{6.21c}$$

Similarly, for the configuration Ω, we have,

$$\begin{aligned}\boldsymbol{\lambda}_1 = &\left(\overline{\varepsilon}_1 + \hat{\xi}_3\overline{\kappa}_2 - \hat{\xi}_2\overline{\kappa}_3 + \partial_{\xi_1}p.\Psi\right)\boldsymbol{d}_1 + \left(\overline{\varepsilon}_2 - \hat{\xi}_3\overline{\kappa}_1 + \partial_{\xi_1}\hat{\xi}_2 + p\Psi\overline{\kappa}_3\right)\boldsymbol{d}_2 \\ &+ \left(\overline{\varepsilon}_3 + \hat{\xi}_2\overline{\kappa}_1 + \partial_{\xi_1}\hat{\xi}_3 - p\Psi\overline{\kappa}_2\right)\boldsymbol{d}_3;\end{aligned} \tag{6.22a}$$

$$\boldsymbol{\lambda}_2 = p.\partial_{\xi_2}\Psi.\boldsymbol{d}_1 + \left(\partial_{\xi_2}\hat{\xi}_2 - 1\right)\boldsymbol{d}_2 + \partial_{\xi_2}\hat{\xi}_3.\boldsymbol{d}_3; \tag{6.22b}$$

$$\boldsymbol{\lambda}_3 = p.\partial_{\xi_3}\Psi.\boldsymbol{d}_1 + \partial_{\xi_3}\hat{\xi}_2.\boldsymbol{d}_2 + \left(\partial_{\xi_3}\hat{\xi}_3 - 1\right)\boldsymbol{d}_3. \tag{6.22c}$$

Here,

$$\partial_{\xi_1}\hat{\xi}_i = -\partial_{\xi_1}\overline{\varepsilon}_1.\nu\xi_i \text{ for } i \in 2,3; \tag{6.23a}$$

$$\partial_{\xi_j}\hat{\xi}_i = (1-\nu\overline{\varepsilon}_1)\delta_{ij} \text{ for } i,j \in 2,3. \tag{6.23b}$$

6.4.2 The director triad and the governing differential equation

To uniquely describe the shear angles and to express the frame $\{\boldsymbol{d}_i\}$ with respect to the fixed frame $\{\boldsymbol{E}_i\}$, we first consider an un-sheared cross-section defined by a *special material adapted frame* (SMAF) field $\{\boldsymbol{T}(\xi_1), \boldsymbol{Y}_{\mathrm{s}}(\xi_1), \boldsymbol{P}_{\mathrm{s}}(\xi_1)\}$ obtained by rotating $\{\boldsymbol{E}_i\}$ frame about $-\boldsymbol{E}_2$ by an angle $\phi_y(\xi_1)$ (yaw angle) followed by rotation about $\boldsymbol{E}_3$ by an angle $\phi_p(\xi_1)$ (pitch angle). Here, $\boldsymbol{T}(\xi_1)$ is the tangent vector field to the mid-curve $\boldsymbol{\varphi}(\xi_1)$ defined as $\boldsymbol{T} = \partial_s\boldsymbol{\varphi} = \frac{1}{1+e}\partial_{\xi_1}\boldsymbol{\varphi}$. Here, s is the deformed arc-length of the beam as defined in section 4.2.2. From (1.27) in section 1.3.3, we can arrive at the relationship between the SMAF and the fixed frame $\{\boldsymbol{E}_i\}$ by substituting $-\phi_y$ in place of ϕ_y (unlike in section 1.3.3, we have rotated the SMAF about $-\boldsymbol{E}_2$), yielding,

$$\begin{bmatrix} \boldsymbol{T} \\ \boldsymbol{Y}_{\mathrm{s}} \\ \boldsymbol{P}_{\mathrm{s}} \end{bmatrix} = \overbrace{\begin{bmatrix} c_{\phi_p}c_{\phi_y} & s_{\phi_p} & c_{\phi_p}s_{\phi_y} \\ -s_{\phi_p}c_{\phi_y} & c_{\phi_p} & -s_{\phi_p}s_{\phi_y} \\ -s_{\phi_y} & 0 & c_{\phi_y} \end{bmatrix}}^{[\boldsymbol{Q}_{\mathrm{s}}]^T_{\boldsymbol{E}_i\otimes\boldsymbol{E}_j}=\Re_{\mathrm{s}}} \begin{bmatrix} \boldsymbol{E}_1 \\ \boldsymbol{E}_2 \\ \boldsymbol{E}_3 \end{bmatrix}. \tag{6.24}$$

From the equation above, we have $\boldsymbol{Q}_{\mathrm{s}} = \boldsymbol{T}\otimes\boldsymbol{E}_1 + \boldsymbol{Y}_{\mathrm{s}}\otimes\boldsymbol{E}_2 + \boldsymbol{P}_{\mathrm{s}}\otimes\boldsymbol{E}_3$. Here we have used same convention as section 1.3.3: $\cos\theta = c_\theta$ and $\sin\theta = s_\theta$, for any angle θ. Both these notations are interchangeably used as per convenience.

Recall the definition of shear angles in section 1.3.3. The three shear angles, denoted by $\gamma_{11}(\xi_1)$, $\frac{\pi}{2} - \gamma_{12}(\xi_1)$ and $\frac{\pi}{2} - \gamma_{13}(\xi_1)$ are subtended by the directors $\boldsymbol{d}_1$, $\boldsymbol{d}_2$ and $\boldsymbol{d}_3$ with the tangent vector $\boldsymbol{T}$. However, this definition does not provide us with unique sheared cross-section. To uniquely define the sheared cross-section, we obtain the director triad by rotating SMAF. To do

so, we define three additional angles $\alpha_1, \alpha_2, \alpha_3$ as angles subtended by the directors $\boldsymbol{d}_1, \boldsymbol{d}_2$, and $\boldsymbol{d}_3$, with the vector $\boldsymbol{Y}_\mathrm{s}$ such that,

$$\begin{bmatrix} \boldsymbol{T} \\ \boldsymbol{Y}_\mathrm{s} \\ \boldsymbol{P}_\mathrm{s} \end{bmatrix} = \overbrace{\begin{bmatrix} c_{\gamma_{11}} & s_{\gamma_{12}} & s_{\gamma_{13}} \\ c_{\alpha_1} & c_{\alpha_2} & c_{\alpha_3} \\ c_{\alpha_3}s_{\gamma_{12}} - c_{\alpha_2}s_{\gamma_{13}} & c_{\alpha_3}c_{\gamma_{11}} - c_{\alpha_1}s_{\gamma_{13}} & c_{\alpha_2}s_{\gamma_{11}} - c_{\alpha_1}s_{\gamma_{12}} \end{bmatrix}}^{[\boldsymbol{Q}^T_\mathrm{sm}]_{\boldsymbol{E}_i\otimes\boldsymbol{E}_j}=[\boldsymbol{Q}_\mathrm{ms}]_{\boldsymbol{E}_i\otimes\boldsymbol{E}_j}=\mathfrak{R}_\mathrm{sm}} \begin{bmatrix} \boldsymbol{d}_1 \\ \boldsymbol{d}_2 \\ \boldsymbol{d}_3 \end{bmatrix}. \tag{6.25}$$

Here, $\boldsymbol{Q}_\mathrm{sm} = \boldsymbol{T} \otimes \boldsymbol{d}_1 + \boldsymbol{Y}_\mathrm{s} \otimes \boldsymbol{d}_2 + \boldsymbol{P}_\mathrm{s} \otimes \boldsymbol{d}_3 = \boldsymbol{Q}^T_\mathrm{ms}$. We aim to relate the director triad $\{\boldsymbol{d}_i\}$ with the fixed reference frame $\{\boldsymbol{E}_i\}$ such that $\boldsymbol{d}_i = \boldsymbol{Q}_\mathrm{m}.\boldsymbol{E}_i$, such that the corresponding direction cosine matrix (refer to section 1.3.2.3) is given by $\mathfrak{R}_\mathrm{m} = [\boldsymbol{Q}_\mathrm{m}]^T_{\boldsymbol{E}_i\otimes\boldsymbol{E}_j}$. Like the result in (1.29), we have,

$$\begin{aligned} \boldsymbol{Q}_\mathrm{m} \equiv \boldsymbol{Q} &= \boldsymbol{Q}_\mathrm{ms}.\boldsymbol{Q}_\mathrm{s} = \boldsymbol{Q}^T_\mathrm{sm}.\boldsymbol{Q}_\mathrm{s}; \\ [\boldsymbol{Q}_\mathrm{m}]^T_{\boldsymbol{E}_i\otimes\boldsymbol{E}_j} &= [\boldsymbol{Q}_\mathrm{sm}]_{\boldsymbol{E}_i\otimes\boldsymbol{E}_j}.[\boldsymbol{Q}_\mathrm{s}]^T_{\boldsymbol{E}_i\otimes\boldsymbol{E}_j}; \\ \mathfrak{R}_\mathrm{m} &= \mathfrak{R}^T_\mathrm{sm}.\mathfrak{R}_\mathrm{s}. \end{aligned} \tag{6.26}$$

The rotation tensor $\boldsymbol{Q}_\mathrm{m}$ is orthogonal if the following constraints on (α_1, α_2, α_3, γ_{11}, γ_{12}, γ_{13}) are imposed:

$$\|\boldsymbol{T}\| = \|\boldsymbol{Y}_\mathrm{s}\| = \|\boldsymbol{P}_\mathrm{s}\| = 1; \quad \partial_{\xi_1}\|\boldsymbol{T}\| = \partial_{\xi_1}\|\boldsymbol{Y}_\mathrm{s}\| = \partial_{\xi_1}\|\boldsymbol{P}_\mathrm{s}\| = 0. \tag{6.27}$$

Figure 6.4 illustrates the discussion carried so far. We define the curvature tensor associated with the beam configuration Ω_1 as $\hat{\boldsymbol{\kappa}} = \partial_{\xi_1}\boldsymbol{Q}_\mathrm{m}.\boldsymbol{Q}^T_\mathrm{m}$ with the associated curvature vector $\boldsymbol{\kappa} = \overline{\kappa}_i\boldsymbol{d}_i$. The components of the curvature vector as a function of the angles (α_1, α_2, α_3, γ_{11}, γ_{12}, γ_{13}) and

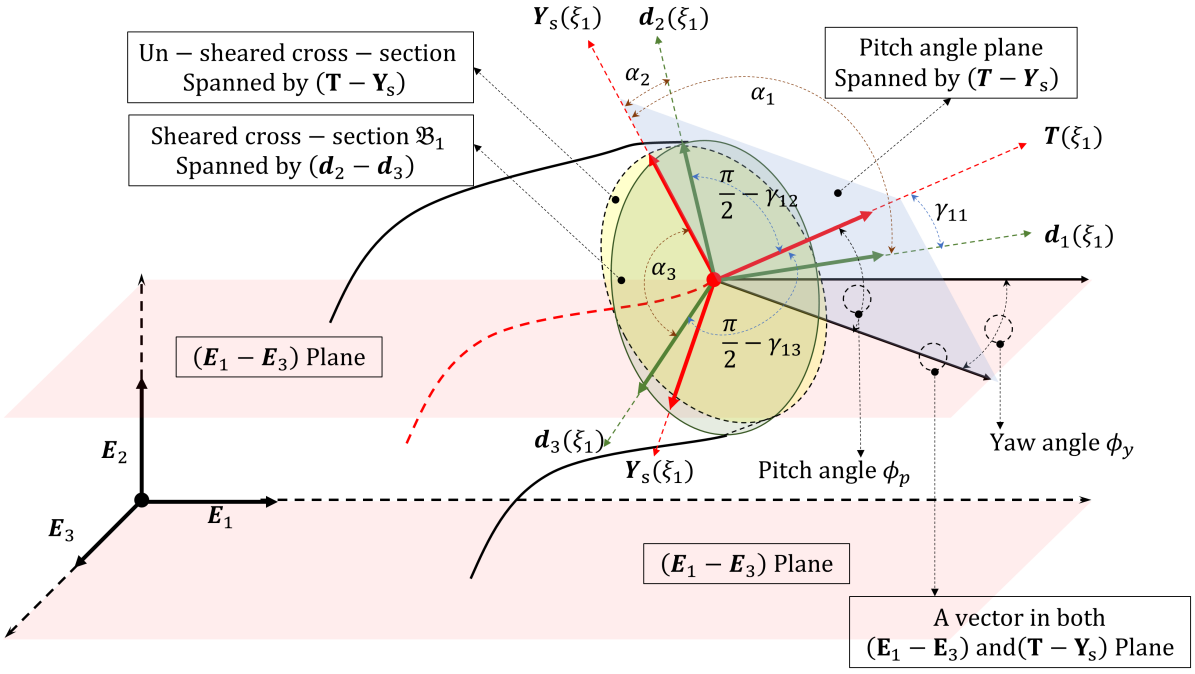

Figure 6.4: Sheared and un-sheared cross-section.

their derivatives can be obtained using the expression for $\boldsymbol{Q}_{\mathrm{m}}$ as:

$$\begin{aligned}\overline{\kappa}_1 = &-\partial_{\xi_1}\alpha_2.c_{\alpha_3}s_{\alpha_2} + \partial_{\xi_1}\alpha_3.c_{\alpha_2}s_{\alpha_3} + \partial_{\xi_1}\gamma_{11}.c_{\alpha_1}s_{\gamma_{11}}(-c_{\alpha_3}s_{\gamma_{12}} + c_{\alpha_2}s_{\gamma_{13}}) - \partial_{\xi_1}\gamma_{12}.c_{\alpha_2^2}c_{\gamma_{12}}s_{\gamma_{13}} \\ &- \partial_{\xi_1}\gamma_{13}.c_{\gamma_{13}}s_{\gamma_{13}} + \partial_{\xi_1}\gamma_{13}.c_{\alpha_3^2}c_{\gamma_{13}}s_{\gamma_{12}} - \partial_{\xi_1}\gamma_{13}.c_{\alpha_2}c_{\alpha_3}c_{\gamma_{13}}s_{\gamma_{13}} + \partial_{\xi_1}\phi_y.(c_{\alpha_2}s_{\gamma_{12}} - c_{\alpha_2}s_{\gamma_{13}}) \\ &- \partial_{\xi_1}\phi_y.(c_{\alpha_1}c_{\phi_p} + c_{\gamma_{11}}s_{\phi_p});\end{aligned} \tag{6.28a}$$

$$\begin{aligned}\overline{\kappa}_2 = \frac{1}{2}\Big(&2\partial_{\xi_1}\alpha_1.c_{\alpha_3}s_{\alpha_1} - 2\partial_{\xi_1}\alpha_3.c_{\alpha_1}s_{\alpha_3} + \partial_{\xi_1}\gamma_{11}.(2 + c_{2\alpha_2} + c_{2\alpha_3})s_{\gamma_{13}} - 2\partial_{\xi_1}\phi_y.\big(c_{\alpha_2}c_{\phi_p} + s_{\gamma_{12}}s_{\phi_p}\big) \\ &+ \partial_{\xi_1}\gamma_{12}.\big(c_{\alpha_1}c_{\alpha_3}s_{2\gamma_{13}} + 2c_{\alpha_2}c_{\gamma_{12}}(-c_{\alpha_3}c_{\gamma_{11}} + c_{\alpha_1}s_{\gamma_{13}})\big) + 2\big(c_{\gamma_{11}}c_{\gamma_{13}}s_{\alpha_3^2} + c_{\alpha_1}c_{\alpha_3}s_{2\gamma_{13}}\big) \\ &+ 2\partial_{\xi_1}\phi_p.(-c_{\alpha_3}c_{\gamma_{11}} + c_{\alpha_1}s_{\gamma_{13}})\Big);\end{aligned} \tag{6.28b}$$

$$\overline{\kappa}_3 = -\partial_{\xi_1}\alpha_1.c_{\alpha_2}s_{\alpha_1} + \partial_{\xi_1}\alpha_2.c_{\alpha_1}s_{\alpha_2} + \partial_{\xi_1}\gamma_{12}.(c_{\alpha_1}c_{\alpha_3}c_{\gamma_{12}}s_{\gamma_{13}} - c_{\alpha_3^2}c_{\gamma_{11}}c_{\gamma_{12}}) - \partial_{\xi_1}\phi_y.(c_{\alpha_3}c_{\phi_p} + s_{\gamma_{13}}s_{\phi_p})$$
$$+ \partial_{\xi_1}\gamma_{13}.(c_{\alpha_2}c_{\alpha_3}c_{\gamma_{11}}c_{\gamma_{13}} - c_{\alpha_1}c_{\alpha_3}c_{\gamma_{13}}s_{\gamma_{12}}) + \partial_{\xi_1}\gamma_{11}.c_{\alpha_3}s_{\gamma_{11}}(c_{\alpha_2}s_{\gamma_{13}} - c_{\alpha_3}s_{\gamma_{12}})$$
$$+ \partial_{\xi_1}\phi_p.(c_{\alpha_2}c_{\gamma_{11}} - c_{\alpha_1}s_{\gamma_{12}}). \tag{6.28c}$$

Like Eq. (2.14), the governing differential equation governing the kinematic evolution of the beam can be obtained using Eq. (4.7) and (4.5) as,

$$\begin{bmatrix} \partial_{\xi_1}\boldsymbol{\varphi} \\ \partial_{\xi_1}\boldsymbol{d}_1 \\ \partial_{\xi_1}\boldsymbol{d}_2 \\ \partial_{\xi_1}\boldsymbol{d}_3 \end{bmatrix} = \begin{bmatrix} 0 & (1+e)c_{\gamma_{11}} & (1+e)s_{\gamma_{12}} & (1+e)s_{\gamma_{13}} \\ 0 & 0 & \overline{\kappa}_3 & -\overline{\kappa}_2 \\ 0 & -\overline{\kappa}_3 & 0 & \overline{\kappa}_1 \\ 0 & \overline{\kappa}_2 & -\overline{\kappa}_1 & 0 \end{bmatrix} \begin{bmatrix} \boldsymbol{\varphi} \\ \boldsymbol{d}_1 \\ \boldsymbol{d}_2 \\ \boldsymbol{d}_3 \end{bmatrix} \tag{6.29}$$

It is worth mentioning that in the absence of shear deformation and the axial extension, we have $\gamma_{1i}(\xi_1) = 0$, $\alpha_1(\xi_1) = \alpha_3(\xi_1) = \frac{\pi}{2}$, $\alpha_2(\xi_1) = 0$ and $e(\xi_1) = 0$, yielding $\{\boldsymbol{d}_i\} = \{\boldsymbol{T}, \boldsymbol{Y}_\mathrm{s}, \boldsymbol{P}_\mathrm{s}\}$, vanishing the axial strain vector $\boldsymbol{\varepsilon} = \boldsymbol{0}$, and simplifying the curvatures as $\overline{\kappa}_1 = -s_{\phi_y}.\partial_{\xi_1}\phi_y$, $\overline{\kappa}_2 = c_{\phi_y}.\partial_{\xi_1}\phi_y$, $\overline{\kappa}_3 = \partial_{\xi_1}\phi_p$, reducing the governing differential equation set to:

$$\begin{bmatrix} \partial_{\xi_1}\boldsymbol{\varphi} \\ \partial_{\xi_1}\boldsymbol{T} \\ \partial_{\xi_1}\boldsymbol{Y}_\mathrm{s} \\ \partial_{\xi_1}\boldsymbol{P}_\mathrm{s} \end{bmatrix} = \begin{bmatrix} 0 & 1 & 0 & 0 \\ 0 & 0 & \partial_{\xi_1}\phi_p & -\partial_{\xi_1}\phi_y.c_{\phi_y} \\ 0 & -\partial_{\xi_1}\phi_p & 0 & -\partial_{\xi_1}\phi_y.s_{\phi_y} \\ 0 & \partial_{\xi_1}\phi_y.c_{\phi_y} & \partial_{\xi_1}\phi_y.s_{\phi_y} & 0 \end{bmatrix} \begin{bmatrix} \boldsymbol{\varphi} \\ \boldsymbol{T} \\ \boldsymbol{Y}_\mathrm{s} \\ \boldsymbol{P}_\mathrm{s} \end{bmatrix}. \tag{6.30}$$

This is exactly the Eq. (5) in Todd et al. [16]. Therefore, the current relationship Eq. (6.29) consistently reduces to the simpler one (6.30) as described in Todd et al. [16]. Equation (6.30) represents a deformation relationship that only considers the curvature-based contributions (bending and torsion).

The matrix in the Eq. (6.29) consist of six unknowns: three components of axial strain vector $\boldsymbol{\varepsilon}$ and three components of the curvature vector $\boldsymbol{\kappa}$. As discussed in section 2.3, once the

quantities $\left(1+\overline{\varepsilon}_1=(1+e)c_{\gamma_{11}},\ \overline{\varepsilon}_2=(1+e)s_{\gamma_{12}},\ \overline{\varepsilon}_3=(1+e)s_{\gamma_{13}},\ \overline{\kappa}_1,\ \overline{\kappa}_2,\ \overline{\kappa}_3\right)$ are known at finite number of cross-sections, the deformed shape of the beam can be estimated by integrating Eq. (6.29). These techniques were discussed in chapter 2 concerning the problem of path estimation. Since there are six unknowns, we need six strain gauges to be attached onto the surface of the beam.

6.4.3 Orientation of the strain gauge in the undeformed state considering circular cross-section

To proceed further, we detail the geometry of beam and the orientation of the strain gauge assumed to develop the shape sensing methodology. We consider a cylindrical beam with circular cross-section of outer radius r. As discussed in section 6.3.1, we assume strain gauges to be attached on the surface at the point $q_0=(\xi_1,\xi_2,\xi_3)\in\mathfrak{S}_0$ such that $\boldsymbol{r}_0=\xi_2\boldsymbol{E}_2+\xi_3\boldsymbol{E}_3$ and $r=\sqrt{\xi_2^2+\xi_3^2}$. We assume that the vector $\boldsymbol{r}_0$ subtends an angle σ with $\boldsymbol{E}_2$, such that $\xi_2=rc_\sigma$, $\xi_3=rs_\sigma$, and $\boldsymbol{t}_0=-s_\mu\boldsymbol{E}_2+c_\mu\boldsymbol{E}_3$. By virtue of the uniform cross-section assumption, we have $\tilde{\mu}=0$, and hence $\tilde{\boldsymbol{t}}=\boldsymbol{E}_1$. Therefore, the strain gauge orientation vector $\boldsymbol{n}_0$ can be obtained as

$$\boldsymbol{n}_0=c_\mu\boldsymbol{E}_1-s_\mu s_\sigma\boldsymbol{E}_2+s_\mu c_\sigma\boldsymbol{E}_3. \tag{6.31}$$

We discuss the scalar strain formula for the configuration Ω_1 and the ideas discussed can be extended to the configurations Ω_4 and Ω. For the deformed configuration Ω_1, we have

$$\boldsymbol{F}_1.\boldsymbol{n_0}=\left((1+\overline{\varepsilon}_1)-\overline{\kappa}_3\xi_2+\overline{\kappa}_2\xi_3\right)c_\mu\boldsymbol{d}_1+(\overline{\varepsilon}_2-\overline{\kappa}_1\xi_3)c_\mu-s_\mu s_\sigma\boldsymbol{d}_2+(\overline{\varepsilon}_3+\overline{\kappa}_1\xi_2)c_\mu+s_\mu c_\sigma\boldsymbol{d}_3. \tag{6.32}$$

To further interpret the expression of scalar strain, we assume $\boldsymbol{n}_0=\boldsymbol{E}_1$, yielding

$$\mathrm{e}_1^{\mathrm{d}}=\sqrt{((1+\overline{\varepsilon}_1)-\overline{\kappa}_3\xi_2+\overline{\kappa}_2\xi_3)^2+(\overline{\varepsilon}_2-\overline{\kappa}_1\xi_3)^2+(\overline{\varepsilon}_3+\overline{\kappa}_1\xi_2)^2}-1. \tag{6.33}$$

Considering only one deformation effect at a time, the expression for scalar strain values are evaluated as follows,

$$\text{Axial deformation :} \qquad \mathfrak{e}_1^{\mathrm{d}}\big|_{\overline{\varepsilon}_1\neq 0} = \overline{\varepsilon}_1; \tag{6.34a}$$

$$\text{Plane bending about } \boldsymbol{E}_3 : \qquad \mathfrak{e}_1^{\mathrm{d}}\big|_{\overline{\kappa}_2\neq 0} = \overline{\kappa}_2\xi_3; \tag{6.34b}$$

$$\text{Plane bending } \boldsymbol{E}_2 : \qquad \mathfrak{e}_1^{\mathrm{d}}\big|_{\overline{\kappa}_3\neq 0} = -\overline{\kappa}_3\xi_2; \tag{6.34c}$$

$$\text{Shear and Axial deformation :} \qquad \mathfrak{e}_1^{\mathrm{d}}\big|_{\overline{\varepsilon}_2,\overline{\varepsilon}_3\neq 0} = \sqrt{(1+\overline{\varepsilon}_1)^2+\overline{\varepsilon}_2^2+\overline{\varepsilon}_3^2}-1; \tag{6.34d}$$

$$\text{Torsion :} \qquad \mathfrak{e}_1^{\mathrm{d}}\big|_{\overline{\kappa}_1\neq 0} = \sqrt{1+\overline{\kappa}_1^2 r^2}-1. \tag{6.34e}$$

The first three expressions considering pure axial and bending deformations are obvious. However, the expressions for $\mathfrak{e}_1^{\mathrm{d}}\big|_{\overline{\varepsilon}_2,\overline{\varepsilon}_3\neq 0}$ and $\mathfrak{e}_1^{\mathrm{d}}\big|_{\overline{\kappa}_1\neq 0}$ seems less obvious. For instance, intuitively, $\overline{\kappa}_1 r = \|\boldsymbol{H}_1.\boldsymbol{n}_0\big|_{\overline{\kappa}_1\neq 0}\|$ should be the scalar strain due to torsion. Here, we carefully note that the strain gauge does not measure the magnitude of the strained vector $\|\boldsymbol{H}_1.\boldsymbol{n}_0\|$, rather it measures the scalar strain defined in Eq. 6.12. For the pure axial deformation and bending, we observe that $\|\boldsymbol{H}_1.\boldsymbol{n}_0\| = \|\boldsymbol{F}_1.\boldsymbol{n}_0\| - 1$, because the deformation happens to be along $\boldsymbol{n}_0 = \boldsymbol{E}_1$. Similarly, for the deformed states Ω_4 and Ω, the expression for the scalar strain $\mathfrak{e}_4^{\mathrm{d}}$ and $\mathfrak{e}^{\mathrm{d}}$ respectively, can be found using Eq. (6.12).

6.4.4 Solution approach

To obtain the approximate solution of the global deformed shapes (Ω_1^h, Ω_4^h, Ω^h), we discretize the structure into N segments ($\overline{n} = 1, 2, ..., N$) with the center of segment $\overline{n}$ located at $\xi_{1_{\overline{n}}}$. Let $\hat{\xi}_{1_{\overline{n}}}$ represents the right boundary of the $\overline{n}^{\text{th}}$ segment, such that $\hat{\xi}_{1_{\overline{n}-1}} < \hat{\xi}_{1_{\overline{n}}}$. We aim at obtaining the estimated deformed configuration of the beam using the finite strain data at the cross-sections located at ξ_{1_n}, with ($n = 1, 2, ..., N$). We assume the origin at $\xi_1 = 0$ is a fixed end and the boundary at $\xi_1 = L$ is a free end. For the assumed boundary conditions, we have, $\xi_{1_n} = \hat{\xi}_{1_{\overline{n}}}$ and $\hat{\xi}_{1_0} = 0$. We also assume $\boldsymbol{Q}_{\mathrm{m}}(0) = \{\boldsymbol{d}_{0i}\} = \{\boldsymbol{E}_i\}$.

From Eq. (6.29), we observe that to determine the estimated mid-curve $\boldsymbol{\varphi}^h(\xi_1)$ and director field $\boldsymbol{Q}^h_{\mathrm{m}}(\xi_1)$, we need only the discrete values of $\left(\overline{\varepsilon}_{1_n},\, \overline{\varepsilon}_{2_n},\, \overline{\varepsilon}_{3_n},\, \overline{\kappa}_{1_n},\, \overline{\kappa}_{2_n},\, \overline{\kappa}_{3_n}\right)$ at N cross sections. However, from the discussion in the previous section, we realize that the scalar strain formula for $\mathfrak{e}^d_1$ is a function of six finite strain quantities $(\overline{\varepsilon}_1,\, \overline{\varepsilon}_2,\, \overline{\varepsilon}_3,\, \overline{\kappa}_1,\, \overline{\kappa}_2,\, \overline{\kappa}_3)$; the scalar strain $\mathfrak{e}^d_4$ is a function of seven finite strain quantities $\left(\overline{\varepsilon}_1,\, \partial_{\xi_1}\overline{\varepsilon}_1,\, \overline{\varepsilon}_2,\, \overline{\varepsilon}_3,\, \overline{\kappa}_1,\, \overline{\kappa}_2,\, \overline{\kappa}_3\right)$; and the quantity $\mathfrak{e}^d$ depends on nine unknowns $\left(\overline{\varepsilon}_1,\, \partial_{\xi_1}\overline{\varepsilon}_1,\, \overline{\varepsilon}_2,\, \overline{\varepsilon}_3,\, \overline{\kappa}_1,\, \overline{\kappa}_2,\, \overline{\kappa}_3,\, p,\, \partial_{\xi_1}p\right)$. Let $\sigma_{n,m}$ and $\mu_{n,m}$ represents the angles defining the orientation of the m^{th} strain gauge at a cross-section located at ξ_{1_n}. Considering the deformed configuration Ω, for the cross-section at ξ_{1_n}, the scalar strain gauge $\mathfrak{e}^{\mathrm{d}}_{n,m}$ at m^{th} strain gauge can be written as a function of $\left(\overline{\varepsilon}_{1_n},\, \partial_{\xi_1}\overline{\varepsilon}_{1_n} = \partial_{\xi_1}\overline{\varepsilon}_1(\xi_{1_n}),\, \overline{\varepsilon}_{2_n},\, \overline{\varepsilon}_{3_n},\, \overline{\kappa}_{1_n},\, \overline{\kappa}_{2_n},\, \overline{\kappa}_{3_n},\, p_n,\, \partial_{\xi_1}p_n = \partial_{\xi_1}p(\xi_{1_n})\right)$ such that:

$$\mathfrak{e}^{\mathrm{d}}_{n,m} = f_m\left(\overline{\varepsilon}_{1_n},\, \partial_{\xi_1}\overline{\varepsilon}_{1_n},\, \overline{\varepsilon}_{2_n},\, \overline{\varepsilon}_{3_n},\, \overline{\kappa}_{1_n},\, \overline{\kappa}_{2_n},\, \overline{\kappa}_{3_n},\, p_n,\, \partial_{\xi_1}p_n;\, \sigma_{n,m},\, \mu_{n,m}\right). \tag{6.35}$$

We note that $\sigma_{n,m}$ and $\mu_{n,m}$ are known. To uniquely evaluate the nine unknowns, we invert the set of $m = 9$ non-linear equations. Similarly, for Ω_1 and Ω_4, we have $m = 6$ and $m = 7$.

6.4.4.1 Approximate solution for the mid-curve position vector and the director triad using SPEG

We only need the discrete value of axial strain and curvatures $\left(\overline{\varepsilon}_{1_n},\, \overline{\varepsilon}_{2_n},\, \overline{\varepsilon}_{3_n},\, \overline{\kappa}_{1_n},\, \overline{\kappa}_{2_n},\, \overline{\kappa}_{3_n}\right)$ to obtain $\left(\boldsymbol{\varphi}^h(\xi_1),\, \boldsymbol{Q}^h_{\mathrm{m}}(\xi_1)\right)$ for any deformed configuration $\left(\Omega^h_1,\, \Omega^h_4,\, \Omega^h\right)$. To estimate the deformed shape using SPEG technique, we consider the co-rotated derivatives of axial strain vector and the curvature vector to vanish for each patch. Equivalently, we truncate the Taylor series expansion of the finite strain quantities about ξ_{1_n} to zeroth order, thereby reducing the system of differential equations (6.29) into a constant-coefficient system such that the solution of the differential equation gives an approximated configuration $\boldsymbol{\Phi}^h_{\overline{n}} = (\boldsymbol{\varphi}^h_{\overline{n}}, \boldsymbol{Q}^h_{\overline{n}}) \equiv (\boldsymbol{\varphi}^h_{\overline{n}}, \{\boldsymbol{d}^h_{i\overline{n}}\}) \in \mathbb{C}_1$ valid in the patch $\overline{n}$. Therefore, N segments would involve solving for $12N$ constants of integration. Imposing continuity in the $(\boldsymbol{\varphi}, \{\boldsymbol{d}_i\})$ fields at the boundary between the segments gives $12(N-1)$

constraints, and an appropriate boundary condition gives the additional 12 conditions. We obtain a solution for $\overline{n}^{\text{th}}$ segment as:

$$\begin{aligned}\boldsymbol{\varphi}^{h}_{\overline{n}}(\xi_1) &= \boldsymbol{A}_{\overline{n}1} + \boldsymbol{A}_{\overline{n}2}\xi_1 + \boldsymbol{A}_{\overline{n}3}\sin\kappa_n\xi_1 + \boldsymbol{A}_{\overline{n}4}\cos\kappa_n\xi_1;\\ \boldsymbol{d}^{h}_{i\overline{n}}(\xi_1) &= \boldsymbol{B}_{\overline{n}i1} + \boldsymbol{B}_{\overline{n}i2}\xi_1 + \boldsymbol{B}_{\overline{n}i3}\sin\kappa_n\xi_1 + \boldsymbol{B}_{\overline{n}i4}\cos\kappa_n\xi_1.\end{aligned} \tag{6.36}$$

In the above equation $\kappa_n = \|\overline{\boldsymbol{\kappa}}_n\|$. We represent the vector coefficients in Eq. (6.36) in a more desirable form given below,

$$\left[[\boldsymbol{A}_{\overline{n}1}]_{\{\boldsymbol{E}_i\}}, [\boldsymbol{A}_{\overline{n}2}]_{\{\boldsymbol{E}_i\}}, [\boldsymbol{A}_{\overline{n}3}]_{\{\boldsymbol{E}_i\}}, [\boldsymbol{A}_{\overline{n}4}]_{\{\boldsymbol{E}_i\}}\right]_{3\times4} = [\boldsymbol{C}_{\overline{n}}]_{3\times4}[\boldsymbol{A}_{\overline{n}}]_{4\times4}; \tag{6.37a}$$

$$\left[[\boldsymbol{B}_{\overline{n}i1}]_{\{\boldsymbol{E}_i\}}, [\boldsymbol{B}_{\overline{n}i2}]_{\{\boldsymbol{E}_i\}}, [\boldsymbol{B}_{\overline{n}i3}]_{\{\boldsymbol{E}_i\}}, [\boldsymbol{B}_{\overline{n}i4}]_{\{\boldsymbol{E}_i\}}\right]_{3\times4} = [\boldsymbol{C}_{\overline{n}}]_{3\times4}[\boldsymbol{B}_{i\overline{n}}]_{4\times4}; \tag{6.37b}$$

In the equation above, the notation $[\boldsymbol{A}_{\overline{n}j}]_{\{\boldsymbol{E}_i\}} = [\boldsymbol{A}_{\overline{n}j}\cdot\boldsymbol{E}_1, \boldsymbol{A}_{\overline{n}j}\cdot\boldsymbol{E}_2, \boldsymbol{A}_{\overline{n}j}\cdot\boldsymbol{E}_3]^T$, represents the component of the coefficient vector $[\boldsymbol{A}_{\overline{n}j}]_{\{\boldsymbol{E}_i\}}$ in $\{\boldsymbol{E}_i\}$ frame. Therefore, the approximated solution is expressed in $\{\boldsymbol{E}_i\}$ frame (Note that the boundary conditions were expressed in $\{\boldsymbol{E}_i\}$ frame). The matrix $[\boldsymbol{C}_{\overline{n}}]$ represents the 12 constants of integration corresponding to $\overline{n}^{\text{th}}$ patch and is determined using continuity conditions or the boundary conditions. The matrices $[\boldsymbol{A}_{\overline{n}}]$ and $[B_{i\overline{n}}]$ (for $i = 1, 2, 3$) contains coefficients that are function of the discrete velocity data $(\boldsymbol{E}_1 + \overline{\boldsymbol{\varepsilon}}_n)$ and $\overline{\boldsymbol{\kappa}}_n$, and are given as:

$$[\boldsymbol{A}_{\overline{n}}] = \begin{bmatrix} \frac{(\overline{\boldsymbol{\kappa}}_n\times(\boldsymbol{E}_1+\overline{\boldsymbol{\varepsilon}}_n))\cdot\boldsymbol{E}_1}{\kappa_n^2} & \frac{((\boldsymbol{E}_1+\overline{\boldsymbol{\varepsilon}}_n)\cdot\overline{\boldsymbol{\kappa}}_n).(\overline{\boldsymbol{\kappa}}_n\cdot\boldsymbol{E}_1)}{\kappa_n^2} & -\frac{(\overline{\boldsymbol{\kappa}}_n\times\overline{\boldsymbol{\kappa}}_n\times(\boldsymbol{E}_1+\overline{\boldsymbol{\varepsilon}}_n))\cdot\boldsymbol{E}_1}{\kappa_n^3} & -\frac{(\overline{\boldsymbol{\kappa}}_n\times(\boldsymbol{E}_1+\overline{\boldsymbol{\varepsilon}}_n)n)\cdot\boldsymbol{E}_1}{\kappa_n^2} \\ \frac{(\overline{\boldsymbol{\kappa}}_n\times(\boldsymbol{E}_1+\overline{\boldsymbol{\varepsilon}}_n))\cdot\boldsymbol{E}_2}{\kappa_n^2} & \frac{((\boldsymbol{E}_1+\overline{\boldsymbol{\varepsilon}}_n)\cdot\overline{\boldsymbol{\kappa}}_n).(\overline{\boldsymbol{\kappa}}_n\cdot\boldsymbol{E}_2)}{\kappa_n^2} & -\frac{(\overline{\boldsymbol{\kappa}}_n\times\overline{\boldsymbol{\kappa}}_n\times(\boldsymbol{E}_1+\overline{\boldsymbol{\varepsilon}}_n))\cdot\boldsymbol{E}_2}{\kappa_n^3} & -\frac{(\overline{\boldsymbol{\kappa}}_n\times(\boldsymbol{E}_1+\overline{\boldsymbol{\varepsilon}}_n))\cdot\boldsymbol{E}_2}{\kappa_n^2} \\ \frac{(\overline{\boldsymbol{\kappa}}_n\times(\boldsymbol{E}_1+\overline{\boldsymbol{\varepsilon}}_n))\cdot\boldsymbol{E}_3}{\kappa_n^2} & \frac{((\boldsymbol{E}_1+\overline{\boldsymbol{\varepsilon}}_n)\cdot\overline{\boldsymbol{\kappa}}_n).(\overline{\boldsymbol{\kappa}}_n\cdot\boldsymbol{E}_3)}{\kappa_n^2} & -\frac{(\overline{\boldsymbol{\kappa}}_n\times\overline{\boldsymbol{\kappa}}_n\times(\boldsymbol{E}_1+\overline{\boldsymbol{\varepsilon}}_n))\cdot\boldsymbol{E}_3}{\kappa_n^3} & -\frac{(\overline{\boldsymbol{\kappa}}_n\times(\boldsymbol{E}_1+\overline{\boldsymbol{\varepsilon}}_n))\cdot\boldsymbol{E}_3}{\kappa_n^2} \\ 1 & 0 & 0 & 0 \end{bmatrix}; \tag{6.38}$$

$$[\boldsymbol{B}_{i\overline{n}}] = \begin{bmatrix} \frac{(\boldsymbol{d}_{i0}+\overline{\boldsymbol{\kappa}}_n\times\overline{\boldsymbol{\kappa}}_n\times\boldsymbol{d}_{i0})\cdot\boldsymbol{E}_1}{\kappa_n^2} & 0 & \frac{(\boldsymbol{d}_{i0}\times\overline{\boldsymbol{\kappa}}_n)\cdot\boldsymbol{E}_1}{\kappa_n} & -\frac{(\overline{\boldsymbol{\kappa}}_n\times\overline{\boldsymbol{\kappa}}_n\times\boldsymbol{d}_{i0})\cdot\boldsymbol{E}_1}{\kappa_n^2} \\ \frac{(\boldsymbol{d}_{i0}+\overline{\boldsymbol{\kappa}}_n\times\overline{\boldsymbol{\kappa}}_n\times\boldsymbol{d}_{i0})\cdot\boldsymbol{E}_2}{\kappa_n^2} & 0 & \frac{(\boldsymbol{d}_{i0}\times\overline{\boldsymbol{\kappa}}_n)\cdot\boldsymbol{E}_2}{\kappa_n} & -\frac{(\overline{\boldsymbol{\kappa}}_n\times\overline{\boldsymbol{\kappa}}_n\times\boldsymbol{d}_{i0})\cdot\boldsymbol{E}_2}{\kappa_n^2} \\ \frac{(\boldsymbol{d}_{i0}+\overline{\boldsymbol{\kappa}}_n\times\overline{\boldsymbol{\kappa}}_n\times\boldsymbol{d}_{i0})\cdot\boldsymbol{E}_3}{\kappa_n^3} & 0 & \frac{(\boldsymbol{d}_{i0}\times\overline{\boldsymbol{\kappa}}_n)\cdot\boldsymbol{E}_3}{\kappa_n} & -\frac{(\overline{\boldsymbol{\kappa}}_n\times\overline{\boldsymbol{\kappa}}_n\times\boldsymbol{d}_{i0})\cdot\boldsymbol{E}_3}{\kappa_n^2} \\ 0 & 0 & 0 & 0 \end{bmatrix}. \tag{6.39}$$

In the equation above $\kappa_n = \|\overline{\boldsymbol{\kappa}}_n\| = \sqrt{\overline{\kappa}_{1_n}^2 + \overline{\kappa}_{2_n}^2 + \overline{\kappa}_{3_n}^2}$. Equation (6.36) yields a helix (which is smooth). We glue the solution of each patch using heavy side function such that the global approximated configuration yielding a continuous solution as,

$$\boldsymbol{\varphi}^h(\xi_1) = \sum_{\overline{n}=1}^{N} \boldsymbol{\varphi}_{\overline{n}}^h(\xi_1) \left[H(\xi_1 - \hat{\xi}_{1\overline{n}-1}) - H(\xi_1 - \hat{\xi}_{1\overline{n}}) \right]; \tag{6.40}$$

$$\boldsymbol{d}_i^h(\xi_1) = \sum_{\overline{n}=1}^{N} \boldsymbol{d}_{i\overline{n}}^h(\xi_1) \left[H(\xi_1 - \hat{\xi}_{1\overline{n}-1}) - H(\xi_1 - \hat{\xi}_{1\overline{n}}) \right]. \tag{6.41}$$

In the equation above $H(\cdot)$ represents Heaviside function. Other higher order techniques listed in section 2.3.2 can also be used to estimate $(\boldsymbol{\varphi}^h(\xi_1), \boldsymbol{Q}_{\mathrm{m}}^h(\xi_1))$ as,

$$\begin{aligned} \boldsymbol{Q}_{\mathrm{m}}^h(\xi_1) &= \exp\left(\int_0^{\xi_1} \hat{\overline{\boldsymbol{\kappa}}}^h(x)\, \mathrm{d}x \right); \\ \boldsymbol{\varphi}^h(t) &= \int_0^t \boldsymbol{Q}^h(x).\left(\overline{\boldsymbol{\varepsilon}}^h(x) + \boldsymbol{E}_1 \right) \mathrm{d}x. \end{aligned} \tag{6.42}$$

6.4.4.2 Estimation of the warping amplitude $p^h(\xi_1)$, mid-curve strain $e^h(\xi_1)$, and shear angles γ_{1i}^h

We obtain p_n by solving the equation set (6.35). The strain e_n and the shear angles γ_{1i_n} can be obtained from the finite strain parameters as:

$$\begin{aligned} e_n &= \sqrt{\overline{\varepsilon}_{1_n}^2 + \overline{\varepsilon}_{2_n}^2 + \overline{\varepsilon}_{3_n}^2} - 1; \\ \gamma_{1i_n} &= \left\{ \begin{array}{ll} \arccos\left(\frac{\overline{\varepsilon}_{i_n}}{1+e_n}\right), & \text{for } i = 1 \\ \arcsin\left(\frac{\overline{\varepsilon}_{i_n}}{1+e_n}\right), & \text{for } i = 2,3 \end{array} \right\}. \end{aligned} \tag{6.43}$$

The approximated fields $p^h(\xi_1)$, $e^h(\xi_1)$, $\gamma_{1i}^h(\xi_1)$ can be obtained by interpolating the discrete quantities p_n, e_n, γ_{1i_n} using techniques listed in table 2.1.

6.4.4.3 Approximated configurations Ω_1^h, Ω_4^h, Ω^h

The approximated deformation maps $\boldsymbol{\phi}_1^h : \boldsymbol{R}_0 \in \Omega_0 \longmapsto \boldsymbol{R} \in \Omega_1^h$, $\boldsymbol{\phi}_4^h : \boldsymbol{R}_0 \in \Omega_0 \longmapsto \boldsymbol{R} \in \Omega_4^h$, and $\boldsymbol{\phi}^h : \boldsymbol{R}_0 \in \Omega_0 \longmapsto \boldsymbol{R} \in \Omega^h$ can be obtained as:

$$\boldsymbol{\phi}_1^h(\boldsymbol{R}_0) = \boldsymbol{\varphi}^h(\xi_1) + \xi_2 \boldsymbol{d}_2^h + \xi_3 \boldsymbol{d}_3^h; \tag{6.44a}$$

$$\boldsymbol{\phi}_4^h(\boldsymbol{R}_0) = \boldsymbol{\varphi}^h(\xi_1) + (1 - \nu\overline{\varepsilon}_1^h)(\xi_2 \boldsymbol{d}_2^h + \xi_3 \boldsymbol{d}_3^h); \tag{6.44b}$$

$$\boldsymbol{\phi}^h(\boldsymbol{R}_0) = \boldsymbol{\varphi}^h(\xi_1) + (1 - \nu\overline{\varepsilon}_1^h)(\xi_2 \boldsymbol{d}_2^h + \xi_3 \boldsymbol{d}_3^h) + p^h \Psi \boldsymbol{d}_1^h. \tag{6.44c}$$

In the equation above, $\overline{\varepsilon}_1^h = (1 + e^h) c_{\gamma_{11_n}}$. In the next section, we show simulations concerning the deformed configurations Ω_1 and Ω_4.

6.4.5 Simulations concerning the deformed state Ω_1

We simulate three-dimensional shapes of varying complexities in deformation. We consider a long rod with the length $L = 300\,m$, and radius $r = 30\,cm$. It is noteworthy that for the deformed state Ω_1, the simulations are completely independent of material properties because inverse shape sensing requires only the kinematic and geometric parameters that define the displacement and strains. To simulate the shape sensing problem, we assume a deformed shape and analytically obtain the finite strain quantities ($\overline{\varepsilon}_{1_n}$, $\overline{\varepsilon}_{2_n}$, $\overline{\varepsilon}_{3_n}$, $\overline{\kappa}_{1_n}$, $\overline{\kappa}_{2_n}$, $\overline{\kappa}_{3_n}$) using the formula for curvatures given in Eq. (6.28) and the definition of material axial strain vector $\overline{\boldsymbol{\varepsilon}} = \boldsymbol{Q}_{\mathrm{m}}^T . \partial_{\xi_1} \boldsymbol{\varphi} - \boldsymbol{E}_i = \overline{\varepsilon}_i \boldsymbol{E}_i$. The strain value at the surface for the assumed deformed shape at set cross-sections for the given directions of strain gauges can be obtained using Eq. (6.43). It was checked that inversion of non-linear equation set (6.35) corresponding to the respective deformed state yields a unique solutions of finite strain terms. To do so we assumed $\sigma_{n,m} = \{\frac{\pi}{4}, \frac{\pi}{2}, \frac{3\pi}{4}, \pi, \frac{5\pi}{4}, \frac{3\pi}{2}\}$ and $\mu_{n,m} = \{\frac{\pi}{4}, -\frac{\pi}{4}, \frac{\pi}{4}, -\frac{\pi}{4}, \frac{\pi}{4}, -\frac{\pi}{4}\}$.

6.4.5.1 Simulation 1

This simulation investigates the effect of curvature and constantly increasing torsion from the fixed end towards the distal end ($0 - 0.75\pi$ radian). The simulation was run for six (3 of them are showed in Fig. 6.5) different cases varying the number of equally spaced strain values to simulate different sensor counts. It is important to note that 6 sensors are required for each cross-section, which implies a total of $6N$ sensors, where N indicates the number of cross-section along the length where these sensors are placed. For simulation 1, N = 3, 5, 10, 20 , 50 and 100 (18, 30, 60, 120 and 600 total sensors respectively) are considered. The distal end was displaced almost by 70 m in both y (along ξ_2) and z (along ξ_3) directions from the initially straight configuration. The imposed configuration is defined by the following parameters:

$$\begin{gathered} \phi_y = \phi_p = \frac{\pi}{8} \sin\left(\frac{\pi\xi_1}{L}\right); \\ e(\xi_1) = 0; \;\; \gamma_{1i} = 0; \;\; \alpha_1 = \frac{\pi}{2}; \;\; \alpha_2 = \frac{0.75\pi\xi_1}{L}; \;\; \alpha_3 = \alpha_1 + \alpha_2. \end{gathered} \tag{6.45}$$

Figure 6.5 compares the exact (imposed) deformed configuration $(\boldsymbol{\varphi}, \{\boldsymbol{d}_i\})$ and the reconstructed configuration $(\boldsymbol{\varphi}^h, \{\boldsymbol{d}_i^h\})$ obtained using the SPEG technique (Eq. (6.40)) for the first simulation. For as few as 5 and 10 cross-sections (spaced approximately 60 m and 30 m respectively), excellent reconstruction is observed with an average (over the full length) root mean square (RMS) error of only 5.2 m and 1.03 m respectively. Secondly for 10 cross-sections, the RMS error for the directors $\boldsymbol{d}_1$, $\boldsymbol{d}_2$, and $\boldsymbol{d}_3$ is merely 0.0078, 0.0056 and 0.0059 respectively, thus predicting the cross-sectional orientation efficiently. If the same simulation is run for the length of cable as 212 m and no torsion for 5 sensor locations (as was performed by Todd et al. [16]), the error comes out to be the same (1.1 m). This clearly reflects the fact that the formulation presented here is a general form that can capture many more mechanical effects as compared to the formulation in Todd et al. [16], which could capture only curvature changes. Increment in number of sensor locations improves the shape reconstruction, thereby reducing the RMS error to as low as 3 mm for 50 sensor locations (1 every 6 m). Figure 6.6 compares the exact component

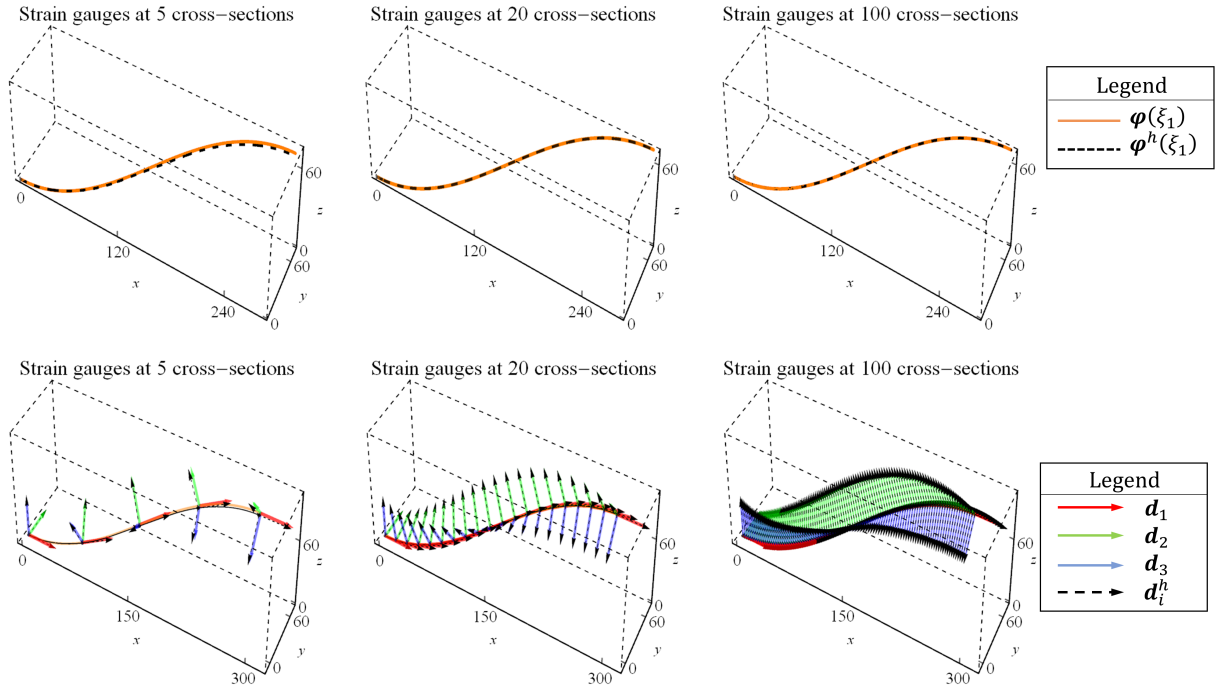

Figure 6.5: Exact and estimated deformed configuration for simulation 1.

of $(\boldsymbol{\varphi}, \boldsymbol{d}_1)$ with the components predicted by $N = 10$ and $N = 50$ strain measurement locations. The figure shows good convergence with the increase of the number of sensors. Since the object in simulation 1 is not deformed in a very complicated shape, 10 sensor locations does a good reconstructing of the shape.

The results presented above are for the ideal case of perfect strain transfer from the structure to the attached strain gauges with certainty in the assumed boundary conditions and no other external noise influence on the system (environmental or numerical). To examine these influences for a first order assessment of robustness, uniformly-distributed random noise was added to the strain values, at a [-5,5] micro-strain level (representative of the most conventional strain gauge systems) and at [-50,50] micro-strain level (severe noise) before being input into the reconstruction algorithm. Fifty such realizations were performed in a Monte Carlo sense, and the average RMS error was computed for different number of sensor counts at each noise level. It is observed that at each sensor count, the noise elevates the error with gradual improvement as

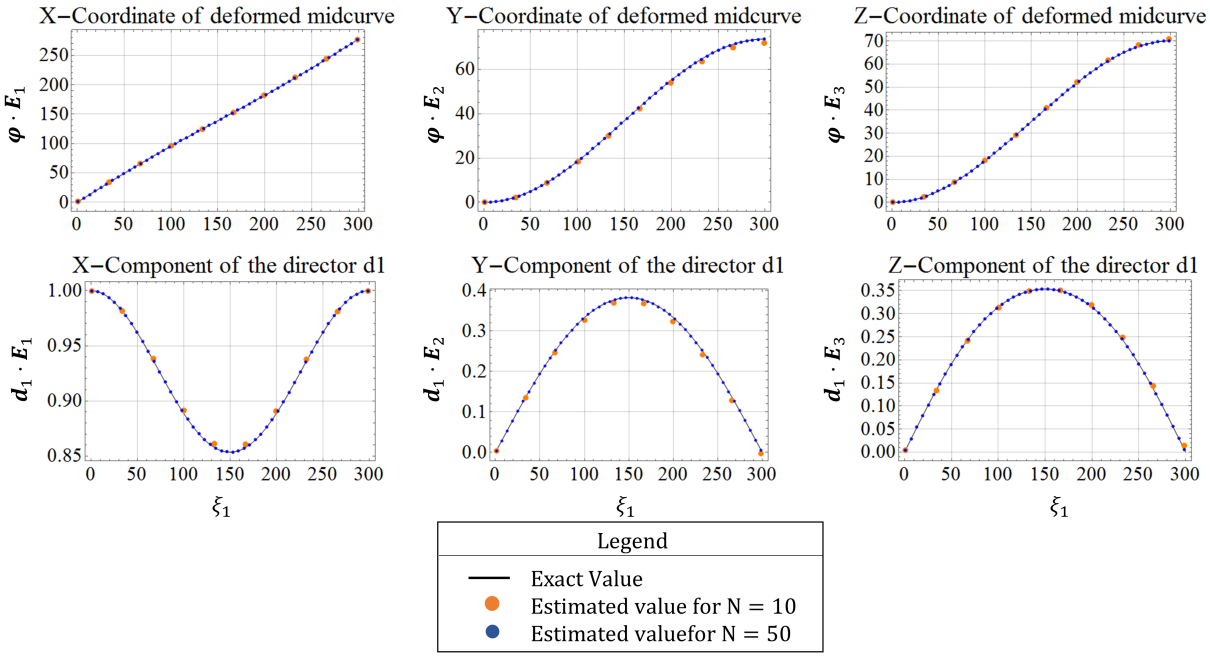

Figure 6.6: Exact and estimated components of mid-curve position vector $\boldsymbol{\varphi}$, and the components of director $\boldsymbol{d}_1$ for simulation 1.

the sensor count increases. Figure 6.7 (right plot) gives the RMS error in the position vector for different noise level and the left plot represents the RMS error plot for the directors considering no external noise. The error when there is no external noise is due to approximation in the estimation. Another source of error is uncertainty in the boundary conditions. Figure 6.7 shows the effect of uncertainty on the specifications of the boundary condition at the proximal end $\xi_1 = 0$, using 100 sensors by choosing 50 random boundary conditions at proximal end over $[-0.0001,\ 0.0001]\ m$, $[-0.01, 0.01]\ m$, $[-0.1, 0.1]\ m$, $[-1, 1]\ m$ and $[-10, 10]\ m$ and obtaining the average RMS value (averaged over 50 simulation) for both the simulations 1 and 2 (discussed in next section). It is clear that with the current approach, the trend remains linear, with the averaged RMS error being proportional to the input boundary condition uncertainty level.

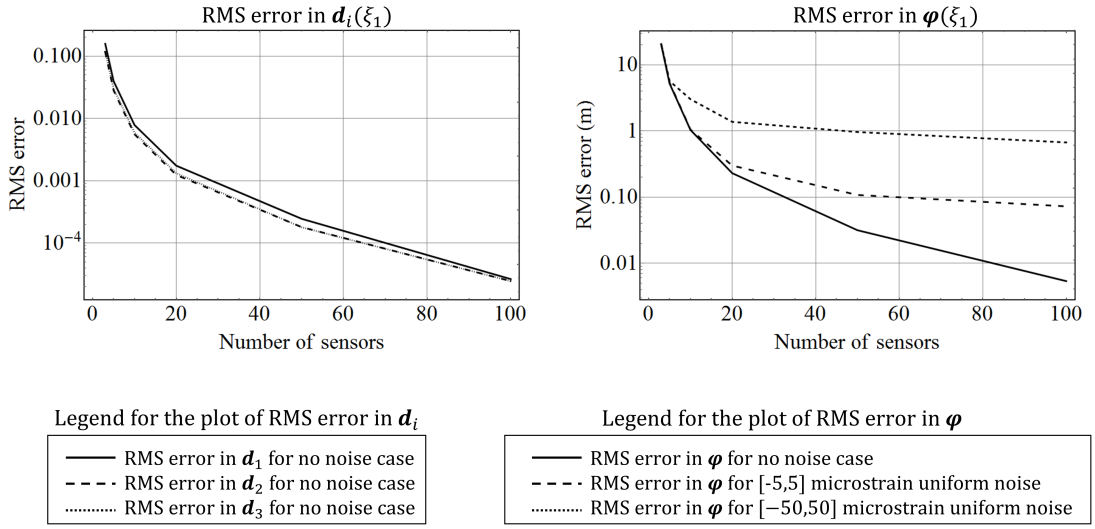

Figure 6.7: Right plot: RMS error in mid-curve position vector for different noise levels; Left plot: RMS error plot for the directors considering no-noise case.

6.4.5.2 Simulation 2

In simulation 2, the object with same geometric and kinematic configuration as in Simulation 1 is subjected to torsion, non-uniform elongation, shear and complex curvature changes, making it more general. The exact/imposed deformed configuration is given by the following,

$$\begin{aligned} \phi_y = \pi \sin\left(\frac{\pi\xi_1}{L}\right);\ \ \phi_p = \pi \sin\left(\frac{\pi\xi_1}{L}\right).\left(1 - 0.5\sin\frac{3.5\pi\xi_1}{L}\right);\\ e(\xi_1) = \frac{20\pi}{L}\cos\left(\frac{\pi\xi_1}{2L}\right);\ \ \gamma_{11} = \frac{\pi\xi_1}{16L};\ \ \gamma_{12} = \frac{\pi\xi_1}{32L};\ \ \alpha_3 = \frac{\pi}{2}\left(1 + \frac{0.2\xi_1}{L}\right). \end{aligned} \tag{6.46}$$

The angles γ_{12}, α_1 and α_2 may be obtained by imposing the constraints defined in Eq. (6.27).

The displacement of the distal end is about 193 m and 116 m in the y and z direction. Since the shape and deformation is complicated, the study is performed for a minimum of 10 sensor locations (with N = 10, 20, 50 and 100) unlike a minimum of 3 sensor locations in simulation 1. The RMS error for the position vector decreases from 9.8 m using 10 sensor locations to 4.8 cm

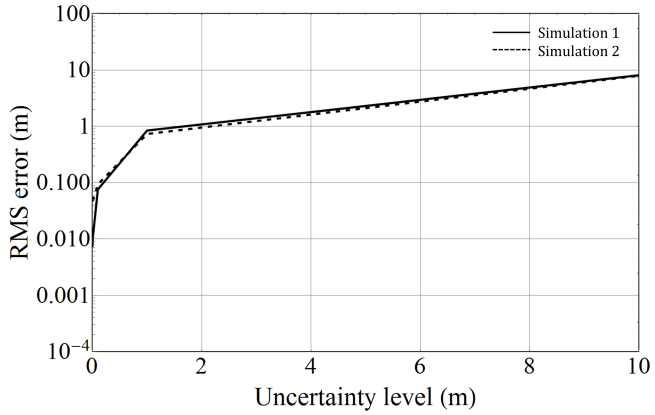

Figure 6.8: Average root mean square error in the shape reconstruction for simulations 1 and 2 as a function of the uncertainty level in the initial displacement conditions at the proximal end.

with 100 sensor locations, representing excellent convergent reconstruction.

The top three plots of Fig. 6.9 compare the exact (imposed) mid-curve with the reconstructed mid-curve for the second simulation and the bottom three plots compares the exact cross sectional orientation with the predicted directors for $N = 10$, 20 and 100. Figure 6.10 represents comparison of the exact component of $(\boldsymbol{\varphi}, \boldsymbol{d}_1)$ with the components predicted by $N = 10$ and $N = 50$ strain measurement locations. Assuming perfect strain transfer between the structure and the strain gauge (no noise and perfect bonding), exact and the predicted angles are observed to coincide because these parameters are directly related to the strain measurements.

The major contributor of error due to the algorithm, for this simulation, is mainly the deformed shape of the mid-curve and the curvatures. The axial, shear and torsion contributions are almost negligible to the RMS error of the position vector to the mid-curve. This observation is made clear from the RMS error plot in Fig. 6.11. This is not a surprising result because the global shape of the structure in this example is still dominated by the curvature; in a simulation dominated by another effect, e.g., a pure axial extension, error would be primarily due to that instead, and using the simplified theory such as in Todd et al. [16] would induce significant error.

Similar pattern of RMS error is observed as in simulation 1 when external noise is added to the structure. The error is much higher for the second simulation as compared to the first

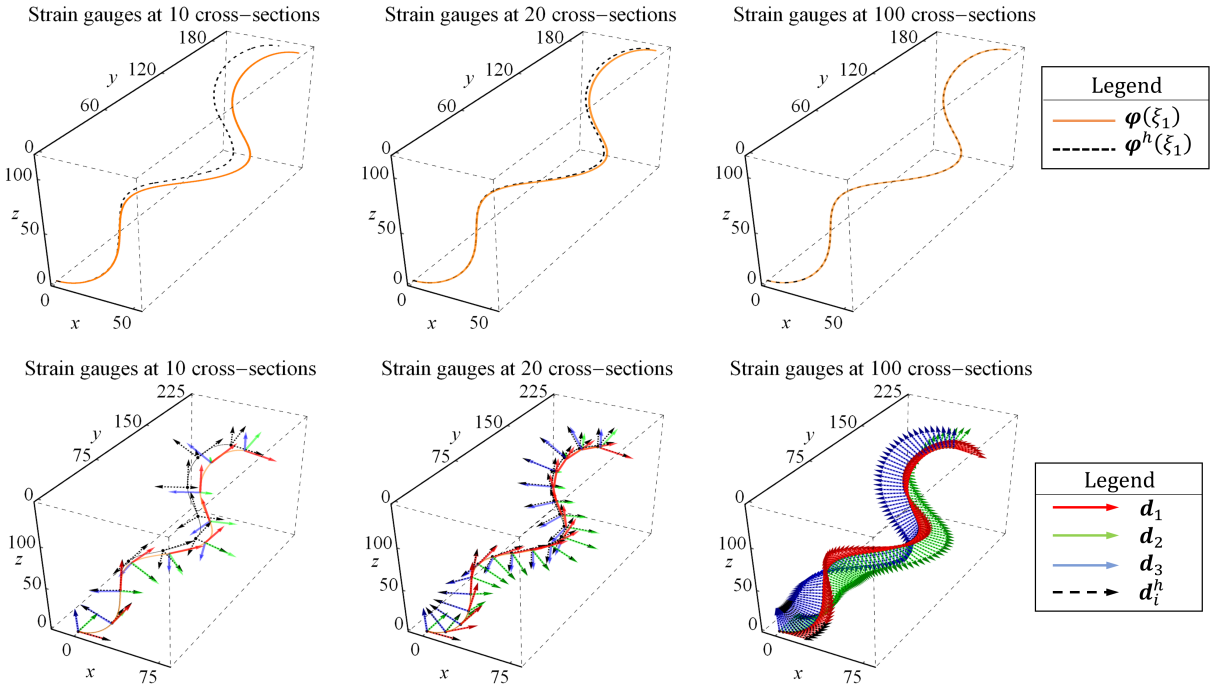

Figure 6.9: Exact and estimated deformed configuration for simulation 2.

because of complicated deformed shape of the mid-curve and the complex curvature. As in Todd et al. [16], the maximum reconstruction error in both of the above simulations was observed at the distal end. It is because the boundary conditions were exactly specified on the proximal end. Error due to the algorithm itself (but not necessarily error due to external influence or measurement noise) then propagates along the object to the maximum at the farthest end from the known condition. Therefore, the error propagation start from the point of specified boundary condition.

6.4.5.3 Simulation 3

In most cable or tether-like structures, curvature is the dominant deformation. The third simulation presents a cable with same cross-section as the previous simulations. We consider a helix with varying radius such that the bottom helix radius is $r_{\text{helix}} = 50\,m$, pitch length is $l_p = 10\pi\,m$, number of turns is $n_{\text{turns}} = 20$. The total length is then given by the total length of $L = 2\pi.n_{turns}\sqrt{r_{\text{spring}}^2 + \left(\frac{l_p}{2\pi}\right)^2} = 6.314\,km$. Apart from these geometric parameters, the deformed

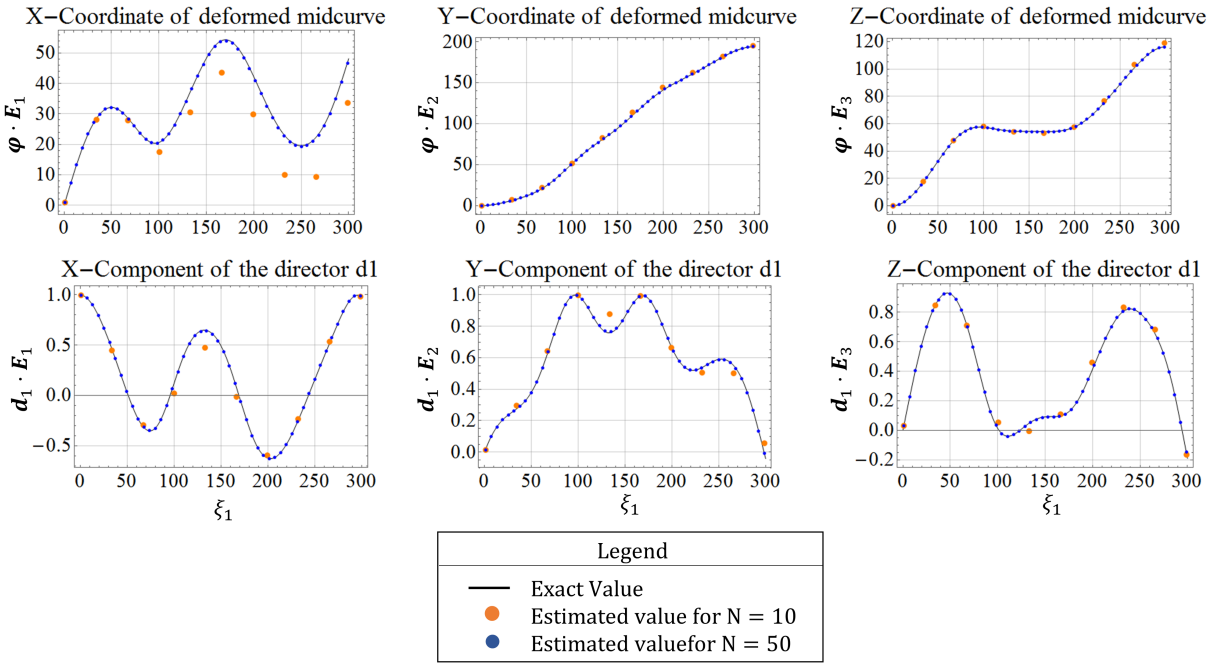

Figure 6.10: Exact and estimated components of the mid-curve position vector $\boldsymbol{\varphi}$ and the director $\boldsymbol{d}_1$ for simulation 2.

state is defined by the following:

$$\begin{gathered}\phi_y = \frac{2\pi n_{\text{turns}}\xi_1}{L};\quad \phi_p = \frac{\pi}{2}\sin\left(\frac{\pi\xi_1}{2L}\right);\\ e(\xi_1) = 0;\quad \gamma_{1i} = 0;\quad \alpha_1 = \alpha_3 = \frac{\pi}{2};\quad \alpha_2 = 0.\end{gathered} \tag{6.47}$$

Significant RMS error of 15.9 m was observed with 50 sensor locations (1 in every 126 m) and it reduced to 0.78 m with 200 sensor locations (1 cross section every 32 m). The predicted shape using 20 sensor locations was not acceptable with tremendous error of 1326 m because of complex shape and curvature changes. Figure 6.12 shows the predicted deformed shape and the directors for $N = 50,\ 100$ and 200 sensor locations. Figure 6.13 shows the comparison between the predicted components of the mid-curve for $N = 50$ and $N = 100$ sensor locations as compared to the exact deformed shape. It is observed that an excellent reconstruction of such a complicated shape is observed with mere $N = 200$ sensor locations.

Furthermore, it is observed that for a constant radius, constant pitch spring only 2

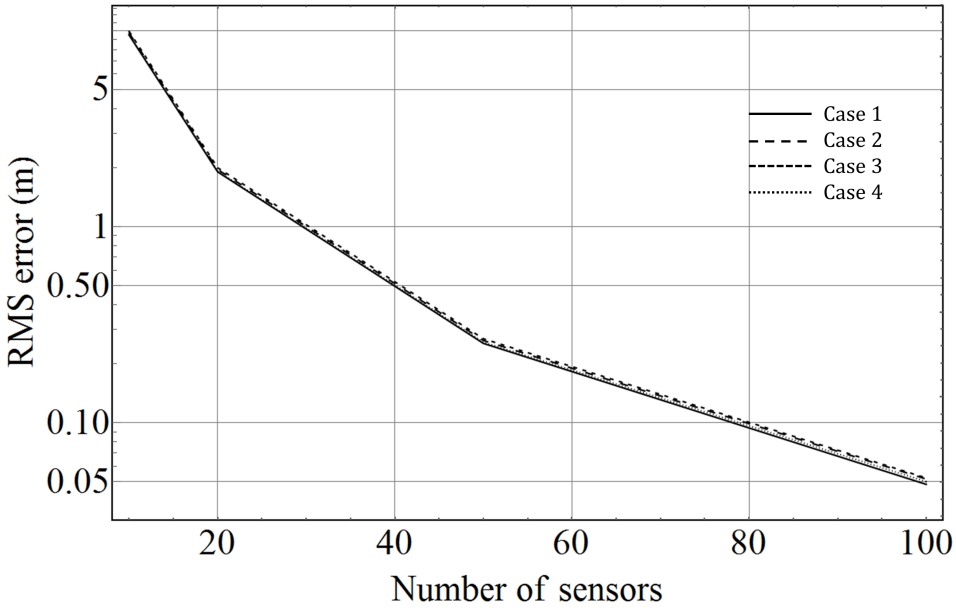

Figure 6.11: Root mean square error for the position vector for simulation 2.

sensor locations (which is the minimum number of sensor locations required) are required to exactly predict the shape. Such a deformed shape is parameterized by constant $\overline{\kappa}_1$ and $\overline{\kappa}_2$ ($\overline{\kappa}_3 = \partial_{\xi_1}\phi_p(\xi_1) = 0$) throughout the length of the cable.

6.4.6 Simulations concerning the deformed state Ω_4

Unlike the simulations in last section concerning the deformed state Ω_1, the shape sensing now depends on the material property ν. To simulate the case, we assume a deformed shape and analytically obtain the finite strain quantities ($\overline{\varepsilon}_{1_n}$, $\partial_{\xi_1}\overline{\varepsilon}_{1_n}$, $\overline{\varepsilon}_{2_n}$, $\overline{\varepsilon}_{3_n}$, $\overline{\kappa}_{1_n}$, $\overline{\kappa}_{2_n}$, $\overline{\kappa}_{3_n}$). The strain value at the surface for the assumed deformed shape at set cross-sections for the given directions of strain gauges can be obtained using Eq. (6.43). It was checked that inversion of set of seven non-linear equation (6.35) corresponding to the respective deformed state yields a unique solutions of finite strain terms. To do so we have assumed $\sigma_{n,m} = \{\frac{\pi}{4}, \frac{\pi}{2}, \frac{3\pi}{4}, \pi, \frac{5\pi}{4}, \frac{3\pi}{2}, \frac{7\pi}{4}\}$ and $\mu_{n,m} = \{\frac{\pi}{4}, -\frac{\pi}{4}, \frac{\pi}{4}, -\frac{\pi}{4}, \frac{\pi}{4}, -\frac{\pi}{4}, \frac{\pi}{4}\}$.

We simulate a 300 m long circular rod with $\nu = 0.3$ and diameter of 30.48 cm to study the effect of multiple curvatures, axial strain, Poisson's deformation, but no shear (thus,

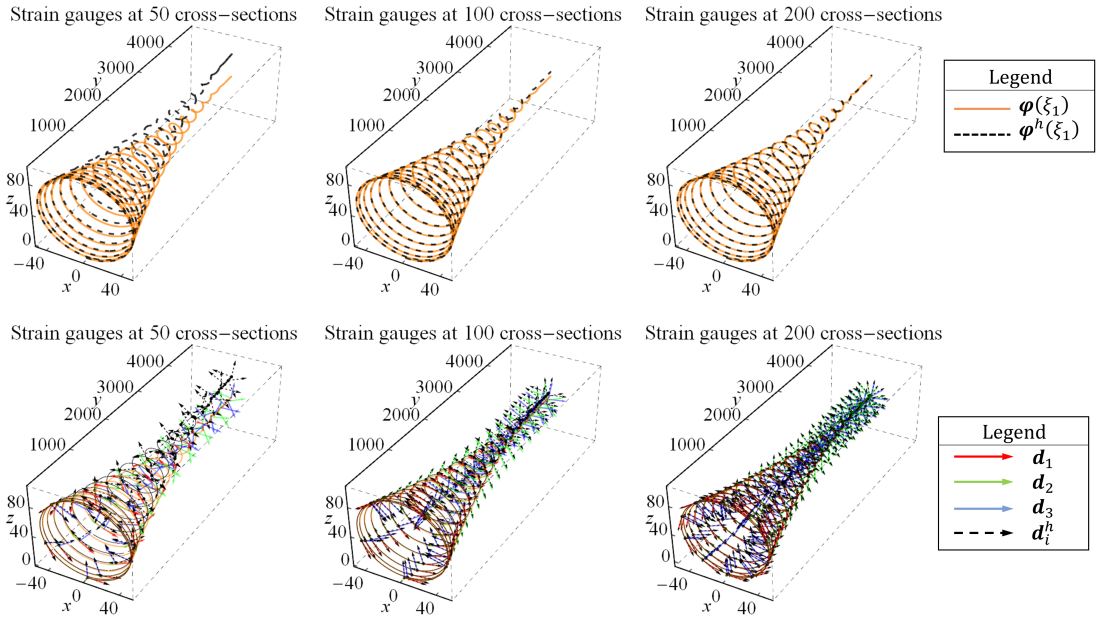

Figure 6.12: Exact and estimated deformed configuration for simulation 3.

$\overline{\varepsilon}_1 = e$; $\overline{\varepsilon}_2 = \overline{\varepsilon}_3 = 0$). The imposed shape is dictated by the following parameters,

$$\phi_y = \phi_p = \frac{\pi}{8}\sin\left(\frac{2.5\pi\xi_1}{L}\right);$$
$$e(\xi_1) = 0.05 + \frac{0.2\xi_1}{L} + \frac{1}{50}\sin\left(\frac{4\pi\xi_1}{L}\right);\quad \gamma_{1i} = 0;\quad \alpha_1 = \frac{\pi}{2};\quad \alpha_2 = \frac{0.75\pi\xi_1}{L};\quad \alpha_3 = \alpha_1 + \alpha_2. \tag{6.48}$$

The assumed mid-curve shape bears two points of degeneracy, yet the algorithm performs robustly. The algorithm is thus without any singularity.

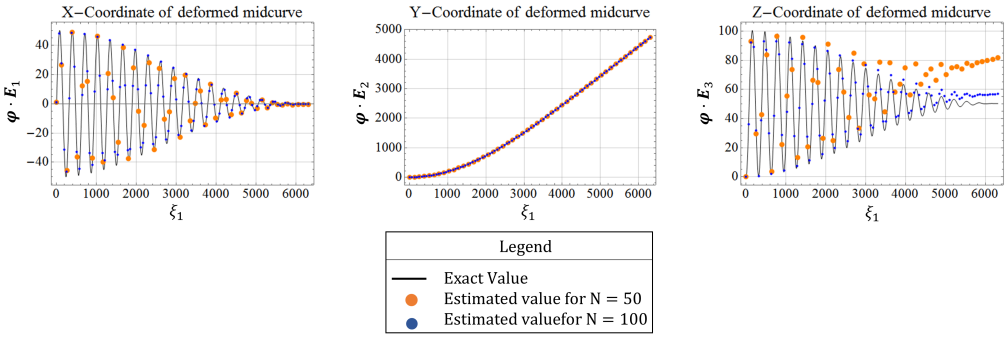

Figure 6.13: Exact and estimated components of mid-curve position vector $\boldsymbol{\varphi}$ and the director $\boldsymbol{d}_1$ for simulation 3.

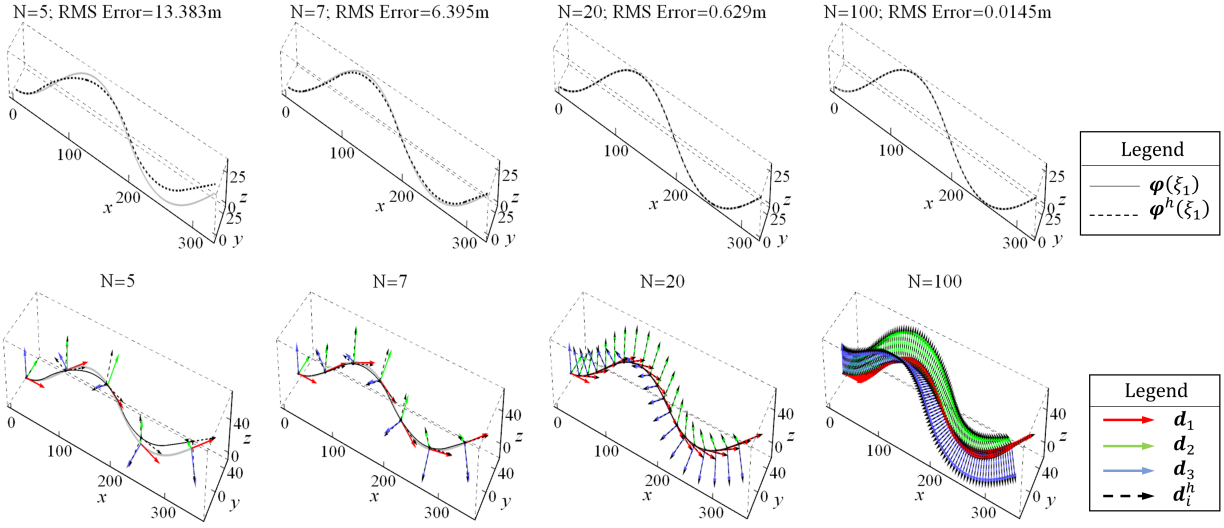

Figure 6.14: Exact and estimated deformed configuration for simulation considering Poisson's deformation along with curvatures and axial strain but no shear.

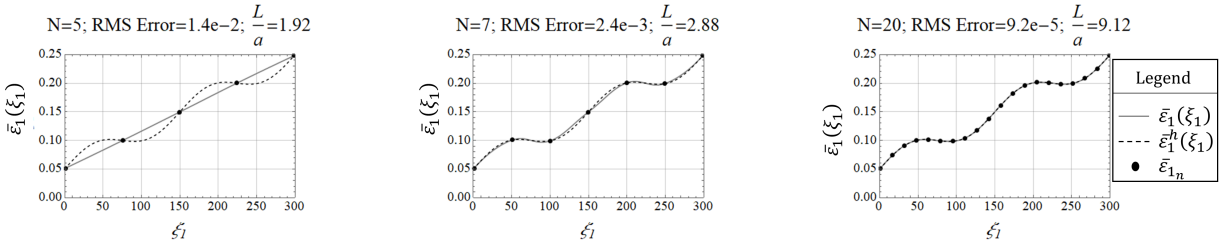

Figure 6.15: Comparison of the components of the exact and approximated axial strain $\bar{\varepsilon}_1$.

The figure 6.14 compares the exact (imposed) mid-curve $\boldsymbol{\varphi}(\xi_1)$ with the approximated mid-curve $\boldsymbol{\varphi}^h(\xi_1)$ and the exact director field $\{\boldsymbol{d}_i\}$ with the approximated field $\{\boldsymbol{d}_i^h\}$, solved using SPEG technique for $N = 5$, 7, 20 and 50 number of cross-sections. The RMS Error is reported on top of the plots. The RMS Error reduces exponentially with the increase in number of cross-section at which strain gauge is attached.

Figure 6.15 and 6.16 compares the exact curvature and axial strain field with the approximated fields. The approximation is obtained using Moving Least Square approximation. In this simulation, we use 2^{nd} order shape function. The parameter L/a in Fig. 6.15 and 6.16 represents the ratio of the undeformed length of beam and the support size chosen for the approximation.

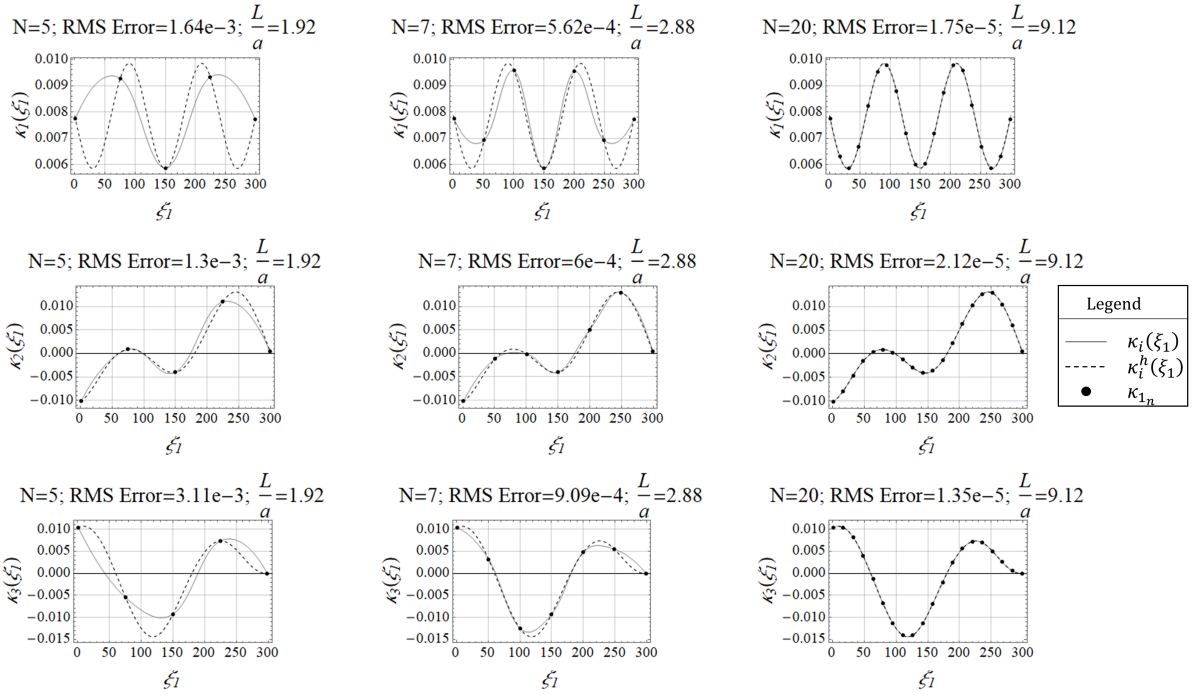

Figure 6.16: Comparison of the components of exact and approximated curvatures.

6.5 Similarities in the path estimation of rigid body (or swarm of rigid bodies) and shape reconstruction of slender structure (like rods)

A rigid body motion and a beam with rigid Euler-Bernoulli's cross-section $\mathfrak{B}_1(\xi_1)$ is defined by an identical configuration space $\mathbb{C}_1 := \mathbb{R}^3 \times SO(3)$. The Cosserat beam is defined by a mid-curve curve $\boldsymbol{\varphi}$ and the director triad field $\{\boldsymbol{d}_i\}$ that defines the orientation of the cross-section. However, the configuration of the beam $\boldsymbol{\Phi}_1 \in \mathbb{C}_1$ is parameterized by the undeformed arc length of the mid-curve, lets call it $\xi_1 \in \mathbb{R}^+$, and the configuration of the moving rigid body $\boldsymbol{\Phi}_2 \in \mathbb{C}_1$ is parameterized by time $t \in \mathbb{R}^+$, such that

$$\begin{aligned}\boldsymbol{\Phi}_1(\xi_1) &:= \left\{(\boldsymbol{\varphi}(\xi_1), \boldsymbol{Q}(\xi_1)) \mid \ \boldsymbol{\varphi} : \mathbb{R}^+ \longrightarrow \mathbb{R}^3, \ \ \boldsymbol{Q} : \mathbb{R}^+ \longrightarrow SO(3)\right\} \in \mathbb{C}_1; \\ \boldsymbol{\Phi}_2(t) &:= \left\{(\boldsymbol{\varphi}(t), \boldsymbol{Q}(t)) \mid \ \boldsymbol{\varphi} : \mathbb{R}^+ \longrightarrow \mathbb{R}^3, \ \ \boldsymbol{Q} : \mathbb{R}^+ \longrightarrow SO(3)\right\} \in \mathbb{C}_1.\end{aligned} \tag{6.49}$$

If s represents the deformed arc-length in the deformed state of the beam or the distance traveled by the moving object, then an analogy can be observed between the axial strain of the mid-curve $e(\xi_1)$ for the beam and the velocity $v(t)$ of the moving object, such that, $\partial_{\xi_1} s = 1 + e(\xi_1)$ for beams, and $\partial_t s = v(t)$ in case of a moving rigid body. Similarly, the velocity vector $\boldsymbol{v} = \partial_t \boldsymbol{\varphi}$ is comparable to the mid-curve axial strain vector of the beam, in the sense that $\partial_{\xi_1} \boldsymbol{\varphi} = \boldsymbol{\varphi} + \boldsymbol{d}_1$.

Like the configuration space, the tangent space of the two systems is identical. The equivalent of angular velocity (spin) tensor $\hat{\boldsymbol{\omega}}(t) = \partial_t \boldsymbol{Q}.\boldsymbol{Q}^T$ is the spin tensor corresponding to the Darboux vector (also called the curvature tensor) $\hat{\boldsymbol{\kappa}}(\xi_1) = \partial_{\xi_1} \boldsymbol{Q}.\boldsymbol{Q}^T$. Therefore, the problem of shape reconstruction of the beam from a finite number of surface strain gauge readings bears a striking similarity with the path estimation of rigid body motion using discrete linear and angular velocity data. In the case of path estimation, the data is obtained in the form of Euler angles (or quaternions) and their derivatives (from the IMU and other sensors), whereas in case of shape sensing, the strain gauge data can be used to obtain the sectional curvatures and mid-curve strains. Furthermore, the problem of *dead reckoning* is common in the case of path estimation and shape sensing as will be seen in this chapter.

A geometrically-exact *Kirchhoff* beam and a rigid body can be defined by an *adapted* frame. If the torsion angle is zero along the beam or if the roll angle field vanishes (which is seldom in case of rigid body motion), SMAF is sufficient to define the orientation. The presence of a torsion field in the beam and roll angle in the rigid body demands GMAF to define the orientation.

A more interesting case arises when we consider the swarm of rigid-bodies (say drones). If the swarm is a *rigid-formation*, the relative positions of *follower* drone is fixed (with vanishing co-rotational derivative) and pre-defined with respect to the *leader* drone. If the *rigid-formation* is planar, the orientation of the plane and the position vector of the leader drone defines the configuration of the system. This is analogous to *Simo-Reissner* beam (refer to: Simo [48] and Reissner [62]) that has *rigid cross-section* and is allowed to have shear deformation (unlike

Euler-Bernoulli beam, where the cross-section is perpendicular to the mid-curve and shear deformations are ignored). In a *leader-follower* model of drone formations, the *follower* drones need not have a fixed relative position with respect to the *leader* drone. However, if the relative positions of follower drones are pre-defined (that is useful for drone light-shows that have gained recent popularity), the system maintains its single-manifold character. This system is similar to *Simo-Reissner* beam with in-plane and out-of-plane cross-sectional deformation with warping and Poisson's transformation being pre-defined. The material frame (MF) can be used to define orientation in these types of problems. The paper by Chadha and Todd [34] (discussed in chapter 4 and 5) is dedicated to developing generalized single-manifold beam kinematics that includes *fully coupled Poisson's and warping effect* (such that the cross-sectional deformation is pre-defined to maintain single-manifold nature of the problem).

The compact approach in defining the shape of the swarm at any given time is accomplished using a partial differential equation. For a system like a swarm of drones, trajectory tracking is essential to define controls for the system so that the shape of swarm converges to the solution of the prescribed differential equation at a given time. Defining the shape as a solution to governing differential equations is compact, communication and memory-efficient, and it helps in developing a local corrective algorithm (distributed control) where one drone corrects its position based on the position of neighboring drones. This process is very much similar to obtaining warping function from the Neumann boundary value problem corresponding to warping in the beam. The local corrective algorithm in case of a swarm of drones is comparable to the compatibility conditions in solid mechanics.

6.6 Summary

This chapter essentially consists of two parts. The first part details the measurement model for strain gauge (finite length and discrete strain gauges) attached to the beam. The kinematics of

the beam described in chapter 5 is exploited to develop a mathematical model for *scalar strain* value that would be observed in strain gauges perfectly attached to the surface (or embedded into the beam). A simple example is illustrated to validate the proposed strain gauge model.

The second part of the chapter deals with three-dimensional shape-reconstruction of slender structures. The idea is to obtain the global shape of the rod using a countable number of strain gauges. The theory detailed in this chapter does not assume the cross-section to be rigid. Therefore, the cross-section could undergo in-plane and out-of-plane deformation. The kinematics considered is simplified as compared to the kinematics of deformed configuration Ω_3 discussed in chapter 4. The contribution of warping and bending towards in-plane deformation is ignored. The contribution of bending induced shear to out-of-plane warping is also ignored.

The finite strain parameters on to which the strain gauge reading depends (like mid-curve axial strain, curvatures, and their derivatives) at a given cross-section can be evaluated from the strain gauges reading by inverting the set of *scalar strain* equations (Eq. (6.12)). Once the material mid-curve strain vector and the curvature vector at discrete cross-section locations are obtained, the mid-curve position vector and the director triads can be estimated using techniques like SPEG developed in chapter 2. This algorithm could potentially be embedded in digital signal processing chips or field-programmable gate array as part of an embedded solution with low power and memory requirements. There are three main sources of error: uncertainty in the boundary condition, noise in the strain measurements, and error due to approximation. Preliminary noise tolerance study and boundary condition uncertainty studies show that the RMS error trends with the extraneous noise due to environmental or measurement noise and with error in specifying the one boundary condition vector required for inertial reference. The suggested reconstruction strategy is convergent and non-singular even if the mid-curve has multiple points or segments of degeneracy.

The discussion on the strain gauge model carried out in the early part of this chapter has been published in the International Journal of Solids and Structures, Mayank Chadha and Michael

D. Todd [34], 2019. The title of this paper is: "A comprehensive kinematic model of single-manifold Cosserat beam structures with application to a finite strain measurement model for strain gauges". The shape reconstruction methodology developed in section 6.4, has been published in the Journal of Applied Mechanics (ASME), Mayank Chadha and Michael D. Todd [17], 2017. The title of this paper is: "A generalized approach for reconstructing the three-dimensional shape of slender structures including the effects of curvature, shear, torsion, and elongation". The conference proceeding titled: "An Improved Shape Reconstruction Methodology for Long Rod Like Structures Using Cosserat Kinematics-Including the Poisson's Effect," published in Nonlinear Dynamics, furthers the theory of shape sensing detailed in [17] by incorporating Poisson's deformation. Conference paper Chadha and Todd [55], presented at International Conference on Experimental Vibration Analysis for Civil Engineering Structures, 2017, focuses on the applications of shape-sensing on pipeline monitoring. The dissertation author is the primary investigator and author of these papers.

Chapter 7

Balance Laws and Variational Formulation of Geometrically-Exact Beam with Enhanced Kinematics

7.1 Introduction and brief literature review on geometrically-exact beam theory

The development of the beam/rod theories idealized by a space curve goes back to two and half centuries ago and was instrumental in accelerating the second industrial revolution (refer Euler and Truesdell [63]). Interestingly, further development of beam theory continues to date. The work by Ericksen and Truesdell [64], Yang et al. [65] and Chadha and Todd [53], among many others in this area, summarizes the developments in the beam theory in the last century. The advanced applications of beam theory like deformation of bio-polymers (for example: Travers et al. [66], Manning et al. [67]), biological structures (for example: Klapper et al. [68]), shape-sensing, robotics, multi-body dynamics (for example: Lang et al. [69]), composite structures (for example: Hodges [70]), contact problems (for example: Meier et al. [71]), thermal problems (for example:

Green and Naghdi [72], Altenbach et al. [73]), micro and nanostructures used in MEMS and NEMS etc., necessitates further development and refinement of this theory. The versatility of the application of beam theory in numerous problems is the core motivation to develop and to refine the existing theories. In the next few paragraphs, we first perform a relevant literature review related to this chapter.

Duhem [74] investigated a kinematic idea that provided a sense of rotation to any material point, such that a point in the object not only has a position vector associated with it but also has an attached triad (not necessarily orthonormal in nature). The attached triad, also called the directors, assigns the sense of rotation to these material points. Darboux [6] exploited the moving frame technique to study surfaces. Cartan further generalized the idea of a frame field (or moving frames) to n-dimensional manifolds in one of the most important constructions in differential geometry, known as *Cartan connections*. The idea was to study Riemannian manifold by means of a moving frame. Influenced from the work of Cosserat brothers [75], Cartan used a moving tetrad frame to investigate 4-dimensional space-time manifold and modified the General Theory of Relativity so as to allows space-time to have torsion in addition to curvature: called Einstein-Cartan Theory (refer to Cartan [9], [8] and Trautman [76]). At a fundamental level, the tetrad frame theory in relativity is very similar to the geometrically-exact shell theory (refer to Simo et al. [77]). We deliberately deviated a bit above to make a strong point that at a deeper level, the kinematics of geometrically-exact beams, shells, and advanced theories like general relativity are kinematically unified under the domain of *differential geometry investigated using moving frames*. In the field of deformation theory, moving frames becomes particularly useful in defining kinematics of micropolar models of continuum mechanics. In such models, a macro element has independent rotational degrees of freedom at the micro-level along with translation considered at a macro level. Unlike traditional continuum mechanics, where each particle has three degrees of freedom associated with it, in micropolar continua, each particle is equipped with 6 degrees of freedom (refer to Eringen [78]). For example, in the case of a beam with rigid

cross-section, each cross-section can be considered as a rigid body that can undergo translation and rotation. The Cosserat rod is a special case of problems in micropolar continua, which is a special restraint case of micromorphic continua. The compiled work by Altenbach and Eremeyev [79] serves as a great reference that covers topics on micro-polar continua (by Altenbach and Eremeyev), Cosserat rods (by Altenbach, Bîrsan and Eremeyev), micromorphic continua (by Samuel Forest), electromagnetism and generalized continua (by Maugin).

It was Eugene and François Cosserat [75] who conceived the idea of moving frames to capture geometrically exact non-linear deformation of the beams (and shells) using framed space curve (therefore called single-manifold beam). Ericksen and Truesdell [64] generalized the Cosserat brothers work to develop a non-linear theory of rods and shells for finite strain. Some of the prominent investigations and research on theory of rods by Hay [80], Cohen [81], Whitman and Desilve [82], Green and Naghdi [83] and [84], Antman et al. [85], [86], and [87], Argyris and Symeonidis [19], [88], and [89], Eric Reissner [90], [91] and [62], and Simo [48].

Among these seminal contributions, the work by Reissner was the first major leap forward towards the *geometrically-exact beam theory*, when he extended *Kirchhoff-Love beam theory* (refer to Love [92]) to also capture shear deformation in addition to bending and torsion in 2D plane [90]. Reissner [62] tackled the 3D problem by further simplifying rotation tensor at a cost of losing geometric exactness. Reissner's work, among many previous ones, ignited researchers in this area and lead to a wave of publications in *geometrically-exact beams* (that can ideally describe any magnitude of displacement and rotations) in and around the 1980s. Amongst them, was a prominent work by Simo [48] that extended the geometrically-exact Reissner's beam to 3D (with geometric-exactness preserved) in the setting of differential geometry (now called *Simo-Reissner beam theory*). In our opinion, Simo [48] succeeded in giving a clear description of non-linear configuration space, the associated tangent space and the exponential maps associated with rotational non-commutative Lie group $SO(3)$. Differential geometry and Lie groups were not an alien concept in the 1980s but these ideas largely remained inaccessible to researchers with an

engineering background. Simo's work established machinery that helped the applied mechanics community in developing an understanding of operating on the tangent space of a non-linear manifold, thus, furthering the research in numerical solutions of the governing equations.

Many papers were published in the same time period concerning finite element formulation of geometrically-exact beams, the primary contributors being: Simo et al. [48], [93], [94] and [95]; Iura et al. [49] and [96]; Cardona et al. [51]; Ibrahimbegovic [52]. These papers considered linearly elastic material and addressed both static and dynamic cases, but they presented different approaches to time-stepping schemes and updating rotation vector: Eulerian (refer to: [93], and [94]), updated Lagrangian (refer to: [51]) and total Lagrangian (refer to: [52], [96] and [97]). Since these papers got published, research tackling the theoretical and computational techniques gained momentum, for examples: problems related to discretization and interpolation approaches (refer to: [98], [99], [100], [101] [102] and [26]), mixed formulation (refer to: [103]), non-linear materials and constitutive law (refer to: [104], [105], [106] and [107]), space and time-integration schemes (refer to: [108], [109] and [110]), initially curved configuration (refer to: [50] and [53]), and enhanced kinematics (refer to: [93], [111], [37] and [34]).

The Cosserat beam with a Euler-Bernoulli rigid cross-section has been well treated in the past. Simo and Vu-Quoc [43] extended their previous work [48] and [95] to incorporate warping using a Saint-Venant warping function. It also included the effect of asymmetrical sections by using the concept of shear-center in the framework of geometrically-exact beams. The works by Carrera et al. [112] and Pagani et al. [113] also tackle warping in a rather general framework of Carrera Unified Formulation (CUF). A very recent paper by Carrera [114] gives CUF for the micropolar beams.

Chapter 4 and 5 investigated and refined the kinematics of Cosserat beams and chapter 6 developed a generalized strain gauge measurement model for prediction of finite strain at any location on the surface of such an object. This development incorporated a fully coupled Poisson's and warping effect along with the classical deformation effects like bending, torsion, shear, and

axial deformation for the case of *finite displacement and strain* (refer to Hay [80]), thus, allowing us to capture a three dimensional, multi-axial strain fields using a single-manifold kinematics (a beam/rod represented by a spatial curve). Numerous works on shear based deformation are founded on Timoshenko's beam theory that assumes a uniform shear distribution (thus restricting the cross-section to remain planar). However, the enhanced kinematics discussed in chapter 4 also considers non-uniform shear deformation due to bending-induced shear. The kinematics of Cosserat beams is derived from the theory of differential geometry of framed space curves. Unlike the traditional geometrically-exact beam theory where the deformation map is a function of the differential invariants (curvatures) of a framed curve, the work presented in chapter 4 considers a deformation map that also depends on the higher-order derivatives of the curvatures and mid-curve strains.

With a more complete kinematics defined, further analysis of the beam can be primarily split into two broad parts: the first part will include developing variational formulation, investigating balance laws (presented in current chapter) and exploring the Hamiltonian structure (presented in chapter 8) of the beam; the second part will focus on numerically solving for the configuration space of the beam (presented in chapter 9 and 10). In order to tangibly solve the problem at hand, we first focus our attention on performing a step-by-step and detailed analysis of the balance laws and the variational formulation of the beam. This investigation becomes interesting, and at the same time challenging, because of the inclusion of *fully coupled Poisson's and warping effect*. In particular, the *bending-induced shear warping* introduces higher-order derivatives of material curvatures (refer to Eq. (5.21) of chapter 5), and the Poisson's effect introduces *mid-curve axial strain* in the deformation map. Hence, the comprehensive kinematics renders the deformation map to be a function of mid-curve axial strain, the curvature vector, and their derivatives, thus making the process of obtaining the variation of these quantities challenging. The reduced section (internal) forces (conjugate to the finite strain terms and their derivatives), inertial and external forces, and the boundary forces are obtained. We also observe that the theory converges to the one

presented in Simo et al.[43] if we ignore the Poisson's effect and bending induced non-uniform shear. The derivation of strong and weak form and their equivalence leads to some very interesting results and relationships that are presented in this chapter.

Finally, we obtain the balance laws for the geometrically-exact beam with a rigid cross-section (a special case) using both an infinitesimal equilibrium equation and the Hamilton-Lagrange principle. We do not specifically assume that the mid-curve passes either through the geometric centroid of the mass centroid of the beam but rather leaves its location general. We obtain the equations for the initially straight configuration and finally achieve the same for an initially curved (but strain-free) reference configuration. To demonstrate the importance of the terms involved in the equation of motion, we interpret the motion as viewed from the director frame of reference. We also obtain the energy conservation law from Hamilton's principle, thereby establishing a transformational link between the total energy and Lagrangian functional for Cosserat beams.

As noted in Mardsen and Hughes [60], we sincerely believe that differential geometry (refer to Kreyszig [14] for beginners; Do Carmo [15] for advanced level; Clelland [115] and Ivey et al. [7] for understanding the method of moving frames) is a natural and unified approach to investigate problems of deformation as it provides construction and a unified language that helps one understand the subject in a more deeper fashion (for example, the tangent bundle of the configuration space represents the state space of dynamical problem). The paper by Simo et al. [116] is a wonderful excursion into the geometric structure of non-linear continuum mechanics. To gain more insights into understanding the behavior of dynamic systems in the realm of differential geometry, readers are recommended to refer to an excellent book by Lee et al. [117]. As much as we are aligned towards using the general tensor analysis in this work, we use differential geometry rather carefully, just enough to elucidate the intended ideas.

Note on Notations: We first quickly present some preliminary definitions and notations: the dot product, ordinary vector product and tensor product of two Euclidean vectors $\boldsymbol{v}_1$ and $\boldsymbol{v}_2$ are

defined as $\boldsymbol{v}_1 \cdot \boldsymbol{v}_2 = \boldsymbol{v}_1^T \boldsymbol{v}_2$, $\boldsymbol{v}_1 \times \boldsymbol{v}_2$, and $\boldsymbol{v}_1 \otimes \boldsymbol{v}_2$ respectively. The expression $\boldsymbol{v}_1^T \boldsymbol{v}_2$ is the matrix representation of the dot product. The usage of $\boldsymbol{v}_1 \cdot \boldsymbol{v}_2$ and $\boldsymbol{v}_1^T \boldsymbol{v}_2$ is contextual and are used interchangeably. The Euclidean norm is represented by $\|.\|$ or the un-bolded version of the symbol (for example, $\|\boldsymbol{v}\| \equiv v$). Secondly, n^{th} order partial derivative with respect to a scalar quantity, ξ_1 for instance, is given by the operator $\frac{\partial^n}{\partial \xi_1^n} = \partial^n_{\xi_1}$. For $n = 1$, we define $\partial^1_{\xi_1} \equiv \partial_{\xi_1}$. A vector, tensor or a matrix is represented by bold symbol and their components are given by indexed un-bolded symbols. The action of a tensor $\boldsymbol{A}$ onto the vector $\boldsymbol{v}$ is represented by $\boldsymbol{A}\boldsymbol{v} \equiv \boldsymbol{A}.\boldsymbol{v}$. The contraction between two tensors $\boldsymbol{A}$ and $\boldsymbol{B}$ is given by $\boldsymbol{A} : \boldsymbol{B} = A_{ij}B_{ij} = \text{trace}(\boldsymbol{B}^T.\boldsymbol{A})$. Vectors when expressed in array form are column in nature. Vertical concatenation of n vectors (for example, of dimension 3×1) $\boldsymbol{v}_1, \boldsymbol{v}_2, ..., \boldsymbol{v}_n$ is represented by the vector $[\boldsymbol{v}_1; \boldsymbol{v}_2; ...; \boldsymbol{v}_n]$ (of dimension $3n \times 1$). The n dimensional Euclidean space is represented by $\mathbb{R}^n$, with $\mathbb{R}^1 = \mathbb{R}$. The space of real number and integers is represented by $\mathbb{R}$ and $\mathbb{Z}$, with $\mathbb{R}^+$ and $\mathbb{Z}^+$ giving the set of positive real numbers and integers (including 0). It is interesting to note that the language that reads-"*The action of a tensor...onto the vector...*"- is acceptable in the field of engineering. However, it would not make much sense in differential geometry. This is because a tensor in differential geometry is defined as multi-linear function that take other tensors, vectors, one-forms etc. as its argument. However, as a matter of convenience, we accept this abuse of notations. These notations are valid for all the chapters hereafter.

7.2 Kinematics

7.2.1 Deformation map and deformation gradient tensor

For the development of mechanics of geometrically-exact beam, we consider the enhanced kinematics discussed in chapter 4 and the deformed configuration Ω_3. For this and the forthcoming chapters, we rename Ω_3 to Ω; $\boldsymbol{\phi}_3$ to $\boldsymbol{\phi}$; $\boldsymbol{R}_3$ to $\boldsymbol{R}$; and $\boldsymbol{F}_3 = \boldsymbol{\lambda}_i^3 \otimes \boldsymbol{E}_i + \boldsymbol{Q} = \boldsymbol{H}_3 + \boldsymbol{Q}$ to $\boldsymbol{F} = \boldsymbol{\lambda}_i \otimes \boldsymbol{E}_i + \boldsymbol{Q} = \boldsymbol{H} + \boldsymbol{Q}$. Bearing this in mind, we briefly discuss the kinematics for continuity

sake. For detailed discussion on kinematics used in this chapter, readers are recommended to read section 4.2 of chapter 4.

Let an open set $\Omega_0 \subset \mathbb{R}^3$ and $\Omega \subset \mathbb{R}^3$ with at least piecewise smooth boundaries $\mathfrak{S}_0 = \mathfrak{B}_0(0) \cup \mathfrak{B}_0(L) \cup_{\forall \xi_1} \Gamma_0(\xi_1)$ and $\mathfrak{S} = \mathfrak{B}(0) \cup \mathfrak{B}(L) \cup_{\forall \xi_1} \Gamma(\xi_1)$ represent the undeformed and deformed configuration of the beam respectively. The final deformed state Ω is defined by the mid-curve $\boldsymbol{\varphi}$ and a family of cross-section $\mathfrak{B}(\xi_1) = \left\{ \left(W(\xi_1, \xi_2, \xi_3), \hat{\xi}_2, \hat{\xi}_3 \right) \in \mathbb{R}^3_{\xi_1} \right\}$. It incorporates a fully coupled Poisson's and warping effect. The deformation map for Ω is given by $\boldsymbol{\phi} : \boldsymbol{R}_0 \in \Omega_0 \longmapsto \boldsymbol{R} \in \Omega$, such that,

$$\begin{aligned} \boldsymbol{\phi}(\boldsymbol{R}_0) = \boldsymbol{R} = \boldsymbol{\varphi}(\xi_1) + \boldsymbol{r}; \\ \boldsymbol{r} = \hat{\xi}_2 \boldsymbol{d}_2(\xi_1) + \hat{\xi}_3 \boldsymbol{d}_3(\xi_1) + W \boldsymbol{d}_1(\xi_1). \end{aligned} \tag{7.1}$$

Here, the vector $\boldsymbol{r}$ gives the position vector of a material point (ξ_2, ξ_3) in the deformed cross-section $\mathfrak{B}(\xi_1)$ with respect to the point $\boldsymbol{\varphi}(\xi_1)$. Let $\Gamma(\xi_1)$ represent the boundary of cross-section $\mathfrak{B}(\xi_1)$, such that $\mathfrak{S} = \mathfrak{B}(0) \cup \mathfrak{B}(L) \cup_{\forall \xi_1} \Gamma(\xi_1)$. As discussed in Eq. (4.25) of chapter 4, the quantities $\hat{\xi}_2$ and $\hat{\xi}_3$ are defined by Poisson's transformation $P_{\xi_1} : (\xi_2, \xi_3) \mapsto (\hat{\xi}_2, \hat{\xi}_3)$.

In general, the mid-curve need not necessarily be the locus of geometric centroid of the beam. It can also be the locus of center of mass or the shear-center. In this chapter, we assume locus of geometric centroid constituting the mid-curve. For homogeneous material with constant mass density, the geometric and mass centroid coincides, vanishing the first geometric and mass moment. This simplifies the computations.

We assume that the contribution of higher order derivative (> 1) of curvatures to warping is negligible. Thus, to facilitate the computation of governing field equations, we consider a simplified warping function for this chapter,

$$\begin{aligned} W(\xi_1, \xi_2, \xi_3) = p(\xi_1)\Psi_1(\xi_2, \xi_3) + \partial_{\xi_1}\overline{\kappa}_2 . \Psi_2(\xi_2, \xi_3) + \partial_{\xi_1}\overline{\kappa}_3 . \Psi_3(\xi_2, \xi_3); \\ W(\xi_1, \xi_2, \xi_3) = p(\xi_1)\Psi_1(\xi_2, \xi_3) + \partial_{\xi_1}\overline{\boldsymbol{\kappa}} . \overline{\boldsymbol{\Psi}}_{23}. \end{aligned} \tag{7.2}$$

In the equation above, $\overline{\boldsymbol{\Psi}}_{23} = \Psi_2(\xi_2, \xi_3)\boldsymbol{E}_2 + \Psi_3(\xi_2, \xi_3)\boldsymbol{E}_3$ and $\partial_{\xi_1}\overline{\boldsymbol{\kappa}} = \partial_{\xi_1}\overline{\kappa}_i . \boldsymbol{E}_i$. The warping

function W mentioned above is a modified version of the warping used in Simo and Vu-Quoc [43], where $p(\xi_1)$ gives the warping amplitude. The coefficients $\partial_{\xi_1}\overline{\kappa}_j$ $(j = 2,3)$ incorporated bending induced non-uniform shear deformation. For the sake of computation, the cross-section dependent functions $\Psi_1(\xi_2,\xi_3)$, $\Psi_2(\xi_2,\xi_3)$ and $\Psi_3(\xi_2,\xi_3)$ are assumed to be known.

We obtain the desirable form of Poisson's transformation in terms of finite strain quantities and the warping function W as

$$\hat{\xi}_i = \left(1 - \nu\left(\overline{\boldsymbol{\varepsilon}}.\boldsymbol{E}_1 + \overline{\boldsymbol{\kappa}}.(\xi_3\boldsymbol{E}_2 - \xi_2\boldsymbol{E}_3) + \partial_{\xi_1}p.\Psi_1 + \partial^2_{\xi_1}\overline{\boldsymbol{\kappa}}.\overline{\boldsymbol{\Psi}}_{23}\right)\right)\xi_i \text{ for } i = 2,3. \tag{7.3}$$

The deformation gradient tensor can then be expressed as,

$$\boldsymbol{F} = \partial_{\xi_i}\boldsymbol{R}\otimes\boldsymbol{E}_i = (\partial_{\xi_i}\boldsymbol{R} - \boldsymbol{d}_i)\otimes\boldsymbol{E}_i + \boldsymbol{Q} = \boldsymbol{\lambda}_i\otimes\boldsymbol{E}_i + \boldsymbol{Q} = \boldsymbol{H} + \boldsymbol{Q}; \tag{7.4a}$$

$$\overline{\boldsymbol{F}} = \overline{\boldsymbol{\lambda}}_i\otimes\boldsymbol{E}_i + \boldsymbol{I}_3 = \overline{\boldsymbol{H}} + \boldsymbol{I}_3. \tag{7.4b}$$

The expressions of the strain vector $\boldsymbol{\lambda}_i$ is described in equation set (4.35).

7.2.2 Revisiting the material and spatial strain vector $\boldsymbol{\lambda}_i$

In this section, we elaborate the expressions of strain vectors $\boldsymbol{\lambda}_i$ and $\overline{\boldsymbol{\lambda}}_i$ in a desirable form. To do so, we present the derivatives of deformed position vector $\boldsymbol{R}$ with respect to material coordinates as

$$\partial_{\xi_1}\boldsymbol{R} = \partial_{\xi_1}\boldsymbol{\varphi} + \boldsymbol{\kappa}\times\boldsymbol{r} + \left(\partial_{\xi_1}\hat{\xi}_2.\boldsymbol{d}_2 + \partial_{\xi_1}\hat{\xi}_3.\boldsymbol{d}_3 + (\partial_{\xi_1}p.\Psi_1 + \partial^2_{\xi_1}\overline{\boldsymbol{\kappa}}.\overline{\boldsymbol{\Psi}}_{23})\boldsymbol{d}_1\right); \tag{7.5a}$$

$$\partial_{\xi_2}\boldsymbol{R} = \partial_{\xi_2}\hat{\xi}_2.\boldsymbol{d}_2 + \partial_{\xi_2}\hat{\xi}_3.\boldsymbol{d}_3 + \left(p.\partial_{\xi_2}\Psi_1 + \partial_{\xi_1}\overline{\boldsymbol{\kappa}}.\partial_{\xi_2}\overline{\boldsymbol{\Psi}}_{23}\right)\boldsymbol{d}_1; \tag{7.5b}$$

$$\partial_{\xi_3}\boldsymbol{R} = \partial_{\xi_3}\hat{\xi}_2.\boldsymbol{d}_2 + \partial_{\xi_3}\hat{\xi}_3.\boldsymbol{d}_3 + \left(p.\partial_{\xi_3}\Psi_1 + \partial_{\xi_1}\overline{\boldsymbol{\kappa}}.\partial_{\xi_3}\overline{\boldsymbol{\Psi}}_{23}\right)\boldsymbol{d}_1. \tag{7.5c}$$

We obtain the derivatives of Poisson's transformed cross-section coordinates $(\hat{\xi}_2,\hat{\xi}_3)$ using Eq. (4.18) and (7.3) as

$$\partial_{\xi_1}\hat{\xi}_2 = \partial_{\xi_1}\overline{\boldsymbol{\varepsilon}}.(-\nu\xi_2\boldsymbol{E}_1) + \partial_{\xi_1}\overline{\boldsymbol{\kappa}}.(\nu\xi_2^2\boldsymbol{E}_3 - \nu\xi_2\xi_3\boldsymbol{E}_2) + \partial^2_{\xi_1}p.(-\nu\xi_2\Psi_1) + \partial^3_{\xi_1}\overline{\boldsymbol{\kappa}}.(-\nu\xi_2\overline{\boldsymbol{\Psi}}_{23}); \tag{7.6a}$$

$$\partial_{\xi_1}\hat{\xi}_3 = \partial_{\xi_1}\overline{\boldsymbol{\varepsilon}}.(-\nu\xi_3\boldsymbol{E}_1) + \partial_{\xi_1}\overline{\boldsymbol{\kappa}}.(\nu\xi_2\xi_3\boldsymbol{E}_3 - \nu\xi_3^2\boldsymbol{E}_2) + \partial^2_{\xi_1}p.(-\nu\xi_3\Psi_1) + \partial^3_{\xi_1}\overline{\boldsymbol{\kappa}}.(-\nu\xi_3\overline{\boldsymbol{\Psi}}_{23}); \quad (7.6b)$$

$$\partial_{\xi_2}\hat{\xi}_2 = 1 + (\overline{\boldsymbol{\varepsilon}}.(-\nu\boldsymbol{E}_1) + \overline{\boldsymbol{\kappa}}.(2\nu\xi_2\boldsymbol{E}_3 - \nu\xi_3\boldsymbol{E}_2) + \partial_{\xi_1}p.(-\nu\Psi_1 - \nu\xi_2.\partial_{\xi_2}\Psi_1) \quad (7.6c)$$

$$+ \partial^2_{\xi_1}\overline{\boldsymbol{\kappa}}.(-\nu\overline{\boldsymbol{\Psi}}_{23} - \nu\xi_2.\partial_{\xi_2}\overline{\boldsymbol{\Psi}}_{23})); \quad (7.6d)$$

$$\partial_{\xi_2}\hat{\xi}_3 = \overline{\boldsymbol{\kappa}}.(\nu\xi_3\boldsymbol{E}_3) + \partial_{\xi_1}p.(-\nu\xi_3.\partial_{\xi_2}\Psi_1) + \partial^2_{\xi_1}\overline{\boldsymbol{\kappa}}.(-\nu\xi_3.\partial_{\xi_2}\overline{\boldsymbol{\Psi}}_{23}); \quad (7.6e)$$

$$\partial_{\xi_3}\hat{\xi}_2 = \overline{\boldsymbol{\kappa}}.(-\nu\xi_2\boldsymbol{E}_2) + \partial_{\xi_1}p.(-\nu\xi_2.\partial_{\xi_3}\Psi_1) + \partial^2_{\xi_1}\overline{\boldsymbol{\kappa}}.(-\nu\xi_2.\partial_{\xi_3}\overline{\boldsymbol{\Psi}}_{23}); \quad (7.6f)$$

$$\partial_{\xi_3}\hat{\xi}_3 = 1 + (\overline{\boldsymbol{\varepsilon}}.(-\nu\boldsymbol{E}_1) + \overline{\boldsymbol{\kappa}}.(\nu\xi_2\boldsymbol{E}_3 - 2\nu\xi_3\boldsymbol{E}_2) + \partial_{\xi_1}p.(-\nu\Psi_1 - \nu\xi_3.\partial_{\xi_3}\Psi_1) \quad (7.6g)$$

$$+ \partial^2_{\xi_1}\overline{\boldsymbol{\kappa}}.(-\nu\overline{\boldsymbol{\Psi}}_{23} - \nu\xi_3.\partial_{\xi_3}\overline{\boldsymbol{\Psi}}_{23})). \quad (7.6h)$$

Substituting the results above into Eq. (7.5) and using the definition of strain vector in Eq. (4.28), we obtain the expressions for material and spatial form of strain vector $\overline{\boldsymbol{\lambda}}_i$ expressed in matrix form as

$$\overline{\mathfrak{L}} = \overline{\boldsymbol{L}}.\overline{\boldsymbol{\epsilon}}; \quad (7.7a)$$

$$\mathfrak{L} = \boldsymbol{L}.\boldsymbol{\epsilon}. \quad (7.7b)$$

where,

$$\begin{aligned}
\overline{\mathfrak{L}} &= \left[\overline{\boldsymbol{\lambda}}_1; \overline{\boldsymbol{\lambda}}_2; \overline{\boldsymbol{\lambda}}_3\right]; \\
\mathfrak{L} &= [\boldsymbol{\lambda}_1; \boldsymbol{\lambda}_2; \boldsymbol{\lambda}_3]; \\
\overline{\boldsymbol{\epsilon}} &= \left[\overline{\boldsymbol{\varepsilon}}; \partial_{\xi_1}\overline{\boldsymbol{\varepsilon}}; \overline{\boldsymbol{\kappa}}; \partial_{\xi_1}\overline{\boldsymbol{\kappa}}; \partial^2_{\xi_1}\overline{\boldsymbol{\kappa}}; \partial^3_{\xi_1}\overline{\boldsymbol{\kappa}}; p; \partial_{\xi_1}p; \partial^2_{\xi_1}p\right]; \\
\boldsymbol{\epsilon} &= \left[\boldsymbol{\varepsilon}; \tilde{\partial}_{\xi_1}\boldsymbol{\varepsilon}; \boldsymbol{\kappa}; \tilde{\partial}_{\xi_1}\boldsymbol{\kappa}; \boldsymbol{Q}.\partial^2_{\xi_1}\overline{\boldsymbol{\kappa}}; \boldsymbol{Q}.\partial^3_{\xi_1}\overline{\boldsymbol{\kappa}}; p; \partial_{\xi_1}p; \partial^2_{\xi_1}p\right];
\end{aligned} \quad (7.8)$$

such that,

$$\begin{aligned}
\mathfrak{L} &= \boldsymbol{Q}_3.\overline{\mathfrak{L}}; \\
\boldsymbol{\epsilon} &= \boldsymbol{\Lambda}.\overline{\boldsymbol{\epsilon}};
\end{aligned} \quad (7.9)$$

where,

$$\boldsymbol{Q}_3 = \begin{bmatrix} \boldsymbol{Q} & \boldsymbol{0}_3 & \boldsymbol{0}_3 \\ \boldsymbol{0}_3 & \boldsymbol{Q} & \boldsymbol{0}_3 \\ \boldsymbol{0}_3 & \boldsymbol{0}_3 & \boldsymbol{Q} \end{bmatrix}; \quad \boldsymbol{\Lambda} = \begin{bmatrix} \boldsymbol{Q} & \boldsymbol{0}_3 & \boldsymbol{0}_3 & \boldsymbol{0}_3 & \boldsymbol{0}_3 & \boldsymbol{0}_3 & \boldsymbol{0}_3 \\ \boldsymbol{0}_3 & \boldsymbol{Q} & \boldsymbol{0}_3 & \boldsymbol{0}_3 & \boldsymbol{0}_3 & \boldsymbol{0}_3 & \boldsymbol{0}_3 \\ \boldsymbol{0}_3 & \boldsymbol{0}_3 & \boldsymbol{Q} & \boldsymbol{0}_3 & \boldsymbol{0}_3 & \boldsymbol{0}_3 & \boldsymbol{0}_3 \\ \boldsymbol{0}_3 & \boldsymbol{0}_3 & \boldsymbol{0}_3 & \boldsymbol{Q} & \boldsymbol{0}_3 & \boldsymbol{0}_3 & \boldsymbol{0}_3 \\ \boldsymbol{0}_3 & \boldsymbol{0}_3 & \boldsymbol{0}_3 & \boldsymbol{0}_3 & \boldsymbol{Q} & \boldsymbol{0}_3 & \boldsymbol{0}_3 \\ \boldsymbol{0}_3 & \boldsymbol{0}_3 & \boldsymbol{0}_3 & \boldsymbol{0}_3 & \boldsymbol{0}_3 & \boldsymbol{Q} & \boldsymbol{0}_3 \\ \boldsymbol{0}_3 & \boldsymbol{0}_3 & \boldsymbol{0}_3 & \boldsymbol{0}_3 & \boldsymbol{0}_3 & \boldsymbol{0}_3 & \boldsymbol{I}_3 \end{bmatrix}. \tag{7.10}$$

Using the result Eq. (3.17a) presented in *Proposition 3.3*, we have, $\boldsymbol{Q}.\partial^n_{\xi_1}\overline{\boldsymbol{\kappa}} = \tilde{\partial}^n_{\xi_1}\boldsymbol{\kappa}$. Therefore,

$$\boldsymbol{\epsilon} = \left[\boldsymbol{\varepsilon}; \tilde{\partial}_{\xi_1}\boldsymbol{\varepsilon}; \boldsymbol{\kappa}; \tilde{\partial}_{\xi_1}\boldsymbol{\kappa}; \tilde{\partial}^2_{\xi_1}\boldsymbol{\kappa}; \tilde{\partial}^3_{\xi_1}\boldsymbol{\kappa}; p; \partial_{\xi_1}p; \partial^2_{\xi_1}p\right]. \tag{7.11}$$

From here on, we call the vectors $\overline{\mathfrak{L}}$ and $\mathfrak{L}$ as material and spatial *concatenated strain vector* respectively. The matrices $\overline{\boldsymbol{L}}$ and $\boldsymbol{L}$ are given as

$$\begin{aligned} \overline{\boldsymbol{L}} &= \begin{bmatrix} \overline{\boldsymbol{L}}^{\boldsymbol{\lambda}_1}_{\boldsymbol{\varepsilon}} & \overline{\boldsymbol{L}}^{\boldsymbol{\lambda}_1}_{\partial_{\xi_1}\boldsymbol{\varepsilon}} & \overline{\boldsymbol{L}}^{\boldsymbol{\lambda}_1}_{\boldsymbol{\kappa}} & \overline{\boldsymbol{L}}^{\boldsymbol{\lambda}_1}_{\partial_{\xi_1}\boldsymbol{\kappa}} & \overline{\boldsymbol{L}}^{\boldsymbol{\lambda}_1}_{\partial^2_{\xi_1}\boldsymbol{\kappa}} & \overline{\boldsymbol{L}}^{\boldsymbol{\lambda}_1}_{\partial^3_{\xi_1}\boldsymbol{\kappa}} & \overline{\boldsymbol{L}}^{\boldsymbol{\lambda}_1}_{p} & \overline{\boldsymbol{L}}^{\boldsymbol{\lambda}_1}_{\partial_{\xi_1}p} & \overline{\boldsymbol{L}}^{\boldsymbol{\lambda}_1}_{\partial^2_{\xi_1}p} \\ \overline{\boldsymbol{L}}^{\boldsymbol{\lambda}_2}_{\boldsymbol{\varepsilon}} & \overline{\boldsymbol{L}}^{\boldsymbol{\lambda}_2}_{\partial_{\xi_1}\boldsymbol{\varepsilon}} & \overline{\boldsymbol{L}}^{\boldsymbol{\lambda}_2}_{\boldsymbol{\kappa}} & \overline{\boldsymbol{L}}^{\boldsymbol{\lambda}_2}_{\partial_{\xi_1}\boldsymbol{\kappa}} & \overline{\boldsymbol{L}}^{\boldsymbol{\lambda}_2}_{\partial^2_{\xi_1}\boldsymbol{\kappa}} & \overline{\boldsymbol{L}}^{\boldsymbol{\lambda}_2}_{\partial^3_{\xi_1}\boldsymbol{\kappa}} & \overline{\boldsymbol{L}}^{\boldsymbol{\lambda}_2}_{p} & \overline{\boldsymbol{L}}^{\boldsymbol{\lambda}_2}_{\partial_{\xi_1}p} & \overline{\boldsymbol{L}}^{\boldsymbol{\lambda}_2}_{\partial^2_{\xi_1}p} \\ \overline{\boldsymbol{L}}^{\boldsymbol{\lambda}_3}_{\boldsymbol{\varepsilon}} & \overline{\boldsymbol{L}}^{\boldsymbol{\lambda}_3}_{\partial_{\xi_1}\boldsymbol{\varepsilon}} & \overline{\boldsymbol{L}}^{\boldsymbol{\lambda}_3}_{\boldsymbol{\kappa}} & \overline{\boldsymbol{L}}^{\boldsymbol{\lambda}_3}_{\partial_{\xi_1}\boldsymbol{\kappa}} & \overline{\boldsymbol{L}}^{\boldsymbol{\lambda}_3}_{\partial^2_{\xi_1}\boldsymbol{\kappa}} & \overline{\boldsymbol{L}}^{\boldsymbol{\lambda}_3}_{\partial^3_{\xi_1}\boldsymbol{\kappa}} & \overline{\boldsymbol{L}}^{\boldsymbol{\lambda}_3}_{p} & \overline{\boldsymbol{L}}^{\boldsymbol{\lambda}_3}_{\partial_{\xi_1}p} & \overline{\boldsymbol{L}}^{\boldsymbol{\lambda}_3}_{\partial^2_{\xi_1}p} \end{bmatrix}; \\ \boldsymbol{L} &= \begin{bmatrix} \boldsymbol{L}^{\boldsymbol{\lambda}_1}_{\boldsymbol{\varepsilon}} & \boldsymbol{L}^{\boldsymbol{\lambda}_1}_{\partial_{\xi_1}\boldsymbol{\varepsilon}} & \boldsymbol{L}^{\boldsymbol{\lambda}_1}_{\boldsymbol{\kappa}} & \boldsymbol{L}^{\boldsymbol{\lambda}_1}_{\partial_{\xi_1}\boldsymbol{\kappa}} & \boldsymbol{L}^{\boldsymbol{\lambda}_1}_{\partial^2_{\xi_1}\boldsymbol{\kappa}} & \boldsymbol{L}^{\boldsymbol{\lambda}_1}_{\partial^3_{\xi_1}\boldsymbol{\kappa}} & \boldsymbol{L}^{\boldsymbol{\lambda}_1}_{p} & \boldsymbol{L}^{\boldsymbol{\lambda}_1}_{\partial_{\xi_1}p} & \boldsymbol{L}^{\boldsymbol{\lambda}_1}_{\partial^2_{\xi_1}p} \\ \boldsymbol{L}^{\boldsymbol{\lambda}_2}_{\boldsymbol{\varepsilon}} & \boldsymbol{L}^{\boldsymbol{\lambda}_2}_{\partial_{\xi_1}\boldsymbol{\varepsilon}} & \boldsymbol{L}^{\boldsymbol{\lambda}_2}_{\boldsymbol{\kappa}} & \boldsymbol{L}^{\boldsymbol{\lambda}_2}_{\partial_{\xi_1}\boldsymbol{\kappa}} & \boldsymbol{L}^{\boldsymbol{\lambda}_2}_{\partial^2_{\xi_1}\boldsymbol{\kappa}} & \boldsymbol{L}^{\boldsymbol{\lambda}_2}_{\partial^3_{\xi_1}\boldsymbol{\kappa}} & \boldsymbol{L}^{\boldsymbol{\lambda}_2}_{p} & \boldsymbol{L}^{\boldsymbol{\lambda}_2}_{\partial_{\xi_1}p} & \boldsymbol{L}^{\boldsymbol{\lambda}_2}_{\partial^2_{\xi_1}p} \\ \boldsymbol{L}^{\boldsymbol{\lambda}_3}_{\boldsymbol{\varepsilon}} & \boldsymbol{L}^{\boldsymbol{\lambda}_3}_{\partial_{\xi_1}\boldsymbol{\varepsilon}} & \boldsymbol{L}^{\boldsymbol{\lambda}_3}_{\boldsymbol{\kappa}} & \boldsymbol{L}^{\boldsymbol{\lambda}_3}_{\partial_{\xi_1}\boldsymbol{\kappa}} & \boldsymbol{L}^{\boldsymbol{\lambda}_3}_{\partial^2_{\xi_1}\boldsymbol{\kappa}} & \boldsymbol{L}^{\boldsymbol{\lambda}_3}_{\partial^3_{\xi_1}\boldsymbol{\kappa}} & \boldsymbol{L}^{\boldsymbol{\lambda}_3}_{p} & \boldsymbol{L}^{\boldsymbol{\lambda}_3}_{\partial_{\xi_1}p} & \boldsymbol{L}^{\boldsymbol{\lambda}_3}_{\partial^2_{\xi_1}p} \end{bmatrix}; \end{aligned} \tag{7.12}$$

such that,

$$\boldsymbol{L} = \boldsymbol{Q}_3.\overline{\boldsymbol{L}}.\boldsymbol{\Lambda}^T. \tag{7.13}$$

We call the quantities $\overline{\boldsymbol{L}}^{\boldsymbol{\lambda}_i}_{\boldsymbol{x}}$ and $\boldsymbol{L}^{\boldsymbol{\lambda}_i}_{\boldsymbol{x}}$ as material and spatial $\boldsymbol{L}$-terms respectively. For $\boldsymbol{x} \in \left\{\boldsymbol{\varepsilon},\ \partial_{\xi_1}\boldsymbol{\varepsilon},\ \boldsymbol{\kappa},\ \partial_{\xi_1}\boldsymbol{\kappa},\ \partial^2_{\xi_1}\boldsymbol{\kappa},\ \partial^3_{\xi_1}\boldsymbol{\kappa},\ \partial_{\xi_1}p,\ \partial_{\xi_1}p,\ \partial^2_{\xi_1}p\right\}$, the quantity $\boldsymbol{L}^{\boldsymbol{\lambda}_i}_{\boldsymbol{x}}$ (or $\overline{\boldsymbol{L}}^{\boldsymbol{\lambda}_i}_{\boldsymbol{x}}$) is associated with the strain term $\boldsymbol{x}$ in the expression of strain vector $\boldsymbol{\lambda}_i$ (or $\overline{\boldsymbol{\lambda}}_i$). For the subscripts $(p,\ \partial_{\xi_1}p,\ \partial^2_{\xi_1}p)$, the

$\boldsymbol{L}$-terms are 3×1 vectors. For all other cases, $\boldsymbol{L}$-terms are 3×3 matrices. The material and spatial $\boldsymbol{L}$-terms are related by the following relationship:

$$\begin{gathered}\boldsymbol{L}_{\boldsymbol{x}}^{\lambda_i} = \boldsymbol{Q}.\overline{\boldsymbol{L}}_{\boldsymbol{x}}^{\lambda_i}.\boldsymbol{Q}^T \text{ and } \overline{\boldsymbol{L}}_{\boldsymbol{x}}^{\lambda_i} = \boldsymbol{Q}^T.\boldsymbol{L}_{\boldsymbol{x}}^{\lambda_i}.\boldsymbol{Q} \text{ for } \boldsymbol{x} \in \{\boldsymbol{\varepsilon},\ \partial_{\xi_1}\boldsymbol{\varepsilon},\ \boldsymbol{\kappa},\ \partial_{\xi_1}\boldsymbol{\kappa},\ \partial_{\xi_1}^2\boldsymbol{\kappa},\ \partial_{\xi_1}^3\boldsymbol{\kappa}\} \\ \boldsymbol{L}_{x}^{\lambda_i} = \boldsymbol{Q}.\overline{\boldsymbol{L}}_{x}^{\lambda_i} \text{ and } \overline{\boldsymbol{L}}_{x}^{\lambda_i} = \boldsymbol{Q}^T.\boldsymbol{L}_{x}^{\lambda_i} \text{ for } x \in \{p,\ \partial_{\xi_1}p,\ \partial_{\xi_1}^2 p\}.\end{gathered} \tag{7.14}$$

The $\boldsymbol{L}$-terms are defined below.

$\boldsymbol{L}$-terms associated with λ_1:

$$\overline{\boldsymbol{L}}_{\boldsymbol{\varepsilon}}^{\lambda_1} = \boldsymbol{I}_3 \qquad \boldsymbol{L}_{\boldsymbol{\varepsilon}}^{\lambda_1} = \boldsymbol{I}_3 \tag{7.15a}$$

$$\overline{\boldsymbol{L}}_{\partial_{\xi_1}\boldsymbol{\varepsilon}}^{\lambda_1} = -\nu\overline{\boldsymbol{r}}_1 \otimes \boldsymbol{E}_1 \qquad \boldsymbol{L}_{\partial_{\xi_1}\boldsymbol{\varepsilon}}^{\lambda_1} = -\nu\boldsymbol{r}_1 \otimes \boldsymbol{d}_1 \tag{7.15b}$$

$$\overline{\boldsymbol{L}}_{\boldsymbol{\kappa}}^{\lambda_1} = \hat{\overline{\boldsymbol{r}}}^T \qquad \boldsymbol{L}_{\boldsymbol{\kappa}}^{\lambda_1} = \hat{\boldsymbol{r}}^T \tag{7.15c}$$

$$\overline{\boldsymbol{L}}_{\partial_{\xi_1}\boldsymbol{\kappa}}^{\lambda_1} = \nu\xi_2\overline{\boldsymbol{r}}_1 \otimes \boldsymbol{E}_3 - \nu\xi_3\overline{\boldsymbol{r}}_1 \otimes \boldsymbol{E}_2 \qquad \boldsymbol{L}_{\partial_{\xi_1}\boldsymbol{\kappa}}^{\lambda_1} = \nu\xi_2\boldsymbol{r}_1 \otimes \boldsymbol{d}_3 - \nu\xi_3\boldsymbol{r}_1 \otimes \boldsymbol{d}_2 \tag{7.15d}$$

$$\overline{\boldsymbol{L}}_{\partial_{\xi_1}^2\boldsymbol{\kappa}}^{\lambda_1} = \boldsymbol{E}_1 \otimes \overline{\boldsymbol{\Psi}}_{23} \qquad \boldsymbol{L}_{\partial_{\xi_1}^2\boldsymbol{\kappa}}^{\lambda_1} = \boldsymbol{d}_1 \otimes \boldsymbol{\Psi}_{23} \tag{7.15e}$$

$$\overline{\boldsymbol{L}}_{\partial_{\xi_1}^3\boldsymbol{\kappa}}^{\lambda_1} = -\nu\overline{\boldsymbol{r}}_1 \otimes \overline{\boldsymbol{\Psi}}_{23} \qquad \boldsymbol{L}_{\partial_{\xi_1}^3\boldsymbol{\kappa}}^{\lambda_1} = -\nu\boldsymbol{r}_1 \otimes \boldsymbol{\Psi}_{23} \tag{7.15f}$$

$$\overline{\boldsymbol{L}}_{p}^{\lambda_1} = \boldsymbol{0}_1 \qquad \boldsymbol{L}_{p}^{\lambda_1} = \boldsymbol{0}_1 \tag{7.15g}$$

$$\overline{\boldsymbol{L}}_{\partial_{\xi_1}p}^{\lambda_1} = \Psi_1\boldsymbol{E}_1 \qquad \boldsymbol{L}_{\partial_{\xi_1}p}^{\lambda_1} = \Psi_1\boldsymbol{d}_1 \tag{7.15h}$$

$$\overline{\boldsymbol{L}}_{\partial_{\xi_1}^2 p}^{\lambda_1} = -\nu\Psi_1\overline{\boldsymbol{r}}_1 \qquad \boldsymbol{L}_{\partial_{\xi_1}^2 p}^{\lambda_1} = -\nu\Psi_1\boldsymbol{r}_1 \tag{7.15i}$$

$\boldsymbol{L}$-terms associated with λ_2:

$$\overline{\boldsymbol{L}}_{\boldsymbol{\varepsilon}}^{\lambda_2} = -\nu\boldsymbol{E}_2 \otimes \boldsymbol{E}_1 \qquad \boldsymbol{L}_{\boldsymbol{\varepsilon}}^{\lambda_2} = -\nu\boldsymbol{d}_2 \otimes \boldsymbol{d}_1 \tag{7.16a}$$

$$\overline{\boldsymbol{L}}_{\partial_{\xi_1}\boldsymbol{\varepsilon}}^{\lambda_2} = \boldsymbol{0}_3 \qquad \boldsymbol{L}_{\partial_{\xi_1}\boldsymbol{\varepsilon}}^{\lambda_2} = \boldsymbol{0}_3 \tag{7.16b}$$

$$\overline{\boldsymbol{L}}^{\lambda_2}_{\boldsymbol{\kappa}} = 2\nu\xi_2\boldsymbol{E}_2\otimes\boldsymbol{E}_3 - \nu\xi_3\boldsymbol{E}_2\otimes\boldsymbol{E}_2 + \nu\xi_3\boldsymbol{E}_3\otimes\boldsymbol{E}_3 \qquad \boldsymbol{L}^{\lambda_2}_{\boldsymbol{\kappa}} = 2\nu\xi_2\boldsymbol{d}_2\otimes\boldsymbol{d}_3 - \nu\xi_3\boldsymbol{d}_2\otimes\boldsymbol{d}_2 + \nu\xi_3\boldsymbol{d}_3\otimes\boldsymbol{d}_3 \tag{7.16c}$$

$$\overline{\boldsymbol{L}}^{\lambda_2}_{\partial_{\xi_1}\boldsymbol{\kappa}} = \boldsymbol{E}_1\otimes\partial_{\xi_2}\overline{\boldsymbol{\Psi}}_{23} \qquad \boldsymbol{L}^{\lambda_2}_{\partial_{\xi_1}\boldsymbol{\kappa}} = \boldsymbol{d}_1\otimes\partial_{\xi_2}\boldsymbol{\Psi}_{23} \tag{7.16d}$$

$$\overline{\boldsymbol{L}}^{\lambda_2}_{\partial^2_{\xi_1}\boldsymbol{\kappa}} = -\nu\boldsymbol{E}_2\otimes\overline{\boldsymbol{\Psi}}_{23} - \nu\overline{\boldsymbol{r}}_1\otimes\partial_{\xi_2}\overline{\boldsymbol{\Psi}}_{23} \qquad \boldsymbol{L}^{\lambda_2}_{\partial^2_{\xi_1}\boldsymbol{\kappa}} = -\nu\boldsymbol{d}_2\otimes\boldsymbol{\Psi}_{23} - \nu\boldsymbol{r}_1\otimes\partial_{\xi_2}\boldsymbol{\Psi}_{23} \tag{7.16e}$$

$$\overline{\boldsymbol{L}}^{\lambda_2}_{\partial^3_{\xi_1}\boldsymbol{\kappa}} = \boldsymbol{0}_3 \qquad \boldsymbol{L}^{\lambda_2}_{\partial^3_{\xi_1}\boldsymbol{\kappa}} = \boldsymbol{0}_3 \tag{7.16f}$$

$$\overline{\boldsymbol{L}}^{\lambda_2}_{p} = \partial_{\xi_2}\Psi_1.\boldsymbol{E}_1 \qquad \boldsymbol{L}^{\lambda_2}_{p} = \partial_{\xi_2}\Psi_1.\boldsymbol{d}_1 \tag{7.16g}$$

$$\overline{\boldsymbol{L}}^{\lambda_2}_{\partial_{\xi_1}p} = -\nu\Psi_1\boldsymbol{E}_2 - \nu\partial_{\xi_2}\Psi_1.\overline{\boldsymbol{r}}_1 \qquad \boldsymbol{L}^{\lambda_2}_{\partial_{\xi_1}p} = -\nu\Psi_1\boldsymbol{d}_2 - \nu\partial_{\xi_2}\Psi_1.\boldsymbol{r}_1 \tag{7.16h}$$

$$\overline{\boldsymbol{L}}^{\lambda_2}_{\partial^2_{\xi_1}p} = \boldsymbol{0}_1 \qquad \boldsymbol{L}^{\lambda_2}_{\partial^2_{\xi_1}p} = \boldsymbol{0}_1 \tag{7.16i}$$

L-terms associated with λ_3:

$$\overline{\boldsymbol{L}}^{\lambda_3}_{\boldsymbol{\varepsilon}} = -\nu\boldsymbol{E}_3\otimes\boldsymbol{E}_1 \qquad \boldsymbol{L}^{\lambda_3}_{\boldsymbol{\varepsilon}} = -\nu\boldsymbol{d}_3\otimes\boldsymbol{d}_1 \tag{7.17a}$$

$$\overline{\boldsymbol{L}}^{\lambda_3}_{\partial_{\xi_1}\boldsymbol{\varepsilon}} = \boldsymbol{0}_3 \qquad \boldsymbol{L}^{\lambda_3}_{\partial_{\xi_1}\boldsymbol{\varepsilon}} = \boldsymbol{0}_3 \tag{7.17b}$$

$$\overline{\boldsymbol{L}}^{\lambda_3}_{\boldsymbol{\kappa}} = -\nu\xi_2\boldsymbol{E}_2\otimes\boldsymbol{E}_2 + \nu\xi_2\boldsymbol{E}_3\otimes\boldsymbol{E}_3 - 2\nu\xi_3\boldsymbol{E}_3\otimes\boldsymbol{E}_2 \qquad \boldsymbol{L}^{\lambda_3}_{\boldsymbol{\kappa}} = -\nu\xi_2\boldsymbol{d}_2\otimes\boldsymbol{d}_2 + \nu\xi_2\boldsymbol{d}_3\otimes\boldsymbol{d}_3 - 2\nu\xi_3\boldsymbol{d}_3\otimes\boldsymbol{d}_2 \tag{7.17c}$$

$$\overline{\boldsymbol{L}}^{\lambda_3}_{\partial_{\xi_1}\boldsymbol{\kappa}} = \boldsymbol{E}_1\otimes\partial_{\xi_3}\overline{\boldsymbol{\Psi}}_{23} \qquad \boldsymbol{L}^{\lambda_3}_{\partial_{\xi_1}\boldsymbol{\kappa}} = \boldsymbol{d}_1\otimes\partial_{\xi_3}\boldsymbol{\Psi}_{23} \tag{7.17d}$$

$$\overline{\boldsymbol{L}}^{\lambda_3}_{\partial^2_{\xi_1}\boldsymbol{\kappa}} = -\nu\boldsymbol{E}_3\otimes\overline{\boldsymbol{\Psi}}_{23} - \nu\overline{\boldsymbol{r}}_1\otimes\partial_{\xi_3}\overline{\boldsymbol{\Psi}}_{23} \qquad \boldsymbol{L}^{\lambda_3}_{\partial^2_{\xi_1}\boldsymbol{\kappa}} = -\nu\boldsymbol{d}_3\otimes\boldsymbol{\Psi}_{23} - \nu\boldsymbol{r}_1\otimes\partial_{\xi_3}\boldsymbol{\Psi}_{23} \tag{7.17e}$$

$$\overline{\boldsymbol{L}}^{\lambda_3}_{\partial^3_{\xi_1}\boldsymbol{\kappa}} = \boldsymbol{0}_3 \qquad \boldsymbol{L}^{\lambda_3}_{\partial^3_{\xi_1}\boldsymbol{\kappa}} = \boldsymbol{0}_3 \tag{7.17f}$$

$$\overline{\boldsymbol{L}}^{\lambda_3}_{p} = \partial_{\xi_3}\Psi_1.\boldsymbol{E}_1 \qquad \boldsymbol{L}^{\lambda_3}_{p} = \partial_{\xi_3}\Psi_1.\boldsymbol{d}_1 \tag{7.17g}$$

$$\overline{\boldsymbol{L}}^{\lambda_3}_{\partial_{\xi_1}p} = -\nu\Psi_1\boldsymbol{E}_3 - \nu\partial_{\xi_3}\Psi_1.\overline{\boldsymbol{r}}_1 \qquad \boldsymbol{L}^{\lambda_3}_{\partial_{\xi_1}p} = -\nu\Psi_1\boldsymbol{d}_3 - \nu\partial_{\xi_3}\Psi_1.\boldsymbol{r}_1 \tag{7.17h}$$

$$\overline{\boldsymbol{L}}^{\lambda_3}_{\partial^2_{\xi_1}p} = \boldsymbol{0}_1 \qquad \boldsymbol{L}^{\lambda_3}_{\partial^2_{\xi_1}p} = \boldsymbol{0}_1 \tag{7.17i}$$

7.3 Configuration and the state space of the beam

Adapting the kinematics discussed above, we find that there are three primary quantities required to defined the configuration Ω: $\boldsymbol{\varphi} \in \mathbb{R}^3$, $\boldsymbol{Q} \in SO(3)$ and $p \in \mathbb{R}$. For static case, the configuration space of the beam Ω is given as

$$\mathbb{C} := \left\{ \boldsymbol{\Phi} = (\boldsymbol{\varphi}, \boldsymbol{Q}, p) : [0, L] \longrightarrow \mathbb{R}^3 \times SO(3) \times \mathbb{R} \right\}. \tag{7.18}$$

For any $\boldsymbol{\Phi}(\xi_1) \in \mathbb{C}$, we define the tangent space $T_{\boldsymbol{\Phi}}\mathbb{C}$ as

$$T_{\boldsymbol{\Phi}}\mathbb{C} := \left\{ \tilde{\boldsymbol{\Phi}} = (\partial_{\xi_1}\boldsymbol{\varphi}, \partial_{\xi_1}\boldsymbol{Q}, \partial_{\xi_1} p) : [0, L] \longrightarrow \mathbb{R}^3 \times T_{\boldsymbol{Q}}SO(3) \times \mathbb{R} \right\}. \tag{7.19}$$

The state space of the beam is defined by the tangent bundle $T\mathbb{C}$ of the configuration space $\mathbb{C}$ as

$$T\mathbb{C} := \left\{ (\boldsymbol{\Phi}, \tilde{\boldsymbol{\Phi}}) | \boldsymbol{\Phi} \in \mathbb{C}, \tilde{\boldsymbol{\Phi}} \in T_{\boldsymbol{\Phi}}\mathbb{C} \right\}. \tag{7.20}$$

As discussed in section 2.2.1 of chapter 2, the curvature associated with the beam can be obtained as,

$$\hat{\boldsymbol{\kappa}} = \partial_{\xi_1}\exp(\hat{\boldsymbol{\theta}}).\exp(-\hat{\boldsymbol{\theta}}) = \left(\frac{\sin\theta}{\theta}\right)\partial_{\xi_1}\hat{\boldsymbol{\theta}} + \left(\frac{1-\cos\theta}{\theta^2}\right)\left[\hat{\boldsymbol{\theta}}, \partial_{\xi_1}\hat{\boldsymbol{\theta}}\right] + (\boldsymbol{\theta}.\partial_{\xi_1}\boldsymbol{\theta})\left(\frac{\theta - \sin\theta}{\theta^3}\right)\hat{\boldsymbol{\theta}}. \tag{7.21}$$

It is interesting to interpret the curvature vector $\boldsymbol{\kappa} = \partial_{\xi_1}\boldsymbol{Q}.\boldsymbol{Q}^T$ and the derivative of rotation vector $\partial_{\xi_1}\boldsymbol{\theta}$ with a physical viewpoint. At an arc-length ξ_1, the director triad $\{\boldsymbol{d}_i(\xi_1)\}$ rotates about the vector $\boldsymbol{\kappa}(\xi_1).\mathrm{d}\xi_1$ to yield the triad at $\{\boldsymbol{d}_i(\xi_1 + \mathrm{d}\xi_1)\}$. Whereas, the triad $\{\boldsymbol{d}_i(\xi_1)\}$ and $\{\boldsymbol{d}_i(\xi_1 + \mathrm{d}\xi_1)\}$ are obtained by finite rotation of the frame $\{\boldsymbol{E}_i\}$ about the rotation vector $\boldsymbol{\theta}(\xi_1)$ and $\boldsymbol{\theta}(\xi_1 + \mathrm{d}\xi_1) = \boldsymbol{\theta}(\xi_1) + \partial_{\xi_1}\boldsymbol{\theta}(\xi_1).\mathrm{d}\xi_1$ respectively. Figure 3.3 (left) illustrates the idea discussed here. In terms of exponential map,

$$\begin{aligned} \boldsymbol{Q}(\xi_1 + \mathrm{d}\xi_1) = \exp(\hat{\boldsymbol{\kappa}}(\xi_1).\mathrm{d}\xi_1).\boldsymbol{Q}(\xi_1) = \exp(\hat{\boldsymbol{\kappa}}(\xi_1).\mathrm{d}\xi_1).\exp(\hat{\boldsymbol{\theta}}(\xi_1)); \\ \boldsymbol{Q}(\xi_1 + \mathrm{d}\xi_1) = \boldsymbol{Q}(\boldsymbol{\theta}(\xi_1 + \mathrm{d}\xi_1)) = \exp(\hat{\boldsymbol{\theta}}(\xi_1) + \partial_{\xi_1}\hat{\boldsymbol{\theta}}(\xi_1).\mathrm{d}\xi_1). \end{aligned} \tag{7.22}$$

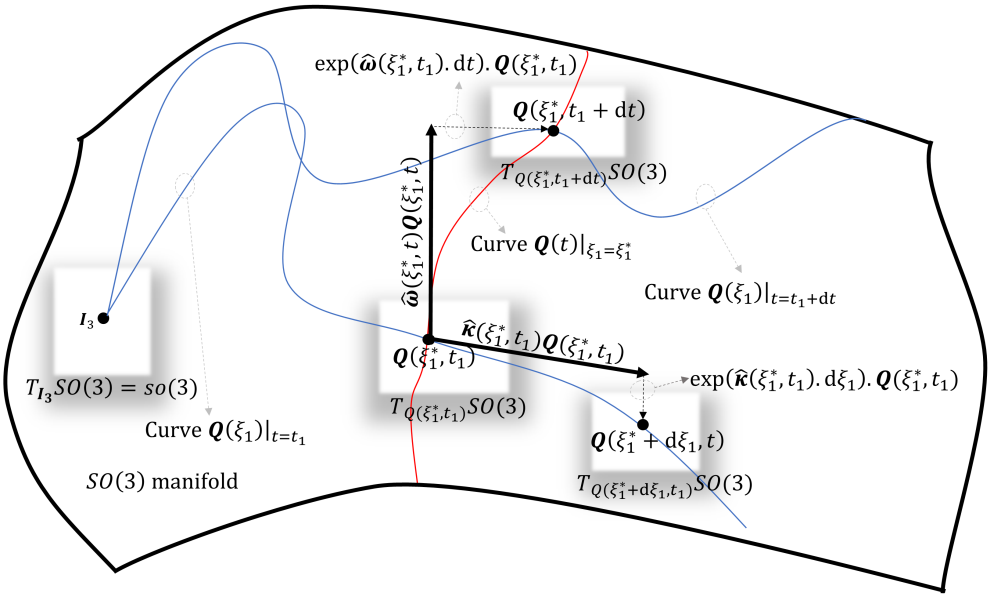

Figure 7.1: Geometric representation of $SO(3)$ manifold, exponential map, tangent plane $T_{\boldsymbol{Q}}SO(3)$, curvature tensor $\hat{\boldsymbol{\kappa}}$, and angular velocity tensor $\hat{\boldsymbol{\omega}}$.

We understand that with slight abuse of notation, we can associate the tangent space with curvature tensor field $\hat{\boldsymbol{\kappa}}(\xi_1)$ (instead of $\partial_{\xi_1}\boldsymbol{Q} = \hat{\boldsymbol{\kappa}}.\boldsymbol{Q}$). The isomorphism between $so(3)$ and $\mathbb{R}^3$ permits one to identify the tensor field $\hat{\boldsymbol{\kappa}}(\xi_1)$ with its corresponding axial vector $\boldsymbol{\kappa}(\xi_1) \in \mathbb{R}^3$. Thus, accepting the abuse of notation, the state space is defined by the set $\left(\boldsymbol{\varphi}, \{\boldsymbol{d}_i\}, p; \partial_{\xi_1}\boldsymbol{\varphi}, \boldsymbol{\kappa}, \partial_{\xi_1} p\right)$. Hence, we redefine the tangent space described in Eq. (7.19) as,

$$T_{\boldsymbol{\Phi}}\mathbb{C} := \left\{\tilde{\boldsymbol{\Phi}} = (\partial_{\xi_1}\boldsymbol{\varphi}, \boldsymbol{\kappa}, \partial_{\xi_1} p) : [0, L] \longrightarrow \mathbb{R}^3 \times \mathbb{R}^3 \times \mathbb{R}\right\}. \tag{7.23}$$

For the dynamic case, we define the configuration space parameterized with arc-length and time (ξ_1, t) as,

$$\mathbb{C} := \left\{\boldsymbol{\Phi} = (\boldsymbol{\varphi}, \boldsymbol{Q}, p) : [0, L] \times \mathbb{R}^+ \longrightarrow \mathbb{R}^3 \times SO(3) \times \mathbb{R}\right\} \tag{7.24}$$

However, it is important to look at the configuration of beam Ω_t at a fixed time $t \in \mathbb{R}^+$ to study curvature vector $\boldsymbol{\kappa}$ and consider a point with constant arc-length to understand the evolution of

director field with time (given by angular velocity tensor $\hat{\boldsymbol{\omega}} = \partial_t \boldsymbol{Q}.\boldsymbol{Q}^T$). Hence,

$$\begin{aligned} \boldsymbol{Q}(\xi_1 + \mathrm{d}\xi_1, t) &= \exp(\hat{\boldsymbol{\kappa}}(\xi_1, t).\mathrm{d}\xi_1).\boldsymbol{Q}(\xi_1, t); \\ \boldsymbol{Q}(\xi_1, t + \mathrm{d}t) &= \exp(\hat{\boldsymbol{\omega}}(\xi_1, t + \mathrm{d}t).\mathrm{d}t).\boldsymbol{Q}(\xi_1, t). \end{aligned} \tag{7.25}$$

Figure 7.1 provides geometric interpretation of result in Eq. (7.25) considering the boundary at $\xi_1 = 0$ to be fixed. We also observe that the geometric structure of angular velocity vector $\boldsymbol{\omega}$ and the curvature vector $\boldsymbol{\kappa}$ is very similar such that $\hat{\boldsymbol{\omega}}.\boldsymbol{Q}, \hat{\boldsymbol{\kappa}}.\boldsymbol{Q} \in T_{\boldsymbol{Q}}SO(3)$.

7.4 Variation

To obtain the virtual work principle (weak form of equilibrium equation), we need to obtain the admissible variation of the deformed configuration. We also must linearize the weak form for numerically solving the system. This shall be covered in chapter 10. However, since both variation and linearization are geometrically similar procedures (that help us operate on the tangent space $T_{\boldsymbol{\Phi}}\mathbb{C}$), we shall carefully describe the variation of deformation map and associated strain quantities here.

7.4.1 Admissible variation of the deformed configuration Ω

To obtain the virtual deformed configuration of the system, we superimpose an admissible variation or admissible infinitesimal (and instantaneous) displacement field $\delta\boldsymbol{\Phi} = (\delta\boldsymbol{\varphi}, \delta\boldsymbol{Q}, \delta p)$ to the configuration $\boldsymbol{\Phi} = (\boldsymbol{\varphi}, \boldsymbol{Q}(\boldsymbol{\theta}), p)$. The varied configuration is then defined by $\boldsymbol{\Phi}_\epsilon = (\boldsymbol{\varphi}_\epsilon, \boldsymbol{Q}_\epsilon, p_\epsilon)$ such that for $\epsilon > 0$, we have,

$$\boldsymbol{\varphi}_\epsilon = \boldsymbol{\varphi} + \epsilon\delta\boldsymbol{\varphi}; \tag{7.26a}$$

$$\boldsymbol{Q}_\epsilon = \boldsymbol{Q}(\boldsymbol{\theta} + \epsilon\delta\boldsymbol{\theta}) = \boldsymbol{Q}(\epsilon\delta\boldsymbol{\alpha}).\boldsymbol{Q}(\boldsymbol{\theta}); \tag{7.26b}$$

$$p_\epsilon = p + \epsilon\delta p. \tag{7.26c}$$

We also note that

$$\delta\boldsymbol{\varphi} = \partial_\epsilon \boldsymbol{\varphi}_\epsilon|_{\epsilon=0};\ \delta\boldsymbol{Q} = \partial_\epsilon \boldsymbol{Q}_\epsilon|_{\epsilon=0};\ \delta p = \partial_\epsilon p_\epsilon|_{\epsilon=0}; \tag{7.27a}$$

$$\delta\boldsymbol{\Phi} = \partial_\epsilon \boldsymbol{\Phi}_\epsilon|_{\epsilon=0}. \tag{7.27b}$$

Unlike the variation in the mid-curve axial vector and the warping amplitude, understanding the variation in the rotation tensor needs some detailed investigation. This is because $\boldsymbol{\varphi} \in \mathbb{R}^3$ and $p \in \mathbb{R}$ belong to linear vector spaces, where as $SO(3)$ is a non-linear manifold. Section 3.3 of chapter 3 discusses variation in the rotation tensor $\boldsymbol{Q}$ in great detail. We recall the following two important results from section 3.3:

$$\begin{aligned} \delta\boldsymbol{Q} &= \delta\hat{\boldsymbol{\alpha}}.\boldsymbol{Q}; \\ \delta\boldsymbol{d}_i &= \delta\hat{\boldsymbol{\alpha}}.\boldsymbol{d}_i = \delta\boldsymbol{\alpha} \times \boldsymbol{d}_i. \end{aligned} \tag{7.28}$$

In the equation above, $\delta\boldsymbol{\alpha}$ represents the *virtual rotation vector in current state*. We redefine $\delta\boldsymbol{\Phi}$ as,

$$\delta\boldsymbol{\Phi} = \left[\delta\boldsymbol{\varphi}; \delta\boldsymbol{\alpha}; \delta p\right]. \tag{7.29}$$

Having understood the varied configuration space, the expressions derived in this section can be directly used to obtain variation of other quantities using straightforward chain rule.

7.4.2 Variation of the strain quantities and their derivatives

In this section, we obtain the variation of finite strain quantities in terms of $(\delta\boldsymbol{\varphi}, \delta\boldsymbol{\alpha}, \delta p)$ and their derivatives. The virtual material strain vectors $\delta\overline{\boldsymbol{\lambda}}_i$ are strain conjugate to material form of first PK stress vectors (discussed later in section 7.5.2). Deriving the expression of $\delta\overline{\boldsymbol{\lambda}}_i$ requires us to first find variation of $\boldsymbol{L}$-terms and $\delta\overline{\boldsymbol{\epsilon}}$ as a function of $(\delta\boldsymbol{\varphi}, \delta\boldsymbol{\alpha}, \delta p)$ and their derivatives.

7.4.2.1 Variation of the finite strain terms

From the definition of axial strain vector $\boldsymbol{\varepsilon}$ and its material counterpart $\overline{\boldsymbol{\varepsilon}}$ in Eq. (4.6), we obtain the variation of these quantities as,

$$\delta\boldsymbol{\varepsilon} = \delta\partial_{\xi_1}\boldsymbol{\varphi} - \delta\hat{\boldsymbol{\alpha}}.\boldsymbol{d}_1; \tag{7.30a}$$

$$\delta\overline{\boldsymbol{\varepsilon}} = \delta(\boldsymbol{Q}^T.\boldsymbol{\varepsilon}) = \boldsymbol{Q}^T\left(\delta\partial_{\xi_1}\boldsymbol{\varphi} + \partial_{\xi_1}\hat{\boldsymbol{\varphi}}.\delta\boldsymbol{\alpha}\right) = \boldsymbol{Q}^T.\tilde{\delta}\boldsymbol{\varepsilon}. \tag{7.30b}$$

Similarly, the variation of spatial and material curvature tensor is given by,

$$\delta\hat{\boldsymbol{\kappa}} = \delta(\partial_{\xi_1}\boldsymbol{Q}.\boldsymbol{Q}^T) = \delta\partial_{\xi_1}\boldsymbol{Q}.\boldsymbol{Q}^T + \partial_{\xi_1}\boldsymbol{Q}.\delta\boldsymbol{Q}^T = \delta\partial_{\xi_1}\hat{\boldsymbol{\alpha}} + [\delta\hat{\boldsymbol{\alpha}},\hat{\boldsymbol{\kappa}}]; \tag{7.31a}$$

$$\delta\hat{\overline{\boldsymbol{\kappa}}} = \delta(\boldsymbol{Q}^T.\partial_{\xi_1}\boldsymbol{Q}) = \delta\boldsymbol{Q}^T.\partial_{\xi_1}\boldsymbol{Q} + \boldsymbol{Q}^T.\delta\partial_{\xi_1}\boldsymbol{Q} = \boldsymbol{Q}^T.\delta\partial_{\xi_1}\hat{\boldsymbol{\alpha}}.\boldsymbol{Q} = \boldsymbol{Q}^T.\tilde{\delta}\hat{\boldsymbol{\kappa}}.\boldsymbol{Q}. \tag{7.31b}$$

The corresponding curvature vector are obtained as,

$$\delta\boldsymbol{\kappa} = \delta\partial_{\xi_1}\boldsymbol{\alpha} + \delta\hat{\boldsymbol{\alpha}}.\boldsymbol{\kappa}; \tag{7.32a}$$

$$\delta\overline{\boldsymbol{\kappa}} = \boldsymbol{Q}^T.\delta\partial_{\xi_1}\boldsymbol{\alpha} = \boldsymbol{Q}^T.\tilde{\delta}\boldsymbol{\kappa}. \tag{7.32b}$$

Like the co-rotated derivatives, $\tilde{\delta}\boldsymbol{\varepsilon} = \left(\delta\partial_{\xi_1}\boldsymbol{\varphi} + \partial_{\xi_1}\hat{\boldsymbol{\varphi}}.\delta\boldsymbol{\alpha}\right)$, $\tilde{\delta}\boldsymbol{\kappa} = \delta\partial_{\xi_1}\boldsymbol{\alpha}$ and $\tilde{\delta}\hat{\boldsymbol{\kappa}} = \delta\partial_{\xi_1}\hat{\boldsymbol{\alpha}}$ defines the co-rotated variation of the curvature vector, axial strain vector and curvature tensor respectively.

7.4.2.2 Variation of the vector $\overline{\boldsymbol{\epsilon}}$

Since the derivative and variation can be used interchangeably, we obtain the following:

$$\delta\partial_{\xi_1}\overline{\boldsymbol{\varepsilon}} = \partial_{\xi_1}\delta\overline{\boldsymbol{\varepsilon}} = \boldsymbol{Q}^T.\left(\delta\partial^2_{\xi_1}\boldsymbol{\varphi} + (\partial^2_{\xi_1}\hat{\boldsymbol{\varphi}} - \hat{\boldsymbol{\kappa}}.\partial_{\xi_1}\hat{\boldsymbol{\varphi}}).\delta\boldsymbol{\alpha} + \partial_{\xi_1}\hat{\boldsymbol{\varphi}}.\delta\partial_{\xi_1}\hat{\boldsymbol{\alpha}} - \hat{\boldsymbol{\kappa}}.\delta\partial_{\xi_1}\boldsymbol{\varphi}\right); \tag{7.33a}$$

$$\delta\partial_{\xi_1}\overline{\boldsymbol{\kappa}} = \partial_{\xi_1}\delta\overline{\boldsymbol{\kappa}} = \boldsymbol{Q}^T.\left(\delta\partial^2_{\xi_1}\boldsymbol{\alpha} - \hat{\boldsymbol{\kappa}}.\delta\partial_{\xi_1}\boldsymbol{\alpha}\right); \tag{7.33b}$$

$$\delta\partial^2_{\xi_1}\overline{\boldsymbol{\kappa}} = \partial_{\xi_1}(\delta\partial_{\xi_1}\overline{\boldsymbol{\kappa}}) = \boldsymbol{Q}^T.\left(\delta\partial^3_{\xi_1}\boldsymbol{\alpha} + (\hat{\boldsymbol{\kappa}}.\hat{\boldsymbol{\kappa}} - \partial_{\xi_1}\hat{\boldsymbol{\kappa}}).\delta\partial_{\xi_1}\boldsymbol{\alpha} - 2\hat{\boldsymbol{\kappa}}.\delta\partial^2_{\xi_1}\boldsymbol{\alpha}\right); \tag{7.33c}$$

$$\begin{aligned}\delta\partial^3_{\xi_1}\overline{\boldsymbol{\kappa}} = \partial_{\xi_1}(\delta\partial^2_{\xi_1}\overline{\boldsymbol{\kappa}}) =& \boldsymbol{Q}^T.(\delta\partial^4_{\xi_1}\boldsymbol{\alpha} + (\partial_{\xi_1}\hat{\boldsymbol{\kappa}}.\hat{\boldsymbol{\kappa}} + 2\hat{\boldsymbol{\kappa}}.\partial_{\xi_1}\hat{\boldsymbol{\kappa}} - \partial^2_{\xi_1}\hat{\boldsymbol{\kappa}} - \hat{\boldsymbol{\kappa}}.\hat{\boldsymbol{\kappa}}.\hat{\boldsymbol{\kappa}}).\delta\partial_{\xi_1}\boldsymbol{\alpha} \\ &+ (3\hat{\boldsymbol{\kappa}}.\hat{\boldsymbol{\kappa}} - 3\partial_{\xi_1}\hat{\boldsymbol{\kappa}}).\delta\partial^2_{\xi}\boldsymbol{\alpha} - 3\hat{\boldsymbol{\kappa}}.\delta\partial^3_{\xi_1}\boldsymbol{\alpha}).\end{aligned} \tag{7.33d}$$

Using the results obtained above, the virtual quantity $\delta\overline{\boldsymbol{\epsilon}}$ can be expressed in the following form:

$$\delta\overline{\boldsymbol{\epsilon}} = \boldsymbol{\Lambda}^T.\boldsymbol{B}_1.\delta\boldsymbol{\Theta} = \boldsymbol{\Lambda}^T.\tilde{\delta}\boldsymbol{\epsilon}, \tag{7.34}$$

where,

$$\delta\boldsymbol{\Theta} = \left[\delta\boldsymbol{\varphi}; \delta\partial_{\xi_1}\boldsymbol{\varphi}; \delta\partial^2_{\xi_1}\boldsymbol{\varphi}; \delta\boldsymbol{\alpha}; \delta\partial_{\xi_1}\boldsymbol{\alpha}; \delta\partial^2_{\xi_1}\boldsymbol{\alpha}; \delta\partial^3_{\xi_1}\boldsymbol{\alpha}; \delta\partial^4_{\xi_1}\boldsymbol{\alpha}; \delta p; \delta\partial_{\xi_1}p; \delta\partial^2_{\xi_1}p\right] \tag{7.35a}$$

$$\delta\overline{\boldsymbol{\epsilon}} = \left[\delta\overline{\boldsymbol{\varepsilon}}; \delta\partial_{\xi_1}\overline{\boldsymbol{\varepsilon}}; \delta\overline{\boldsymbol{\kappa}}; \delta\partial_{\xi_1}\overline{\boldsymbol{\kappa}}; \delta\partial^2_{\xi_1}\overline{\boldsymbol{\kappa}}; \delta\partial^3_{\xi_1}\overline{\boldsymbol{\kappa}}; \delta p; \delta\partial_{\xi_1}p; \delta\partial^2_{\xi_1}p\right]; \tag{7.35b}$$

$$\begin{aligned}\tilde{\delta}\boldsymbol{\epsilon} &= \left[\tilde{\delta}\boldsymbol{\varepsilon}; \boldsymbol{Q}.\delta\partial_{\xi_1}\overline{\boldsymbol{\varepsilon}}; \tilde{\delta}\boldsymbol{\kappa}; \boldsymbol{Q}.\delta\partial_{\xi_1}\overline{\boldsymbol{\kappa}}; \boldsymbol{Q}.\delta\partial^2_{\xi_1}\overline{\boldsymbol{\kappa}}; \boldsymbol{Q}.\delta\partial^3_{\xi_1}\overline{\boldsymbol{\kappa}}; \delta p; \delta\partial_{\xi_1}p; \delta\partial^2_{\xi_1}p\right]; \\ &= \left[\tilde{\delta}\boldsymbol{\varepsilon}; \tilde{\delta}\tilde{\partial}_{\xi_1}\boldsymbol{\varepsilon}; \tilde{\delta}\boldsymbol{\kappa}; \tilde{\delta}\tilde{\partial}_{\xi_1}\boldsymbol{\kappa}; \tilde{\delta}\tilde{\partial}^2_{\xi_1}\boldsymbol{\kappa}; \tilde{\delta}\tilde{\partial}^3_{\xi_1}\boldsymbol{\kappa}; \delta p; \delta\partial_{\xi_1}p; \delta\partial^2_{\xi_1}p\right].\end{aligned} \tag{7.35c}$$

In Eq. (7.34), the transformation matrix $\boldsymbol{\Lambda}$ left-translates the quantity $\delta\overline{\boldsymbol{\epsilon}}$ to obtain co-rotationally varied vector $\tilde{\delta}\boldsymbol{\epsilon}$.

The virtual vector $\delta\boldsymbol{\Theta}$ can be related to $\delta\boldsymbol{\Phi}$ by means of a differential operator $\boldsymbol{B}_2$ (of size 27×7), such that,

$$\delta\boldsymbol{\Theta} = \boldsymbol{B}_2.\delta\boldsymbol{\Phi}. \tag{7.36}$$

The Eq. (7.34) can then be re-written as,

$$\begin{aligned}\delta\overline{\boldsymbol{\epsilon}} &= \boldsymbol{\Lambda}^T.\boldsymbol{B}_1.\boldsymbol{B}_2.\delta\boldsymbol{\Phi}; \\ \tilde{\delta}\boldsymbol{\epsilon} &= \boldsymbol{B}_1.\boldsymbol{B}_2.\delta\boldsymbol{\Phi}.\end{aligned} \tag{7.37}$$

The expanded description of the matrix $\boldsymbol{B}_1$ is given below.

$$\boldsymbol{B}_1 = \begin{bmatrix} \mathbf{0}_3 & \boldsymbol{I}_3 & \mathbf{0}_3 & \partial_{\xi_1}\hat{\boldsymbol{\varphi}} & \mathbf{0}_3 & \mathbf{0}_3 & \mathbf{0}_3 & \mathbf{0}_3 & \mathbf{0}_3 \\ \mathbf{0}_3 & -\hat{\boldsymbol{\kappa}} & \boldsymbol{I}_3 & \left(\partial^2_{\xi_1}\hat{\boldsymbol{\varphi}} - \hat{\boldsymbol{\kappa}}.\partial_{\xi_1}\hat{\boldsymbol{\varphi}}\right) & \partial_{\xi_1}\hat{\boldsymbol{\varphi}} & \mathbf{0}_3 & \mathbf{0}_3 & \mathbf{0}_3 & \mathbf{0}_3 \\ \mathbf{0}_3 & \mathbf{0}_3 & \mathbf{0}_3 & \mathbf{0}_3 & \boldsymbol{I}_3 & \mathbf{0}_3 & \mathbf{0}_3 & \mathbf{0}_3 & \mathbf{0}_3 \\ \mathbf{0}_3 & \mathbf{0}_3 & \mathbf{0}_3 & \mathbf{0}_3 & -\hat{\boldsymbol{\kappa}} & \boldsymbol{I}_3 & \mathbf{0}_3 & \mathbf{0}_3 & \mathbf{0}_3 \\ \mathbf{0}_3 & \mathbf{0}_3 & \mathbf{0}_3 & \mathbf{0}_3 & \left(\hat{\boldsymbol{\kappa}}.\hat{\boldsymbol{\kappa}} - \partial_{\xi_1}\hat{\boldsymbol{\kappa}}\right) & -2\hat{\boldsymbol{\kappa}} & \boldsymbol{I}_3 & \mathbf{0}_3 & \mathbf{0}_3 \\ \mathbf{0}_3 & \mathbf{0}_3 & \mathbf{0}_3 & \mathbf{0}_3 & \begin{pmatrix} \partial_{\xi_1}\hat{\boldsymbol{\kappa}}.\hat{\boldsymbol{\kappa}} + 2\hat{\boldsymbol{\kappa}}.\partial_{\xi_1}\hat{\boldsymbol{\kappa}} \\ -\partial^2_{\xi_1}\hat{\boldsymbol{\kappa}} - \hat{\boldsymbol{\kappa}}.\hat{\boldsymbol{\kappa}}.\hat{\boldsymbol{\kappa}} \end{pmatrix} & 3\left(\hat{\boldsymbol{\kappa}}.\hat{\boldsymbol{\kappa}} - \partial_{\xi_1}\hat{\boldsymbol{\kappa}}\right) & -3\hat{\boldsymbol{\kappa}} & \boldsymbol{I}_3 & \mathbf{0}_3 \\ \mathbf{0}_3 & \mathbf{0}_3 & \mathbf{0}_3 & \mathbf{0}_3 & \mathbf{0}_3 & \mathbf{0}_3 & \mathbf{0}_3 & \mathbf{0}_3 & \boldsymbol{I}_3 \end{bmatrix}. \tag{7.38}$$

The matrix $\boldsymbol{B}_2$ consist of differential operators and is given by,

$$\boldsymbol{B}_2^T = \begin{bmatrix} \boldsymbol{I}_3 & \partial_{\xi_1}.\boldsymbol{I}_3 & \partial^2_{\xi_1}.\boldsymbol{I}_3 & \mathbf{0}_3 & \mathbf{0}_3 & \mathbf{0}_3 & \mathbf{0}_3 & \mathbf{0}_3 & \mathbf{0}_1 & \mathbf{0}_1 & \mathbf{0}_1 \\ \mathbf{0}_3 & \mathbf{0}_3 & \mathbf{0}_3 & \boldsymbol{I}_3 & \partial_{\xi_1}.\boldsymbol{I}_3 & \partial^2_{\xi_1}.\boldsymbol{I}_3 & \partial^3_{\xi_1}.\boldsymbol{I}_3 & \partial^4_{\xi_1}.\boldsymbol{I}_3 & \mathbf{0}_1 & \mathbf{0}_1 & \mathbf{0}_1 \\ \mathbf{0}_1^T & \mathbf{0}_1^T & \mathbf{0}_1^T & \mathbf{0}_1^T & \mathbf{0}_1^T & \mathbf{0}_1^T & \mathbf{0}_1^T & \mathbf{0}_1^T & 1 & \partial_{\xi_1} & \partial^2_{\xi_1} \end{bmatrix}. \tag{7.39}$$

Here,

$$\partial^n_{\xi_1}.\boldsymbol{I}_3 = \begin{bmatrix} \partial^n_{\xi_1} & 0 & 0 \\ 0 & \partial^n_{\xi_1} & 0 \\ 0 & 0 & \partial^n_{\xi_1}. \end{bmatrix} \tag{7.40}$$

7.4.2.3 Variation of the strain vector $\overline{\lambda}_i$ and the concatenated strain vector $\overline{\mathfrak{L}}$

From Eq. (7.7a), we have,

$$\delta\overline{\mathfrak{L}} = \delta\overline{\mathfrak{L}}.\overline{\boldsymbol{\epsilon}} + \overline{\mathfrak{L}}.\delta\overline{\boldsymbol{\epsilon}}. \tag{7.41}$$

We realize that, except for $\delta \boldsymbol{L}_{\boldsymbol{\kappa}}^{\boldsymbol{\lambda}_1} = \delta \hat{\overline{\boldsymbol{r}}}^T$, the variation in all other $\boldsymbol{L}$-terms are $\boldsymbol{0}_3$. Thus, we have,

$$\delta \overline{\mathfrak{Q}}.\overline{\boldsymbol{\epsilon}} = [\delta \boldsymbol{L}_{\boldsymbol{\kappa}}^{\boldsymbol{\lambda}_1}.\overline{\boldsymbol{\kappa}}; \boldsymbol{0}_1; \boldsymbol{0}_1] = [\delta \hat{\overline{\boldsymbol{r}}}^T.\overline{\boldsymbol{\kappa}}; \boldsymbol{0}_1; \boldsymbol{0}_1] \tag{7.42}$$

The material form of the position vector of $\boldsymbol{r}$ is given by,

$$\overline{\boldsymbol{r}} = \boldsymbol{Q}^T.\boldsymbol{r} = \hat{\xi}_2 \boldsymbol{E}_2 + \hat{\xi}_3 \boldsymbol{E}_3 + W \boldsymbol{E}_3. \tag{7.43}$$

From the equation above, we have,

$$\begin{aligned}
\delta \hat{\overline{\boldsymbol{r}}}^T &= \left(\delta \overline{\boldsymbol{\varepsilon}}.(-\nu \boldsymbol{E}_1) + \delta \overline{\boldsymbol{\kappa}}.(-\nu \xi_3 \boldsymbol{E}_2 + \nu \xi_2 \boldsymbol{E}_3) + \delta \partial^2_{\xi_1} \overline{\boldsymbol{\kappa}}.(-\nu \overline{\boldsymbol{\Psi}}_{23}) + \delta \partial_{\xi_1} p.(-\nu \Psi_1)\right) \hat{\overline{\boldsymbol{r}}}_1^T \\
&\quad + \left(\delta p.(-\Psi_1) + \delta \partial_{\xi_1} \overline{\boldsymbol{\kappa}}.\overline{\boldsymbol{\Psi}}_{23}\right) \hat{\boldsymbol{E}}_1^T; \qquad (7.44a) \\
\delta \hat{\overline{\boldsymbol{r}}}^T.\overline{\boldsymbol{\kappa}} &= \left(-\nu \hat{\overline{\boldsymbol{\kappa}}}.\overline{\boldsymbol{r}}_1 \otimes \boldsymbol{E}_1\right).\delta \overline{\boldsymbol{\varepsilon}} + \left(\nu \hat{\overline{\boldsymbol{\kappa}}}.\overline{\boldsymbol{r}}_1 \otimes (\xi_2 \boldsymbol{E}_3 - \xi_3 \boldsymbol{E}_2)\right).\delta \overline{\boldsymbol{\kappa}} + \left(\hat{\overline{\boldsymbol{\kappa}}} \boldsymbol{E}_1 \otimes \overline{\boldsymbol{\Psi}}_{23}\right).\delta \partial_{\xi_1} \overline{\boldsymbol{\kappa}} \\
&\quad + \left(-\nu \hat{\overline{\boldsymbol{\kappa}}}.\overline{\boldsymbol{r}}_1 \otimes \overline{\boldsymbol{\Psi}}_{23}\right).\delta \partial^2_{\xi_1} \overline{\boldsymbol{\kappa}} + \delta p \left(\Psi_1 \hat{\overline{\boldsymbol{\kappa}}}.\overline{\boldsymbol{E}}_1\right) + \delta \partial_{\xi_1} p.\left(-\nu \Psi_1 \hat{\overline{\boldsymbol{\kappa}}}.\overline{\boldsymbol{r}}_1\right) \qquad (7.44b) \\
&= \overline{\boldsymbol{M}}_{\boldsymbol{\varepsilon}}^{\boldsymbol{\lambda}_1}.\delta \overline{\boldsymbol{\varepsilon}} + \overline{\boldsymbol{M}}_{\boldsymbol{\kappa}}^{\boldsymbol{\lambda}_1}.\delta \overline{\boldsymbol{\kappa}} + \overline{\boldsymbol{M}}_{\partial_{\xi_1}\boldsymbol{\kappa}}^{\boldsymbol{\lambda}_1}.\delta \partial_{\xi_1} \overline{\boldsymbol{\kappa}} + \overline{\boldsymbol{M}}_{\partial^2_{\xi_1}\boldsymbol{\kappa}}^{\boldsymbol{\lambda}_1}.\delta \partial^2_{\xi_1} \overline{\boldsymbol{\kappa}} + \overline{\boldsymbol{M}}_{p}^{\boldsymbol{\lambda}_1}.\delta p + \overline{\boldsymbol{M}}_{\partial_{\xi_1} p}^{\boldsymbol{\lambda}_1}.\delta \partial_{\xi_1} p.
\end{aligned}$$

Like $\boldsymbol{L}$-terms, we call $\overline{\boldsymbol{M}}_{(.)}^{\boldsymbol{\lambda}_i}$ as $\boldsymbol{M}$-terms. The expression of $\boldsymbol{M}$-terms are given as follows,

$$\overline{\boldsymbol{M}}_{\boldsymbol{\varepsilon}}^{\boldsymbol{\lambda}_1} = -\nu \hat{\overline{\boldsymbol{\kappa}}}.\overline{\boldsymbol{r}}_1 \otimes \boldsymbol{E}_1 \qquad \boldsymbol{M}_{\boldsymbol{\varepsilon}}^{\boldsymbol{\lambda}_1} = -\nu \hat{\boldsymbol{\kappa}}.\boldsymbol{r}_1 \otimes \boldsymbol{d}_1 \tag{7.45a}$$

$$\overline{\boldsymbol{M}}_{\boldsymbol{\kappa}}^{\boldsymbol{\lambda}_1} = \nu \hat{\overline{\boldsymbol{\kappa}}}.\overline{\boldsymbol{r}}_1 \otimes (\xi_2 \boldsymbol{E}_3 - \xi_3 \boldsymbol{E}_2) \qquad \boldsymbol{M}_{\boldsymbol{\kappa}}^{\boldsymbol{\lambda}_1} = \nu \hat{\boldsymbol{\kappa}}.\boldsymbol{r}_1 \otimes (\xi_2 \boldsymbol{d}_3 - \xi_3 \boldsymbol{d}_2) \tag{7.45b}$$

$$\overline{\boldsymbol{M}}_{\partial_{\xi_1}\boldsymbol{\kappa}}^{\boldsymbol{\lambda}_1} = \hat{\overline{\boldsymbol{\kappa}}}.\boldsymbol{E}_1 \otimes \overline{\boldsymbol{\Psi}}_{23} \qquad \boldsymbol{M}_{\partial_{\xi_1}\boldsymbol{\kappa}}^{\boldsymbol{\lambda}_1} = \hat{\boldsymbol{\kappa}}.\boldsymbol{d}_1 \otimes \boldsymbol{\Psi}_{23} \tag{7.45c}$$

$$\overline{\boldsymbol{M}}_{\partial^2_{\xi_1}\boldsymbol{\kappa}}^{\boldsymbol{\lambda}_1} = -\nu \hat{\overline{\boldsymbol{\kappa}}}.\overline{\boldsymbol{r}}_1 \otimes \overline{\boldsymbol{\Psi}}_{23} \qquad \boldsymbol{M}_{\partial^2_{\xi_1}\boldsymbol{\kappa}}^{\boldsymbol{\lambda}_1} = -\nu \hat{\boldsymbol{\kappa}}.\boldsymbol{r}_1 \otimes \boldsymbol{\Psi}_{23} \tag{7.45d}$$

$$\overline{\boldsymbol{M}}_{p}^{\boldsymbol{\lambda}_1} = \Psi_1 \hat{\overline{\boldsymbol{\kappa}}}.\overline{\boldsymbol{E}}_1 \qquad \boldsymbol{M}_{p}^{\boldsymbol{\lambda}_1} = \Psi_1 \hat{\boldsymbol{\kappa}}.\boldsymbol{d}_1 \tag{7.45e}$$

$$\overline{\boldsymbol{M}}_{\partial_{\xi_1} p}^{\boldsymbol{\lambda}_1} = -\nu \Psi_1 \hat{\overline{\boldsymbol{\kappa}}}.\overline{\boldsymbol{r}}_1 \qquad \boldsymbol{M}_{\partial_{\xi_1} p}^{\boldsymbol{\lambda}_1} = -\nu \Psi_1 \hat{\boldsymbol{\kappa}}.\boldsymbol{r}_1. \tag{7.45f}$$

Combining equations (7.42) and (7.44b), we have

$$\delta \overline{\mathfrak{Q}}.\overline{\boldsymbol{\epsilon}} = \overline{\boldsymbol{M}}.\delta \overline{\boldsymbol{\epsilon}}, \tag{7.46}$$

where,

$$\overline{\boldsymbol{M}} = \begin{bmatrix} \overline{\boldsymbol{M}}_{\boldsymbol{\varepsilon}}^{\boldsymbol{\lambda}_1} & \mathbf{0}_3 & \overline{\boldsymbol{M}}_{\boldsymbol{\kappa}}^{\boldsymbol{\lambda}_1} & \overline{\boldsymbol{M}}_{\partial_{\xi_1}\boldsymbol{\kappa}}^{\boldsymbol{\lambda}_1} & \overline{\boldsymbol{M}}_{\partial^2_{\xi_1}\boldsymbol{\kappa}}^{\boldsymbol{\lambda}_1} & \mathbf{0}_3 & \overline{\boldsymbol{M}}_{p}^{\boldsymbol{\lambda}_1} & \overline{\boldsymbol{M}}_{\partial_{\xi_1} p}^{\boldsymbol{\lambda}_1} & \mathbf{0}_1 \\ \mathbf{0}_3 & \mathbf{0}_3 & \mathbf{0}_3 & \mathbf{0}_3 & \mathbf{0}_3 & \mathbf{0}_3 & \mathbf{0}_1 & \mathbf{0}_1 & \mathbf{0}_1 \\ \mathbf{0}_3 & \mathbf{0}_3 & \mathbf{0}_3 & \mathbf{0}_3 & \mathbf{0}_3 & \mathbf{0}_3 & \mathbf{0}_1 & \mathbf{0}_1 & \mathbf{0}_1 \end{bmatrix}. \tag{7.47}$$

Similar to Eq. (7.13), we define the spatial form of $\boldsymbol{M}$ matrix as,

$$\boldsymbol{M} = \boldsymbol{Q}_3.\overline{\boldsymbol{M}}.\boldsymbol{\Lambda}^T, \tag{7.48}$$

such that,

$$\boldsymbol{M} = \begin{bmatrix} \boldsymbol{M}_{\boldsymbol{\varepsilon}}^{\boldsymbol{\lambda}_1} & \mathbf{0}_3 & \boldsymbol{M}_{\boldsymbol{\kappa}}^{\boldsymbol{\lambda}_1} & \boldsymbol{M}_{\partial_{\xi_1}\boldsymbol{\kappa}}^{\boldsymbol{\lambda}_1} & \boldsymbol{M}_{\partial^2_{\xi_1}\boldsymbol{\kappa}}^{\boldsymbol{\lambda}_1} & \mathbf{0}_3 & \boldsymbol{M}_{p}^{\boldsymbol{\lambda}_1} & \boldsymbol{M}_{\partial_{\xi_1} p}^{\boldsymbol{\lambda}_1} & \mathbf{0}_1 \\ \mathbf{0}_3 & \mathbf{0}_3 & \mathbf{0}_3 & \mathbf{0}_3 & \mathbf{0}_3 & \mathbf{0}_3 & \mathbf{0}_1 & \mathbf{0}_1 & \mathbf{0}_1 \\ \mathbf{0}_3 & \mathbf{0}_3 & \mathbf{0}_3 & \mathbf{0}_3 & \mathbf{0}_3 & \mathbf{0}_3 & \mathbf{0}_1 & \mathbf{0}_1 & \mathbf{0}_1 \end{bmatrix}, \tag{7.49}$$

and

$$\begin{gathered} \boldsymbol{M}_{\boldsymbol{x}}^{\boldsymbol{\lambda}_i} = \boldsymbol{Q}.\overline{\boldsymbol{M}}_{\boldsymbol{x}}^{\boldsymbol{\lambda}_i}.\boldsymbol{Q}^T \text{ and } \overline{\boldsymbol{M}}_{\boldsymbol{x}}^{\boldsymbol{\lambda}_i} = \boldsymbol{Q}^T.\boldsymbol{M}_{\boldsymbol{x}}^{\boldsymbol{\lambda}_i}.\boldsymbol{Q} \text{ for } \boldsymbol{x} \in \{\boldsymbol{\varepsilon},\ \boldsymbol{\kappa},\ \partial_{\xi_1}\boldsymbol{\kappa},\ \partial^2_{\xi_1}\boldsymbol{\kappa}\} \\ \boldsymbol{M}_{x}^{\boldsymbol{\lambda}_i} = \boldsymbol{Q}.\overline{\boldsymbol{M}}_{x}^{\boldsymbol{\lambda}_i} \text{ and } \overline{\boldsymbol{M}}_{x}^{\boldsymbol{\lambda}_i} = \boldsymbol{Q}^T.\boldsymbol{M}_{x}^{\boldsymbol{\lambda}_i} \text{ for } x \in \{p,\ \partial_{\xi_1} p\} \end{gathered}. \tag{7.50}$$

Substituting Eq. (7.46) into Eq. (7.41), we get

$$\delta\overline{\mathfrak{L}} = \left[\delta\overline{\boldsymbol{\lambda}}_1; \delta\overline{\boldsymbol{\lambda}}_2; \delta\overline{\boldsymbol{\lambda}}_3\right] = \left(\overline{\boldsymbol{L}} + \overline{\boldsymbol{M}}\right).\delta\overline{\boldsymbol{\epsilon}} \tag{7.51}$$

We define the co-rotoational variation of the concatenated strain vector $\mathfrak{L}$ as

$$\begin{aligned} \tilde{\delta}\mathfrak{L} &= \left[\tilde{\delta}\boldsymbol{\lambda}_1; \tilde{\delta}\boldsymbol{\lambda}_2; \tilde{\delta}\boldsymbol{\lambda}_3\right] = \boldsymbol{Q}_3.\delta\overline{\mathfrak{L}} = \boldsymbol{Q}_3.\left(\overline{\boldsymbol{L}} + \overline{\boldsymbol{M}}\right).\delta\overline{\boldsymbol{\epsilon}} \\ &= \left(\boldsymbol{Q}_3.\left(\overline{\boldsymbol{L}} + \overline{\boldsymbol{M}}\right).\boldsymbol{\Lambda}^T\right).\tilde{\delta}\boldsymbol{\epsilon} = (\boldsymbol{L} + \boldsymbol{M}).\tilde{\delta}\boldsymbol{\epsilon}. \end{aligned} \tag{7.52}$$

We finally note that the variation of deformation gradient tensor is obtained as

$$\begin{gathered} \delta\boldsymbol{F} = \tilde{\delta}\boldsymbol{F} + \delta\boldsymbol{Q}.\overline{\boldsymbol{F}} = \tilde{\delta}\boldsymbol{F} + \delta\hat{\boldsymbol{\alpha}}.\boldsymbol{F}; \\ \tilde{\delta}\boldsymbol{F} = \boldsymbol{Q}.\delta\overline{\boldsymbol{F}} = \tilde{\delta}\boldsymbol{\lambda}_i \otimes \boldsymbol{E}_i; \\ \delta\overline{\boldsymbol{F}} = \delta\overline{\boldsymbol{\lambda}}_i \otimes \boldsymbol{E}_i. \end{gathered} \tag{7.53}$$

7.4.3 Variation of displacement field

We need the variation of displacement field to evaluate the virtual work done by external loads. We define the displacement field $\boldsymbol{u}(\xi_1, \xi_2, \xi_3)$ as $\boldsymbol{u} = \boldsymbol{R} - \boldsymbol{R}_0$. Since, $\delta\boldsymbol{R}_0 = \boldsymbol{0}_1$, we have $\delta\boldsymbol{u} = \delta\boldsymbol{R}$. Thus, from Eq. (7.1),

$$\delta\boldsymbol{R} = \delta\boldsymbol{\varphi} + \delta\boldsymbol{r}; \tag{7.54a}$$

$$\delta\boldsymbol{r} = \tilde{\delta}\boldsymbol{r} + \delta\hat{\boldsymbol{\alpha}}.\boldsymbol{r}; \tag{7.54b}$$

$$\tilde{\delta}\boldsymbol{r} = \delta\hat{\xi}_2\boldsymbol{d}_2 + \delta\hat{\xi}_3\boldsymbol{d}_3 + \delta W\boldsymbol{d}_1, \tag{7.54c}$$

where,

$$\begin{aligned}
\delta\hat{\xi}_2 &= \delta\overline{\boldsymbol{\varepsilon}}.(-\nu\xi_2\boldsymbol{E}_1) + \delta\overline{\boldsymbol{\kappa}}.(\nu\xi_2^2\boldsymbol{E}_3 - \nu\xi_2\xi_3\boldsymbol{E}_2) + \delta\partial^2_{\xi_1}\overline{\boldsymbol{\kappa}}.(-\nu\xi_2\overline{\boldsymbol{\Psi}}_{23}) + \delta\partial_{\xi_1}p(-\nu\xi_2\Psi_1);\\
\delta\hat{\xi}_3 &= \delta\overline{\boldsymbol{\varepsilon}}.(-\nu\xi_3\boldsymbol{E}_1) + \delta\overline{\boldsymbol{\kappa}}.(\nu\xi_2\xi_3\boldsymbol{E}_3 - \nu\xi_3^2\boldsymbol{E}_2) + \delta\partial^2_{\xi_1}\overline{\boldsymbol{\kappa}}.(-\nu\xi_3\overline{\boldsymbol{\Psi}}_{23}) + \delta\partial_{\xi_1}p(-\nu\xi_3\Psi_1);\\
\delta W &= \delta p.\Psi_1 + \delta\partial_{\xi_1}\overline{\boldsymbol{\kappa}}.\overline{\boldsymbol{\Psi}}_{23}.
\end{aligned} \tag{7.55}$$

Using the results discussed above, we expand the expression for $\tilde{\delta}\boldsymbol{r}$ in Eq. (7.54c) in a desirable form that will be used later:

$$\begin{aligned}
\tilde{\delta}\boldsymbol{r} &= \boldsymbol{L}^{\boldsymbol{\lambda}_1}_{\partial_{\xi_1}\boldsymbol{\varepsilon}}.\tilde{\delta}\boldsymbol{\varepsilon} + \boldsymbol{L}^{\boldsymbol{\lambda}_1}_{\partial_{\xi_1}\boldsymbol{\kappa}}.\tilde{\delta}\boldsymbol{\kappa} + \boldsymbol{L}^{\boldsymbol{\lambda}_1}_{\partial^2_{\xi_1}\boldsymbol{\kappa}}.(\boldsymbol{Q}.\delta\partial_{\xi_1}\overline{\boldsymbol{\kappa}}) + \boldsymbol{L}^{\boldsymbol{\lambda}_1}_{\partial^3_{\xi_1}\boldsymbol{\kappa}}.(\boldsymbol{Q}.\delta\partial^2_{\xi_1}\overline{\boldsymbol{\kappa}}) + \delta p.\boldsymbol{L}^{\boldsymbol{\lambda}_1}_{\partial_{\xi_1}p} + \delta\partial_{\xi_1}p.\boldsymbol{L}^{\boldsymbol{\lambda}_1}_{\partial^2_{\xi_1}p};\\
&= \boldsymbol{L}^{\boldsymbol{\lambda}_1}_{\partial_{\xi_1}\boldsymbol{\varepsilon}}.\tilde{\delta}\boldsymbol{\varepsilon} + \boldsymbol{L}^{\boldsymbol{\lambda}_1}_{\partial_{\xi_1}\boldsymbol{\kappa}}.\tilde{\delta}\boldsymbol{\kappa} + \boldsymbol{L}^{\boldsymbol{\lambda}_1}_{\partial^2_{\xi_1}\boldsymbol{\kappa}}.(\tilde{\delta}\tilde{\partial}_{\xi_1}\boldsymbol{\kappa}) + \boldsymbol{L}^{\boldsymbol{\lambda}_1}_{\partial^3_{\xi_1}\boldsymbol{\kappa}}.(\tilde{\delta}\tilde{\partial}^2_{\xi_1}\boldsymbol{\kappa}) + \delta p.\boldsymbol{L}^{\boldsymbol{\lambda}_1}_{\partial_{\xi_1}p} + \delta\partial_{\xi_1}p.\boldsymbol{L}^{\boldsymbol{\lambda}_1}_{\partial^2_{\xi_1}p}.
\end{aligned} \tag{7.56}$$

7.5 Weak form of governing differential equation for the deformed state Ω

7.5.1 General virtual work principle

We define the unsymmetric two-point first Piola Kirchoff stress tensor $\boldsymbol{S}$ referenced to the undeformed configuration Ω_0 such that the associated stress vectors $\boldsymbol{S}_i$ are given by

$$\boldsymbol{S}_i = \boldsymbol{S}.\boldsymbol{E}_i = \overline{S}_{ij}\boldsymbol{d}_j; \tag{7.57a}$$

$$\boldsymbol{S} = \boldsymbol{S}_i \otimes \boldsymbol{E}_i = \overline{S}_{ij}\boldsymbol{d}_j \otimes \boldsymbol{E}_i. \tag{7.57b}$$

The infinitesimal equilibrium equation for a general continuum referenced to the undeformed configuration Ω_0 is given as

$$\begin{gathered} \mathrm{Div}\boldsymbol{S} + \rho_0\boldsymbol{b} = \rho_0\partial_t^2\boldsymbol{R}; \\ \text{or} \\ \partial_{\xi_1}\boldsymbol{S}_1 + \partial_{\xi_2}\boldsymbol{S}_2 + \partial_{\xi_3}\boldsymbol{S}_3 + \rho_0\boldsymbol{b} = \rho_0\partial_t^2\boldsymbol{R}. \end{gathered} \tag{7.58}$$

Here, Div is divergence operator referenced to the configuration Ω_0. The quantities $\rho_0(\xi_1, \xi_2, \xi_3) = \rho_0$ and $\boldsymbol{b}(\xi_1, \xi_2, \xi_3) = \boldsymbol{b}$ give the mass density field in the undeformed state and the body force per unit mass of the body respectively. We can write the point-wise equilibrium equation described in Eq. (7.58) in an integral form as

$$\int_\Omega \delta\boldsymbol{u}.\left(\mathrm{Div}\boldsymbol{S} + \rho_0\boldsymbol{b} - \rho_0\partial_t^2\boldsymbol{R}\right)\mathrm{d}\Omega = 0. \tag{7.59}$$

Since $\boldsymbol{F} = \boldsymbol{I}_3 + \mathrm{Grad}(\boldsymbol{u})$, we have $\delta\boldsymbol{F} = \mathrm{Grad}(\delta\boldsymbol{u})$. Here, Grad is the gradient operator with respect to the configuration Ω_0. Using this result and divergence theorem on Eq. (7.59), we get

the general virtual work principle as,

$$\begin{aligned} \delta \mathrm{U}_{\text{strain}} + \delta \mathrm{W}_{\text{inertial}} &= \delta \mathrm{W}_{\text{ext}}; \\ G(\boldsymbol{\Phi}, \delta\boldsymbol{\Phi}) = \delta \mathrm{U}_{\text{strain}} + \delta \mathrm{W}_{\text{inertial}} - \delta \mathrm{W}_{\text{ext}} &= 0, \end{aligned} \tag{7.60}$$

where,

$$\delta \mathrm{U}_{\text{strain}} = \int_{\Omega_0} \boldsymbol{S} : \delta \boldsymbol{F} \, \mathrm{d}\Omega_0 = \int_{\Omega_0} \text{trace}\left(\boldsymbol{S}^T.\delta \boldsymbol{F}\right) \mathrm{d}\Omega_0; \tag{7.61a}$$

$$\delta \mathrm{W}_{\text{inertial}} = \int_{\Omega_0} \rho_0 \delta \boldsymbol{u}.\partial_t^2 \boldsymbol{R} \, \mathrm{d}\Omega_0; \tag{7.61b}$$

$$\delta \mathrm{W}_{\text{ext}} = \int_{\Xi_0} \delta \boldsymbol{u}.(\boldsymbol{S}.\boldsymbol{N}) \, \mathrm{d}\Xi_0 + \int_{\Omega_0} \delta \boldsymbol{u}.\boldsymbol{b} \, \mathrm{d}\Omega_0 = \delta \mathrm{W}^{\text{st}}_{\text{ext}} + \delta \mathrm{W}^{\text{b}}_{\text{ext}}. \tag{7.61c}$$

The virtual work due to external forces is contributed by surface tractions ($\delta \mathrm{W}^{\text{st}}_{\text{ext}}$) and body forces ($\delta \mathrm{W}^{\text{b}}_{\text{ext}}$). In the equation above, $\boldsymbol{N}$ represents the normal vector to the surface Ξ_0 of the beam.

7.5.2 Virtual strain energy

The expression of strain energy in Eq. (7.61a) can be further simplified by using Eq. (7.53)

$$\delta \mathrm{U}_{\text{strain}} = \int_{\Omega_0} \boldsymbol{S} : \delta \boldsymbol{F} \, \mathrm{d}\Omega_0 = \int_{\Omega_0} \boldsymbol{S} : \tilde{\delta} \boldsymbol{F} \, \mathrm{d}\Omega_0 + \int_{\Omega_0} \boldsymbol{S} : (\delta \hat{\boldsymbol{\alpha}}.\boldsymbol{F}) \, \mathrm{d}\Omega_0. \tag{7.62}$$

We observe that $\boldsymbol{S} : (\delta \hat{\boldsymbol{\alpha}}.\boldsymbol{F}) = \boldsymbol{S}\boldsymbol{F}^T : \delta \hat{\boldsymbol{\alpha}} = 0$. This is because, $\boldsymbol{S}\boldsymbol{F}^T$ is symmetric and $\delta \hat{\boldsymbol{\alpha}}$ is an anti-symmetric matrix. We define the concatenated stress vector $\mathfrak{G} = [\boldsymbol{S}_1; \boldsymbol{S}_2; \boldsymbol{S}_3]$ and its material counterpart $\overline{\mathfrak{G}} = \left[\overline{\boldsymbol{S}}_1; \overline{\boldsymbol{S}}_2; \overline{\boldsymbol{S}}_3\right]$, such that $\mathfrak{G} = \boldsymbol{Q}_3.\overline{\mathfrak{G}}$. This further simplifies Eq. (7.62) to

$$\begin{aligned} \delta \mathrm{U}_{\text{strain}} &= \int_{\Omega_0} \boldsymbol{S} : \tilde{\delta} \boldsymbol{F} \, \mathrm{d}\Omega_0 = \int_{\Omega_0} \boldsymbol{S}_i.\tilde{\delta} \boldsymbol{\lambda}_i \, \mathrm{d}\Omega_0 = \int_{\Omega_0} \overline{\boldsymbol{S}}_i.\delta \overline{\boldsymbol{\lambda}}_i \, \mathrm{d}\Omega_0; \\ \delta \mathrm{U}_{\text{strain}} &= \int_{\Omega_0} \mathfrak{G}.\tilde{\delta} \mathfrak{L} \, \mathrm{d}\Omega_0 = \int_{\Omega_0} \overline{\mathfrak{G}}.\delta \overline{\mathfrak{L}} \, \mathrm{d}\Omega_0. \end{aligned} \tag{7.63}$$

Using the results in Eq. (7.51) and (7.52) we have,

$$\delta \mathrm{U}_{\text{strain}} = \int_{\Omega_0} \tilde{\delta} \boldsymbol{\epsilon}.\left((\boldsymbol{L} + \boldsymbol{M})^T.\mathfrak{G}\right) \, \mathrm{d}\Omega_0 = \int_0^L \tilde{\delta} \boldsymbol{\epsilon}.\mathfrak{R} \, \mathrm{d}\xi_1; \tag{7.64a}$$

$$\delta \mathrm{U}_{\text{strain}} = \int_{\Omega_0} \delta\overline{\boldsymbol{\epsilon}}.\left((\overline{\boldsymbol{L}}+\overline{\boldsymbol{M}})^T.\overline{\mathfrak{G}}\right)\,\mathrm{d}\Omega_0 = \int_0^L \delta\overline{\boldsymbol{\epsilon}}.\overline{\mathfrak{N}}\,\mathrm{d}\xi_1. \tag{7.64b}$$

We define the spatial and material reduced section force vectors $\mathfrak{N}(\xi_1)$ and $\overline{\mathfrak{N}}(\xi_1)$ as

$$\begin{aligned}
\mathfrak{N} &= [\mathfrak{N}_{\boldsymbol{\varepsilon}}; \mathfrak{N}_{\partial_{\xi_1}\boldsymbol{\varepsilon}}; \mathfrak{N}_{\boldsymbol{\kappa}}; \mathfrak{N}_{\partial_{\xi_1}\boldsymbol{\kappa}}; \mathfrak{N}_{\partial^2_{\xi_1}\boldsymbol{\kappa}}; \mathfrak{N}_{\partial^3_{\xi_1}\boldsymbol{\kappa}}; \mathfrak{N}_p; \mathfrak{N}_{\partial_{\xi_1}p}; \mathfrak{N}_{\partial^2_{\xi_1}p}] = \int_{\mathfrak{B}_0} (\boldsymbol{L}+\boldsymbol{M})^T.\mathfrak{G}\,\mathrm{d}\mathfrak{B}_0;\\
\overline{\mathfrak{N}} &= [\overline{\mathfrak{N}}_{\boldsymbol{\varepsilon}}; \overline{\mathfrak{N}}_{\partial_{\xi_1}\boldsymbol{\varepsilon}}; \overline{\mathfrak{N}}_{\boldsymbol{\kappa}}; \overline{\mathfrak{N}}_{\partial_{\xi_1}\boldsymbol{\kappa}}; \overline{\mathfrak{N}}_{\partial^2_{\xi_1}\boldsymbol{\kappa}}; \overline{\mathfrak{N}}_{\partial^3_{\xi_1}\boldsymbol{\kappa}}; \overline{\mathfrak{N}}_p; \overline{\mathfrak{N}}_{\partial_{\xi_1}p}; \overline{\mathfrak{N}}_{\partial^2_{\xi_1}p}] = \int_{\mathfrak{B}_0} (\overline{\boldsymbol{L}}+\overline{\boldsymbol{M}})^T.\overline{\mathfrak{G}}\,\mathrm{d}\mathfrak{B}_0,
\end{aligned} \tag{7.65}$$

such that

$$\mathfrak{N} = \boldsymbol{\Lambda}.\overline{\mathfrak{N}}. \tag{7.66}$$

The expressions of material and spatial reduced section forces are given as follows,

$$\mathfrak{N}_{\boldsymbol{\varepsilon}} = \int_{\mathfrak{B}_0} (\boldsymbol{L}_{\boldsymbol{\varepsilon}}^{\boldsymbol{\lambda}_1} + \boldsymbol{M}_{\boldsymbol{\varepsilon}}^{\boldsymbol{\lambda}_1})^T.\boldsymbol{S}_1 + (\boldsymbol{L}_{\boldsymbol{\varepsilon}}^{\boldsymbol{\lambda}_2})^T.\boldsymbol{S}_2 + (\boldsymbol{L}_{\boldsymbol{\varepsilon}}^{\boldsymbol{\lambda}_3})^T.\boldsymbol{S}_3\,\mathrm{d}\mathfrak{B}_0 \tag{7.67a}$$

$$\mathfrak{N}_{\partial_{\xi_1}\boldsymbol{\varepsilon}} = \int_{\mathfrak{B}_0} (\boldsymbol{L}_{\partial_{\xi_1}\boldsymbol{\varepsilon}}^{\boldsymbol{\lambda}_1})^T.\boldsymbol{S}_1\,\mathrm{d}\mathfrak{B}_0 \tag{7.67b}$$

$$\mathfrak{N}_{\boldsymbol{\kappa}} = \int_{\mathfrak{B}_0} (\boldsymbol{L}_{\boldsymbol{\kappa}}^{\boldsymbol{\lambda}_1} + \boldsymbol{M}_{\boldsymbol{\kappa}}^{\boldsymbol{\lambda}_1})^T.\boldsymbol{S}_1 + (\boldsymbol{L}_{\boldsymbol{\kappa}}^{\boldsymbol{\lambda}_2})^T.\boldsymbol{S}_2 + (\boldsymbol{L}_{\boldsymbol{\kappa}}^{\boldsymbol{\lambda}_3})^T.\boldsymbol{S}_3\,\mathrm{d}\mathfrak{B}_0 \tag{7.67c}$$

$$\mathfrak{N}_{\partial_{\xi_1}\boldsymbol{\kappa}} = \int_{\mathfrak{B}_0} (\boldsymbol{L}_{\partial_{\xi_1}\boldsymbol{\kappa}}^{\boldsymbol{\lambda}_1} + \boldsymbol{M}_{\partial_{\xi_1}\boldsymbol{\kappa}}^{\boldsymbol{\lambda}_1})^T.\boldsymbol{S}_1 + (\boldsymbol{L}_{\partial_{\xi_1}\boldsymbol{\kappa}}^{\boldsymbol{\lambda}_2})^T.\boldsymbol{S}_2 + (\boldsymbol{L}_{\partial_{\xi_1}\boldsymbol{\kappa}}^{\boldsymbol{\lambda}_3})^T.\boldsymbol{S}_3\,\mathrm{d}\mathfrak{B}_0 \tag{7.67d}$$

$$\mathfrak{N}_{\partial^2_{\xi_1}\boldsymbol{\kappa}} = \int_{\mathfrak{B}_0} (\boldsymbol{L}_{\partial^2_{\xi_1}\boldsymbol{\kappa}}^{\boldsymbol{\lambda}_1} + \boldsymbol{M}_{\partial^2_{\xi_1}\boldsymbol{\kappa}}^{\boldsymbol{\lambda}_1})^T.\boldsymbol{S}_1 + (\boldsymbol{L}_{\partial^2_{\xi_1}\boldsymbol{\kappa}}^{\boldsymbol{\lambda}_2})^T.\boldsymbol{S}_2 + (\boldsymbol{L}_{\partial^2_{\xi_1}\boldsymbol{\kappa}}^{\boldsymbol{\lambda}_3})^T.\boldsymbol{S}_3\,\mathrm{d}\mathfrak{B}_0 \tag{7.67e}$$

$$\mathfrak{N}_{\partial^3_{\xi_1}\boldsymbol{\kappa}} = \int_{\mathfrak{B}_0} (\boldsymbol{L}_{\partial^3_{\xi_1}\boldsymbol{\kappa}}^{\boldsymbol{\lambda}_1})^T.\boldsymbol{S}_1\,\mathrm{d}\mathfrak{B}_0 \tag{7.67f}$$

$$\mathfrak{N}_p = \int_{\mathfrak{B}_0} \boldsymbol{M}_p^{\boldsymbol{\lambda}_1}.\boldsymbol{S}_1 + \boldsymbol{L}_p^{\boldsymbol{\lambda}_2}.\boldsymbol{S}_2 + \boldsymbol{L}_p^{\boldsymbol{\lambda}_3}.\boldsymbol{S}_3\,\mathrm{d}\mathfrak{B}_0 \tag{7.67g}$$

$$\mathfrak{N}_{\partial_{\xi_1}p} = \int_{\mathfrak{B}_0} (\boldsymbol{L}_{\partial_{\xi_1}p}^{\boldsymbol{\lambda}_1} + \boldsymbol{M}_{\partial_{\xi_1}p}^{\boldsymbol{\lambda}_1}).\boldsymbol{S}_1 + \boldsymbol{L}_{\partial_{\xi_1}p}^{\boldsymbol{\lambda}_2}.\boldsymbol{S}_2 + \boldsymbol{L}_{\partial_{\xi_1}p}^{\boldsymbol{\lambda}_3}.\boldsymbol{S}_3\,\mathrm{d}\mathfrak{B}_0 \tag{7.67h}$$

$$\mathfrak{N}_{\partial^2_{\xi_1}p} = \int_{\mathfrak{B}_0} \boldsymbol{L}_{\partial^2_{\xi_1}p}^{\boldsymbol{\lambda}_1}.\boldsymbol{S}_1\,\mathrm{d}\mathfrak{B}_0; \tag{7.67i}$$

and,

$$\overline{\mathfrak{N}}_{\boldsymbol{\varepsilon}} = \int_{\mathfrak{B}_0} (\overline{\boldsymbol{L}}_{\boldsymbol{\varepsilon}}^{\boldsymbol{\lambda}_1} + \overline{\boldsymbol{M}}_{\boldsymbol{\varepsilon}}^{\boldsymbol{\lambda}_1})^T.\overline{\boldsymbol{S}}_1 + (\overline{\boldsymbol{L}}_{\boldsymbol{\varepsilon}}^{\boldsymbol{\lambda}_2})^T.\overline{\boldsymbol{S}}_2 + (\overline{\boldsymbol{L}}_{\boldsymbol{\varepsilon}}^{\boldsymbol{\lambda}_3})^T.\overline{\boldsymbol{S}}_3\,\mathrm{d}\mathfrak{B}_0 \tag{7.68a}$$

$$\overline{\mathfrak{N}}_{\partial_{\xi_1}\boldsymbol{\varepsilon}} = \int_{\mathfrak{B}_0} (\overline{\boldsymbol{L}}_{\partial_{\xi_1}\boldsymbol{\varepsilon}}^{\boldsymbol{\lambda}_1})^T.\overline{\boldsymbol{S}}_1\,\mathrm{d}\mathfrak{B}_0 \tag{7.68b}$$

$$\overline{\mathfrak{R}}_{\boldsymbol{\kappa}} = \int_{\mathfrak{B}_0} (\overline{\boldsymbol{L}}_{\boldsymbol{\kappa}}^{\boldsymbol{\lambda}_1} + \overline{\boldsymbol{M}}_{\boldsymbol{\kappa}}^{\boldsymbol{\lambda}_1})^T.\overline{\boldsymbol{S}}_1 + (\overline{\boldsymbol{L}}_{\boldsymbol{\kappa}}^{\boldsymbol{\lambda}_2})^T.\overline{\boldsymbol{S}}_2 + (\overline{\boldsymbol{L}}_{\boldsymbol{\kappa}}^{\boldsymbol{\lambda}_3})^T.\overline{\boldsymbol{S}}_3 \, \mathrm{d}\mathfrak{B}_0 \tag{7.68c}$$

$$\overline{\mathfrak{R}}_{\partial_{\xi_1}\boldsymbol{\kappa}} = \int_{\mathfrak{B}_0} (\overline{\boldsymbol{L}}_{\partial_{\xi_1}\boldsymbol{\kappa}}^{\boldsymbol{\lambda}_1} + \overline{\boldsymbol{M}}_{\partial_{\xi_1}\boldsymbol{\kappa}}^{\boldsymbol{\lambda}_1})^T.\overline{\boldsymbol{S}}_1 + (\overline{\boldsymbol{L}}_{\partial_{\xi_1}\boldsymbol{\kappa}}^{\boldsymbol{\lambda}_2})^T.\overline{\boldsymbol{S}}_2 + (\overline{\boldsymbol{L}}_{\partial_{\xi_1}\boldsymbol{\kappa}}^{\boldsymbol{\lambda}_3})^T.\overline{\boldsymbol{S}}_3 \, \mathrm{d}\mathfrak{B}_0 \tag{7.68d}$$

$$\overline{\mathfrak{R}}_{\partial_{\xi_1}^2\boldsymbol{\kappa}} = \int_{\mathfrak{B}_0} (\overline{\boldsymbol{L}}_{\partial_{\xi_1}^2\boldsymbol{\kappa}}^{\boldsymbol{\lambda}_1} + \overline{\boldsymbol{M}}_{\partial_{\xi_1}^2\boldsymbol{\kappa}}^{\boldsymbol{\lambda}_1})^T.\overline{\boldsymbol{S}}_1 + (\overline{\boldsymbol{L}}_{\partial_{\xi_1}^2\boldsymbol{\kappa}}^{\boldsymbol{\lambda}_2})^T.\overline{\boldsymbol{S}}_2 + (\overline{\boldsymbol{L}}_{\partial_{\xi_1}^2\boldsymbol{\kappa}}^{\boldsymbol{\lambda}_3})^T.\overline{\boldsymbol{S}}_3 \, \mathrm{d}\mathfrak{B}_0 \tag{7.68e}$$

$$\overline{\mathfrak{R}}_{\partial_{\xi_1}^3\boldsymbol{\kappa}} = \int_{\mathfrak{B}_0} (\overline{\boldsymbol{L}}_{\partial_{\xi_1}^3\boldsymbol{\kappa}}^{\boldsymbol{\lambda}_1})^T.\overline{\boldsymbol{S}}_1 \, \mathrm{d}\mathfrak{B}_0 \tag{7.68f}$$

$$\overline{\mathfrak{R}}_{p} = \int_{\mathfrak{B}_0} \overline{\boldsymbol{M}}_{p}^{\boldsymbol{\lambda}_1}.\overline{\boldsymbol{S}}_1 + \overline{\boldsymbol{L}}_{p}^{\boldsymbol{\lambda}_2}.\overline{\boldsymbol{S}}_2 + \overline{\boldsymbol{L}}_{p}^{\boldsymbol{\lambda}_3}.\overline{\boldsymbol{S}}_3 \, \mathrm{d}\mathfrak{B}_0 \tag{7.68g}$$

$$\overline{\mathfrak{R}}_{\partial_{\xi_1}p} = \int_{\mathfrak{B}_0} (\overline{\boldsymbol{L}}_{\partial_{\xi_1}p}^{\boldsymbol{\lambda}_1} + \overline{\boldsymbol{M}}_{\partial_{\xi_1}p}^{\boldsymbol{\lambda}_1}).\overline{\boldsymbol{S}}_1 + \overline{\boldsymbol{L}}_{\partial_{\xi_1}p}^{\boldsymbol{\lambda}_2}.\overline{\boldsymbol{S}}_2 + \overline{\boldsymbol{L}}_{\partial_{\xi_1}p}^{\boldsymbol{\lambda}_3}.\overline{\boldsymbol{S}}_3 \, \mathrm{d}\mathfrak{B}_0 \tag{7.68h}$$

$$\overline{\mathfrak{R}}_{\partial_{\xi_1}^2 p} = \int_{\mathfrak{B}_0} \overline{\boldsymbol{L}}_{\partial_{\xi_1}^2 p}^{\boldsymbol{\lambda}_1}.\overline{\boldsymbol{S}}_1 \, \mathrm{d}\mathfrak{B}_0. \tag{7.68i}$$

Using Eq. (7.37), we finally arrive at the desired matrix form of virtual strain energy expression that is useful in the process of linearization as

$$\delta \mathrm{U}_{\mathrm{strain}} = \int_0^L \delta\boldsymbol{\Phi}^T \boldsymbol{B}_2^T \boldsymbol{B}_1^T \mathfrak{R} \, \mathrm{d}\xi_1. \tag{7.69}$$

The equation above is written in matrix format. For clarity, we note that $\delta\boldsymbol{\Phi}^T \boldsymbol{B}_2^T \boldsymbol{B}_1^T \mathfrak{R} = \delta\boldsymbol{\Phi}.\left(\boldsymbol{B}_2^T \boldsymbol{B}_1^T \mathfrak{R}\right)$.

7.5.3 Virtual work done due to external and inertial forces

7.5.3.1 Virtual work done due to external forces

The virtual work due to external forces is contributed by surface traction and body force. We first consider the surface traction term:

$$\begin{aligned} \delta \mathrm{W}_{\mathrm{ext}}^{\mathrm{st}} &= \int_{\mathfrak{S}_0} \delta\boldsymbol{u}.(\boldsymbol{S}.\boldsymbol{N}) \, \mathrm{d}\mathfrak{S}_0 \\ &= \int_0^L \left(\int_{\mathfrak{B}_0(\xi_1+\mathrm{d}\xi_1)} \delta\boldsymbol{u}.\boldsymbol{S}_1 \, \mathrm{d}\mathfrak{B}_0 - \int_{\mathfrak{B}_0(\xi_1)} \delta\boldsymbol{u}.\boldsymbol{S}_1 \, \mathrm{d}\mathfrak{B}_0 + \int_{\Gamma_0(\xi_1)} \delta\boldsymbol{u}.(\boldsymbol{S}.\boldsymbol{N}) \, \mathrm{d}\Gamma_0 \right) \mathrm{d}\xi_1 \end{aligned} \tag{7.70}$$

Recall the expression of $\delta\boldsymbol{u} = \delta\boldsymbol{\varphi} + \delta\hat{\boldsymbol{\alpha}}.\boldsymbol{r} + \tilde{\delta}\boldsymbol{r}$ as discussed in section 7.4.3. We simplify the first two integrals to obtain boundary terms. We note the following results:

$$\begin{aligned}
&\int_{\mathfrak{B}_0(\xi_1+\mathrm{d}\xi_1)} \delta\boldsymbol{\varphi}.\boldsymbol{S}_1 \,\mathrm{d}\mathfrak{B}_0 - \int_{\mathfrak{B}_0(\xi_1)} \delta\boldsymbol{\varphi}.\boldsymbol{S}_1 \,\mathrm{d}\mathfrak{B}_0 = \partial_{\xi_1}\left(\delta\boldsymbol{\varphi}.\boldsymbol{B}_{\boldsymbol{\varphi}}\right)\,\mathrm{d}\xi_1 \\
&\int_{\mathfrak{B}_0(\xi_1+\mathrm{d}\xi_1)} (\delta\hat{\boldsymbol{\alpha}}.\boldsymbol{r}).\boldsymbol{S}_1 \,\mathrm{d}\mathfrak{B}_0 - \int_{\mathfrak{B}_0(\xi_1)} (\delta\hat{\boldsymbol{\alpha}}.\boldsymbol{r}).\boldsymbol{S}_1 \,\mathrm{d}\mathfrak{B}_0 = \partial_{\xi_1}\left(\delta\boldsymbol{\alpha}.\boldsymbol{B}_{\boldsymbol{\alpha}}\right)\,\mathrm{d}\xi_1 \\
&\int_{\mathfrak{B}_0(\xi_1+\mathrm{d}\xi_1)} \tilde{\delta}\boldsymbol{r}.\boldsymbol{S}_1 \,\mathrm{d}\mathfrak{B}_0 - \int_{\mathfrak{B}_0(\xi_1)} \tilde{\delta}\boldsymbol{r}.\boldsymbol{S}_1 \,\mathrm{d}\mathfrak{B}_0 = \partial_{\xi_1}(\tilde{\delta}\boldsymbol{\varepsilon}.\boldsymbol{B}_{\boldsymbol{\varepsilon}} + \tilde{\delta}\boldsymbol{\kappa}.\boldsymbol{B}_{\boldsymbol{\kappa}} + (\boldsymbol{Q}.\delta\partial_{\xi_1}\overline{\boldsymbol{\kappa}}).\boldsymbol{B}_{\partial_{\xi_1}\boldsymbol{\kappa}} \\
&\qquad + (\boldsymbol{Q}.\delta\partial^2_{\xi_1}\overline{\boldsymbol{\kappa}}).\boldsymbol{B}_{\partial^2_{\xi_1}\boldsymbol{\kappa}} + \delta p.B_p + \delta\partial_{\xi_1}p.B_{\partial_{\xi_1}p})\,\mathrm{d}\xi_1.
\end{aligned} \tag{7.71}$$

Here, the quantities $\boldsymbol{B}_{(.)}$ and $B_{(.)}$ represents the reduced end boundary force terms. Therefore, the virtual work due to end boundary terms associated with the traction $\delta\mathrm{W}^{\mathrm{st}}_{\mathrm{ext}}\big|_{\mathfrak{B}(0)\cup\mathfrak{B}(L)}$ is given by

$$\begin{aligned}
\delta\mathrm{W}^{\mathrm{st}}_{\mathrm{ext}}\big|_{\mathfrak{B}(0)\cup\mathfrak{B}(L)} &= \int_0^L \left(\int_{\mathfrak{B}_0(\xi_1+\mathrm{d}\xi_1)} \delta\boldsymbol{u}.\boldsymbol{S}_1 \,\mathrm{d}\mathfrak{B}_0 - \int_{\mathfrak{B}_0(\xi_1)} \delta\boldsymbol{u}.\boldsymbol{S}_1 \,\mathrm{d}\mathfrak{B}_0\right)\,\mathrm{d}\xi_1 \\
&= \big[\delta\boldsymbol{\varphi}.\boldsymbol{B}_{\boldsymbol{\varphi}} + \delta\boldsymbol{\alpha}.\boldsymbol{B}_{\boldsymbol{\alpha}} + \tilde{\delta}\boldsymbol{\varepsilon}.\boldsymbol{B}_{\boldsymbol{\varepsilon}} + \tilde{\delta}\boldsymbol{\kappa}.\boldsymbol{B}_{\boldsymbol{\kappa}} + (\boldsymbol{Q}.\delta\partial_{\xi_1}\overline{\boldsymbol{\kappa}}).\boldsymbol{B}_{\partial_{\xi_1}\boldsymbol{\kappa}} \\
&\quad + (\boldsymbol{Q}.\delta\partial^2_{\xi_1}\overline{\boldsymbol{\kappa}}).\boldsymbol{B}_{\partial^2_{\xi_1}\boldsymbol{\kappa}} + \delta p.B_p + \delta\partial_{\xi_1}p.B_{\partial_{\xi_1}p}\big]^L_0
\end{aligned} \tag{7.72}$$

Note that $\boldsymbol{B}_{\boldsymbol{\varphi}}$, $\boldsymbol{B}_{\boldsymbol{\alpha}}$ and B_p represents the reduced section force, moment and bi-shear as in Simo et al. [43] (given by $\boldsymbol{n}$, $\boldsymbol{m}$ and N_f).

We now consider the virtual work due to surface traction on the peripheral boundary $\cup_{\forall\xi_1}\Gamma_0(\xi_1)$, denoted by $\delta\mathrm{W}^{\mathrm{st}}_{\mathrm{ext}}\big|_{\cup_{\forall\xi_1}\Gamma_0(\xi_1)}$. We have,

$$\begin{aligned}
\delta\mathrm{W}^{\mathrm{st}}_{\mathrm{ext}}\big|_{\cup_{\forall\xi_1}\Gamma_0(\xi_1)} &= \int_0^L \left(\int_{\Gamma_0(\xi_1)} \delta\boldsymbol{u}.(\boldsymbol{S}.\boldsymbol{N})\,\mathrm{d}\Gamma_0\right)\,\mathrm{d}\xi_1 \\
&= \int_0^L (\delta\boldsymbol{\varphi}.\boldsymbol{N}^{\mathrm{st}}_{\boldsymbol{\varphi}} + \delta\boldsymbol{\alpha}.\boldsymbol{N}^{\mathrm{st}}_{\boldsymbol{\alpha}} + \tilde{\delta}\boldsymbol{\varepsilon}.\boldsymbol{N}^{\mathrm{st}}_{\boldsymbol{\varepsilon}} + \tilde{\delta}\boldsymbol{\kappa}.\boldsymbol{N}^{\mathrm{st}}_{\boldsymbol{\kappa}} + (\boldsymbol{Q}.\delta\partial_{\xi_1}\overline{\boldsymbol{\kappa}}).\boldsymbol{N}^{\mathrm{st}}_{\partial_{\xi_1}\boldsymbol{\kappa}} \\
&\quad + (\boldsymbol{Q}.\delta\partial^2_{\xi_1}\overline{\boldsymbol{\kappa}}).\boldsymbol{N}^{\mathrm{st}}_{\partial^2_{\xi_1}\boldsymbol{\kappa}} + \delta p.N^{\mathrm{st}}_p + \delta\partial_{\xi_1}p.N^{\mathrm{st}}_{\partial_{\xi_1}p})\,\mathrm{d}\xi_1.
\end{aligned} \tag{7.73}$$

In the equation above, the quantities $\boldsymbol{N}^{\mathrm{st}}_{(.)}$ and $N^{\mathrm{st}}_{(.)}$ represents the reduced external force due to surface traction (represented by the super script st). Similarly, the virtual work due to body force

field $\boldsymbol{b}$ is obtained as,

$$\delta \mathrm{W}^{\mathrm{b}}_{\mathrm{ext}} = \int_0^L (\delta\boldsymbol{\varphi}.\boldsymbol{N}^{\mathrm{b}}_{\boldsymbol{\varphi}} + \delta\boldsymbol{\alpha}.\boldsymbol{N}^{\mathrm{b}}_{\boldsymbol{\alpha}} + \tilde{\delta}\boldsymbol{\varepsilon}.\boldsymbol{N}^{\mathrm{b}}_{\boldsymbol{\varepsilon}} + \tilde{\delta}\boldsymbol{\kappa}.\boldsymbol{N}^{\mathrm{b}}_{\boldsymbol{\kappa}} + (\boldsymbol{Q}.\delta\partial_{\xi_1}\overline{\boldsymbol{\kappa}}).\boldsymbol{N}^{\mathrm{b}}_{\partial_{\xi_1}\boldsymbol{\kappa}} + (\boldsymbol{Q}.\delta\partial^2_{\xi_1}\overline{\boldsymbol{\kappa}}).\boldsymbol{N}^{\mathrm{b}}_{\partial^2_{\xi_1}\boldsymbol{\kappa}} + \delta p.N^{\mathrm{b}}_{p} + \delta\partial_{\xi_1}p.N^{\mathrm{b}}_{\partial_{\xi_1}p})\,\mathrm{d}\xi_1. \tag{7.74}$$

The quantities $\boldsymbol{N}^{\mathrm{b}}_{(.)}$ and $N^{\mathrm{b}}_{(.)}$ represents the reduced external force due to body force (represented by the super script b). Hence,

$$\delta \mathrm{W}_{\mathrm{ext}} = \left(\delta \mathrm{W}^{\mathrm{st}}_{\mathrm{ext}}\big|_{\cup_{\forall\xi_1}\Gamma_0(\xi_1)} + \delta \mathrm{W}^{\mathrm{b}}_{\mathrm{ext}}\right) + \delta \mathrm{W}^{\mathrm{st}}_{\mathrm{ext}}\big|_{\mathfrak{B}(0)\cup\mathfrak{B}(L)}. \tag{7.75}$$

Defining the (total) reduced external forces as $\boldsymbol{N}_{(.)} = \boldsymbol{N}^{\mathrm{st}}_{(.)} + \boldsymbol{N}^{\mathrm{b}}_{(.)}$ and $N_{(.)} = N^{\mathrm{st}}_{(.)} + N^{\mathrm{b}}_{(.)}$, we have,

$$\left(\delta \mathrm{W}^{\mathrm{st}}_{\mathrm{ext}}\big|_{\cup_{\forall\xi_1}\Gamma_0(\xi_1)} + \delta \mathrm{W}^{\mathrm{b}}_{\mathrm{ext}}\right) = \int_0^L (\delta\boldsymbol{\varphi}.\boldsymbol{N}_{\boldsymbol{\varphi}} + \delta\boldsymbol{\alpha}.\boldsymbol{N}_{\boldsymbol{\alpha}} + \tilde{\delta}\boldsymbol{\varepsilon}.\boldsymbol{N}_{\boldsymbol{\varepsilon}} + \tilde{\delta}\boldsymbol{\kappa}.\boldsymbol{N}_{\boldsymbol{\kappa}} + (\boldsymbol{Q}.\delta\partial_{\xi_1}\overline{\boldsymbol{\kappa}}).\boldsymbol{N}_{\partial_{\xi_1}\boldsymbol{\kappa}} + (\boldsymbol{Q}.\delta\partial^2_{\xi_1}\overline{\boldsymbol{\kappa}}).\boldsymbol{N}_{\partial^2_{\xi_1}\boldsymbol{\kappa}} + \delta p.N_p + \delta\partial_{\xi_1}p.N_{\partial_{\xi_1}p})\,\mathrm{d}\xi_1. \tag{7.76}$$

To proceed further, we intend to obtain the virtual work in terms of the virtual quantities $\delta\boldsymbol{\varphi}, \delta\boldsymbol{\alpha}$ and δp and their derivatives. Using Eq. (7.30b), (7.32b), (7.33b) and (7.33c), we re-write Eq. (7.72) and (7.76) in matrix form as

$$\begin{aligned}
\delta \mathrm{W}^{\mathrm{st}}_{\mathrm{ext}}\big|_{\mathfrak{B}(0)\cup\mathfrak{B}(L)} &= \left[\delta\boldsymbol{\Theta}.(\boldsymbol{B}_3\mathfrak{B}_f)\right]_0^L = \left[\delta\boldsymbol{\Theta}^T\boldsymbol{B}_3\mathfrak{B}_f\right]_0^L = \left[\delta\boldsymbol{\Phi}^T\boldsymbol{B}_2^T\boldsymbol{B}_3\mathfrak{B}_f\right]_0^L;\\
\left(\delta \mathrm{W}^{\mathrm{st}}_{\mathrm{ext}}\big|_{\cup_{\forall\xi_1}\Gamma_0(\xi_1)} + \delta \mathrm{W}^{\mathrm{b}}_{\mathrm{ext}}\right) &= \int_0^L \delta\boldsymbol{\Theta}.(\boldsymbol{B}_3\boldsymbol{N}_f)\,\mathrm{d}\xi_1 = \int_0^L \delta\boldsymbol{\Theta}^T\boldsymbol{B}_3\boldsymbol{N}_f\,\mathrm{d}\xi_1\\
&= \int_0^L \delta\boldsymbol{\Phi}^T\boldsymbol{B}_2^T\boldsymbol{B}_3\boldsymbol{N}_f\,\mathrm{d}\xi_1;
\end{aligned} \tag{7.77}$$

where,

$$\begin{aligned}
\mathfrak{B}_f &= [\boldsymbol{B}_{\boldsymbol{\varphi}}; \boldsymbol{B}_{\boldsymbol{\varepsilon}}; \boldsymbol{B}_{\boldsymbol{\alpha}}; \boldsymbol{B}_{\boldsymbol{\kappa}}; \boldsymbol{B}_{\partial_{\xi_1}\boldsymbol{\kappa}}; \boldsymbol{B}_{\partial^2_{\xi_1}\boldsymbol{\kappa}}; B_p; B_{\partial_{\xi_1}p}];\\
\boldsymbol{N}_f &= [\boldsymbol{N}_{\boldsymbol{\varphi}}; \boldsymbol{N}_{\boldsymbol{\varepsilon}}; \boldsymbol{N}_{\boldsymbol{\alpha}}; \boldsymbol{N}_{\boldsymbol{\kappa}}; \boldsymbol{N}_{\partial_{\xi_1}\boldsymbol{\kappa}}; \boldsymbol{N}_{\partial^2_{\xi_1}\boldsymbol{\kappa}}; N_p; N_{\partial_{\xi_1}p}].
\end{aligned} \tag{7.78}$$

The vectors $\mathfrak{B}_f$ and $\boldsymbol{N}_f$ represent concatenated end *boundary forces* and *reduced external forces*

respectively. The expressions of *boundary forces* and *reduced external forces* are given as,

$$\boldsymbol{B}_{\boldsymbol{\varphi}} = \int_{\mathfrak{B}_0} (\boldsymbol{L}_{\boldsymbol{\varepsilon}}^{\boldsymbol{\lambda}_1})^T . \boldsymbol{S}_1 \, \mathrm{d}\mathfrak{B}_0; \tag{7.79a}$$

$$\boldsymbol{B}_{\boldsymbol{\alpha}} = \int_{\mathfrak{B}_0} (\boldsymbol{L}_{\boldsymbol{\kappa}}^{\boldsymbol{\lambda}_1})^T . \boldsymbol{S}_1 \, \mathrm{d}\mathfrak{B}_0; \tag{7.79b}$$

$$\boldsymbol{B}_{\boldsymbol{\varepsilon}} = \int_{\mathfrak{B}_0} (\boldsymbol{L}_{\partial_{\xi_1}\boldsymbol{\varepsilon}}^{\boldsymbol{\lambda}_1})^T . \boldsymbol{S}_1 \, \mathrm{d}\mathfrak{B}_0; \tag{7.79c}$$

$$\boldsymbol{B}_{\boldsymbol{\kappa}} = \int_{\mathfrak{B}_0} (\boldsymbol{L}_{\partial_{\xi_1}\boldsymbol{\kappa}}^{\boldsymbol{\lambda}_1})^T . \boldsymbol{S}_1 \, \mathrm{d}\mathfrak{B}_0; \tag{7.79d}$$

$$\boldsymbol{B}_{\partial_{\xi_1}\boldsymbol{\kappa}} = \int_{\mathfrak{B}_0} (\boldsymbol{L}_{\partial_{\xi_1}^2\boldsymbol{\kappa}}^{\boldsymbol{\lambda}_1})^T . \boldsymbol{S}_1 \, \mathrm{d}\mathfrak{B}_0; \tag{7.79e}$$

$$\boldsymbol{B}_{\partial_{\xi_1}^2\boldsymbol{\kappa}} = \int_{\mathfrak{B}_0} (\boldsymbol{L}_{\partial_{\xi_1}^3\boldsymbol{\kappa}}^{\boldsymbol{\lambda}_1})^T . \boldsymbol{S}_1 \, \mathrm{d}\mathfrak{B}_0; \tag{7.79f}$$

$$B_p = \int_{\mathfrak{B}_0} \boldsymbol{L}_{\partial_{\xi_1} p}^{\boldsymbol{\lambda}_1} . \boldsymbol{S}_1 \, \mathrm{d}\mathfrak{B}_0; \tag{7.79g}$$

$$B_{\partial_{\xi_1} p} = \int_{\mathfrak{B}_0} \boldsymbol{L}_{\partial_{\xi_1}^2 p}^{\boldsymbol{\lambda}_1} . \boldsymbol{S}_1 \, \mathrm{d}\mathfrak{B}_0; \tag{7.79h}$$

and,

$$\boldsymbol{N}_{\boldsymbol{\varphi}} = \boldsymbol{N}_{\boldsymbol{\varphi}}^{\mathrm{st}} + \boldsymbol{N}_{\boldsymbol{\varphi}}^{\mathrm{b}} = \int_{\Gamma_0} (\boldsymbol{L}_{\boldsymbol{\varepsilon}}^{\boldsymbol{\lambda}_1})^T . (\boldsymbol{S} . \boldsymbol{N}) \, \mathrm{d}\Gamma_0 + \int_{\mathfrak{B}_0} \rho_0 (\boldsymbol{L}_{\boldsymbol{\varepsilon}}^{\boldsymbol{\lambda}_1})^T . \boldsymbol{b} \, \mathrm{d}\mathfrak{B}_0; \tag{7.80a}$$

$$\boldsymbol{N}_{\boldsymbol{\alpha}} = \boldsymbol{N}_{\boldsymbol{\alpha}}^{\mathrm{st}} + \boldsymbol{N}_{\boldsymbol{\alpha}}^{\mathrm{b}} = \int_{\Gamma_0} (\boldsymbol{L}_{\boldsymbol{\kappa}}^{\boldsymbol{\lambda}_1})^T . (\boldsymbol{S} . \boldsymbol{N}) \, \mathrm{d}\Gamma_0 + \int_{\mathfrak{B}_0} \rho_0 (\boldsymbol{L}_{\boldsymbol{\kappa}}^{\boldsymbol{\lambda}_1})^T . \boldsymbol{b} \, \mathrm{d}\mathfrak{B}_0; \tag{7.80b}$$

$$\boldsymbol{N}_{\boldsymbol{\varepsilon}} = \boldsymbol{N}_{\boldsymbol{\varepsilon}}^{\mathrm{st}} + \boldsymbol{N}_{\boldsymbol{\varepsilon}}^{\mathrm{b}} = \int_{\Gamma_0} (\boldsymbol{L}_{\partial_{\xi_1}\boldsymbol{\varepsilon}}^{\boldsymbol{\lambda}_1})^T . (\boldsymbol{S} . \boldsymbol{N}) \, \mathrm{d}\Gamma_0 + \int_{\mathfrak{B}_0} \rho_0 (\boldsymbol{L}_{\partial_{\xi_1}\boldsymbol{\varepsilon}}^{\boldsymbol{\lambda}_1})^T . \boldsymbol{b} \, \mathrm{d}\mathfrak{B}_0; \tag{7.80c}$$

$$\boldsymbol{N}_{\boldsymbol{\kappa}} = \boldsymbol{N}_{\boldsymbol{\kappa}}^{\mathrm{st}} + \boldsymbol{N}_{\boldsymbol{\kappa}}^{\mathrm{b}} = \int_{\Gamma_0} (\boldsymbol{L}_{\partial_{\xi_1}\boldsymbol{\kappa}}^{\boldsymbol{\lambda}_1})^T . (\boldsymbol{S} . \boldsymbol{N}) \, \mathrm{d}\Gamma_0 + \int_{\mathfrak{B}_0} \rho_0 (\boldsymbol{L}_{\partial_{\xi_1}\boldsymbol{\kappa}}^{\boldsymbol{\lambda}_1})^T . \boldsymbol{b} \, \mathrm{d}\mathfrak{B}_0; \tag{7.80d}$$

$$\boldsymbol{N}_{\partial_{\xi_1}\boldsymbol{\kappa}} = \boldsymbol{N}_{\partial_{\xi_1}\boldsymbol{\kappa}}^{\mathrm{st}} + \boldsymbol{N}_{\partial_{\xi_1}\boldsymbol{\kappa}}^{\mathrm{b}} = \int_{\Gamma_0} (\boldsymbol{L}_{\partial_{\xi_1}^2\boldsymbol{\kappa}}^{\boldsymbol{\lambda}_1})^T . (\boldsymbol{S} . \boldsymbol{N}) \, \mathrm{d}\Gamma_0 + \int_{\mathfrak{B}_0} \rho_0 (\boldsymbol{L}_{\partial_{\xi_1}^2\boldsymbol{\kappa}}^{\boldsymbol{\lambda}_1})^T . \boldsymbol{b} \, \mathrm{d}\mathfrak{B}_0; \tag{7.80e}$$

$$\boldsymbol{N}_{\partial_{\xi_1}^2\boldsymbol{\kappa}} = \boldsymbol{N}_{\partial_{\xi_1}^2\boldsymbol{\kappa}}^{\mathrm{st}} + \boldsymbol{N}_{\partial_{\xi_1}^2\boldsymbol{\kappa}}^{\mathrm{b}} = \int_{\Gamma_0} (\boldsymbol{L}_{\partial_{\xi_1}^3\boldsymbol{\kappa}}^{\boldsymbol{\lambda}_1})^T . (\boldsymbol{S} . \boldsymbol{N}) \, \mathrm{d}\Gamma_0 + \int_{\mathfrak{B}_0} \rho_0 (\boldsymbol{L}_{\partial_{\xi_1}^3\boldsymbol{\kappa}}^{\boldsymbol{\lambda}_1})^T . \boldsymbol{b} \, \mathrm{d}\mathfrak{B}_0; \tag{7.80f}$$

$$N_p = N_p^{\mathrm{st}} + N_p^{\mathrm{b}} = \int_{\Gamma_0} \boldsymbol{L}_{\partial_{\xi_1} p}^{\boldsymbol{\lambda}_1} . (\boldsymbol{S} . \boldsymbol{N}) \, \mathrm{d}\Gamma_0 + \int_{\mathfrak{B}_0} \rho_0 \boldsymbol{L}_{\partial_{\xi_1} p}^{\boldsymbol{\lambda}_1} . \boldsymbol{b} \, \mathrm{d}\mathfrak{B}_0; \tag{7.80g}$$

$$N_{\partial_{\xi_1} p} = N_{\partial_{\xi_1} p}^{\mathrm{st}} + N_{\partial_{\xi_1} p}^{\mathrm{b}} = \int_{\Gamma_0} \boldsymbol{L}_{\partial_{\xi_1}^2 p}^{\boldsymbol{\lambda}_1} . (\boldsymbol{S} . \boldsymbol{N}) \, \mathrm{d}\Gamma_0 + \int_{\mathfrak{B}_0} \rho_0 \boldsymbol{L}_{\partial_{\xi_1}^2 p}^{\boldsymbol{\lambda}_1} . \boldsymbol{b} \, \mathrm{d}\mathfrak{B}_0. \tag{7.80h}$$

The matrix $\boldsymbol{B}_3$ is given as,

$$\boldsymbol{B}_3 = \begin{bmatrix} \boldsymbol{I}_3 & \boldsymbol{0}_3 & \boldsymbol{0}_3 & \boldsymbol{0}_3 & \boldsymbol{0}_3 & \boldsymbol{0}_3 & \boldsymbol{0}_1 & \boldsymbol{0}_1 \\ \boldsymbol{0}_3 & \boldsymbol{I}_3 & \boldsymbol{0}_3 & \boldsymbol{0}_3 & \boldsymbol{0}_3 & \boldsymbol{0}_3 & \boldsymbol{0}_1 & \boldsymbol{0}_1 \\ \boldsymbol{0}_3 & \boldsymbol{0}_3 & \boldsymbol{0}_3 & \boldsymbol{0}_3 & \boldsymbol{0}_3 & \boldsymbol{0}_3 & \boldsymbol{0}_1 & \boldsymbol{0}_1 \\ \boldsymbol{0}_3 & -\partial_{\xi_1}\hat{\boldsymbol{\varphi}} & \boldsymbol{I}_3 & \boldsymbol{0}_3 & \boldsymbol{0}_3 & \boldsymbol{0}_3 & \boldsymbol{0}_1 & \boldsymbol{0}_1 \\ \boldsymbol{0}_3 & \boldsymbol{0}_3 & \boldsymbol{0}_3 & \boldsymbol{I}_3 & \hat{\boldsymbol{\kappa}} & (\hat{\boldsymbol{\kappa}}.\hat{\boldsymbol{\kappa}} + \partial_{\xi_1}\hat{\boldsymbol{\kappa}}) & \boldsymbol{0}_1 & \boldsymbol{0}_1 \\ \boldsymbol{0}_3 & \boldsymbol{0}_3 & \boldsymbol{0}_3 & \boldsymbol{0}_3 & \boldsymbol{I}_3 & 2\hat{\boldsymbol{\kappa}} & \boldsymbol{0}_1 & \boldsymbol{0}_1 \\ \boldsymbol{0}_3 & \boldsymbol{0}_3 & \boldsymbol{0}_3 & \boldsymbol{0}_3 & \boldsymbol{0}_3 & \boldsymbol{I}_3 & \boldsymbol{0}_1 & \boldsymbol{0}_1 \\ \boldsymbol{0}_3 & \boldsymbol{0}_3 & \boldsymbol{0}_3 & \boldsymbol{0}_3 & \boldsymbol{0}_3 & \boldsymbol{0}_3 & \boldsymbol{0}_1 & \boldsymbol{0}_1 \\ \boldsymbol{0}_1^T & \boldsymbol{0}_1^T & \boldsymbol{0}_1^T & \boldsymbol{0}_1^T & \boldsymbol{0}_1^T & \boldsymbol{0}_1^T & 1 & 0 \\ \boldsymbol{0}_1^T & \boldsymbol{0}_1^T & \boldsymbol{0}_1^T & \boldsymbol{0}_1^T & \boldsymbol{0}_1^T & \boldsymbol{0}_1^T & 0 & 1 \\ \boldsymbol{0}_1^T & \boldsymbol{0}_1^T & \boldsymbol{0}_1^T & \boldsymbol{0}_1^T & \boldsymbol{0}_1^T & \boldsymbol{0}_1^T & 0 & 0 \end{bmatrix} \tag{7.81}$$

7.5.3.2 Virtual work done due to inertial forces

We realize that the body force $\boldsymbol{b}$ and the acceleration $\partial_t^2\boldsymbol{R}$ is defined over the volume Ω_0. Therefore, like the expression of virtual work contribution due to body force in Eq. (7.74), we arrive at the following

$$\begin{aligned} \delta \mathrm{W}_{\text{inertial}} = \int_0^L (&\delta\boldsymbol{\varphi}.\boldsymbol{\mathfrak{F}}_{\boldsymbol{\varphi}} + \delta\boldsymbol{\alpha}.\boldsymbol{\mathfrak{F}}_{\boldsymbol{\alpha}} + \tilde{\delta}\boldsymbol{\varepsilon}.\boldsymbol{\mathfrak{F}}_{\boldsymbol{\varepsilon}} + \tilde{\delta}\boldsymbol{\kappa}.\boldsymbol{\mathfrak{F}}_{\boldsymbol{\kappa}} + (\boldsymbol{Q}.\delta\partial_{\xi_1}\overline{\boldsymbol{\kappa}}).\boldsymbol{\mathfrak{F}}_{\partial_{\xi_1}\boldsymbol{\kappa}} + (\boldsymbol{Q}.\delta\partial_{\xi_1}^2\overline{\boldsymbol{\kappa}}).\boldsymbol{\mathfrak{F}}_{\partial_{\xi_1}^2\boldsymbol{\kappa}} \\ &+ \delta p.\mathfrak{F}_p + \delta\partial_{\xi_1}p.\mathfrak{F}_{\partial_{\xi_1}p})\,\mathrm{d}\xi_1. \end{aligned} \tag{7.82}$$

The expressions of the inertial forces $\boldsymbol{\mathfrak{F}}_{(.)}$ and $\mathfrak{F}_{(.)}$ are given as,

$$\boldsymbol{\mathfrak{F}}_{\boldsymbol{\varphi}} = \int_{\Omega_0} \rho_0 (\boldsymbol{L}_{\boldsymbol{\varepsilon}}^{\boldsymbol{\lambda}_1})^T.\partial_t^2\boldsymbol{R}\,\mathrm{d}\Omega_0 \tag{7.83a}$$

$$\boldsymbol{\mathfrak{F}}_{\boldsymbol{\alpha}} = \int_{\Omega_0} \rho_0 (\boldsymbol{L}_{\boldsymbol{\kappa}}^{\boldsymbol{\lambda}_1})^T.\partial_t^2\boldsymbol{R}\,\mathrm{d}\Omega_0 \tag{7.83b}$$

$$\boldsymbol{\mathfrak{F}}_{\boldsymbol{\varepsilon}} = \int_{\Omega_0} \rho_0 (\boldsymbol{L}_{\partial_{\xi_1}\boldsymbol{\varepsilon}}^{\boldsymbol{\lambda}_1})^T.\partial_t^2\boldsymbol{R}\,\mathrm{d}\Omega_0 \tag{7.83c}$$

$$\mathfrak{F}_{\boldsymbol{\kappa}} = \int_{\Omega_0} \rho_0 (\boldsymbol{L}^{\boldsymbol{\lambda}_1}_{\partial_{\xi_1}\boldsymbol{\kappa}})^T . \partial_t^2 \boldsymbol{R} \, \mathrm{d}\Omega_0 \tag{7.83d}$$

$$\mathfrak{F}_{\partial_{\xi_1}\boldsymbol{\kappa}} = \int_{\Omega_0} \rho_0 (\boldsymbol{L}^{\boldsymbol{\lambda}_1}_{\partial^2_{\xi_1}\boldsymbol{\kappa}})^T . \partial_t^2 \boldsymbol{R} \, \mathrm{d}\Omega_0 \tag{7.83e}$$

$$\mathfrak{F}_{\partial^2_{\xi_1}\boldsymbol{\kappa}} = \int_{\Omega_0} \rho_0 (\boldsymbol{L}^{\boldsymbol{\lambda}_1}_{\partial^3_{\xi_1}\boldsymbol{\kappa}})^T . \partial_t^2 \boldsymbol{R} \, \mathrm{d}\Omega_0 \tag{7.83f}$$

$$\mathfrak{F}_p = \int_{\Omega_0} \rho_0 \boldsymbol{L}^{\boldsymbol{\lambda}_1}_{\partial_{\xi_1} p} . \partial_t^2 \boldsymbol{R} \, \mathrm{d}\Omega_0 \tag{7.83g}$$

$$\mathfrak{F}_{\partial_{\xi_1} p} = \int_{\Omega_0} \rho_0 \boldsymbol{L}^{\boldsymbol{\lambda}_1}_{\partial^2_{\xi_1} p} . \partial_t^2 \boldsymbol{R} \, \mathrm{d}\Omega_0 \tag{7.83h}$$

Substituting for the expressions of $\tilde{\delta}\boldsymbol{\varepsilon}$, $\tilde{\delta}\boldsymbol{\kappa}$, $\boldsymbol{Q}.\delta\partial_{\xi_1}\overline{\boldsymbol{\kappa}}$ and $\boldsymbol{Q}.\delta\partial^2_{\xi_1}\overline{\boldsymbol{\kappa}}$ as in equations (7.30b), (7.32b), (7.33b) and (7.33c), we condense Eq. (7.82) into a more desirable matrix form as

$$\delta \mathrm{W}_{\text{inertial}} = \int_0^L \delta\boldsymbol{\Phi}^T \boldsymbol{B}_2^T \boldsymbol{B}_3 \mathfrak{F} \, \mathrm{d}\xi_1; \tag{7.84}$$

where,

$$\mathfrak{F} = [\mathfrak{F}_{\boldsymbol{\varphi}}; \mathfrak{F}_{\boldsymbol{\alpha}}; \mathfrak{F}_{\boldsymbol{\varepsilon}}; \mathfrak{F}_{\boldsymbol{\kappa}}; \mathfrak{F}_{\partial_{\xi_1}\boldsymbol{\kappa}}; \mathfrak{F}_{\partial^2_{\xi_1}\boldsymbol{\kappa}}; \mathfrak{F}_p; \mathfrak{F}_{\partial_{\xi_1} p}]. \tag{7.85}$$

7.5.4 Virtual work principle revisited

We restate the weak form of governing differential equation (7.60) for the beam kinematics at hand by using the expression of virtual strain energy in Eq. (7.69), virtual work due to external forces in Eq. (7.75) and (7.77) and the virtual work contribution due to inertial work obtained in Eq. (7.84) as,

$$G(\boldsymbol{\Phi}, \delta\boldsymbol{\Phi}) = \int_0^L \delta\boldsymbol{\Phi}^T \boldsymbol{B}_2^T (\boldsymbol{B}_1^T \mathfrak{N} + \boldsymbol{B}_3 \mathfrak{F} - \boldsymbol{B}_3 \boldsymbol{N}_f) \, \mathrm{d}\xi_1 - \delta \mathrm{W}^{\text{st}}_{\text{ext}}\big|_{\mathfrak{B}(0)\cup\mathfrak{B}(L)} = 0; \tag{7.86}$$

7.6 Strong form of governing differential equation for the deformed state Ω

In this section, we derive the strong form (governing differential equations) from the weak form using the equivalence between the two forms. The strong form essentially represents the local balance laws governing the deformation of beam. The analysis carried in the following section can be summarized in two steps. Firstly, we transform the weak form in Eq. (7.86) using integration by parts to obtain an equation of the form

$$G(\boldsymbol{\Phi}, \delta\boldsymbol{\Phi}) = \int_0^L \delta\boldsymbol{\Phi}^T [\mathfrak{E}_{\boldsymbol{\varphi}}; \mathfrak{E}_{\boldsymbol{\alpha}}; \mathfrak{E}_p] \, \mathrm{d}\xi_1 = \int_0^L \delta\boldsymbol{\varphi}.\mathfrak{E}_{\boldsymbol{\varphi}} + \delta\boldsymbol{\alpha}.\mathfrak{E}_{\boldsymbol{\alpha}} + \delta p.\mathfrak{E}_p \, \mathrm{d}\xi_1 = 0. \tag{7.87}$$

The arbitrary nature of the virtual displacement field implies $\mathfrak{E}_{\boldsymbol{\varphi}} = \mathbf{0}_1$,$\mathfrak{E}_{\boldsymbol{\alpha}} = \mathbf{0}_1$ and $\mathfrak{E}_p = 0$, resulting in the conservation of linear, angular momentum and balance of bi-moment respectively. Secondly, since the strong form equations are local in nature, the boundary terms arising due to integration by part of the integral $\int_0^L \delta\boldsymbol{\Phi}^T \boldsymbol{B}_2^T (\boldsymbol{B}_1^T \mathfrak{N} + \boldsymbol{B}_3 \mathfrak{F} - \boldsymbol{B}_3 \boldsymbol{N}_f) \, \mathrm{d}\xi_1$ must be $-\delta \mathrm{W}_{\mathrm{ext}}^{\mathrm{st}}\big|_{\mathfrak{B}(0)\cup\mathfrak{B}(L)}$ such that no boundary term appears in the transformed equation of the form (7.87). We carefully prove that the boundary terms vanish in the transformation of Eq. (7.86) into the form described in Eq. (7.87).

7.6.1 Relationship between L and M terms

For our further analysis, we present the following useful identities.

Identity set 1:

$$\partial_{\xi_1} \boldsymbol{L}^{\boldsymbol{\lambda}_1}_{\partial^2_{\xi_1} p} = \boldsymbol{M}^{\boldsymbol{\lambda}_1}_{\partial_{\xi_1} p} \tag{7.88a}$$

$$\partial_{\xi_2} \boldsymbol{L}^{\boldsymbol{\lambda}_1}_{\partial^2_{\xi_1} p} = \boldsymbol{L}^{\boldsymbol{\lambda}_2}_{\partial_{\xi_1} p} \tag{7.88b}$$

$$\partial_{\xi_3} \boldsymbol{L}^{\boldsymbol{\lambda}_1}_{\partial^2_{\xi_1} p} = \boldsymbol{L}^{\boldsymbol{\lambda}_3}_{\partial_{\xi_1} p} \tag{7.88c}$$

$$\partial_{\xi_2} \boldsymbol{L}^{\boldsymbol{\lambda}_1}_{\partial_{\xi_1} \boldsymbol{\varepsilon}} = \boldsymbol{L}^{\boldsymbol{\lambda}_2}_{\boldsymbol{\varepsilon}} \Rightarrow \partial_{\xi_2} (\boldsymbol{L}^{\boldsymbol{\lambda}_1}_{\partial_{\xi_1} \boldsymbol{\varepsilon}})^T = (\boldsymbol{L}^{\boldsymbol{\lambda}_2}_{\boldsymbol{\varepsilon}})^T \tag{7.88d}$$

$$\partial_{\xi_3} \boldsymbol{L}^{\boldsymbol{\lambda}_1}_{\partial_{\xi_1} \boldsymbol{\varepsilon}} = \boldsymbol{L}^{\boldsymbol{\lambda}_3}_{\boldsymbol{\varepsilon}} \Rightarrow \partial_{\xi_3} (\boldsymbol{L}^{\boldsymbol{\lambda}_1}_{\partial_{\xi_1} \boldsymbol{\varepsilon}})^T = (\boldsymbol{L}^{\boldsymbol{\lambda}_3}_{\boldsymbol{\varepsilon}})^T \tag{7.88e}$$

$$\partial_{\xi_2} \boldsymbol{L}^{\boldsymbol{\lambda}_1}_{\partial_{\xi_1} \boldsymbol{\kappa}} = \boldsymbol{L}^{\boldsymbol{\lambda}_2}_{\boldsymbol{\kappa}} \Rightarrow \partial_{\xi_2} (\boldsymbol{L}^{\boldsymbol{\lambda}_1}_{\partial_{\xi_1} \boldsymbol{\kappa}})^T = (\boldsymbol{L}^{\boldsymbol{\lambda}_2}_{\boldsymbol{\kappa}})^T \tag{7.88f}$$

$$\partial_{\xi_3} \boldsymbol{L}^{\boldsymbol{\lambda}_1}_{\partial_{\xi_1} \boldsymbol{\kappa}} = \boldsymbol{L}^{\boldsymbol{\lambda}_3}_{\boldsymbol{\kappa}} \Rightarrow \partial_{\xi_3} (\boldsymbol{L}^{\boldsymbol{\lambda}_1}_{\partial_{\xi_1} \boldsymbol{\kappa}})^T = (\boldsymbol{L}^{\boldsymbol{\lambda}_3}_{\boldsymbol{\kappa}})^T \tag{7.88g}$$

$$\partial_{\xi_2} \boldsymbol{L}^{\boldsymbol{\lambda}_1}_{\partial^2_{\xi_1} \boldsymbol{\kappa}} = \boldsymbol{L}^{\boldsymbol{\lambda}_2}_{\partial_{\xi_1} \boldsymbol{\kappa}} \Rightarrow \partial_{\xi_2} (\boldsymbol{L}^{\boldsymbol{\lambda}_1}_{\partial^2_{\xi_1} \boldsymbol{\kappa}})^T = (\boldsymbol{L}^{\boldsymbol{\lambda}_2}_{\partial_{\xi_1} \boldsymbol{\kappa}})^T \tag{7.88h}$$

$$\partial_{\xi_3} \boldsymbol{L}^{\boldsymbol{\lambda}_1}_{\partial^2_{\xi_1} \boldsymbol{\kappa}} = \boldsymbol{L}^{\boldsymbol{\lambda}_3}_{\partial_{\xi_1} \boldsymbol{\kappa}} \Rightarrow \partial_{\xi_3} (\boldsymbol{L}^{\boldsymbol{\lambda}_1}_{\partial^2_{\xi_1} \boldsymbol{\kappa}})^T = (\boldsymbol{L}^{\boldsymbol{\lambda}_3}_{\partial_{\xi_1} \boldsymbol{\kappa}})^T \tag{7.88i}$$

$$\partial_{\xi_2} \boldsymbol{L}^{\boldsymbol{\lambda}_1}_{\partial^3_{\xi_1} \boldsymbol{\kappa}} = \boldsymbol{L}^{\boldsymbol{\lambda}_2}_{\partial^2_{\xi_1} \boldsymbol{\kappa}} \Rightarrow \partial_{\xi_2} (\boldsymbol{L}^{\boldsymbol{\lambda}_1}_{\partial^3_{\xi_1} \boldsymbol{\kappa}})^T = (\boldsymbol{L}^{\boldsymbol{\lambda}_2}_{\partial^2_{\xi_1} \boldsymbol{\kappa}})^T \tag{7.88j}$$

$$\partial_{\xi_3} \boldsymbol{L}^{\boldsymbol{\lambda}_1}_{\partial^3_{\xi_1} \boldsymbol{\kappa}} = \boldsymbol{L}^{\boldsymbol{\lambda}_3}_{\partial^2_{\xi_1} \boldsymbol{\kappa}} \Rightarrow \partial_{\xi_3} (\boldsymbol{L}^{\boldsymbol{\lambda}_1}_{\partial^3_{\xi_1} \boldsymbol{\kappa}})^T = (\boldsymbol{L}^{\boldsymbol{\lambda}_3}_{\partial^2_{\xi_1} \boldsymbol{\kappa}})^T \tag{7.88k}$$

Identity set 2: For a vector $\boldsymbol{v} \in \mathbb{R}^3$, the following holds:

$$(\boldsymbol{M}^{\boldsymbol{\lambda}_1}_{\boldsymbol{\varepsilon}})^T . \boldsymbol{v} = -(\boldsymbol{L}^{\boldsymbol{\lambda}_1}_{\partial_{\xi_1} \boldsymbol{\varepsilon}})^T . \hat{\boldsymbol{\kappa}} . \boldsymbol{v} \tag{7.89a}$$

$$(\boldsymbol{M}^{\boldsymbol{\lambda}_1}_{\boldsymbol{\kappa}})^T . \boldsymbol{v} = -(\boldsymbol{L}^{\boldsymbol{\lambda}_1}_{\partial_{\xi_1} \boldsymbol{\kappa}})^T . \hat{\boldsymbol{\kappa}} . \boldsymbol{v} \tag{7.89b}$$

$$(\boldsymbol{M}^{\boldsymbol{\lambda}_1}_{\partial_{\xi_1} \boldsymbol{\kappa}})^T . \boldsymbol{v} = -(\boldsymbol{L}^{\boldsymbol{\lambda}_1}_{\partial^2_{\xi_1} \boldsymbol{\kappa}})^T . \hat{\boldsymbol{\kappa}} . \boldsymbol{v} \tag{7.89c}$$

$$(\boldsymbol{M}^{\boldsymbol{\lambda}_1}_{\partial^2_{\xi_1} \boldsymbol{\kappa}})^T . \boldsymbol{v} = -(\boldsymbol{L}^{\boldsymbol{\lambda}_1}_{\partial^3_{\xi_1} \boldsymbol{\kappa}})^T . \hat{\boldsymbol{\kappa}} . \boldsymbol{v} \tag{7.89d}$$

Proof of the identities mentioned above are rather straightforward and follows from the definition of $\boldsymbol{L}$ and $\boldsymbol{M}$ terms.

Identity set 3:

$$\tilde{\partial}_{\xi_1} \int_{\mathfrak{B}_0} \left(\boldsymbol{L}^{\boldsymbol{\lambda}_1}_{\partial_{\xi_1} \boldsymbol{\varepsilon}} \right)^T . \boldsymbol{S}_1 \, \mathrm{d}\mathfrak{B}_0 = \int_{\mathfrak{B}_0} \left(\boldsymbol{L}^{\boldsymbol{\lambda}_1}_{\partial_{\xi_1} \boldsymbol{\varepsilon}} \right)^T . \partial_{\xi_1} \boldsymbol{S}_1 \, \mathrm{d}\mathfrak{B}_0 + \int_{\mathfrak{B}_0} \left(\boldsymbol{M}^{\boldsymbol{\lambda}_1}_{\boldsymbol{\varepsilon}} \right)^T . \boldsymbol{S}_1 \, \mathrm{d}\mathfrak{B}_0 \tag{7.90a}$$

$$\tilde{\partial}_{\xi_1} \int_{\mathfrak{B}_0} \left(\boldsymbol{L}^{\boldsymbol{\lambda}_1}_{\partial_{\xi_1} \boldsymbol{\kappa}} \right)^T . \boldsymbol{S}_1 \, \mathrm{d}\mathfrak{B}_0 = \int_{\mathfrak{B}_0} \left(\boldsymbol{L}^{\boldsymbol{\lambda}_1}_{\partial_{\xi_1} \boldsymbol{\kappa}} \right)^T . \partial_{\xi_1} \boldsymbol{S}_1 \, \mathrm{d}\mathfrak{B}_0 + \int_{\mathfrak{B}_0} \left(\boldsymbol{M}^{\boldsymbol{\lambda}_1}_{\boldsymbol{\kappa}} \right)^T . \boldsymbol{S}_1 \, \mathrm{d}\mathfrak{B}_0 \tag{7.90b}$$

$$\tilde{\partial}^2_{\xi_1} \int_{\mathfrak{B}_0} \left(\boldsymbol{L}^{\lambda_1}_{\partial^2_{\xi_1}\boldsymbol{\kappa}}\right)^T .\boldsymbol{S}_1 \, \mathrm{d}\mathfrak{B}_0 = \tilde{\partial}_{\xi_1} \int_{\mathfrak{B}_0} \left(\boldsymbol{L}^{\lambda_1}_{\partial^2_{\xi_1}\boldsymbol{\kappa}}\right)^T .\partial_{\xi_1}\boldsymbol{S}_1 \, \mathrm{d}\mathfrak{B}_0 + \tilde{\partial}_{\xi_1} \int_{\mathfrak{B}_0} \left(\boldsymbol{M}^{\lambda_1}_{\partial_{\xi_1}\boldsymbol{\kappa}}\right)^T .\boldsymbol{S}_1 \, \mathrm{d}\mathfrak{B}_0 \quad (7.90c)$$

$$\tilde{\partial}^3_{\xi_1} \int_{\mathfrak{B}_0} \left(\boldsymbol{L}^{\lambda_1}_{\partial^3_{\xi_1}\boldsymbol{\kappa}}\right)^T .\boldsymbol{S}_1 \, \mathrm{d}\mathfrak{B}_0 = \tilde{\partial}^2_{\xi_1} \int_{\mathfrak{B}_0} \left(\boldsymbol{L}^{\lambda_1}_{\partial^3_{\xi_1}\boldsymbol{\kappa}}\right)^T .\partial_{\xi_1}\boldsymbol{S}_1 \, \mathrm{d}\mathfrak{B}_0 + \tilde{\partial}^2_{\xi_1} \int_{\mathfrak{B}_0} \left(\boldsymbol{M}^{\lambda_1}_{\partial^2_{\xi_1}\boldsymbol{\kappa}}\right)^T .\boldsymbol{S}_1 \, \mathrm{d}\mathfrak{B}_0 \quad (7.90d)$$

Proof of identity (7.90a) **and** (7.90b)**:** Observe, $\tilde{\partial}_{\xi_1}\left(\boldsymbol{L}^{\lambda_1}_{\partial_{\xi_1}\boldsymbol{\varepsilon}}\right)^T = \boldsymbol{0}_3$. Recall the relation between derivative of a spatial tensor (or matrix) and the corresponding co-rotational derivative in (3.4). Following which, we have,

$$\partial_{\xi_1}\left(\boldsymbol{L}^{\lambda_1}_{\partial_{\xi_1}\boldsymbol{\varepsilon}}\right)^T = \hat{\boldsymbol{\kappa}}.\left(\boldsymbol{L}^{\lambda_1}_{\partial_{\xi_1}\boldsymbol{\varepsilon}}\right)^T - \left(\boldsymbol{L}^{\lambda_1}_{\partial_{\xi_1}\boldsymbol{\varepsilon}}\right)^T .\hat{\boldsymbol{\kappa}} + \tilde{\partial}_{\xi_1}\left(\boldsymbol{L}^{\lambda_1}_{\partial_{\xi_1}\boldsymbol{\varepsilon}}\right)^T = \hat{\boldsymbol{\kappa}}.\left(\boldsymbol{L}^{\lambda_1}_{\partial_{\xi_1}\boldsymbol{\varepsilon}}\right)^T - \left(\boldsymbol{L}^{\lambda_1}_{\partial_{\xi_1}\boldsymbol{\varepsilon}}\right)^T .\hat{\boldsymbol{\kappa}}; \quad (7.91)$$

Using the result above, we get

$$\begin{aligned}\tilde{\partial}_{\xi_1} \int_{\mathfrak{B}_0} \left(\boldsymbol{L}^{\lambda_1}_{\partial_{\xi_1}\boldsymbol{\varepsilon}}\right)^T .\boldsymbol{S}_1 \, \mathrm{d}\mathfrak{B}_0 &= \partial_{\xi_1} \int_{\mathfrak{B}_0} \left(\boldsymbol{L}^{\lambda_1}_{\partial_{\xi_1}\boldsymbol{\varepsilon}}\right)^T .\boldsymbol{S}_1 \, \mathrm{d}\mathfrak{B}_0 - \int_{\mathfrak{B}_0} \left(\hat{\boldsymbol{\kappa}}.\left(\boldsymbol{L}^{\lambda_1}_{\partial_{\xi_1}\boldsymbol{\varepsilon}}\right)^T\right).\boldsymbol{S}_1 \, \mathrm{d}\mathfrak{B}_0; \\ &= \int_{\mathfrak{B}_0} \left(\boldsymbol{L}^{\lambda_1}_{\partial_{\xi_1}\boldsymbol{\varepsilon}}\right)^T .\partial_{\xi_1}\boldsymbol{S}_1 \, \mathrm{d}\mathfrak{B}_0 - \int_{\mathfrak{B}_0} \left(\boldsymbol{L}^{\lambda_1}_{\partial_{\xi_1}\boldsymbol{\varepsilon}}\right)^T .\hat{\boldsymbol{\kappa}}.\boldsymbol{S}_1 \, \mathrm{d}\mathfrak{B}_0.\end{aligned} \quad (7.92)$$

Identity (7.89a) implies

$$\int_{\mathfrak{B}_0} \left(\boldsymbol{M}^{\lambda_1}_{\boldsymbol{\varepsilon}}\right)^T .\boldsymbol{S}_1 \, \mathrm{d}\mathfrak{B}_0 = -\int_{\mathfrak{B}_0} \left(\boldsymbol{L}^{\lambda_1}_{\partial_{\xi_1}\boldsymbol{\varepsilon}}\right)^T .\hat{\boldsymbol{\kappa}}.\boldsymbol{S}_1 \, \mathrm{d}\mathfrak{B}_0. \quad (7.93)$$

Combining equations 7.92 and 7.93 proves the identity (7.90a). Following an exactly similar procedure yields identity (7.90b). □

Proof of identity (7.90c) **and** (7.90d)**:** We note the following:

$$\tilde{\partial}_{\xi_1}\left(\boldsymbol{L}^{\lambda_1}_{\partial^2_{\xi_1}\boldsymbol{\kappa}}\right)^T = \boldsymbol{0}_3; \quad (7.94a)$$

$$\int_{\mathfrak{B}_0} \left(\boldsymbol{M}^{\lambda_1}_{\partial_{\xi_1}\boldsymbol{\kappa}}\right)^T .\boldsymbol{S}_1 \, \mathrm{d}\mathfrak{B}_0 = -\int_{\mathfrak{B}_0} \left(\boldsymbol{L}^{\lambda_1}_{\partial^2_{\xi_1}\boldsymbol{\kappa}}\right)^T .\hat{\boldsymbol{\kappa}}.\boldsymbol{S}_1 \, \mathrm{d}\mathfrak{B}_0. \quad (7.94b)$$

The relation (7.94b) follows from identity (7.89d). Consider the RHS of identity (7.90c). Using equations (7.94a) and (7.94b), we have

$$
\begin{aligned}
\text{RHS} &= \tilde{\partial}_{\xi_1}\left(\int_{\mathfrak{B}_0}\left(\boldsymbol{L}^{\boldsymbol{\lambda}_1}_{\partial^2_{\xi_1}\boldsymbol{\kappa}}\right)^T.\partial_{\xi_1}\boldsymbol{S}_1+\left(\boldsymbol{M}^{\boldsymbol{\lambda}_1}_{\partial_{\xi_1}\boldsymbol{\kappa}}\right)^T.\boldsymbol{S}_1\,\mathrm{d}\mathfrak{B}_0\right)\\
&= \tilde{\partial}_{\xi_1}\left(\int_{\mathfrak{B}_0}\left(\boldsymbol{L}^{\boldsymbol{\lambda}_1}_{\partial^2_{\xi_1}\boldsymbol{\kappa}}\right)^T.(\partial_{\xi_1}\boldsymbol{S}_1-\hat{\boldsymbol{\kappa}}.\boldsymbol{S}_1)\,\mathrm{d}\mathfrak{B}_0\right)\\
&= \tilde{\partial}_{\xi_1}\left(\int_{\mathfrak{B}_0}\left(\boldsymbol{L}^{\boldsymbol{\lambda}_1}_{\partial^2_{\xi_1}\boldsymbol{\kappa}}\right)^T.(\tilde{\partial}_{\xi_1}\boldsymbol{S}_1)\,\mathrm{d}\mathfrak{B}_0\right)\\
&= \tilde{\partial}^2_{\xi_1}\int_{\mathfrak{B}_0}\left(\boldsymbol{L}^{\boldsymbol{\lambda}_1}_{\partial^2_{\xi_1}\boldsymbol{\kappa}}\right)^T.\boldsymbol{S}_1\,\mathrm{d}\mathfrak{B}_0=\text{LHS}
\end{aligned}
\tag{7.95}
$$

The last step follows from the fact that co-rotational derivative abides with the product rule of derivatives. This completes the proof of identity (7.90c). Along similar lines, identity (7.90d) can be proved. □

7.6.2 Further manipulation of weak form

7.6.2.1 Further manipulation of virtual strain energy

The expression of $\delta \mathrm{U}_{\text{strain}}$ in Eq. (7.64a) can be expanded as:

$$
\begin{aligned}
\delta \mathrm{U}_{\text{strain}} = \int_0^L \big(&\mathfrak{N}_{\boldsymbol{\varepsilon}}.\tilde{\delta}\boldsymbol{\varepsilon}+\mathfrak{N}_{\partial_{\xi_1}\boldsymbol{\varepsilon}}.(\boldsymbol{Q}.\delta\partial_{\xi_1}\overline{\boldsymbol{\varepsilon}})+\mathfrak{N}_{\boldsymbol{\kappa}}.\tilde{\delta}\boldsymbol{\kappa}+\mathfrak{N}_{\partial_{\xi_1}\boldsymbol{\kappa}}.(\boldsymbol{Q}.\delta\partial_{\xi_1}\overline{\boldsymbol{\kappa}})+\mathfrak{N}_{\partial^2_{\xi_1}\boldsymbol{\kappa}}.(\boldsymbol{Q}.\delta\partial^2_{\xi_1}\overline{\boldsymbol{\kappa}})\\
&+\mathfrak{N}_{\partial^3_{\xi_1}\boldsymbol{\kappa}}.(\boldsymbol{Q}.\delta\partial^3_{\xi_1}\overline{\boldsymbol{\kappa}})+\mathfrak{N}_p.p+\mathfrak{N}_{\partial_{\xi_1}p}.\partial_{\xi_1}p+\mathfrak{N}_{\partial^2_{\xi_1}p}.\partial^2_{\xi_1}p\big)\,\mathrm{d}\xi_1.
\end{aligned}
\tag{7.96}
$$

We note that the strain conjugates of the reduced section forces are spatial quantities obtained by left translation of material finite-strain terms and their derivatives. Using the expressions for $\tilde{\delta}\boldsymbol{\varepsilon}$, $\tilde{\delta}\boldsymbol{\kappa}$, $\boldsymbol{Q}.\delta\partial_{\xi_1}\overline{\boldsymbol{\kappa}}$, $\boldsymbol{Q}.\delta\partial^2_{\xi_1}\overline{\boldsymbol{\kappa}}$ and $\boldsymbol{Q}.\delta\partial^3_{\xi_1}\overline{\boldsymbol{\kappa}}$ in equations (7.30b), (7.32b), (7.33b), (7.33c) and (7.33d), followed by integration by part on the integrals in (7.96) and simplifying using the definition of the operator $\tilde{\partial}^n_{\xi_1}$ (refer to *Proposition 1* in Chadha and Todd [35]), we obtain the following:

$$\delta \mathrm{U}_{\mathrm{strain}} = \int_0^L \partial_{\xi_1}\big(- \mathfrak{R}_{\boldsymbol{\varepsilon}} + \tilde{\delta}_{\xi_1}\mathfrak{R}_{\partial_{\xi_1}\boldsymbol{\varepsilon}}\big).\delta\boldsymbol{\varphi}\ \mathrm{d}\xi_1 + \int_0^L \big(\mathfrak{R}_p - \partial_{\xi_1}\mathfrak{R}_{\partial_{\xi_1}p} + \partial^2_{\xi_1}\mathfrak{R}_{\partial^2_{\xi_1}p}\big).\delta p\ \mathrm{d}\xi_1$$
$$+ \int_0^L \left(\partial_{\xi_1}\big(- \mathfrak{R}_{\boldsymbol{\kappa}} + \tilde{\delta}_{\xi_1}\mathfrak{R}_{\partial_{\xi_1}\boldsymbol{\kappa}} - \tilde{\delta}^2_{\xi_1}\mathfrak{R}_{\partial^2_{\xi_1}\boldsymbol{\kappa}} + \tilde{\delta}^3_{\xi_1}\mathfrak{R}_{\partial^3_{\xi_1}\boldsymbol{\kappa}}\big) - \partial_{\xi_1}\hat{\boldsymbol{\varphi}}.\big(\mathfrak{R}_{\boldsymbol{\varepsilon}} - \tilde{\delta}_{\xi_1}\mathfrak{R}_{\partial_{\xi_1}\boldsymbol{\varepsilon}}\big)\right).\delta\boldsymbol{\alpha}\ \mathrm{d}\xi_1 \quad (7.97)$$
$$+ \delta \mathrm{U}^*_{\mathrm{strain}}.$$

In the equation above, $\delta \mathrm{U}^*_{\mathrm{strain}}$ gives the sum of boundary terms that originated by virtue of integration by part, such that,

$$\delta \mathrm{U}^*_{\mathrm{strain}} = \delta \mathrm{U}^*_{\mathrm{strain}\boldsymbol{\varphi}} + \delta \mathrm{U}^*_{\mathrm{strain}\boldsymbol{\alpha}} + \delta \mathrm{U}^*_{\mathrm{strain}p} \quad (7.98)$$

where,

$$\begin{aligned}
\delta \mathrm{U}^*_{\mathrm{strain}\boldsymbol{\varphi}} &= \left[\delta\boldsymbol{\varphi}.\big(\mathfrak{R}_{\boldsymbol{\varepsilon}} - \tilde{\delta}_{\xi_1}\mathfrak{R}_{\partial_{\xi_1}\boldsymbol{\varepsilon}}\big)\right]_0^L + \left[\delta\partial_{\xi_1}\boldsymbol{\varphi}.\mathfrak{R}_{\partial_{\xi_1}\boldsymbol{\varepsilon}}\right]_0^L - \left[\delta\boldsymbol{\alpha}.\big(\partial_{\xi_1}\hat{\boldsymbol{\varphi}}.\mathfrak{R}_{\partial_{\xi_1}\boldsymbol{\varepsilon}}\big)\right]_0^L;\\
\delta \mathrm{U}^*_{\mathrm{strain}\boldsymbol{\alpha}} &= \left[\delta\boldsymbol{\alpha}.\big(\mathfrak{R}_{\boldsymbol{\kappa}} - \tilde{\delta}_{\xi_1}\mathfrak{R}_{\partial_{\xi_1}\boldsymbol{\kappa}} + \tilde{\delta}^2_{\xi_1}\mathfrak{R}_{\partial^2_{\xi_1}\boldsymbol{\kappa}} - \tilde{\delta}^3_{\xi_1}\mathfrak{R}_{\partial^3_{\xi_1}\boldsymbol{\kappa}}\big)\right]_0^L + \left[\delta\partial_{\xi_1}\boldsymbol{\alpha}.\big(\mathfrak{R}_{\partial_{\xi_1}\boldsymbol{\kappa}} - \tilde{\delta}_{\xi_1}\mathfrak{R}_{\partial^2_{\xi_1}\boldsymbol{\kappa}}\big)\right]_0^L\\
&\quad + \left[\delta\partial^2_{\xi_1}\boldsymbol{\alpha}.\big(\mathfrak{R}_{\partial^2_{\xi_1}\boldsymbol{\kappa}} - \tilde{\delta}_{\xi_1}\mathfrak{R}_{\partial^3_{\xi_1}\boldsymbol{\kappa}} + 2\hat{\boldsymbol{\kappa}}.\mathfrak{R}_{\partial^3_{\xi_1}\boldsymbol{\kappa}}\big)\right]_0^L + \left[\delta\partial^3_{\xi_1}\boldsymbol{\alpha}.\mathfrak{R}_{\partial^3_{\xi_1}\boldsymbol{\kappa}}\right]_0^L;\\
\delta \mathrm{U}^*_{\mathrm{strain}p} &= \left[\delta p.\big(\mathfrak{R}_{\partial_{\xi_1}p} - \partial_{\xi_1}\mathfrak{R}_{\partial^2_{\xi_1}p}\big)\right]_0^L + \left[\delta\partial_{\xi_1}p.\mathfrak{R}_{\partial^2_{\xi_1}p}\right]_0^L.
\end{aligned} \quad (7.99)$$

7.6.2.2 Further manipulation of virtual work done due to external and inertial forces

Equations (7.76) and (7.82) can be re-written by substituting the expressions of $\tilde{\delta}\boldsymbol{\varepsilon}$, $\tilde{\delta}\boldsymbol{\kappa}$, $\boldsymbol{Q}.\delta\partial_{\xi_1}\overline{\boldsymbol{\kappa}}$ and $\boldsymbol{Q}.\delta\partial^2_{\xi_1}\overline{\boldsymbol{\kappa}}$ in equations (7.30b), (7.32b), (7.33b) and (7.33c) respectively, such that

$$\begin{aligned}
\left(\delta \mathrm{W}^{\mathrm{st}}_{\mathrm{ext}}\big|_{\cup_{\forall\xi_1}\Gamma_0(\xi_1)} + \delta \mathrm{W}^{\mathrm{b}}_{\mathrm{ext}}\right) = \int_0^L \Big(&\delta\boldsymbol{\varphi}.\boldsymbol{N}_{\boldsymbol{\varphi}} + \delta\partial_{\xi_1}\boldsymbol{\varphi}.\boldsymbol{N}_{\boldsymbol{\varepsilon}} + \delta p.N_p + \delta\partial_{\xi_1}p.N_{\partial_{\xi_1}p}\\
&+ \delta\boldsymbol{\alpha}.\Big(\boldsymbol{N}_{\boldsymbol{\alpha}} - \partial_{\xi_1}\hat{\boldsymbol{\varphi}}.\boldsymbol{N}_{\varepsilon}\Big) + \delta\partial_{\xi_1}\boldsymbol{\alpha}.\Big(\boldsymbol{N}_{\boldsymbol{\kappa}} + \hat{\boldsymbol{\kappa}}.\boldsymbol{N}_{\partial_{\xi_1}\boldsymbol{\kappa}} + \big(\hat{\boldsymbol{\kappa}}.\hat{\boldsymbol{\kappa}} + \partial_{\xi_1}\hat{\boldsymbol{\kappa}}\big).\boldsymbol{N}_{\partial^2_{\xi_1}\boldsymbol{\kappa}}\Big)\\
&+ \delta\partial^2_{\xi_1}\boldsymbol{\alpha}.\big(\boldsymbol{N}_{\partial_{\xi_1}\boldsymbol{\kappa}} + 2(\hat{\boldsymbol{\kappa}}.\boldsymbol{N}_{\partial^2_{\xi_1}\boldsymbol{\kappa}})\big) + \delta\partial^3_{\xi_1}\boldsymbol{\alpha}.\boldsymbol{N}_{\partial^2_{\xi_1}\boldsymbol{\kappa}}\Big)\ \mathrm{d}\xi_1;
\end{aligned} \quad (7.100a)$$

$$\delta \mathrm{W}_{\text{inertial}} = \int_0^L \Big(\delta\boldsymbol{\varphi}.\mathfrak{F}_{\boldsymbol{\varphi}} + \delta\partial_{\xi_1}\boldsymbol{\varphi}.\mathfrak{F}_{\boldsymbol{\varepsilon}} + \delta p.\mathfrak{F}_p + \delta\partial_{\xi_1} p.\mathfrak{F}_{\partial_{\xi_1} p} + \delta\boldsymbol{\alpha}.\Big(\mathfrak{F}_{\boldsymbol{\alpha}} - \partial_{\xi_1}\hat{\boldsymbol{\varphi}}.\mathfrak{F}_{\varepsilon}\Big) + \delta\partial_{\xi_1}\boldsymbol{\alpha}.\Big(\mathfrak{F}_{\boldsymbol{\kappa}} + \hat{\boldsymbol{\kappa}}.\mathfrak{F}_{\partial_{\xi_1}\boldsymbol{\kappa}} + \big(\hat{\boldsymbol{\kappa}}.\hat{\boldsymbol{\kappa}} + \partial_{\xi_1}\hat{\boldsymbol{\kappa}}\big).\mathfrak{F}_{\partial^2_{\xi_1}\boldsymbol{\kappa}}\Big) + \delta\partial^2_{\xi_1}\boldsymbol{\alpha}.\big(\mathfrak{F}_{\partial_{\xi_1}\boldsymbol{\kappa}} + 2(\hat{\boldsymbol{\kappa}}.\mathfrak{F}_{\partial^2_{\xi_1}\boldsymbol{\kappa}})\big) + \delta\partial^3_{\xi_1}\boldsymbol{\alpha}.\mathfrak{F}_{\partial^2_{\xi_1}\boldsymbol{\kappa}}\Big)\,\mathrm{d}\xi_1. \tag{7.100b}$$

Carrying integration by part on equation set (7.100) followed by further simplification yields

$$\begin{aligned}\Big(\delta \mathrm{W}^{\text{st}}_{\text{ext}}\big|_{\cup_{\forall\xi_1}\Gamma_0(\xi_1)} + \delta \mathrm{W}^{\text{b}}_{\text{ext}}\Big) = \int_0^L \Big(&\delta\boldsymbol{\varphi}.\big(\boldsymbol{N}_{\boldsymbol{\varphi}} - \partial_{\xi_1}\boldsymbol{N}_{\boldsymbol{\varepsilon}}\big) + \delta p.\big(N_p - \partial_{\xi_1} N_{\partial_{\xi_1} p}\big) \\ &\delta\boldsymbol{\alpha}.\big(\boldsymbol{N}_{\boldsymbol{\alpha}} - \partial_{\xi_1}\hat{\boldsymbol{\varphi}}.\boldsymbol{N}_{\boldsymbol{\varepsilon}} - \partial_{\xi_1}(\boldsymbol{N}_{\boldsymbol{\kappa}} - \tilde{\partial}_{\xi_1}\boldsymbol{N}_{\partial_{\xi_1}\boldsymbol{\kappa}} + \tilde{\partial}^2_{\xi_1}\boldsymbol{N}_{\partial^2_{\xi_1}\boldsymbol{\kappa}}))\Big)\,\mathrm{d}\xi_1 + \delta \mathrm{W}^{*}_{\text{ext}};\end{aligned} \tag{7.101a}$$

$$\begin{aligned}\delta \mathrm{W}_{\text{inertial}} = \int_0^L \Big(&\delta\boldsymbol{\varphi}.\big(\mathfrak{F}_{\boldsymbol{\varphi}} - \partial_{\xi_1}\mathfrak{F}_{\boldsymbol{\varepsilon}}\big) + \delta p.\big(\mathfrak{F}_p - \partial_{\xi_1}\mathfrak{F}_{\partial_{\xi_1} p}\big) \\ &\delta\boldsymbol{\alpha}.\big(\mathfrak{F}_{\boldsymbol{\alpha}} - \partial_{\xi_1}\hat{\boldsymbol{\varphi}}.\mathfrak{F}_{\boldsymbol{\varepsilon}} - \partial_{\xi_1}(\mathfrak{F}_{\boldsymbol{\kappa}} - \tilde{\partial}_{\xi_1}\mathfrak{F}_{\partial_{\xi_1}\boldsymbol{\kappa}} + \tilde{\partial}^2_{\xi_1}\mathfrak{F}_{\partial^2_{\xi_1}\boldsymbol{\kappa}}))\Big)\Big)\,\mathrm{d}\xi_1 + \delta \mathrm{W}^{*}_{\text{inertial}}.\end{aligned} \tag{7.101b}$$

Here, $\delta \mathrm{W}^{*}_{\text{ext}}$ and $\delta \mathrm{W}^{*}_{\text{inertial}}$ represent the boundary terms arising due to integration by part and are given by,

$$\begin{aligned}\delta \mathrm{W}^{*}_{\text{ext}} = &\Big[\delta\boldsymbol{\varphi}.\boldsymbol{N}_{\boldsymbol{\varepsilon}} + \delta\boldsymbol{\alpha}.\big(\boldsymbol{N}_{\boldsymbol{\kappa}} - \tilde{\partial}_{\xi_1}\boldsymbol{N}_{\partial_{\xi_1}\boldsymbol{\kappa}} + \tilde{\partial}^2_{\xi_1}\boldsymbol{N}_{\partial^2_{\xi_1}\boldsymbol{\kappa}}\big)\Big]_0^L + \Big[\delta\partial^2_{\xi_1}\boldsymbol{\alpha}.\boldsymbol{N}_{\partial^2_{\xi_1}\boldsymbol{\kappa}} + \delta p.N_{\partial_{\xi_1} p}\Big]_0^L \\ &+ \Big[\delta\partial_{\xi_1}\boldsymbol{\alpha}.\big(\boldsymbol{N}_{\partial_{\xi_1}\boldsymbol{\kappa}} - \tilde{\partial}_{\xi_1}\boldsymbol{N}_{\partial^2_{\xi_1}\boldsymbol{\kappa}} + \hat{\boldsymbol{\kappa}}.\boldsymbol{N}_{\partial^2_{\xi_1}\boldsymbol{\kappa}}\big)\Big]_0^L;\end{aligned} \tag{7.102a}$$

$$\begin{aligned}\delta \mathrm{W}^{*}_{\text{inertial}} = &\Big[\delta\boldsymbol{\varphi}.\mathfrak{F}_{\boldsymbol{\varepsilon}} + \delta\boldsymbol{\alpha}.\big(\mathfrak{F}_{\boldsymbol{\kappa}} - \tilde{\partial}_{\xi_1}\mathfrak{F}_{\partial_{\xi_1}\boldsymbol{\kappa}} + \tilde{\partial}^2_{\xi_1}\mathfrak{F}_{\partial^2_{\xi_1}\boldsymbol{\kappa}}\big)\Big]_0^L + \Big[\delta\partial^2_{\xi_1}\boldsymbol{\alpha}.\mathfrak{F}_{\partial^2_{\xi_1}\boldsymbol{\kappa}} + \delta p.\mathfrak{F}_{\partial_{\xi_1} p}\Big]_0^L \\ &+ \Big[\delta\partial_{\xi_1}\boldsymbol{\alpha}.\big(\mathfrak{F}_{\partial_{\xi_1}\boldsymbol{\kappa}} - \tilde{\partial}_{\xi_1}\mathfrak{F}_{\partial^2_{\xi_1}\boldsymbol{\kappa}} + \hat{\boldsymbol{\kappa}}.\mathfrak{F}_{\partial^2_{\xi_1}\boldsymbol{\kappa}}\big)\Big]_0^L.\end{aligned} \tag{7.102b}$$

7.6.3 Conservation laws

7.6.3.1 Revisiting the weak form

Using the results from last two sections 7.6.2.2 and 7.6.2.2, the weak form of equilibrium equation can be written in the form of Eq. (7.87) as

$$G(\boldsymbol{\Phi}, \delta\boldsymbol{\Phi}) = \int_0^L \delta\boldsymbol{\varphi}.\mathfrak{E}_{\boldsymbol{\varphi}} + \delta\boldsymbol{\alpha}.\mathfrak{E}_{\boldsymbol{\alpha}} + \delta p.\mathfrak{E}_p\,\mathrm{d}\xi_1 + G^{*} = 0, \tag{7.103}$$

where,

$$G^* = \delta \mathrm{U}^*_{\text{strain}} + \delta \mathrm{W}^*_{\text{inertial}} - \delta \mathrm{W}^*_{\text{ext}} - \delta \mathrm{W}^{\text{st}}_{\text{ext}}\big|_{\mathfrak{B}(0)\cup\mathfrak{B}(L)}; \tag{7.104}$$

and

$$\mathfrak{E}_{\boldsymbol{\varphi}} = \partial_{\xi_1}\boldsymbol{n} + \boldsymbol{N}_{\boldsymbol{\varphi}} - \mathfrak{F}_{\boldsymbol{\varphi}}; \tag{7.105a}$$

$$\mathfrak{E}_{\boldsymbol{\alpha}} = \partial_{\xi_1}\boldsymbol{m} + \partial_{\xi_1}\hat{\boldsymbol{\varphi}}.\boldsymbol{n} + \boldsymbol{N}_{\boldsymbol{\alpha}} - \mathfrak{F}_{\boldsymbol{\alpha}}; \tag{7.105b}$$

$$\mathfrak{E}_p = \partial_{\xi_1} M_\Psi - \mathfrak{N}_p + \boldsymbol{N}_p - \mathfrak{F}_p. \tag{7.105c}$$

In Eq. (7.105c), $\mathfrak{N}_p$ represents the bi-shear. Here we define the reduced cross-section force, moment vector, and the bi-moment as

$$\boldsymbol{n} = \left(\left(\mathfrak{N}_{\boldsymbol{\varepsilon}} - \tilde{\partial}_{\xi_1}\mathfrak{N}_{\partial_{\xi_1}\boldsymbol{\varepsilon}}\right) + \left(\mathfrak{F}_{\boldsymbol{\varepsilon}} - \boldsymbol{N}_{\boldsymbol{\varepsilon}}\right)\right); \tag{7.106a}$$

$$\begin{aligned}\boldsymbol{m} = &\left(\mathfrak{N}_{\boldsymbol{\kappa}} - \tilde{\partial}_{\xi_1}\mathfrak{N}_{\partial_{\xi_1}\boldsymbol{\kappa}} + \tilde{\partial}^2_{\xi_1}\mathfrak{N}_{\partial^2_{\xi_1}\boldsymbol{\kappa}} - \tilde{\partial}^3_{\xi_1}\mathfrak{N}_{\partial^3_{\xi_1}\boldsymbol{\kappa}}\right) + \left(\mathfrak{F}_{\boldsymbol{\kappa}} - \tilde{\partial}_{\xi_1}\mathfrak{F}_{\partial_{\xi_1}\boldsymbol{\kappa}} + \tilde{\partial}^2_{\xi_1}\mathfrak{F}_{\partial^2_{\xi_1}\boldsymbol{\kappa}}\right);\\ &- \left(\boldsymbol{N}_{\boldsymbol{\kappa}} - \tilde{\partial}_{\xi_1}\boldsymbol{N}_{\partial_{\xi_1}\boldsymbol{\kappa}} + \tilde{\partial}^2_{\xi_1}\boldsymbol{N}_{\partial^2_{\xi_1}\boldsymbol{\kappa}}\right);\end{aligned} \tag{7.106b}$$

$$M_\Psi = \left(\left(\mathfrak{N}_{\partial_{\xi_1}p} - \partial_{\xi_1}\mathfrak{N}_{\partial^2_{\xi_1}p}\right) + \left(\mathfrak{F}_{\partial_{\xi_1}p} - N_{\partial_{\xi_1}p}\right)\right). \tag{7.106c}$$

Remark 7.1: It remains to be proven that the term G^* in Eq. (7.103) vanishes. This result should not come as a surprise because the strong form describes local equilibrium of forces. However, it is interesting (and also necessary, as it provides check for correctness of the work discussed so far) to prove that $G^* = 0$. The proof is carried out in section 7.6.3.2.

Remark 7.2: Assuming that $G^* = 0$, the arbitrary nature of the virtual displacement field $\delta\boldsymbol{\Phi}$ leads us to conservation of linear and angular momentum and the balance laws for bi-shear and bi-moment: $\mathfrak{E}_{\boldsymbol{\varphi}} = \boldsymbol{0}_1$, $\mathfrak{E}_{\boldsymbol{\alpha}} = \boldsymbol{0}_1$ and $\mathfrak{E}_p = 0$, respectively. The strong form of equation described in Eq. set (7.105) appears similar to the governing equations discussed in Simo and Vu-Quoc [43], except for the definition of reduced section forces and bi-moment $\boldsymbol{n}$, $\boldsymbol{m}$ and M_Ψ. The fact that

reduced forces in Eq. (7.106), contains inertial and external force terms is distracting. However, the results obtained in the process of proving $G^* = 0$, helps us to simplify $\boldsymbol{n}$, $\boldsymbol{m}$ and M_Ψ (refer to section 7.6.3.3) to a desirable form independent of inertial and external force terms.

Remark 7.3: We obtain the velocity and acceleration vectors as

$$\begin{aligned} \partial_t \boldsymbol{R} &= \partial_t \boldsymbol{\varphi} + \tilde{\partial}_t \boldsymbol{r} + \boldsymbol{\omega} \times \boldsymbol{r}; \\ \partial_t^2 \boldsymbol{R} &= \partial_t^2 \boldsymbol{\varphi} + \tilde{\partial}_t^2 \boldsymbol{r} + \boldsymbol{\omega} \times (\boldsymbol{\omega} \times \boldsymbol{r}) + 2\boldsymbol{\omega} \times \tilde{\partial}_t \boldsymbol{r} + \partial_t \boldsymbol{\omega} \times \boldsymbol{r}. \end{aligned} \tag{7.107}$$

In case of Cosserat beam with rigid cross-section (refer to section 6.5 of Chadha and Todd [53]), the Coriolis force and non-inertial force due to cross-sectional deformation vanishes because $\tilde{\partial}_t \boldsymbol{r}_1 = 0$ and $\tilde{\partial}_t^2 \boldsymbol{r}_1 = 0$. Secondly, if the locus of geometric centroid coincided with the center of mass locus for a beam with rigid cross-section, the centrifugal and Euler force vanishes because $\int_{\mathfrak{B}_0} \rho_0 . \boldsymbol{r}_1 \, \mathrm{d}\mathfrak{B}_0 = 0$. However, for the deformed state Ω, we have non-zero Coriolis force $\left(-2\boldsymbol{\omega} \times \int_{\mathfrak{B}_0} \rho_0 . \tilde{\partial}_t \boldsymbol{r} \, \mathrm{d}\mathfrak{B}_0 \neq 0\right)$, non-inertial force due to cross-sectional deformation $\left(-\int_{\mathfrak{B}_0} \rho_0 . \tilde{\partial}_t^2 \boldsymbol{r} \, \mathrm{d}\mathfrak{B}_0 \neq 0\right)$, Euler force $\left(-\partial_t \boldsymbol{\omega} \times \int_{\mathfrak{B}_0} \rho_0 . \boldsymbol{r} \, \mathrm{d}\mathfrak{B}_0 \neq 0\right)$ and centrifugal force $\left(-\boldsymbol{\omega} \times \left(\boldsymbol{\omega} \times \int_{\mathfrak{B}_0} \rho_0 . \boldsymbol{r} \, \mathrm{d}\mathfrak{B}_0\right) \neq 0\right)$ in addition to impressed force $\left(\partial_{\xi_1} \boldsymbol{n} + \boldsymbol{N}_{\boldsymbol{\varphi}}\right)$, Einstein force due to translation $\left(-\int_{\mathfrak{B}_0} \rho_0 . \partial_t^2 \boldsymbol{\varphi} \, \mathrm{d}\mathfrak{B}_0\right)$ such that the sum of impressed and the non-inertial forces yields Eq. (7.105a).

7.6.3.2 Vanishing G^*

Theorem 1: For an arbitrarily displacement field $\delta\boldsymbol{\Theta}$, $G^* = 0$.

Proof: The term G^* in Eq. (7.104) can be written in the form presented below,

$$G^* = \left[\delta\boldsymbol{\varphi} . \boldsymbol{g}_{\boldsymbol{\varphi}} + \delta\boldsymbol{\alpha} . \boldsymbol{g}_{\boldsymbol{\alpha}} + \delta\partial_{\xi_1}\boldsymbol{\alpha} . \boldsymbol{g}_{\partial_{\xi_1}\boldsymbol{\alpha}} + \delta\partial_{\xi_1}^2\boldsymbol{\alpha} . \boldsymbol{g}_{\partial_{\xi_1}^2\boldsymbol{\alpha}} + \delta p . g_p\right]_0^L. \tag{7.108}$$

The displacement field is arbitrary but admissible. Provided we have displacement prescribed boundary conditions, G^* vanishes due to admissibility requirement. However, for a general case,

proving theorem 1 requires,

$$g_p = 0;\ \boldsymbol{g}_{\boldsymbol{\varphi}} = \mathbf{0}_1;\ \boldsymbol{g}_{\boldsymbol{\alpha}} = \mathbf{0}_1;\ \boldsymbol{g}_{\partial_{\xi_1}\boldsymbol{\alpha}} = \mathbf{0}_1;\ \boldsymbol{g}_{\partial^2_{\xi_1}\boldsymbol{\alpha}} = \mathbf{0}_1. \tag{7.109}$$

We prove that all these conditions are true. The expressions of $\boldsymbol{g}_{(.)}$ and g_p are stated as required during the proof.

Proof: $g_p = 0$

We have,

$$\begin{aligned} g_p &= g_{p1} + g_{p2} + g_{p3}; \\ g_{p1} &= \left(\mathfrak{N}_{\partial_{\xi_1} p} - \partial_{\xi_1}\mathfrak{N}_{\partial^2_{\xi_1} p}\right) - B_p; \\ g_{p2} &= \mathfrak{F}_{\partial_{\xi_1} p} - N^{\mathrm{b}}_{\partial_{\xi_1} p}; \\ g_{p3} &= -N^{\mathrm{st}}_{\partial_{\xi_1} p}. \end{aligned} \tag{7.110}$$

Substituting for the expressions of reduced forces given in appendix 7.128 and using the relationship (7.88a), we manipulate the expression of g_{p1} as,

$$\begin{aligned} g_{p1} &= \int_{\mathfrak{B}_0} \left(\boldsymbol{M}^{\boldsymbol{\lambda}_1}_{\partial_{\xi_1} p}.\boldsymbol{S}_1 + \boldsymbol{L}^{\boldsymbol{\lambda}_2}_{\partial_{\xi_1} p}.\boldsymbol{S}_2 + \boldsymbol{L}^{\boldsymbol{\lambda}_3}_{\partial_{\xi_1} p}.\boldsymbol{S}_3\right) \mathrm{d}\mathfrak{B}_0 - \partial_{\xi_1}\int_{\mathfrak{B}_0} \boldsymbol{L}^{\boldsymbol{\lambda}_1}_{\partial^2_{\xi_1} p}.\boldsymbol{S}_1 \,\mathrm{d}\mathfrak{B}_0 \\ &= \int_{\mathfrak{B}_0} \left(\boldsymbol{L}^{\boldsymbol{\lambda}_2}_{\partial_{\xi_1} p}.\boldsymbol{S}_2 + \boldsymbol{L}^{\boldsymbol{\lambda}_3}_{\partial_{\xi_1} p}.\boldsymbol{S}_3\right) \mathrm{d}\mathfrak{B}_0 - \int_{\mathfrak{B}_0} \boldsymbol{L}^{\boldsymbol{\lambda}_1}_{\partial^2_{\xi_1} p}.\partial_{\xi_1}\boldsymbol{S}_1 \,\mathrm{d}\mathfrak{B}_0. \end{aligned} \tag{7.111}$$

Using stress equilibrium equation (Eq. (7.58)), we further analyze the expression of g_{p2} as,

$$g_{p2} = \int_{\mathfrak{B}_0} \boldsymbol{L}^{\boldsymbol{\lambda}_1}_{\partial^2_{\xi_1} p}.(\rho_0.\partial_t^2\boldsymbol{R} - \rho_0.\boldsymbol{b}) \,\mathrm{d}\mathfrak{B}_0 = \int_{\mathfrak{B}_0} \boldsymbol{L}^{\boldsymbol{\lambda}_1}_{\partial^2_{\xi_1} p}.(\partial_{\xi_1}\boldsymbol{S}_1 + \partial_{\xi_2}\boldsymbol{S}_2 + \partial_{\xi_3}\boldsymbol{S}_3) \,\mathrm{d}\mathfrak{B}_0. \tag{7.112}$$

Finally, we apply divergence theorem on the expression of g_{p3} and use the relations established in Eq. (7.88b) and (7.88c) , yielding

$$\begin{aligned} g_{p3} &= -\int_{\Gamma_0} \boldsymbol{L}^{\boldsymbol{\lambda}_1}_{\partial^2_{\xi_1} p}.(\boldsymbol{S}.\boldsymbol{N}) \,\mathrm{d}\Gamma_0 \\ &= -\int_{\mathfrak{B}_0} \partial_{\xi_2}\boldsymbol{L}^{\boldsymbol{\lambda}_1}_{\partial^2_{\xi_1} p}.\boldsymbol{S}_2 + \partial_{\xi_3}\boldsymbol{L}^{\boldsymbol{\lambda}_1}_{\partial^2_{\xi_1} p}.\boldsymbol{S}_3 + \boldsymbol{L}^{\boldsymbol{\lambda}_1}_{\partial^2_{\xi_1} p}.(\partial_{\xi_2}\boldsymbol{S}_2 + \partial_{\xi_3}\boldsymbol{S}_3) \,\mathrm{d}\mathfrak{B}_0 \\ &= -\int_{\mathfrak{B}_0} \boldsymbol{L}^{\boldsymbol{\lambda}_2}_{\partial_{\xi_1} p}.\boldsymbol{S}_2 + \boldsymbol{L}^{\boldsymbol{\lambda}_3}_{\partial_{\xi_1} p}.\boldsymbol{S}_3 + \boldsymbol{L}^{\boldsymbol{\lambda}_1}_{\partial^2_{\xi_1} p}.(\partial_{\xi_2}\boldsymbol{S}_2 + \partial_{\xi_3}\boldsymbol{S}_3) \,\mathrm{d}\mathfrak{B}_0. \end{aligned} \tag{7.113}$$

Adding up the expressions of g_{p1}, g_{p2} and g_{p3} in equations (7.111), (7.112) and (7.113), we get, $g_p = 0$.

Proof: $\boldsymbol{g_\varphi = 0}_1$

We have,

$$\begin{aligned}
\boldsymbol{g}_{\boldsymbol{\varphi}} &= \boldsymbol{g}_{\boldsymbol{\varphi}1} + \boldsymbol{g}_{\boldsymbol{\varphi}2} + \boldsymbol{g}_{\boldsymbol{\varphi}3};\\
\boldsymbol{g}_{\boldsymbol{\varphi}1} &= \mathfrak{N}_{\boldsymbol{\varepsilon}} - \tilde{\partial}_{\xi_1}\mathfrak{N}_{\partial_{\xi_1}\boldsymbol{\varepsilon}} - \boldsymbol{B}_{\boldsymbol{\varphi}};\\
\boldsymbol{g}_{\boldsymbol{\varphi}2} &= \mathfrak{F}_{\boldsymbol{\varepsilon}} - \boldsymbol{N}^{\mathrm{b}}_{\boldsymbol{\varepsilon}};\\
\boldsymbol{g}_{\boldsymbol{\varphi}3} &= -\boldsymbol{N}^{\mathrm{st}}_{\boldsymbol{\varepsilon}}.
\end{aligned} \tag{7.114}$$

Realizing $\tilde{\partial}_{\xi_1}\mathfrak{N}_{\partial_{\xi_1}\boldsymbol{\varepsilon}} = \tilde{\partial}_{\xi_1}\left(\int_{\mathfrak{B}_0}\left(\boldsymbol{L}^{\boldsymbol{\lambda}_1}_{\partial_{\xi_1}\boldsymbol{\varepsilon}}\right)^T.\boldsymbol{S}_1\,\mathrm{d}\mathfrak{B}_0\right)$, we manipulate the expression of $\boldsymbol{g}_{\boldsymbol{\varphi}1}$ using identity (7.90a) to obtain

$$\boldsymbol{g}_{\boldsymbol{\varphi}1} = \int_{\mathfrak{B}_0}\left(\left(\boldsymbol{L}^{\boldsymbol{\lambda}_2}_{\boldsymbol{\varepsilon}}\right)^T.\boldsymbol{S}_2 + \left(\boldsymbol{L}^{\boldsymbol{\lambda}_3}_{\boldsymbol{\varepsilon}}\right)^T.\boldsymbol{S}_3 - \left(\boldsymbol{L}^{\boldsymbol{\lambda}_1}_{\partial_{\xi_1}\boldsymbol{\varepsilon}}\right)^T.\partial_{\xi_1}\boldsymbol{S}_1\right)\mathrm{d}\mathfrak{B}_0. \tag{7.115}$$

Using stress equilibrium equation (Eq. (7.58)), we expand the expression of $\boldsymbol{g}_{\boldsymbol{\varphi}2}$ to obtain,

$$\boldsymbol{g}_{\boldsymbol{\varphi}2} = \int_{\mathfrak{B}_0}\rho_0\left(\boldsymbol{L}^{\boldsymbol{\lambda}_1}_{\partial_{\xi_1}\boldsymbol{\varepsilon}}\right)^T.(\partial_t^2\boldsymbol{R} - \boldsymbol{b})\,\mathrm{d}\mathfrak{B}_0 = \int_{\mathfrak{B}_0}\left(\boldsymbol{L}^{\boldsymbol{\lambda}_1}_{\partial_{\xi_1}\boldsymbol{\varepsilon}}\right)^T.(\partial_{\xi_1}\boldsymbol{S}_1 + \partial_{\xi_2}\boldsymbol{S}_2 + \partial_{\xi_3}\boldsymbol{S}_3)\,\mathrm{d}\mathfrak{B}_0. \tag{7.116}$$

Using divergence theorem, the results in Eq. (7.88d) and (7.88e) on to the expression of $\boldsymbol{g}_{\boldsymbol{\varphi}3}$, we obtain,

$$\begin{aligned}
\boldsymbol{g}_{\boldsymbol{\varphi}3} &= -\int_{\Gamma_0}\left(\boldsymbol{L}^{\boldsymbol{\lambda}_1}_{\partial_{\xi_1}\boldsymbol{\varepsilon}}\right)^T.(\boldsymbol{S}.\boldsymbol{N})\,\mathrm{d}\Gamma_0\\
&= -\int_{\mathfrak{B}_0}\partial_{\xi_2}\left(\boldsymbol{L}^{\boldsymbol{\lambda}_1}_{\partial_{\xi_1}\boldsymbol{\varepsilon}}\right)^T.\boldsymbol{S}_2 + \partial_{\xi_3}\left(\boldsymbol{L}^{\boldsymbol{\lambda}_1}_{\partial_{\xi_1}\boldsymbol{\varepsilon}}\right)^T.\boldsymbol{S}_3 + \left(\boldsymbol{L}^{\boldsymbol{\lambda}_1}_{\partial_{\xi_1}\boldsymbol{\varepsilon}}\right)^T.(\partial_{\xi_2}\boldsymbol{S}_2 + \partial_{\xi_3}\boldsymbol{S}_3)\,\mathrm{d}\mathfrak{B}_0\\
&= -\int_{\mathfrak{B}_0}\left(\boldsymbol{L}^{\boldsymbol{\lambda}_2}_{\boldsymbol{\varepsilon}}\right)^T.\boldsymbol{S}_2 + \left(\boldsymbol{L}^{\boldsymbol{\lambda}_3}_{\boldsymbol{\varepsilon}}\right)^T.\boldsymbol{S}_3 + \left(\boldsymbol{L}^{\boldsymbol{\lambda}_1}_{\partial_{\xi_1}\boldsymbol{\varepsilon}}\right)^T.(\partial_{\xi_2}\boldsymbol{S}_2 + \partial_{\xi_3}\boldsymbol{S}_3)\,\mathrm{d}\mathfrak{B}_0.
\end{aligned} \tag{7.117}$$

Equations (7.115), (7.116) and (7.117) adds up to give $\boldsymbol{g}_{\boldsymbol{\varphi}} = \boldsymbol{0}_1$.

Proof: $\boldsymbol{g}_{\alpha} = \mathbf{0}_1$

Consider

$$
\begin{aligned}
\boldsymbol{g}_{\alpha} &= \boldsymbol{g}_{\alpha 1} + \boldsymbol{g}_{\alpha 2} + \boldsymbol{g}_{\alpha 3};\\
\boldsymbol{g}_{\alpha 1} &= \left(\mathfrak{N}_{\boldsymbol{\kappa}} - \tilde{\partial}_{\xi_1}\mathfrak{N}_{\partial_{\xi_1}\boldsymbol{\kappa}} + \tilde{\partial}^2_{\xi_1}\mathfrak{N}_{\partial^2_{\xi_1}\boldsymbol{\kappa}} - \tilde{\partial}^3_{\xi_1}\mathfrak{N}_{\partial^3_{\xi_1}\boldsymbol{\kappa}}\right) - \boldsymbol{B}_{\alpha};\\
\boldsymbol{g}_{\alpha 2} &= \left(\mathfrak{F}_{\boldsymbol{\kappa}} - \tilde{\partial}_{\xi_1}\mathfrak{F}_{\partial_{\xi_1}\boldsymbol{\kappa}} + \tilde{\partial}^2_{\xi_1}\mathfrak{F}_{\partial^2_{\xi_1}\boldsymbol{\kappa}}\right) - \left(\boldsymbol{N}^{\mathrm{b}}_{\boldsymbol{\kappa}} - \tilde{\partial}_{\xi_1}\boldsymbol{N}^{\mathrm{b}}_{\partial_{\xi_1}\boldsymbol{\kappa}} + \tilde{\partial}^2_{\xi_1}\boldsymbol{N}^{\mathrm{b}}_{\partial^2_{\xi_1}\boldsymbol{\kappa}}\right);\\
\boldsymbol{g}_{\alpha 3} &= -\left(\boldsymbol{N}^{\mathrm{st}}_{\boldsymbol{\kappa}} - \tilde{\partial}_{\xi_1}\boldsymbol{N}^{\mathrm{st}}_{\partial_{\xi_1}\boldsymbol{\kappa}} + \tilde{\partial}^2_{\xi_1}\boldsymbol{N}^{\mathrm{st}}_{\partial^2_{\xi_1}\boldsymbol{\kappa}}\right).
\end{aligned}
\tag{7.118}
$$

Like the previous proves, we arrive at the following,

$$
\begin{aligned}
\boldsymbol{g}_{\alpha 2} + \boldsymbol{g}_{\alpha 3} &= \left(\int_{\mathfrak{B}_0}\left(\boldsymbol{L}^{\boldsymbol{\lambda}_1}_{\partial_{\xi_1}\boldsymbol{\kappa}}\right)^T.\partial_{\xi_1}\boldsymbol{S}_1\,\mathrm{d}\mathfrak{B}_0 - \int_{\mathfrak{B}_0}\left(\left(\boldsymbol{L}^{\boldsymbol{\lambda}_2}_{\boldsymbol{\kappa}}\right)^T.\boldsymbol{S}_2 + \left(\boldsymbol{L}^{\boldsymbol{\lambda}_3}_{\boldsymbol{\kappa}}\right)^T.\boldsymbol{S}_3\right)\,\mathrm{d}\mathfrak{B}_0\right)\\
&- \tilde{\partial}_{\xi_1}\left(\int_{\mathfrak{B}_0}\left(\boldsymbol{L}^{\boldsymbol{\lambda}_1}_{\partial^2_{\xi_1}\boldsymbol{\kappa}}\right)^T.\partial_{\xi_1}\boldsymbol{S}_1\,\mathrm{d}\mathfrak{B}_0 - \int_{\mathfrak{B}_0}\left(\left(\boldsymbol{L}^{\boldsymbol{\lambda}_2}_{\partial_{\xi_1}\boldsymbol{\kappa}}\right)^T.\boldsymbol{S}_2 + \left(\boldsymbol{L}^{\boldsymbol{\lambda}_3}_{\partial_{\xi_1}\boldsymbol{\kappa}}\right)^T.\boldsymbol{S}_3\right)\,\mathrm{d}\mathfrak{B}_0\right)\\
&+ \tilde{\partial}^2_{\xi_1}\left(\int_{\mathfrak{B}_0}\left(\boldsymbol{L}^{\boldsymbol{\lambda}_1}_{\partial^3_{\xi_1}\boldsymbol{\kappa}}\right)^T.\partial_{\xi_1}\boldsymbol{S}_1\,\mathrm{d}\mathfrak{B}_0 - \int_{\mathfrak{B}_0}\left(\left(\boldsymbol{L}^{\boldsymbol{\lambda}_2}_{\partial^2_{\xi_1}\boldsymbol{\kappa}}\right)^T.\boldsymbol{S}_2 + \left(\boldsymbol{L}^{\boldsymbol{\lambda}_3}_{\partial^2_{\xi_1}\boldsymbol{\kappa}}\right)^T.\boldsymbol{S}_3\right)\,\mathrm{d}\mathfrak{B}_0\right).
\end{aligned}
\tag{7.119}
$$

Substituting for the expression of reduced section forces defined in appendix 7.128 into $\boldsymbol{g}_{\alpha 1}$, we get,

$$
\begin{aligned}
\boldsymbol{g}_{\alpha 1} &= \left(\int_{\mathfrak{B}_0}\left(\left(\boldsymbol{M}^{\boldsymbol{\lambda}_1}_{\boldsymbol{\kappa}}\right)^T.\boldsymbol{S}_1 + \left(\boldsymbol{L}^{\boldsymbol{\lambda}_2}_{\boldsymbol{\kappa}}\right)^T.\boldsymbol{S}_2 + \left(\boldsymbol{L}^{\boldsymbol{\lambda}_3}_{\boldsymbol{\kappa}}\right)^T.\boldsymbol{S}_3\right)\,\mathrm{d}\mathfrak{B}_0\right)\\
&- \tilde{\partial}_{\xi_1}\left(\int_{\mathfrak{B}_0}\left(\left(\boldsymbol{L}^{\boldsymbol{\lambda}_1}_{\partial_{\xi_1}\boldsymbol{\kappa}} + \boldsymbol{M}^{\boldsymbol{\lambda}_1}_{\partial_{\xi_1}\boldsymbol{\kappa}}\right)^T.\boldsymbol{S}_1 + \left(\boldsymbol{L}^{\boldsymbol{\lambda}_2}_{\partial_{\xi_1}\boldsymbol{\kappa}}\right)^T.\boldsymbol{S}_2 + \left(\boldsymbol{L}^{\boldsymbol{\lambda}_3}_{\partial_{\xi_1}\boldsymbol{\kappa}}\right)^T.\boldsymbol{S}_3\right)\,\mathrm{d}\mathfrak{B}_0\right)\\
&+ \tilde{\partial}^2_{\xi_1}\left(\int_{\mathfrak{B}_0}\left(\left(\boldsymbol{L}^{\boldsymbol{\lambda}_1}_{\partial^2_{\xi_1}\boldsymbol{\kappa}} + \boldsymbol{M}^{\boldsymbol{\lambda}_1}_{\partial^2_{\xi_1}\boldsymbol{\kappa}}\right)^T.\boldsymbol{S}_1 + \left(\boldsymbol{L}^{\boldsymbol{\lambda}_2}_{\partial^2_{\xi_1}\boldsymbol{\kappa}}\right)^T.\boldsymbol{S}_2 + \left(\boldsymbol{L}^{\boldsymbol{\lambda}_3}_{\partial^2_{\xi_1}\boldsymbol{\kappa}}\right)^T.\boldsymbol{S}_3\right)\,\mathrm{d}\mathfrak{B}_0\right)\\
&- \tilde{\partial}^3_{\xi_1}\left(\int_{\mathfrak{B}_0}\left(\boldsymbol{L}^{\boldsymbol{\lambda}_1}_{\partial^3_{\xi_1}\boldsymbol{\kappa}}\right)^T.\boldsymbol{S}_1\,\mathrm{d}\mathfrak{B}_0\right).
\end{aligned}
\tag{7.120}
$$

Summing up the equations (7.119) and (7.120) followed by considering the identities (7.90b), (7.90c) and (7.90d), we get $\boldsymbol{g}_{\alpha} = \mathbf{0}_1$.

Proof: $\boldsymbol{g}_{\partial_{\xi_1}\alpha} = \mathbf{0}_1$

The equation set below presents the expression of $\boldsymbol{g}_{\partial_{\xi_1}\alpha}$ in a desirable form that facilitate the

proof.

$$\boldsymbol{g}_{\partial_{\xi_1}\boldsymbol{\alpha}} = \boldsymbol{g}_{\partial_{\xi_1}\boldsymbol{\alpha}1} + \boldsymbol{g}_{\partial_{\xi_1}\boldsymbol{\alpha}2} + \boldsymbol{g}_{\partial_{\xi_1}\boldsymbol{\alpha}3}; \tag{7.121a}$$

$$\begin{aligned}\boldsymbol{g}_{\partial_{\xi_1}\boldsymbol{\alpha}1} = &\overbrace{\left(\boldsymbol{\mathfrak{N}}_{\partial_{\xi_1}\boldsymbol{\kappa}} - \boldsymbol{B}_{\boldsymbol{\kappa}}\right)}^{\boldsymbol{g}^a_{\partial_{\xi_1}\boldsymbol{\alpha}1}} + \overbrace{\left(-\left(\partial_{\xi_1}\boldsymbol{\mathfrak{N}}_{\partial^2_{\xi_1}\boldsymbol{\kappa}} - 2(\hat{\boldsymbol{\kappa}}.\boldsymbol{\mathfrak{N}}_{\partial^2_{\xi_1}\boldsymbol{\kappa}})\right) - \hat{\boldsymbol{\kappa}}.\boldsymbol{B}_{\partial_{\xi_1}\boldsymbol{\kappa}}\right)}^{\boldsymbol{g}^b_{\partial_{\xi_1}\boldsymbol{\alpha}1}} \\ &+ \overbrace{\left(\partial^2_{\xi_1}\boldsymbol{\mathfrak{N}}_{\partial^3_{\xi_1}\boldsymbol{\kappa}} - 3\partial_{\xi_1}\left(\hat{\boldsymbol{\kappa}}.\boldsymbol{\mathfrak{N}}_{\partial^3_{\xi_1}\boldsymbol{\kappa}}\right) + \left((2\hat{\boldsymbol{\kappa}}.\hat{\boldsymbol{\kappa}} + 2\partial_{\xi_1}\hat{\boldsymbol{\kappa}})\right).\boldsymbol{\mathfrak{N}}_{\partial^3_{\xi_1}\boldsymbol{\kappa}}\right)}^{\boldsymbol{g}^c_{\partial_{\xi_1}\boldsymbol{\alpha}1}};\end{aligned} \tag{7.121b}$$

$$\boldsymbol{g}_{\partial_{\xi_1}\boldsymbol{\alpha}2} = \left(\boldsymbol{\mathfrak{F}}_{\partial_{\xi_1}\boldsymbol{\kappa}} + \hat{\boldsymbol{\kappa}}.\boldsymbol{\mathfrak{F}}_{\partial^2_{\xi_1}\boldsymbol{\kappa}} - \tilde{\partial}_{\xi_1}\boldsymbol{\mathfrak{F}}_{\partial^2_{\xi_1}\boldsymbol{\kappa}}\right) - \left(\boldsymbol{N}^{\mathrm{b}}_{\partial_{\xi_1}\boldsymbol{\kappa}} + \hat{\boldsymbol{\kappa}}.\boldsymbol{N}^{\mathrm{b}}_{\partial^2_{\xi_1}\boldsymbol{\kappa}} - \tilde{\partial}_{\xi_1}\boldsymbol{N}^{\mathrm{b}}_{\partial^2_{\xi_1}\boldsymbol{\kappa}}\right); \tag{7.121c}$$

$$\boldsymbol{g}_{\partial_{\xi_1}\boldsymbol{\alpha}3} = -\left(\boldsymbol{N}^{\mathrm{st}}_{\partial_{\xi_1}\boldsymbol{\kappa}} + \hat{\boldsymbol{\kappa}}.\boldsymbol{N}^{\mathrm{st}}_{\partial^2_{\xi_1}\boldsymbol{\kappa}} - \tilde{\partial}_{\xi_1}\boldsymbol{N}^{\mathrm{st}}_{\partial^2_{\xi_1}\boldsymbol{\kappa}}\right). \tag{7.121d}$$

We manipulate the expression of $\boldsymbol{g}_{\partial_{\xi_1}\boldsymbol{\alpha}2} + \boldsymbol{g}_{\partial_{\xi_1}\boldsymbol{\alpha}3}$ as in previous proves, such that

$$\begin{aligned}\boldsymbol{g}_{\partial_{\xi_1}\boldsymbol{\alpha}2} + \boldsymbol{g}_{\partial_{\xi_1}\boldsymbol{\alpha}3} &= \left(\boldsymbol{\mathfrak{F}}_{\partial_{\xi_1}\boldsymbol{\kappa}} + \hat{\boldsymbol{\kappa}}.\boldsymbol{\mathfrak{F}}_{\partial^2_{\xi_1}\boldsymbol{\kappa}} - \tilde{\partial}_{\xi_1}\boldsymbol{\mathfrak{F}}_{\partial^2_{\xi_1}\boldsymbol{\kappa}}\right) - \left(\boldsymbol{N}_{\partial_{\xi_1}\boldsymbol{\kappa}} + \hat{\boldsymbol{\kappa}}.\boldsymbol{N}_{\partial^2_{\xi_1}\boldsymbol{\kappa}} - \tilde{\partial}_{\xi_1}\boldsymbol{N}_{\partial^2_{\xi_1}\boldsymbol{\kappa}}\right) \\ &= \left(\boldsymbol{\mathfrak{F}}_{\partial_{\xi_1}\boldsymbol{\kappa}} - \boldsymbol{N}_{\partial_{\xi_1}\boldsymbol{\kappa}}\right) - (\tilde{\partial}_{\xi_1} - \hat{\partial}_{\xi_1})\left(\boldsymbol{\mathfrak{F}}_{\partial^2_{\xi_1}\boldsymbol{\kappa}} - \boldsymbol{N}_{\partial^2_{\xi_1}\boldsymbol{\kappa}}\right) \\ &= \left(\int_{\mathfrak{B}_0}\left(\boldsymbol{L}^{\boldsymbol{\lambda}_1}_{\partial^2_{\xi_1}\boldsymbol{\kappa}}\right)^T.\partial_{\xi_1}\boldsymbol{S}_1\,\mathrm{d}\mathfrak{B}_0 - \int_{\mathfrak{B}_0}\left(\left(\boldsymbol{L}^{\boldsymbol{\lambda}_2}_{\partial_{\xi_1}\boldsymbol{\kappa}}\right)^T.\boldsymbol{S}_2 + \left(\boldsymbol{L}^{\boldsymbol{\lambda}_3}_{\partial_{\xi_1}\boldsymbol{\kappa}}\right)^T.\boldsymbol{S}_3\right)\,\mathrm{d}\mathfrak{B}_0\right) \\ &\quad - (\tilde{\partial}_{\xi_1} - \hat{\partial}_{\xi_1})\left(\int_{\mathfrak{B}_0}\left(\boldsymbol{L}^{\boldsymbol{\lambda}_1}_{\partial^3_{\xi_1}\boldsymbol{\kappa}}\right)^T.\partial_{\xi_1}\boldsymbol{S}_1\,\mathrm{d}\mathfrak{B}_0 - \int_{\mathfrak{B}_0}\left(\left(\boldsymbol{L}^{\boldsymbol{\lambda}_2}_{\partial^2_{\xi_1}\boldsymbol{\kappa}}\right)^T.\boldsymbol{S}_2 + \left(\boldsymbol{L}^{\boldsymbol{\lambda}_3}_{\partial^2_{\xi_1}\boldsymbol{\kappa}}\right)^T.\boldsymbol{S}_3\right)\,\mathrm{d}\mathfrak{B}_0\right).\end{aligned} \tag{7.122}$$

We now simplify the terms associated with $\boldsymbol{g}_{\partial_{\xi_1}\boldsymbol{\alpha}1}$. We have,

$$\boldsymbol{g}^a_{\partial_{\xi_1}\boldsymbol{\alpha}1} = \boldsymbol{\mathfrak{N}}_{\partial_{\xi_1}\boldsymbol{\kappa}} - \boldsymbol{B}_{\boldsymbol{\kappa}} = \int_{\mathfrak{B}_0}\left(\boldsymbol{M}^{\boldsymbol{\lambda}_1}_{\partial_{\xi_1}\boldsymbol{\kappa}}\right)^T.\boldsymbol{S}_1 + \left(\boldsymbol{L}^{\boldsymbol{\lambda}_2}_{\partial_{\xi_1}\boldsymbol{\kappa}}\right)^T.\boldsymbol{S}_2 + \left(\boldsymbol{L}^{\boldsymbol{\lambda}_3}_{\partial_{\xi_1}\boldsymbol{\kappa}}\right)^T.\boldsymbol{S}_3\,\mathrm{d}\mathfrak{B}_0. \tag{7.123}$$

Similarly,

$$
\begin{aligned}
\boldsymbol{g}^{b}_{\partial_{\xi_1}\boldsymbol{\alpha}1} &= -\big(\partial_{\xi_1}\mathfrak{R}_{\partial^2_{\xi_1}\boldsymbol{\kappa}} - 2(\hat{\boldsymbol{\kappa}}.\mathfrak{R}_{\partial^2_{\xi_1}\boldsymbol{\kappa}})\big) - \hat{\boldsymbol{\kappa}}.\boldsymbol{B}_{\partial_{\xi_1}\boldsymbol{\kappa}} \\
&= -\big(\partial_{\xi_1}\mathfrak{R}_{\partial^2_{\xi_1}\boldsymbol{\kappa}} - (\hat{\boldsymbol{\kappa}}.\mathfrak{R}_{\partial^2_{\xi_1}\boldsymbol{\kappa}})\big) + \hat{\boldsymbol{\kappa}}.(\mathfrak{R}_{\partial^2_{\xi_1}\boldsymbol{\kappa}} - \boldsymbol{B}_{\partial_{\xi_1}\boldsymbol{\kappa}}) \\
&= -\tilde{\partial}_{\xi_1}\mathfrak{R}_{\partial^2_{\xi_1}\boldsymbol{\kappa}} + \hat{\partial}_{\xi_1}(\mathfrak{R}_{\partial^2_{\xi_1}\boldsymbol{\kappa}} - \boldsymbol{B}_{\partial_{\xi_1}\boldsymbol{\kappa}}) \\
&= -(\tilde{\partial}_{\xi_1} - \hat{\partial}_{\xi_1})\left(\int_{\mathfrak{B}_0}\left(\boldsymbol{M}^{\boldsymbol{\lambda}_1}_{\partial^2_{\xi_1}\boldsymbol{\kappa}}\right)^T.\boldsymbol{S}_1 + \left(\boldsymbol{L}^{\boldsymbol{\lambda}_2}_{\partial^2_{\xi_1}\boldsymbol{\kappa}}\right)^T.\boldsymbol{S}_2 + \left(\boldsymbol{L}^{\boldsymbol{\lambda}_3}_{\partial^2_{\xi_1}\boldsymbol{\kappa}}\right)^T.\boldsymbol{S}_3\ \mathrm{d}\mathfrak{B}_0\right) \\
&\quad - \tilde{\partial}_{\xi_1}\left(\int_{\mathfrak{B}_0}\left(\boldsymbol{L}^{\boldsymbol{\lambda}_1}_{\partial^2_{\xi_1}\boldsymbol{\kappa}}\right)^T.\boldsymbol{S}_1\ \mathrm{d}\mathfrak{B}_0\right).
\end{aligned}
\tag{7.124}
$$

In a similar fashion, we manipulate the expression of $\boldsymbol{g}^{c}_{\partial_{\xi_1}\boldsymbol{\alpha}1}$ as follows,

$$
\begin{aligned}
\boldsymbol{g}^{c}_{\partial_{\xi_1}\boldsymbol{\alpha}1} &= \tilde{\partial}^2_{\xi_1}\mathfrak{R}_{\partial^3_{\xi_1}\boldsymbol{\kappa}} - \hat{\boldsymbol{\kappa}}.\tilde{\partial}_{\xi_1}\mathfrak{R}_{\partial^3_{\xi_1}\boldsymbol{\kappa}} = (\tilde{\partial}_{\xi_1} - \hat{\partial}_{\xi_1})\tilde{\partial}_{\xi_1}\mathfrak{R}_{\partial^3_{\xi_1}\boldsymbol{\kappa}} \\
&= (\tilde{\partial}_{\xi_1} - \hat{\partial}_{\xi_1})\tilde{\partial}_{\xi_1}\left(\int_{\mathfrak{B}_0}\left(\boldsymbol{L}^{\boldsymbol{\lambda}_1}_{\partial^3_{\xi_1}\boldsymbol{\kappa}}\right)^T.\boldsymbol{S}_1\ \mathrm{d}\mathfrak{B}_0\right) \\
&= (\tilde{\partial}_{\xi_1} - \hat{\partial}_{\xi_1})\left(\int_{\mathfrak{B}_0}\left(\left(\boldsymbol{L}^{\boldsymbol{\lambda}_1}_{\partial^3_{\xi_1}\boldsymbol{\kappa}}\right)^T.\partial_{\xi_1}\boldsymbol{S}_1 - \left(\boldsymbol{L}^{\boldsymbol{\lambda}_1}_{\partial^3_{\xi_1}\boldsymbol{\kappa}}\right)^T.\hat{\boldsymbol{\kappa}}.\boldsymbol{S}_1\right)\mathrm{d}\mathfrak{B}_0\right) \\
&= (\tilde{\partial}_{\xi_1} - \hat{\partial}_{\xi_1})\left(\int_{\mathfrak{B}_0}\left(\left(\boldsymbol{L}^{\boldsymbol{\lambda}_1}_{\partial^3_{\xi_1}\boldsymbol{\kappa}}\right)^T.\partial_{\xi_1}\boldsymbol{S}_1 + \left(\boldsymbol{M}^{\boldsymbol{\lambda}_1}_{\partial^2_{\xi_1}\boldsymbol{\kappa}}\right)^T.\boldsymbol{S}_1\right)\mathrm{d}\mathfrak{B}_0\right).
\end{aligned}
\tag{7.125}
$$

The last equality in the above equation holds by virtue of identity (7.89d). Summing up equations (7.122), (7.123), (7.124) and (7.125) yields $\boldsymbol{g}_{\partial_{\xi_1}\boldsymbol{\alpha}} = \boldsymbol{0}_1$.

Proof: $\boldsymbol{g}_{\partial^2_{\xi_1}\boldsymbol{\alpha}} = \boldsymbol{0}_1$

Like before, we define,

$$
\begin{aligned}
\boldsymbol{g}_{\partial^2_{\xi_1}\boldsymbol{\alpha}} &= \boldsymbol{g}_{\partial^2_{\xi_1}\boldsymbol{\alpha}1} + \boldsymbol{g}_{\partial^2_{\xi_1}\boldsymbol{\alpha}2} + \boldsymbol{g}_{\partial^2_{\xi_1}\boldsymbol{\alpha}3}; \\
\boldsymbol{g}_{\partial^2_{\xi_1}\boldsymbol{\alpha}1} &= \left(\mathfrak{R}_{\partial^2_{\xi_1}\boldsymbol{\kappa}} - \tilde{\partial}_{\xi_1}\mathfrak{R}_{\partial^3_{\xi_1}\boldsymbol{\kappa}}\right) - \boldsymbol{B}_{\partial_{\xi_1}\boldsymbol{\kappa}} \\
\boldsymbol{g}_{\partial^2_{\xi_1}\boldsymbol{\alpha}2} &= \mathfrak{F}_{\partial^2_{\xi_1}\boldsymbol{\kappa}} - \boldsymbol{N}^{\mathrm{b}}_{\partial^2_{\xi_1}\boldsymbol{\kappa}}; \\
\boldsymbol{g}_{\partial^2_{\xi_1}\boldsymbol{\alpha}3} &= -\boldsymbol{N}^{\mathrm{st}}_{\partial^2_{\xi_1}\boldsymbol{\kappa}}.
\end{aligned}
\tag{7.126}
$$

Substituting for the expressions of reduced forced from appendix 7.128 into the equation above, we have,

$$\begin{aligned}
\boldsymbol{g}_{\partial^2_{\xi_1}\alpha 1} &= \int_{\mathfrak{B}_0} \left(\boldsymbol{L}^{\boldsymbol{\lambda}_1}_{\partial^2_{\xi_1}\boldsymbol{\kappa}}\right)^T .\partial_{\xi_1}\boldsymbol{S}_1 \, \mathrm{d}\mathfrak{B}_0 - \int_{\mathfrak{B}_0} \left(\left(\boldsymbol{L}^{\boldsymbol{\lambda}_2}_{\partial^2_{\xi_1}\boldsymbol{\kappa}}\right)^T .\boldsymbol{S}_2 + \left(\boldsymbol{L}^{\boldsymbol{\lambda}_3}_{\partial^2_{\xi_1}\boldsymbol{\kappa}}\right)^T .\boldsymbol{S}_3\right) \mathrm{d}\mathfrak{B}_0 \\
\boldsymbol{g}_{\partial^2_{\xi_1}\alpha 2} &+ \boldsymbol{g}_{\partial^2_{\xi_1}\alpha 3} = -\boldsymbol{g}_{\partial^2_{\xi_1}\alpha 1}.
\end{aligned} \tag{7.127}$$

This completes the proof. Hence, $G^* = 0$. □

7.6.3.3 Simplified reduced section force, couple and bi-moment: $\boldsymbol{n}$, $\boldsymbol{m}$ and M_Ψ

The expression of $\boldsymbol{n}$, $\boldsymbol{m}$ and M_Ψ as defined in (7.106a), (7.106b) and (7.106c) can be further reduced by using equation set (7.114), (7.118) and (7.110) respectively yielding

$$\begin{aligned}
\boldsymbol{n} &= \boldsymbol{g}_{\boldsymbol{\varphi}} + \boldsymbol{B}_{\boldsymbol{\varphi}} = \boldsymbol{B}_{\boldsymbol{\varphi}} = \int_{\mathfrak{B}_0} \left(\boldsymbol{L}^{\boldsymbol{\lambda}_1}_{\boldsymbol{\varepsilon}}\right)^T .\boldsymbol{S}_1 \, \mathrm{d}\mathfrak{B}_0 = \int_{\mathfrak{B}_0} \boldsymbol{S}_1 \, \mathrm{d}\mathfrak{B}_0; \\
\boldsymbol{m} &= \boldsymbol{g}_{\boldsymbol{\alpha}} + \boldsymbol{B}_{\boldsymbol{\alpha}} = \boldsymbol{B}_{\boldsymbol{\alpha}} = \int_{\mathfrak{B}_0} \left(\boldsymbol{L}^{\boldsymbol{\lambda}_1}_{\boldsymbol{\kappa}}\right)^T .\boldsymbol{S}_1 \, \mathrm{d}\mathfrak{B}_0 = \int_{\mathfrak{B}_0} \boldsymbol{r} \times \boldsymbol{S}_1 \, \mathrm{d}\mathfrak{B}_0; \\
M_\Psi &= g_p + B_p = B_p = \int_{\mathfrak{B}_0} \boldsymbol{L}^{\boldsymbol{\lambda}_1}_{\partial_{\xi_1} p} .\boldsymbol{S}_1 \, \mathrm{d}\mathfrak{B}_0.
\end{aligned} \tag{7.128}$$

As expected, the expression of reduced section force, couple and bi-moment is independent of any external and inertial force terms. The reduced forces obtained above are identical to the respective quantities discussed in Simo and Vu-Quoc. [43].

7.7 Balance laws for the deformed configuration Ω_1: A special case

The chapter so far has focused on the general beam configuration Ω that allows the cross-section to deform. A special case of a deformed state that is of interest to engineers is the beam configuration Ω_1 that assumes the cross-section to be rigid. Slender structures are predominated by mid-curve deformation governed by bending, shear and axial strain. Therefore,

in many applications, it is safe to assume the cross-section to be rigid. This section is dedicated to carefully investigating the balance laws associated with the deformed state Ω_1.

Recall, the configuration space for Ω_1 is $\mathbb{R}^3 \times SO(3)$. The primary unknowns are the mid-curve position vector and the rotation tensor field. The beam subjected to rigid cross-section is governed by balance of linear and angular momentum (there is no warping, hence we do not have balance law for bi-shear and bi-moment). As in (7.128), the internal force and moment vector (refer to Fig. 7.2) for this case is defined as,

$$\begin{aligned} \boldsymbol{n} &= \int_{\mathfrak{B}_0} \boldsymbol{S}_1 \, \mathrm{d}\mathfrak{B}_0; \\ \boldsymbol{m} &= \int_{\mathfrak{B}_0} \boldsymbol{r}_1 \times \boldsymbol{S}_1 \, \mathrm{d}\mathfrak{B}_0. \end{aligned} \tag{7.129}$$

The infinitesimal equilibrium equation for a general continuum problem referenced to the

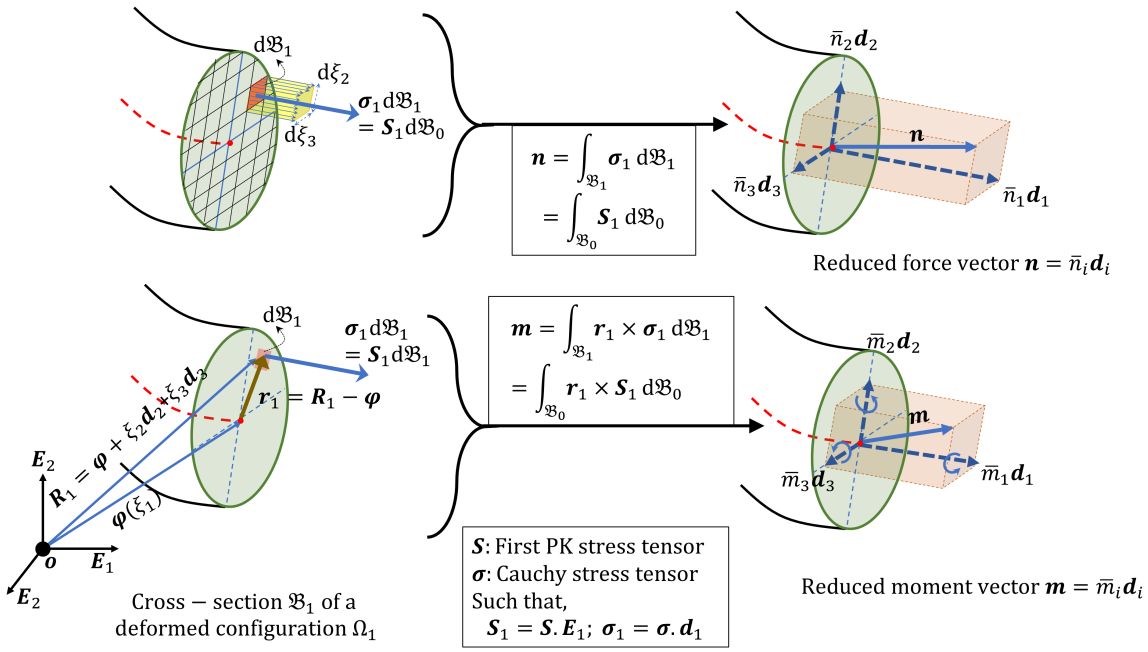

Figure 7.2: Reduced section force and moment for the deformed state Ω_1.

configuration Ω_0 for this case of deformation is given by:

$$\mathrm{Div}\boldsymbol{S} + \rho_0 \boldsymbol{b} = \rho_0 \partial_t^2 \boldsymbol{R}_1. \tag{7.130}$$

Integrating above equation over the entire undeformed domain Ω_0 followed by the application of Green's theorem to get the boundary terms gives the balance of linear momentum equation. Similarly, taking the cross product of the lever arm $(\boldsymbol{R}_1 - \boldsymbol{v})$ with all the terms in Eq. (7.130), followed by the integration over the entire domain gives the angular momentum balance equation with respect to any arbitrary point p defined by the fixed vector $\boldsymbol{v}$, such that

$$\int_{\Gamma_0} \boldsymbol{S}.\boldsymbol{N}\ \mathrm{d}\Gamma_0 + \int_{\Omega_0} \rho_0 \boldsymbol{b}\ \mathrm{d}\Omega_0 = \int_{\Omega_0} \rho_0 \partial_t^2 \boldsymbol{R}_1\ \mathrm{d}\Omega_0, \tag{7.131a}$$

$$\int_{\Gamma_0} (\boldsymbol{R}_1 - \boldsymbol{v}) \times (\boldsymbol{S}.\boldsymbol{N})\ \mathrm{d}\Gamma_0 + \int_{\Omega_0} \rho_0 (\boldsymbol{R}_1 - \boldsymbol{v}) \times \boldsymbol{b}\ \mathrm{d}\Omega_0 = \int_{\Omega_0} \rho_0 (\boldsymbol{R}_1 - \boldsymbol{v}) \times \partial_t^2 \boldsymbol{R}_1\ \mathrm{d}\Omega_0. \tag{7.131b}$$

7.7.1 Strong form obtained by balance of force and moment on a unit arc-length element referenced to initially straight configuration

7.7.1.1 Balance of linear momentum

To obtain the governing differential equation that holds at every deformed cross-section $\mathfrak{B}_1(\xi_1)$, we exploit the fact that the conservation equations (7.131a) and (7.131b) obtained for the entire beam are also valid for the unit arc-length element of the beam (bounded by the cross-section $\mathfrak{B}_0(\xi_1)$, $\mathfrak{B}_0(\xi_1 + \mathrm{d}\xi_1)$, and the peripheral boundary Γ_0 in the un-deformed state), since equilibrium of the structure as a whole implies the equilibrium of a reduced element in Ω_0. Therefore, the conservation of linear momentum for a unit arc-length element is given by,

$$\overbrace{\int_{\Omega_0} \rho_0 \partial_t^2 \boldsymbol{R}_1\ \mathrm{d}\Omega_0}^{\substack{\text{Term F3:}\\ \text{Inertial force term.}}} = \overbrace{\int_{\mathfrak{B}_0(\xi_1)} \boldsymbol{S}.\boldsymbol{N}(\xi_1)\ \mathrm{d}\mathfrak{B}_0 + \int_{\mathfrak{B}_0(\xi_1+\mathrm{d}\xi_1)} \boldsymbol{S}.\boldsymbol{N}(\xi_1 + \mathrm{d}\xi_1)\ \mathrm{d}\mathfrak{B}_0}^{\substack{\text{Term F1:}\\ \text{The reduced internal force at the cross-sectional boundary}\\ \mathfrak{B}_0(\xi_1) \text{ and } \mathfrak{B}_0(\xi_1+\mathrm{d}\xi_1) \text{ referred to unit arc-length reduced element.}}} + \overbrace{\int_{\Gamma_0} \boldsymbol{S}.\boldsymbol{N}\ \mathrm{d}\Gamma_0 + \int_{\Omega_0} \rho_0 \boldsymbol{b}\ \mathrm{d}\Omega_0}^{\substack{\text{Term F2:}\\ \text{The reduced external force due to}\\ \text{body force and surface traction.}}}. \tag{7.132}$$

For the domain of unit arc-length reduced element (refer to Fig. 7.3), the volume integral of any

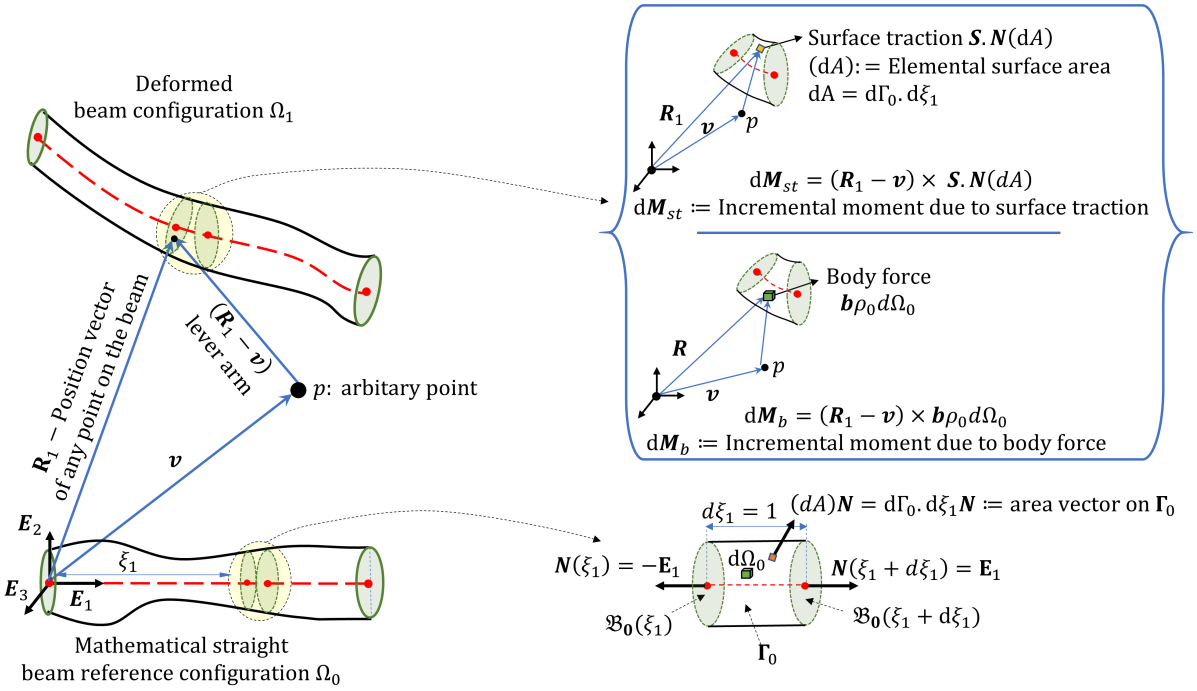

Figure 7.3: Unit arc-length element of the initially straight beam and incremental moment about an arbitrary point.

function $\boldsymbol{X}(\xi_1, \xi_2, \xi_3)$ would become integral over the cross section $\mathfrak{B}_0(\xi_1)$ as

$$\lim_{\mathrm{d}\xi_1 \to 1} \int_{\Omega_0} \boldsymbol{X}(\xi_1, \xi_2, \xi_3)\, \mathrm{d}\Omega_0 = \int_{\mathfrak{B}_0(\xi_1)} \boldsymbol{X}(\xi_1, \xi_2, \xi_3)\, \mathrm{d}\mathfrak{B}_0. \tag{7.133}$$

The stress vectors at the cross-sections $\mathfrak{B}_1(\xi_1)$ and $\mathfrak{B}_1(\xi_1 + \mathrm{d}\xi_1)$ (with the corresponding undeformed cross-sections being $\mathfrak{B}_0(\xi_1)$ and $\mathfrak{B}_0(\xi_1 + \mathrm{d}\xi_1)$) are given by the following,

$$\begin{aligned} [\boldsymbol{S}.\boldsymbol{N}]_{\mathfrak{B}_0(\xi_1)} &= \boldsymbol{S}.\boldsymbol{N}(\xi_1) = -\boldsymbol{S}.\boldsymbol{E}_1 = -\boldsymbol{S}_1, \\ [\boldsymbol{S}.\boldsymbol{N}]_{\mathfrak{B}_0(\xi_1 + \mathrm{d}\xi_1)} &= \boldsymbol{S}.\boldsymbol{N}(\xi_1 + \mathrm{d}\xi_1) = \boldsymbol{S}.\boldsymbol{E}_1 = \boldsymbol{S}_1. \end{aligned} \tag{7.134}$$

Term F1 and F2 can be simplified using the result (7.134) and the definition of reduced sectional force $\boldsymbol{n}$ and moment $\boldsymbol{m}$ in Eq. (7.128) to obtain,

$$\text{Term F1} = \lim_{\mathrm{d}\xi_1 \to 1} \left[\boldsymbol{n}(\xi_1 + \mathrm{d}\xi_1) - \boldsymbol{n}(\xi_1)\right] = \partial_{\xi_1} \boldsymbol{n}(\xi_1); \tag{7.135}$$

$$\text{Term F2} = \int_{\Gamma_0} \boldsymbol{S}.\boldsymbol{N}\ \mathrm{d}\Gamma_0 + \int_{\mathfrak{B}_0} \rho_0 \boldsymbol{b}\ \ \mathrm{d}\mathfrak{B}_0 = \boldsymbol{N}_{\boldsymbol{\varphi}}(\xi_1). \tag{7.136}$$

Like the result stated in *remark 7.3*, the velocity and acceleration vector for the deformed state can be written as,

$$\begin{aligned} \partial_t \boldsymbol{R}_1(\xi_1,\xi_2,\xi_3) &= \partial_t \boldsymbol{\varphi}(\xi_1) + \boldsymbol{\omega}(\xi_1) \times \boldsymbol{r}_1; \\ \partial_t^2 \boldsymbol{R}_1(\xi_1,\xi_2,\xi_3) &= \partial_t^2 \boldsymbol{\varphi}(\xi_1) + \partial_t \boldsymbol{\omega}(\xi_1) \times \boldsymbol{r}_1 + \boldsymbol{\omega}(\xi_1) \times \boldsymbol{\omega}(\xi_1) \times \boldsymbol{r}_1. \end{aligned} \tag{7.137}$$

Using these results, the term F3 is obtained as,

$$\text{Term F3} = \mathfrak{F}_{\boldsymbol{\varphi}} = \mu_0 \partial_t^2 \boldsymbol{\varphi} + \partial_t \boldsymbol{\omega} \times \boldsymbol{\Upsilon}_0 + \boldsymbol{\omega} \times \boldsymbol{\omega} \times \boldsymbol{\Upsilon}_0, \tag{7.138}$$

where,

$$\mu_0(\xi_1) = \int_{\mathfrak{B}_0} \rho_0\ \mathrm{d}\mathfrak{B}_0, \tag{7.139}$$

$$\boldsymbol{\Upsilon}_0(\xi_1) = \int_{\mathfrak{B}_0} \rho_0 \boldsymbol{r}_1\ \mathrm{d}\mathfrak{B}_0 = \left(\int_{\mathfrak{B}_0} \rho_0 \xi_2\ \mathrm{d}\mathfrak{B}_0 \right) \boldsymbol{d}_2 + \left(\int_{\mathfrak{B}_0} \rho_0 \xi_3\ \mathrm{d}\mathfrak{B}_0 \right) \boldsymbol{d}_3. \tag{7.140}$$

The first term ($\mu_0 \partial_t^2 \boldsymbol{\varphi}$) in Eq. (7.138) represents the inertial force due to translation acting at the point where the mid-curve intersect the cross-section $\mathfrak{B}_1$. The term μ_0 represents the mass density per unit arc-length in the initially straight configuration Ω_0. The occurrence of second term is because of the fact that, in general the mid-curve may not coincide with the mass centroid. These terms would vanish for the untwisted straight beam Ω_0 of homogeneous material if the beam mid-curve is chosen as the loci of mass centroid, which in this case would coincide with the geometric centroid. If the initial configuration of the beam were curved Ω_c, these terms would vanish only if the mass centroid were chosen as the mid-curve, as in this case the loci of geometric centroid may not coincide with the mass centroid.

Combining Eqs. (7.132)–(7.140) gives the reduced linear momentum conservation equation of the moving beam at section $\mathfrak{B}_1(\xi_1)$ referred to the initially straight configuration Ω_0 as

$$\partial_{\xi_1} \boldsymbol{n}(\xi_1) + \boldsymbol{N}_{\boldsymbol{\varphi}}(\xi_1) = \mathfrak{F}_{\boldsymbol{\varphi}}(\xi_1). \tag{7.141}$$

7.7.1.2 Balance of angular momentum

The angular momentum conservation for the unit arc-length element can be written as:

$$\overbrace{\int_{\mathfrak{B}_0(\xi_1)} (\boldsymbol{R}_1 - \boldsymbol{v}) \times \big(\boldsymbol{S}.\boldsymbol{N}\big)\, \mathrm{d}\mathfrak{B}_0 + \int_{\mathfrak{B}_0(\xi_1+\mathrm{d}\xi_1)} (\boldsymbol{R}_1 - \boldsymbol{v}) \times \big(\boldsymbol{S}.\boldsymbol{N}\big)\, \mathrm{d}\mathfrak{B}_0}^{\substack{\text{Term M1:}\\ \text{The reduced internal moment at the cross-sectional boundary } \mathfrak{B}_0 \text{ and } \mathfrak{B}_0(\xi_1+\mathrm{d}\xi_1)\\ \text{referred to unit arc-length reduced element about a fixed arbitrary point } p.}} +$$
$$\underbrace{\int_{\Gamma_0} (\boldsymbol{R}_1 - \boldsymbol{v}) \times \big(\boldsymbol{S}.\boldsymbol{N}\big) d\Gamma_0 + \int_{\Omega_0} \rho_0 (\boldsymbol{R}_1 - \boldsymbol{v}) \times \boldsymbol{b}\, d\Omega_0}_{\substack{\text{Term M2:}\\ \text{The reduced external moment about a fixed arbitrary}\\ \text{point } p \text{ due to the body force and surface traction.}}} = \underbrace{\int_{\Omega_0} \rho_0 (\boldsymbol{R}_1 - \boldsymbol{v}) \times \partial_t^2 \boldsymbol{R}\, \mathrm{d}\Omega_0}_{\substack{\text{Term M3:}\\ \text{Inertial term corresponding to}\\ \text{moment about point } p.}}. \tag{7.142}$$

It is sensible to define the moment about the mid-curve such that the lever arm is $\boldsymbol{r}_1 = (\boldsymbol{R}_1 - \boldsymbol{\varphi})$. Therefore, from the definition of reduced force and moment as in Eqs. (7.128), and using the result in Eq. (7.134), Term M1 may be simplified as

$$\begin{aligned}
\text{Term M1} =& \int_{\mathfrak{B}_0(\xi_1)} (\boldsymbol{R}_1 - \boldsymbol{\varphi}) \times (\boldsymbol{S}.\boldsymbol{N})\, \mathrm{d}\mathfrak{B}_0 + \int_{\mathfrak{B}_0(\xi_1)} (\boldsymbol{\varphi} - \boldsymbol{v}) \times (\boldsymbol{S}.\boldsymbol{N})\, \mathrm{d}\mathfrak{B}_0 \\
&+ \int_{\mathfrak{B}_0(\xi_1+\mathrm{d}\xi_1)} (\boldsymbol{R}_1 - \boldsymbol{\varphi}) \times (\boldsymbol{S}.\boldsymbol{N})\, \mathrm{d}\mathfrak{B}_0 + \int_{\mathfrak{B}_0(\xi_1+\mathrm{d}\xi_1)} (\boldsymbol{\varphi} - \boldsymbol{v}) \times (\boldsymbol{S}.\boldsymbol{N})\, \mathrm{d}\mathfrak{B}_0 \\
=& \lim_{\mathrm{d}\xi_1 \to 1} (\boldsymbol{m}(\xi_1 + \mathrm{d}\xi_1) - \boldsymbol{m}(\xi_1)) \\
&+ \lim_{\mathrm{d}\xi_1 \to 1} \left(\int_{\mathfrak{B}_0(\xi_1+\mathrm{d}\xi_1)} (\boldsymbol{\varphi} - \boldsymbol{v}) \times \boldsymbol{S}_1\, \mathrm{d}\mathfrak{B}_0 - \int_{\mathfrak{B}_0(\xi_1)} (\boldsymbol{\varphi} - \boldsymbol{v}) \times \boldsymbol{S}_1\, \mathrm{d}\mathfrak{B}_0 \right) \\
=& \partial_{\xi_1} \boldsymbol{m} + \partial_{\xi_1} \boldsymbol{\varphi} \times \boldsymbol{n} + (\boldsymbol{\varphi} - \boldsymbol{v}) \times \partial_{\xi_1} \boldsymbol{n}.
\end{aligned} \tag{7.143}$$

For a unit arc-length element, Term M2 and Term M3 may be simplified using Eq. (7.133) as

$$\begin{aligned}
\text{Term M2} &= \int_{\Gamma_0} (\boldsymbol{R}_1 - \boldsymbol{v}) \times (\boldsymbol{S}.\boldsymbol{N})\, \mathrm{d}\Gamma_0 + \int_{\mathfrak{B}_0} \rho_0 (\boldsymbol{R}_1 - \boldsymbol{v}) \times \boldsymbol{b}\, \mathrm{d}\mathfrak{B}_0 \\
&= \boldsymbol{N}_{\boldsymbol{\alpha}}(\xi_1) + \int_{\Gamma_0} (\boldsymbol{\varphi} - \boldsymbol{v}) \times (\boldsymbol{S}.\boldsymbol{N})\, \mathrm{d}\Gamma_0 + \int_{\mathfrak{B}_0} \rho_0 (\boldsymbol{\varphi} - \boldsymbol{v}) \times \boldsymbol{b}\, \mathrm{d}\mathfrak{B}_0.
\end{aligned} \tag{7.144}$$

where,

$$\boldsymbol{N}_{\boldsymbol{\alpha}}(\xi_1) = \int_{\Gamma_0} (\boldsymbol{r}_1) \times (\boldsymbol{S}.\boldsymbol{N})\, \mathrm{d}\Gamma_0 + \int_{\mathfrak{B}_0} \rho_0 (\boldsymbol{r}_1) \times \boldsymbol{b}\, \mathrm{d}\mathfrak{B}_0. \tag{7.145}$$

The quantity $\boldsymbol{N}_\alpha$ represents the reduced moment due to surface traction on peripheral boundary Γ_0 and body force about the point on the mid-curve.

Similarly,

$$\text{Term M3} = \overbrace{\int_{\mathfrak{B}_0} \rho_0(\boldsymbol{R} - \boldsymbol{\varphi}) \times \partial_t^2 \boldsymbol{R}_1 \, \mathrm{d}\mathfrak{B}_0}^{\text{Term M3a}} + \int_{\mathfrak{B}_0} \rho_0(\boldsymbol{\varphi} - \boldsymbol{v}) \times \partial_t^2 \boldsymbol{R}_1 \, \mathrm{d}\mathfrak{B}_0. \tag{7.146}$$

Term M3a represents the reduced moment due to the inertial force about point on the mid-curve. Noting the expression for $\partial_t^2 \boldsymbol{R}_1$ and $\boldsymbol{\Upsilon}_0$ as in Eq. (7.137) and (7.140), Term M3a can be simplified as

$$\begin{aligned}
\text{Term M3a} &= \int_{\mathfrak{B}_0} \rho_0(\boldsymbol{r}_1 \times \partial_t^2 \boldsymbol{R}_1) \, \mathrm{d}\mathfrak{B}_0 \\
&= \boldsymbol{\Upsilon}_0 \times \partial_t^2 \boldsymbol{\varphi} - \int_{\mathfrak{B}_0} \rho_0 \boldsymbol{r}_1 \times (\boldsymbol{r}_1 \times \partial_t \boldsymbol{\omega}) \, \mathrm{d}\mathfrak{B}_0 + \int_{\mathfrak{B}_0} \rho_0 \boldsymbol{r}_1 \times \boldsymbol{\omega} \times (\boldsymbol{\omega} \times \boldsymbol{r}_1) \, \mathrm{d}\mathfrak{B}_0 \\
&= \boldsymbol{\Upsilon}_0 \times \partial_t^2 \boldsymbol{\varphi} + \left(\int_{\mathfrak{B}_0} \rho_0 \hat{\boldsymbol{r}}_1^T . \hat{\boldsymbol{r}}_1 \, \mathrm{d}\mathfrak{B}_0 \right) . \partial_t \boldsymbol{\omega} + \boldsymbol{\omega} \times \left(\int_{\mathfrak{B}_0} \rho_0 \hat{\boldsymbol{r}}_1^T . \hat{\boldsymbol{r}}_1 \, \mathrm{d}\mathfrak{B}_0 \right) . \boldsymbol{\omega} \\
&= \boldsymbol{\Upsilon}_0 \times \partial_t^2 \boldsymbol{\varphi} + \boldsymbol{I}_0 . \partial_t^2 \boldsymbol{\omega} + \boldsymbol{\omega} \times \boldsymbol{I}_0 . \boldsymbol{\omega}
\end{aligned} \tag{7.147}$$

The spatial quantity $\boldsymbol{I}_0 = \int_{\mathfrak{B}_0} \rho_0 \hat{\boldsymbol{r}}_1^T . \hat{\boldsymbol{r}}_1 \, \mathrm{d}\mathfrak{B}_0$ is the second mass moment of inertia tensor per unit arc length of the straight configuration Ω_0. It is associated with the distribution of mass across the cross section. The vector $(\boldsymbol{\varphi} - \boldsymbol{v})$ is independent of the parameters ξ_2 and ξ_3. Keeping this in mind and combining all the equations above yields,

$$\begin{aligned}
&\overbrace{\partial_{\xi_1} \boldsymbol{m} + \partial_{\xi_1} \boldsymbol{\varphi} \times \boldsymbol{n} + \boldsymbol{\mathfrak{N}}_\alpha - (\boldsymbol{\Upsilon}_0 \times \partial_t^2 \boldsymbol{\varphi} + \boldsymbol{I}_0 . \partial_t \boldsymbol{\omega} + \boldsymbol{\omega} \times \boldsymbol{I}_0 \boldsymbol{\omega})}^{\text{Equation M1}} + \\
&\underbrace{(\boldsymbol{\varphi} - \boldsymbol{v}) \times \left(\partial_{\xi_1} \boldsymbol{n} + \int_{\Gamma_0} \boldsymbol{S} . \boldsymbol{N} \, \mathrm{d}\Gamma_0 + \int_{\mathfrak{B}_0} \rho_0 \boldsymbol{b} \, \mathrm{d}\mathfrak{B}_0 - \int_{\mathfrak{B}_0} \rho_0 \partial_t^2 \boldsymbol{R}_1 \, \mathrm{d}\mathfrak{B}_0 \right)}_{\text{Equation M2}} = 0.
\end{aligned} \tag{7.148}$$

It is clear that term Equation M2 contains terms consisting of $(\boldsymbol{\varphi} - \boldsymbol{v})$, which must vanish in order to obtain angular momentum balance law with respect to moment taken about the point on the

mid-curve. It is clear from the linear momentum conservation equation (7.141) that the Equation M2 vanishes. Therefore, the reduced strong form of angular momentum conservation referenced to Ω_0 is given as

$$\partial_{\xi_1} \boldsymbol{m} + \partial_{\xi_1} \boldsymbol{\varphi} \times \boldsymbol{n} + \boldsymbol{N}_{\alpha} = \mathfrak{F}_{\alpha}, \tag{7.149}$$

The quantity $\mathfrak{F}_{\alpha}$ represents reduced moment acting at the cross-section $\mathfrak{B}_1$ about point on the mid-curve due to inertial forces. Refer to section 7.7.6 for further discussion on inertial forces.

7.7.2 Strong form referenced to initially curved configuration

To derive the balance law referenced to Ω_c we transform the limits of the integrals in the strong form obtained in previous section to the configuration Ω_c. Consider that the unit arc-length element for curved beam configuration Ω_c is defined by the boundary $\Gamma_c \cup \mathfrak{B}_c(\xi_1) \cup \mathfrak{B}_c(\xi_1 + \mathrm{d}\xi_1)$. To proceed further, it is required to establish a relation between the stress tensors $\boldsymbol{S}$ and $\boldsymbol{S}_c$ (first PK stress tensor referenced to initially curved configuration). We utilize the relationship between the Cauchy stress tensor $\boldsymbol{\sigma}$, and the first PK stress tensors $\boldsymbol{S}$ and $\boldsymbol{S_c}$ (refer to Lai et al. [118]). We have,

$$\boldsymbol{\sigma} = \frac{1}{\det(\boldsymbol{F}_r)} \boldsymbol{S}_c . \boldsymbol{F}_r^T = \frac{1}{\det(\boldsymbol{F}_1)} \boldsymbol{S} . {\boldsymbol{F}_1}^T; \tag{7.150}$$

$$\boldsymbol{S} = \det(\boldsymbol{F}_c) . \boldsymbol{S}_c . \boldsymbol{F}_c^{-T}. \tag{7.151}$$

The area vector on the surface boundary $\boldsymbol{N}\mathrm{d}\Gamma_0$ and $\boldsymbol{N}_c\mathrm{d}\Gamma_c$ in the configurations Ω_0 and Ω_c, respectively, is related by Nanson's relation as

$$\boldsymbol{N}\mathrm{d}\Gamma_0 = \frac{1}{\det(\boldsymbol{F}_c)} \boldsymbol{F}_c^T . \boldsymbol{N}_c . \mathrm{d}\Gamma_c. \tag{7.152}$$

Using Eq. (7.151) and (7.152) and the result in Eq. (4.47), the reduced linear momentum conservation equation referenced to the curved configuration Ω_c is obtained as,

$$\partial_{\xi_1} \boldsymbol{n} + \boldsymbol{N}_{\alpha} = \mathfrak{F}_{\boldsymbol{\varphi}}^c. \tag{7.153}$$

Here,

$$
\begin{aligned}
\boldsymbol{N}_{\boldsymbol{\varphi}} &= \int_{\Gamma_0} \boldsymbol{S}_c.\boldsymbol{N}_c \, \mathrm{d}\Gamma_c + \int_{\mathfrak{B}_c} \det(\boldsymbol{F}_c)\rho_c \boldsymbol{b} \, \mathrm{d}\mathfrak{B}_c = \int_{\Gamma_0} \boldsymbol{S}.\boldsymbol{N} \, \mathrm{d}\Gamma_0 + \int_{\mathfrak{B}_0} \rho_0 \boldsymbol{b} \, \mathrm{d}\mathfrak{B}_0; \\
\mathfrak{F}^c_{\boldsymbol{\varphi}} &= \mu_c \partial_t^2 \boldsymbol{\varphi} + \boldsymbol{\omega} \times (\boldsymbol{\omega} \times \boldsymbol{\Upsilon}_c) + \partial_t \boldsymbol{\omega} \times \boldsymbol{\Upsilon}_c; \\
\mu_c &= \int_{\mathfrak{B}_c} \det(\boldsymbol{F}_c)\rho_c \, \mathrm{d}\mathfrak{B}_c; \\
\boldsymbol{\Upsilon}_c &= \left(\int_{\mathfrak{B}_c} \det(\boldsymbol{F}_c)\rho_c \xi_2 \, \mathrm{d}\mathfrak{B}_c \right) \boldsymbol{d}_2 + \left(\int_{\mathfrak{B}_c} \det(\boldsymbol{F}_c)\rho_c \xi_3 \, \mathrm{d}\mathfrak{B}_c \right) \boldsymbol{d}_3.
\end{aligned}
\tag{7.154}
$$

Since the deformation is referenced to Ω_c, the angular velocity tensor for this case is defined as $\hat{\boldsymbol{\omega}} = \partial_t \boldsymbol{Q}_r.\boldsymbol{Q}_r^T$. Along the similar lines, we observe that the reduced angular momentum conservation equation referenced to Ω_c has similar form as Eq.(7.149), such that,

$$
\partial_{\xi_1} \boldsymbol{m} + \partial_{\xi_1} \boldsymbol{\varphi} \times \boldsymbol{n} + \boldsymbol{N}_{\boldsymbol{\alpha}} = \mathfrak{F}^c_{\boldsymbol{\alpha}},
\tag{7.155}
$$

where,

$$
\boldsymbol{N}_{\boldsymbol{\alpha}} = \int_{\Gamma_c} \boldsymbol{r}_1 \times (\boldsymbol{S}_c.\boldsymbol{N}_c) d\Gamma_c + \int_{\mathfrak{B}_c} \det(\boldsymbol{F}_c)\rho_c (\boldsymbol{r}_1 \times \boldsymbol{b}) \, \mathrm{d}\mathfrak{B}_c;
\tag{7.156}
$$

$$
\mathfrak{F}^c_{\boldsymbol{\alpha}} = \boldsymbol{\Upsilon}_c \times \partial_t^2 \boldsymbol{\varphi} + \boldsymbol{I}_c.\partial_t \boldsymbol{\omega} + \boldsymbol{\omega} \times (\boldsymbol{I}_c.\boldsymbol{\omega});
\tag{7.157}
$$

$$
\boldsymbol{I}_c = \int_{\mathfrak{B}_c} \rho_c (\hat{\boldsymbol{r}}_1^T.\hat{\boldsymbol{r}}_1) \, \mathrm{d}\mathfrak{B}_c.
\tag{7.158}
$$

The parameter $\boldsymbol{\Upsilon}_c$ defines the first mass moment vector and $\boldsymbol{I}_c$ defines the second mass moment of inertia tensor considering the curved reference configuration Ω_c.

7.7.3 Weak form and virtual work principle

Along the lines of section 7.5, the virtual work principle for deformed state Ω_1 is given by Eq. (7.60), such that

$$
\begin{aligned}
\delta \mathrm{U}_{\mathrm{strain}} &= \int_{\Omega_0} \boldsymbol{S} : \delta \boldsymbol{F}_1 \, \mathrm{d}\Omega_0 = \int_0^L \left(\boldsymbol{n} \cdot \tilde{\delta}\boldsymbol{\varepsilon} + \boldsymbol{m} \cdot \tilde{\delta}\boldsymbol{\kappa} \right) \, \mathrm{d}\xi_1 \\
&= \int_0^L \left(\overline{\boldsymbol{n}} \cdot \delta\overline{\boldsymbol{\varepsilon}} + \overline{\boldsymbol{m}} \cdot \delta\overline{\boldsymbol{\kappa}} \right) \, \mathrm{d}\xi_1;
\end{aligned}
\tag{7.159a}
$$

$$\delta \mathrm{W}_{\text{inertial}} = \int_{\Omega_0} \rho_0 \delta \boldsymbol{u} \cdot \partial_t^2 \boldsymbol{R}_1 \, \mathrm{d}\Omega_0 = \int_0^L \left(\delta \boldsymbol{\varphi} \cdot \mathfrak{F}_{\boldsymbol{\varphi}} + \delta \boldsymbol{\alpha} \cdot \mathfrak{F}_{\boldsymbol{\alpha}} \right) \, \mathrm{d}\xi_1; \tag{7.159b}$$

$$\begin{aligned} \delta \mathrm{W}_{\text{ext}} &= \int_{\Im_0} \delta \boldsymbol{u} \cdot (\boldsymbol{S}.\boldsymbol{N}) \, \mathrm{d}\Im_0 + \int_{\Omega_0} \delta \boldsymbol{u} \cdot \boldsymbol{b} \, \mathrm{d}\Omega_0 \\ &= \int_0^L \left(\delta \boldsymbol{\varphi} \cdot \boldsymbol{N}_{\boldsymbol{\varphi}} + \delta \boldsymbol{\varphi} \cdot \boldsymbol{N}_{\boldsymbol{\alpha}} \right) \, \mathrm{d}\xi_1 + \left[\delta \boldsymbol{\varphi} \cdot \boldsymbol{n} + \delta \boldsymbol{\alpha} \cdot \boldsymbol{m} \right]_0^L . \end{aligned}$$

The equation (7.60) defines the general virtual work principle which states that if the body in dynamic equilibrium is subjected to a virtual displacement at a given instant of time, the virtual work done due to the real external forces δW_{ext} (Traction and body force) is stored as virtual strain energy δU_{strain} and virtual work due to the inertial forces on the body $\delta W_{\text{inertial}}$. The virtual work principle, when the deformation of the beam is referenced to the curved configuration would then become,

$$\delta U^c_{\text{strain}} + \delta W^c_{\text{inertial}} = \delta W_{\text{ext}}; \tag{7.160}$$

where,

$$\delta U^c_{\text{strain}} = \int_0^L \left(\boldsymbol{n} \cdot \tilde{\delta} \boldsymbol{\varepsilon}_r + \boldsymbol{m} \cdot \tilde{\delta} \boldsymbol{\kappa}_r \right) \, \mathrm{d}\xi_1 = \int_0^L \left(\overline{\boldsymbol{n}} \cdot \delta \overline{\boldsymbol{\varepsilon}}_r + \overline{\boldsymbol{m}} \cdot \delta \overline{\boldsymbol{\kappa}}_r \right) \, \mathrm{d}\xi_1, \tag{7.161}$$

$$\delta W^c_{\text{inertial}} = \int_0^L \left(\delta \boldsymbol{\varphi} \cdot \mathfrak{F}^c_{\boldsymbol{\varphi}} + \delta \boldsymbol{\alpha} \cdot \mathfrak{F}^c_{\boldsymbol{\alpha}} \right) \, \mathrm{d}\xi_1. \tag{7.162}$$

The quantities $\boldsymbol{\varepsilon}_r = \partial_{\xi_1} \boldsymbol{\varphi} - \boldsymbol{d}_{c_1}$ and $\hat{\boldsymbol{\kappa}}_r = \partial_{\xi_1} \boldsymbol{Q}_r . \boldsymbol{Q}_r^T$ gives the mid-curve axial strain and the curvature vector of the deformed state Ω_1 referenced to the curved reference state Ω_c. The virtual external work δW_{ext} remains the same for both the reference configuration Ω_0 and Ω_c. The expression for the strain energy and the inertial work changes because the strain and the inertial effect depends on the initial configuration of the beam considered.

7.7.4 Equivalence of the weak and strong form of equilibrium equation

Section 7.6 was dedicated to obtaining the strong form of governing differential equations for the general deformed state Ω from the weak form. In this section, we do the opposite. We obtain the weak form for the beam Ω_1 referenced to the undeformed state Ω_0 using the strong

form derived in the section 7.7.1.

The linear and angular momentum conservation principle for the beam Ω_1 is obtained in Eq. (7.141) and (7.149). The weak form of equation described in section 7.7.3 can be obtained in a purely mathematical sense from the strong form. This shows the equivalence of strong and weak form and also validate the results obtained in section 7.7.3. We take a similar approach as delineated in Hughes [119]. The linear momentum equation (7.141) is associated with the mid-curve deformation. Therefore, the weight function used to obtain residual form of reduced equilibrium equation is the virtual displacement of the mid-curve $\delta\boldsymbol{\varphi}$. Similarly, the angular momentum equation (7.149) is associated with the curvatures of the cross-section, thus making virtual rotation $\delta\boldsymbol{\alpha}$ as the natural choice for the weight function. Note that $\delta\boldsymbol{\varphi}$ and $\delta\boldsymbol{\alpha}$ are admissible and are related to $\delta\boldsymbol{u}$ in the sense that $\delta\boldsymbol{u} = \delta\boldsymbol{\varphi} + \delta\boldsymbol{\alpha} \times \boldsymbol{r}_1$. The residual form of equilibrium equation referenced to the straight configuration Ω_0 can be written as,

$$\int_0^L \left(\delta\boldsymbol{\varphi} \cdot \left(\partial_{\xi_1}\boldsymbol{n} + \boldsymbol{N}_{\boldsymbol{\varphi}} - \mathfrak{F}_{\boldsymbol{\varphi}}\right) + \delta\boldsymbol{\alpha} \cdot \left(\partial_{\xi_1}\boldsymbol{m} + \partial_{\xi_1}\boldsymbol{\varphi} \times \boldsymbol{n} + \boldsymbol{N}_{\boldsymbol{\alpha}} - \mathfrak{F}_{\boldsymbol{\alpha}}\right)\right) \, \mathrm{d}\xi_1 = 0. \tag{7.163}$$

Using Green's theorem and the property of the triple product of vectors, following results hold,

$$\begin{aligned}
\int_0^L (\delta\boldsymbol{\varphi}.\partial_{\xi_1}\boldsymbol{n}) \, \mathrm{d}\xi_1 &= \left[\delta\boldsymbol{\varphi}.\boldsymbol{n}\right]_{\xi_1=0}^{\xi_1=L} - \int_0^L (\delta\partial_{\xi_1}\boldsymbol{\varphi}.\boldsymbol{n}) \, \mathrm{d}\xi_1, \\
\int_0^L (\delta\boldsymbol{\alpha}.\partial_{\xi_1}\boldsymbol{m}) d\xi_1 &= \left[\delta\boldsymbol{\alpha}.\boldsymbol{m}\right]_{\xi_1=0}^{\xi_1=L} - \int_0^L (\delta\partial_{\xi_1}\boldsymbol{\alpha}.\boldsymbol{m}) \, \mathrm{d}\xi_1, \\
\int_0^L \delta\boldsymbol{\alpha}.(\partial_{\xi_1}\boldsymbol{\varphi} \times \boldsymbol{n}) \, \mathrm{d}\xi_1 &= \int_0^L \boldsymbol{n}.(\delta\boldsymbol{\alpha} \times \partial_{\xi_1}\boldsymbol{\varphi}) \, \mathrm{d}\xi_1.
\end{aligned} \tag{7.164}$$

Therefore, using the results in Eq. (7.164) with Eq. (7.163), the residual form of equilibrium equation simplifies to the following,

$$\begin{aligned}
&\int_0^L \left(\left(\delta\partial_{\xi_1}\boldsymbol{\varphi} - \delta\boldsymbol{\alpha} \times \partial_{\xi_1}\boldsymbol{\varphi}\right) \cdot \boldsymbol{n} + \delta\partial_{\xi_1}\boldsymbol{\alpha} \cdot \boldsymbol{m}\right) \, \mathrm{d}\xi_1 + \int_0^L (\delta\boldsymbol{\varphi} \cdot \mathfrak{F}_{\boldsymbol{\varphi}} + \delta\boldsymbol{\alpha} \cdot \mathfrak{F}_{\boldsymbol{\alpha}}) \, \mathrm{d}\xi_1 \\
&\qquad = \left[\delta\boldsymbol{\varphi} \cdot \boldsymbol{n}\right]_{\xi_1=0}^{\xi_1=L} + \left[\delta\boldsymbol{\alpha} \cdot \boldsymbol{m}\right]_{\xi_1=0}^{\xi_1=L} + \int_0^L (\delta\boldsymbol{\varphi} \cdot \boldsymbol{N}_{\boldsymbol{\varphi}} + \delta\boldsymbol{\alpha} \cdot \boldsymbol{N}_{\boldsymbol{\alpha}}) \, \mathrm{d}\xi_1.
\end{aligned} \tag{7.165}$$

Using the expression for $\tilde{\delta}\boldsymbol{\varepsilon}$ and $\tilde{\delta}\boldsymbol{\kappa}$ mentioned in section 7.4.2.1, the above equation becomes,

$$\begin{aligned}&\int_0^L \left(\tilde{\delta}\boldsymbol{\varepsilon}\cdot\boldsymbol{n}+\tilde{\delta}\boldsymbol{\kappa}\cdot\boldsymbol{m}\right)\,\mathrm{d}\xi_1+\int_0^L(\delta\boldsymbol{\varphi}\cdot\mathfrak{F}_{\boldsymbol{\varphi}}+\delta\boldsymbol{\alpha}\cdot\mathfrak{F}_{\boldsymbol{\alpha}})d\xi_1\\&=\left[\delta\boldsymbol{\varphi}\cdot\boldsymbol{n}\right]_{\xi_1=0}^{\xi_1=L}+\left[\delta\boldsymbol{\alpha}\cdot\boldsymbol{m}\right]_{\xi_1=0}^{\xi_1=L}+\int_0^L(\delta\boldsymbol{\varphi}\cdot\boldsymbol{N}_{\boldsymbol{\varepsilon}}+\delta\boldsymbol{\alpha}\cdot\boldsymbol{N}_{\boldsymbol{\alpha}})\,\mathrm{d}\xi_1.\end{aligned}\tag{7.166}$$

which is exactly same as the weak form mentioned in Eq. (7.159) derived using the infinitesimal Lagrangian equation of motion thereby validating the former approach.

7.7.5 Strong form of equations derived from Hamilton's equation

Hamilton's Principle (refer to Rao [120]) can be used to evaluate the dynamic equation of motion. The principle assumes that the configuration of the deformed beam is exactly known at time t_1 and t_2. Therefore, the variational field $\delta\boldsymbol{u}(t_1,\xi_1,\xi_2,\xi_3)=\boldsymbol{0}$ and $\delta\boldsymbol{u}(t_2,\xi_1,\xi_2,\xi_3)=\boldsymbol{0}$. There are infinitesimal configurations that the beam can have at any time t ($t\neq t_1$and t_2), each configuration deviating from the correct one by an arbitrary but admissible displacement field $\delta\boldsymbol{u}(t,\xi_1,\xi_2,\xi_3)=\delta\boldsymbol{\varphi}(t,\xi_1)+\delta\boldsymbol{\alpha}(t,\xi_1)\times\boldsymbol{r}_1(\xi_1,\xi_2,\xi_3)$, where $\delta\boldsymbol{\varphi}$ defines the admissible variation in the midcurve and the vector $\delta\boldsymbol{\alpha}$ parametrizes the variation in the director frame. The exact deformed configuration at any time $t_1<t<t_2$ is determined by making the *action A* stationary, defined as,

$$A=\int_{t_1}^{t_2}\mathbb{L}dt=\int_{t_1}^{t_2}(T-U_{\text{strain}}+W_{\text{ext}})\,\mathrm{d}t.\tag{7.167}$$

where, the functional $\mathbb{L}$ is called the *Lagrangian* of the system. The principle states that,

$$\delta\int_{t_1}^{t_2}(T-U_{\text{strain}}+W_{\text{ext}})\,\mathrm{d}t=\overbrace{\int_{t_1}^{t_2}\delta T\,\mathrm{d}t}^{\text{Term 1}}-\overbrace{\int_{t_1}^{t_2}\delta U_{\text{strain}}\,\mathrm{d}t}^{\text{Term 2}}+\overbrace{\int_{t_1}^{t_2}\delta W_{\text{ext}}\,\mathrm{d}t}^{\text{Term 3}}=0.\tag{7.168}$$

To proceed further with the simplification of the equation above, we consider each of these terms independently.

7.7.5.1 Term 1: Simplification of kinetic energy term

The total kinetic energy of the beam referenced to Ω_0 can be written using Eq. (7.137) as,

$$T = \frac{1}{2}\int_{\Omega_0} \rho_0 \partial_t \boldsymbol{u} \cdot \partial_t \boldsymbol{u}\ \mathrm{d}\Omega_0 = \frac{1}{2}\int_{\Omega_0} \rho_0 \partial_t \boldsymbol{R}_1 \cdot \partial_t \boldsymbol{R}_1\ \mathrm{d}\Omega_0 = \frac{1}{2}\int_{\Omega_0} \rho_0 (\partial_t \boldsymbol{\varphi} + \partial_t \boldsymbol{r}_1)\cdot(\partial_t \boldsymbol{\varphi} + \partial_t \boldsymbol{r}_1)\ \mathrm{d}\Omega_0. \tag{7.169}$$

Therefore,

$$\delta\int_{t_1}^{t_2} T\ \mathrm{d}t = \int_{t_1}^{t_2}\int_{\Omega_0} \rho_0 \left(\delta\partial_t\boldsymbol{\varphi}\cdot\partial_t\boldsymbol{\varphi} + \delta\partial_t\boldsymbol{\varphi}\cdot\partial_t\boldsymbol{r}_1 + \partial_t\boldsymbol{\varphi}\cdot\delta\partial_t\boldsymbol{r}_1 + \delta\partial_t\boldsymbol{r}_1\cdot\partial_t\boldsymbol{r}_1\right)\ \mathrm{d}\Omega_0\mathrm{d}t. \tag{7.170}$$

We subject Eq. (7.170) to integration by parts with respect to time and note that $\delta\boldsymbol{\varphi}(t_1) = \delta\boldsymbol{\varphi}(t_2) = \delta\boldsymbol{\alpha}(t_1) = \delta\boldsymbol{\alpha}(t_2) = \mathbf{0}$. Therefore $\delta\boldsymbol{r}_1(t_1) = \delta\boldsymbol{\alpha}(t_1)\times\boldsymbol{r}_1 = \mathbf{0}$ and $\delta\boldsymbol{r}_1(t_2) = \mathbf{0}$. This leads to,

$$\delta\int_{t_1}^{t_2} T\ dt = -\int_{t_1}^{t_2}\int_{\Omega_0} \left(\delta\boldsymbol{\varphi}\cdot\partial_t^2\boldsymbol{\varphi} + \delta\boldsymbol{\varphi}\cdot\partial_t^2\boldsymbol{r}_1 + \partial_t^2\boldsymbol{\varphi}\cdot\delta\boldsymbol{r}_1 + \delta\boldsymbol{r}_1\cdot\partial_t^2\boldsymbol{r}_1\right)\ \mathrm{d}\Omega_0\mathrm{d}t. \tag{7.171}$$

We make note of the following relations,

$$\partial_t^2\boldsymbol{\varphi}\cdot\delta\boldsymbol{r}_1 = \partial_t^2\boldsymbol{\varphi}\cdot(\delta\boldsymbol{\alpha}\times\boldsymbol{r}_1) = \delta\boldsymbol{\alpha}\cdot\left(\boldsymbol{r}_1\times\partial_t^2\boldsymbol{\varphi}\right); \tag{7.172}$$

$$\delta\boldsymbol{r}_1\cdot\partial_t^2\boldsymbol{r}_1 = \delta\boldsymbol{\alpha}\cdot\left(\boldsymbol{r}_1\times\partial_t^2\boldsymbol{r}_1\right) \tag{7.173}$$

Substituting (7.172) and (7.173) in Eq. (7.171), and realizing that $\delta\boldsymbol{\varphi}$, $\delta\boldsymbol{\alpha}$, $\delta\boldsymbol{\omega}$ and $\delta\partial_t\boldsymbol{\omega}$ are function of (ξ_1, t) only, we obtain,

$$\delta\int_{t_1}^{t_2} T\ \mathrm{d}t = -\int_{t_1}^{t_2}\int_0^L \delta\boldsymbol{\varphi}\cdot\overbrace{\left(\partial_t^2\boldsymbol{\varphi}.\overbrace{\left(\int_{\mathfrak{B}_0}\rho_0\ \mathrm{d}\mathfrak{B}_0\right)}^{\mu_0} + \overbrace{\left(\int_{\mathfrak{B}_0}\rho_0\partial_t\boldsymbol{r}_1\ \mathrm{d}\mathfrak{B}_0\right)}^{\partial_t\boldsymbol{\omega}\times\boldsymbol{\Upsilon}_0+\boldsymbol{\omega}\times\boldsymbol{\omega}\times\boldsymbol{\Upsilon}_0}\right)}^{\mathfrak{F}_{\boldsymbol{\varphi}}}\mathrm{d}\xi_1\mathrm{d}t \tag{7.174}$$

$$-\int_{t_1}^{t_2}\int_0^L \delta\boldsymbol{\alpha}\cdot\overbrace{\left(\overbrace{\left(\int_{\mathfrak{B}_0}\rho_0\boldsymbol{r}_1\,\mathrm{d}\mathfrak{B}_0\right)}^{\boldsymbol{\Upsilon}_0}\times\partial_t\boldsymbol{\varphi}+\overbrace{\left(\int_{\mathfrak{B}_0}\rho_0(\boldsymbol{r}_1\times\partial_t\boldsymbol{r}_1)\,\mathrm{d}\mathfrak{B}_0\right)}^{\boldsymbol{I}_0.\partial_t\boldsymbol{\omega}+\boldsymbol{\omega}\times\boldsymbol{I}_0.\boldsymbol{\omega}}\right)}^{\mathfrak{F}_{\boldsymbol{\alpha}}}\mathrm{d}\xi_1\mathrm{d}t.$$

Therefore,

$$\delta\int_{t_1}^{t_2}T\,\mathrm{d}t=-\int_{t_1}^{t_2}\int_0^L\left(\delta\boldsymbol{\varphi}\cdot\mathfrak{F}_{\boldsymbol{\varphi}}+\delta\boldsymbol{\alpha}\cdot\mathfrak{F}_{\boldsymbol{\alpha}}\right)\,\mathrm{d}\xi_1\,dt. \tag{7.175}$$

7.7.5.2 Term 2: Simplification of potential energy term

We simplify the virtual strain energy defined in Eq. (7.159) as,

$$\int_{t_1}^{t_2}\delta U_{\text{strain}}\,\mathrm{d}t=\int_{t_1}^{t_2}\int_0^L\left(\left(\delta\partial_{\xi_1}\boldsymbol{\varphi}-\delta\boldsymbol{\alpha}\times\partial_{\xi_1}\boldsymbol{\varphi}\right)\cdot\boldsymbol{n}+\delta\partial_{\xi_1}\boldsymbol{\alpha}\cdot\boldsymbol{m}\right)\,\mathrm{d}\xi_1\mathrm{d}t. \tag{7.176}$$

Rearranging the terms and carrying out integration by parts with respect to ξ_1, we obtain,

$$\int_{t_1}^{t_2}\delta U_{\text{strain}}\,\mathrm{d}t=-\int_{t_1}^{t_2}\int_0^L\delta\boldsymbol{\varphi}\cdot\partial_{\xi_1}\boldsymbol{n}+\delta\boldsymbol{\alpha}\cdot(\partial_{\xi_1}\boldsymbol{\varphi}\times\boldsymbol{n}+\partial_{\xi_1}\boldsymbol{m})\,\mathrm{d}\xi_1\,\mathrm{d}t+\int_{t_1}^{t_2}(\delta\boldsymbol{\varphi}\cdot\boldsymbol{n}+\delta\boldsymbol{\alpha}\cdot\boldsymbol{m})_{\xi_1=0}^{\xi_1=L}\,\mathrm{d}t \tag{7.177}$$

7.7.5.3 Term 3: Simplification of external work term

The body force field $\boldsymbol{b}$ and the surface traction are the external forces in the body. The external force term in Hamilton's equation can be written as,

$$\int_{t_1}^{t_2}\delta W_{\text{ext}}\,\mathrm{d}t=\overbrace{\int_{t_1}^{t_2}\int_{\Omega_0}\rho_0(\delta\boldsymbol{u}\cdot\boldsymbol{b})d\Omega_0\mathrm{d}t}^{\text{Term 3.1}}+\overbrace{\int_{t_1}^{t_2}\int_0^L\int_{\Gamma_0}(\delta\boldsymbol{u}\cdot(\boldsymbol{S}.\boldsymbol{N}))\,d\Gamma_0\,\mathrm{d}\xi_1\mathrm{d}t}^{\text{Term 3.2}} \tag{7.178}$$

Term 3.1 and *Term 3.2* can be simplified by substituting for the expression of $\delta\boldsymbol{u}$, yielding,

$$\int_{t_1}^{t_2}\int_{\Omega_0}\rho_0(\delta\boldsymbol{u}\cdot\boldsymbol{b})\,\mathrm{d}\xi_1\mathrm{d}t=\int_{t_1}^{t_2}\int_0^L\delta\boldsymbol{\varphi}\cdot\left(\int_{\mathfrak{B}_0}\rho_0\boldsymbol{b}\,\mathrm{d}\mathfrak{B}_0\right)+\delta\boldsymbol{\alpha}\cdot\left(\int_{\mathfrak{B}_0}\rho_0(\boldsymbol{r}_1\times\boldsymbol{b})\,\mathrm{d}\mathfrak{B}_0\right)\,\mathrm{d}\xi_1\mathrm{d}t; \tag{7.179}$$

$$\int_{t_1}^{t_2}\int_0^L\int_{\Gamma_0}(\delta\boldsymbol{u}\cdot(\boldsymbol{S}.\boldsymbol{N}))\ \mathrm{d}\Gamma_0\,\mathrm{d}\xi_1\mathrm{d}t=\int_{t_1}^{t_2}\int_0^L\delta\boldsymbol{\varphi}\cdot\left(\int_{\Gamma_0}\boldsymbol{S}.\boldsymbol{N}\ \mathrm{d}\Gamma_0\right)+\delta\boldsymbol{\alpha}\cdot\left(\int_{\Gamma_0}\boldsymbol{r}_1\times(\boldsymbol{S}.\boldsymbol{N})\,\mathrm{d}\Gamma_0\right)\mathrm{d}\xi_1\mathrm{d}t. \tag{7.180}$$

Combing Eq.(7.178)–(7.180) and noting the definition of reduced external force $\mathfrak{F}_{\boldsymbol{\varphi}}$ and moment $\mathfrak{F}_{\boldsymbol{\alpha}}$ in Eq. (7.136) and (7.144) respectively, we get,

$$\int_{t_1}^{t_2}\delta W_{\text{ext}}\ \mathrm{d}t=\int_{t_1}^{t_2}\int_0^L\left(\delta\boldsymbol{\varphi}\cdot\mathfrak{F}_{\boldsymbol{\varphi}}+\delta\boldsymbol{\alpha}\cdot\mathfrak{F}_{\boldsymbol{\alpha}}\right)\ \mathrm{d}\xi_1\mathrm{d}t. \tag{7.181}$$

7.7.5.4 Governing equations of motion and boundary terms

The Hamilton's equation for the Cosserat beam can be realized by combining Eq. (7.168), (7.175), (7.177), and (7.181), giving

$$\int_{t_1}^{t_2}\int_0^L\left(\delta\boldsymbol{\varphi}\cdot\left(\partial_{\xi_1}\boldsymbol{n}+\boldsymbol{N}_{\boldsymbol{\varphi}}-\mathfrak{F}_{\boldsymbol{\varphi}}\right)+\delta\boldsymbol{\alpha}\cdot\left(\partial_{\xi_1}\boldsymbol{m}+\partial_{\xi_1}\boldsymbol{\varphi}\times\boldsymbol{n}+\boldsymbol{N}_{\boldsymbol{\alpha}}-\mathfrak{F}_{\boldsymbol{\alpha}}\right)\right)\ \mathrm{d}\xi_1\mathrm{d}t+\int_{t_1}^{t_2}\left(\delta\boldsymbol{\varphi}\cdot\boldsymbol{n}+\delta\boldsymbol{\alpha}\cdot\boldsymbol{m}\right)_{\xi_1=0}^{\xi_1=L}\ \mathrm{d}t=0. \tag{7.182}$$

Realizing that $\delta\boldsymbol{\varphi}$ and $\delta\boldsymbol{\alpha}$ are arbitrary virtual quantities at time t, for Eq. (7.182) to hold good for all $\delta\boldsymbol{\varphi}$ and $\delta\boldsymbol{\alpha}$, following must be true,

$$\partial_{\xi_1}\boldsymbol{n}+\boldsymbol{N}_{\boldsymbol{\varphi}}-\mathfrak{F}_{\boldsymbol{\varphi}}=0, \tag{7.183}$$

$$\partial_{\xi_1}\boldsymbol{m}+\partial_{\xi_1}\boldsymbol{\varphi}\times\boldsymbol{n}+\boldsymbol{N}_{\boldsymbol{\alpha}}-\mathfrak{F}_{\boldsymbol{\alpha}}=0, \tag{7.184}$$

$$\left[\delta\boldsymbol{\varphi}\cdot\boldsymbol{n}\right]_{\xi_1=0}^{\xi_1=L}=0, \tag{7.185}$$

$$\left[\delta\boldsymbol{\alpha}\cdot\boldsymbol{m}\right]_{\xi_1=0}^{\xi_1=L}=0. \tag{7.186}$$

Equations (7.183) and (7.184) represent linear momentum conservation and angular momentum conservation law referenced to straight configuration Ω_0 respectively. It is not surprising that the result is same as obtained from infinitesimal equilibrium equation in section 7.7.1 as in Eq. (7.141) and (7.149). Secondly, the equations (7.185) and (7.186) represent the general boundary

condition at $\xi_1 = 0$ and $\xi_1 = L$. For instance, if the left boundary is fixed and the right boundary is free, $\boldsymbol{\varphi}(0) = \boldsymbol{\theta}(0) = \mathbf{0}$ and $\boldsymbol{n}(L) = \boldsymbol{m}(L) = \mathbf{0}$. Note that $\delta\boldsymbol{\alpha}$ parameterize the variational rotation of director frame that has rotation of $\boldsymbol{Q}(\boldsymbol{\theta})$ in equilibrium state. Therefore, for the fixed end, $\delta\boldsymbol{\alpha}(0) = \mathbf{0}$ implies $\boldsymbol{\theta}(0) = \mathbf{0}$ at all time t.

7.7.6 Interpretation of equation of motion from D'Alembert's Principle– Motion viewed from the director frame

In general, to interpret motion from the non-inertial frame, we define the *impressed forces* as the forces that are imposed on the system due to external effects and due to the configuration of the system. In the case of the Cosserat beam, the body force, traction (external forces), and the internal stresses (due to deformed configuration) are the sources of the *impressed forces*. We define the *forces of inertia referenced to a frame in consideration* as the forces resisted by the structure by virtue of inertia, as observed from the frame considered. Lastly the *Einstein forces* or the *apparent forces* are defined as the forces experienced by the object due to non-inertial nature of the frame of reference. To establish the state of equilibrium, the *impressed forces*, *Einstein forces*, and the *forces of inertia referenced to a frame in consideration* are considered simultaneously. This law is referred to as the D'Alembert's Principle.

Owing to the single manifold nature of the problem, the motion of the Cosserat beam is simplified to motion of the mid-curve. Each point of the mid-curve has a rigid section attached to it. Therefore, the equation of motions developed in section 7.7.1 can be thought of as the equilibrium equation of a unit arc-length element with the mass μ_0 idealized as a rigid section $\mathfrak{B}_1(\xi_1)$, with the mass μ_0 distributed homogeneously throughout the section.

We have assumed that the mid-curve may not necessarily be the locus mass centroid. For the cross-section $\mathfrak{B}_1(\xi_1)$, any point is defined by the position vector $\boldsymbol{r}_1$. Let the point CM represents the mass centroid located by the vector $\boldsymbol{r}_{cm} = \frac{\boldsymbol{\Upsilon}_0}{\mu_0}$. The figure below illustrates the discussion.

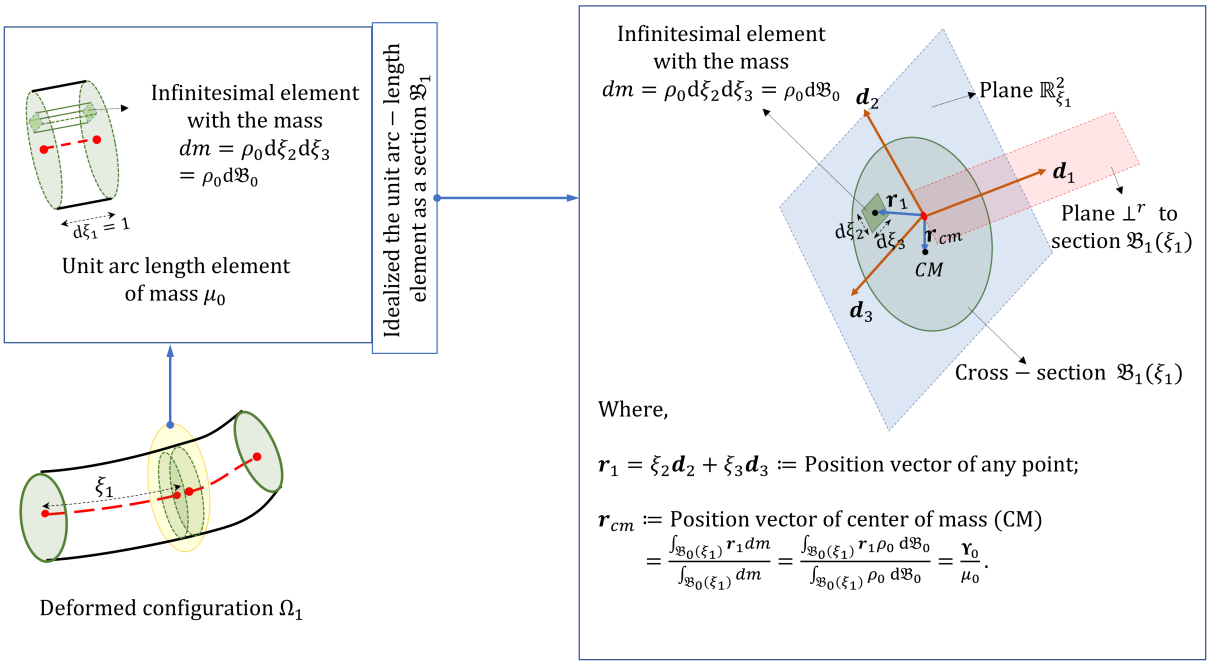

Figure 7.4: Reduced element of unit arc-length idealized as a rigid section with the mass μ_0.

The conservation of linear momentum equation (7.141) represents the translational equilibrium of the mass μ_0. The mass μ_0 is static with respect to the frame $\{\boldsymbol{d}_i\}$ because the section is rigid. The frame $\{\boldsymbol{d}_i\}$ is translating with the translational acceleration of $\partial_t^2 \boldsymbol{\varphi}$ and is rotating with the angular acceleration $\partial_t \boldsymbol{\omega}$ referenced to the fixed inertial frame $\{\boldsymbol{E}_i\}$. The mass μ_0 experiences the following forces,

1. The *impressed force* $= \partial_{\xi_1} \boldsymbol{n} + \boldsymbol{N}_{\boldsymbol{\varphi}}$.
2. The *force of inertia* w.r.t the frame $\{\boldsymbol{d}_i\} = -\mu_0 \tilde{\partial}_t^2 \boldsymbol{r}_{cm} = \boldsymbol{0}$.
3. The *Einstein force* due to translation $= -\mu_0 \partial_t^2 \boldsymbol{\varphi}$.
4. The *centrifugal force* $= -\boldsymbol{\omega} \times \boldsymbol{\omega} \times (\mu_0 \boldsymbol{r}_{cm}) = -\boldsymbol{\omega} \times \boldsymbol{\omega} \times (\boldsymbol{\Upsilon}_0)$.
5. The *Euler force* $= -\partial_t \boldsymbol{\omega} \times (\mu_0 \boldsymbol{r}_{cm}) = -\partial_t \boldsymbol{\omega} \times (\boldsymbol{\Upsilon}_0)$.
6. The *Coriolis force* $= -2\boldsymbol{\omega} \times (\mu_0 \tilde{\partial}_t \boldsymbol{r}_{cm}) = \boldsymbol{0}$.

Summing these forces yields linear momentum conservation law.

The conservation of angular momentum Eq. (7.149) represents the moment balance of the section $\mathfrak{B}_1(\xi_1)$. If the force on the elemental mass $\rho_0 \mathrm{d}\xi_2 \mathrm{d}\xi_3 = \rho_0 \mathrm{d}\mathfrak{B}_0 = \rho_0 \mathrm{d}\mathfrak{B}_1$ located at point on the section, positioned by the vector $\boldsymbol{r}_1$, is $\mathrm{d}\boldsymbol{F}$, then the total reduced moment of the section is $\int_{\mathfrak{B}_1} \boldsymbol{r}_1 \times \mathrm{d}\boldsymbol{F}$. Therefore,

1. The reduced moment due to the *impressed forces* $= \boldsymbol{m}_{,\xi_1} + \boldsymbol{\varphi}_{,\xi_1} \times \boldsymbol{n} + \boldsymbol{N}_{\boldsymbol{\alpha}}$.
2. The reduced moment due to *force of inertia* w.r.t the frame $\{\boldsymbol{d}_i\} = -\int_{\mathfrak{B}_1} \rho_0 \boldsymbol{r}_1 \times \tilde{\partial}_t^2 \boldsymbol{r}_1 \, \mathrm{d}\mathfrak{B}_1 = \boldsymbol{0}$. The parameter $\tilde{\partial}_t^2 \boldsymbol{r}_1$ represents the acceleration of a point w.r.t the frame $\{\boldsymbol{d}_i\}$. It vanishes since the configuration Ω_1 assume rigid cross-section.
3. The reduced moment due to the translational *Einstein force* $= -\int_{\mathfrak{B}_1} \rho_0 \boldsymbol{r}_1 \times \partial_t^2 \boldsymbol{\varphi} \mathrm{d}\mathfrak{B}_1 = -\boldsymbol{\Upsilon}_0 \times \partial_t^2 \boldsymbol{\varphi}$.
4. The reduced moment due to the *centrifugal force* $= -\int_{\mathfrak{B}_1} \boldsymbol{r}_1 \times (\boldsymbol{\omega} \times \boldsymbol{\omega} \times (\boldsymbol{r}_1 \rho_0 \mathrm{d}\mathfrak{B}_1))$ $= -\boldsymbol{\omega} \times \boldsymbol{I}_0.\boldsymbol{\omega}$.
5. The reduced moment due to the *Euler force* $= -\int_{\mathfrak{B}_1} \boldsymbol{r}_1 \times (\partial_t \boldsymbol{\omega} \times (\boldsymbol{r}_1 \rho_0 \mathrm{d}\mathfrak{B}_1)) = \boldsymbol{I}_0.\partial_t \boldsymbol{\omega}$.
6. The moment due to the *Coriolis force* is $\boldsymbol{0}$ because $\tilde{\partial}_t \boldsymbol{r}_1 = \boldsymbol{0}$.

It is noteworthy that the *Coriolis force* and the *force of inertia* w.r.t $\{\boldsymbol{d}_i\}$ (and the respective moments) vanishes because we have ignored the *Poisson's* and the *warping effect*. As discussed in *remark 7.3*, if the cross-section is allowed to deform, we will have these two forces (and the respective moments). Secondly, if the locus of mass centroid was considered as the mid-curve, the mass μ_0 would not experience *centrifugal force* and *Euler force*.

7.7.7 Conservation of energy and time invariance

The Hamilton formulation of least action holds if the *impressed forces* are *monogenic* in nature (refer Lanczos [121]). Therefore, work functions for the forces can be defined. The work function need not necessarily be conservative for the applicability of Hamilton's principle. Table

Table 7.1: Forces and their respective work functions

Force	**Work function**
Body force	$W^{\mathrm{b}}_{\mathrm{ext}} = \int_{\Omega_0} \rho_0 (\boldsymbol{u} \cdot \boldsymbol{b})\, \mathrm{d}\Omega_0$
Surface traction	$W^{\mathrm{st}}_{\mathrm{ext}} = \int_0^L \int_{\Gamma_0} (\boldsymbol{u} \cdot (\boldsymbol{S}.\boldsymbol{N}))\ \mathrm{d}\Gamma_0\ \mathrm{d}\xi_1$
Internal stress	$U_{\mathrm{strain}} = \int_{\Omega_0} F_{1ij} S_{ij}\, \mathrm{d}\Omega_0 = \int_{\Omega_0} U\, \mathrm{d}\Omega_0$
Inertial force	$T = \frac{1}{2} \int_{\Omega_0} \rho_0 \partial_t \boldsymbol{R}_1 \cdot \partial_t \boldsymbol{R}_1\, \mathrm{d}\Omega_0 = \frac{1}{2} \int_{\Omega_0} \rho_0 \partial_t \boldsymbol{u} \cdot \partial_t \boldsymbol{u}\, \mathrm{d}\Omega_0$

7.1 lists the work function for all the forces considering the straight beam as the undeformed state. In table 7.1, U represents the strain energy density. Secondly, the work function for external force used in Eq. (7.168) can be written as $W_{\mathrm{ext}} = W^{\mathrm{b}}_{\mathrm{ext}} + W^{\mathrm{st}}_{\mathrm{ext}}$.

We may arrive at the Energy conservation law and the conditions associated with it by considering the real infinitesimal displacement $\mathrm{d}\boldsymbol{u} = \partial_t \boldsymbol{u} \mathrm{d}t$ as the variational field in the Hamilton's equation (7.168). This unique consideration no longer guarantees the virtual displacement at time t_1 and t_2 to vanish. Therefore, for $\delta\boldsymbol{u} \rightarrow d\boldsymbol{u}$, the Hamilton's principle modifies to,

$$\delta A = \delta \int_{t_1}^{t_2} \mathbb{L}\ \mathrm{d}t = \int_{\Omega_0} \rho_0 \Big[\partial_t \boldsymbol{u} \cdot \delta \boldsymbol{u} \Big]_{t=t_1}^{t=t_2} d\Omega_0. \tag{7.187}$$

Using table 7.1, the left hand side of the above equation can be simplified for $\delta\boldsymbol{u} \rightarrow d\boldsymbol{u}$ as,

$$\begin{aligned}
\delta A &= \int_{t_1}^{t_2} \left(\int_{\Omega_0} \left(\rho_0 \partial_t \boldsymbol{u} \cdot \delta \partial_t \boldsymbol{u} - \delta U + \rho_0 \delta \boldsymbol{u} \cdot \boldsymbol{b} \right) \mathrm{d}\Omega_0 + \int_0^L \int_{\Gamma_0} \big(\delta \boldsymbol{u} \cdot (\boldsymbol{S}.\boldsymbol{N}) \big) d\Gamma_0\, d\xi_1 \right) \mathrm{d}t \\
&= \left(\int_{t_1}^{t_2} \int_{\Omega_0} \left(\rho_0 \partial_t \boldsymbol{u} \cdot \partial_t^2 \boldsymbol{u} - dU + \rho_0 \partial_t \boldsymbol{u}.\boldsymbol{b} \right) \mathrm{d}\Omega_0 + \int_0^L \int_{\Gamma_0} \big(\partial_t \boldsymbol{u}.(\boldsymbol{S}.\boldsymbol{N}) \big) d\Gamma_0\, d\xi_1\, \mathrm{d}t \right) \mathrm{d}t \\
&= \left(\int_{t_1}^{t_2} \left(\partial_t T - \partial_t U_{\mathrm{strain}} + \partial_t W^{\mathrm{b}}_{\mathrm{ext}} + \partial_t W^{\mathrm{st}}_{\mathrm{ext}} \right) \mathrm{d}t \right) \mathrm{d}t = \Big[T - U_{\mathrm{strain}} + W_{\mathrm{external}} \Big]_{t_1}^{t_2} \mathrm{d}t.
\end{aligned} \tag{7.188}$$

It was possible to simplify Eq. (7.188) by assuming the traction and body forces to be constant with time. This was done to obtain a simplified form of energy as $(T - U_{\mathrm{strain}} + W_{\mathrm{ext}})$. The second step of (7.188) shows the general energy conservation law. We can evaluate the right hand side of Eq. (7.187) for $\delta\boldsymbol{u} \rightarrow d\boldsymbol{u}$ as,

$$\int_{\Omega_0} \rho_0 \Big[\partial_t \boldsymbol{u} \delta \boldsymbol{u} \Big]_{t=t_1}^{t=t_2} \mathrm{d}\Omega_0 = \Big[\int_{\Omega_0} \rho_0 \partial_t \boldsymbol{u}.\partial_t \boldsymbol{u}\ \mathrm{d}\Omega_0 \Big]_{t=t_1}^{t=t_2} \mathrm{d}t = \Big[2T \Big]_{t=t_1}^{t=t_2} \mathrm{d}t. \tag{7.189}$$

Therefore, from Eqs. (7.187)–(7.189), we have

$$\left[\int_{\Omega_0} \rho_0 \partial_t \boldsymbol{u}.\partial_t \boldsymbol{u}\ \mathrm{d}\Omega_0 - \mathbb{L}\right]_{t=t_1}^{t=t_2} = \left[T - W_{\text{ext}} + U_{\text{strain}}\right]_{t=t_1}^{t=t_2} = 0. \tag{7.190}$$

This implies that the quantity $(T - W_{\text{ext}} + U_{\text{strain}})$ is conserved. This quantity is energy $\mathbb{H}$ (or Hamiltonian). It is clear that the external work W_{ext} adds energy to the system. This energy is used to deform the beam (stored as strain energy U_{strain}) and to bring the motion in the beam (stored as kinetic energy T), implying $W_{\text{ext}} = U_{\text{strain}} + T$. Therefore, a relationship between the Lagrangian and the Hamilton can be established for Continuum problem as,

$$\int_{\Omega_0} \rho_0 \partial_t \boldsymbol{u}.\partial_t \boldsymbol{u}\ \mathrm{d}\Omega_0 - \mathbb{L} = \mathbb{H}. \tag{7.191}$$

The above equation establishes a relationship between the Lagrangian and Hamiltonian functional. It is well known from the classical mechanics of discrete bodies that both the functionals are related by Legendre transformation [121]. The continuum is an infinite degree of freedom system. If we assume the beam to be composed of infinite particle each of mass $m_i = \rho_0 \Delta\Omega_{0_i}$, located by $\boldsymbol{u_i}$, the Lagrangian takes the form,

$$\mathbb{L} = \sum_{i=1}^{\infty} \frac{1}{2} m_i \partial_t \boldsymbol{u}_i.\partial_t \boldsymbol{u}_i - U_{\text{strain}} + W_{\text{ext}}. \tag{7.192}$$

Note that only the kinetic energy is function of velocity. We define the *generalized momentum* of the i^{th} particle as $\boldsymbol{p}_i = (\rho_0 \Delta\Omega_{0_i})\partial_t \boldsymbol{u}_i = \frac{\partial \mathbb{L}}{\partial \partial_t \boldsymbol{u}_i}$. The Legendre transformation applied to the Lagrangian is therefore, written as,

$$\sum_{i=1}^{\infty} \frac{\partial \mathbb{L}}{\partial \partial_t \boldsymbol{u}_i} \cdot \partial_t \boldsymbol{u}_i - \mathbb{L} = \sum_{i=1}^{\infty} \boldsymbol{p}_i \cdot \partial_t \boldsymbol{u}_i - \mathbb{L} = \mathbb{H}. \tag{7.193}$$

For the continuum case,

$$\sum_{i=1}^{\infty} \boldsymbol{p}_i \cdot \partial_t \boldsymbol{u}_i = \lim_{\substack{n\to\infty \\ \Delta\Omega_i^s \to d\Omega_{0_i}}} \sum_{i=1}^{n} \rho_0 \partial_t \boldsymbol{u}_i \cdot \partial_t \boldsymbol{u}_i \Delta\Omega_{0_i} = \int_{\Omega_0} \rho_0 \partial_t \boldsymbol{u} \cdot \partial_t \boldsymbol{u} d\Omega_0. \tag{7.194}$$

Therefore, for continuum case, Eq. (7.193) is same as Eq. (7.191).

We were able to obtain the Energy conservation law from Hamilton's Principle by considering the differential displacement as the virtual displacement. We can choose this special case of variation only if the Lagrangian does not have explicit time dependence. If the Lagrangian has explicit time dependence, then the variation in Lagrangian occurs at a specific time t, whereas the differential change in Lagrangian occurs in a duration of dt. Therefore, for the Energy of the system to be conserved, the system must be *scleronomic* and the forces must be *conservative* in addition to *monogenic*. If the external forces are time-dependent, it would imply the presence of an external source of energy which is not taken into account, leading to the addition of unaccounted energy in the system. The energy conservation arises from the time invariance symmetry of nature. Therefore, our understanding is in accordance with Noether's theorem.

The Hamiltonian structure of the general beam configuration Ω is not as straightforward as the discussion in this section. Therefore, we dedicate the next chapter to exhaustively discuss the Poisson bracket formulation and general Legendre transformation.

7.8 Summary

This chapter details the variational formulation of geometrically-exact Cosserat beams with deforming cross-section. In this regard, the current chapter is a sequel to chapter 4.

To arrive at the virtual work principle, the variation of necessary quantities are evaluated. The attempt to capture fully coupled Poisson's and warping effect (including bending induced non-uniform shear) results in the dependence of deformation map on derivatives of curvature fields (up to second-order). This makes the calculation of variations rather demanding. Detailed calculations of variations of kinematic quantities required to obtain the weak form are performed.

The next part of this chapter deals with deriving the weak equilibrium equation in a form desirable to computationally solve the problem. This beam model has higher regularity requirements as compared to the conventional Simo-Reissner beam. It was expected to obtain

an exactly similar balance of linear momentum, angular momentum, and bi-moment as given in Simo and Vu-Quoc [43]. Despite using an advanced kinematic model, the strong form, when expressed using the first PK stress tensor, does not change.

Finally, the variational formulation and balance laws of the beam with a rigid cross-section (a special case) are discussed in detail.

The discussion carried out in this chapter is planned to be published in a journal titled: "Mathematical theory of a higher-order geometrically-exact beam with a deforming cross-section". The content of section 7.7 is part of a publication in the International Journal of Solids and Structures authored by Mayank Chadha and Michael D. Todd, titled: "An introductory treatise on reduced balance laws of Cosserat beams". The dissertation author is the primary investigator and author of this paper.

Chapter 8

The Poisson Bracket Formulation

8.1 Introduction

This chapter deals with the *Poisson bracket* formulation associated with the beam kinematics discussed in chapter 4. The Poisson bracket formulation constitutes a part of the variational analysis of a mechanical system. In this sense, this chapter is a continuation of the last chapter. Simo et al. [116] details the Hamiltonian structure of general continua, geometrically-exact rods with rigid cross-section, and geometrically-exact shells. We define the Hamiltonian structure of geometrically exact beam with enhanced kinematics and deformable cross-section in terms of the canonical conjugate variables (as is indicated in Marsden and Hughes [60]).

We discuss the cotangent space, phase space and cotangent bundle associated with beam configuration mentioned in Eq. (7.18). We also define the Poisson bracket associated with the cotangent bundle or phase space of the system. Poisson brackets essentially help one study flows on phase space and the *generators* associated with such flows, and they facilitate the development of canonical transformations. Canonically transformed phase space coordinates preserve the Poisson geometry associated with the system or equivalently they preserve the Hamiltonian structure of the system. We obtain the Hamiltonian via Legendre transformation of the Lagrangian.

Finally, the Hamiltonian form of equilibrium equations is obtained.

8.2 The cotangent space, phase space, and cotangent bundle

Recall *remark 4.1* in chapter 4, where we discussed how we got away with making use of one-form and cotangent space associated with $\mathbb{R}^3$ ($T_{\phi(p)}\Omega$ to be specific, for $\phi(p) \in \Omega$) using the concept of the dot product. However, to define phase space associated with the configuration space of the beam, we need to describe the cotangent space $T^*_{\boldsymbol{\Phi}}\mathbb{C}$ (identified with the product space $(\mathbb{R}^3)^* \times T^*_Q SO(3) \times \mathbb{R}^*$) dual to the tangent space $T_{\boldsymbol{\Phi}}\mathbb{C}$.

Consider $\boldsymbol{v}^* = v_i \boldsymbol{E}_i^* \in (\mathbb{R}^3)^*$ and $\boldsymbol{u} = u_i \boldsymbol{E}_i \in \mathbb{R}^3$. Here, $\boldsymbol{E}_i^*$ is the one-form (or covector) associated with the vector $\boldsymbol{E}_i$ such that $\boldsymbol{E}_i^*(\boldsymbol{E}_j) = \boldsymbol{E}_i.\boldsymbol{E}_j = \delta_{ij}$. We define the duality $\langle \cdot | \cdot \rangle_{\mathbb{R}^3} : (\mathbb{R}^3)^* \times \mathbb{R}^3 \longrightarrow \mathbb{R}$ by means of dot product, such that,

$$\langle \boldsymbol{v}^* | \boldsymbol{u} \rangle_{\mathbb{R}^3} = \boldsymbol{v}^*(\boldsymbol{u}) = \boldsymbol{v}.\boldsymbol{u} \tag{8.1}$$

Here, $\boldsymbol{v} = v_i \boldsymbol{E}_i$ is dual to $\boldsymbol{v}^*$. From here on, any quantity with $*$ as super-script represent a covector. Essentially, the duality defined above is an identity metric on the tangent space of $\mathbb{R}^3$. Therefore, we can identify $\left(\mathbb{R}^3\right)^* \equiv \mathbb{R}^3$ via the Euclidean dot product. Similarly, we realize that $\mathbb{R}^* \equiv \mathbb{R}$. However, to avoid confusion, we maintain our nomenclature of using $*$ as super-script representing an element of dual space. Therefore, if $v^* \in \mathbb{R}^*$ (with $v^* = v$) and $u \in \mathbb{R}$, the duality $\langle \cdot | \cdot \rangle_{\mathbb{R}} : \mathbb{R}^* \times \mathbb{R} \longrightarrow \mathbb{R}$ by means of product as,

$$\langle v^* | u \rangle_{\mathbb{R}} = v^*(u) = vu \tag{8.2}$$

We define $so(3)^* \equiv T^*_{\boldsymbol{I}_3} SO(3)$ as the cotangent space to $so(3)$ such that for $\hat{\boldsymbol{A}}^* = \hat{A}_{ij} \boldsymbol{E}_i^* \otimes \boldsymbol{E}_j^* \in so(3)^*$ and $\hat{\boldsymbol{B}} = \hat{B}_{ij} \boldsymbol{E}_i \otimes \boldsymbol{E}_j \in so(3)$, we define the duality $\langle \cdot | \cdot \rangle_{so(3)} : so(3)^* \times so(3) \longrightarrow \mathbb{R}$ as follows,

$$\langle \hat{\boldsymbol{A}}^* | \hat{\boldsymbol{B}} \rangle_{so(3)} = \hat{\boldsymbol{A}}^* \left(\hat{\boldsymbol{B}} \right) = \frac{1}{2} \hat{\boldsymbol{A}} : \hat{\boldsymbol{B}} = \frac{1}{2} \hat{A}_{ij} \hat{B}_{ij} = \boldsymbol{A}.\boldsymbol{B}. \tag{8.3}$$

Here, $\boldsymbol{A} = A_{ij}\boldsymbol{E}_i \otimes \boldsymbol{E}_j \in T_{\boldsymbol{Q}}SO(3)$ is the tangent vector dual to $\boldsymbol{A}^*$. Since $\hat{\boldsymbol{A}}$ and $\hat{\boldsymbol{B}}$ are skew-symmetric, let $\boldsymbol{A}$ and $\boldsymbol{B}$ represent the associated axial vectors. Using the duality defined above, we can rewrite the metric $\|\log(\boldsymbol{Q}(\boldsymbol{\theta}))\|$ defined in Eq. (1.18) as

$$\|\log(\boldsymbol{Q}(\boldsymbol{\theta}))\| = \sqrt{\left\langle \hat{\boldsymbol{\theta}}^* \middle| \hat{\boldsymbol{\theta}} \right\rangle_{so(3)}}. \tag{8.4}$$

Let $\boldsymbol{A}_{\boldsymbol{Q}} = \boldsymbol{Q}.\hat{\boldsymbol{A}} \in T_{\boldsymbol{Q}}SO(3)$ and $\boldsymbol{B}_{\boldsymbol{Q}} = \boldsymbol{Q}.\hat{\boldsymbol{B}} \in T_{\boldsymbol{Q}}SO(3)$ be obtained by left translating the quantities $\hat{\boldsymbol{A}}$ and $\hat{\boldsymbol{B}}$. We note that the quantities $\boldsymbol{A}_{\boldsymbol{Q}}$ and $\boldsymbol{B}_{\boldsymbol{Q}}$ are not skew-symmetric. For the cotangent vector $\boldsymbol{A}^*_{\boldsymbol{Q}} \in T^*_{\boldsymbol{Q}}SO(3)$, dual to the tangent vector $\boldsymbol{A}_{\boldsymbol{Q}}$, we define the duality $\langle\cdot|\cdot\rangle_{T_{\boldsymbol{Q}}SO(3)} : T^*_{\boldsymbol{Q}}SO(3) \times T_{\boldsymbol{Q}}SO(3) \longrightarrow \mathbb{R}$ as,

$$\left\langle \boldsymbol{A}^*_{\boldsymbol{Q}} \middle| \boldsymbol{B}_{\boldsymbol{Q}} \right\rangle_{T_{\boldsymbol{Q}}SO(3)} = \boldsymbol{A}^*_{\boldsymbol{Q}}(\boldsymbol{B}_{\boldsymbol{Q}}) = \frac{1}{2}\boldsymbol{A}_{\boldsymbol{Q}} : \boldsymbol{B}_{\boldsymbol{Q}}. \tag{8.5}$$

We also observe the left-invariant nature of the metric (or duality) discussed in Eq. (8.3) and (8.5) such that

$$\left\langle \boldsymbol{A}^*_{\boldsymbol{Q}} \middle| \boldsymbol{B}_{\boldsymbol{Q}} \right\rangle_{T_{\boldsymbol{Q}}SO(3)} = \left\langle \hat{\boldsymbol{A}}^* \middle| \hat{\boldsymbol{B}} \right\rangle_{so(3)}. \tag{8.6}$$

Similarly, the duality associated with $T^*_{\boldsymbol{\Phi}}\mathbb{C}$ and $T_{\boldsymbol{\Phi}}\mathbb{C}$ is given by:

$$\langle\cdot|\cdot\rangle_{T_{\boldsymbol{\Phi}}\mathbb{C}} = \langle\cdot|\cdot\rangle_{\mathbb{R}^3} + \langle\cdot|\cdot\rangle_{T_{\boldsymbol{Q}}SO(3)} + \langle\cdot|\cdot\rangle_{\mathbb{R}}. \tag{8.7}$$

We note that the dualities discussed above are commutative in the sense that

$$\left\langle \boldsymbol{A}^*_{\boldsymbol{Q}} \middle| \boldsymbol{B}_{\boldsymbol{Q}} \right\rangle_{T_{\boldsymbol{Q}}SO(3)} = \left\langle \boldsymbol{B}^*_{\boldsymbol{Q}} \middle| \boldsymbol{A}_{\boldsymbol{Q}} \right\rangle_{T_{\boldsymbol{Q}}SO(3)} \text{ and } \langle \boldsymbol{v}^* | \boldsymbol{u} \rangle_{\mathbb{R}^3} = \langle \boldsymbol{u}^* | \boldsymbol{v} \rangle_{\mathbb{R}^3}. \tag{8.8}$$

This brings us to the definition of cotangent bundle $T^*\mathbb{C}$ dual to $T^*\mathbb{C}$ associated with the configuration $\mathbb{C}$. For $\tilde{\boldsymbol{\Phi}}^* \in T^*_{\boldsymbol{\Phi}}\mathbb{C}$ and $\boldsymbol{\Phi} \in \mathbb{C}$, we have,

$$T^*\mathbb{C} := \left\{ (\boldsymbol{\Phi}, \tilde{\boldsymbol{\Phi}}^*) | \boldsymbol{\Phi} \in \mathbb{C}, \tilde{\boldsymbol{\Phi}}^* \in T^*_{\boldsymbol{\Phi}}\mathbb{C} \right\}. \tag{8.9}$$

The $T\mathbb{C}$ gives the state space and $T^*\mathbb{C}$ gives the phase space. For simplicity, we assume displacement prescribed boundary and no external force for the analysis in the coming sections.

8.3 The Lagrangian and Hamiltonian

Usually, the Lagrangian is defined as $\mathbb{L} : T\mathbb{C} \longrightarrow \mathbb{R}$. The Hamiltonian $\mathbb{H} : T^*\mathbb{C} \longrightarrow \mathbb{R}$ is obtained by means of Legendre transformation of Lagrangian via the change of variables $(\boldsymbol{\Phi}, \tilde{\boldsymbol{\Phi}}) \mapsto (\boldsymbol{\Phi}, \tilde{\boldsymbol{\Phi}}^*)$. However, the kinematics of the beam at hand not only depends on the configuration space but also on the spatial (with respect to ξ_1) derivatives of $(\boldsymbol{\varphi}, \boldsymbol{Q}, p)$. Therefore, we take a more general approach to obtain Hamiltonian from the Lagrangian. We start with defining the Lagrangian in terms of *passive* and *active* coordinates. The coordinates that takes part in Legendre transformation are called as *active* coordinates (refer to chapter 6 of Lanczos [121]).

Definition 8.1: Let the set $\mathfrak{q}$ and $\mathfrak{a}$ define the field of passive and active variables respectively with $\overline{\mathfrak{q}}$ and $\overline{\mathfrak{a}}$ being their respective material forms. These sets are given by:

$$\begin{aligned}
\mathfrak{q} &= \{\boldsymbol{\varphi}, \boldsymbol{Q},\ p,\ \boldsymbol{\varepsilon},\ \boldsymbol{\kappa},\ \boldsymbol{Q}.\partial_{\xi_1}\overline{\boldsymbol{\varepsilon}},\ \boldsymbol{Q}.\partial_{\xi_1}\overline{\boldsymbol{\kappa}},\ \boldsymbol{Q}.\partial^2_{\xi_1}\overline{\boldsymbol{\kappa}},\ \boldsymbol{Q}.\partial^3_{\xi_1}\overline{\boldsymbol{\kappa}},\ \partial_{\xi_1}p,\ \partial^2_{\xi_1}p\};\\
\overline{\mathfrak{q}} &= \{\boldsymbol{Q}^T.\boldsymbol{\varphi},\ \boldsymbol{I}_3,\ p,\ \overline{\boldsymbol{\varepsilon}},\ \overline{\boldsymbol{\kappa}},\ \partial_{\xi_1}\overline{\boldsymbol{\varepsilon}},\ \partial_{\xi_1}\overline{\boldsymbol{\kappa}},\ \partial^2_{\xi_1}\overline{\boldsymbol{\kappa}},\ \partial^3_{\xi_1}\overline{\boldsymbol{\kappa}},\ \partial_{\xi_1}p,\ \partial^2_{\xi_1}p\};\\
\mathfrak{a} &= \{\partial_t\boldsymbol{\varphi},\ \boldsymbol{\omega},\ \partial_t p,\ \tilde{\partial}_t\boldsymbol{\varepsilon},\ \tilde{\partial}_t\boldsymbol{\kappa},\ \boldsymbol{Q}.\partial_t(\partial_{\xi_1}\overline{\boldsymbol{\kappa}}),\ \boldsymbol{Q}.\partial_t(\partial^2_{\xi_1}\overline{\boldsymbol{\kappa}}),\ \partial_t(\partial_{\xi_1}p)\};\\
\overline{\mathfrak{a}} &= \{\boldsymbol{Q}^T.\partial_t\boldsymbol{\varphi},\ \overline{\boldsymbol{\omega}},\ \partial_t p,\ \partial_t\overline{\boldsymbol{\varepsilon}},\ \partial_t\overline{\boldsymbol{\kappa}},\ \partial_t(\partial_{\xi_1}\overline{\boldsymbol{\kappa}}),\ \partial_t(\partial^2_{\xi_1}\overline{\boldsymbol{\kappa}}),\ \partial_t(\partial_{\xi_1}p)\}.
\end{aligned} \tag{8.10}$$

We note that $(\mathfrak{q}_1, \mathfrak{q}_2, \mathfrak{q}_3) \in \mathbb{C}$ and $(\mathfrak{a}_1, \mathfrak{a}_{2\boldsymbol{Q}}, \mathfrak{a}_3) \in T_{\boldsymbol{\Phi}}\mathbb{C}$, where $\mathfrak{a}_{2\boldsymbol{Q}} = \hat{\mathfrak{a}}_2.\boldsymbol{Q}$. Finally, we define $\hat{\overline{\mathfrak{a}}}_2 = \boldsymbol{Q}^T.\hat{\mathfrak{a}}_2.\boldsymbol{Q}$.

Definition 8.2: The Lagrangian $\mathbb{L} : (\mathfrak{q}; \mathfrak{a}) \mapsto \mathbb{R}$ associated with the beam is defined as

$$\mathbb{L} = \mathrm{T}(\mathfrak{a}) - \mathrm{U}_{\mathrm{strain}}(\mathfrak{q}). \tag{8.11}$$

Here, T and $\mathrm{U}_{\mathrm{strain}}$ gives the kinetic energy and strain energy stored in the system respectively. T can be obtained using the result (7.107) as

$$\mathrm{T} = \int_{\Omega_0} \rho_0 \partial_t\boldsymbol{R}.\partial_t\boldsymbol{R}\ \mathrm{d}\Omega_0 = \frac{1}{2}\int_0^L \sum_{i=1}^{8} \mathfrak{a}_i.(\mathbb{I}_i\mathfrak{a}_i)\ \mathrm{d}\xi_1 = \frac{1}{2}\int_0^L \sum_{i=1}^{8} \overline{\mathfrak{a}}_i.(\overline{\mathbb{I}}_i\overline{\mathfrak{a}}_i)\ \mathrm{d}\xi_1. \tag{8.12}$$

Here,

$$\mathbb{I}_1 = \int_{\mathfrak{B}_0} \rho_0 \, \mathrm{d}\mathfrak{B}_0; \tag{8.13a}$$

$$\mathbb{I}_2 = \int_{\mathfrak{B}_0} \rho_0 \hat{\boldsymbol{r}}^T.\hat{\boldsymbol{r}} \, \mathrm{d}\mathfrak{B}_0; \tag{8.13b}$$

$$\mathbb{I}_3 = \int_{\mathfrak{B}_0} \rho_0 \boldsymbol{L}^{\boldsymbol{\lambda}_1}_{\partial_{\xi_1} p}.\boldsymbol{L}^{\boldsymbol{\lambda}_1}_{\partial_{\xi_1} p} \, \mathrm{d}\mathfrak{B}_0; \tag{8.13c}$$

$$\mathbb{I}_4 = \int_{\mathfrak{B}_0} \rho_0 (\boldsymbol{L}^{\boldsymbol{\lambda}_1}_{\partial_{\xi_1} \boldsymbol{\varepsilon}})^T.\boldsymbol{L}^{\boldsymbol{\lambda}_1}_{\partial_{\xi_1} \boldsymbol{\varepsilon}} \, \mathrm{d}\mathfrak{B}_0; \tag{8.13d}$$

$$\mathbb{I}_5 = \int_{\mathfrak{B}_0} \rho_0 (\boldsymbol{L}^{\boldsymbol{\lambda}_1}_{\partial_{\xi_1} \boldsymbol{\kappa}})^T.\boldsymbol{L}^{\boldsymbol{\lambda}_1}_{\partial_{\xi_1} \boldsymbol{\kappa}} \, \mathrm{d}\mathfrak{B}_0; \tag{8.13e}$$

$$\mathbb{I}_6 = \int_{\mathfrak{B}_0} \rho_0 (\boldsymbol{L}^{\boldsymbol{\lambda}_1}_{\partial^2_{\xi_1} \boldsymbol{\kappa}})^T.\boldsymbol{L}^{\boldsymbol{\lambda}_1}_{\partial^2_{\xi_1} \boldsymbol{\kappa}} \, \mathrm{d}\mathfrak{B}_0; \tag{8.13f}$$

$$\mathbb{I}_7 = \int_{\mathfrak{B}_0} \rho_0 (\boldsymbol{L}^{\boldsymbol{\lambda}_1}_{\partial^3_{\xi_1} \boldsymbol{\kappa}})^T.\boldsymbol{L}^{\boldsymbol{\lambda}_1}_{\partial^3_{\xi_1} \boldsymbol{\kappa}} \, \mathrm{d}\mathfrak{B}_0; \tag{8.13g}$$

$$\mathbb{I}_8 = \int_{\mathfrak{B}_0} \rho_0 \boldsymbol{L}^{\boldsymbol{\lambda}_1}_{\partial^2_{\xi_1} p}.\boldsymbol{L}^{\boldsymbol{\lambda}_1}_{\partial^2_{\xi_1} p} \, \mathrm{d}\mathfrak{B}_0. \tag{8.13h}$$

Define the material quantity $\bar{\mathbb{I}}_i = \boldsymbol{Q}^T.\mathbb{I}_i.\boldsymbol{Q}$. For $i \in \{1, 3, 8\}$, we have $\bar{\mathbb{I}}_i = \mathbb{I}_i$. Also observe that $\bar{\mathbb{I}}_2$ is dependent on $(p, \overline{\varepsilon}_1, \overline{\boldsymbol{\kappa}}, \partial_{\xi_1}\overline{\boldsymbol{\kappa}}, \partial^2_{\xi_1}\overline{\boldsymbol{\kappa}})$. For ρ_0 = constant, we have

$$\mathbb{I}_1 = \rho_0 \int_{\mathfrak{B}_0} \mathrm{d}\mathfrak{B}_0 = \rho_0 A, \text{ where } A = \text{Area of cross section } \mathfrak{B}_0; \tag{8.14a}$$

$$\mathbb{I}_2 = \rho_0 \int_{\mathfrak{B}_0} \hat{\boldsymbol{r}}^T.\hat{\boldsymbol{r}} \, \mathrm{d}\mathfrak{B}_0 = \rho_0 \boldsymbol{I}, \text{ where } \boldsymbol{I} = \text{spatial moment of inertia matrix ;} \tag{8.14b}$$

$$\mathbb{I}_3 = \rho_0 \int_{\mathfrak{B}_0} \Psi_1^2 \, \mathrm{d}\mathfrak{B}_0 = \rho_0 \Xi, \text{ where } \Xi = \text{warping constant of Vlasov.} \tag{8.14c}$$

The strong form of equations obtained in section 7.6 can be obtained by stationarizing the action provided $\delta\boldsymbol{u}(t_1) = \delta\boldsymbol{u}(t_2) = 0$, such that (refer section 6 of Chadha and Todd [53])

$$\delta \int_{t_1}^{t_2} \mathbb{L} \, \mathrm{d}t = 0. \tag{8.15}$$

To obtain canonical coordinates using Legendre transformation, we assume each $\mathfrak{a}_i$ as independent quantities and we note the following result that can be easily proved using the chain rule.

Proposition 8.1: For a function of form $g(\mathfrak{a}_i) = \overline{g}(\boldsymbol{Q}.\overline{\mathfrak{a}}_i)$ for $i \in \{1,2,4,5,6,7\}$ and a function of form $f(\mathfrak{a}_{2\boldsymbol{Q}}) = \overline{f}(\hat{\overline{\mathfrak{a}}}_2)$, the following are true:

$$\frac{\partial g}{\partial \mathfrak{a}_i} = \boldsymbol{Q}.\frac{\partial \overline{g}}{\partial \overline{\mathfrak{a}}_i}; \tag{8.16a}$$

$$\frac{\partial f}{\partial \mathfrak{a}_{2\boldsymbol{Q}}} = \boldsymbol{Q}.\frac{\partial \overline{f}}{\partial \hat{\overline{\mathfrak{a}}}_2}. \tag{8.16b}$$

Definition 8.3: Define the set $\mathfrak{p}$ of canonical momentum coordinates corresponding to the active variable set $\mathfrak{a}$ obtained by Legendre transformation $\mathbb{F}$ as,

$$\mathbb{F}\mathbb{L}(\mathfrak{a}_i) = \mathfrak{p}_i = \partial_{\xi_1}\frac{\partial \mathbb{L}}{\partial \mathfrak{a}_i} \tag{8.17}$$

Using the fact that $\bar{\mathbb{I}}_i$ is symmetric, and the result in *proposition 8.1*, we get $\mathfrak{p}_i = \mathbb{I}_i\mathfrak{a}_i$ (Einstein summation is suppressed). Let $\overline{\mathfrak{p}}$ represent the material form of canonical momentum coordinates. We note that the kinetic energy depends on the first component of $\partial_t\overline{\boldsymbol{\varepsilon}}$ and on the second and third components of $\partial_t\overline{\boldsymbol{\kappa}}, \partial_t(\partial_{\xi_1}\overline{\boldsymbol{\kappa}})$ and, $\partial_t(\partial^2_{\xi_1}\overline{\boldsymbol{\kappa}})$. We assume that the canonical momentum coordinate for all the zero active coordinates (for example, $\partial_t\overline{\kappa}_1 = 0$) is zero, for example $\overline{\mathfrak{p}}_4 = (\bar{\mathbb{I}}_{4_{11}}\partial_t\overline{\varepsilon}_1, 0, 0)^T$ and $\mathfrak{p}_4 = \boldsymbol{Q}.(\bar{\mathbb{I}}_{4_{11}}\partial_t\overline{\varepsilon}_1, 0, 0)^T$. As such, the non-zero active coordinates can then be uniquely defined as a function of their corresponding canonical coordinate and vice-versa. This is equivalent to the fact that if the active coordinate consists of non-zero terms only, then the determinant of Hessian of the Lagrangian with respect to the active coordinate is non-zero. Using the result (8.16b), we get the following:

$$\begin{gathered}\frac{\partial \overline{f}}{\partial \overline{\mathfrak{a}}_2} = (\bar{\mathbb{I}}_2\overline{\boldsymbol{\omega}}) \implies \frac{\partial \overline{f}}{\partial \hat{\overline{\mathfrak{a}}}_2} = \widehat{(\bar{\mathbb{I}}_2\overline{\boldsymbol{\omega}})}; \\ \mathfrak{p}_{2\boldsymbol{Q}} = \frac{\partial \mathbb{L}}{\partial \mathfrak{a}_{2\boldsymbol{Q}}} = \boldsymbol{Q}.\widehat{(\bar{\mathbb{I}}_2\overline{\boldsymbol{\omega}})}.\end{gathered} \tag{8.18}$$

Definition 8.4: The Hamiltonian $\mathbb{H} : (\mathfrak{q}, \mathfrak{p}^*) \mapsto \mathbb{R}$ is defined in terms of canonical coordinates as

$$\mathbb{H} = \int_0^L \sum_{i=1}^{8} \mathfrak{p}_i.\mathfrak{a}_i \, \mathrm{d}\xi_1 - \mathbb{L} = \int_0^L H(\mathfrak{q}, \mathfrak{p}) \, \mathrm{d}\xi_1 = \mathrm{T}(\mathfrak{p}) + \mathrm{U}_{\mathrm{strain}}(\mathfrak{q}) = \text{Total energy}. \tag{8.19}$$

Here $H(\mathfrak{q}, \mathfrak{p})$ is energy per unit arc length or energy density.

Definition 8.5: Define the inverse Legendre transformation $\mathbb{F}^{-1}$ as

$$\mathbb{F}^{-1}\mathbb{H}(\mathfrak{p}_i) = \mathfrak{a}_i = \partial_{\xi_1}\frac{\partial \mathbb{H}}{\partial \mathfrak{p}_i} = \frac{\partial H}{\partial \mathfrak{p}_i}. \tag{8.20}$$

8.4 Canonical bracket

Poisson brackets are defined on phase space. The definition of Poisson's bracket consist of mix of *partial derivatives of functional* of form $f(\mathfrak{q}; \mathfrak{p})$ (example of such function is Hamiltonian) with respect to parameters defining configuration space $(\boldsymbol{\varphi}, \boldsymbol{Q}, p) \equiv (\mathfrak{q}_1, \mathfrak{q}_2, \mathfrak{q}_3)$ and parameters defining cotangent space $(\mathfrak{p}_1, \mathfrak{p}_{2\boldsymbol{Q}}, \mathfrak{p}_3)$. Therefore, in order to state Poisson bracket on $T^*\mathbb{C}$, we first define *partial functional derivatives* of such functional (we consider Hamiltonian as the functional of interest). Refer to appendix A of Engel et al. [122] for detailed discussion on funtional derivatives.

Definition 8.6: The varied passive and canonical variables is defined as $\mathfrak{q}_{i\epsilon} = \mathfrak{q}_i + \epsilon\delta\mathfrak{q}_i$ and $\mathfrak{p}_{i\epsilon} = \mathfrak{p}_i + \epsilon\delta\mathfrak{p}_i$. We have $\mathfrak{q}_\epsilon = \{\mathfrak{q}_{i\epsilon}\}$ and $\mathfrak{p}_\epsilon = \{\mathfrak{p}_{i\epsilon}\}$ such that $\mathfrak{p}_{2\boldsymbol{Q}\epsilon} = \boldsymbol{Q}.\hat{\mathfrak{p}}_{2\epsilon} = \boldsymbol{Q}.\widehat{(\boldsymbol{Q}^T.\mathfrak{p}_{2\epsilon})}$.

Definition 8.7: For a pure displacement boundary, following are the partial functional derivative $\frac{\delta H}{\delta \mathfrak{p}_i}$ of Hamiltonian (density) $H(\mathfrak{q}; \mathfrak{p})$ with respect to parameters defining cotangent space $(\mathfrak{p}_1, \mathfrak{p}_{2\boldsymbol{Q}}, \mathfrak{p}_3)$ as:

$$\frac{\mathrm{d}}{\mathrm{d}\epsilon}\mathbb{H}(\mathfrak{q}; (\mathfrak{p}_{1\epsilon}, \mathfrak{p}_i))\bigg|_{\epsilon=0} = \int_0^L \left\langle \frac{\delta H}{\delta \mathfrak{p}_1}^* \middle| \delta\mathfrak{p}_1 \right\rangle_{\mathbb{R}^3} \mathrm{d}\xi_1 = \int_0^L \frac{\delta H}{\delta \mathfrak{p}_1}.\delta\mathfrak{p}_1 \, \mathrm{d}\xi_1 \tag{8.21a}$$

$$\frac{\mathrm{d}}{\mathrm{d}\epsilon}\mathbb{H}(\mathfrak{q}; (\mathfrak{p}_{2\boldsymbol{Q}\epsilon}, \mathfrak{p}_i))\bigg|_{\epsilon=0} = \int_0^L \left\langle \frac{\delta H}{\delta \mathfrak{p}_{2\boldsymbol{Q}}}^* \middle| \delta\mathfrak{p}_{2\boldsymbol{Q}} \right\rangle_{T_{\boldsymbol{Q}}SO(3)} \mathrm{d}\xi_1 = \frac{1}{2}\int_0^L \frac{\delta H}{\delta \mathfrak{p}_{2\boldsymbol{Q}}} : \delta\mathfrak{p}_{2\boldsymbol{Q}} \, \mathrm{d}\xi_1 \tag{8.21b}$$

$$\frac{\mathrm{d}}{\mathrm{d}\epsilon}\mathbb{H}(\mathfrak{q}; (\mathfrak{p}_{3\epsilon}, \mathfrak{p}_i))\bigg|_{\epsilon=0} = \int_0^L \left\langle \frac{\delta H}{\delta \mathfrak{p}_3}^* \middle| \delta\mathfrak{p}_3 \right\rangle_{\mathbb{R}} \mathrm{d}\xi_1 = \int_0^L \frac{\delta H}{\delta \mathfrak{p}_3}.\delta\mathfrak{p}_3 \, \mathrm{d}\xi_1 \tag{8.21c}$$

Like the result in Eq. (8.16b), we have:

$$\frac{\delta H}{\delta \mathfrak{p}_2 \boldsymbol{Q}} = \boldsymbol{Q}.\frac{\partial H}{\partial \hat{\bar{\mathfrak{p}}}_2}. \tag{8.22}$$

Remark 8.1: This result holds because, $\mathfrak{p}_i$ for $i \neq 2$ does not have any functional dependence on $\mathfrak{p}_2$. However, the elements of $\mathfrak{q}$ and $\mathfrak{p}$ do have dependence on the spatial and time derivatives of $(\mathfrak{q}_1, \mathfrak{q}_2, \mathfrak{q}_3)$. To define partial functional derivatives of H with respect to $(\mathfrak{q}_1, \mathfrak{q}_2, \mathfrak{q}_3)$, we treat the pairs $(\mathfrak{q}_1, \mathfrak{p}_1)$, $(\mathfrak{q}_2, \mathfrak{p}_2\boldsymbol{Q})$ and $(\mathfrak{q}_3, \mathfrak{p}_3)$ as independent quantities. This is crucial as it allows us to operate on cotangent bundle. As a result, even though, for example, $\partial_t \boldsymbol{\varphi}$ is functionally dependent on $\boldsymbol{\varphi}$, the corresponding canonical quantity $\mathfrak{p}_1$ is considered to be independent of $\boldsymbol{\varphi}$. On the other hand, the direct dependence of $\mathfrak{p}_2$ on $\mathfrak{q}_3$ is consider while evaluating $\frac{\delta H}{\delta p}$. We also note that since $(\mathfrak{q}_1, \mathfrak{q}_2, \mathfrak{q}_3)$ defines the configuration space, we do not consider $\mathfrak{p}_i$ for $i > 3$ to be functionally independent on the configuration space. As was pointed in section 3 of Simo et al. [116], defining the functional derivative of $H(\mathfrak{q}; \mathfrak{p})$ with respect to parameters on configuration space requires some caution. This is because the cotangent bundle is not a simple product space. Accordingly definition 5 can be written as:

$$\mathbb{F}^{-1}\mathbb{H}(\mathfrak{p}_i) = \mathfrak{a}_i = \frac{\delta H}{\delta \mathfrak{p}_i} \tag{8.23}$$

Definition 8.8: For a change $\mathfrak{q}_i \mapsto \mathfrak{q}_{i\epsilon} = \mathfrak{q}_i + \epsilon\delta\mathfrak{q}_i$ (with $i \in 1, 2, 3$), let $\mathfrak{p}_{(\mathfrak{q}_{i\epsilon})} = \{\mathfrak{p}_{j(\mathfrak{q}_{i\epsilon})}\}$ and $\mathfrak{q}_{j(\mathfrak{q}_{i\epsilon})}$ (for $j \neq 1, 2, 3$) define the associated canonical and passive quantities respectively.

Definition 8.9: For a pure displacement boundary, the partial functional derivatives $\frac{\delta H}{\delta \mathfrak{q}_i}$ of Hamiltonian density $H(\mathfrak{q}; \mathfrak{p})$ with respect to parameters defining cotangent space $(\mathfrak{q}_1, \mathfrak{q}_2, \mathfrak{q}_3)$ are given as:

$$\frac{\mathrm{d}}{\mathrm{d}\epsilon}\mathbb{H}((\mathfrak{q}_{1\epsilon}, \mathfrak{q}_{i(\mathfrak{q}_{1\epsilon})}); \mathfrak{p}_{(\mathfrak{q}_{1\epsilon})})\bigg|_{\epsilon=0} = \int_0^L \left\langle \frac{\delta H}{\delta \mathfrak{q}_1}^* \middle| \delta\mathfrak{q}_1 \right\rangle_{\mathbb{R}^3} \mathrm{d}\xi_1 = \int_0^L \frac{\delta H}{\delta \boldsymbol{\varphi}}.\delta\boldsymbol{\varphi}\ \mathrm{d}\xi_1 \tag{8.24a}$$

$$\frac{\mathrm{d}}{\mathrm{d}\epsilon}\mathbb{H}((\mathfrak{q}_{2\epsilon}, \mathfrak{q}_{i(\mathfrak{q}_{2\epsilon})}); \mathfrak{p}_{(\mathfrak{q}_{2\epsilon})})\bigg|_{\epsilon=0} = \int_0^L \left\langle \frac{\delta H}{\delta \mathfrak{q}_2}^* \middle| \delta\mathfrak{q}_2 \right\rangle_{T_{\boldsymbol{Q}}SO(3)} \mathrm{d}\xi_1 = \frac{1}{2}\int_0^L \frac{\delta H}{\delta \boldsymbol{Q}} : \delta\boldsymbol{Q}\ \mathrm{d}\xi_1 \tag{8.24b}$$

$$\frac{\mathrm{d}}{\mathrm{d}\epsilon}\mathbb{H}((\mathfrak{q}_{3\epsilon}, \mathfrak{q}_{i(\mathfrak{q}_{3\epsilon})}); \mathfrak{p}_{(\mathfrak{q}_{2\epsilon})})\bigg|_{\epsilon=0} = \int_0^L \left\langle \frac{\delta H^*}{\delta \mathfrak{q}_3} \middle| \delta\mathfrak{q}_3 \right\rangle_{\mathbb{R}} \mathrm{d}\xi_1 = \int_0^L \frac{\delta H}{\delta p}.\delta p \, \mathrm{d}\xi_1. \tag{8.24c}$$

Proposition 8.2: The following holds:

$$\frac{\mathrm{d}\mathfrak{p}_1}{\mathrm{d}t} = \mathfrak{F}_{\boldsymbol{\varphi}} \tag{8.25a}$$

$$\frac{\mathrm{d}\mathfrak{p}_2}{\mathrm{d}t} = \mathfrak{F}_{\boldsymbol{\alpha}} \tag{8.25b}$$

$$\frac{\mathrm{d}\mathfrak{p}_3}{\mathrm{d}t} = \frac{\mathrm{d}^2 p}{\mathrm{d}t^2}.\int_{\mathfrak{B}_0} \rho_0 \Psi_1^2 \, \mathrm{d}\mathfrak{B}_0 = \mathbb{I}_3 \frac{\mathrm{d}^2 p}{\mathrm{d}t^2} = \mathfrak{F}_{p1}. \tag{8.25c}$$

Proof: Proof of *proposition 8.2* follows from a straightforward calculation and application of chain rule. We leave proving (8.25a) and (8.25c) to the readers. Realizing $\tilde{\partial}_t \mathbb{I}_2 = \mathbf{0}_3$ and $\tilde{\partial}_t \boldsymbol{\omega} = \frac{\mathrm{d}\boldsymbol{\omega}}{\mathrm{d}t} - \boldsymbol{\omega} \times \boldsymbol{\omega} = \frac{\mathrm{d}\boldsymbol{\omega}}{\mathrm{d}t}$, we can prove the result (8.25b) as

$$\frac{\mathrm{d}\mathfrak{p}_2}{\mathrm{d}t} = \frac{\mathrm{d}\mathbb{I}_2.\boldsymbol{\omega}}{\mathrm{d}t} = \tilde{\partial}_t(\mathbb{I}_2.\boldsymbol{\omega}) + \boldsymbol{\omega} \times \mathbb{I}_2.\boldsymbol{\omega} = \mathbb{I}_2.\frac{\mathrm{d}\boldsymbol{\omega}}{\mathrm{d}t} + \boldsymbol{\omega} \times \mathbb{I}_2.\boldsymbol{\omega} = \mathfrak{F}_{\boldsymbol{\alpha}}. \tag{8.26}$$

Hence proved. □

Proposition 8.4: With the definition of Hamiltonian and its partial functional derivatives in equation set (8.19) and (8.24) respectively, the following holds true:

$$\frac{\delta H}{\delta \mathfrak{q}_1} = -(\mathfrak{E}_{\boldsymbol{\varphi}} + \mathfrak{F}_{\boldsymbol{\varphi}}) \tag{8.27a}$$

$$\frac{\delta H}{\delta \mathfrak{q}_{2\boldsymbol{Q}}} = -\boldsymbol{Q}.(\hat{\mathfrak{E}}_{\boldsymbol{\alpha}} + \hat{\mathfrak{F}}_{\boldsymbol{\alpha}}), \text{ where } \hat{\mathfrak{E}}_{\boldsymbol{\alpha}} = \widehat{\boldsymbol{Q}^T.\mathfrak{E}_{\boldsymbol{\alpha}}} \text{ and } \hat{\mathfrak{F}}_{\boldsymbol{\alpha}} = \widehat{\boldsymbol{Q}^T.\mathfrak{F}_{\boldsymbol{\alpha}}} \tag{8.27b}$$

$$\frac{\delta H}{\delta \mathfrak{q}_3} = -(\mathfrak{E}_p + \mathfrak{F}_p) \tag{8.27c}$$

$$\frac{\delta H}{\delta \mathfrak{q}_2} = -(\mathfrak{E}_{\boldsymbol{\alpha}} + \mathfrak{F}_{\boldsymbol{\alpha}}) \tag{8.27d}$$

Proof: Recall *remark 8.1*, that stated the need to consider $(\mathfrak{q}_i, \mathfrak{p}_i)$ as independent quantities while considering partial functional derivative of H with respect to $\mathfrak{q}_1, \mathfrak{q}_{2\boldsymbol{Q}}, \mathfrak{q}_3$. Keeping that in mind, for the curve $\epsilon : \boldsymbol{\Phi} \mapsto \boldsymbol{\Phi} + \epsilon\delta\boldsymbol{\Phi}$ (keeping the respective canonical coordinates fixed), the variation of

Hamiltonian in the direction of $\delta\mathbf{\Phi}$ is given as,

$$\delta\mathbb{H}|_{(\{\mathfrak{p}_1,\mathfrak{p}_{2\boldsymbol{Q}},\mathfrak{p}_3\}=\text{fixed})} = \int_0^L \left\langle \frac{\delta H^*}{\delta \mathfrak{q}_1} \middle| \delta\mathfrak{q}_1 \right\rangle_{\mathbb{R}^3} + \left\langle \frac{\delta H^*}{\delta \mathfrak{q}_2} \middle| \delta\mathfrak{q}_2 \right\rangle_{T_{\boldsymbol{Q}}SO(3)} + \left\langle \frac{\delta H^*}{\delta \mathfrak{q}_3} \middle| \delta\mathfrak{q}_3 \right\rangle_{\mathbb{R}} \mathrm{d}\xi_1. \tag{8.28}$$

Since strain energy does not have any dependence on the canonical quantities $\mathfrak{p}$, we have

$$\begin{aligned}
\delta\mathrm{U}_{\text{strain}}|_{(\{\mathfrak{p}_1,\mathfrak{p}_{2\boldsymbol{Q}},\mathfrak{p}_3\}=\text{fixed})} = \delta\mathrm{U}_{\text{strain}} &= \int_0^L \partial_{\xi_1}\big(- \mathfrak{N}_{\boldsymbol{\varepsilon}} + \tilde{\partial}_{\xi_1}\mathfrak{N}_{\partial_{\xi_1}\boldsymbol{\varepsilon}}\big)\cdot\delta\boldsymbol{\varphi}\ \mathrm{d}\xi_1 \\
&+ \int_0^L \big(\mathfrak{N}_p - \partial_{\xi_1}\mathfrak{N}_{\partial_{\xi_1}p} + \partial^2_{\xi_1}\mathfrak{N}_{\partial^2_{\xi_1}p}\big).\delta p\ \mathrm{d}\xi_1 \\
&+ \int_0^L \left(\partial_{\xi_1}\big(- \mathfrak{N}_{\boldsymbol{\kappa}} + \tilde{\partial}_{\xi_1}\mathfrak{N}_{\partial_{\xi_1}\boldsymbol{\kappa}} - \tilde{\partial}^2_{\xi_1}\mathfrak{N}_{\partial^2_{\xi_1}\boldsymbol{\kappa}} + \tilde{\partial}^3_{\xi_1}\mathfrak{N}_{\partial^3_{\xi_1}\boldsymbol{\kappa}}\big) - \partial_{\xi_1}\hat{\boldsymbol{\varphi}}.\big(\mathfrak{N}_{\boldsymbol{\varepsilon}} - \tilde{\partial}_{\xi_1}\mathfrak{N}_{\partial_{\xi_1}\boldsymbol{\varepsilon}}\big)\right)\cdot\delta\boldsymbol{\alpha}\ \mathrm{d}\xi_1.
\end{aligned} \tag{8.29}$$

Substituting for the expression of velocity vector in Eq. (7.107) into Eq. (8.12) and carrying out integration by parts yields

$$\begin{aligned}
\delta\mathrm{T} = \int_0^L \Big(\delta\boldsymbol{\varphi}\cdot\big(- \mathfrak{F}_{\boldsymbol{\varphi}} - \partial_{\xi_1}\mathfrak{F}_{\boldsymbol{\varepsilon}}\big) + \delta p.\big(- \mathfrak{F}_p - \partial_{\xi_1}\mathfrak{F}_{\partial_{\xi_1}p}\big) \\
\delta\boldsymbol{\alpha}\cdot\big(- \mathfrak{F}_{\boldsymbol{\alpha}} - \partial_{\xi_1}\hat{\boldsymbol{\varphi}}.\mathfrak{F}_{\boldsymbol{\varepsilon}} - \partial_{\xi_1}(\mathfrak{F}_{\boldsymbol{\kappa}} - \tilde{\partial}_{\xi_1}\mathfrak{F}_{\partial_{\xi_1}\boldsymbol{\kappa}} + \tilde{\partial}^2_{\xi_1}\mathfrak{F}_{\partial^2_{\xi_1}\boldsymbol{\kappa}})\big)\Big)\ \mathrm{d}\xi_1.
\end{aligned} \tag{8.30}$$

However, the terms $-\int_0^L \left(\delta\boldsymbol{\varphi}.\mathfrak{F}_{\boldsymbol{\varphi}} + \delta\boldsymbol{\alpha}.\mathfrak{F}_{\boldsymbol{\alpha}} + \delta p.\mathfrak{F}_p\right)\ \mathrm{d}\xi_1$ are obtained by considering the terms $\partial_t\boldsymbol{\varphi} = \mathfrak{a}_1 = \mathbb{I}_1^{-1}\mathfrak{p}_1$, $\boldsymbol{\omega} = \mathfrak{a}_2 = \mathbb{I}_2^{-1}\mathfrak{p}_2$ and $\partial_t p = \mathfrak{a}_3 = \mathbb{I}_3^{-1}\mathfrak{p}_3$ to be functionally dependent on the configuration space. Therefore, we can obtain $\delta\mathrm{T}|_{(\{\mathfrak{p}_1,\mathfrak{p}_{2\boldsymbol{Q}},\mathfrak{p}_3\}=\text{fixed})}$ by ignoring these terms, yielding

$$\begin{aligned}
\delta\mathrm{T}|_{(\{\mathfrak{p}_1,\mathfrak{p}_{2\boldsymbol{Q}},\mathfrak{p}_3\}=\text{fixed})} = \int_0^L \delta\boldsymbol{\varphi}\Big(- \partial_{\xi_1}\mathfrak{F}_{\boldsymbol{\varepsilon}}\Big) + \delta p.\big(- \mathfrak{F}_p + \mathfrak{F}_{p1} - \partial_{\xi_1}\mathfrak{F}_{\partial_{\xi_1}p}\big) \\
\delta\boldsymbol{\alpha}.\big(- \partial_{\xi_1}\hat{\boldsymbol{\varphi}}.\mathfrak{F}_{\boldsymbol{\varepsilon}} - \partial_{\xi_1}(\mathfrak{F}_{\boldsymbol{\kappa}} - \tilde{\partial}_{\xi_1}\mathfrak{F}_{\partial_{\xi_1}\boldsymbol{\kappa}} + \tilde{\partial}^2_{\xi_1}\mathfrak{F}_{\partial^2_{\xi_1}\boldsymbol{\kappa}})\big)\Big)\ \mathrm{d}\xi_1.
\end{aligned} \tag{8.31}$$

From the definition of Hamiltonian in Eq. (8.19), we have

$$\delta\mathbb{H}|_{(\{\mathfrak{p}_1,\mathfrak{p}_{2\boldsymbol{Q}},\mathfrak{p}_3\}=\text{fixed})} = \delta\mathrm{T}|_{(\{\mathfrak{p}_1,\mathfrak{p}_{2\boldsymbol{Q}},\mathfrak{p}_3\}=\text{fixed})} + \delta\mathrm{U}_{\text{strain}}|_{(\{\mathfrak{p}_1,\mathfrak{p}_{2\boldsymbol{Q}},\mathfrak{p}_3\}=\text{fixed})}. \tag{8.32}$$

We use the expression of $\delta\mathrm{U}_{\text{strain}}$ Eq. (7.97) and the results in Eq. set (7.105) to obtain:

$$\delta\mathbb{H}|_{(\{\mathfrak{p}_1,\mathfrak{p}_{2\boldsymbol{Q}},\mathfrak{p}_3\}=\text{fixed})} = -\int_0^L (\mathfrak{E}_{\boldsymbol{\varphi}} + \mathfrak{F}_{\boldsymbol{\varphi}}).\delta\boldsymbol{\alpha} + (\mathfrak{E}_{\boldsymbol{\alpha}} + \mathfrak{F}_{\boldsymbol{\alpha}}).\delta\boldsymbol{\alpha} + (\mathfrak{E}_p + \mathfrak{F}_{p1}).\delta p\ \mathrm{d}\xi_1 \tag{8.33}$$

Eq. (8.28) and (8.32) proves the results (8.27a) and (8.27c). To prove (8.27b), we consider

$$(\mathfrak{E}_\alpha + \mathfrak{F}_\alpha).\delta\boldsymbol{\alpha} = (\overline{\mathfrak{E}}_\alpha + \overline{\mathfrak{F}}_\alpha).\delta\overline{\boldsymbol{\alpha}} = (\hat{\overline{\mathfrak{E}}}_\alpha + \hat{\overline{\mathfrak{F}}}_\alpha).\delta\hat{\overline{\boldsymbol{\alpha}}} = \left\langle \boldsymbol{Q}.(\hat{\overline{\mathfrak{E}}}_\alpha + \hat{\overline{\mathfrak{F}}}_\alpha) \middle| \delta\boldsymbol{Q} \right\rangle_{T_{\boldsymbol{Q}}SO(3)} \tag{8.34}$$

This proves the result (8.27b). Using chain rule, like Eq. (8.22), we have

$$\frac{\delta H}{\delta \mathfrak{p}_{2\boldsymbol{Q}}} = \boldsymbol{Q}.\frac{\delta H}{\delta \hat{\overline{\mathfrak{p}}}_2}; \tag{8.35a}$$

$$\frac{\delta H}{\delta \mathfrak{p}_2} = \boldsymbol{Q}.\frac{\delta H}{\delta \overline{\mathfrak{p}}_2}. \tag{8.35b}$$

Since $\hat{\overline{\mathfrak{p}}}_2 \in so(3)$, we realize that $\frac{\delta H}{\delta \hat{\overline{\mathfrak{p}}}_2} = \widehat{\left(\frac{\delta H}{\delta \overline{\mathfrak{p}}_2}\right)}$. Using the result obtained above and in (8.27b), we have:

$$\frac{\delta H}{\delta \hat{\overline{\mathfrak{p}}}_2} = (\hat{\overline{\mathfrak{E}}}_\alpha + \hat{\overline{\mathfrak{F}}}_\alpha) \implies \frac{\delta H}{\delta \overline{\mathfrak{p}}_2} = -(\overline{\mathfrak{E}}_\alpha + \overline{\mathfrak{F}}_\alpha) \implies \frac{\delta H}{\delta \mathfrak{p}_2} = -(\mathfrak{E}_\alpha + \mathfrak{F}_\alpha). \tag{8.36}$$

This completes the proof of *proposition 8.4*. □

Note that a more direct approach towards obtaining partial functional derivatives of Hamiltonian with respect to configuration space is by considering a general function $\mathbb{H} = \int_0^L H(\mathfrak{q}, \mathfrak{p})\, \mathrm{d}\xi_1$ and obtaining $\delta\mathbb{H}|_{(\{\mathfrak{p}_1, \mathfrak{p}_{2\boldsymbol{Q}}, \mathfrak{p}_3\}=\text{fixed})}$ by carrying integration by parts of all functionally dependent quantities (keeping $(\mathfrak{p}_1, \mathfrak{p}_{2\boldsymbol{Q}}, \mathfrak{p}_3)$ fixed) to obtain result of form (8.28). Such proof would require defining strain energy in an integral form using for example, a free-energy function characterizing hyperelastic response. Readers are recommended to refer section 5 of Simo et al. [116] that deploys this approach for beam with rigid cross-section.

Corollary 8.1: *Proposition 8.3* and *8.4* along with the strong form of equilibrium equation stated section 7.6.3.1 yields:

$$\frac{\mathrm{d}\mathfrak{p}_1}{\mathrm{d}t} = -\frac{\delta H}{\delta \mathfrak{q}_1} \tag{8.37a}$$

$$\frac{\mathrm{d}\mathfrak{p}_2}{\mathrm{d}t} = -\frac{\delta H}{\delta \mathfrak{q}_2} \tag{8.37b}$$

$$\frac{\mathrm{d}\mathfrak{p}_3}{\mathrm{d}t} = -\frac{\delta H}{\delta \mathfrak{q}_3} \tag{8.37c}$$

The equation set (8.37) along with the inverse Legendre transformation (8.23) gives *Hamiltonian equation of motion*. Note that there are 7 equations constituting the strong form (3 for linear momentum conservation, 3 for angular momentum conservation and 1 for the balance of bi-moment and bi-shear), where as, there are 14 equations constituting Hamiltonian form. This brings us to the definition of Poisson bracket. □

Definition 8.10 : Consider $(\boldsymbol{\Phi}, \tilde{\boldsymbol{\Phi}}) \in T^*\mathbb{C}$ such that $\boldsymbol{\Phi} = \{\mathfrak{q}_1, \mathfrak{q}_2, \mathfrak{q}_3\} \in \mathbb{C}$ and $\tilde{\boldsymbol{\Phi}}^* = \{\mathfrak{p}_1^*, \mathfrak{p}_{2\boldsymbol{Q}}^*, \mathfrak{p}_3^*\} \in T^*_{\boldsymbol{\Phi}}\mathbb{C}$. For the functions of form $F, G : T^*\mathbb{C} \longrightarrow \mathbb{R}$ or $F, G \in \mathfrak{f}(T^*\mathbb{C})$, such that $F(\boldsymbol{\Phi}, \tilde{\boldsymbol{\Phi}}) = \int_0^L f(\boldsymbol{\Phi}, \tilde{\boldsymbol{\Phi}})\, \mathrm{d}\xi_1$ and $G(\boldsymbol{\Phi}, \tilde{\boldsymbol{\Phi}}) = \int_0^L g(\boldsymbol{\Phi}, \tilde{\boldsymbol{\Phi}})\, \mathrm{d}\xi_1$, the Poisson bracket $\{.,.\} : \mathfrak{f}(T^*\mathbb{C}) \times \mathfrak{f}(T^*\mathbb{C}) \longrightarrow \mathbb{R}$ is defined as:

$$
\begin{aligned}
\{F, G\} &= \int_0^L \left\langle \frac{\delta f}{\delta \boldsymbol{\Phi}}^* \middle| \frac{\delta g}{\delta \tilde{\boldsymbol{\Phi}}} \right\rangle_{T_{\boldsymbol{\Phi}}\boldsymbol{C}} - \left\langle \frac{\delta g}{\delta \boldsymbol{\Phi}}^* \middle| \frac{\delta f}{\delta \tilde{\boldsymbol{\Phi}}} \right\rangle_{T_{\boldsymbol{\Phi}}\boldsymbol{C}} \mathrm{d}\xi_1 \\
\{F, G\} &= \int_0^L \left(\left\langle \frac{\delta f}{\delta \mathfrak{q}_1}^* \middle| \frac{\delta g}{\delta \mathfrak{p}_1} \right\rangle_{\mathbb{R}^3} - \left\langle \frac{\delta f}{\delta \mathfrak{q}_1}^* \middle| \frac{\delta g}{\delta \mathfrak{p}_1} \right\rangle_{\mathbb{R}^3} \right) + \left(\left\langle \frac{\delta f}{\delta \mathfrak{q}_2}^* \middle| \frac{\delta g}{\delta \mathfrak{p}_{2\boldsymbol{Q}}} \right\rangle_{T_{\boldsymbol{Q}}SO(3)} - \left\langle \frac{\delta g}{\delta \mathfrak{q}_2}^* \middle| \frac{\delta f}{\delta \mathfrak{p}_{2\boldsymbol{Q}}} \right\rangle_{T_{\boldsymbol{Q}}SO(3)} \right) \\
&\quad + \left(\left\langle \frac{\delta f}{\delta \mathfrak{p}_3}^* \middle| \frac{\delta g}{\delta \mathfrak{q}_3} \right\rangle_{\mathbb{R}} - \left\langle \frac{\delta f}{\delta \mathfrak{p}_3}^* \middle| \frac{\delta g}{\delta \mathfrak{q}_3} \right\rangle_{\mathbb{R}} \right) \mathrm{d}\xi_1 \\
\{F, G\} &= \int_0^L \frac{\delta f}{\delta \boldsymbol{\varphi}} . \frac{\delta g}{\delta \mathfrak{p}_1} - \frac{\delta g}{\delta \boldsymbol{\varphi}} . \frac{\delta f}{\delta \mathfrak{p}_1} \, \mathrm{d}\xi_1 + \frac{1}{2} \int_0^L \frac{\delta f}{\delta \boldsymbol{Q}} : \frac{\delta g}{\delta \mathfrak{p}_{2\boldsymbol{Q}}} - \frac{\delta g}{\delta \boldsymbol{Q}} : \frac{\delta f}{\delta \mathfrak{p}_{2\boldsymbol{Q}}} \, \mathrm{d}\xi_1 \\
&\quad + \int_0^L \frac{\delta f}{\delta p} . \frac{\delta g}{\delta \mathfrak{p}_3} - \frac{\delta g}{\delta p} . \frac{\delta f}{\delta \mathfrak{p}_3} \, \mathrm{d}\xi_1
\end{aligned}
\tag{8.38}
$$

Theorem 8.1: The following are equivalent

1. The strong form of equilibrium equations ($\mathfrak{E}_{\boldsymbol{\varphi}} = \mathbf{0}_1, \mathfrak{E}_{\boldsymbol{\alpha}} = \mathbf{0}_1, \mathfrak{E}_p = 0$);

2. Hamilton's principle of stationary action defined by Eq. (8.15);

3. The Hamiltonian equation of motion given by equation set (8.23) and (8.37);

4. Hamiltonian equation in their Poisson bracket formulation given by $\frac{\mathrm{d}F}{\mathrm{d}t} = \{F, \mathbb{H}\}$ for all $F = \int_0^L f \, \mathrm{d}\xi_1 \in \mathfrak{f}(T^*\mathbb{C})$.

Proof: We had used the strong form (statement 1) to establish Hamiltonian equation (statement 3) in *corollary 8.1*. We can obtain strong form of equation using by stationarizing the action as indicated in Eq. (8.15) and substituting for the expression of virtual kinetic energy and virtual strain energy in (8.30) and (7.97) respectively. We prove statement 4. By chain rule, we have

$$\frac{\mathrm{d}F}{\mathrm{d}t} = \int_0^L \left(\frac{\delta f}{\delta \mathfrak{q}_1} . \mathfrak{a}_1 + \frac{1}{2} \frac{\delta f}{\delta \mathfrak{q}_2} : (\boldsymbol{Q} \hat{\tilde{\mathfrak{a}}}_2 \boldsymbol{Q}) + \frac{\delta f}{\delta \mathfrak{q}_3} . \mathfrak{a}_3 \right) + \left(\frac{\delta f}{\delta \mathfrak{p}_1} . \frac{\mathrm{d}\mathfrak{p}_1}{\mathrm{d}t} + \frac{\delta f}{\delta \mathfrak{p}_2} . \frac{\mathrm{d}\mathfrak{p}_2}{\mathrm{d}t} + \frac{\delta f}{\delta \mathfrak{p}_3} . \frac{\mathrm{d}\mathfrak{p}_3}{\mathrm{d}t} \right) \mathrm{d}\xi_1 \quad (8.39)$$

Using Hamiltonian equations (8.23) and (8.37), the equation above simplifies to $\frac{\mathrm{d}F}{\mathrm{d}t} = \{F, \mathbb{H}\}$, thereby proving theorem 8.1. □

Remark 8.2: The Poisson bracket defined in (8.38) satisfies the following properties: anti-commutativity, bilinearity, Leibniz's rule and Jacobi identity. Refer chapter on *canonical transformation* in Goldstein et al. [123]. Using anti-commutative property, we arrive at energy conservation law as $\frac{\mathrm{d}\mathbb{H}}{\mathrm{d}t} = \{\mathbb{H}, \mathbb{H}\} = 0 \implies \frac{\mathrm{d}\mathbb{H}}{\mathrm{d}t} = 0$. This is true because the energy density H (or the total energy $\mathbb{H}$ and the Lagrangian $\mathbb{L}$) does not have explicit time dependence, thereby implying time invariant symmetry. Thus, the equations derived in the last section are for *scleronomic* system. However, if we consider time dependent external forces (for example, non-conservative forces like follower loads) and damping, it would imply the presence of unaccounted source of energy, such that $\frac{\partial \mathbb{H}}{\partial t} \neq 0$. Therefore, the general Poisson bracket form of equilibrium equation is $\frac{\mathrm{d}F}{\mathrm{d}t} = \{F, \mathbb{H}\} + \frac{\partial F}{\partial t}$. Lastly, we note that for infinitesimal motion considered on phase space and using Hamiltonian form of equations, we have

$$\begin{aligned} \boldsymbol{\Phi}(t) &= \boldsymbol{\Phi}(t=0) + t \frac{\mathrm{d}\boldsymbol{\Phi}}{\mathrm{d}t}\Big|_{t=0} = \boldsymbol{\Phi}(t=0) + t \frac{\delta H}{\delta \tilde{\boldsymbol{\Phi}}}\Big|_{t=0} \\ \tilde{\boldsymbol{\Phi}}(t) &= \tilde{\boldsymbol{\Phi}}(t=0) + t \frac{\mathrm{d}\tilde{\boldsymbol{\Phi}}}{\mathrm{d}t}\Big|_{t=0} = \tilde{\boldsymbol{\Phi}}(t=0) - t \frac{\delta H}{\delta \boldsymbol{\Phi}}\Big|_{t=0}. \end{aligned} \quad (8.40)$$

Thus, $\left(\frac{\delta H}{\delta \tilde{\mathbf{\Phi}}}, -\frac{\delta H}{\delta \mathbf{\Phi}}\right)$ can be thought as two component of tangent vector to the curve representing time evolution of the system on phase space at $t = 0$. Therefore, we can consider time evolution as a canonical transformation on coordinates $(\mathbf{\Phi}(t = 0), \tilde{\mathbf{\Phi}}(t = 0)) \longrightarrow (\mathbf{\Phi}(t), \tilde{\mathbf{\Phi}}(t))$ generated by Hamiltonian.

8.5 Summary

This chapter dealt with the Hamiltonian structure of geometrically-exact beams with enhanced kinematics. The phase space and the associated duality (or metric) are defined. The Hamiltonian is obtained from Lagrangian via change of coordinates from state space to phase space carried by means of Legendre transformation. The Hamiltonian form of equations are obtained, Poisson bracket formulation is described and the equivalence between various forms of balance laws are stated.

The discussion carried out in this chapter is planned to be published in a journal titled: "Mathematical theory of a higher-order geometrically-exact beam with a deforming cross-section". The dissertation author is the primary investigator and author of this paper.

Chapter 9

Multi-Axial Linear Constitutive Law for Small Strain

9.1 Introduction

In this chapter, the time- and rate-independent, multi-axial linear constitutive relations restricted to large deformation but small strain assumption is considered. We first establish the relationship between the material form of first Piola-Kirchhoff stress tensor $\boldsymbol{S}$ and the material form of the symmetric part of the strain tensor $\boldsymbol{H}$ using the linear constitutive law for isotropic Saint-Venant/Kirchhoff material. Finally, the reduced constitutive law pertaining to the single-manifold beam model is developed that relates the reduced internal forces $\overline{\mathfrak{N}}$ with the conjugate strain vector $\overline{\boldsymbol{\epsilon}}$.

9.2 Saint-Venant/Kirchhoff constitutive law for small strains

In this section, we define the multi-axial linearly elastic constitutive law considering large deformation but small strain. Recall, the expression of material form of deformation

gradient tensor in Eq. (7.4b): $\overline{\boldsymbol{F}} = \boldsymbol{I}_3 + \overline{\boldsymbol{H}}$. The small strain assumption is imposed by assuming $\|\overline{\boldsymbol{H}}\| = O(\epsilon)$ for a small parameter $\epsilon > 0$ such that $\lim_{\epsilon\to 0} \frac{O(\epsilon)}{\epsilon} =$ constant. Keeping this in mind, we can linearize the material deformation gradient tensor about $\boldsymbol{I}_3$, such that,

$$\overline{\boldsymbol{F}}_\epsilon = \boldsymbol{I}_3 + \left.\frac{\partial \overline{\boldsymbol{F}}}{\partial \epsilon}\right|_{\epsilon=0} .\epsilon + O(\epsilon^2) = \boldsymbol{I}_3 + \epsilon\overline{\boldsymbol{H}} + O(\epsilon^2). \tag{9.1}$$

The spatial form can be obtained by linearizing $\boldsymbol{F}$ about $\boldsymbol{Q}$, or simply by left translation of $\overline{\boldsymbol{F}}_\epsilon$ as:

$$\boldsymbol{F}_\epsilon = \boldsymbol{Q} + \epsilon\boldsymbol{H} + O(\epsilon^2). \tag{9.2}$$

It is advantageous to postulate linear isotropic constitutive law (Saint-Venant/Kirchhoff material) by relating the linear part of second PK stress tensor $\boldsymbol{T} = T_{ij}\boldsymbol{E}_i \otimes \boldsymbol{E}_j$ with the linear part of the corresponding strain conjugate: Lagrangian strain tensor (symmetric) $\boldsymbol{E} = E_{ij}\boldsymbol{E}_i \otimes \boldsymbol{E}_j$. This is because of the material nature of these quantities. We have (refer to Marsden et al. [60]):

$$\begin{aligned} \boldsymbol{T} &= 2G\boldsymbol{E} + \lambda \text{trace}(\boldsymbol{E}); \\ T_{ij} &= (G(\delta_{ik}\delta_{jl} + \delta_{il}\delta_{jk}) + \lambda\delta_{ij}\delta_{kl})E_{kl} = (2G\delta_{ik}\delta_{jl} + \lambda\delta_{ij}\delta_{kl})E_{kl}. \end{aligned} \tag{9.3}$$

Here, G and $\lambda = \frac{E\nu}{(1+\nu)(1-2\nu)}$ are the Lamé's constant. The quantities G and E represents shear and Young's modulus respectively.

Proposition 9.1: Up to order $O(\epsilon)$, the following holds: $\overline{\boldsymbol{S}} = \boldsymbol{T}$ and $\boldsymbol{E} = \frac{1}{2}(\overline{\boldsymbol{H}} + \overline{\boldsymbol{H}}^T) = \overline{\boldsymbol{H}}^S$.

Proof: For small strain, we assume the Lagrangian strain tensor of order $O(\epsilon)$; that's saying $\boldsymbol{E}_\epsilon = \epsilon\boldsymbol{E}$. Using the relationship between $\boldsymbol{E}$ and $\boldsymbol{F}$, and the result in Eq. (9.1), we have:

$$\boldsymbol{E}_\epsilon = \frac{1}{2}(\boldsymbol{F}_\epsilon^T.\boldsymbol{F}_\epsilon - \boldsymbol{I}_3) = \frac{1}{2}(\overline{\boldsymbol{F}}_\epsilon^T.\overline{\boldsymbol{F}}_\epsilon - \boldsymbol{I}_3). \tag{9.4}$$

From Eq. (9.1), we have:

$$\overline{\boldsymbol{F}}_\epsilon^T = \boldsymbol{I}_3 + \epsilon\overline{\boldsymbol{H}}^T + O(\epsilon^2); \tag{9.5a}$$

$$\overline{\boldsymbol{F}}_{\epsilon}^{T}.\overline{\boldsymbol{F}}_{\epsilon} = \boldsymbol{I}_3 + \epsilon\overline{\boldsymbol{H}} + \epsilon\overline{\boldsymbol{H}}^{T} + O(\epsilon^2); \tag{9.5b}$$

$$\det(\boldsymbol{F}) = \det(\boldsymbol{Q} + \epsilon\boldsymbol{H} + O(\epsilon^2)) = 1 + \epsilon.\det(\boldsymbol{H}) + O(\epsilon^2). \tag{9.5c}$$

Using the results (9.4) and (9.5), up to order $O(\epsilon)$, we get:

$$\begin{aligned} \boldsymbol{E}_{\epsilon} &= \epsilon\frac{1}{2}\left(\overline{\boldsymbol{H}} + \overline{\boldsymbol{H}}^{T}\right) = \epsilon\overline{\boldsymbol{H}}^{S} \\ \boldsymbol{E} &= \overline{\boldsymbol{H}}^{S} \end{aligned} \tag{9.6}$$

To prove $\overline{\boldsymbol{S}} = \boldsymbol{T}$ up to order $O(\epsilon)$, we start with the Cauchy stress tensor $\boldsymbol{\sigma}$, which for small strain is of order $O(\epsilon)$, implying $\boldsymbol{\sigma}_{\epsilon} = \epsilon\boldsymbol{\sigma}$. Recall the relationship of $\boldsymbol{S}$ and $\boldsymbol{T}$ with $\boldsymbol{\sigma}$ (refer to Lai et al. [118]):

$$\begin{aligned} \boldsymbol{S} &= \det(\boldsymbol{F}).\boldsymbol{F}^{-1}.\boldsymbol{\sigma}.\boldsymbol{F}^{-T}; \\ \boldsymbol{T} &= \det(\boldsymbol{F}).\boldsymbol{\sigma}.\boldsymbol{F}^{-T}. \end{aligned} \tag{9.7}$$

Using (9.1), we have

$$\overline{\boldsymbol{F}}_{\epsilon}^{-T} = \boldsymbol{I}_3 + \epsilon\overline{\boldsymbol{H}}^{-T} + O(\epsilon^2); \tag{9.8a}$$

$$\overline{\boldsymbol{F}}_{\epsilon}^{-1} = \boldsymbol{Q}^{T} + \epsilon\boldsymbol{H}^{-1} + O(\epsilon^2); \tag{9.8b}$$

$$\det(\boldsymbol{F}) = \det(\boldsymbol{Q} + \epsilon\boldsymbol{H} + O(\epsilon^2)) = 1 + \epsilon.\det(\boldsymbol{H}) + O(\epsilon^2). \tag{9.8c}$$

Therefore, using Eq. (9.7) and equation set (9.8), we arrive at the following for small strain case:

$$\begin{aligned} \boldsymbol{S}_{\epsilon} &= \epsilon\boldsymbol{S} = \epsilon(\boldsymbol{Q}^{T}.\boldsymbol{\sigma}.\boldsymbol{Q}); \\ \boldsymbol{T}_{\epsilon} &= \epsilon\boldsymbol{T} = \epsilon(\boldsymbol{\sigma}.\boldsymbol{Q}). \end{aligned} \tag{9.9}$$

From Eq. (9.9), up to order $O(\epsilon)$, we get $\overline{\boldsymbol{S}} = \boldsymbol{T}$. Hence proved. □

This brings us to the definition of constitutive relation in terms of $\overline{\boldsymbol{S}}$ and $\overline{\boldsymbol{H}}^{S}$. Using Eq. (9.3) and the *proposition 9.1*, we have:

$$\begin{aligned} \overline{\boldsymbol{S}} &= 2G\overline{\boldsymbol{H}}^{S} + \lambda.\text{trace}\left(\overline{\boldsymbol{H}}^{S}\right); \\ \overline{S}_{ij} &= (2G\delta_{ik}\delta_{jl} + \lambda\delta_{ij}\delta_{kl})\overline{H}_{kl}^{S}. \end{aligned} \tag{9.10}$$

The definition of symmetric matrix $\overline{\boldsymbol{H}}^S$ yields:

$$\overline{\boldsymbol{H}}^S = \frac{1}{2}(\overline{\boldsymbol{\lambda}}_i \otimes \boldsymbol{E}_i + \boldsymbol{E}_i \otimes \overline{\boldsymbol{\lambda}}_i) = \frac{1}{2}(\overline{\lambda}_{ij} + \overline{\lambda}_{ji})\boldsymbol{E}_i \otimes \boldsymbol{E}_j. \tag{9.11}$$

Using the constitutive law given by (9.10) and the expression of $\overline{H}^S_{kl}$ in Eq. (9.11), we express the material form of stress vector $\overline{\boldsymbol{S}}_i$ in terms of material form of strain vectors $\overline{\boldsymbol{\lambda}}_i$ as:

$$\begin{bmatrix} \overline{\boldsymbol{S}}_1 \\ \overline{\boldsymbol{S}}_2 \\ \overline{\boldsymbol{S}}_3 \end{bmatrix} = \overbrace{\begin{bmatrix} \overline{\boldsymbol{C}}_{11} & \overline{\boldsymbol{C}}_{12} & \overline{\boldsymbol{C}}_{13} \\ \overline{\boldsymbol{C}}_{21} & \overline{\boldsymbol{C}}_{22} & \overline{\boldsymbol{C}}_{23} \\ \overline{\boldsymbol{C}}_{31} & \overline{\boldsymbol{C}}_{32} & \overline{\boldsymbol{C}}_{33} \end{bmatrix}}^{\overline{\boldsymbol{C}}} \begin{bmatrix} \overline{\boldsymbol{\lambda}}_1 \\ \overline{\boldsymbol{\lambda}}_2 \\ \overline{\boldsymbol{\lambda}}_3 \end{bmatrix}; \tag{9.12}$$

$$\overline{\mathfrak{S}} = \overline{\boldsymbol{C}}.\overline{\mathfrak{L}}.$$

In spatial form, the stress vectors can be related to the spatial strain vectors as follows

$$\begin{aligned} \mathfrak{S} &= \boldsymbol{C}.\mathfrak{L}; \\ \boldsymbol{C} &= \boldsymbol{Q}_3.\overline{\boldsymbol{C}}.\boldsymbol{Q}_3^T. \end{aligned} \tag{9.13}$$

The matrices $\overline{\boldsymbol{C}}_{ij}$ are constant material matrix and are defined below.

$$\begin{aligned}
\overline{\boldsymbol{C}}_{11} &= \begin{bmatrix} \tilde{\lambda} & 0 & 0 \\ 0 & G & 0 \\ 0 & 0 & G \end{bmatrix}; \quad \overline{\boldsymbol{C}}_{12} = \begin{bmatrix} 0 & \lambda & 0 \\ G & 0 & 0 \\ 0 & 0 & 0 \end{bmatrix}; \quad \overline{\boldsymbol{C}}_{13} = \begin{bmatrix} 0 & 0 & \lambda \\ 0 & 0 & 0 \\ G & 0 & 0 \end{bmatrix}; \\
\overline{\boldsymbol{C}}_{21} &= \begin{bmatrix} 0 & G & 0 \\ \lambda & 0 & 0 \\ 0 & 0 & 0 \end{bmatrix}; \quad \overline{\boldsymbol{C}}_{22} = \begin{bmatrix} G & 0 & 0 \\ 0 & \tilde{\lambda} & 0 \\ 0 & 0 & G \end{bmatrix}; \quad \overline{\boldsymbol{C}}_{23} = \begin{bmatrix} 0 & 0 & 0 \\ 0 & 0 & \lambda \\ 0 & G & 0 \end{bmatrix}; \\
\overline{\boldsymbol{C}}_{31} &= \begin{bmatrix} 0 & 0 & G \\ 0 & 0 & 0 \\ \lambda & 0 & 0 \end{bmatrix}; \quad \overline{\boldsymbol{C}}_{32} = \begin{bmatrix} 0 & 0 & 0 \\ 0 & 0 & G \\ 0 & \lambda & 0 \end{bmatrix}; \quad \overline{\boldsymbol{C}}_{33} = \begin{bmatrix} G & 0 & 0 \\ 0 & G & 0 \\ 0 & 0 & \tilde{\lambda} \end{bmatrix}.
\end{aligned} \tag{9.14}$$

Here, $\tilde{\lambda} = 2G + \lambda$. The spatial constitutive matrix is given as:

$$\boldsymbol{C} = \begin{bmatrix} \boldsymbol{C}_{11} & \boldsymbol{C}_{12} & \boldsymbol{C}_{13} \\ \boldsymbol{C}_{21} & \boldsymbol{C}_{22} & \boldsymbol{C}_{23} \\ \boldsymbol{C}_{31} & \boldsymbol{C}_{32} & \boldsymbol{C}_{33} \end{bmatrix} = \boldsymbol{Q}_3.\overline{\boldsymbol{C}}.\boldsymbol{Q}_3^T; \text{ where } \boldsymbol{C}_{ij} = \boldsymbol{Q}.\overline{\boldsymbol{C}}_{ij}.\boldsymbol{Q}^T. \tag{9.15}$$

9.3 Reduced constitutive law

The goal is to obtain a linear relationship between the internal force vector $\overline{\mathfrak{N}}$ with the vector $\overline{\boldsymbol{\epsilon}}$. We ignore terms of $O(\epsilon^2)$ in the expression of $\overline{\boldsymbol{\lambda}}_i$. To start with, we make use of following two observation to redefine the internal force vector for first order strain:

First, we realize that except for $\overline{\boldsymbol{L}}_{\boldsymbol{\kappa}}^{\boldsymbol{\lambda}_i}$, all the other $\overline{\boldsymbol{L}}_{(.)}^{\boldsymbol{\lambda}_i}$ are independent of any strain measurements. Realizing $\overline{\boldsymbol{S}}_1 \longrightarrow O(\epsilon)$, we have

$$\left(\int_{\mathfrak{B}_0} \overline{\boldsymbol{L}}_{\boldsymbol{\kappa}}^{\boldsymbol{\lambda}_i} . \overline{\boldsymbol{S}}_1 \, \mathrm{d}\mathfrak{B}_0 \right)_{\boldsymbol{\epsilon}} = \epsilon . \int_{\mathfrak{B}_0} \hat{\overline{\boldsymbol{r}}}_1^T . \overline{\boldsymbol{S}}_1 \, \mathrm{d}\mathfrak{B}_0 + O(\epsilon^2). \tag{9.16}$$

Therefore, from here on $\overline{\boldsymbol{L}}_{\boldsymbol{\kappa}}^{\boldsymbol{\lambda}_i} = \hat{\overline{\boldsymbol{r}}}_1^T$. Secondly, we note that the $\boldsymbol{M}$-matrix are of order $O(\epsilon)$. Therefore,

$$\int_{\mathfrak{B}_0} \overline{\boldsymbol{M}}_{(.)}^{\boldsymbol{\lambda}_1} . \boldsymbol{S}_1 \, \mathrm{d}\mathfrak{B}_0 \longrightarrow O(\epsilon^2). \tag{9.17}$$

Using Eq. (9.16) and (9.17), we redefine the material form of reduced forces, initially defined in Eq. (7.65) as: $\overline{\mathfrak{N}} = \int_{\mathfrak{B}_0} \overline{\boldsymbol{L}}^T . \overline{\mathfrak{G}} \, \mathrm{d}\mathfrak{B}_0$, where $\overline{\boldsymbol{L}}$ is defined in Eq. (7.12) with $\overline{\boldsymbol{L}}_{\boldsymbol{\kappa}}^{\boldsymbol{\lambda}_i} = \hat{\overline{\boldsymbol{r}}}_1^T$. Using Eq. (9.12) and the relation given in Eq. (7.7a) we have:

$$\overline{\mathfrak{N}} = \int_{\mathfrak{B}_0} \overline{\boldsymbol{L}}^T . \overline{\boldsymbol{C}} . \overline{\mathfrak{L}} \, \mathrm{d}\mathfrak{B}_0 = \int_{\mathfrak{B}_0} \overline{\boldsymbol{L}}^T . \overline{\boldsymbol{C}} . \overline{\boldsymbol{L}} . \overline{\boldsymbol{\epsilon}} \, \mathrm{d}\mathfrak{B}_0 = \overbrace{\left(\int_{\mathfrak{B}_0} \overline{\boldsymbol{L}}^T . \overline{\boldsymbol{C}} . \overline{\boldsymbol{L}} \, \mathrm{d}\mathfrak{B}_0 \right)}^{\overline{\mathfrak{C}}} . \overline{\boldsymbol{\epsilon}} = \overline{\mathfrak{C}} . \overline{\boldsymbol{\epsilon}}. \tag{9.18}$$

The symmetric matrix $\overline{\mathfrak{C}}$ relates the reduced force vectors with the finite strains and their derivatives. The constitutive matrix $\overline{\mathfrak{C}}$ is defined below. The spatial form can be written as $\mathfrak{C} = \boldsymbol{\Lambda} . \overline{\mathfrak{C}} . \boldsymbol{\Lambda}^T$.

$\mathfrak{C}$ matrix and definitions of some constants

$$\overline{\mathfrak{C}} = \begin{bmatrix} \overline{\mathfrak{C}}_{11} & \overline{\mathfrak{C}}_{12} & \overline{\mathfrak{C}}_{13} & \overline{\mathfrak{C}}_{14} & \overline{\mathfrak{C}}_{15} & \overline{\mathfrak{C}}_{16} & \overline{\mathfrak{C}}_{17} & \overline{\mathfrak{C}}_{18} & \overline{\mathfrak{C}}_{19} \\ \overline{\mathfrak{C}}_{21} & \overline{\mathfrak{C}}_{22} & \overline{\mathfrak{C}}_{23} & \overline{\mathfrak{C}}_{24} & \overline{\mathfrak{C}}_{25} & \overline{\mathfrak{C}}_{26} & \overline{\mathfrak{C}}_{27} & \overline{\mathfrak{C}}_{28} & \overline{\mathfrak{C}}_{29} \\ \overline{\mathfrak{C}}_{31} & \overline{\mathfrak{C}}_{32} & \overline{\mathfrak{C}}_{33} & \overline{\mathfrak{C}}_{34} & \overline{\mathfrak{C}}_{35} & \overline{\mathfrak{C}}_{36} & \overline{\mathfrak{C}}_{37} & \overline{\mathfrak{C}}_{38} & \overline{\mathfrak{C}}_{39} \\ \overline{\mathfrak{C}}_{41} & \overline{\mathfrak{C}}_{42} & \overline{\mathfrak{C}}_{43} & \overline{\mathfrak{C}}_{44} & \overline{\mathfrak{C}}_{45} & \overline{\mathfrak{C}}_{46} & \overline{\mathfrak{C}}_{47} & \overline{\mathfrak{C}}_{48} & \overline{\mathfrak{C}}_{49} \\ \overline{\mathfrak{C}}_{51} & \overline{\mathfrak{C}}_{52} & \overline{\mathfrak{C}}_{53} & \overline{\mathfrak{C}}_{54} & \overline{\mathfrak{C}}_{55} & \overline{\mathfrak{C}}_{56} & \overline{\mathfrak{C}}_{57} & \overline{\mathfrak{C}}_{58} & \overline{\mathfrak{C}}_{59} \\ \overline{\mathfrak{C}}_{61} & \overline{\mathfrak{C}}_{62} & \overline{\mathfrak{C}}_{63} & \overline{\mathfrak{C}}_{64} & \overline{\mathfrak{C}}_{65} & \overline{\mathfrak{C}}_{66} & \overline{\mathfrak{C}}_{67} & \overline{\mathfrak{C}}_{68} & \overline{\mathfrak{C}}_{69} \\ \overline{\mathfrak{C}}_{71}^{T} & \overline{\mathfrak{C}}_{72}^{T} & \overline{\mathfrak{C}}_{73}^{T} & \overline{\mathfrak{C}}_{74}^{T} & \overline{\mathfrak{C}}_{75}^{T} & \overline{\mathfrak{C}}_{76}^{T} & \overline{\mathfrak{C}}_{77} & \overline{\mathfrak{C}}_{78} & \overline{\mathfrak{C}}_{79} \\ \overline{\mathfrak{C}}_{81}^{T} & \overline{\mathfrak{C}}_{82}^{T} & \overline{\mathfrak{C}}_{83}^{T} & \overline{\mathfrak{C}}_{84}^{T} & \overline{\mathfrak{C}}_{85}^{T} & \overline{\mathfrak{C}}_{86}^{T} & \overline{\mathfrak{C}}_{87} & \overline{\mathfrak{C}}_{88} & \overline{\mathfrak{C}}_{89} \\ \overline{\mathfrak{C}}_{91}^{T} & \overline{\mathfrak{C}}_{92}^{T} & \overline{\mathfrak{C}}_{93}^{T} & \overline{\mathfrak{C}}_{94}^{T} & \overline{\mathfrak{C}}_{95}^{T} & \overline{\mathfrak{C}}_{96}^{T} & \overline{\mathfrak{C}}_{97} & \overline{\mathfrak{C}}_{98} & \overline{\mathfrak{C}}_{99} \end{bmatrix}. \tag{9.19}$$

We define the following:

$$\begin{aligned} &\tilde{\lambda} = 2G + \lambda; \\ &c_1 = 4\nu^2(G + \lambda) - 4\nu\lambda; \\ &c_2 = -\lambda\nu + 2\nu^2(G + \lambda); \\ &c_3 = 9\lambda\nu^2 - 6\lambda\nu + 9G\nu^2; \\ &c_4 = 3\lambda\nu^2 + 3G\nu^2 - \lambda\nu; \\ &c_5 = \tilde{\lambda} + c_1 + c_2; \\ &c_6 = \tilde{\lambda} + c_1; \\ &I_{22} = \int_{\mathfrak{B}_0} \xi_3^2 \, \mathrm{d}\mathfrak{B}_0; \quad I_{33} = \int_{\mathfrak{B}_0} \xi_2^2 \, \mathrm{d}\mathfrak{B}_0; \quad I_{23} = -\int_{\mathfrak{B}_0} \xi_2\xi_3 \, \mathrm{d}\mathfrak{B}_0; \quad I_{11} = I_{22} + I_{33}. \\ &\mathrm{Grad}\Psi_i = \partial_{\xi_2}\Psi_i \boldsymbol{E}_2 + \partial_{\xi_3}\Psi_i \boldsymbol{E}_3. \end{aligned} \tag{9.20}$$

Matrices associated with the reduced force $\overline{\mathfrak{N}}_{\boldsymbol{\varepsilon}}$:

The reduced force vector $\overline{\mathfrak{N}}_{\boldsymbol{\varepsilon}}$ can be written as,

$$\overline{\mathfrak{N}}_{\boldsymbol{\varepsilon}} = \overline{\mathfrak{C}}_{11}.\overline{\boldsymbol{\varepsilon}} + \overline{\mathfrak{C}}_{12}.\partial_{\xi_1}\overline{\boldsymbol{\varepsilon}} + \overline{\mathfrak{C}}_{13}.\overline{\boldsymbol{\kappa}} + \overline{\mathfrak{C}}_{14}.\partial_{\xi_1}\overline{\boldsymbol{\kappa}} + \overline{\mathfrak{C}}_{15}.\partial^2_{\xi_1}\overline{\boldsymbol{\kappa}} + \overline{\mathfrak{C}}_{16}.\partial^3_{\xi_1}\overline{\boldsymbol{\kappa}} + p.\overline{\mathfrak{C}}_{17} + \partial_{\xi_1}p.\overline{\mathfrak{C}}_{18} + \partial^2_{\xi_1}p.\overline{\mathfrak{C}}_{19}. \tag{9.21}$$

Here:

$$\overline{\mathfrak{C}}_{11} = \begin{bmatrix} (\tilde{\lambda}+c_1)A & 0 & 0 \\ 0 & GA & 0 \\ 0 & 0 & GA \end{bmatrix}; \quad \overline{\mathfrak{C}}_{12} = \overline{\mathfrak{C}}_{13} = \mathbf{0}_3;$$

$$\overline{\mathfrak{C}}_{14} = \begin{bmatrix} 0 & 0 & 0 \\ 0 & -G\nu I_{23} + G\displaystyle\int_{\mathfrak{B}_0} \partial_{\xi_2}\Psi_2 \, \mathrm{d}\mathfrak{B}_0 & G\nu I_{33} + G\displaystyle\int_{\mathfrak{B}_0} \partial_{\xi_2}\Psi_3 \, \mathrm{d}\mathfrak{B}_0 \\ 0 & -G\nu I_{22} + G\displaystyle\int_{\mathfrak{B}_0} \partial_{\xi_3}\Psi_2 \, \mathrm{d}\mathfrak{B}_0 & -G\nu I_{23} + G\displaystyle\int_{\mathfrak{B}_0} \partial_{\xi_3}\Psi_3 \, \mathrm{d}\mathfrak{B}_0 \end{bmatrix};$$

$$\overline{\mathfrak{C}}_{15} = \begin{bmatrix} 0 & \begin{pmatrix} (\tilde{\lambda}+c_1)\displaystyle\int_{\mathfrak{B}_0} \Psi_2 \, \mathrm{d}\mathfrak{B}_0 \\ +c_2\displaystyle\int_{\mathfrak{B}_0} \mathrm{Grad}\Psi_2.\overline{\boldsymbol{r}}_1 \, \mathrm{d}\mathfrak{B}_0 \end{pmatrix} & \begin{pmatrix} (\tilde{\lambda}+c_1)\displaystyle\int_{\mathfrak{B}_0} \Psi_3 \, \mathrm{d}\mathfrak{B}_0 \\ +c_2\displaystyle\int_{\mathfrak{B}_0} \mathrm{Grad}\Psi_3.\overline{\boldsymbol{r}}_1 \, \mathrm{d}\mathfrak{B}_0 \end{pmatrix} \\ 0 & 0 & 0 \\ 0 & 0 & 0 \end{bmatrix};$$

$$\overline{\mathfrak{C}}_{16} = \begin{bmatrix} 0 & 0 & 0 \\ 0 & -G\nu\displaystyle\int_{\mathfrak{B}_0} \xi_2\Psi_2 \, \mathrm{d}\mathfrak{B}_0 & -G\nu\displaystyle\int_{\mathfrak{B}_0} \xi_2\Psi_3 \, \mathrm{d}\mathfrak{B}_0 \\ 0 & -G\nu\displaystyle\int_{\mathfrak{B}_0} \xi_3\Psi_2 \, \mathrm{d}\mathfrak{B}_0 & -G\nu\displaystyle\int_{\mathfrak{B}_0} \xi_3\Psi_3 \, \mathrm{d}\mathfrak{B}_0 \end{bmatrix};$$

$$\overline{\mathfrak{C}}_{17} = \begin{bmatrix} 0 \\ G\int_{\mathfrak{B}_0} \partial_{\xi_2}\Psi_1 \, \mathrm{d}\mathfrak{B}_0 \\ G\int_{\mathfrak{B}_0} \partial_{\xi_3}\Psi_1 \, \mathrm{d}\mathfrak{B}_0 \end{bmatrix}; \overline{\mathfrak{C}}_{18} = \begin{bmatrix} \left((\tilde{\lambda} + c_1)\int_{\mathfrak{B}_0} \Psi_1 \, \mathrm{d}\mathfrak{B}_0 \right) \\ \left(+c_2 \int_{\mathfrak{B}_0} \mathrm{Grad}\Psi_1 . \overline{\boldsymbol{r}}_1 \, \mathrm{d}\mathfrak{B}_0 \right) \\ 0 \\ 0 \end{bmatrix}; \overline{\mathfrak{C}}_{19} = \begin{bmatrix} 0 \\ -G\nu\int_{\mathfrak{B}_0} \xi_2\Psi_1 \, \mathrm{d}\mathfrak{B}_0 \\ -G\nu\int_{\mathfrak{B}_0} \xi_3\Psi_1 \, \mathrm{d}\mathfrak{B}_0 \end{bmatrix}.$$

Matrices associated with the reduced force $\overline{\mathfrak{N}}_{\partial_{\xi_1}\boldsymbol{\varepsilon}}$:

The reduced force vector $\overline{\mathfrak{N}}_{\partial_{\xi_1}\boldsymbol{\varepsilon}}$ can be written as,

$$\overline{\mathfrak{N}}_{\partial_{\xi_1}\boldsymbol{\varepsilon}} = \overline{\mathfrak{C}}_{21}.\overline{\boldsymbol{\varepsilon}} + \overline{\mathfrak{C}}_{22}.\partial_{\xi_1}\overline{\boldsymbol{\varepsilon}} + \overline{\mathfrak{C}}_{23}.\overline{\boldsymbol{\kappa}} + \overline{\mathfrak{C}}_{24}.\partial_{\xi_1}\overline{\boldsymbol{\kappa}} + \overline{\mathfrak{C}}_{25}.\partial^2_{\xi_1}\overline{\boldsymbol{\kappa}} + \overline{\mathfrak{C}}_{26}.\partial^3_{\xi_1}\overline{\boldsymbol{\kappa}} + p.\overline{\mathfrak{C}}_{27} + \partial_{\xi_1}p.\overline{\mathfrak{C}}_{28} + \partial^2_{\xi_1}p.\overline{\mathfrak{C}}_{29}. \tag{9.22}$$

Here:

$$\overline{\mathfrak{C}}_{21} = \mathbf{0}_3; \quad \overline{\mathfrak{C}}_{22} = \begin{bmatrix} G\nu^2 I_{11} & 0 & 0 \\ 0 & 0 & 0 \\ 0 & 0 & 0 \end{bmatrix}; \quad \overline{\mathfrak{C}}_{23} = \mathbf{0}_3;$$

$$\overline{\mathfrak{C}}_{24} = \begin{bmatrix} 0 & \left(G\nu^2 \int_{\mathfrak{B}_0} \xi_3(\xi_3^2 - \xi_2^2) \, \mathrm{d}\mathfrak{B}_0 \right) & \left(-G\nu^2 \int_{\mathfrak{B}_0} \xi_2(\xi_3^2 + \xi_2^2) \, \mathrm{d}\mathfrak{B}_0 \right) \\ & \left(-G\nu \int_{\mathfrak{B}_0} \mathrm{Grad}\Psi_2 . \overline{\boldsymbol{r}}_1 \, \mathrm{d}\mathfrak{B}_0 \right) & \left(-G\nu \int_{\mathfrak{B}_0} \mathrm{Grad}\Psi_3 . \overline{\boldsymbol{r}}_1 \, \mathrm{d}\mathfrak{B}_0 \right) \\ 0 & 0 & 0 \\ 0 & 0 & 0 \end{bmatrix};$$

$$\overline{\mathfrak{C}}_{25} = \mathbf{0}_3; \quad \overline{\mathfrak{C}}_{26} = \begin{bmatrix} 0 & G\nu^2 \int_{\mathfrak{B}_0} (\xi_3^2 + \xi_2^2)\Psi_2 \, \mathrm{d}\mathfrak{B}_0 & G\nu^2 \int_{\mathfrak{B}_0} (\xi_3^2 + \xi_2^2)\Psi_3 \, \mathrm{d}\mathfrak{B}_0 \\ 0 & 0 & 0 \\ 0 & 0 & 0 \end{bmatrix};$$

$$\overline{\mathfrak{C}}_{27} = \begin{bmatrix} -G\nu \int_{\mathfrak{B}_0} \text{Grad}\Psi_1.\overline{\boldsymbol{r}}_1 \, \text{d}\mathfrak{B}_0 \\ 0 \\ 0 \end{bmatrix}; \quad \overline{\mathfrak{C}}_{28} = \mathbf{0}_1; \quad \overline{\mathfrak{C}}_{29} = \begin{bmatrix} G\nu^2 \int_{\mathfrak{B}_0} (\xi_2^2 + \xi_3^2)\Psi_1 \, \text{d}\mathfrak{B}_0 \\ 0 \\ 0 \end{bmatrix}.$$

Matrices associated with the reduced force $\overline{\mathfrak{N}}_{\boldsymbol{\kappa}}$:

The reduced force vector $\overline{\mathfrak{N}}_{\boldsymbol{\kappa}}$ can be written as,

$$\overline{\mathfrak{N}}_{\boldsymbol{\kappa}} = \overline{\mathfrak{C}}_{31}.\overline{\boldsymbol{\varepsilon}} + \overline{\mathfrak{C}}_{32}.\partial_{\xi_1}\overline{\boldsymbol{\varepsilon}} + \overline{\mathfrak{C}}_{33}.\overline{\boldsymbol{\kappa}} + \overline{\mathfrak{C}}_{34}.\partial_{\xi_1}\overline{\boldsymbol{\kappa}} + \overline{\mathfrak{C}}_{35}.\partial^2_{\xi_1}\overline{\boldsymbol{\kappa}} + \overline{\mathfrak{C}}_{36}.\partial^3_{\xi_1}\overline{\boldsymbol{\kappa}} + p.\overline{\mathfrak{C}}_{37} + \partial_{\xi_1}p.\overline{\mathfrak{C}}_{38} + \partial^2_{\xi_1}p.\overline{\mathfrak{C}}_{39}. \tag{9.23}$$

Here:

$$\overline{\mathfrak{C}}_{31} = \overline{\mathfrak{C}}_{32} = \mathbf{0}_3; \quad \overline{\mathfrak{C}}_{33} = \begin{bmatrix} GI_{11} & 0 & 0 \\ 0 & \tilde{\lambda}I_{22} & \tilde{\lambda}I_{23} \\ 0 & \tilde{\lambda}I_{23} & \tilde{\lambda}I_{33} \end{bmatrix} + \begin{bmatrix} 0 & 0 & 0 \\ 0 & G\nu^2 I_{11} + c_3 I_{22} & c_3 I_{23} \\ 0 & c_3 I_{23} & G\nu^2 I_{11} + c_3 I_{33} \end{bmatrix};$$

$$\overline{\mathfrak{C}}_{34} = \begin{bmatrix} 0 & \begin{pmatrix} -2G\nu \int_{\mathfrak{B}_0} \xi_2\xi_3^2 \, \text{d}\mathfrak{B}_0 \\ +G\boldsymbol{E}_1. \int_{\mathfrak{B}_0} \overline{\boldsymbol{r}}_1 \times \text{Grad}\Psi_2 \, \text{d}\mathfrak{B}_0 \end{pmatrix} & \left(G\boldsymbol{E}_1. \int_{\mathfrak{B}_0} \overline{\boldsymbol{r}}_1 \times \text{Grad}\Psi_3 \, \text{d}\mathfrak{B}_0 \right) \\ 0 & 0 & 0 \\ 0 & 0 & 0 \end{bmatrix};$$

$$\overline{\mathfrak{C}}_{35} = \begin{bmatrix} 0 & 0 & 0 \\ 0 & \overline{\mathfrak{C}}_{35_{22}} & \overline{\mathfrak{C}}_{35_{23}} \\ 0 & \overline{\mathfrak{C}}_{35_{32}} & \overline{\mathfrak{C}}_{35_{33}} \end{bmatrix}; \quad \overline{\mathfrak{C}}_{36} = \mathbf{0}_3 \quad \text{with,}$$

$$\overline{\mathfrak{C}}_{35_{22}} = c_5 \int_{\mathfrak{B}_0} \xi_3\Psi_2 \, \text{d}\mathfrak{B}_0 + G\nu^2 \int_{\mathfrak{B}_0} (\xi_2^2 + \xi_3^2).\partial_{\xi_3}\Psi_2 \, \text{d}\mathfrak{B}_0 + c_4 \int_{\mathfrak{B}_0} \xi_3(\overline{\boldsymbol{r}}_1.\text{Grad}\Psi_2) \, \text{d}\mathfrak{B}_0;$$

$$\overline{\mathfrak{C}}_{35_{23}} = c_5 \int_{\mathfrak{B}_0} \xi_3\Psi_3 \, \text{d}\mathfrak{B}_0 + G\nu^2 \int_{\mathfrak{B}_0} (\xi_2^2 + \xi_3^2).\partial_{\xi_3}\Psi_3 \, \text{d}\mathfrak{B}_0 + c_4 \int_{\mathfrak{B}_0} \xi_3(\overline{\boldsymbol{r}}_1.\text{Grad}\Psi_3) \, \text{d}\mathfrak{B}_0;$$

$$\overline{\mathfrak{C}}_{35_{32}} = -c_5 \int_{\mathfrak{B}_0} \xi_2 \Psi_2 \, \mathrm{d}\mathfrak{B}_0 - G\nu^2 \int_{\mathfrak{B}_0} (\xi_2^2 + \xi_3^2).\partial_{\xi_2}\Psi_2 \, \mathrm{d}\mathfrak{B}_0 - c_4 \int_{\mathfrak{B}_0} \xi_2(\overline{\boldsymbol{r}}_1.\mathrm{Grad}\Psi_2) \, \mathrm{d}\mathfrak{B}_0;$$
$$\overline{\mathfrak{C}}_{35_{32}} = -c_5 \int_{\mathfrak{B}_0} \xi_2 \Psi_3 \, \mathrm{d}\mathfrak{B}_0 - G\nu^2 \int_{\mathfrak{B}_0} (\xi_2^2 + \xi_3^2).\partial_{\xi_2}\Psi_3 \, \mathrm{d}\mathfrak{B}_0 - c_4 \int_{\mathfrak{B}_0} \xi_2(\overline{\boldsymbol{r}}_1.\mathrm{Grad}\Psi_3) \, \mathrm{d}\mathfrak{B}_0;$$

$$\overline{\mathfrak{C}}_{37} = \begin{bmatrix} G\boldsymbol{E}_1.\displaystyle\int_{\mathfrak{B}_0} \overline{\boldsymbol{r}}_1 \times \mathrm{Grad}\Psi_1 \, \mathrm{d}\mathfrak{B}_0 \\ 0 \\ 0 \end{bmatrix}; \quad \overline{\mathfrak{C}}_{38} = \begin{bmatrix} 0 \\ \overline{\mathfrak{C}}_{38_2} \\ \overline{\mathfrak{C}}_{38_3} \end{bmatrix}; \quad \overline{\mathfrak{C}}_{39} = \mathbf{0}_1 \text{ with,}$$
$$\overline{\mathfrak{C}}_{38_2} = c_5 \int_{\mathfrak{B}_0} \xi_3 \Psi_1 \, \mathrm{d}\mathfrak{B}_0 + G\nu^2 \int_{\mathfrak{B}_0} (\xi_2^2 + \xi_3^2).\partial_{\xi_3}\Psi_1 \, \mathrm{d}\mathfrak{B}_0 + c_4 \int_{\mathfrak{B}_0} \xi_3(\overline{\boldsymbol{r}}_1.\mathrm{Grad}\Psi_1) \, \mathrm{d}\mathfrak{B}_0;$$
$$\overline{\mathfrak{C}}_{38_3} = -c_5 \int_{\mathfrak{B}_0} \xi_2 \Psi_1 \, \mathrm{d}\mathfrak{B}_0 - G\nu^2 \int_{\mathfrak{B}_0} (\xi_2^2 + \xi_3^2).\partial_{\xi_2}\Psi_1 \, \mathrm{d}\mathfrak{B}_0 - c_4 \int_{\mathfrak{B}_0} \xi_2(\overline{\boldsymbol{r}}_1.\mathrm{Grad}\Psi_1) \, \mathrm{d}\mathfrak{B}_0.$$

Matrices associated with the reduced force $\overline{\mathfrak{N}}_{\partial_{\xi_1}\boldsymbol{\kappa}}$:

The reduced force vector $\overline{\mathfrak{N}}_{\partial_{\xi_1}\boldsymbol{\kappa}}$ can be written as,

$$\overline{\mathfrak{N}}_{\partial_{\xi_1}\boldsymbol{\kappa}} = \overline{\mathfrak{C}}_{41}.\overline{\boldsymbol{\varepsilon}} + \overline{\mathfrak{C}}_{42}.\partial_{\xi_1}\overline{\boldsymbol{\varepsilon}} + \overline{\mathfrak{C}}_{43}.\overline{\boldsymbol{\kappa}} + \overline{\mathfrak{C}}_{44}.\partial_{\xi_1}\overline{\boldsymbol{\kappa}} + \overline{\mathfrak{C}}_{45}.\partial^2_{\xi_1}\overline{\boldsymbol{\kappa}} + \overline{\mathfrak{C}}_{46}.\partial^3_{\xi_1}\overline{\boldsymbol{\kappa}} + p.\overline{\mathfrak{C}}_{47} + \partial_{\xi_1}p.\overline{\mathfrak{C}}_{48} + \partial^2_{\xi_1}p.\overline{\mathfrak{C}}_{49}. \tag{9.24}$$

Here:

$$\overline{\mathfrak{C}}_{41} = \overline{\mathfrak{C}}^T_{14}; \quad \overline{\mathfrak{C}}_{42} = \overline{\mathfrak{C}}^T_{24}; \quad \overline{\mathfrak{C}}_{43} = \overline{\mathfrak{C}}^T_{34};$$

$$\overline{\mathfrak{C}}_{44} = \begin{bmatrix} 0 & 0 & 0 \\ 0 & \overline{\mathfrak{C}}_{44_{22}} & \overline{\mathfrak{C}}_{44_{23}} \\ 0 & \overline{\mathfrak{C}}_{44_{32}} & \overline{\mathfrak{C}}_{44_{33}} \end{bmatrix}; \quad \overline{\mathfrak{C}}_{45} = \mathbf{0}_3 \text{ where,}$$
$$\begin{aligned}\overline{\mathfrak{C}}_{44_{22}} =& G\nu^2 \int_{\mathfrak{B}_0} \xi_3^2(\xi_2^2 + \xi_3^2) \, \mathrm{d}\mathfrak{B}_0 + 2G\nu \int_{\mathfrak{B}_0} \xi_2\xi_3.\partial_{\xi_2}\Psi_2 - \xi_3^2.\partial_{\xi_3}\Psi_2 \, \mathrm{d}\mathfrak{B}_0 \\ &+ G \int_{\mathfrak{B}_0} \|\mathrm{Grad}\Psi_2\|^2 \, \mathrm{d}\mathfrak{B}_0;\end{aligned}$$

$$\overline{\mathfrak{C}}_{44_{23}} = \mathfrak{C}_{44_{32}} = G\nu^2 \int_{\mathfrak{B}_0} \xi_2\xi_3(\xi_2^2 - \xi_3^2)\,\mathrm{d}\mathfrak{B}_0 + G\int_{\mathfrak{B}_0} \partial_{\xi_3}\Psi_2.\partial_{\xi_3}\Psi_3 + \partial_{\xi_2}\Psi_2.\partial_{\xi_2}\Psi_3\,\mathrm{d}\mathfrak{B}_0$$
$$+ G\nu\int_{\mathfrak{B}_0} (\xi_2^2.\partial_{\xi_2}\Psi_2 + \xi_2\xi_3.\partial_{\xi_3}\Psi_2) + (\xi_2\xi_3.\partial_{\xi_2}\Psi_3 - \xi_3^2.\partial_{\xi_3}\Psi_3)\,\mathrm{d}\mathfrak{B}_0;$$
$$\overline{\mathfrak{C}}_{44_{33}} = G\nu^2 \int_{\mathfrak{B}_0} \xi_2^2(\xi_2^2 + \xi_3^2)\,\mathrm{d}\mathfrak{B}_0 + 2G\nu\int_{\mathfrak{B}_0} \xi_2\xi_3.\partial_{\xi_3}\Psi_3 + \xi_2^2.\partial_{\xi_2}\Psi_3\,\mathrm{d}\mathfrak{B}_0$$
$$+ G\int_{\mathfrak{B}_0} \|\mathrm{Grad}\Psi_3\|^2\,\mathrm{d}\mathfrak{B}_0;$$

$$\overline{\mathfrak{C}}_{46} = \begin{bmatrix} 0 & 0 & 0 \\ 0 & \overline{\mathfrak{C}}_{46_{22}} & \overline{\mathfrak{C}}_{46_{23}} \\ 0 & \overline{\mathfrak{C}}_{46_{32}} & \overline{\mathfrak{C}}_{47_{33}} \end{bmatrix} \text{ with,}$$
$$\overline{\mathfrak{C}}_{46_{22}} = -G\nu^2 \int_{\mathfrak{B}_0} \xi_3(\xi_2^2 - \xi_3^2)\Psi_2\,\mathrm{d}\mathfrak{B}_0 - G\nu\int_{\mathfrak{B}_0} \Psi_2(\overline{\boldsymbol{r}}_1.\mathrm{Grad}\Psi_2)\,\mathrm{d}\mathfrak{B}_0;$$
$$\overline{\mathfrak{C}}_{46_{23}} = -G\nu^2 \int_{\mathfrak{B}_0} \xi_3(\xi_2^2 - \xi_3^2)\Psi_3\,\mathrm{d}\mathfrak{B}_0 - G\nu\int_{\mathfrak{B}_0} \Psi_3(\overline{\boldsymbol{r}}_1.\mathrm{Grad}\Psi_2)\,\mathrm{d}\mathfrak{B}_0;$$
$$\overline{\mathfrak{C}}_{46_{32}} = -G\nu^2 \int_{\mathfrak{B}_0} \xi_2(\xi_2^2 + \xi_3^2)\Psi_2\,\mathrm{d}\mathfrak{B}_0 - G\nu\int_{\mathfrak{B}_0} \Psi_2(\overline{\boldsymbol{r}}_1.\mathrm{Grad}\Psi_3)\,\mathrm{d}\mathfrak{B}_0;$$
$$\overline{\mathfrak{C}}_{46_{33}} = -G\nu^2 \int_{\mathfrak{B}_0} \xi_2(\xi_2^2 + \xi_3^2)\Psi_3\,\mathrm{d}\mathfrak{B}_0 - G\nu\int_{\mathfrak{B}_0} \Psi_3(\overline{\boldsymbol{r}}_1.\mathrm{Grad}\Psi_3)\,\mathrm{d}\mathfrak{B}_0;$$

$$\overline{\mathfrak{C}}_{47} = \begin{bmatrix} 0 \\ \overline{\mathfrak{C}}_{47_2} \\ \overline{\mathfrak{C}}_{47_3} \end{bmatrix}; \quad \overline{\mathfrak{C}}_{48} = \mathbf{0}_1; \quad \overline{\mathfrak{C}}_{49} = \begin{bmatrix} 0 \\ \overline{\mathfrak{C}}_{49_2} \\ \overline{\mathfrak{C}}_{49_3} \end{bmatrix} \text{ where,}$$
$$\overline{\mathfrak{C}}_{47_2} = G\nu\int_{\mathfrak{B}_0} \xi_2\xi_3.\partial_{\xi_2}\Psi_1 - \xi_3^2.\partial_{\xi_3}\Psi_1\,\mathrm{d}\mathfrak{B}_0 + G\int_{\mathfrak{B}_0} \partial_{\xi_3}\Psi_1.\partial_{\xi_3}\Psi_2 + \partial_{\xi_2}\Psi_1.\partial_{\xi_2}\Psi_2\,\mathrm{d}\mathfrak{B}_0;$$
$$\overline{\mathfrak{C}}_{47_3} = G\nu\int_{\mathfrak{B}_0} \xi_2(\overline{\boldsymbol{r}}_1.\mathrm{Grad}\Psi_1)\,\mathrm{d}\mathfrak{B}_0 + G\int_{\mathfrak{B}_0} \partial_{\xi_3}\Psi_1.\partial_{\xi_3}\Psi_3 + \partial_{\xi_2}\Psi_1.\partial_{\xi_2}\Psi_3\,\mathrm{d}\mathfrak{B}_0;$$

and

$$\overline{\mathfrak{C}}_{49_2} = -G\nu\int_{\mathfrak{B}_0} \Psi_1(\overline{\boldsymbol{r}}_1.\mathrm{Grad}\Psi_2)\,\mathrm{d}\mathfrak{B}_0 - G\nu^2\int_{\mathfrak{B}_0} \xi_3(\xi_2^2 - \xi_3^2)\Psi_1\,\mathrm{d}\mathfrak{B}_0;$$
$$\overline{\mathfrak{C}}_{49_3} = -G\nu\int_{\mathfrak{B}_0} \Psi_1(\overline{\boldsymbol{r}}_1.\mathrm{Grad}\Psi_3)\,\mathrm{d}\mathfrak{B}_0 - G\nu^2\int_{\mathfrak{B}_0} \xi_2(\xi_2^2 + \xi_3^2)\Psi_1\,\mathrm{d}\mathfrak{B}_0.$$

Matrices associated with the reduced force $\overline{\mathfrak{R}}_{\partial^2_{\xi_1}\boldsymbol{\kappa}}$:

The reduced force vector $\overline{\mathfrak{R}}_{\partial_{\xi_1}\boldsymbol{\kappa}}$ can be written as,

$$\overline{\mathfrak{R}}_{\partial_{\xi_1}\boldsymbol{\kappa}} = \overline{\mathfrak{C}}_{51}.\overline{\boldsymbol{\varepsilon}} + \overline{\mathfrak{C}}_{52}.\partial_{\xi_1}\overline{\boldsymbol{\varepsilon}} + \overline{\mathfrak{C}}_{53}.\overline{\boldsymbol{\kappa}} + \overline{\mathfrak{C}}_{54}.\partial_{\xi_1}\overline{\boldsymbol{\kappa}} + \overline{\mathfrak{C}}_{55}.\partial^2_{\xi_1}\overline{\boldsymbol{\kappa}} + \overline{\mathfrak{C}}_{56}.\partial^3_{\xi_1}\overline{\boldsymbol{\kappa}} + p.\overline{\mathfrak{C}}_{57} + \partial_{\xi_1}p.\overline{\mathfrak{C}}_{58} + \partial^2_{\xi_1}p.\overline{\mathfrak{C}}_{59}. \tag{9.25}$$

Here:

$$\overline{\mathfrak{C}}_{51} = \overline{\mathfrak{C}}^T_{15}; \quad \overline{\mathfrak{C}}_{52} = \overline{\mathfrak{C}}^T_{25}; \quad \overline{\mathfrak{C}}_{53} = \overline{\mathfrak{C}}^T_{35}; \quad \overline{\mathfrak{C}}_{54} = \overline{\mathfrak{C}}^T_{45};$$

$$\overline{\mathfrak{C}}_{55} = \begin{bmatrix} 0 & 0 & 0 \\ 0 & \overline{\mathfrak{C}}_{55_{22}} & \overline{\mathfrak{C}}_{55_{23}} \\ 0 & \overline{\mathfrak{C}}_{55_{32}} & \overline{\mathfrak{C}}_{55_{33}} \end{bmatrix} \text{ where,}$$

$$\begin{aligned}
\overline{\mathfrak{C}}_{55_{22}} =& c_6 \int_{\mathfrak{B}_0} \Psi_2^2 \, \mathrm{d}\mathfrak{B}_0 + 2c_2 \int_{\mathfrak{B}_0} \Psi_2(\overline{\boldsymbol{r}}_1.\mathrm{Grad}\Psi_2) \, \mathrm{d}\mathfrak{B}_0 + G\nu^2 \int_{\mathfrak{B}_0} \xi_2^2(\partial_{\xi_3}\Psi_2)^2 + \xi_3^2(\partial_{\xi_2}\Psi_2)^2 \, \mathrm{d}\mathfrak{B}_0 \\
&+ \tilde{\lambda}\nu^2 \int_{\mathfrak{B}_0} \xi_3^2(\partial_{\xi_3}\Psi_2)^2 + \xi_2^2(\partial_{\xi_2}\Psi_2)^2 \, \mathrm{d}\mathfrak{B}_0 + 2(G+\lambda)\nu^2 \int_{\mathfrak{B}_0} \xi_2\xi_3.\partial_{\xi_3}\Psi_2.\partial_{\xi_2}\Psi_2 \, \mathrm{d}\mathfrak{B}_0; \\
\overline{\mathfrak{C}}_{55_{23}} = \overline{\mathfrak{C}}_{55_{32}} =& c_6 \int_{\mathfrak{B}_0} \Psi_2\Psi_3 \, \mathrm{d}\mathfrak{B}_0 + c_2 \int_{\mathfrak{B}_0} \Psi_2(\overline{\boldsymbol{r}}_1.\mathrm{Grad}\Psi_3) + \Psi_3(\overline{\boldsymbol{r}}_1.\mathrm{Grad}\Psi_2) \, \mathrm{d}\mathfrak{B}_0 \\
&+ G\nu^2 \int_{\mathfrak{B}_0} \xi_2^2(\partial_{\xi_3}\Psi_2.\partial_{\xi_3}\Psi_3) + \xi_3^2(\partial_{\xi_2}\Psi_2.\partial_{\xi_2}\Psi_3) \, \mathrm{d}\mathfrak{B}_0 \\
&+ \tilde{\lambda}\nu^2 \int_{\mathfrak{B}_0} \xi_3^2(\partial_{\xi_3}\Psi_2.\partial_{\xi_3}\Psi_3) + \xi_2^2(\partial_{\xi_2}\Psi_2.\partial_{\xi_2}\Psi_3) \, \mathrm{d}\mathfrak{B}_0 \\
&+ (G+\lambda)\nu^2 \int_{\mathfrak{B}_0} \xi_2\xi_3.(\partial_{\xi_3}\Psi_3.\partial_{\xi_2}\Psi_2 + \partial_{\xi_3}\Psi_2.\partial_{\xi_2}\Psi_3) \, \mathrm{d}\mathfrak{B}_0; \\
\overline{\mathfrak{C}}_{55_{33}} =& c_6 \int_{\mathfrak{B}_0} \Psi_3^2 \, \mathrm{d}\mathfrak{B}_0 + 2c_2 \int_{\mathfrak{B}_0} \Psi_3(\overline{\boldsymbol{r}}_1.\mathrm{Grad}\Psi_3) \, \mathrm{d}\mathfrak{B}_0 + G\nu^2 \int_{\mathfrak{B}_0} \xi_2^2(\partial_{\xi_3}\Psi_3)^2 + \xi_3^2(\partial_{\xi_2}\Psi_3)^2 \, \mathrm{d}\mathfrak{B}_0 \\
&+ \tilde{\lambda}\nu^2 \int_{\mathfrak{B}_0} \xi_3^2(\partial_{\xi_3}\Psi_3)^2 + \xi_2^2(\partial_{\xi_2}\Psi_3)^2 \, \mathrm{d}\mathfrak{B}_0 + 2(G+\lambda)\nu^2 \int_{\mathfrak{B}_0} \xi_2\xi_3.\partial_{\xi_3}\Psi_3.\partial_{\xi_2}\Psi_3 \, \mathrm{d}\mathfrak{B}_0;
\end{aligned}$$

$$\overline{\mathfrak{C}}_{56} = \mathbf{0}_3; \quad \overline{\mathfrak{C}}_{57} = \mathbf{0}_1; \quad \overline{\mathfrak{C}}_{58} = \begin{bmatrix} 0 \\ \overline{\mathfrak{C}}_{58_2} \\ \overline{\mathfrak{C}}_{58_3} \end{bmatrix}; \quad \overline{\mathfrak{C}}_{59} = \mathbf{0}_1 \text{ where,}$$

$$\begin{aligned}
\overline{\mathfrak{C}}_{58_2} =& c_2 \int_{\mathfrak{B}_0} \Psi_2(\overline{\boldsymbol{r}}_1.\text{Grad}\Psi_1)\, \mathrm{d}\mathfrak{B}_0 + G\nu^2 \int_{\mathfrak{B}_0} \xi_2^2(\partial_{\xi_3}\Psi_2.\partial_{\xi_3}\Psi_1) + \xi_3^2(\partial_{\xi_2}\Psi_2.\partial_{\xi_2}\Psi_1)\, \mathrm{d}\mathfrak{B}_0 \\
&+ \tilde{\lambda}\nu^2 \int_{\mathfrak{B}_0} \xi_3^2(\partial_{\xi_3}\Psi_2.\partial_{\xi_3}\Psi_1) + \xi_2^2(\partial_{\xi_2}\Psi_2.\partial_{\xi_2}\Psi_1)\, \mathrm{d}\mathfrak{B}_0 \\
&+ (G+\lambda)\nu^2 \int_{\mathfrak{B}_0} \xi_2\xi_3.(\partial_{\xi_3}\Psi_2.\partial_{\xi_2}\Psi_1 + \partial_{\xi_2}\Psi_2.\partial_{\xi_3}\Psi_1)\, \mathrm{d}\mathfrak{B}_0; \\
\overline{\mathfrak{C}}_{58_3} =& c_2 \int_{\mathfrak{B}_0} \Psi_3(\overline{\boldsymbol{r}}_1.\text{Grad}\Psi_1)\, \mathrm{d}\mathfrak{B}_0 + G\nu^2 \int_{\mathfrak{B}_0} \xi_2^2(\partial_{\xi_3}\Psi_3.\partial_{\xi_3}\Psi_1) + \xi_3^2(\partial_{\xi_2}\Psi_3.\partial_{\xi_2}\Psi_1)\, \mathrm{d}\mathfrak{B}_0 \\
&+ \tilde{\lambda}\nu^2 \int_{\mathfrak{B}_0} \xi_3^2(\partial_{\xi_3}\Psi_3.\partial_{\xi_3}\Psi_1) + \xi_2^2(\partial_{\xi_2}\Psi_3.\partial_{\xi_2}\Psi_1)\, \mathrm{d}\mathfrak{B}_0 \\
&+ (G+\lambda)\nu^2 \int_{\mathfrak{B}_0} \xi_2\xi_3.(\partial_{\xi_3}\Psi_3.\partial_{\xi_2}\Psi_1 + \partial_{\xi_2}\Psi_3.\partial_{\xi_3}\Psi_1)\, \mathrm{d}\mathfrak{B}_0.
\end{aligned}$$

Matrices associated with the reduced force $\overline{\mathfrak{N}}_{\partial^3_{\xi_1}\boldsymbol{\kappa}}$:

The reduced force vector $\overline{\mathfrak{N}}_{\partial^3_{\xi_1}\boldsymbol{\kappa}}$ can be written as,

$$\overline{\mathfrak{N}}_{\partial^3_{\xi_1}\boldsymbol{\kappa}} = \overline{\mathfrak{C}}_{61}.\overline{\boldsymbol{\varepsilon}} + \overline{\mathfrak{C}}_{62}.\partial_{\xi_1}\overline{\boldsymbol{\varepsilon}} + \overline{\mathfrak{C}}_{63}.\overline{\boldsymbol{\kappa}} + \overline{\mathfrak{C}}_{64}.\partial_{\xi_1}\overline{\boldsymbol{\kappa}} + \overline{\mathfrak{C}}_{65}.\partial^2_{\xi_1}\overline{\boldsymbol{\kappa}} + \overline{\mathfrak{C}}_{66}.\partial^3_{\xi_1}\overline{\boldsymbol{\kappa}} + p.\overline{\mathfrak{C}}_{67} + \partial_{\xi_1}p.\overline{\mathfrak{C}}_{68} + \partial^2_{\xi_1}p.\overline{\mathfrak{C}}_{69}. \tag{9.26}$$

Here,

$$\overline{\mathfrak{C}}_{61} = \overline{\mathfrak{C}}^T_{16}; \quad \overline{\mathfrak{C}}_{62} = \overline{\mathfrak{C}}^T_{26}; \quad \overline{\mathfrak{C}}_{63} = \overline{\mathfrak{C}}^T_{36}; \quad \overline{\mathfrak{C}}_{64} = \overline{\mathfrak{C}}^T_{46};$$

$$\overline{\mathfrak{C}}_{66} = \begin{bmatrix} 0 & 0 & 0 \\ 0 & G\nu^2 \int_{\mathfrak{B}_0} (\xi_2^2+\xi_3^2)\Psi_2^2\, \mathrm{d}\mathfrak{B}_0 & G\nu^2 \int_{\mathfrak{B}_0} (\xi_2^2+\xi_3^2)\Psi_2\Psi_3 \\ 0 & G\nu^2 \int_{\mathfrak{B}_0} (\xi_2^2+\xi_3^2)\Psi_2\Psi_3\, \mathrm{d}\mathfrak{B}_0 & G\nu^2 \int_{\mathfrak{B}_0} (\xi_2^2+\xi_3^2)\Psi_3^2\, \mathrm{d}\mathfrak{B}_0 \end{bmatrix}$$

$$\overline{\mathfrak{C}}_{67} = \begin{bmatrix} 0 \\ -G\nu \int_{\mathfrak{B}_0} \Psi_2(\overline{\boldsymbol{r}}_1.\mathrm{Grad}\Psi_1)\,\mathrm{d}\mathfrak{B}_0 \\ -G\nu \int_{\mathfrak{B}_0} \Psi_3(\overline{\boldsymbol{r}}_1.\mathrm{Grad}\Psi_1)\,\mathrm{d}\mathfrak{B}_0 \end{bmatrix}; \quad \overline{\mathfrak{C}}_{68} = \mathbf{0}_1; \quad \overline{\mathfrak{C}}_{69} = \begin{bmatrix} 0 \\ G\nu^2 \int_{\mathfrak{B}_0} \Psi_1\Psi_3(\xi_2^2 + \xi_3^2)\,\mathrm{d}\mathfrak{B}_0 \\ G\nu^2 \int_{\mathfrak{B}_0} \Psi_1\Psi_2(\xi_2^2 + \xi_3^2)\,\mathrm{d}\mathfrak{B}_0 \end{bmatrix}.$$

Matrices associated with the reduced force $\overline{\mathfrak{N}}_p$:

The bi-shear $\overline{\mathfrak{N}}_p$ can be written as,

$$\overline{\mathfrak{N}}_p = \overline{\mathfrak{C}}_{71}\cdot\overline{\boldsymbol{\varepsilon}} + \overline{\mathfrak{C}}_{72}\cdot\partial_{\xi_1}\overline{\boldsymbol{\varepsilon}} + \overline{\mathfrak{C}}_{73}\cdot\overline{\boldsymbol{\kappa}} + \overline{\mathfrak{C}}_{74}\cdot\partial_{\xi_1}\overline{\boldsymbol{\kappa}} + \overline{\mathfrak{C}}_{75}\cdot\partial^2_{\xi_1}\overline{\boldsymbol{\kappa}} + \overline{\mathfrak{C}}_{76}\cdot\partial^3_{\xi_1}\overline{\boldsymbol{\kappa}} + p.\overline{\mathfrak{C}}_{77} + \partial_{\xi_1}p.\overline{\mathfrak{C}}_{78} + \partial^2_{\xi_1}p.\overline{\mathfrak{C}}_{79}. \tag{9.27}$$

Here:

$$\overline{\mathfrak{C}}_{71} = \overline{\mathfrak{C}}_{17}; \quad \overline{\mathfrak{C}}_{72} = \overline{\mathfrak{C}}_{27}; \quad \overline{\mathfrak{C}}_{73} = \overline{\mathfrak{C}}_{37}; \quad \overline{\mathfrak{C}}_{74} = \overline{\mathfrak{C}}_{47}; \quad \overline{\mathfrak{C}}_{75} = \overline{\mathfrak{C}}_{57}; \quad \overline{\mathfrak{C}}_{76} = \overline{\mathfrak{C}}_{67};$$

$$\overline{\mathfrak{C}}_{77} = G\int_{\mathfrak{B}_0} \|\mathrm{Grad}\Psi_1\|^2\,\mathrm{d}\mathfrak{B}_0; \quad \overline{\mathfrak{C}}_{78} = 0; \quad \overline{\mathfrak{C}}_{79} = -\nu G\int_{\mathfrak{B}_0} \Psi_1(\overline{\boldsymbol{r}}_1.\mathrm{Grad}\Psi_1)\,\mathrm{d}\mathfrak{B}_0.$$

Matrices associated with the reduced force $\overline{\mathfrak{N}}_{\partial_{\xi_1}p}$:

The bi-moment $\overline{\mathfrak{N}}_{\partial_{\xi_1}p}$ can be written as,

$$\overline{\mathfrak{N}}_{\partial_{\xi_1}p} = \overline{\mathfrak{C}}_{81}\cdot\overline{\boldsymbol{\varepsilon}} + \overline{\mathfrak{C}}_{82}\cdot\partial_{\xi_1}\overline{\boldsymbol{\varepsilon}} + \overline{\mathfrak{C}}_{83}\cdot\overline{\boldsymbol{\kappa}} + \overline{\mathfrak{C}}_{84}\cdot\partial_{\xi_1}\overline{\boldsymbol{\kappa}} + \overline{\mathfrak{C}}_{85}\cdot\partial^2_{\xi_1}\overline{\boldsymbol{\kappa}} + \overline{\mathfrak{C}}_{86}.\partial^3_{\xi_1}\overline{\boldsymbol{\kappa}} + p.\overline{\mathfrak{C}}_{87} + \partial_{\xi_1}p.\overline{\mathfrak{C}}_{88} + \partial^2_{\xi_1}p.\overline{\mathfrak{C}}_{89}. \tag{9.28}$$

Here:

$$\overline{\mathfrak{C}}_{81} = \overline{\mathfrak{C}}_{18}; \quad \overline{\mathfrak{C}}_{82} = \overline{\mathfrak{C}}_{28}; \quad \overline{\mathfrak{C}}_{83} = \overline{\mathfrak{C}}_{38}; \quad \overline{\mathfrak{C}}_{84} = \overline{\mathfrak{C}}_{48}; \quad \overline{\mathfrak{C}}_{85} = \overline{\mathfrak{C}}_{58}; \quad \overline{\mathfrak{C}}_{86} = \overline{\mathfrak{C}}_{68}; \quad \overline{\mathfrak{C}}_{87} = \overline{\mathfrak{C}}_{78};$$

$$\begin{aligned}\overline{\mathfrak{C}}_{88} =& c_6\int_{\mathfrak{B}_0} \Psi_1^2\,\mathrm{d}\mathfrak{B}_0 + 2c_2\int_{\mathfrak{B}_0} \Psi_1(\overline{\boldsymbol{r}}_1.\mathrm{Grad}\Psi_1)\,\mathrm{d}\mathfrak{B}_0 + G\nu^2\int_{\mathfrak{B}_0} \xi_2^2(\partial_{\xi_3}\Psi_1)^2 + \xi_3^2(\partial_{\xi_2}\Psi_1)^2\,\mathrm{d}\mathfrak{B}_0 \\ &+ \tilde{\lambda}\nu^2\int_{\mathfrak{B}_0} \xi_3^2(\partial_{\xi_3}\Psi_1)^2 + \xi_2^2(\partial_{\xi_2}\Psi_1)^2\,\mathrm{d}\mathfrak{B}_0 + 2(G+\lambda)\nu^2\int_{\mathfrak{B}_0} \xi_2\xi_3.\partial_{\xi_3}\Psi_1.\partial_{\xi_2}\Psi_1\,\mathrm{d}\mathfrak{B}_0;\end{aligned}$$

$\overline{\mathfrak{C}}_{89} = 0.$

Matrices associated with the reduced force $\overline{\mathfrak{N}}_{\partial^2_{\xi_1} p}$:

The reduced force $\overline{\mathfrak{N}}_{\partial^2_{\xi_1} p}$ can be written as,

$$\overline{\mathfrak{N}}_{\partial^2_{\xi_1} p} = \overline{\mathfrak{C}}_{91} \cdot \overline{\boldsymbol{\varepsilon}} + \overline{\mathfrak{C}}_{92} \cdot \partial_{\xi_1} \overline{\boldsymbol{\varepsilon}} + \overline{\mathfrak{C}}_{93} \cdot \overline{\boldsymbol{\kappa}} + \overline{\mathfrak{C}}_{94} \cdot \partial_{\xi_1} \overline{\boldsymbol{\kappa}} + \overline{\mathfrak{C}}_{95} \cdot \partial^2_{\xi_1} \overline{\boldsymbol{\kappa}} + \overline{\mathfrak{C}}_{96} \cdot \partial^3_{\xi_1} \overline{\boldsymbol{\kappa}} + p.\overline{\mathfrak{C}}_{97} + \partial_{\xi_1} p.\overline{\mathfrak{C}}_{98} + \partial^2_{\xi_1} p.\overline{\mathfrak{C}}_{99}. \tag{9.29}$$

Here:

$$\begin{aligned}
&\overline{\mathfrak{C}}_{91} = \overline{\mathfrak{C}}_{19}; \quad \overline{\mathfrak{C}}_{92} = \overline{\mathfrak{C}}_{29}; \quad \overline{\mathfrak{C}}_{93} = \overline{\mathfrak{C}}_{39}; \quad \overline{\mathfrak{C}}_{94} = \overline{\mathfrak{C}}_{49}; \\
&\overline{\mathfrak{C}}_{95} = \overline{\mathfrak{C}}_{59}; \quad \overline{\mathfrak{C}}_{96} = \overline{\mathfrak{C}}_{69}; \quad \overline{\mathfrak{C}}_{97} = \overline{\mathfrak{C}}_{79}; \quad \overline{\mathfrak{C}}_{98} = \overline{\mathfrak{C}}_{89}; \\
&\overline{\mathfrak{C}}_{99} = G\nu^2 \int_{\mathfrak{B}_0} (\xi_2^2 + \xi_3^2) \Psi_1^2 \, \mathrm{d}\mathfrak{B}_0.
\end{aligned}$$

Remark 9.1: Owing to the linear elastic and small strain assumption, the matrix $\overline{\boldsymbol{C}}$ and $\overline{\mathfrak{C}}$ are symmetric. However, $\overline{\mathfrak{C}}$ matrix in the form defined above is singular. We observe that the second and third components of $\overline{\mathfrak{N}}_{\partial_{\xi_1} \boldsymbol{\varepsilon}}$ and the first component of $\overline{\mathfrak{N}}_{\partial_{\xi_1} \boldsymbol{\kappa}}$, $\overline{\mathfrak{N}}_{\partial^2_{\xi_1} \boldsymbol{\kappa}}$ and $\overline{\mathfrak{N}}_{\partial^3_{\xi_1} \boldsymbol{\kappa}}$ are zero. Therefore, the 5, 6, 10, 13, and 16th rows and columns of $\overline{\mathfrak{C}}$ are zero. However the global material stiffness matrix obtained in next chapter is not singular.

9.4 Summary

This chapter deals with obtaining a reduced linear constitutive model for isotropic Kirchhoff material for the single-manifold geometrically-exact beam. At a continuum level, the relationship between the material form of first PK stress tensor $\boldsymbol{S}$ and the material form of the symmetric part of the strain tensor $\boldsymbol{H}$ is obtained. Finally, the reduced constitutive law for a one-dimensional beam is derived. The constitutive law described in Simo et al. [48] and [93] are recovered considering the simplified kinematics used in those papers.

The discussion carried out in this chapter is planned to be published in a journal titled: "Mathematical theory of a higher-order geometrically-exact beam with a deforming cross-section". The dissertation author is the primary investigator and author of this paper.

Chapter 10

Finite Element Formulation

10.1 Introduction

To numerically solve the higher-order geometrically-exact beam with enhanced kinematics, we restrict to static case and use multi-axial linear material constitutive law valid for large deformation but limited to small strains relating to the reduced forces to their corresponding finite strain counterpart (presented in chapter 9). Linearization of weak form is detailed followed by matrix formulation of the equation of motion. For simplicity, we assume displacement prescribed boundary conditions. We update the rotation tensor in Eulerian sense using an *incremental current rotation vector*. As was noted in Cardona et al. [51], this choice of updating leads to non-symmetric geometric stiffness. We obtain and update curvature and its derivatives using the results presented in chapter 3.

10.2 Consistent linearization

10.2.1 Linearization of weak form

The linearized part of the functional $G(\boldsymbol{\Phi}, \delta\boldsymbol{\Phi})$ at the configuration $\boldsymbol{\Phi}^{\#}$ in the direction of $\Delta\boldsymbol{\Phi}$, such that $\boldsymbol{\Phi}_\epsilon = \boldsymbol{\Phi}^{\#} + \epsilon\Delta\boldsymbol{\Phi}$, is given as,

$$G(\boldsymbol{\Phi}, \delta\boldsymbol{\Phi}) = \delta \mathrm{U}_{\text{strain}} - \delta \mathrm{W}_{\text{ext}} = \int_0^L \delta\boldsymbol{\Phi}^T \boldsymbol{B}_2^T \boldsymbol{B}_1^T \mathfrak{N} \, \mathrm{d}\xi_1 - \int_0^L \delta\boldsymbol{\Phi}^T \boldsymbol{B}_2^T \boldsymbol{B}_3 \boldsymbol{N}_f \, \mathrm{d}\xi_1 = 0. \tag{10.1}$$

$$L[G(\boldsymbol{\Phi}, \delta\boldsymbol{\Phi})]_{(\boldsymbol{\Phi}^{\#}, \Delta\boldsymbol{\Phi})} = G(\boldsymbol{\Phi}^{\#}, \delta\boldsymbol{\Phi}) + \mathrm{D}G(\boldsymbol{\Phi}^{\#}, \delta\boldsymbol{\Phi}).\Delta\boldsymbol{\Phi}. \tag{10.2}$$

In the equation above, $\mathrm{D}G(\boldsymbol{\Phi}^{\#}, \delta\boldsymbol{\Phi}).\Delta\boldsymbol{\Phi}$ is the Frećhet differential defined by directional derivative formula as,

$$\mathrm{D}G(\boldsymbol{\Phi}^{\#}, \delta\boldsymbol{\Phi}).\Delta\boldsymbol{\Phi} = \left.\frac{\mathrm{d}G(\boldsymbol{\Phi}_\epsilon, \delta\boldsymbol{\Phi})}{\mathrm{d}\epsilon}\right|_{\epsilon=0}. \tag{10.3}$$

In Eq. (10.2), the term $G(\boldsymbol{\Phi}^{\#}, \delta\boldsymbol{\Phi})$ is responsible for the unbalanced forces, whereas the term $\mathrm{D}G(\boldsymbol{\Phi}^{\#}, \delta\boldsymbol{\Phi}).\Delta\boldsymbol{\Phi}$ (linear in $\Delta\boldsymbol{\Phi}$) yields the tangent stiffness matrix. For simplicity, we assume that $\boldsymbol{\Phi}^{\#} = \boldsymbol{\Phi}$ and define the linear increment in the weak form ΔG as,

$$\begin{gathered}\mathrm{D}G(\boldsymbol{\Phi}^{\#}, \delta\boldsymbol{\Phi}).\Delta\boldsymbol{\Phi} = \Delta G(\boldsymbol{\Phi}^{\#}, \delta\boldsymbol{\Phi}) = \Delta G(\boldsymbol{\Phi}, \delta\boldsymbol{\Phi})\big|_{\boldsymbol{\Phi}=\boldsymbol{\Phi}^{\#}} = \Delta G(\boldsymbol{\Phi}, \delta\boldsymbol{\Phi}); \\ \Delta G(\boldsymbol{\Phi}, \delta\boldsymbol{\Phi}) = \Delta\delta \mathrm{U}_{\text{strain}} - \Delta\delta \mathrm{W}_{\text{ext}}.\end{gathered} \tag{10.4}$$

10.2.2 Linearization of virtual strain energy

The expression of virtual strain energy can be written using Eq. (7.69) as,

$$\delta \mathrm{U}_{\text{strain}} = \int_0^L \delta\boldsymbol{\Phi}^T \boldsymbol{B}_2^T \boldsymbol{B}_1^T \mathfrak{N} \, \mathrm{d}\xi_1 = \int_0^L \delta\boldsymbol{\Phi}^T \boldsymbol{B}_2^T \boldsymbol{B}_1^T \boldsymbol{\Lambda} \overline{\mathfrak{N}} \, \mathrm{d}\xi_1. \tag{10.5}$$

Thus, the linearized virtual strain energy is obtained as,

$$\Delta\delta \mathrm{U}_{\mathrm{strain}} = \overbrace{\int_0^L \delta\boldsymbol{\Phi}^T \boldsymbol{B}_2^T \boldsymbol{B}_1^T \boldsymbol{\Lambda} \Delta\overline{\mathfrak{N}} \, \mathrm{d}\xi_1}^{\Delta\delta \mathrm{U}_{\mathrm{strain1}}} + \overbrace{\int_0^L \delta\boldsymbol{\Phi}^T \boldsymbol{B}_2^T \boldsymbol{B}_1^T \Delta\boldsymbol{\Lambda} \overline{\mathfrak{N}} \, \mathrm{d}\xi_1}^{\Delta\delta \mathrm{U}_{\mathrm{strain2}}} + \overbrace{\int_0^L \delta\boldsymbol{\Phi}^T \boldsymbol{B}_2^T \Delta\boldsymbol{B}_1^T \boldsymbol{\Lambda} \overline{\mathfrak{N}} \, \mathrm{d}\xi_1}^{\Delta\delta \mathrm{U}_{\mathrm{strain3}}} . \tag{10.6}$$

Since the process of linearization is similar to the variation, using Eq. (7.37), we get $\Delta\overline{\boldsymbol{\epsilon}} = \boldsymbol{\Lambda}^T \boldsymbol{B}_1 \boldsymbol{B}_2 \Delta\boldsymbol{\Phi}$. Using the constitutive law given in Eq. (9.18), we can obtain the linear increment in the material internal force vector as,

$$\Delta\overline{\mathfrak{N}} = \overline{\mathfrak{C}} \Delta\overline{\boldsymbol{\epsilon}} = \overline{\mathfrak{C}} \boldsymbol{\Lambda}^T \boldsymbol{B}_1 \boldsymbol{B}_2 \Delta\boldsymbol{\Phi}. \tag{10.7}$$

Thus,

$$\begin{aligned} \Delta\delta \mathrm{U}_{\mathrm{strain1}} &= \mathrm{D}\delta \mathrm{U}_{\mathrm{strain1}}(\boldsymbol{\Phi}, \delta\boldsymbol{\Phi}).\Delta\boldsymbol{\Phi} \\ &= \int_0^L \delta\boldsymbol{\Phi}^T \boldsymbol{B}_2^T \boldsymbol{B}_1^T \boldsymbol{\Lambda} \overline{\mathfrak{C}} \boldsymbol{\Lambda}^T \boldsymbol{B}_1 \boldsymbol{B}_2 \Delta\boldsymbol{\Phi} \, \mathrm{d}\xi_1 = \int_0^L \delta\boldsymbol{\Phi}^T \boldsymbol{B}_2^T \boldsymbol{B}_1^T \mathfrak{C} \boldsymbol{B}_1 \boldsymbol{B}_2 \Delta\boldsymbol{\Phi} \, \mathrm{d}\xi_1. \end{aligned} \tag{10.8}$$

Similarly, we have $\Delta\boldsymbol{Q} = \Delta\hat{\boldsymbol{\alpha}}.\boldsymbol{Q}$, using which, the following is obtained,

$$\begin{aligned} \Delta\boldsymbol{\Lambda}\overline{\mathfrak{N}} &= [\Delta\hat{\boldsymbol{\alpha}}.\mathfrak{N}_{\boldsymbol{\varepsilon}}; \Delta\hat{\boldsymbol{\alpha}}.\mathfrak{N}_{\partial_{\xi_1}\boldsymbol{\varepsilon}}; \Delta\hat{\boldsymbol{\alpha}}.\mathfrak{N}_{\boldsymbol{\kappa}}; \Delta\hat{\boldsymbol{\alpha}}.\mathfrak{N}_{\partial_{\xi_1}\boldsymbol{\kappa}}; \Delta\hat{\boldsymbol{\alpha}}.\mathfrak{N}_{\partial^2_{\xi_1}\boldsymbol{\kappa}}; \Delta\hat{\boldsymbol{\alpha}}.\mathfrak{N}_{\partial^3_{\xi_1}\boldsymbol{\kappa}}; 0; 0; 0] \\ &= \boldsymbol{B}_4 \Delta\boldsymbol{\Theta} = \boldsymbol{B}_4 \boldsymbol{B}_2 \Delta\boldsymbol{\Phi}. \end{aligned} \tag{10.9}$$

Here,

$$\boldsymbol{B}_4 = \begin{bmatrix} \mathbf{0}_3 & \mathbf{0}_3 & \mathbf{0}_3 & -\hat{\mathfrak{N}}_{\boldsymbol{\varepsilon}} & \mathbf{0}_3 & \mathbf{0}_3 & \mathbf{0}_3 & \mathbf{0}_3 & \mathbf{0}_3 \\ \mathbf{0}_3 & \mathbf{0}_3 & \mathbf{0}_3 & -\hat{\mathfrak{N}}_{\partial_{\xi_1}\boldsymbol{\varepsilon}} & \mathbf{0}_3 & \mathbf{0}_3 & \mathbf{0}_3 & \mathbf{0}_3 & \mathbf{0}_3 \\ \mathbf{0}_3 & \mathbf{0}_3 & \mathbf{0}_3 & -\hat{\mathfrak{N}}_{\boldsymbol{\kappa}} & \mathbf{0}_3 & \mathbf{0}_3 & \mathbf{0}_3 & \mathbf{0}_3 & \mathbf{0}_3 \\ \mathbf{0}_3 & \mathbf{0}_3 & \mathbf{0}_3 & -\hat{\mathfrak{N}}_{\partial_{\xi_1}\boldsymbol{\kappa}} & \mathbf{0}_3 & \mathbf{0}_3 & \mathbf{0}_3 & \mathbf{0}_3 & \mathbf{0}_3 \\ \mathbf{0}_3 & \mathbf{0}_3 & \mathbf{0}_3 & -\hat{\mathfrak{N}}_{\partial^2_{\xi_1}\boldsymbol{\kappa}} & \mathbf{0}_3 & \mathbf{0}_3 & \mathbf{0}_3 & \mathbf{0}_3 & \mathbf{0}_3 \\ \mathbf{0}_3 & \mathbf{0}_3 & \mathbf{0}_3 & -\hat{\mathfrak{N}}_{\partial^3_{\xi_1}\boldsymbol{\kappa}} & \mathbf{0}_3 & \mathbf{0}_3 & \mathbf{0}_3 & \mathbf{0}_3 & \mathbf{0}_3 \\ \mathbf{0}_3 & \mathbf{0}_3 & \mathbf{0}_3 & \mathbf{0}_3 & \mathbf{0}_3 & \mathbf{0}_3 & \mathbf{0}_3 & \mathbf{0}_3 & \mathbf{0}_3 \end{bmatrix} \tag{10.10}$$

Thus,

$$\Delta\delta \mathrm{U}_{\text{strain2}} = \mathrm{D}\delta \mathrm{U}_{\text{strain2}}(\boldsymbol{\Phi}, \delta\boldsymbol{\Phi}).\Delta\boldsymbol{\Phi} = \int_0^L \delta\boldsymbol{\Phi}^T \boldsymbol{B}_2^T \boldsymbol{B}_1^T \boldsymbol{B}_4 \boldsymbol{B}_2 \Delta\boldsymbol{\Phi} \, \mathrm{d}\xi_1. \tag{10.11}$$

Finally, to derive the expression of $\Delta\delta \mathrm{U}_{\text{strain3}}$, we consider the following results:

$$\begin{aligned}
&\Delta\boldsymbol{\kappa} = \Delta\partial_{\xi_1}\boldsymbol{\alpha} - \hat{\boldsymbol{\kappa}}.\Delta\boldsymbol{\alpha};\\
&\Delta\partial_{\xi_1}\boldsymbol{\kappa} = \Delta\partial^2_{\xi_1}\boldsymbol{\alpha} + \hat{\boldsymbol{\kappa}}.\Delta\partial_{\xi_1}\boldsymbol{\alpha} - \partial_{\xi_1}\hat{\boldsymbol{\kappa}}.\Delta\boldsymbol{\alpha};\\
&\Delta\partial^2_{\xi_1}\boldsymbol{\kappa} = \Delta\partial^3_{\xi_1}\boldsymbol{\alpha} - \hat{\boldsymbol{\kappa}}.\Delta\partial^2_{\xi_1}\boldsymbol{\alpha} - 2\partial_{\xi_1}\hat{\boldsymbol{\kappa}}.\Delta\partial_{\xi_1}\boldsymbol{\alpha} - \partial^2_{\xi_1}\hat{\boldsymbol{\kappa}}.\Delta\boldsymbol{\alpha}.
\end{aligned} \tag{10.12}$$

For $\hat{\boldsymbol{A}}, \hat{\boldsymbol{B}} \in so(3)$ with their corresponding axial vectors $\boldsymbol{A}, \boldsymbol{B} \in \mathbb{R}^3$ and the vector $\boldsymbol{v} \in \mathbb{R}^3$, we note the following identities:

$$\begin{aligned}
&\hat{\boldsymbol{A}}.\hat{\boldsymbol{B}}.\boldsymbol{v} = -\hat{\boldsymbol{A}}.\hat{\boldsymbol{v}}.\boldsymbol{B} = -\left[\hat{\boldsymbol{B}}, \hat{\boldsymbol{v}}\right].\boldsymbol{A};\\
&\hat{\boldsymbol{B}}.\hat{\boldsymbol{A}}.\hat{\boldsymbol{A}}.\boldsymbol{v} = \left[\widehat{\hat{\boldsymbol{A}}.\boldsymbol{v}}, \hat{\boldsymbol{A}}\right].\boldsymbol{B} = \left[\left[\hat{\boldsymbol{A}}, \hat{\boldsymbol{v}}\right], \hat{\boldsymbol{A}}\right].\boldsymbol{B}.
\end{aligned} \tag{10.13}$$

Using results in Eq. (10.12) and (10.13) along with the expression of $\boldsymbol{B}_1^T$ in Eq. (7.38), we obtain

$$\Delta\boldsymbol{B}_1^T\mathfrak{N} = \boldsymbol{B}_5\Delta\boldsymbol{\Theta} = \boldsymbol{B}_5\boldsymbol{B}_2\Delta\boldsymbol{\Phi}. \tag{10.14}$$

The matrix $\boldsymbol{B}_5$ is defined as follows,

$$\boldsymbol{B}_5 = \begin{bmatrix}
\boldsymbol{0}_3 & \boldsymbol{0}_3 & \boldsymbol{0}_3 & \boldsymbol{0}_3 & \boldsymbol{0}_3 & \boldsymbol{0}_3 & \boldsymbol{0}_3 & \boldsymbol{0}_3 & \boldsymbol{0}_3\\
\boldsymbol{0}_3 & \boldsymbol{0}_3 & \boldsymbol{0}_3 & \boldsymbol{B}_{5_{24}} & \boldsymbol{B}_{5_{25}} & \boldsymbol{0}_3 & \boldsymbol{0}_3 & \boldsymbol{0}_3 & \boldsymbol{0}_3\\
\boldsymbol{0}_3 & \boldsymbol{0}_3 & \boldsymbol{0}_3 & \boldsymbol{0}_3 & \boldsymbol{0}_3 & \boldsymbol{0}_3 & \boldsymbol{0}_3 & \boldsymbol{0}_3 & \boldsymbol{0}_3\\
\boldsymbol{0}_3 & \boldsymbol{B}_{5_{42}} & \boldsymbol{B}_{5_{43}} & \boldsymbol{B}_{5_{44}} & \boldsymbol{B}_{5_{45}} & \boldsymbol{0}_3 & \boldsymbol{0}_3 & \boldsymbol{0}_3 & \boldsymbol{0}_3\\
\boldsymbol{0}_3 & \boldsymbol{B}_{5_{52}} & \boldsymbol{0}_3 & \boldsymbol{B}_{5_{54}} & \boldsymbol{B}_{5_{55}} & \boldsymbol{B}_{5_{56}} & \boldsymbol{B}_{5_{57}} & \boldsymbol{0}_3 & \boldsymbol{0}_3\\
\boldsymbol{0}_3 & \boldsymbol{0}_3 & \boldsymbol{0}_3 & \boldsymbol{B}_{5_{64}} & \boldsymbol{B}_{5_{65}} & \boldsymbol{B}_{5_{66}} & \boldsymbol{0}_3 & \boldsymbol{0}_3 & \boldsymbol{0}_3\\
\boldsymbol{0}_3 & \boldsymbol{0}_3 & \boldsymbol{0}_3 & \boldsymbol{B}_{5_{74}} & \boldsymbol{B}_{5_{75}} & \boldsymbol{0}_3 & \boldsymbol{0}_3 & \boldsymbol{0}_3 & \boldsymbol{0}_3\\
\boldsymbol{0}_3 & \boldsymbol{0}_3 & \boldsymbol{0}_3 & \boldsymbol{0}_3 & \boldsymbol{0}_3 & \boldsymbol{0}_3 & \boldsymbol{0}_3 & \boldsymbol{0}_3 & \boldsymbol{0}_3\\
\boldsymbol{0}_3 & \boldsymbol{0}_3 & \boldsymbol{0}_3 & \boldsymbol{0}_3 & \boldsymbol{0}_3 & \boldsymbol{0}_3 & \boldsymbol{0}_3 & \boldsymbol{0}_3 & \boldsymbol{0}_3
\end{bmatrix} \tag{10.15}$$

where,

$$\boldsymbol{B}_{5_{24}} = \hat{\mathfrak{N}}_{\partial_{\xi_1}\boldsymbol{\varepsilon}}.\hat{\boldsymbol{\kappa}};$$

$$\boldsymbol{B}_{5_{25}} = -\hat{\mathfrak{N}}_{\partial_{\xi_1}\boldsymbol{\varepsilon}};$$

$$\boldsymbol{B}_{5_{42}} = \hat{\mathfrak{N}}_{\boldsymbol{\varepsilon}} + \left[\hat{\boldsymbol{\kappa}}, \hat{\mathfrak{N}}_{\partial_{\xi_1}\boldsymbol{\varepsilon}}\right];$$

$$\boldsymbol{B}_{5_{43}} = \hat{\mathfrak{N}}_{\partial_{\xi_1}\boldsymbol{\varepsilon}};$$

$$\boldsymbol{B}_{5_{44}} = -\partial_{\xi_1}\hat{\boldsymbol{\varphi}}.\hat{\mathfrak{N}}_{\partial_{\xi_1}\boldsymbol{\varepsilon}}.\hat{\boldsymbol{\kappa}};$$

$$\boldsymbol{B}_{5_{45}} = \partial_{\xi_1}\hat{\boldsymbol{\varphi}}.\hat{\mathfrak{N}}_{\partial_{\xi_1}\boldsymbol{\varepsilon}};$$

$$\boldsymbol{B}_{5_{52}} = \hat{\mathfrak{N}}_{\partial_{\xi_1}\boldsymbol{\varepsilon}};$$

$$\begin{aligned}\boldsymbol{B}_{5_{54}} =& \Big(\hat{\mathfrak{N}}_{\partial_{\xi_1}\boldsymbol{\kappa}} + \left[\hat{\boldsymbol{\kappa}}, \hat{\mathfrak{N}}_{\partial^2_{\xi_1}\boldsymbol{\kappa}}\right] + \hat{\boldsymbol{\kappa}}.\hat{\mathfrak{N}}_{\partial^2_{\xi_1}\boldsymbol{\kappa}} + \hat{\boldsymbol{\kappa}}.\left[\hat{\boldsymbol{\kappa}}, \hat{\mathfrak{N}}_{\partial^3_{\xi_1}\boldsymbol{\kappa}}\right] + \left[\hat{\boldsymbol{\kappa}}, [\hat{\boldsymbol{\kappa}}, \hat{\mathfrak{N}}_{\partial^3_{\xi_1}\boldsymbol{\kappa}}]\right] + \hat{\boldsymbol{\kappa}}.\hat{\boldsymbol{\kappa}}.\hat{\mathfrak{N}}_{\partial^3_{\xi_1}\boldsymbol{\kappa}} \\ &+ \left[\partial_{\xi_1}\hat{\boldsymbol{\kappa}}, \hat{\mathfrak{N}}_{\partial^3_{\xi_1}\boldsymbol{\kappa}}\right] + 2\partial_{\xi_1}\hat{\boldsymbol{\kappa}}.\hat{\mathfrak{N}}_{\partial^3_{\xi_1}\boldsymbol{\kappa}}\Big).\hat{\boldsymbol{\kappa}} + \Big(\hat{\mathfrak{N}}_{\partial^2_{\xi_1}\boldsymbol{\kappa}} + \hat{\boldsymbol{\kappa}}.\hat{\mathfrak{N}}_{\partial^3_{\xi_1}\boldsymbol{\kappa}} + 2\left[\hat{\boldsymbol{\kappa}}, \hat{\mathfrak{N}}_{\partial^3_{\xi_1}\boldsymbol{\kappa}}\right]\Big).\partial_{\xi_1}\hat{\boldsymbol{\kappa}} \\ &+ \hat{\mathfrak{N}}_{\partial^3_{\xi_1}\boldsymbol{\kappa}}.\partial^2_{\xi_1}\hat{\boldsymbol{\kappa}};\end{aligned}$$

$$\begin{aligned}\boldsymbol{B}_{5_{55}} =& -\Big(\hat{\mathfrak{N}}_{\partial_{\xi_1}\boldsymbol{\kappa}} + \left[\hat{\boldsymbol{\kappa}}, \hat{\mathfrak{N}}_{\partial^2_{\xi_1}\boldsymbol{\kappa}}\right] + \hat{\boldsymbol{\kappa}}.\hat{\mathfrak{N}}_{\partial^2_{\xi_1}\boldsymbol{\kappa}} + \hat{\boldsymbol{\kappa}}.\left[\hat{\boldsymbol{\kappa}}, \hat{\mathfrak{N}}_{\partial^3_{\xi_1}\boldsymbol{\kappa}}\right] + \left[\hat{\boldsymbol{\kappa}}, [\hat{\boldsymbol{\kappa}}, \hat{\mathfrak{N}}_{\partial^3_{\xi_1}\boldsymbol{\kappa}}]\right] + \hat{\boldsymbol{\kappa}}.\hat{\boldsymbol{\kappa}}.\hat{\mathfrak{N}}_{\partial^3_{\xi_1}\boldsymbol{\kappa}} \\ &+ \left[\partial_{\xi_1}\hat{\boldsymbol{\kappa}}, \hat{\mathfrak{N}}_{\partial^3_{\xi_1}\boldsymbol{\kappa}}\right] + 2\partial_{\xi_1}\hat{\boldsymbol{\kappa}}.\hat{\mathfrak{N}}_{\partial^3_{\xi_1}\boldsymbol{\kappa}}\Big) + \Big(\hat{\mathfrak{N}}_{\partial^2_{\xi_1}\boldsymbol{\kappa}} + \hat{\boldsymbol{\kappa}}.\hat{\mathfrak{N}}_{\partial^3_{\xi_1}\boldsymbol{\kappa}} + 2\left[\hat{\boldsymbol{\kappa}}, \hat{\mathfrak{N}}_{\partial^3_{\xi_1}\boldsymbol{\kappa}}\right]\Big).\hat{\boldsymbol{\kappa}} \\ &+ 2\hat{\mathfrak{N}}_{\partial^3_{\xi_1}\boldsymbol{\kappa}}.\partial_{\xi_1}\hat{\boldsymbol{\kappa}};\end{aligned}$$

$$\boldsymbol{B}_{5_{56}} = \hat{\mathfrak{N}}_{\partial^3_{\xi_1}\boldsymbol{\kappa}}.\hat{\boldsymbol{\kappa}} - \Big(\hat{\mathfrak{N}}_{\partial^2_{\xi_1}\boldsymbol{\kappa}} + \hat{\boldsymbol{\kappa}}.\hat{\mathfrak{N}}_{\partial^3_{\xi_1}\boldsymbol{\kappa}} + 2\left[\hat{\boldsymbol{\kappa}}, \hat{\mathfrak{N}}_{\partial^3_{\xi_1}\boldsymbol{\kappa}}\right]\Big);$$

$$\boldsymbol{B}_{5_{57}} = -\hat{\mathfrak{N}}_{\partial^3_{\xi_1}\boldsymbol{\kappa}};$$

$$\boldsymbol{B}_{5_{64}} = 3\hat{\mathfrak{N}}_{\partial^3_{\xi_1}\boldsymbol{\kappa}}.\partial_{\xi_1}\hat{\boldsymbol{\kappa}} + \Big(2\hat{\mathfrak{N}}_{\partial^2_{\xi_1}\boldsymbol{\kappa}} + 3\left[\hat{\boldsymbol{\kappa}}, \hat{\mathfrak{N}}_{\partial^3_{\xi_1}\boldsymbol{\kappa}}\right] + 3\hat{\boldsymbol{\kappa}}.\hat{\mathfrak{N}}_{\partial^3_{\xi_1}\boldsymbol{\kappa}}\Big).\hat{\boldsymbol{\kappa}};$$

$$\boldsymbol{B}_{5_{65}} = -\Big(2\hat{\mathfrak{N}}_{\partial^2_{\xi_1}\boldsymbol{\kappa}} + 3\left[\hat{\boldsymbol{\kappa}}, \hat{\mathfrak{N}}_{\partial^3_{\xi_1}\boldsymbol{\kappa}}\right] + 3\hat{\boldsymbol{\kappa}}.\hat{\mathfrak{N}}_{\partial^3_{\xi_1}\boldsymbol{\kappa}}\Big) + 3\hat{\mathfrak{N}}_{\partial^3_{\xi_1}\boldsymbol{\kappa}}.\hat{\boldsymbol{\kappa}};$$

$$\boldsymbol{B}_{5_{66}} = -3\hat{\mathfrak{N}}_{\partial^3_{\xi_1}\boldsymbol{\kappa}};$$

$$\boldsymbol{B}_{5_{74}} = 3\hat{\mathfrak{N}}_{\partial^3_{\xi_1}\boldsymbol{\kappa}}.\hat{\boldsymbol{\kappa}};$$

$$\boldsymbol{B}_{5_{75}} = -3\hat{\mathfrak{N}}_{\partial^3_{\xi_1}\boldsymbol{\kappa}}.$$

Therefore, we have,

$$\Delta\delta \mathrm{U}_{\mathrm{strain3}} = \mathrm{D}\delta \mathrm{U}_{\mathrm{strain3}}(\boldsymbol{\Phi}, \delta\boldsymbol{\Phi}).\Delta\boldsymbol{\Phi} = \int_0^L \delta\boldsymbol{\Phi}^T \boldsymbol{B}_2^T \boldsymbol{B}_5 \boldsymbol{B}_2 \Delta\boldsymbol{\Phi} \, \mathrm{d}\xi_1. \tag{10.16}$$

Finally, if $\boldsymbol{B}_6 = \boldsymbol{B}_5 + \boldsymbol{B}_1^T.\boldsymbol{B}_4$, we define:

$$\Delta\delta \mathrm{U}_{\mathrm{strain23}} = \Delta\delta \mathrm{U}_{\mathrm{strain2}} + \Delta\delta \mathrm{U}_{\mathrm{strain3}} = \mathrm{D}\delta \mathrm{U}_{\mathrm{strain23}}(\boldsymbol{\Phi}, \delta\boldsymbol{\Phi}).\Delta\boldsymbol{\Phi} = \int_0^L \delta\boldsymbol{\Phi}^T \boldsymbol{B}_2^T \boldsymbol{B}_6 \boldsymbol{B}_2 \Delta\boldsymbol{\Phi} \, \mathrm{d}\xi_1. \tag{10.17}$$

Therefore, from Eq. (10.6), (10.8) and (10.17), we get,

$$\Delta\delta \mathrm{U}_{\mathrm{strain}} = \int_0^L \delta\boldsymbol{\Phi}^T \boldsymbol{B}_2^T \boldsymbol{B}_1^T \mathfrak{C} \boldsymbol{B}_1 \boldsymbol{B}_2 \Delta\boldsymbol{\Phi} \, \mathrm{d}\xi_1 + \int_0^L \delta\boldsymbol{\Phi}^T \boldsymbol{B}_2^T \boldsymbol{B}_6 \boldsymbol{B}_2 \Delta\boldsymbol{\Phi} \, \mathrm{d}\xi_1. \tag{10.18}$$

The term $\Delta\delta \mathrm{U}_{\mathrm{strain1}}$ leads to the symmetric material stiffness matrix whereas, the term $\Delta\delta \mathrm{U}_{\mathrm{strain23}}$ yields geometric stiffness matrix (not necessarily symmetric).

10.2.3 Linearization of virtual external work done

From the expression of virtual external work, we have:

$$\Delta\delta \mathrm{W}_{\mathrm{ext}} = \overbrace{\int_0^L \delta\boldsymbol{\Phi}^T \boldsymbol{B}_2^T \Delta\boldsymbol{B}_3 \boldsymbol{N}_f \, \mathrm{d}\xi_1}^{\Delta\delta \mathrm{W}_{\mathrm{ext1}}} + \overbrace{\int_0^L \delta\boldsymbol{\Phi}^T \boldsymbol{B}_2^T \boldsymbol{B}_3 \Delta\boldsymbol{N}_f \, \mathrm{d}\xi_1}^{\Delta\delta \mathrm{W}_{\mathrm{ext2}}}. \tag{10.19}$$

The term $\Delta\delta \mathrm{W}_{\mathrm{ext1}}$ arises due to geometric dependence of $\Delta\delta \mathrm{W}_{\mathrm{ext}}$; whereas the term $\Delta\delta \mathrm{W}_{\mathrm{ext2}}$ is due to non-conservative nature of the external forces. We can represent $\Delta\boldsymbol{B}_3\boldsymbol{N}_f$ and $\boldsymbol{B}_3\Delta\boldsymbol{N}_f$ in a more desirable form:

$$\begin{aligned} \Delta\boldsymbol{B}_3\boldsymbol{N}_f &= \boldsymbol{B}_7\Delta\boldsymbol{\Theta} = \boldsymbol{B}_7\boldsymbol{B}_2\Delta\boldsymbol{\Phi}; \\ \boldsymbol{B}_3\Delta\boldsymbol{N}_f &= \boldsymbol{B}_8\Delta\boldsymbol{\Theta} = \boldsymbol{B}_8\boldsymbol{B}_2\Delta\boldsymbol{\Phi}. \end{aligned} \tag{10.20}$$

The matrix $\boldsymbol{B}_7$ is defined as,

$$\boldsymbol{B}_7 = \begin{bmatrix} \mathbf{0}_3 & \mathbf{0}_3 & \mathbf{0}_3 & \mathbf{0}_3 & \mathbf{0}_3 & \mathbf{0}_3 & \mathbf{0}_3 & \mathbf{0}_3 & \mathbf{0}_3 \\ \mathbf{0}_3 & \mathbf{0}_3 & \mathbf{0}_3 & \mathbf{0}_3 & \mathbf{0}_3 & \mathbf{0}_3 & \mathbf{0}_3 & \mathbf{0}_3 & \mathbf{0}_3 \\ \mathbf{0}_3 & \mathbf{0}_3 & \mathbf{0}_3 & \mathbf{0}_3 & \mathbf{0}_3 & \mathbf{0}_3 & \mathbf{0}_3 & \mathbf{0}_3 & \mathbf{0}_3 \\ \mathbf{0}_3 & \boldsymbol{B}_{7_{42}} & \mathbf{0}_3 & \mathbf{0}_3 & \mathbf{0}_3 & \mathbf{0}_3 & \mathbf{0}_3 & \mathbf{0}_3 & \mathbf{0}_3 \\ \mathbf{0}_3 & \mathbf{0}_3 & \mathbf{0}_3 & \boldsymbol{B}_{7_{54}} & \boldsymbol{B}_{7_{55}} & \boldsymbol{B}_{7_{56}} & \mathbf{0}_3 & \mathbf{0}_3 & \mathbf{0}_3 \\ \mathbf{0}_3 & \mathbf{0}_3 & \mathbf{0}_3 & \boldsymbol{B}_{7_{64}} & \boldsymbol{B}_{7_{65}} & \mathbf{0}_3 & \mathbf{0}_3 & \mathbf{0}_3 & \mathbf{0}_3 \\ \mathbf{0}_3 & \mathbf{0}_3 & \mathbf{0}_3 & \mathbf{0}_3 & \mathbf{0}_3 & \mathbf{0}_3 & \mathbf{0}_3 & \mathbf{0}_3 & \mathbf{0}_3 \\ \mathbf{0}_3 & \mathbf{0}_3 & \mathbf{0}_3 & \mathbf{0}_3 & \mathbf{0}_3 & \mathbf{0}_3 & \mathbf{0}_3 & \mathbf{0}_3 & \mathbf{0}_3 \\ \mathbf{0}_3 & \mathbf{0}_3 & \mathbf{0}_3 & \mathbf{0}_3 & \mathbf{0}_3 & \mathbf{0}_3 & \mathbf{0}_3 & \mathbf{0}_3 & \mathbf{0}_3 \end{bmatrix}. \tag{10.21}$$

where,

$$\boldsymbol{B}_{7_{42}} = \hat{\boldsymbol{N}}_{\boldsymbol{\varepsilon}}; \tag{10.22a}$$

$$\boldsymbol{B}_{7_{54}} = \left(\hat{\boldsymbol{N}}_{\partial_{\xi_1}\boldsymbol{\kappa}} + \left[\hat{\boldsymbol{\kappa}}, \hat{\boldsymbol{N}}_{\partial^2_{\xi_1}\boldsymbol{\kappa}}\right] + \hat{\boldsymbol{\kappa}}.\hat{\boldsymbol{N}}_{\partial^2_{\xi_1}\boldsymbol{\kappa}}\right).\hat{\boldsymbol{\kappa}} + \hat{\boldsymbol{N}}_{\partial^2_{\xi_1}\boldsymbol{\kappa}}.\partial_{\xi_1}\hat{\boldsymbol{\kappa}}; \tag{10.22b}$$

$$\boldsymbol{B}_{7_{55}} = \hat{\boldsymbol{N}}_{\partial^2_{\xi_1}\boldsymbol{\kappa}}.\hat{\boldsymbol{\kappa}} - \left(\hat{\boldsymbol{N}}_{\partial_{\xi_1}\boldsymbol{\kappa}} + \left[\hat{\boldsymbol{\kappa}}, \hat{\boldsymbol{N}}_{\partial^2_{\xi_1}\boldsymbol{\kappa}}\right] + \hat{\boldsymbol{\kappa}}.\hat{\boldsymbol{N}}_{\partial^2_{\xi_1}\boldsymbol{\kappa}}\right); \tag{10.22c}$$

$$\boldsymbol{B}_{7_{56}} = -\hat{\boldsymbol{N}}_{\partial^2_{\xi_1}\boldsymbol{\kappa}}; \tag{10.22d}$$

$$\boldsymbol{B}_{7_{64}} = 2\hat{\boldsymbol{N}}_{\partial^2_{\xi_1}\boldsymbol{\kappa}}.\hat{\boldsymbol{\kappa}}; \tag{10.22e}$$

$$\boldsymbol{B}_{7_{65}} = -2\hat{\boldsymbol{N}}_{\partial^2_{\xi_1}\boldsymbol{\kappa}}. \tag{10.22f}$$

The matrix $\boldsymbol{B}_8$ depends on the characteristic of external loading (for example: follower load, pressure load, etc) and is determined on a case by case basis. Therefore, using Eq. (10.19) and (10.20), we have:

$$\Delta\delta \mathrm{W}_{\mathrm{ext}} = \int_0^L \delta\boldsymbol{\Phi}^T \boldsymbol{B}_2^T \boldsymbol{B}_7 \boldsymbol{B}_2 \Delta\boldsymbol{\Phi}\, \mathrm{d}\xi_1 + \int_0^L \delta\boldsymbol{\Phi}^T \boldsymbol{B}_2^T \boldsymbol{B}_8 \boldsymbol{B}_2 \Delta\boldsymbol{\Phi}\, \mathrm{d}\xi_1. \tag{10.23}$$

10.2.4 Example of concentrated follower load and moment

To demonstrate treatment of concentrated and follower load, we consider a case of external loading where we have a concentrated follower load and moment acting at $\xi_1 = \xi_1^{\#}$, such that $\boldsymbol{N}_{\varphi}(\xi_1) = \boldsymbol{Q}.\overline{\boldsymbol{N}}_{\varphi}\delta(\xi_1 - \xi_1^{\#})$ and $\boldsymbol{N}_{\alpha}(\xi_1) = \boldsymbol{Q}.\overline{\boldsymbol{N}}_{\alpha}\delta(\xi_1 - \xi_1^{\#})$. Here, $\delta(\xi_1 - \xi_1^{\#})$ is Dirac delta function. We assume all the other loads constituting $\boldsymbol{N}_f$ to be zero. We have,

$$\begin{aligned} \Delta\boldsymbol{N}_{\varphi}(\xi_1) &= \Delta\hat{\boldsymbol{\alpha}}.\boldsymbol{N}_{\varphi}.\delta(\xi_1 - \xi_1^{\#}) = -\hat{\boldsymbol{N}}_{\varphi}.\Delta\boldsymbol{\alpha}.\delta(\xi_1 - \xi_1^{\#}); \\ \Delta\boldsymbol{N}_{\alpha}(\xi_1) &= \Delta\hat{\boldsymbol{\alpha}}.\boldsymbol{N}_{\alpha}.\delta(\xi_1 - \xi_1^{\#}) = -\hat{\boldsymbol{N}}_{\alpha}.\Delta\boldsymbol{\alpha}.\delta(\xi_1 - \xi_1^{\#}). \end{aligned} \tag{10.24}$$

The linearized external force $\Delta\boldsymbol{N}_f$ and the matrix $\boldsymbol{B}_8$ can then be written as,

$$\begin{aligned} \Delta\boldsymbol{N}_f &= \boldsymbol{B}_9.\boldsymbol{B}_2.\Delta\boldsymbol{\Phi}.\delta(\xi_1 - \xi_1^{\#}); \\ \boldsymbol{B}_8 &= \boldsymbol{B}_3.\boldsymbol{B}_9. \end{aligned} \tag{10.25}$$

The matrix $\boldsymbol{B}_9$ is given below,

$$\boldsymbol{B}_9 = \begin{bmatrix} \mathbf{0}_3 & \mathbf{0}_3 & \mathbf{0}_3 & -\hat{\boldsymbol{N}}_{\varphi} & \mathbf{0}_3 & \mathbf{0}_3 & \mathbf{0}_3 & \mathbf{0}_3 \\ \mathbf{0}_3 & \mathbf{0}_3 & \mathbf{0}_3 & \mathbf{0}_3 & \mathbf{0}_3 & \mathbf{0}_3 & \mathbf{0}_3 & \mathbf{0}_3 \\ \mathbf{0}_3 & \mathbf{0}_3 & \mathbf{0}_3 & -\hat{\boldsymbol{N}}_{\alpha} & \mathbf{0}_3 & \mathbf{0}_3 & \mathbf{0}_3 & \mathbf{0}_3 \\ \mathbf{0}_3 & \mathbf{0}_3 & \mathbf{0}_3 & \mathbf{0}_3 & \mathbf{0}_3 & \mathbf{0}_3 & \mathbf{0}_3 & \mathbf{0}_3 \\ \mathbf{0}_3 & \mathbf{0}_3 & \mathbf{0}_3 & \mathbf{0}_3 & \mathbf{0}_3 & \mathbf{0}_3 & \mathbf{0}_3 & \mathbf{0}_3 \\ \mathbf{0}_3 & \mathbf{0}_3 & \mathbf{0}_3 & \mathbf{0}_3 & \mathbf{0}_3 & \mathbf{0}_3 & \mathbf{0}_3 & \mathbf{0}_3 \\ \mathbf{0}_1^T & \mathbf{0}_1^T & \mathbf{0}_1^T & \mathbf{0}_1^T & \mathbf{0}_1^T & \mathbf{0}_1^T & \mathbf{0}_1^T & \mathbf{0}_1^T \\ \mathbf{0}_1^T & \mathbf{0}_1^T & \mathbf{0}_1^T & \mathbf{0}_1^T & \mathbf{0}_1^T & \mathbf{0}_1^T & \mathbf{0}_1^T & \mathbf{0}_1^T \end{bmatrix}. \tag{10.26}$$

10.3 Discretization and Galerkin form of equilibrium equation

We discretize the domain using N_e elements. Any element e consist of N_{en} number of nodes and has length $L_e = \xi^e_{1b} - \xi^e_{1a}$, where, ξ^e_{1b} and ξ^e_{1a} are the arc-length of the first and last node of the element e, such that $\xi^e_{1b} > \xi^e_{1a}$ and $\xi^e_1 \in [\xi^e_{1a}, \xi^e_{1b}]$. We approximate the admissible incremental displacement field $\Delta\mathbf{\Phi}$ by a finite dimensional subspace that is subset of the variationally admissible tangent space. The incremental displacement field $(\Delta\boldsymbol{\varphi}^e, \Delta\boldsymbol{\alpha}^e, \Delta p^e)$ restricted to element e can then be interpolated by means of shape functions as:

$$\Delta\boldsymbol{\varphi}^e = \sum_{I=1}^{N_{en}} N_I \Delta\boldsymbol{\varphi}^e_I; \quad \Delta\boldsymbol{\alpha}^e = \sum_{I=1}^{N_{en}} N_I \Delta\boldsymbol{\alpha}^e_I; \quad \Delta p^e = \sum_{I=1}^{N_{en}} N_I \Delta p^e_I. \tag{10.27}$$

Here, $\Delta\boldsymbol{\varphi}^e_I$, $\Delta\boldsymbol{\alpha}^e_I$ and Δp^e_I represents the nodal incremental dispacement, vortivity and warping amplitude at node I of element e respectively; N_I is the shape-function associated with I^{th} node.

10.3.1 Unbalanced force vector

We first obtain the *nodal internal load vector* $\boldsymbol{f}^e_{\text{int}I}$. The approximated virtual strain energy can be written as

$$\begin{aligned}\delta \mathrm{U}^h_{\text{strain}} &= \sum_{e=1}^{N_e} \left(\sum_{I=1}^{N_{en}} \int_{\xi^e_{1a}}^{\xi^e_{1b}} \delta\mathbf{\Phi}_I^{e^T} \mathbb{B}_I^T \boldsymbol{B}_1^{e^T} \mathfrak{N}^e \, \mathrm{d}\xi_1 \right) \\ &= \sum_{e=1}^{N_e} \sum_{I=1}^{N_{en}} \delta\mathbf{\Phi}_I^{e^T} \overbrace{\left(\int_{\xi^e_{1a}}^{\xi^e_{1b}} \mathbb{B}_I^T \boldsymbol{B}_1^{e^T} \mathfrak{N}^e \, \mathrm{d}\xi_1 \right)}^{\boldsymbol{f}^e_{\text{int}I}} = \sum_{e=1}^{N_e} \sum_{I=1}^{N_{en}} \delta\mathbf{\Phi}_I^{e^T} \boldsymbol{f}^e_{\text{int}I}.\end{aligned} \tag{10.28}$$

The matrix $\mathbb{B}_I$, defined below, consists of the shape-functions and its derivatives. The superscript e on any quantity represents the restriction of that quantity on element e.

$$\mathbb{B}_I = \begin{bmatrix} N_I \boldsymbol{I}_3 & \mathbf{0}_3 & \mathbf{0}_1 \\ \partial_{\xi_1} N_I . \boldsymbol{I}_3 & \mathbf{0}_3 & \mathbf{0}_1 \\ \partial^2_{\xi_1} N_I . \boldsymbol{I}_3 & \mathbf{0}_3 & \mathbf{0}_1 \\ \mathbf{0}_3 & N_I \boldsymbol{I}_3 & \mathbf{0}_1 \\ \mathbf{0}_3 & \partial_{\xi_1} N_I . \boldsymbol{I}_3 & \mathbf{0}_1 \\ \mathbf{0}_3 & \partial^2_{\xi_1} N_I . \boldsymbol{I}_3 & \mathbf{0}_1 \\ \mathbf{0}_3 & \partial^3_{\xi_1} N_I . \boldsymbol{I}_3 & \mathbf{0}_1 \\ \mathbf{0}_3 & \partial^4_{\xi_1} N_I . \boldsymbol{I}_3 & \mathbf{0}_1 \\ \mathbf{0}_1^T & \mathbf{0}_1^T & N_I \\ \mathbf{0}_1^T & \mathbf{0}_1^T & \partial_{\xi_1} N_I \\ \mathbf{0}_1^T & \mathbf{0}_1^T & \partial^2_{\xi_1} N_I \end{bmatrix} . \text{ Here, } \partial^n_{\xi_1} N_I . \boldsymbol{I}_3 = \begin{bmatrix} \partial^n_{\xi_1} N_I & 0 & 0 \\ 0 & \partial^n_{\xi_1} N_I & 0 \\ 0 & 0 & \partial^n_{\xi_1} N_I \end{bmatrix} . \tag{10.29}$$

In order to define incremental load steps necessary for numerical formulation, we first define the load coefficient $\mathfrak{X} \in [0, 1]$ with $\boldsymbol{N}_f(\mathfrak{X}) = \mathfrak{X} \boldsymbol{N}_{f0}$, such that:

$$\delta \mathrm{W}_{\mathrm{ext}}(\mathfrak{X}) = \mathfrak{X} \delta \mathrm{W}_{\mathrm{ext0}} = \mathfrak{X} \int_0^L \delta \boldsymbol{\Phi}^T \boldsymbol{B}_2^T \boldsymbol{B}_3 \boldsymbol{N}_{f0} \, \mathrm{d}\xi_1 . \tag{10.30}$$

The approximated virtual external work is obtained as:

$$\begin{aligned} \delta \mathrm{W}^h_{\mathrm{ext0}} &= \sum_{e=1}^{N_e} \sum_{I=1}^{N_{en}} \delta \boldsymbol{\Phi}_I^{e^T} \overbrace{\left(\int_{\xi^e_{1a}}^{\xi^e_{1b}} \mathbb{B}_I^T \boldsymbol{B}_3 \boldsymbol{N}^e_{f0} \, \mathrm{d}\xi_1 \right)}^{\boldsymbol{f}^e_{\mathrm{ext0}I}} = \sum_{e=1}^{N_e} \sum_{I=1}^{N_{en}} \delta \boldsymbol{\Phi}_I^{e^T} \boldsymbol{f}^e_{\mathrm{ext0}I} . \\ \delta \mathrm{W}^h_{\mathrm{ext}}(\mathfrak{X}) &= \sum_{e=1}^{N_e} \sum_{I=1}^{N_{en}} \delta \boldsymbol{\Phi}_I^{e^T} \boldsymbol{f}^e_{\mathrm{ext}I}(\mathfrak{X}) ; \text{ where } \boldsymbol{f}^e_{\mathrm{ext}I}(\mathfrak{X}) = \mathfrak{X} \boldsymbol{f}^e_{\mathrm{ext0}I} . \end{aligned} \tag{10.31}$$

The expression of internal and external force vectors: $\boldsymbol{f}^e_{\mathrm{int}I}$ and $\boldsymbol{f}^e_{\mathrm{ext}I}(\mathfrak{X})$ are defined below,

$$\boldsymbol{f}^e_{\mathrm{int}I} = \int_{\xi^e_{1a}}^{\xi^e_{1b}} \mathbb{B}_I^T \boldsymbol{B}_1^{e^T} \boldsymbol{\mathfrak{R}}^e \, \mathrm{d}\xi_1 = \left[\boldsymbol{f}^e_{\mathrm{int}I1} ; \quad \boldsymbol{f}^e_{\mathrm{int}I2} ; \quad \boldsymbol{f}^e_{\mathrm{int}I3} \right] . \tag{10.32}$$

Here,

$$f^e_{\text{int}I1} = \int_{\xi^e_{1a}}^{\xi^e_{1b}} \left(\partial_{\xi_1} N_I (\mathfrak{R}^e_{\boldsymbol{\varepsilon}} + \hat{\boldsymbol{\kappa}}.\mathfrak{R}^e_{\partial_{\xi_1}\boldsymbol{\varepsilon}}) + \partial^2_{\xi_1} N_I \mathfrak{R}^e_{\partial_{\xi_1}\boldsymbol{\varepsilon}} \right) \mathrm{d}\xi_1; \tag{10.33}$$

$$\begin{aligned} f^e_{\text{int}I2} = \int_{\xi^e_{1a}}^{\xi^e_{1b}} \Bigg(& N_I \left(-\partial_{\xi_1}\hat{\boldsymbol{\varphi}}.\mathfrak{R}^e_{\boldsymbol{\varepsilon}} - \left(\partial^2_{\xi_1}\hat{\boldsymbol{\varphi}} + \partial_{\xi_1}\hat{\boldsymbol{\varphi}}.\hat{\boldsymbol{\kappa}} \right).\mathfrak{R}^e_{\partial_{\xi_1}\boldsymbol{\varepsilon}} \right) + \partial_{\xi_1} N_I . \Big(\mathfrak{R}^e_{\boldsymbol{\kappa}} - \partial_{\xi_1}\hat{\boldsymbol{\varphi}}.\mathfrak{R}^e_{\partial_{\xi_1}\boldsymbol{\varepsilon}} + \hat{\boldsymbol{\kappa}}.\mathfrak{R}^e_{\partial_{\xi_1}\boldsymbol{\kappa}} \\ & + \left(\hat{\boldsymbol{\kappa}}.\hat{\boldsymbol{\kappa}} + \partial_{\xi_1}\hat{\boldsymbol{\kappa}} \right).\mathfrak{R}^e_{\partial^2_{\xi_1}\boldsymbol{\kappa}} + \left(\hat{\boldsymbol{\kappa}}.\partial_{\xi_1}\hat{\boldsymbol{\kappa}} + 2\partial_{\xi_1}\hat{\boldsymbol{\kappa}}.\hat{\boldsymbol{\kappa}} + \partial^2_{\xi_1}\hat{\boldsymbol{\kappa}} + \hat{\boldsymbol{\kappa}}.\hat{\boldsymbol{\kappa}}.\hat{\boldsymbol{\kappa}} \right).\mathfrak{R}^e_{\partial^3_{\xi_1}\boldsymbol{\kappa}} \Big) \\ & + \partial^2_{\xi_1} N_I \left(\mathfrak{R}^e_{\partial_{\xi_1}\boldsymbol{\kappa}} + 2\hat{\boldsymbol{\kappa}}.\mathfrak{R}^e_{\partial^2_{\xi_1}\boldsymbol{\kappa}} + 3\left(\hat{\boldsymbol{\kappa}}.\hat{\boldsymbol{\kappa}} + \partial_{\xi_1}\hat{\boldsymbol{\kappa}} \right).\mathfrak{R}^e_{\partial^3_{\xi_1}\boldsymbol{\kappa}} \right) + \partial^3_{\xi_1} N_I \left(\mathfrak{R}^e_{\partial^2_{\xi_1}\boldsymbol{\kappa}} + 3\hat{\boldsymbol{\kappa}}.\mathfrak{R}^e_{\partial^3_{\xi_1}\boldsymbol{\kappa}} \right) \\ & + \partial^4_{\xi_1} N_I . \mathfrak{R}^e_{\partial^3_{\xi_1}\boldsymbol{\kappa}} \Bigg) \mathrm{d}\xi_1. \end{aligned} \tag{10.34}$$

$$f^e_{\text{int}I3} = \int_{\xi^e_{1a}}^{\xi^e_{1b}} \left(N_I . \mathfrak{N}^e_p + \partial_{\xi_1} N_I . \mathfrak{N}^e_{\partial_{\xi_1} p} + \partial^2_{\xi_1} N_I . \mathfrak{N}^e_{\partial^2_{\xi_1} p} \right) \mathrm{d}\xi_1. \tag{10.35}$$

Similarly,

$$\begin{aligned} \boldsymbol{f}^e_{\text{ext}I}(\mathfrak{X}) &= \int_{\xi^e_{1a}}^{\xi^e_{1b}} \mathbb{B}^T_I \boldsymbol{B}_3 \boldsymbol{N}^e_f(\mathfrak{X})\, \mathrm{d}\xi_1 = \left[\boldsymbol{f}^e_{\text{ext}I1};\quad \boldsymbol{f}^e_{\text{ext}I2};\quad \boldsymbol{f}^e_{\text{ext}I3} \right] \\ &= \int_{\xi^e_{1a}}^{\xi^e_{1b}} \begin{bmatrix} N_I . \boldsymbol{N}^e_{\boldsymbol{\varphi}}(\mathfrak{X}) + \partial_{\xi_1} N_I . \boldsymbol{N}^e_{\boldsymbol{\varepsilon}}(\mathfrak{X}) \\ \begin{pmatrix} N_I . \left(\boldsymbol{N}^e_{\boldsymbol{\alpha}}(\mathfrak{X}) - \partial_{\xi_1}\hat{\boldsymbol{\varphi}}.\boldsymbol{N}^e_{\boldsymbol{\varepsilon}}(\mathfrak{X}) \right) + \partial^2_{\xi_1} N_I . \boldsymbol{N}^e_{\partial^2_{\xi_1}\boldsymbol{\kappa}}(\mathfrak{X}) \\ + \partial_{\xi_1} N_I . (\boldsymbol{N}^e_{\boldsymbol{\kappa}}(\mathfrak{X}) + \hat{\boldsymbol{\kappa}}.\boldsymbol{N}^e_{\partial_{\xi_1}\boldsymbol{\kappa}}(\mathfrak{X}) + (\hat{\boldsymbol{\kappa}}.\hat{\boldsymbol{\kappa}} + \partial_{\xi_1}\hat{\boldsymbol{\kappa}}).\boldsymbol{N}^e_{\partial^2_{\xi_1}\boldsymbol{\kappa}}(\mathfrak{X}) \end{pmatrix} \\ N_I . N^e_p(\mathfrak{X}) + \partial_{\xi_1} N_I . N^e_{\partial_{\xi_1} p}(\mathfrak{X}) \end{bmatrix} \mathrm{d}\xi_1 \end{aligned}. \tag{10.36}$$

The unbalanced force vector associated with element e at node I is defined as:

$$\boldsymbol{P}^e_I(\boldsymbol{\Phi}^e, \mathfrak{X}) = \boldsymbol{f}^e_{\text{ext}I}(\boldsymbol{\Phi}^e, \mathfrak{X}) - \boldsymbol{f}^e_{\text{int}I}(\boldsymbol{\Phi}^e). \tag{10.37}$$

10.3.2 Element tangent stiffness

The approximated form of linearized virtual strain energy defined in Eq. (10.18) is given by:

$$\begin{aligned}\Delta\delta \mathrm{U}^h_{\text{strain}} &= \Delta\delta \mathrm{U}^h_{\text{strain1}} + \Delta\delta \mathrm{U}^h_{\text{strain23}} \\ &= \sum_{e=1}^{N_e}\sum_{I=1}^{N_{en}}\sum_{J=1}^{N_{en}} \delta\boldsymbol{\Phi}_I^{e^T}\left(\overbrace{\int_{\xi^e_{1a}}^{\xi^e_{1b}} \mathbb{B}_I^T \boldsymbol{B}_1^{e^T}\mathfrak{C}\boldsymbol{B}_1^e\mathbb{B}_J \,\mathrm{d}\xi_1}^{\boldsymbol{K}^e_{\mathrm{m}IJ}} + \overbrace{\int_{\xi^e_{1a}}^{\xi^e_{1b}} \mathbb{B}_I^T \boldsymbol{B}_6^e\mathbb{B}_J \,\mathrm{d}\xi_1}^{\boldsymbol{K}^e_{\mathrm{g}IJ}}\right)\Delta\boldsymbol{\Phi}_J^e \\ &= \sum_{e=1}^{N_e}\sum_{I=1}^{N_{en}}\sum_{J=1}^{N_{en}} \delta\boldsymbol{\Phi}_I^{e^T}\boldsymbol{K}^e_{\text{int}IJ}\Delta\boldsymbol{\Phi}_J^e.\end{aligned} \tag{10.38}$$

Here, the element tangential stiffness matrix corresponding to internal loads $\boldsymbol{K}^e_{\text{int}IJ} = \boldsymbol{K}^e_{\mathrm{m}IJ} + \boldsymbol{K}^e_{\mathrm{g}IJ}$ consist of a symmetric material part $\boldsymbol{K}^e_{mIJ}$ and a geometric part $\boldsymbol{K}^e_{\mathrm{g}IJ}$ (not necessarily symmetric. Similarly, the contribution to stiffness matrix due to external loads can be obtained by using Eq. (10.23), such that the approximated linearized virtual work is obtained as:

$$\begin{aligned}\Delta\delta \mathrm{W}^h_{\text{ext}}(\mathfrak{X}) &= \mathfrak{X}\Delta\delta \mathrm{W}^h_{\text{ext0}} \\ &= \sum_{e=1}^{N_e}\sum_{I=1}^{N_{en}}\sum_{J=1}^{N_{en}} \delta\boldsymbol{\Phi}_I^{e^T}\left(\overbrace{\int_{\xi^e_{1a}}^{\xi^e_{1b}} \mathbb{B}_I^T \boldsymbol{B}_7^e\mathbb{B}_J \,\mathrm{d}\xi_1}^{\boldsymbol{K}^e_{\text{ext1}IJ}} + \overbrace{\int_{\xi^e_{1a}}^{\xi^e_{1b}} \mathbb{B}_I^T \boldsymbol{B}_8^e\mathbb{B}_J \,\mathrm{d}\xi_1}^{\boldsymbol{K}^e_{\text{ext2}IJ}}\right)\Delta\boldsymbol{\Phi}_J^e \\ &= \sum_{e=1}^{N_e}\sum_{I=1}^{N_{en}}\sum_{J=1}^{N_{en}} \delta\boldsymbol{\Phi}_I^{e^T}\boldsymbol{K}^e_{\text{ext}IJ}\Delta\boldsymbol{\Phi}_J^e.\end{aligned} \tag{10.39}$$

Here, the element tangential stiffness matrix corresponding to internal loads $\boldsymbol{K}^e_{\text{ext}IJ} = \boldsymbol{K}^e_{\text{ext1}IJ} + \boldsymbol{K}^e_{\text{ext2}IJ}$ consist of two parts: the matrix $\boldsymbol{K}^e_{\text{ext1}IJ}$ gives contribution due to dependence of external work on the configuration of the system, assuming the force vectors are conservative; whereas, the matrix $\boldsymbol{K}^e_{\text{ext2}IJ}$ is due to non-conservative nature of the external forces. The element stiffness

matrix is given as:

$$\begin{aligned}\boldsymbol{K}^e_{IJ}(\boldsymbol{\Phi}^e,\mathfrak{X}) &= \boldsymbol{K}^e_{\text{int}IJ}(\boldsymbol{\Phi}^e) - \boldsymbol{K}^e_{\text{ext}IJ}(\boldsymbol{\Phi}^e,\mathfrak{X}) \\ &= \boldsymbol{K}^e_{\text{m}IJ}(\boldsymbol{\Phi}^e) + \boldsymbol{K}^e_{\text{g}IJ}(\boldsymbol{\Phi}^e) - \boldsymbol{K}^e_{\text{ext1}IJ}(\boldsymbol{\Phi}^e,\mathfrak{X}) - \boldsymbol{K}^e_{\text{ext2}IJ}(\boldsymbol{\Phi}^e,\mathfrak{X}).\end{aligned} \tag{10.40}$$

10.3.3 Matrix form of linearized equation of motion and iterative solution

The unbalanced force vector and the element tangent stiffness can be assembled using assembly operator $\mathbb{A}$ such that the global stiffness and global unbalanced force is obtained as:

$$\begin{aligned}&\boldsymbol{K} = \mathbb{A}(\boldsymbol{K}^e_{IJ}); \\ &\boldsymbol{P}(\boldsymbol{\Phi},\mathfrak{X}) = \mathbb{A}(\boldsymbol{P}^e_I) = \mathfrak{X}\mathbb{A}(\boldsymbol{f}^e_{\text{ext}0I}(\boldsymbol{\Phi}^e)) - \mathbb{A}(\boldsymbol{f}^e_{\text{int}I}(\boldsymbol{\Phi}^e)) = \mathfrak{X}\boldsymbol{f}_{\text{ext}0}(\boldsymbol{\Phi}) - \boldsymbol{f}_{\text{int}}(\boldsymbol{\Phi}).\end{aligned} \tag{10.41}$$

We use standard Newton Raphson's iterative procedure. We divide the external loading into n load steps. Let $\boldsymbol{\Phi}_n$ represents the discretized form of degrees of freedom vector at load step n, such that $\Delta\boldsymbol{\Phi}_n = \boldsymbol{\Phi}_{n+1} - \boldsymbol{\Phi}_n$. At equilibrium state corresponding to load step n (converged state), the unbalanced force vanishes, i.e., $\boldsymbol{P}(\boldsymbol{\Phi}_n,\mathfrak{X}_n) = \boldsymbol{0}$. Provided the n^{th} load step has converged, we aim to find $\Delta\boldsymbol{\Phi}_n$, such that $\boldsymbol{P}(\boldsymbol{\Phi}_{n+1},\mathfrak{X}_{n+1}) = \boldsymbol{0}$. At i^{th} iteration, we can linearize the equation $\boldsymbol{P}(\boldsymbol{\Phi}_{n+1},\mathfrak{X}_{n+1}) = \boldsymbol{0}$ about $\boldsymbol{P}(\boldsymbol{\Phi}^i_{n+1},\mathfrak{X}^i_{n+1})$, such that $\boldsymbol{\Phi}^{i+1}_{n+1} = \boldsymbol{\Phi}^i_{n+1} + \Delta\boldsymbol{\Phi}^{i+1}_n$ and $\mathfrak{X}^i_{n+1} = \mathfrak{X}_n$ as:

$$\boldsymbol{P}(\boldsymbol{\Phi}^{i+1}_{n+1},\mathfrak{X}_{n+1}) = \boldsymbol{P}(\boldsymbol{\Phi}^i_{n+1},\mathfrak{X}_n) + \left.\frac{\partial\boldsymbol{P}}{\partial\boldsymbol{\Phi}}\right|_{(\boldsymbol{\Phi}^i_{n+1},\mathfrak{X}_n)}.\Delta\boldsymbol{\Phi}^{i+1}_n + \left.\frac{\partial\boldsymbol{P}}{\partial\mathfrak{X}}\right|_{(\boldsymbol{\Phi}^i_{n+1},\mathfrak{X}_n)}.(\mathfrak{X}_{n+1} - \mathfrak{X}_n) = \boldsymbol{0}. \tag{10.42}$$

We define the global tangent stiffness matrix (obtained in (10.41)) and obtain the following results from Eq. (10.41),

$$\begin{aligned}&\boldsymbol{P}(\boldsymbol{\Phi}^i_{n+1},\mathfrak{X}_n) = \mathfrak{X}_n\boldsymbol{f}_{\text{ext}0}(\boldsymbol{\Phi}^i_{n+1}) - \boldsymbol{f}_{\text{int}}(\boldsymbol{\Phi}^i_{n+1}); \\ &\boldsymbol{K}(\boldsymbol{\Phi}^i_{n+1},\mathfrak{X}_n) = -\left.\frac{\partial\boldsymbol{P}(\boldsymbol{\Phi}_{n+1},\mathfrak{X}_{n+1})}{\partial\boldsymbol{\Phi}_{n+1}}\right|_{(\boldsymbol{\Phi}^i_{n+1},\mathfrak{X}_n)}; \\ &\boldsymbol{f}_{\text{ext}0}(\boldsymbol{\Phi}^i_{n+1}) = \left.\frac{\partial\boldsymbol{P}(\boldsymbol{\Phi}_{n+1},\mathfrak{X}_{n+1})}{\partial\mathfrak{X}_{n+1}}\right|_{(\boldsymbol{\Phi}^i_{n+1},\mathfrak{X}_n)}.\end{aligned} \tag{10.43}$$

Substituting the results obtained above into the equation (10.42), we get:

$$\boldsymbol{K}(\boldsymbol{\Phi}^i_{n+1}, \mathfrak{X}_n).\Delta\boldsymbol{\Phi}^{i+1}_n = \mathfrak{X}_{n+1}\boldsymbol{f}_{\text{ext0}}(\boldsymbol{\Phi}^i_{n+1}) - \boldsymbol{f}_{\text{int}}(\boldsymbol{\Phi}^i_{n+1}) = \boldsymbol{P}(\boldsymbol{\Phi}^i_{n+1}, \mathfrak{X}_{n+1}). \tag{10.44}$$

10.4 Updating the axial strain vector, curvature vector and their derivatives

10.4.1 Updating configuration

Solving equation (10.44), yields an incremental change in configuration space due to deformation, say $\Delta\boldsymbol{\Phi} = \{\Delta\boldsymbol{\Phi}, \Delta\boldsymbol{\alpha}, \Delta p\}$.The derivatives of these increments can be obtained by using the approximation in Eq. 10.27 such that $\partial^n_{\xi_1}\Delta\boldsymbol{\Phi}^e(\xi^e_1) = \partial^n_{\xi_1}N_I(\xi^e_1).\Delta\boldsymbol{\Phi}^e$, $\partial^n_{\xi_1}\Delta\boldsymbol{\alpha}^e(\xi^e_1) = \partial^n_{\xi_1}N_I(\xi^e_1).\Delta\boldsymbol{\alpha}^e_I$ and $\partial^n_{\xi_1}\Delta p^e(\xi^e_1) = \partial^n_{\xi_1}N_I(\xi^e_1).\Delta p^e_I$. Let the *initial* and *final* configuration be given as $\boldsymbol{\Phi}_{\text{i}} = \{\boldsymbol{\Phi}_{\text{i}}, \boldsymbol{Q}_{\text{i}}, p_{\text{i}}\}$ and $\boldsymbol{\Phi}_{\text{f}} = \{\boldsymbol{\Phi}_{\text{f}}, \boldsymbol{Q}_{\text{f}}, p_{\text{f}}\}$, such that:

$$\boldsymbol{\varphi}_{\text{f}} = \boldsymbol{\varphi}_{\text{i}} + \Delta\boldsymbol{\varphi}; \quad \partial^n_{\xi_1}\boldsymbol{\varphi}_{\text{f}} = \partial^n_{\xi_1}\boldsymbol{\varphi}_{\text{i}} + \partial^n_{\xi_1}\Delta\boldsymbol{\varphi} \tag{10.45a}$$

$$p_{\text{f}} = p_{\text{i}} + \Delta p; \quad \partial^n_{\xi_1}p_{\text{f}} = \partial^n_{\xi_1}p_{\text{i}} + \partial^n_{\xi_1}\Delta p \tag{10.45b}$$

$$\boldsymbol{Q}_{\text{f}} = \exp(\Delta\hat{\boldsymbol{\alpha}}).\boldsymbol{Q}_{\text{i}} = \boldsymbol{Q}_{+}.\boldsymbol{Q}_{\text{i}} \text{ where, } \boldsymbol{Q}_{+} = \exp(\Delta\hat{\boldsymbol{\alpha}}). \tag{10.45c}$$

From the expressions of $\boldsymbol{B}_i$ with $i \in \{1,3,4,5,6\}$ defined in previous sections, the following quantities other than the configuration space itself need to be updated: $\partial_{\xi_1}\boldsymbol{\varphi}, \partial^2_{\xi_1}\boldsymbol{\varphi}, \hat{\boldsymbol{\kappa}}, \partial_{\xi_1}\hat{\boldsymbol{\kappa}}$, and $\partial^2_{\xi_1}\hat{\boldsymbol{\kappa}}$ and the finite strain quantities constituting $\overline{\boldsymbol{\epsilon}}$. Once we update $\overline{\boldsymbol{\epsilon}}$, we can obtain the material (and then spatial) form of internal force vector, eventually getting the updates $\boldsymbol{B}_i$ with $i \in \{4,5,6\}$.

10.4.2 Updating axial strain, curvature and its derivatives

Readers are refereed back to chapter 3 that details method for obtaining and updating the higher-order derivatives of curvature. So far, we have obtained all the elements constituting the

concatenated strain vector $\overline{\boldsymbol{\epsilon}}$ except for $\overline{\boldsymbol{\varepsilon}}$ and $\partial_{\xi_1}\overline{\boldsymbol{\varepsilon}}$. These can be obtained using the definition of axial strain vector in Eq. (4.6), such that:

$$\overline{\boldsymbol{\varepsilon}} = \boldsymbol{Q}^T.\partial_{\xi_1}\boldsymbol{\varphi} - \boldsymbol{E}_1; \tag{10.46a}$$

$$\partial_{\xi_1}\overline{\boldsymbol{\varepsilon}} = \boldsymbol{Q}^T.\left(\partial^2_{\xi_1}\boldsymbol{\varphi} - \hat{\boldsymbol{\kappa}}.\partial_{\xi_1}\boldsymbol{\varphi}\right) = \boldsymbol{Q}^T.(\tilde{\partial}_{\xi_1}\partial_{\xi_1}\boldsymbol{\varphi}). \tag{10.46b}$$

Using the results in *Proposition 3.3*, presented in chapter 3, we get $\partial_{\xi_1}\overline{\boldsymbol{\varepsilon}} = \boldsymbol{Q}^T.\tilde{\partial}_{\xi_1}\boldsymbol{\varepsilon}$. The co-rotational derivative can be obtained from Eq. (10.46b) as $\tilde{\partial}_{\xi_1}\boldsymbol{\varepsilon} = \tilde{\partial}_{\xi_1}(\partial_{\xi_1}\boldsymbol{\varphi})$. Using *Proposition 3.1* (that also defines the operator $\hat{\partial}_{\xi_1}$ used below) presented in chapter 3, we have the following,

$$\tilde{\partial}^n_{\xi_1}\boldsymbol{\varepsilon} = \tilde{\partial}^n_{\xi_1}(\partial_{\xi_1}\boldsymbol{\varphi}) = (\partial_{\xi_1} - \hat{\partial}_{\xi_1})^n(\partial_{\xi_1}\boldsymbol{\varphi}); \tag{10.47a}$$

$$\partial^n_{\xi_1}\overline{\boldsymbol{\varepsilon}} = \boldsymbol{Q}^T.\tilde{\partial}^n_{\xi_1}(\partial_{\xi_1}\boldsymbol{\varphi}) = \boldsymbol{Q}^T.\left(\sum_{i=0}^{n}(-1)^{(n-i)}C^n_i\partial^n_{\xi_1}\hat{\partial}^{(n-i)}_{\xi_1}\right)\partial_{\xi_1}\boldsymbol{\varphi}. \tag{10.47b}$$

The following section presents few numerical example concerning the formulation described so far.

10.5 Numerical examples

We consider three numerical examples based on the formulation described in this chapter using the constitutive model defined in chapter 9. The set of problems chosen emphasizes on a large 3D deformation of beam/framed structure.

We realize that the weak form demands C^3 continuity in $\Delta\boldsymbol{\alpha}$; C^1 continuity in $\Delta\boldsymbol{\phi}$ and Δp. To maintain a global C^3 continuity in the incremental rotation angle, a seventh order polynomial is required (for example: eight, seventh-order Hermite polynomials obtained by imposing Kronecker-delta properties at the element junction; or considering seventh-order Lagrangian-polynomials on an eight-noded element). However, concerning the computational cost and the fact that we are not using Gauss-Lobatto quadrature (the integration points include the element end nodes), we use fourth-order Lagrangian polynomial (committing Variational crime) as it satisfies the minimum

requirement for the weak form to be square-integrable. Secondly, it satisfies the compatibility requirement and yields a continuous curvature and mid-curve axial-strain vector at the element junctions. We use a full Newton-Raphson iterative solution procedure with uniformly reduced Gauss-Legendre quadrature to avoid shear-locking.

We consider the tolerance of 10^{-5} in the Euclidean norm of force residue $\|\boldsymbol{P}(\boldsymbol{\Phi})\| = \|\mathfrak{X}\boldsymbol{f}_{\text{ext0}}(\boldsymbol{\Phi}) - \boldsymbol{f}_{\text{int}}(\boldsymbol{\Phi})\|$ as a measure of convergence. The numerical results, including the deformation map and finite strains, obtained by the current formulation (referred to as Chadha-Todd (CT) beam) are compared with the Simo-Reissener beam model (SR) described in [48], Simo Vu-Quoc beam model (SV) discussed in [43], and Crisfield co-rotational formulation detailed in [124]. As per the description of deformed configuration in chapter 4, the SR beam is defined by the configuration Ω_1; the SV beam is defined by a special case of configuration Ω_2 that considers non-uniform St. Venant warping but ignores bending induced shear contribution to warping; the CT beam is described by the state $\Omega \equiv \Omega_3$; and the CF beam is a special case of SR (defined by Ω_1) that ignores the shear deformation. We also note that SV and CT beam converges if we ignore Poisson's deformation and warping due to bending induced shear; SR and CF beam formulation converges if shear deformation is ignores; and all the four beams converge if the structure is infinitely slender.

In the following simulations, we consider rectangular cross-section with the edge dimensions $b \times d$, such that $d \geq b$. The warping function Ψ_1 pertaining to the torsion can be obtained using the Neumann boundary value problem defined in Eq. (4.13). There exists a closed form solution of this differential equation for rectangular cross-section (refer to Sokolnikoff [38]) given by:

$$\begin{aligned} \Psi_1(\xi_2, \xi_3) &= \xi_2\xi_3 - \frac{8d^2}{\pi^3}\sum_{n=0}^{\infty}\frac{(-1)^n \sin(k_n\xi_2)\sinh(k_n\xi_3)}{(2n+1)^3\cosh(k_n b)}; \\ k_n &= \frac{(2n+1)\pi}{d} \quad \text{for} \quad n = 0, 1, 2, ... \end{aligned} \tag{10.48}$$

The Fig. 10.1a illustrates the warping function Ψ_{1a} for a square cross-section with the edge dimension 0.5 units obtained by solving the concerned Neumann boundary value problem.

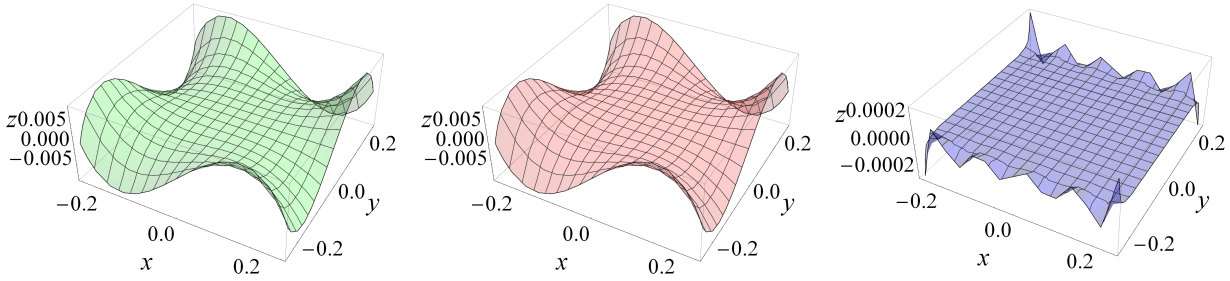

(a) Warping function Ψ_{1a} (b) Warping function Ψ_{1b} (c) Error $\Psi_{1a} - \Psi_{1b}$

Figure 10.1: Saint Venant's warping function for a square cross-section.

Similarly, Fig. 10.1b represents the warping function Ψ_{1b} obtained using Eq. (10.48) considering $0 \leq n \leq 3$. We observe from Fig. 10.1c that Eq. (10.48) with $0 \leq n \leq 3$ gives an excellent estimate of the warping function Ψ_1.

The bending induced shear warping functions are obtained in chapter 5 described in Eq. (5.29). We consider the non-linear parts of warping functions defined in Eq. (5.29) as Ψ_2 and Ψ_3. This is because the uniform shear deformation of the cross-section is taken care of by the director triad. Therefore, we have:

$$\Psi_3 = -\frac{E}{2G}\left(\frac{\xi_2^3}{3}\right); \quad \Psi_2 = -\frac{E}{2G}\left(\frac{\xi_3^3}{3}\right). \tag{10.49}$$

10.5.1 Numerical example 1: Cantilever beam subjected to conservative concentrated end load

For simulation 1, we consider a cantilever beam with a uniform square cross-section with edge length 0.5 units subjected to the conservative concentrated load $\boldsymbol{N}_{\boldsymbol{\varphi}} = [18; 5; 5]$ units and $\boldsymbol{N}_{\boldsymbol{\alpha}} = [120; 500; 200]$ units at end node. The beam has the material and geometric properties as: $E = 150 \times 10^3$ units, $L = 10$ units, $G = 62.5 \times 10^3$ units and $\nu = 0.2$. The Vlasov warping constant for this case is significantly small: $\overline{\mathfrak{C}}_{88} = 0.796$.

We run the simulations considering 15 elements, fourth-order Lagrangian polynomial and

30 load steps (implying $\mathfrak{X}_{n+1} - \mathfrak{X}_n = \frac{1}{30}$). The CT beam shows an excellent rate of convergence. Table 4 gives the norm of force residue for the selective load step.

Table 10.1: Numerical example 1: Force residue for the load steps (5, 10, 20, 30) obtained using the Chadha-Todd (CT) beam model

Iterations	**Load step 5**	**Load step 10**	**Load step 20**	**Load step 30**
0	1.840211×10^{1}	1.840211×10^{1}	1.840211×10^{1}	1.840211×10^{1}
1	6.345199×10^{2}	6.114772×10^{2}	1.816455×10^{3}	6.963457×10^{2}
2	2.065176×10^{0}	2.282938×10^{0}	1.141781×10^{1}	1.576687×10^{0}
3	2.637549×10^{-2}	1.091766×10^{-1}	4.058497×10^{0}	2.615883×10^{-1}
4	1.318676×10^{-5}	6.821832×10^{-5}	1.037867×10^{-3}	2.640774×10^{-5}
5	1.759103×10^{-7}	1.817813×10^{-7}	1.127938×10^{-5}	1.740689×10^{-7}
6	–	–	1.881784×10^{-7}	–

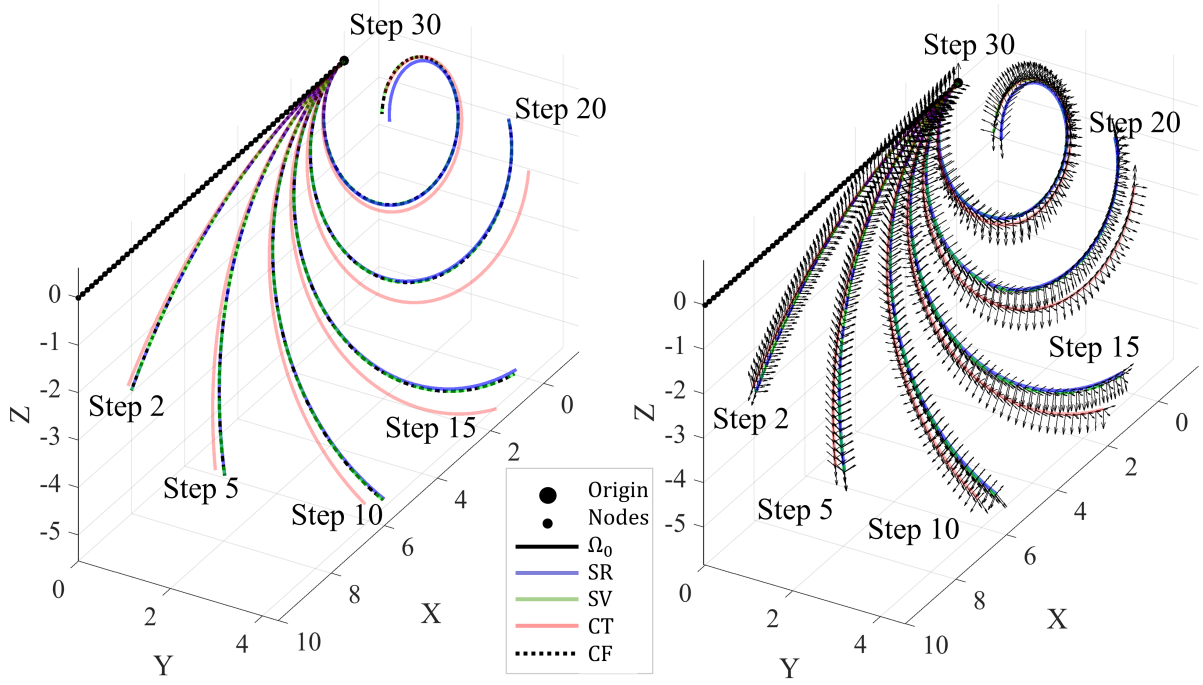

Figure 10.2: Numerical example 1: Deformed configuration.

Figure 10.2 represents the mid-curve and director triad field of the considered beam for selective load steps respectively. The plot compares the undeformed state Ω_0 and the deformed state obtained using SR, SV, CT, and CF beam models.

The error $e_{\boldsymbol{\varphi}}$ and $e_{\boldsymbol{Q}}$ (as defined in Eq. (2.33a) and (2.36a)) of SR and SV beam relative to the CT beam for four different load steps are plotted in the figures 10.3 and 10.4.

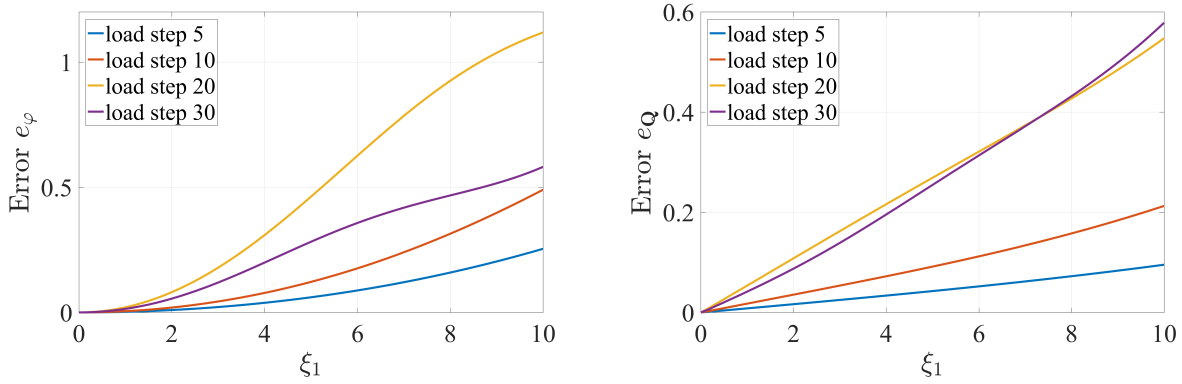

(a) Error in mid-curve position vector (b) Error in the rotation tensor field

Figure 10.3: Numerical example 1: Error in the Simo-Reissener beam relative to the Chadha-Todd beam.

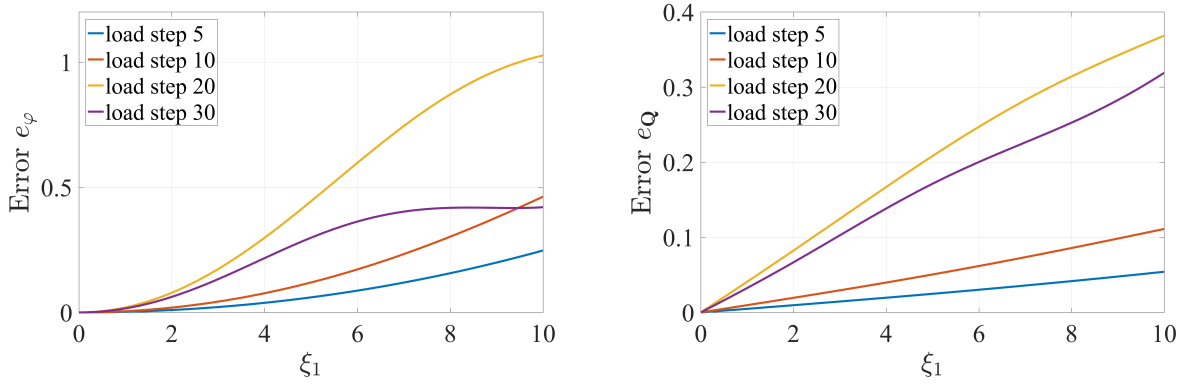

(a) Error in mid-curve position vector (b) Error in the rotation tensor field

Figure 10.4: Numerical example 1: Error in the Simo Vu-Quoc beam relative to the Chadha-Todd beam.

There is significant difference in the position vector of the mid-curve obtained using CT beam model relative to SR, CF, and SV beams. This is primarily because the bending stiffness for CT beam (described in Eq. (9.23)) is greater than the bending section modulus for SR, SV, and CF beam by a factor of $f = \left(\frac{3\nu^2+2\nu-2}{4\nu^2+2\nu-2} + \frac{\nu^2}{2(1+\nu)}\left(\frac{I_{11}}{I_{xx}}\right)\right) \geq 1$, such that $\overline{\mathfrak{C}}_{33_{xx}} = fEI_{xx}$, where the subscript xx is either 22 or 33 (refer to Fig. 10.8).

Secondly, CT beam is flexible in torsion relative to the other beam models. We also observe that the error e_{φ}, increases with the arc-length ξ_1, or equivalently $\frac{\partial e_{\varphi}}{\partial \xi_1} > 0$. This phenomenon is very similar to the problem of dead-reckoning (also called a coning effect) in path-estimation. In

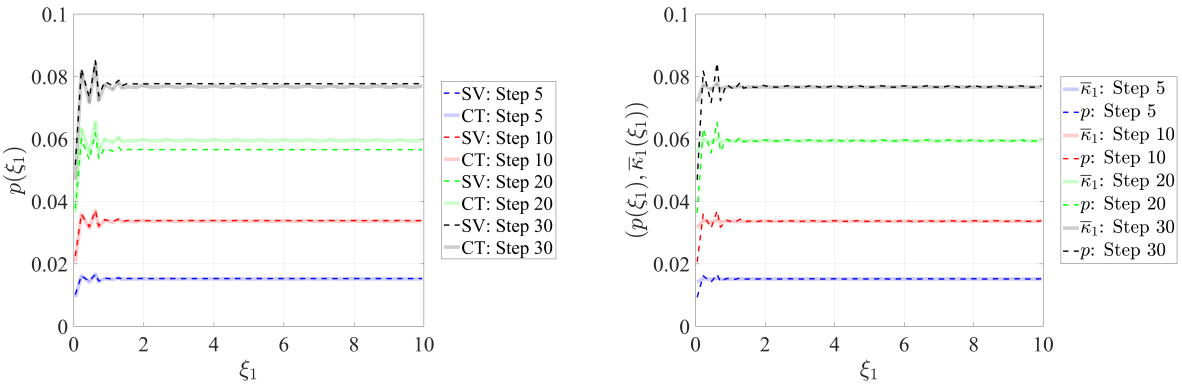

(a) p for CT and SV beam

(b) p and $\overline{\kappa}_1$ for CT

Figure 10.5: Numerical example 1: Torsional curvature and warping amplitude.

Fig. 10.5a, we observe that CT and SV predicts almost the same warping amplitude p. This is because the parameters $\overline{\mathfrak{C}}_{78}$, $\overline{\mathfrak{C}}_{79}$, $\overline{\mathfrak{C}}_{89}$, $\overline{\mathfrak{C}}_{99}$, $\overline{\mathfrak{C}}_{98}$, $\overline{\mathfrak{C}}_{97}$ are small for the considered cross-section. We observe oscillations in the warping amplitude p near the boundary. The beam is subjected to conservative torsional moment, leading to constant warping amplitude away from the boundary. Since the aforementioned material constants $\overline{\mathfrak{C}}_{ij}$ are negligible and the cross-section is symmetric (shear center and the centroid of the cross-section coincides), the warping amplitude $p(\xi_1)$ converges with the torsional curvature field $\overline{\kappa}_1(\xi_1)$ as depicted in Fig. 10.5b.

Figure 10.6 shows the curvatures (left column) and axial strain components (right column) for load steps (5, 10, 20, 30) obtained using Simo-Reissener (SR), Simo Vu-Quoc (SV) and Chadha-Todd (CT) beam models. Figure 10.7 illustrates the shear angle field for load steps (5, 10, 20, 30) obtained using SR, SV, and CT beam models.

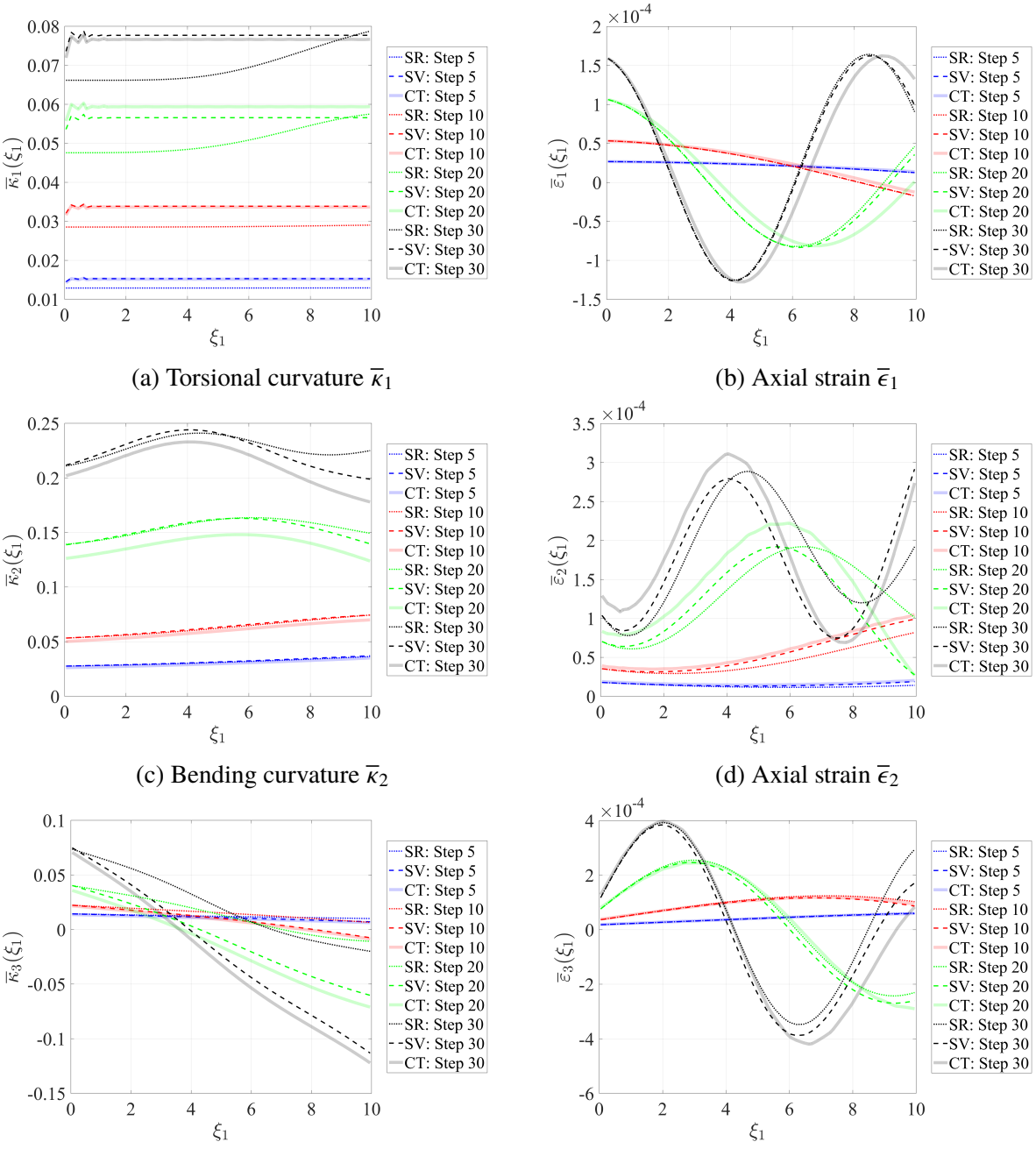

(a) Torsional curvature $\overline{\kappa}_1$

(b) Axial strain $\overline{\epsilon}_1$

(c) Bending curvature $\overline{\kappa}_2$

(d) Axial strain $\overline{\epsilon}_2$

(e) Bending curvature $\overline{\kappa}_3$

(f) Axial strain $\overline{\epsilon}_3$

Figure 10.6: Numerical example 1: Components of the material curvature vector (left column) and the axial strain vector (right column).

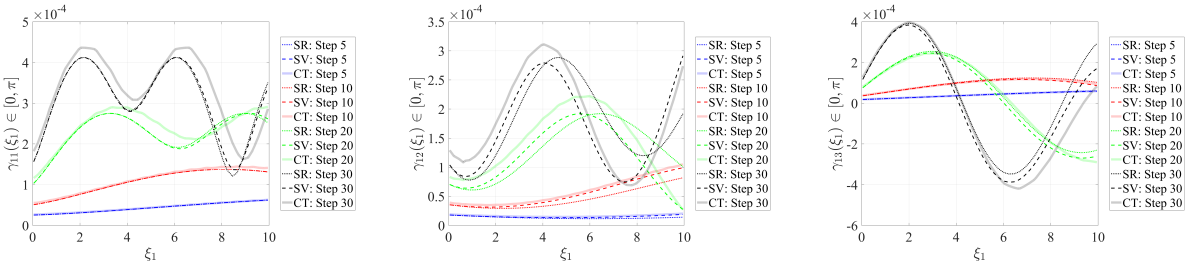

(a) Shear angle γ_{11} (b) Shear angle γ_{12} (c) Shear angle γ_{13}

Figure 10.7: Numerical example 1: Shear angles.

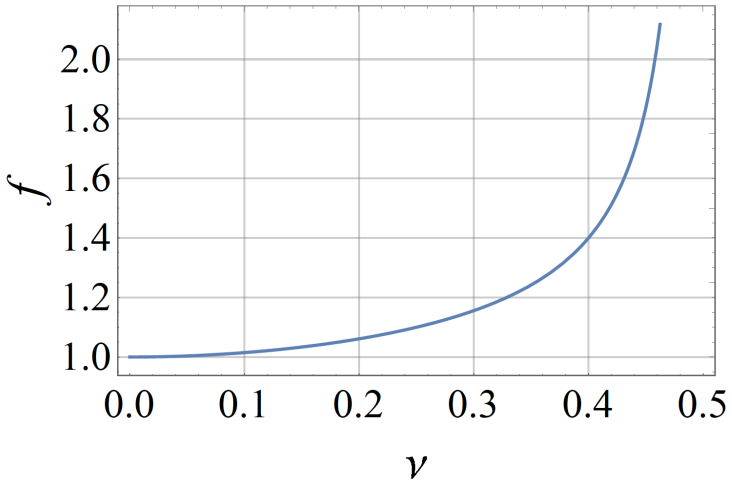

Figure 10.8: Factor f as a function of Poisson's ratio for a square cross-section.

10.5.2 Numerical example 2: Cantilever beam subjected to pure torsion and elongation

We consider a beam with the same geometry and material property as for example 1 discussed in section 10.5.1, except for the cross-section. For current example, we consider a rectangular cross-section with the dimensions $b = 0.5$ units and $d = 4b = 2 = \frac{L}{5}$ units. The Vlasov constant for the considered cross-section is $\overline{\mathfrak{C}}_{88} = 1261.65$. The beam is subjected to torsion of 10000 units and an axial pull of 10000 units at the free end. This structure can not be considered as a slender beam because the depth of the cross-section is 20% of its length. The

goal of this example is to demonstrate the performance of the CT beam relative to SV, SR, and CF beam when Poisson's and warping effects are dominant. We expect a significant deviation of CT and SV beam relative to the SR and CF beam. Like before, we consider 30 load steps, 15 elements, and fourth-order Lagrangian polynomial.

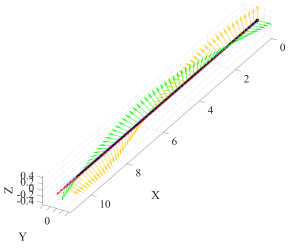

(a) Deformed state for SR and CF beam

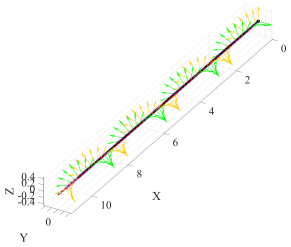

(b) Deformed state for SV beam

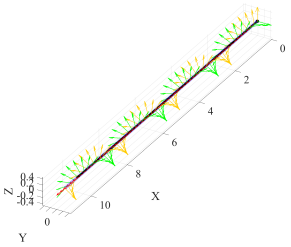

(c) Deformed state for CT beam

Figure 10.9: Numerical example 2: Deformed state.

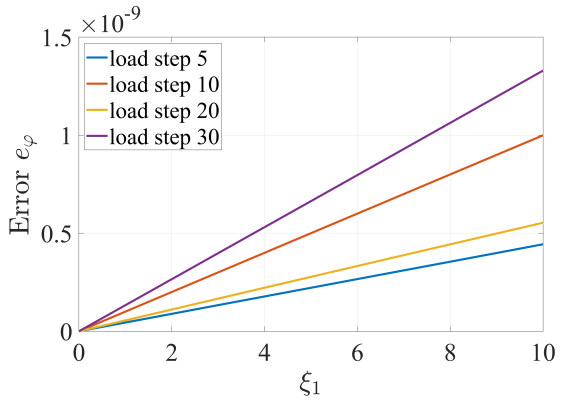

(a) Error in mid-curve position vector

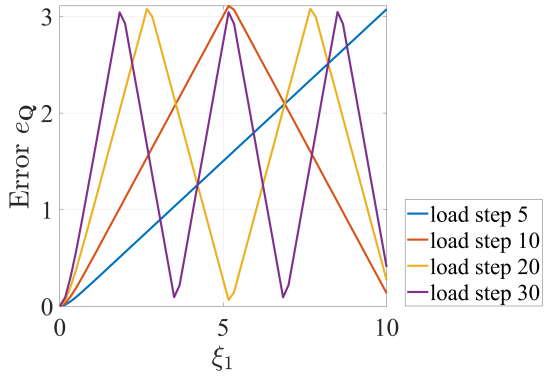

(b) Error in the rotation tensor field

Figure 10.10: Numerical example 2: Error in the Simo-Reissener beam relative to the Chadha-Todd beam.

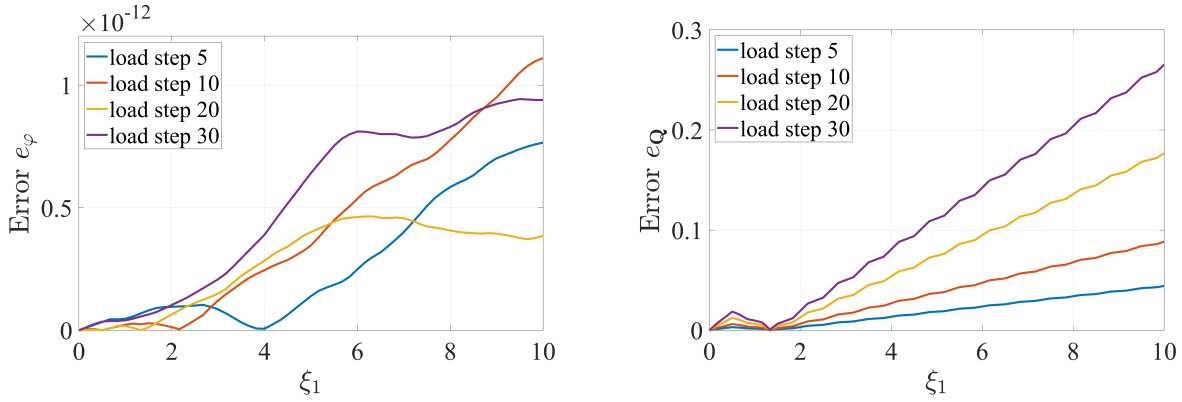

(a) Error in mid-curve position vector

(b) Error in the rotation tensor field

Figure 10.11: Numerical example 2: Error in the Simo Vu-Quoc beam relative to the Chadha-Todd beam.

Figure 10.9 represents the deformed state for SR (and CF), SV and CT beam models. We observe a few expected results. The error in $e_{\boldsymbol{\varphi}}$ is negligible for SR (Fig. 10.10a) and SV (Fig. 10.11a) beams. This is because the mid-cure of the beam is effected by pure elongation. However, as observed in figures 10.9 and 10.10b, there is significant error in rotation triad obtained for SR and CF beam relative to CT beam (or even SV beam). Unlike example 1, we observe a notable error in the rotation triad obtained using the SV beam model relative to the CT beam. We can infer from figure 10.9a that the deviation of the director triad in the SR beam relative to the CT beam (obtained at the Gauss points) increases linearly along the length of the beam. However, at first glimpse, the triangular shape of the error plot $e_{\boldsymbol{Q}}$ (Fig. 10.10b) depicts a linear increase followed by a decrease in the error. This observation is misleading and contradicting to our previous inference. The wave nature of error plot $e_{\boldsymbol{Q}}$ is due to a local homeomorphism of exponential map discussed in section 1.3.2.2. In fact, the error plot 10.10b does show continuous increase of error since $e_{\boldsymbol{Q}} \in [0, \pi]$.

We attribute large error in the deformation map predicted by SR beam to the fact that the considered structure can no longer be considered slender and the deformation is significantly effected by fully coupled Poisson's and warping effect. The inclusion of all deformation effects in the CT beam makes it more flexible (or less stiff).

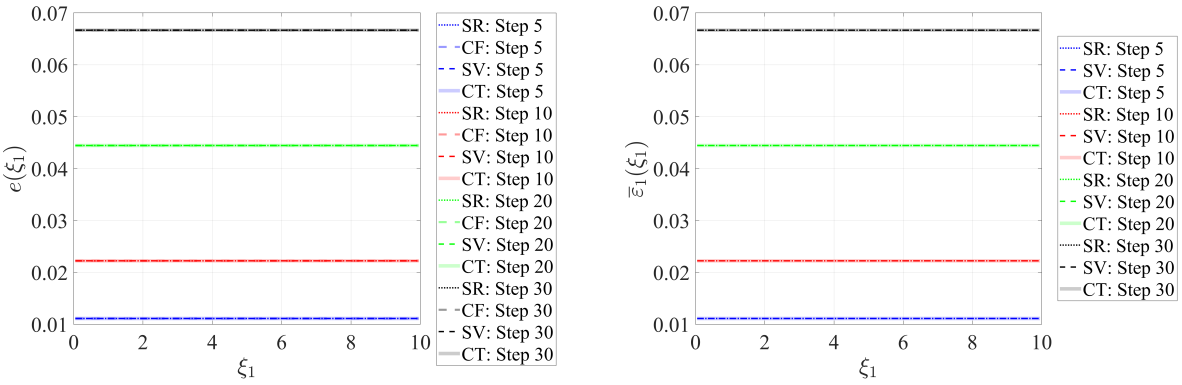

(a) Mid-curve axial strain e (b) Axial-strain $\overline{\varepsilon}_1$

Figure 10.12: Numerical example 2: Axial strains.

Figure 10.12 shows the first component of the axial strain vector $\overline{\varepsilon}_1$ and the mid-curve axial strain e. Since the beam is not subjected to bending and shear, $\overline{\varepsilon}_2 = \overline{\varepsilon}_3 = 0$, $\overline{\kappa}_2 = \overline{\kappa}_3 = 0$, and $\overline{\varepsilon}_1 = e$. As expected, we observe that all four beams have excellent agreement on the mid-curve deformation and the axial strains.

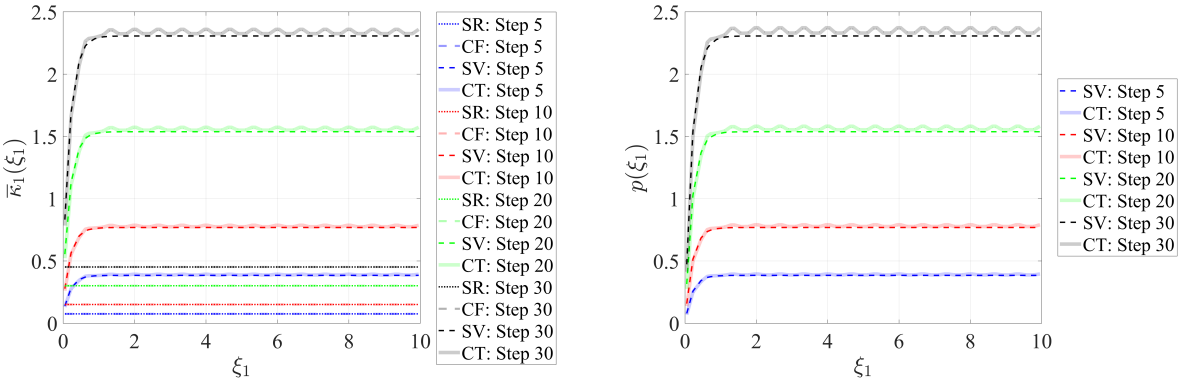

(a) Curvature $\overline{\kappa}_1$ (b) Warping constant p

Figure 10.13: Numerical example 2: Torsional curvature and warping amplitude.

Figure 10.13a illustrates the torsional curvature field obtained using SR, CF, SV, and CT beam model; and Fig. 10.13b illustrates the warping amplitude obtained using SV and CT for the load steps in the multiple of five. We make the following observations. Firstly, we observe a significant underestimation of the torsional curvature obtained by the SR or CF beam. This is

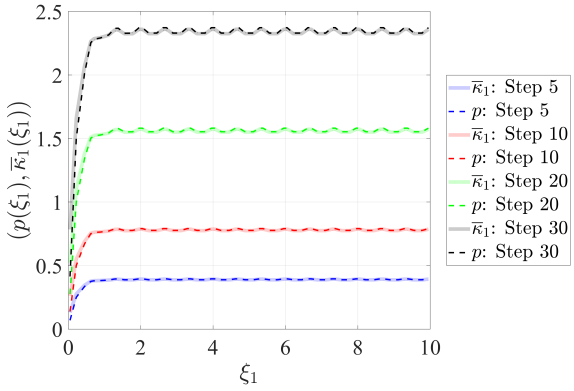

Figure 10.14: Numerical example 2: Warping amplitude and torsional curvature for CT beam.

because the beam is no longer slender. The CT and SV beams are more flexible in torsion relative to SR and CF beam. In case of uniform torsion, we have $p = \overline{\kappa}_1$. If T represents torsion at the end node (here, $T = 10000$ units), the torsional curvature converges to a constant value for CT and SV beam as $\overline{\kappa}_1(L) = \frac{T}{\overline{\mathfrak{C}}_{33_{11}} + \overline{\mathfrak{C}}_{37_{11}}} = 2.306$ (note that $\overline{\mathfrak{C}}_{37_{11}} < 0$), whereas, the curvature for SR and CF beam can be obtained as $\overline{\kappa}_1(L) = \frac{T}{\overline{\mathfrak{C}}_{33_{11}}} = 0.456$.

Secondly, for the given loading, we anticipate a constant torsion field (as in SR beam), but the torsional curvature transitions from zero to constant value in SV and CT beam. Similar is the case with the warping amplitude. We also know that for uniform torsion, the warping amplitude equals the torsional curvature, as observed in Fig. 10.14. The fixed boundary on the left end implies $p(0) = 0$. Seemingly, the warping amplitude guides the value of torsional curvature leading to an anomaly in the value of curvature near the boundary. Thirdly, we observe oscillations in the torsional curvature and warping amplitude in plot 10.13. We suspect that the oscillation in the warping amplitude is because of the dependence of bi-shear on $\partial^2_{\xi_1} p$. Since the quantity $\partial^2_{\xi_1} p$ is highly oscillatory at Gauss points it leads to oscillations in the warping amplitude. The derivatives of warping amplitude obtained at the Gauss points recorded after the convergence of the load step is shown in Fig. 10.15. As noted before, in the case of uniform torsion, the torsional curvature is guided by the warping amplitude. Therefore, we observe the same oscillations in $\overline{\kappa}_1(\xi_1)$.

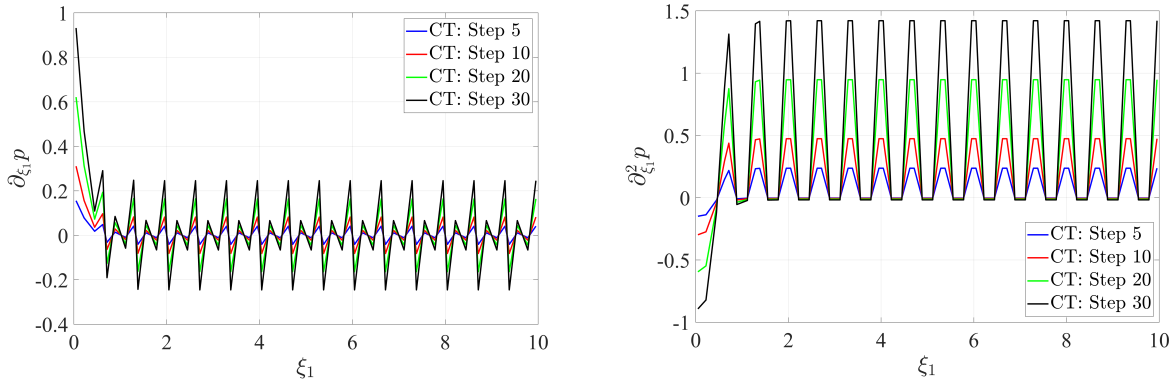

(a) $\partial_{\xi_1} p$ (b) $\partial^2_{\xi_1} p$

Figure 10.15: Numerical example 2: First and second derivatives of warping amplitude at Gauss points for CT beam.

10.5.3 Numerical example 3: 3D frame subjected to concentrated conservative loads at multiple nodes

We consider a structure with the geometry depicted in figure 10.16 subjected to two different cases of loading and cross-section. The local element frames are defined by $\{\boldsymbol{e}_i\}$. The only global to local transformation that we make here is for the material matrix $\overline{\mathfrak{C}}$. We consider 150 load steps for this example.

10.5.3.1 Case 1

For case 1, we consider a moderately slender structure with the cross-sectional dimension as $b = 0.5$ units and $d = 5b$ units. We subject the structure to 3 times the load showed in figure 10.16. Figure 10.17 illustrates the deformed shape for various load-steps using CT, SV, SR, and CF beam models. As is expected, SR and CF formulation yields a very similar deformation field.

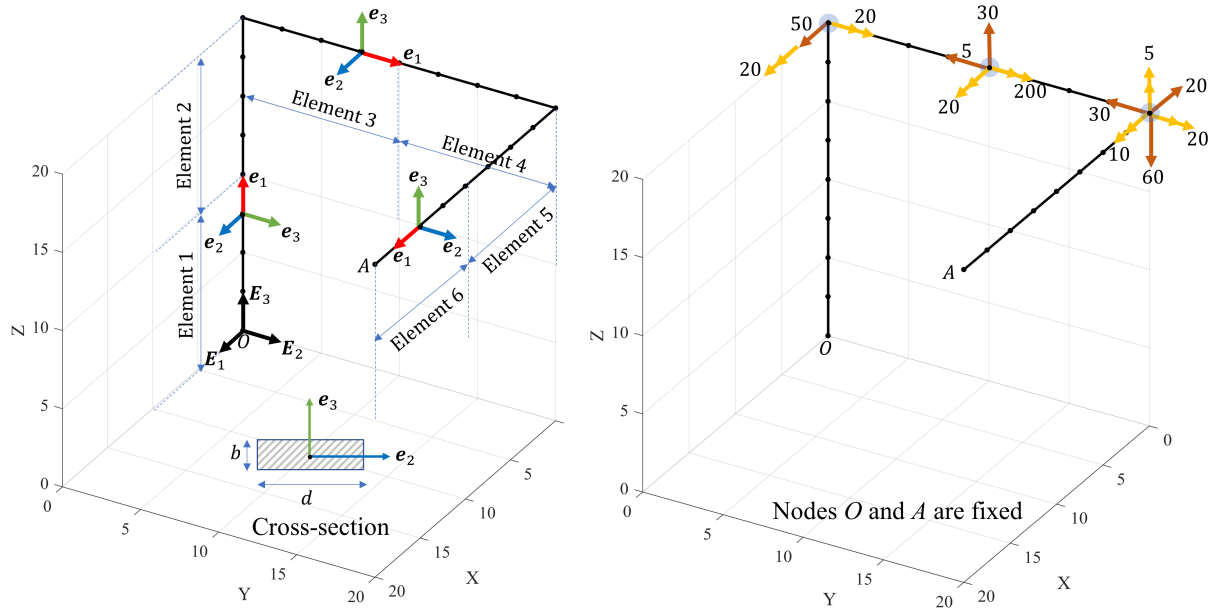

Figure 10.16: Numerical example 3: Geometry and load pattern.

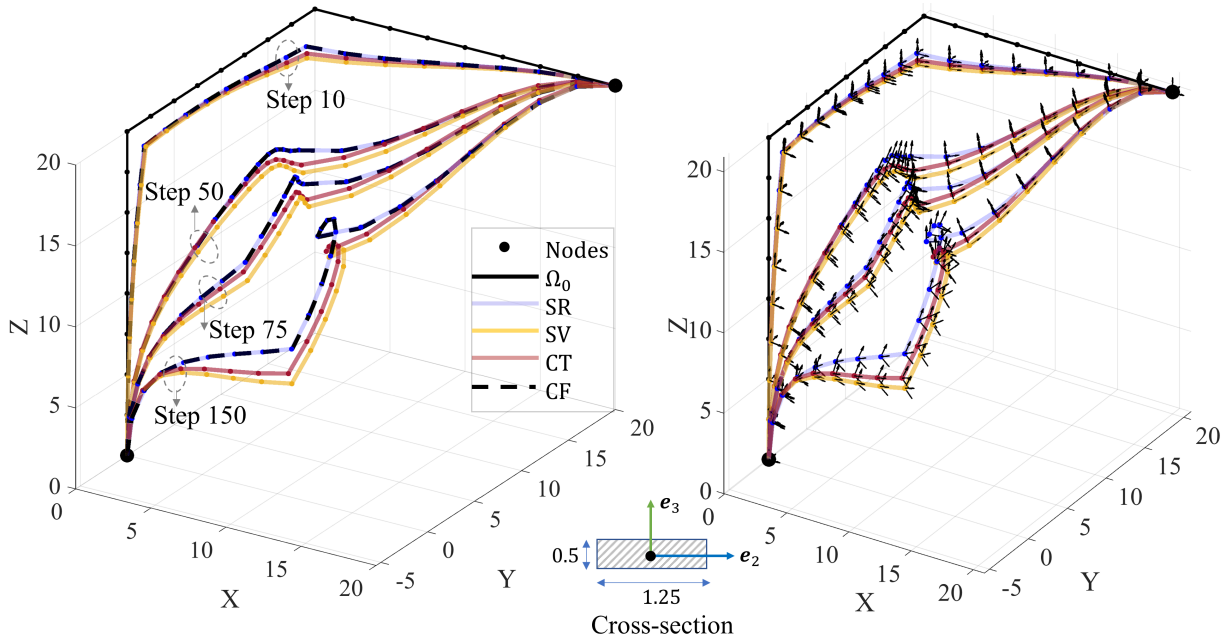

Figure 10.17: Numerical example 3, case 1: Deformed configuration.

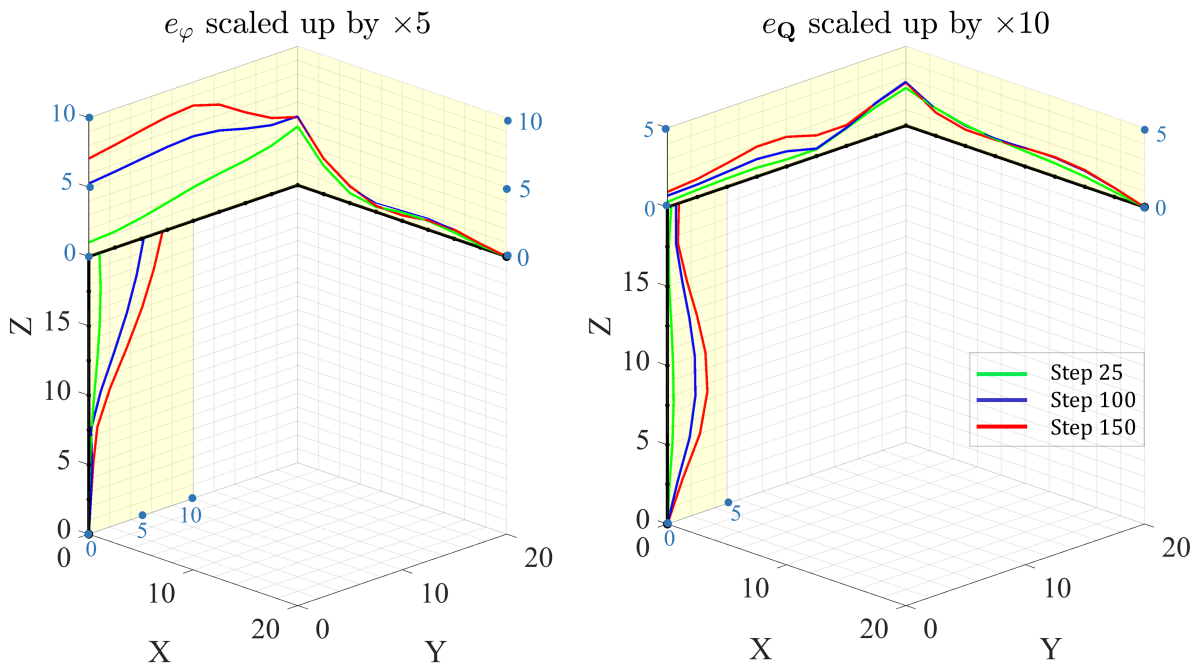

Figure 10.18: Numerical example 3, case 1: Error in the Simo-Reissener beam relative to the Chadha-Todd beam.

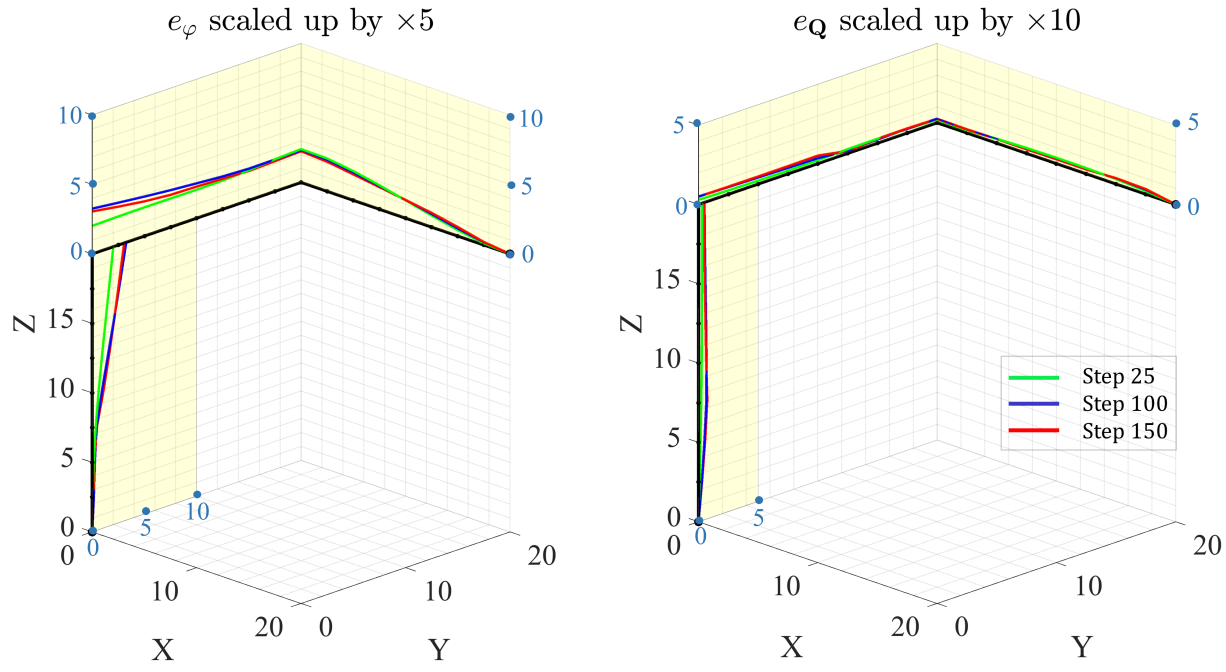

Figure 10.19: Numerical example 3, case 1: Error in the Simo Vu-Quoc beam relative to the Chadha-Todd beam.

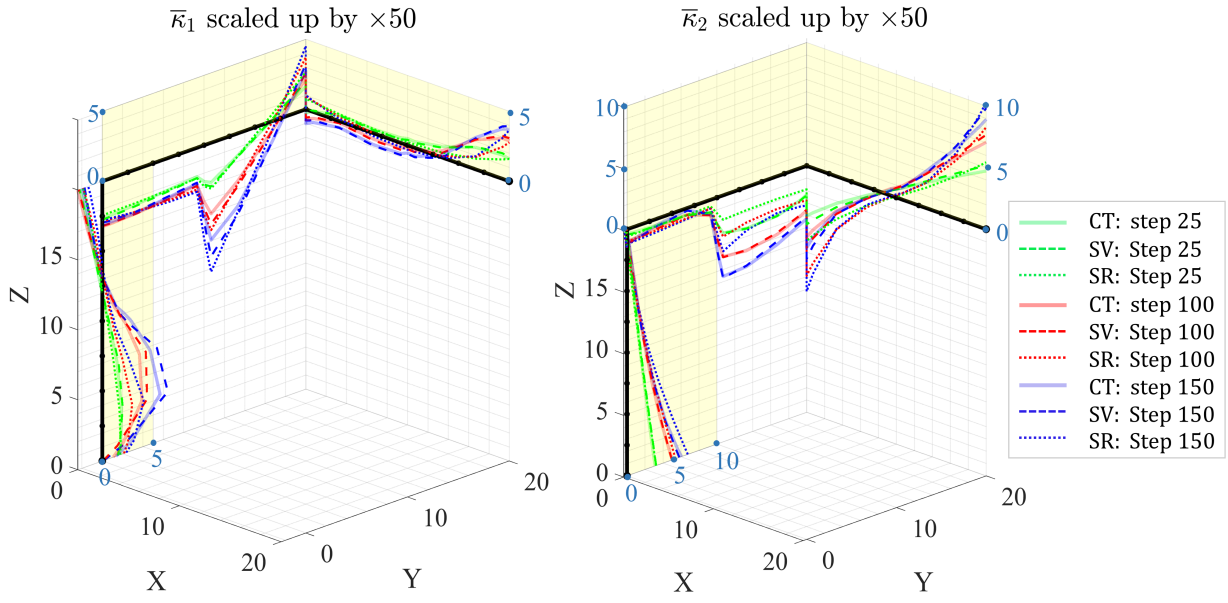

Figure 10.20: Numerical example 3, case 1: The component of material curvatures $\overline{\kappa}_1$, and $\overline{\kappa}_2$ in global coordinates.

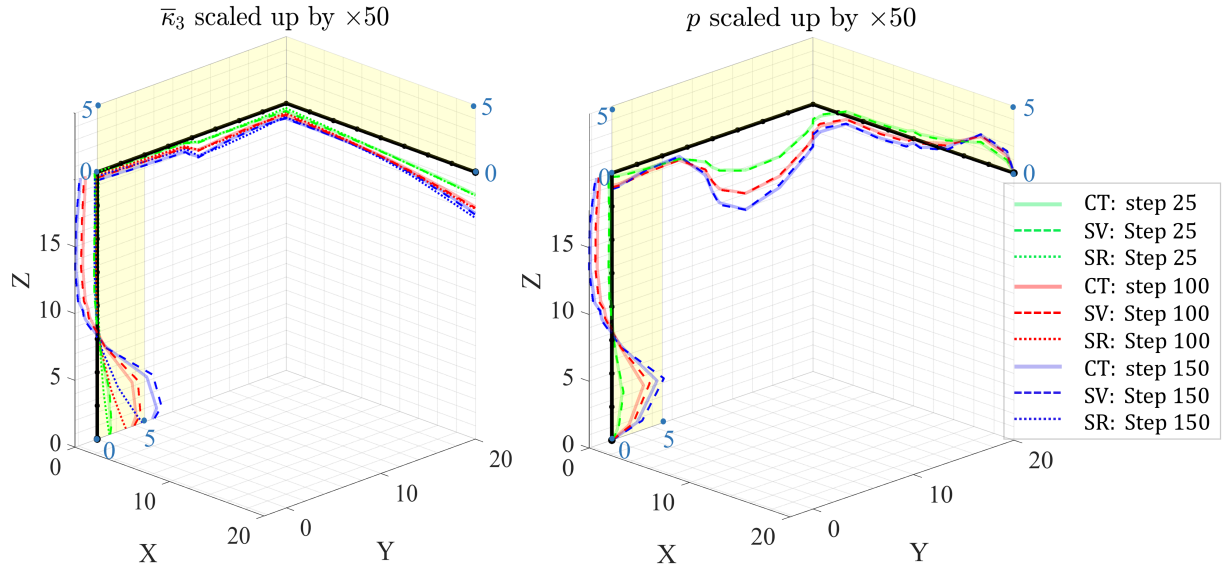

Figure 10.21: Numerical example 3, case 1: The component of material curvature $\overline{\kappa}_3$ in global coordinates, and warping amplitude p.

Figure 10.17 and 10.18 shows the error in the mid-curve position vector and rotation triads predicted by SR and SV beams relative to CT beam respectively. CT beam prediction is closer to SV beam as compared to SR beam. The figure 10.19 and 10.20 compares the curvature and warping amplitude fields interpolated linearly from their values at the Gauss points obtained by CT, SV, and SR beam models for various load steps. The yellow plane represents the positive plot. We note that the strain fields are in global coordinate system, for example, in local element coordinate system, $\overline{\kappa}_1$ represents bending curvature about $\boldsymbol{e}_2$ for elements 1, 2, 3, and 4, whereas it represents torsional curvature for elements 5 and 6. Similarly, the torsional curvature for elements 1 and 2 is given by $\overline{\kappa}_3$, for elements 3 and 4 by $\overline{\kappa}_2$ (the local and global system aligns for elements 4 and 5). A clear resemblance in the warping amplitude p can be observed with $\overline{\kappa}_3$ for elements 1 and 2; with $\overline{\kappa}_2$ for elements 3 and 4; and with $\overline{\kappa}_1$ for elements 5 and 6.

10.5.3.2 Case 2

For case 2, we consider a more slender structure with the cross-sectional dimension as $b = 0.2$ units and $d = 8b$ units. We subject the structure to 2 times the load showed in figure 10.16. Figure 10.22 illustrates the deformed shape for various load-steps using CT, SV, SR, and CF beam models.

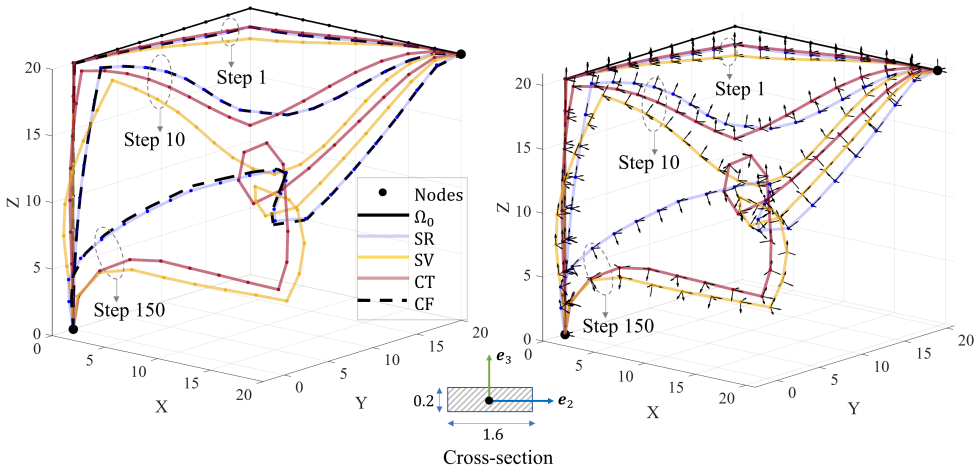

Figure 10.22: Numerical example 3, case 2: Deformed configuration.

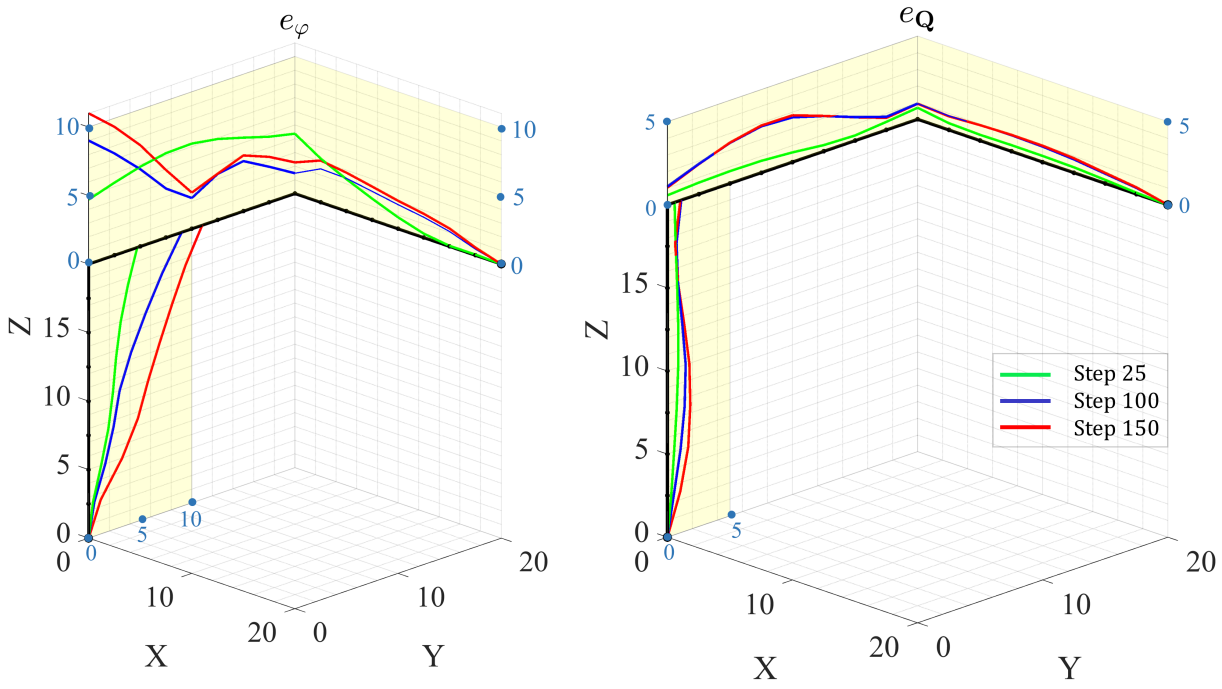

Figure 10.23: Numerical example 3, case 2: Error in the Simo-Reissener beam relative to the Chadha-Todd beam.

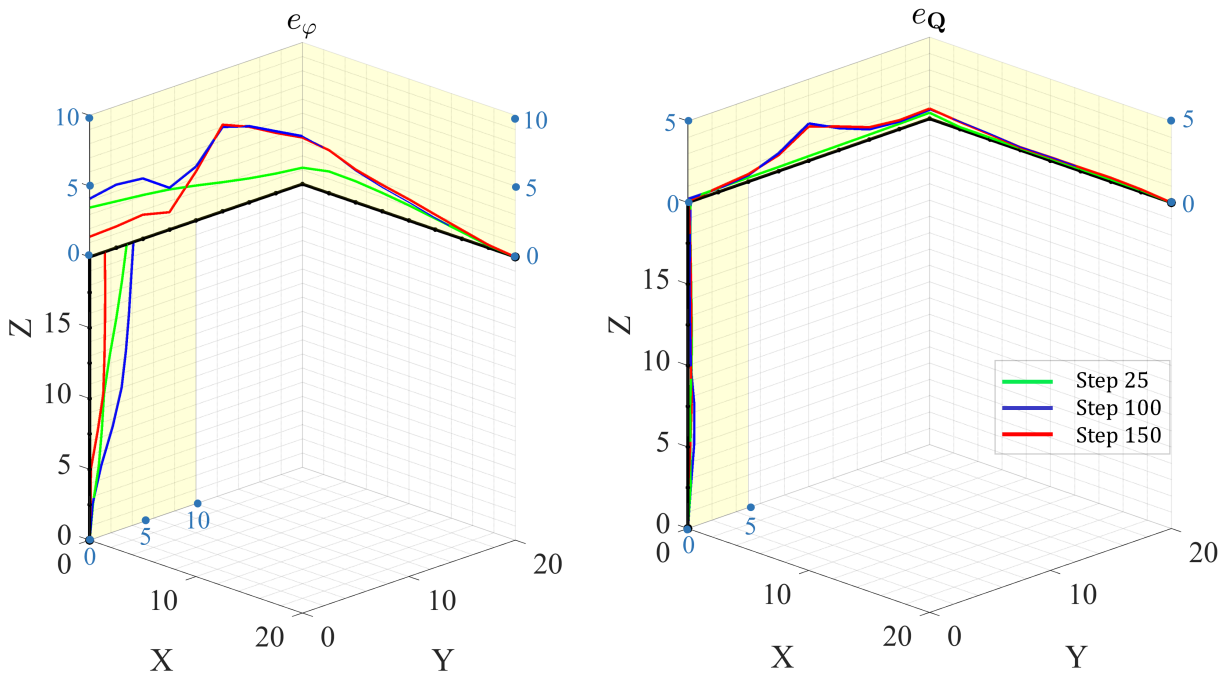

Figure 10.24: Numerical example 3, case 2: Error in the Simo Vu-Quoc beam relative to the Chadha-Todd beam.

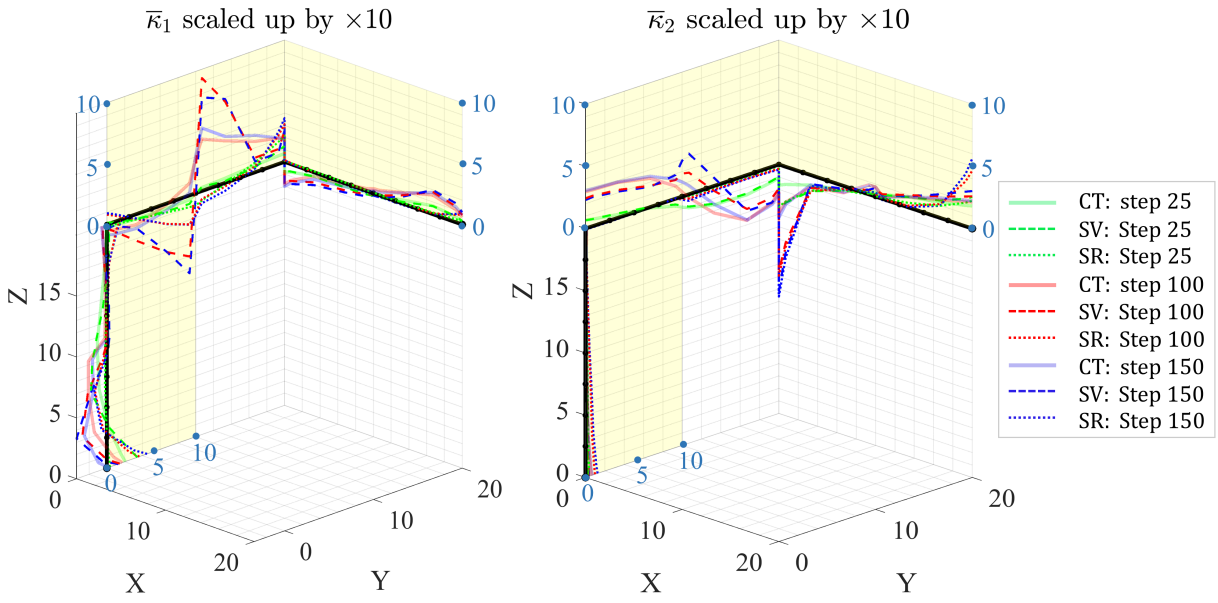

Figure 10.25: Numerical example 3, case 2: The component of the material curvatures $\overline{\kappa}_1$, and $\overline{\kappa}_2$ in global coordinates.

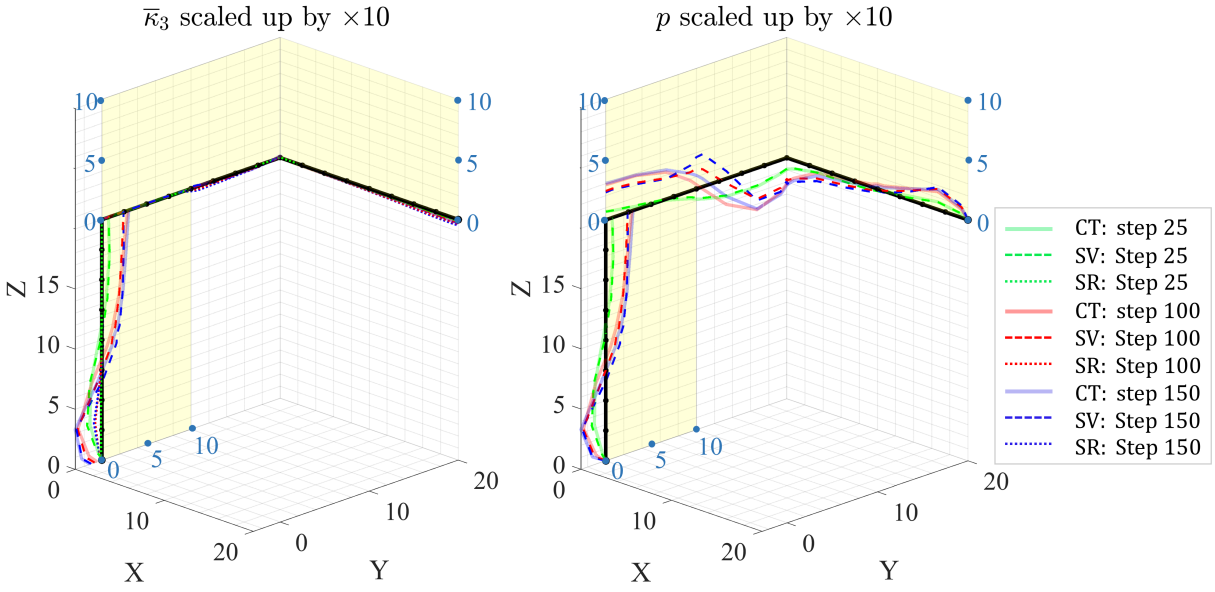

Figure 10.26: Numerical example 3, case 2: The component of the material curvature $\overline{\kappa}_3$ in global coordinates, and warping amplitude p.

As is expected, SR and CF formulation yields a very close displacement field. The difference in the displacement fields obtained by various beam models are very prominent in this example because the slenderness of the structure brings out the affect of fully coupled Poisson's and warping effect in the displacement and strain fields.

10.6 Summary

This chapter delineates the consistent linearization of the weak form of the equilibrium equation discussed in chapter 7. The material and geometric stiffness matrices, external and internal force vectors are obtained. The matrix form of equilibrium equations is derived and solved using Newton Raphson's iterative algorithm using uniformly reduced Gauss quadrature. For the considered constitutive model, the material stiffness matrix is symmetric, whereas, in general, the geometric stiffness is not symmetric. Finally, numerical simulation for conservative and non-conservative loading is presented.

The discussion carried out in this chapter is planned to be published in a journal titled: "Mathematical theory of a higher-order geometrically-exact beam with a deforming cross-section". The dissertation author is the primary investigator and author of this paper.

Chapter 11

Modal analysis

11.1 Introduction

In this chapter, we investigate linear dynamics, focusing on modal analysis, for the considered beam. There are seven unknowns in our beam model: three components of the mid-curve position vector $\boldsymbol{\varphi}$, three components of rotation vector $\boldsymbol{\theta}$, and the warping amplitude p. Therefore, in this chapter, we arrive at seven uncoupled and non-dimensionalized governing differential equations describing the evolution of these seven degrees of freedom. We solve these Euler-Lagrangian equations to obtain mode shapes for various boundary conditions.

11.2 Euler-Lagrangian equations of motion

For the purpose of linear dynamics, we assume that the deformation is small, such that the oscillations occur about the undeformed state Ω_0. Therefore, it is safe to assume $\boldsymbol{Q} = \boldsymbol{I}_3$ or equivalently, $\boldsymbol{d}_i = \boldsymbol{E}_i$. The deformed mid-curve position vector is given by $\boldsymbol{\varphi} = \boldsymbol{\varphi}_0 + \boldsymbol{x}$, where $\boldsymbol{x} = x_i \boldsymbol{E}_i$ is the the mid-curve displacement vector. For small deformation, from Eq. 2.3, we have, $\lim_{\boldsymbol{\theta}\to\boldsymbol{0}} \hat{\boldsymbol{\kappa}} = \partial_{\xi_1} \hat{\boldsymbol{\theta}}$. Thus, $\kappa_i = \overline{\kappa}_i = \partial_{\xi_1} \theta_i$. The angle θ_1 represents torsional deformation, whereas,

the angles θ_2 and θ_3 quantifies bending. The deformation map is then defined as:

$$\boldsymbol{R}(\xi_1, \xi_2, \xi_3) = \boldsymbol{\varphi} + \boldsymbol{r} = \boldsymbol{R}_0 + \boldsymbol{u}. \tag{11.1}$$

The components of the displacement vector $\boldsymbol{u} = u_i \boldsymbol{E}_i$ are given as:

$$\begin{aligned} u_1 &= x_1 - (1 - \nu\epsilon_l)\xi_2\theta_3 + (1 - \nu\epsilon_l)\xi_3\theta_2 + p\Psi_1 + \partial^2_{\xi_1}\theta_2.\Psi_2 + \partial^2_{\xi_1}\theta_3.\Psi_3; \\ u_2 &= x_2 - (1 - \nu\epsilon_l)\xi_3\theta_1 - \nu\epsilon_l\xi_2; \\ u_3 &= x_3 - (1 - \nu\epsilon_l)\xi_2\theta_1 - \nu\epsilon_l\xi_3. \end{aligned} \tag{11.2}$$

where,

$$\epsilon_l = \partial_{\xi_1} x_1 - \xi_2.\partial_{\xi_1}\theta_3 + \xi_3.\partial_{\xi_1}\theta_2 + \partial_{\xi_1} p.\Psi_1 \tag{11.3}$$

The quantity ϵ_l is same as $\boldsymbol{\lambda}_1^2 \cdot \boldsymbol{d}_1$ defined in Eq. 4.33, but for the linear small deformation case. We extend our small deformation assumption to the following:

1. Contributions to Poisson's effect due to bending and warping deformations are negligible as compared to axial strains. Therefore,

$$\epsilon_l = \partial_{\xi_1} x_1. \tag{11.4}$$

2. Contributions of Poisson's deformation on to bending and torsion are negligible. Therefore, the deformation map simplifies to the following,

$$\begin{aligned} u_1 &= x_1 - \xi_2\theta_3 + \xi_3\theta_2 + p\Psi_1 + \partial^2_{\xi_1}\theta_2.\Psi_2 + \partial^2_{\xi_1}\theta_3.\Psi_3; \\ u_2 &= x_2 - \xi_3\theta_1 - \nu\partial_{\xi_1} x_1.\xi_2; \\ u_3 &= x_3 - \xi_2\theta_1 - \nu\partial_{\xi_1} x_1.\xi_3. \end{aligned} \tag{11.5}$$

3. The contribution of bending induced shear non-uniform warping is negligible. The section constant arising out of non-uniform shear warping is negligible as compared to other section

constant. The deformation map further simplifies to,

$$\begin{aligned} u_1 &= x_1 - \xi_2\theta_3 + \xi_3\theta_2 + p\Psi_1; \\ u_2 &= x_2 - \xi_3\theta_1 - \nu\partial_{\xi_1}x_1.\xi_2; \\ u_3 &= x_3 - \xi_2\theta_1 - \nu\partial_{\xi_1}x_1.\xi_3. \end{aligned} \tag{11.6}$$

4. To proceed further, we also assume the section to be symmetric to at least one principle axes.

Considering linear isotropic St. Venant's Kirchhoff material, we define the symmetric Cauchy stress tensor $\boldsymbol{\sigma}$ and its strain conjugate $\boldsymbol{\tau}$ as:

$$\begin{aligned} \tau_{ij} &= \frac{1}{2}\left(\partial_{\xi_i}u_j + \partial_{\xi_j}u_i\right); \\ \sigma_{ij} &= 2G\tau_{ij} + \left(\frac{E\nu}{(1+\nu)(1-2\nu)}\right)\tau_{kk}\delta_{ij}. \end{aligned} \tag{11.7}$$

Using the deformation map defined in Eq. (11.6), and the definition of stress-strain in Eq. (11.7), the strain energy U_{strain}, kinetic energy T and external work W_{ext} can be obtained as:

$$\begin{aligned} U_{\text{strain}} =& \frac{1}{2}\int_\Omega \boldsymbol{\sigma} : \boldsymbol{\tau}\, \mathrm{d}\Omega \\ =& \frac{1}{2}\int_0^L \Big(EA(\partial_{\xi_1}x_1)^2 + GA(\partial_{\xi_1}x_3 + \theta_2)^2 + GA(\partial_{\xi_1}x_2 - \theta_3)^2 + G(I_{11} - I_k)(\partial_{\xi_1}\theta_1)^2 \\ &+ EI_{22}(\partial_{\xi_1}\theta_2)^2 + EI_{33}(\partial_{\xi_1}\theta_3)^2 + GI_k(p - \partial_{\xi_1}\theta_1)^2 + E\Xi.(\partial_{\xi_1}p)^2 \\ &+ \left(\frac{GI_{11}\nu^2}{1+\nu}\right)(\partial^2_{\xi_1}x_1)^2\Big)\,\mathrm{d}\xi_1; \end{aligned} \tag{11.8}$$

$$\begin{aligned} T =& \frac{1}{2}\int_0^L \rho\Big(A(\partial_t x_1^2 + \partial_t x_2^2 + \partial_t x_3^2) + I_{33}(\partial_t\theta_3)^2 + I_{22}(\partial_t\theta_2)^2 + I_{11}(\partial_t\theta_1)^2 \\ &+ \nu^2 I_{11}(\partial_t\partial_{\xi_1}x_1)^2 + \Xi\partial_t p^2\Big)\,\mathrm{d}\xi_1; \end{aligned} \tag{11.9}$$

$$W_{\text{ext}} = \int_0^L (N_1x_1 + N_2x_2 + N_3x_3 + M_1\theta_1 + M_2\theta_2 + M_3\theta_3 + N_p p)\,\mathrm{d}\xi_1. \tag{11.10}$$

In the equation above,

$$\begin{aligned} A = \int_{\mathfrak{B}} \mathrm{d}\mathfrak{B};\ I_{22} = \int_{\mathfrak{B}} \xi_2^2\ \mathrm{d}\mathfrak{B};\ I_{33} = \int_{\mathfrak{B}} \xi_3^2\ \mathrm{d}\mathfrak{B};\ I_{11} = I_{22} + I_{33}; \\ \Xi = \int_{\mathfrak{B}} \Psi_1^2\ \mathrm{d}\mathfrak{B};\ I_k = \int_{\mathfrak{B}} \partial_{\xi_2}\Psi_1^2 + \partial_{\xi_3}\Psi_1^2\ \mathrm{d}\mathfrak{B} = \int_{\mathfrak{B}} (\xi_2\partial_{\xi_3}\Psi_1 - \xi_3\partial_{\xi_2}\Psi_1)\ \mathrm{d}\mathfrak{B}. \end{aligned} \tag{11.11}$$

The external force and moment vectors are given by:

$$\begin{aligned} \boldsymbol{N}(\xi_1) = N_i(\xi_1)\boldsymbol{E}_i = \int_\Gamma \boldsymbol{\sigma}.\boldsymbol{n}\ \mathrm{d}\Gamma + \int_\Omega \rho\boldsymbol{b}\ \mathrm{d}\Omega; \\ \boldsymbol{M}(\xi_1) = M_i(\xi_1)\boldsymbol{E}_i = \int_\Gamma \boldsymbol{r}\times\boldsymbol{\sigma}.\boldsymbol{n}\ \mathrm{d}\Gamma + \int_\Omega \rho\boldsymbol{r}\times\boldsymbol{b}\ \mathrm{d}\Omega; \\ N_p = \boldsymbol{E}_1 \cdot \left(\int_\Gamma \Psi_1\boldsymbol{\sigma}.\boldsymbol{n}\ \mathrm{d}\Gamma + \int_\Omega \rho\Psi_1\boldsymbol{b}\ \mathrm{d}\Omega \right). \end{aligned} \tag{11.12}$$

We note that, for the case of small linear deformation case, the integration in the above equation set can be carried out with respect to the undeformed state Ω_0, with the boundary Γ_0. The vector $\boldsymbol{n}$ gives the surface normal vector.

We arrive at the governing equations of motion using Hamiltonian's principle, such that the action $\mathfrak{A}$ is stationarized:

$$\delta\mathfrak{A} = \delta(T - U_{\text{strain}} + W_{\text{ext}}) = 0. \tag{11.13}$$

We obtain seven coupled Euler-Lagrangian equations of motion with the respective boundary conditions. The governing equations and the boundary conditions for the axial deformation is obtained as:

$$\begin{aligned} \left(\frac{G\nu^2 I_{11}}{1+\nu}\right)\partial_{\xi_1}^4 x_1 - (EA)\partial_{\xi_1}^2 x_1 - (\rho I_{11}\nu^2)\partial_t^2\partial_{\xi_1}^2 x_1 + (\rho A)\partial_t^2 x_1 = N_1; \\ \left[\left(-EA\partial_{\xi_1}x_1 - (\rho I_{11}\nu^2)\partial_t^2\partial_{\xi_1}x_1 + \left(\frac{G\nu^2 I_{11}}{1+\nu}\right)\partial_{\xi_1}^3 x_1\right)\delta x_1\right]_0^L = 0; \\ \left[\left(\left(\frac{G\nu^2 I_{11}}{1+\nu}\right)\partial_{\xi_1}^2 x_1\right)\delta\partial_{\xi_1}x_1\right]_0^L = 0. \end{aligned} \tag{11.14}$$

The coupled equations for the torsion angle θ_1 and warping amplitude p are obtained as:

$$\begin{gathered}\rho\Xi\partial_t^2 p - E\Xi\partial_{\xi_1}^2 p + GI_k(p - \partial_{\xi_1}\theta_1) = N_p; \\ \left[E\Xi\partial_{\xi_1} p.\delta p\right]_0^L = 0;\end{gathered} \tag{11.15}$$

and,

$$\begin{gathered}\rho I_{11}\partial_t^2\theta_1 - \partial_{\xi_1}\left(GI_{11}\partial_{\xi_1}\theta_1 - GI_k p\right) = M_1; \\ \left[\left(GI_{11}\partial_{\xi_1}\theta_1 - GI_k p\right).\delta\theta_1\right]_0^L = 0.\end{gathered} \tag{11.16}$$

The coupled equations for the bending angle θ_2 and the mid-curve deformation component x_3 are obtained as:

$$\begin{gathered}\rho A\partial_t^2 x_3 - GA.\partial_{\xi_1}\left(\theta_2 + \partial_{\xi_1} x_3\right) = N_3; \\ \left[\left(GA(\theta_2 + \partial_{\xi_1} x_3)\right).\delta x_3\right]_0^L = 0;\end{gathered} \tag{11.17}$$

and,

$$\begin{gathered}\rho I_{22}\partial_t^2\theta_2 + GA(\theta_2 + \partial_{\xi_1} x_3) - EI_{22}\partial_{\xi_1}^2\theta_2 = M_2; \\ \left[\left(EI_{22}\partial_{\xi_1}\theta_2\right).\delta\theta_2\right]_0^L = 0.\end{gathered} \tag{11.18}$$

The coupled equations for the bending angle θ_3 and the mid-curve deformation component x_2 is obtained as:

$$\begin{gathered}\rho A\partial_t^2 x_2 + GA\partial_{\xi_1}\left(\theta_3 - \partial_{\xi_1} x_2\right) = N_2; \\ \left[\left(GA(\theta_3 - \partial_{\xi_1} x_2)\right).\delta x_2\right]_0^L = 0;\end{gathered} \tag{11.19}$$

and,

$$\begin{gathered}\rho I_{33}\partial_t^2\theta_3 + GA(\theta_3 - \partial_{\xi_1} x_2) - EI_{33}\partial_{\xi_1}^2\theta_3 = M_3; \\ \left[\left(EI_{33}\partial_{\xi_1}\theta_3\right).\delta\theta_3\right]_0^L = 0.\end{gathered} \tag{11.20}$$

11.3 Modal analysis

To proceed further with the modal analysis, we non-dimensionalize the Euler-Lagrangian equations of motion obtained in the previous section. We represent the mode shapes corresponding to a non-dimensionalized degree of freedom by adding a tilde on the quantity. For example $\tilde{\theta}_{1n}$ and

$\tilde{p}_n$ represents the n^{th} mode shape corresponding to θ_1 and non-dimensionalized warping amplitude $\overline{p}$ (defined later) respectively. Secondly, we use $\sin(\alpha) = s_\alpha$ and $\cos(\alpha) = c_\alpha$ interchangeably. Lastly, we define shorthand notation of hyperbolic functions as $\sinh(\alpha) = \text{sh}_\alpha$ and $\cosh(\alpha) = \text{ch}_\alpha$ that is used interchangeably.

11.3.1 Mode shape for θ_1 and p

We consider the following definition of dimensionless quantities:

$$\begin{aligned}
&\overline{\xi}_1 = \frac{\xi_1}{L};\ \overline{t} = t\sqrt{\frac{E\Xi}{\rho I_{11} L^4}};\ \overline{p} = pL;\ \theta_1(\xi_1, t) = \theta_1(\overline{\xi}_1, \overline{t}) = \theta_1;\\
&\beta^2 = \frac{E}{G};\ \gamma^2 = \frac{\Xi}{I_{11}L^2};\ \alpha^2 = \frac{I_k}{I_{11}};\ \overline{N}_p = \frac{N_p L}{G I_{11}};\ \overline{M}_1 = \frac{M_1 L^2}{G I_{11}}.
\end{aligned} \tag{11.21}$$

We note that if $I_k < 0$, then α is a complex number. Substituting these quantities into equations (11.15) and (11.16), we get non-dimensionalized but coupled equations as:

$$\begin{aligned}
\beta^2\gamma^4\partial^2_{\overline{t}}\overline{p} - \beta^2\gamma^2\partial^2_{\overline{\xi}_1}\overline{p} + \alpha^2(\overline{p} - \partial_{\overline{\xi}_1}\theta_1) &= \overline{N}_p;\\
\left[\partial_{\overline{\xi}_1}\overline{p}.\delta\overline{p}\right]^1_0 &= 0;
\end{aligned} \tag{11.22}$$

and,

$$\begin{aligned}
\beta^2\gamma^2\partial^2_{\overline{t}}\theta_1 - \partial^2_{\overline{\xi}_1}\theta_1 + \alpha^2\partial_{\overline{\xi}_1}\overline{p} &= \overline{M}_1;\\
\left[\left(\partial_{\overline{\xi}_1}\theta_1 - \alpha^2\overline{p}\right).\delta\theta_1\right]^1_0 &= 0.
\end{aligned} \tag{11.23}$$

The non-dimensionalized uncoupled Euler-Lagrangian equations can be obtained from Eq. (11.22) and (11.23) as:

$$\begin{aligned}
\beta^4\gamma^6\partial^4_{\overline{t}}\overline{p} + \alpha^2\beta^2\gamma^2\partial^2_{\overline{t}}\overline{p} - \beta^2\gamma^4(\beta^2+1)\partial^2_{\overline{\xi}_1}\partial^2_{\overline{t}}\overline{p} + \beta^2\gamma^2\partial^4_{\overline{\xi}_1}\overline{p} + \alpha^2(\alpha^2-1)\partial^2_{\overline{\xi}_1}\overline{p}&\\
= \alpha^2\partial_{\overline{\xi}_1}\overline{M}_1 + \beta^2\gamma^2\partial^2_{\overline{t}}\overline{N}_p - \partial^2_{\overline{\xi}_1}\overline{N}_p;&
\end{aligned} \tag{11.24}$$

$$\begin{aligned}
-\beta^4\gamma^6\partial^4_{\overline{t}}\theta_1 - \alpha^2\beta^2\gamma^2\partial^2_{\overline{t}}\theta_1 + \beta^2\gamma^4(\beta^2+1)\partial^2_{\overline{\xi}_1}\partial^2_{\overline{t}}\theta_1 - \beta^2\gamma^2\partial^4_{\overline{\xi}_1}\theta_1 - \alpha^2(\alpha^2-1)\partial^2_{\overline{\xi}_1}\theta_1&\\
= -\alpha^2\overline{M}_1 - \beta^2\gamma^4\partial^2_{\overline{t}}\overline{M}_1 + \beta^2\gamma^2\partial^2_{\overline{\xi}_1}\overline{M}_1 + \alpha^2\partial_{\overline{\xi}_1}\overline{N}_p.&
\end{aligned} \tag{11.25}$$

For modal analysis, we consider the case of free vibration and assume all the external forces to vanish. We assume a solution of form $\overline{p} = e^{\lambda\overline{\xi}_1}\cos\overline{\omega}\overline{t}$ (or similar form of θ_1) and substitute it in Eq. (11.24), yielding the characteristic equations:

$$(-1+\alpha^2)\lambda^2 + \left(\frac{\beta^2\gamma^2}{\alpha^2}\right)\lambda^4 - (\beta^2\gamma^2)\overline{\omega}^2 + \left(\frac{\beta^2\gamma^4}{\alpha^2}\right)(\beta^2+1)\lambda^2\overline{\omega}^2 + \left(\frac{\beta^4\gamma^6}{\alpha^2}\right)\overline{\omega}^4 = 0. \tag{11.26}$$

The characteristic equation leads to four complex roots:

$$\lambda_{1,2} = \pm i\mathfrak{s}_1; \tag{11.27}$$

$$\lambda_{3,4} = \pm i\mathfrak{s}_2. \tag{11.28}$$

where,

$$\mathfrak{s}_1 = \sqrt{\frac{\alpha^2\left(\alpha^2 + \sqrt{\frac{\beta^4\left(\beta^2-1\right)^2\gamma^8\overline{\omega}^4}{\alpha^4} + \frac{2\beta^2\gamma^4\overline{\omega}^2\left(\alpha^2\left(\beta^2+1\right)+\beta^2-1\right)}{\alpha^2} + \left(\alpha^2-1\right)^2} - 1\right)}{2\beta^2\gamma^2} + \frac{1}{2}\left(\beta^2+1\right)\gamma^2\overline{\omega}^2}; \tag{11.29}$$

$$\mathfrak{s}_2 = \sqrt{\frac{\alpha^4 - \alpha^2\left(\sqrt{\frac{\beta^4\left(\beta^2-1\right)^2\gamma^8\overline{\omega}^4}{\alpha^4} + \frac{2\beta^2\gamma^4\overline{\omega}^2\left(\alpha^2\left(\beta^2+1\right)+\beta^2-1\right)}{\alpha^2} + \left(\alpha^2-1\right)^2} + 1\right) + \beta^2\left(\beta^2+1\right)\gamma^4\overline{\omega}^2}{2\beta^2\gamma^2}}. \tag{11.30}$$

Here, $\mathfrak{s}_1, \mathfrak{s}_2 \in \mathbb{R}$. Therefore, the mode shapes can be written as:

$$\begin{aligned}
\overline{p} &= \left(\mathfrak{c}_1\cos\left(\mathfrak{s}_1\overline{\xi}_1\right) + \mathfrak{c}_2\sin\left(\mathfrak{s}_1\overline{\xi}_1\right) + \mathfrak{c}_3\cos\left(\mathfrak{s}_2\overline{\xi}_1\right) + \mathfrak{c}_4\sin\left(\mathfrak{s}_2\overline{\xi}_1\right)\right)\cos\left(\overline{\omega}\overline{t}\right); \\
\theta_1 &= \left(\mathfrak{c}_5\cos\left(\mathfrak{s}_1\overline{\xi}_1\right) + \mathfrak{c}_6\sin\left(\mathfrak{s}_1\overline{\xi}_1\right) + \mathfrak{c}_7\cos\left(\mathfrak{s}_2\overline{\xi}_1\right) + \mathfrak{c}_8\sin\left(\mathfrak{s}_2\overline{\xi}_1\right)\right)\cos\overline{\omega}\overline{t}.
\end{aligned} \tag{11.31}$$

There are nine unknowns: eight $\mathfrak{c}_i$ and the natural frequency $\overline{\omega}$ that is embedded in $\mathfrak{s}_1$ and $\mathfrak{s}_2$. Eight constants can be specified by applying four boundary conditions and four continuity conditions. The continuity conditions makes sure that the assumed solutions in (11.31) must solve the coupled equation (11.22) and (11.23). To realize various mode shapes, we assume For

$\beta^2 = 2.4$, $\gamma^2 = 2.88 \times 10^{-2}$ and $\alpha^2 = -0.923$.

11.3.1.1 Fixed-fixed boundary condition

For fixed-fixed boundary, we have

$$\begin{aligned} \overline{p}(0,\bar{t}) = \overline{p}(1,\bar{t}) = 0; \\ \theta_1(0,\bar{t}) = \theta_1(1,\bar{t}) = 0. \end{aligned} \tag{11.32}$$

We impose these boundary conditions on the Eq. (11.31) and ensure continuity as mentioned before. We obtain eight conditions that can be represented in the form given below:

$$\boldsymbol{Z}.\boldsymbol{c} = \mathbf{0}, \quad \text{where,} \tag{11.33a}$$

$$\boldsymbol{c} = [\mathfrak{c}_1; \mathfrak{c}_2; \mathfrak{c}_3; \mathfrak{c}_4; \mathfrak{c}_5; \mathfrak{c}_6; \mathfrak{c}_7; \mathfrak{c}_8]; \tag{11.33b}$$

$$\boldsymbol{Z} = \begin{bmatrix} 1 & 0 & 1 & 0 & 0 & 0 & 0 & 0 \\ c_{\mathfrak{s}_1} & s_{\mathfrak{s}_1} & c_{\mathfrak{s}_2} & s_{\mathfrak{s}_2} & 0 & 0 & 0 & 0 \\ 0 & 0 & 0 & 0 & 1 & 0 & 1 & 0 \\ 0 & 0 & 0 & 0 & c_{\mathfrak{s}_1} & s_{\mathfrak{s}_1} & c_{\mathfrak{s}_2} & s_{\mathfrak{s}_2} \\ 0 & \mathfrak{s}_1^2 - \chi^2 & 0 & 0 & -\alpha^2\mathfrak{s}_1 & 0 & 0 & 0 \\ \mathfrak{s}_1^2 - \chi^2 & 0 & 0 & 0 & 0 & \alpha^2\mathfrak{s}_1 & 0 & 0 \\ 0 & 0 & 0 & \mathfrak{s}_2^2 - \chi^2 & 0 & 0 & -\alpha^2\mathfrak{s}_2 & 0 \\ 0 & 0 & \mathfrak{s}_2^2 - \chi^2 & 0 & 0 & 0 & 0 & \alpha^2\mathfrak{s}_2 \end{bmatrix}. \tag{11.33c}$$

$$\chi = \beta\gamma\overline{\omega}. \tag{11.33d}$$

For equation (11.33a) to hold, we require the determinant of $\boldsymbol{Z}$ matrix to vanish, yielding

$$\begin{aligned} \det(\boldsymbol{Z}) = &\frac{1}{2}\Bigg(2\mathfrak{s}_1 s_{\mathfrak{s}_2}\left(\chi^2 - \mathfrak{s}_2^2\right)\left(\mathfrak{s}_2 s_{\mathfrak{s}_2}\left(\mathfrak{s}_1^2 - \chi^2\right) + \mathfrak{s}_1 s_{\mathfrak{s}_1}(\chi - \mathfrak{s}_2)(\chi + \mathfrak{s}_2)\right) \\ &+ \mathfrak{s}_2\left(\mathfrak{s}_1^2 - \chi^2\right)\left(2\mathfrak{s}_2 s_{\mathfrak{s}_1} s_{\mathfrak{s}_2}\left(\mathfrak{s}_1^2 - \chi^2\right) + \mathfrak{s}_1\left(-4c_{\mathfrak{s}_1}c_{\mathfrak{s}_2} + c_{2\mathfrak{s}_2} + 3\right)\left(\chi^2 - \mathfrak{s}_2^2\right)\right)\Bigg) = 0. \end{aligned} \tag{11.34}$$

We solve the above equation to obtain the natural frequencies $\overline{\omega}$ of which the first five are $\overline{\omega} = \{8.912, 23.527, 26.406, 38.114, 43.133\}$. The natural frequency ω can be obtained using the equality $\overline{\omega}\overline{t} = \omega t$. The mode shape or the Eigenfunction is only determinable up to the arbitrary scaling constant. Therefore, we obtain seven constants by solving any seven equations in the equation set Eq. (11.33a) and normalize the mode shape to obtain the eighth constant. Figure 11.1 illustrates the first five mode shapes.

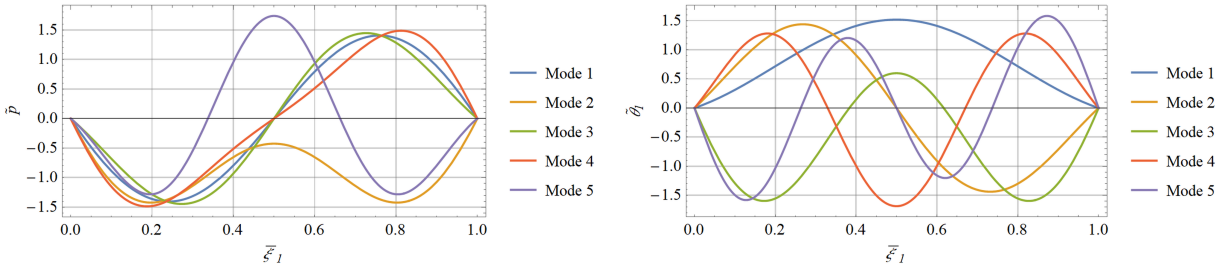

(a) Mode shapes $\tilde{p}_n$ for $1 \leq n \leq 5$

(b) Mode shapes $\tilde{\theta}_{1n}$ for $1 \leq n \leq 5$

Figure 11.1: Mode shapes for the warping amplitude $\overline{p}$ and θ_1 considering the fixed-fixed boundary.

11.3.1.2 Fixed-free boundary condition

At the fixed boundary, we have displacement boundary conditions, whereas at the free boundary, we impose the force boundary conditions, such that

$$\begin{gathered} \overline{p}(0,\bar{t}) = \theta_1(0,\bar{t}) = 0; \\ \partial_{\bar{\xi}_1}\overline{p}(1,\bar{t}) = 0;\ \partial_{\bar{\xi}_1}\theta_1(1,\bar{t}) - \alpha^2\partial_{\bar{\xi}_1}\overline{p}(1,\bar{t}) = 0 \end{gathered} \tag{11.35}$$

We obtain eight simultaneous equations in the coefficient c_i that can be written in the form defined in Eq. (11.33a), such that:

$$\boldsymbol{Z} = \begin{bmatrix} 1 & 0 & 1 & 0 & 0 & 0 & 0 & 0 \\ 0 & 0 & 0 & 0 & -\mathfrak{s}_1 s_{\mathfrak{s}_1} & \mathfrak{s}_1 c_{\mathfrak{s}_1} & -\mathfrak{s}_2 s_{\mathfrak{s}_2} & \mathfrak{s}_2 c_{\mathfrak{s}_2} \\ 0 & 0 & 0 & 0 & 1 & 0 & 1 & 0 \\ -\mathfrak{s}_1 s_{\mathfrak{s}_1} & \mathfrak{s}_1 c_{\mathfrak{s}_1} & -\mathfrak{s}_2 s_{\mathfrak{s}_2} & \mathfrak{s}_2 c_{\mathfrak{s}_2} & -\alpha^2 c_{\mathfrak{s}_1} & -\alpha^2 s_{\mathfrak{s}_1} & -\alpha^2 c_{\mathfrak{s}_2} & -\alpha^2 s_{\mathfrak{s}_2} \\ 0 & \mathfrak{s}_1^2 - \chi^2 & 0 & 0 & -\alpha^2 \mathfrak{s}_1 & 0 & 0 & 0 \\ \mathfrak{s}_1^2 - \chi^2 & 0 & 0 & 0 & 0 & \alpha^2 \mathfrak{s}_1 & 0 & 0 \\ 0 & 0 & 0 & \mathfrak{s}_2^2 - \chi^2 & 0 & 0 & -\alpha^2 \mathfrak{s}_2 & 0 \\ 0 & 0 & \mathfrak{s}_2^2 - \chi^2 & 0 & 0 & 0 & 0 & \alpha^2 \mathfrak{s}_2 \end{bmatrix}. \tag{11.36}$$

The zero determinant condition yields,

$$\begin{aligned} \det(\boldsymbol{Z}) = &- \mathfrak{s}_1 \mathfrak{s}_2 c_{\mathfrak{s}_1} c_{\mathfrak{s}_2} \left(-2\mathfrak{s}_1^2 \chi^2 - 2\mathfrak{s}_2^2 \chi^2 + \mathfrak{s}_1^4 + \mathfrak{s}_2^4 + 2\chi^4\right) - 2\mathfrak{s}_1 \mathfrak{s}_2 \left(\mathfrak{s}_1^2 - \chi^2\right)\left(\chi^2 - \mathfrak{s}_2^2\right) \\ &- \left(\mathfrak{s}_1^2 + \mathfrak{s}_2^2\right) s_{\mathfrak{s}_1} s_{\mathfrak{s}_2} \left(\mathfrak{s}_1^2 - \chi^2\right)\left(\mathfrak{s}_2^2 - \chi^2\right) = 0. \end{aligned} \tag{11.37}$$

We solve the Eq. (11.37) for $\overline{\omega}$, yielding the first five non-dimensional natural frequencies as $\overline{\omega} = \{11.888,\ 17.956,\ 31.622,\ 34.408,\ 46.462\}$. The mode shapes can be obtained using the approach described in section 11.3.1.1. Figures 11.2 illustrates the first five mode shape for fixed-free boundary.

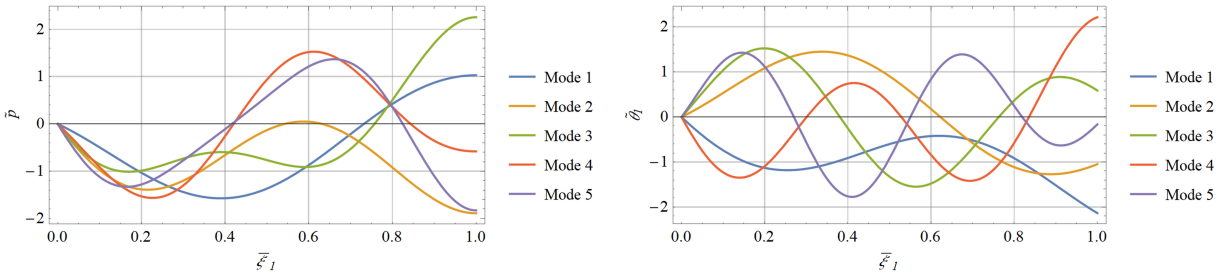

(a) Mode shapes $\tilde{p}_n$ for $1 \leq n \leq 5$

(b) Mode shapes $\tilde{\theta}_{1n}$ for $1 \leq n \leq 5$

Figure 11.2: Mode shapes for the warping amplitude $\overline{p}$ and θ_1 considering the fixed-free boundary.

11.3.1.3 Free-free boundary condition

We assume force boundary condition at both ends as,

$$\begin{aligned} \partial_{\overline{\xi}_1}\overline{p}(0,\overline{t}) = 0;\ \partial_{\overline{\xi}_1}\theta_1(0,\overline{t}) - \alpha^2\partial_{\overline{\xi}_1}\overline{p}(0,\overline{t}) = 0; \\ \partial_{\overline{\xi}_1}\overline{p}(1,\overline{t}) = 0,\ \partial_{\overline{\xi}_1}\theta_1(1,\overline{t}) - \alpha^2\partial_{\overline{\xi}_1}\overline{p}(1,\overline{t}) = 0. \end{aligned} \tag{11.38}$$

The $\boldsymbol{Z}$ matrix obtained after imposing these boundary conditions along with the continuity conditions is:

$$\boldsymbol{Z} = \begin{bmatrix} 0 & 0 & 0 & 0 & 0 & \mathfrak{s}_1 & 0 & \mathfrak{s}_2 \\ 0 & 0 & 0 & 0 & -\mathfrak{s}_1 s_{\mathfrak{s}_1} & \mathfrak{s}_1 c_{\mathfrak{s}_1} & -\mathfrak{s}_2 s_{\mathfrak{s}_2} & \mathfrak{s}_2 c_{\mathfrak{s}_2} \\ 0 & \mathfrak{s}_1 & 0 & \mathfrak{s}_2 & -\alpha^2 & 0 & -\alpha^2 & 0 \\ -\mathfrak{s}_1 s_{\mathfrak{s}_1} & \mathfrak{s}_1 c_{\mathfrak{s}_1} & -\mathfrak{s}_2 s_{\mathfrak{s}_2} & \mathfrak{s}_2 c_{\mathfrak{s}_2} & -\alpha^2 c_{\mathfrak{s}_1} & -\alpha^2 s_{\mathfrak{s}_1} & -\alpha^2 c_{\mathfrak{s}_2} & -\alpha^2 s_{\mathfrak{s}_2} \\ 0 & \mathfrak{s}_1^2 - \chi^2 & 0 & 0 & -\alpha^2\mathfrak{s}_1 & 0 & 0 & 0 \\ \mathfrak{s}_1^2 - \chi^2 & 0 & 0 & 0 & 0 & \alpha^2\mathfrak{s}_1 & 0 & 0 \\ 0 & 0 & 0 & \mathfrak{s}_2^2 - \chi^2 & 0 & 0 & -\alpha^2\mathfrak{s}_2 & 0 \\ 0 & 0 & \mathfrak{s}_2^2 - \chi^2 & 0 & 0 & 0 & 0 & \alpha^2\mathfrak{s}_2 \end{bmatrix} \tag{11.39}$$

The zero determinant condition yields,

$$\begin{aligned} \det(\boldsymbol{Z}) =& 2\mathfrak{s}_2\mathfrak{s}_1^3\left(c_{\mathfrak{s}_1}c_{\mathfrak{s}_2} - 1\right)\left(\mathfrak{s}_2^2 - \chi^2\right) + 2\mathfrak{s}_2\mathfrak{s}_1\chi^2\left(c_{\mathfrak{s}_1}c_{\mathfrak{s}_2} - 1\right)\left(\chi^2 - \mathfrak{s}_2^2\right) + s_{\mathfrak{s}_1}s_{\mathfrak{s}_2}\mathfrak{s}_1^2\chi^4 \\ & - 2s_{\mathfrak{s}_1}s_{\mathfrak{s}_2}\mathfrak{s}_1^4\chi^2 + s_{\mathfrak{s}_1}s_{\mathfrak{s}_2}\left(\mathfrak{s}_2^3 - \mathfrak{s}_2\chi^2\right)^2 + s_{\mathfrak{s}_1}s_{\mathfrak{s}_2}\mathfrak{s}_1^6 = 0. \end{aligned} \tag{11.40}$$

We solve the Eq. (11.40) for $\overline{\omega}$, using same parameters used before, yielding the first six non-dimensional natural frequencies as $\overline{\omega} = \{0,\ 12.272,\ 22.480,\ 26.003,\ 39.726,\ 41.778\}$. We note that $\overline{\omega} = 0$ is a trivial solution to the previously discussed boundary conditions. However, for this boundary condition, the Eigenfunction corresponding to $\overline{\omega} = 0$ reflects the rigid body mode for θ_1. Figure 11.3 illustrates the first six mode shape for fixed-free boundary.

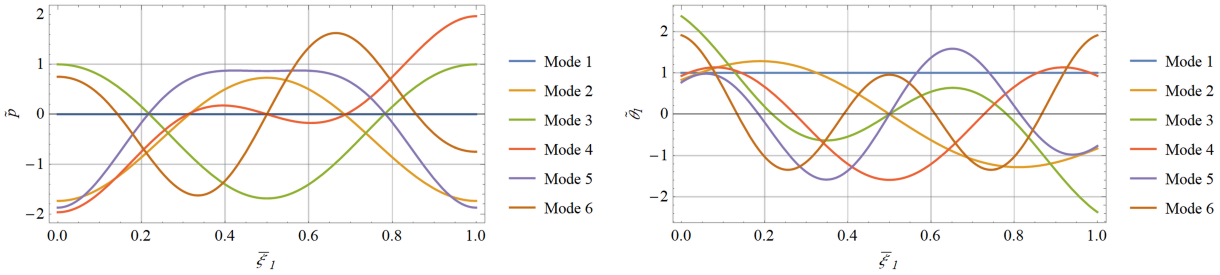

(a) Mode shapes $\tilde{p}_n$ for $1 \leq n \leq 6$

(b) Mode shapes $\tilde{\theta}_{1n}$ for $1 \leq n \leq 6$

Figure 11.3: Mode shapes for the warping amplitude $\overline{p}$ and θ_1 considering the free-free boundary.

11.3.2 Mode shape for θ_2 and x_3

We consider the following definition of dimensionless quantities:

$$\overline{\xi}_1 = \frac{\xi_1}{L};\ \overline{t} = t\sqrt{\frac{EI_{22}}{\rho AL^4}};\ \overline{x}_3 = \frac{x_3}{L};\ \theta_2(\xi_1, t) = \theta_2(\overline{\xi}_1, \theta_t) = \theta_2;\ \beta^2 = \frac{E}{G};\ R^2_{\xi_2} = \frac{I_{22}}{AL^2}. \tag{11.41}$$

In the equation above, R_{ξ_2} defines the radius of gyration of the cross-section about $\boldsymbol{E}_2$ axis. Substituting these quantities into the Euler-Lagrangian equations for θ_2 and x_3 in Eq. (11.17) and (11.18) leads to the non-dimensional equations of motion as,

$$\begin{aligned} \beta^2 R^2_{\xi_2} \partial^2_{\overline{t}} \overline{x}_3 - \partial^2_{\overline{\xi}_1} \overline{x}_3 - \partial_{\overline{\xi}_1} \theta_2 &= \overline{N}_3; \\ \left[(\partial_{\overline{\xi}_1} \overline{x}_3 + \theta_2).\delta\overline{x}_3\right]^1_0 &= 0; \end{aligned} \tag{11.42}$$

and,

$$\begin{aligned} \beta^2 R^4_{\xi_2} \partial^2_{\overline{t}} \theta_2 - \beta^2 R^2_{\xi_2} \partial^2_{\overline{\xi}_1} \theta_2 + \theta_2 + \partial_{\overline{\xi}_1} \overline{x}_3 &= \overline{M}_2; \\ \left[\partial_{\overline{\xi}_1} \theta_2.\delta\theta_2\right]^1_0 &= 0. \end{aligned} \tag{11.43}$$

We can obtained the uncoupled non-dimensionalized set of governing equations like before. We assume a solution of form $\overline{x}_3 = e^{\lambda\overline{\xi}_1} \cos\overline{\omega}\overline{t}$ (or similar form of θ_2) and substitute it in the uncoupled non-dimensionalized equation yielding the characteristic equations:

$$\lambda^2\overline{\omega}^2 \left(-\beta^2 R^2_{\xi_2} - R^2_{\xi_2}\right) - \beta^2\overline{\omega}^4 R^4_{\xi_2} + \overline{\omega}^2 - \lambda^4 = 0; \tag{11.44}$$

The characteristic equation leads to four roots (2 complex and two real):

$$\lambda_{1,2} = \pm i\sqrt{\frac{1}{2}\overline{\omega}\left(\left(\beta^2+1\right)\overline{\omega}R_{\xi_2}^2 + \sqrt{\left(\beta^2-1\right)^2\overline{\omega}^2R_{\xi_2}^4+4}\right)} = \pm i\mathfrak{s}_1; \tag{11.45}$$

$$\lambda_{3,4} = \pm i\sqrt{\frac{1}{2}\overline{\omega}\left(\left(-\beta^2-1\right)\overline{\omega}R_{\xi_2}^2 + \sqrt{\left(\beta^2-1\right)^2\overline{\omega}^2R_{\xi_2}^4+4}\right)} = \pm\mathfrak{s}_2. \tag{11.46}$$

Here, $\mathfrak{s}_1, \mathfrak{s}_2 \in \mathbb{R}$. Therefore, the mode shapes can be written as:

$$\begin{aligned}\overline{x}_3 &= \left(\mathfrak{c}_1\cos\left(\mathfrak{s}_1\overline{\xi}_1\right) + \mathfrak{c}_2\sin\left(\mathfrak{s}_1\overline{\xi}_1\right) + \mathfrak{c}_3\cosh\left(\mathfrak{s}_2\overline{\xi}_1\right) + \mathfrak{c}_4\sinh\left(\mathfrak{s}_2\overline{\xi}_1\right)\right)\cos\left(\overline{\omega}\overline{t}\right);\\ \theta_2 &= \left(\mathfrak{c}_5\cos\left(\mathfrak{s}_1\overline{\xi}_1\right) + \mathfrak{c}_6\sin\left(\mathfrak{s}_1\overline{\xi}_1\right) + \mathfrak{c}_7\cosh\left(\mathfrak{s}_2\overline{\xi}_1\right) + \mathfrak{c}_8\sinh\left(\mathfrak{s}_2\overline{\xi}_1\right)\right)\cos\overline{\omega}\overline{t}.\end{aligned} \tag{11.47}$$

As before, there are nine unknowns: eight $\mathfrak{c}_i$ and the natural frequency $\overline{\omega}$ that is embedded in $\mathfrak{s}_1$ and $\mathfrak{s}_2$. Eight constants can be specified by applying four boundary conditions and four continuity conditions. The continuity conditions makes sure that the assumed solutions in (11.47), must solve the coupled equation (11.42) and (11.43). To investigate mode shapes for various boundaries, we assume $R_{\xi_2} = 0.0289$ and $\beta^2 = 2.4$.

11.3.2.1 Pinned-pinned boundary condition:

We enforce the following boundary conditions:

$$\begin{aligned}&\overline{x}_3(0,\overline{t}) = 0;\ \partial_{\overline{\xi}_1}\theta_2(0,\overline{t}) = 0;\\ &\overline{x}_3(1,\overline{t}) = 0;\ \partial_{\overline{\xi}_1}\theta_2(1,\overline{t}) = 0.\end{aligned} \tag{11.48}$$

We obtain eight simultaneous equations in $\mathfrak{c}_i$ by enforcing the boundary conditions and continuity conditions, that can be written in the form $\boldsymbol{Z}.\boldsymbol{c} = \boldsymbol{0}$. The vanishing determinant of $\boldsymbol{Z}$ matrix yields,

$$\det\left(\boldsymbol{Z}\right) = \mathfrak{s}_1^2\mathfrak{s}_2^2\left(\mathfrak{s}_1^2+\mathfrak{s}_2^2\right)^2 s_{\mathfrak{s}_1}\mathrm{sh}_{\mathfrak{s}_2} = 0. \tag{11.49}$$

The non trivial solution for the equation above is $\mathfrak{s}_1 = n\pi$, where $n \in \mathbb{Z}^+ - \{0\}$. Solving the equation above for $\mathfrak{s}_1 - n\pi$ yields two group of natural frequencies $\overline{\omega}$ as,

$$\overline{\omega} = \sqrt{\frac{\pi^2\left(\beta^2+1\right)n^2R_{\xi_2}^2 - \sqrt{\pi^4\left(\beta^2-1\right)^2 n^4 R_{\xi_2}^4 + 2\pi^2\left(\beta^2+1\right)n^2R_{\xi_2}^2 + 1} + 1}{2\beta^2 R_{\xi_2}^4}};$$
$$\overline{\omega} = \sqrt{\frac{\pi^2\left(\beta^2+1\right)n^2R_{\xi_2}^2 + \sqrt{\pi^4\left(\beta^2-1\right)^2 n^4 R_{\xi_2}^4 + 2\pi^2\left(\beta^2+1\right)n^2R_{\xi_2}^2 + 1} + 1}{2\beta^2 R_{\xi_2}^4}}. \tag{11.50}$$

The first set of natural frequencies corresponds to bending about $\boldsymbol{E}_2$, whereas the second set of natural frequencies corresponds to shear mode. The first set of natural frequencies are $\overline{\omega} = \{9.727, 37.372, 79.286, 131.479, 190.672\}$, whereas the shear mode frequencies are $\overline{\omega} = \{755.083, 786.158, 833.756, 893.834, 963.046\}$. In this case, we obtain an analytic form of mode shapes $\tilde{x}_{3n}$ and $\tilde{\theta}_{2n}$ as,

$$\begin{aligned}\tilde{x}_{3n} &= \mathfrak{c}_2 \sin(\pi n \overline{\xi}_1);\\ \tilde{\theta}_{2n} &= -\mathfrak{c}_2\left(\frac{\pi^2 n^2 - \beta^2\overline{\omega}^2 R_{\xi_2}^2}{\pi n}\right)\cos(\pi n\overline{\xi}_1).\end{aligned} \tag{11.51}$$

The normalized mode shapes are obtained as:

$$\begin{aligned}\tilde{x}_{3n} &= \sqrt{2}\sin(\pi n \overline{\xi}_1);\\ \tilde{\theta}_{2n} &= -\sqrt{2}\cos(\pi n\overline{\xi}_1).\end{aligned} \tag{11.52}$$

For simplicity, we have used the displacement variables $\overline{x}_3$ and θ_2 as the variable representing the mode shapes. Figure 11.4 illustrates the first five mode shapes.

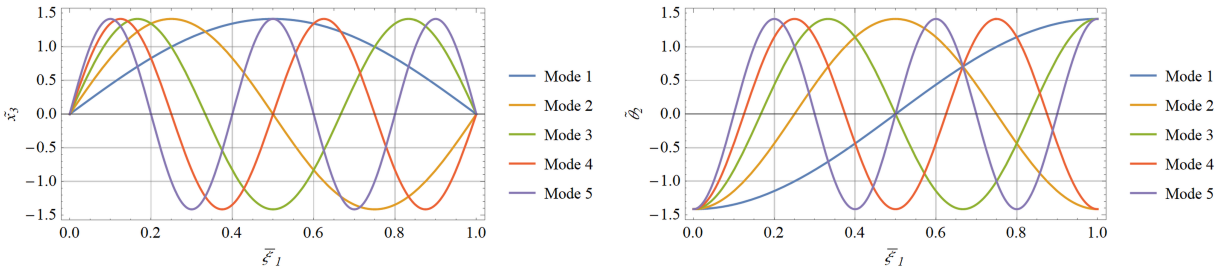

(a) Mode shapes $\tilde{x}_{3n}$ for $1 \le n \le 5$ (b) Mode shapes $\tilde{\theta}_{2n}$ for $1 \le n \le 5$

Figure 11.4: Mode shapes for $\overline{x}_3$ and θ_2 considering the pinned-pinned boundary.

11.3.2.2 Fixed-fixed boundary condition

We impose the following boundary conditions:

$$\begin{aligned} \overline{x}_3(0,\bar{t}) = \theta_2(0,\bar{t}) = 0; \\ \overline{x}_3(1,\bar{t}) = \theta_2(1,\bar{t}) = 0; . \end{aligned} \tag{11.53}$$

The determinant condition on the $\boldsymbol{Z}$ matrix arrived at by enforcing the boundary conditions and the continuity requirements is given by:

$$\begin{aligned} \det(\boldsymbol{Z}) = &-\frac{1}{2}\mathfrak{s}_1\mathfrak{s}_2\left(4\mathrm{ch}_{\mathfrak{s}_1}\mathrm{ch}_{\mathfrak{s}_2} - \mathrm{ch}_{2\mathfrak{s}_2} - 3\right)\left(\mathfrak{s}_1^2 - \beta^2\overline{\omega}^2 R_{\xi_2}^2\right)\left(\beta^2\overline{\omega}^2 R_{\xi_2}^2 + \mathfrak{s}_2^2\right) \\ &+ \mathfrak{s}_1\mathrm{sh}_{\mathfrak{s}_2}\left(\beta^2\overline{\omega}^2 R_{\xi_2}^2 + \mathfrak{s}_2^2\right)\left(\beta^2\overline{\omega}^2 R_{\xi_2}^2\left(\mathfrak{s}_2\mathrm{sh}_{\mathfrak{s}_2} + \mathfrak{s}_1 s_{\mathfrak{s}_1}\right) + \mathfrak{s}_1\mathfrak{s}_2\left(\mathfrak{s}_2 s_{\mathfrak{s}_1} - \mathfrak{s}_1\mathrm{sh}_{\mathfrak{s}_2}\right)\right) \\ &+ s_{\mathfrak{s}_1}\mathfrak{s}_2^2\mathrm{sh}_{\mathfrak{s}_2}\left(-\left(\mathfrak{s}_1^2 - \beta^2\overline{\omega}^2 R_{\xi_2}^2\right)^2\right) = 0. \end{aligned} \tag{11.54}$$

The natural frequencies can be by solving above equation. The first five natural frequencies are obtained as $\overline{\omega} = \{21.172, 54.727, 99.706, 152.466, 210.595\}$ (assuming $R_{\xi_2} = 0.0289$ and $\beta^2 = 2.4$). Figure 11.5 illustrates the first five mode shapes for this case.

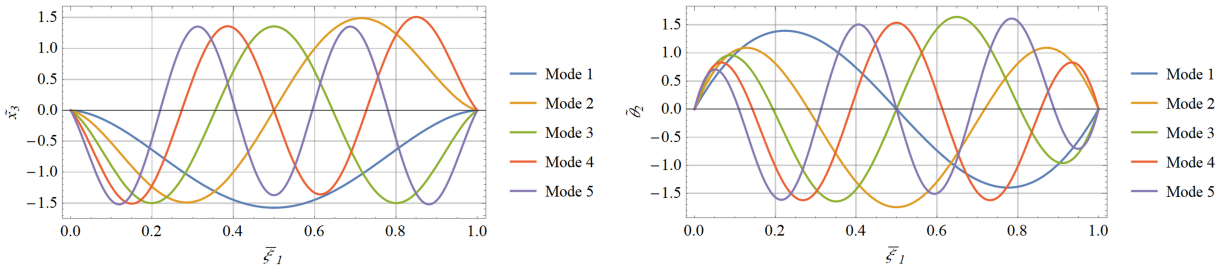

(a) Mode shapes $\tilde{x}_{3n}$ for $1 \leq n \leq 5$ (b) Mode shapes $\tilde{\theta}_{2n}$ for $1 \leq n \leq 5$

Figure 11.5: Mode shapes for $\overline{x}_3$ and θ_2 considering the fixed-fixed boundary.

11.3.2.3 Fixed-free boundary condition

The boundary conditions for this case are:

$$\begin{aligned} \overline{x}_3(0,\bar{t}) = \theta_2(0,\bar{t}) = 0; \\ \partial_{\bar{\xi}_1}\theta_2(1,\bar{t}) = 0;\ \theta_2(1,\bar{t}) + \partial_{\bar{\xi}_1}\overline{x}_3(1,\bar{t}) = 0. \end{aligned} \tag{11.55}$$

The determinant condition on the $\boldsymbol{Z}$ matrix yields:

$$\begin{aligned}\det(\boldsymbol{Z}) =& \mathfrak{s}_1\mathfrak{s}_2\mathrm{ch}_{\mathfrak{s}_1}\mathrm{ch}_{\mathfrak{s}_2}\left(2\beta^4\overline{\omega}^4R_{\xi_2}^4+2\beta^2\left(\mathfrak{s}_2^2-\mathfrak{s}_1^2\right)\overline{\omega}^2R_{\xi_2}^2+\mathfrak{s}_1^4+\mathfrak{s}_2^4\right)\\ &+2\mathfrak{s}_1\mathfrak{s}_2\left(\mathfrak{s}_1^2-\beta^2\overline{\omega}^2R_{\xi_2}^2\right)\left(\beta^2\overline{\omega}^2R_{\xi_2}^2+\mathfrak{s}_2^2\right)\\ &+\left(\mathfrak{s}_1^2-\mathfrak{s}_2^2\right)s_{\mathfrak{s}_1}\mathrm{sh}_{\mathfrak{s}_2}\left(\beta^2\overline{\omega}^2R_{\xi_2}^2-\mathfrak{s}_1^2\right)\left(\beta^2\overline{\omega}^2R_{\xi_2}^2+\mathfrak{s}_2^2\right)=0.\end{aligned} \tag{11.56}$$

The first five non-dimensional natural frequencies, for same parameters R_{ξ_2} and β, obtained by solving the equation above are $\overline{\omega}=\{3.492,21.040,55.712,101.807,156.041\}$. Figure below illustrates the mode shapes.

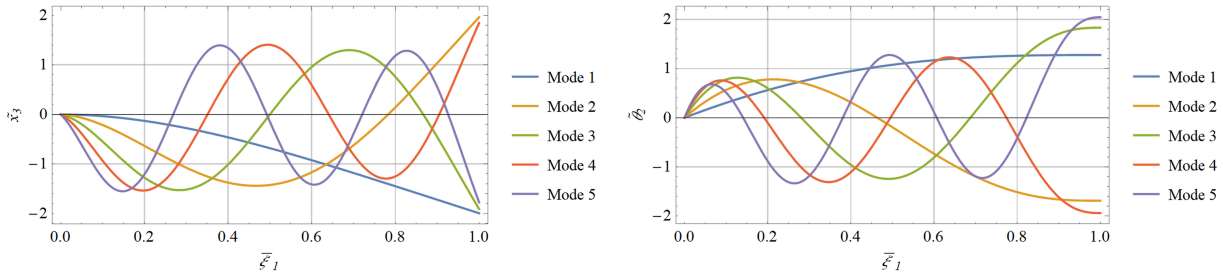

(a) Mode shapes $\tilde{x}_{3n}$ for $1 \leq n \leq 5$

(b) Mode shapes $\tilde{\theta}_{2n}$ for $1 \leq n \leq 5$

Figure 11.6: Mode shapes for $\overline{x}_3$ and θ_2 considering the fixed-free boundary.

11.3.2.4 Free-free boundary condition

The boundary conditions for this case are:

$$\begin{aligned}&\partial_{\overline{\xi}_1}\theta_2(0,\overline{t})=0;\ \theta_2(0,\overline{t})+\partial_{\overline{\xi}_1}\overline{x}_3(0,\overline{t})=0;\\ &\partial_{\overline{\xi}_1}\theta_2(1,\overline{t})=0;\ \theta_2(1,\overline{t})+\partial_{\overline{\xi}_1}\overline{x}_3(1,\overline{t})=0.\end{aligned} \tag{11.57}$$

The vanishing determinant condition for this case is:

$$\begin{aligned}\det(\boldsymbol{Z}) =& -2\mathfrak{s}_1\mathfrak{s}_2\mathrm{ch}_{\mathfrak{s}_1}\mathrm{ch}_{\mathfrak{s}_2}\left(\mathfrak{s}_1^2-\beta^2\overline{\omega}^2R_{\xi_2}^2\right)\left(\beta^2\overline{\omega}^2R_{\xi_2}^2+\mathfrak{s}_2^2\right)+2\mathfrak{s}_1\mathfrak{s}_2\left(\mathfrak{s}_1^2-\beta^2\overline{\omega}^2R_{\xi_2}^2\right)\left(\beta^2\overline{\omega}^2R_{\xi_2}^2+\mathfrak{s}_2^2\right)\\ &+s_{\mathfrak{s}_1}\mathrm{sh}_{\mathfrak{s}_2}\left(\beta^4\left(\mathfrak{s}_1^2-\mathfrak{s}_2^2\right)\overline{\omega}^4R_{\xi_2}^4-2\beta^2\left(\mathfrak{s}_1^4+\mathfrak{s}_2^4\right)\overline{\omega}^2R_{\xi_2}^2+\mathfrak{s}_1^6-\mathfrak{s}_2^6\right)=0.\end{aligned} \tag{11.58}$$

Solving the above equation for previously assumed parameters yields the natural frequency, the first six of them being $\overline{\omega} = \{0,\ 21.660,\ 56.656,\ 104.022,\ 159.795,\ 221.170\}$. The Eigenfunction corresponding to $\overline{\omega} = 0$ represents the rigid body mode for θ_2 and $\overline{x}_3$. The figure below presents the mode shapes.

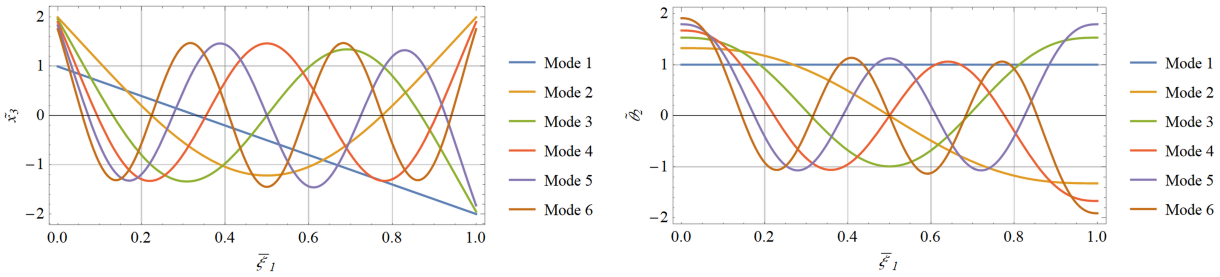

(a) Mode shapes $\tilde{x}_{3n}$ for $1 \leq n \leq 6$ (b) Mode shapes $\tilde{\theta}_{2n}$ for $1 \leq n \leq 6$

Figure 11.7: Mode shapes for $\overline{x}_3$ and θ_2 considering the free-free boundary.

11.3.3 Mode shape for θ_3 and x_2

We consider the following definition of dimensionless quantities:

$$\overline{\xi}_1 = \frac{\xi_1}{L};\ \overline{t} = t\sqrt{\frac{EI_{33}}{\rho AL^4}};\ \overline{x}_2 = \frac{x_2}{L};\ \theta_3(\xi_1, t) = \theta_3(\overline{\xi}_1, \theta_t) = \theta_3;\ \beta^2 = \frac{E}{G};\ R^2_{\xi_3} = \frac{I_{33}}{AL^2}. \tag{11.59}$$

In the equation above, R_{ξ_3} defines the radius of gyration of the cross-section about $\boldsymbol{E}_3$ axis. Substituting these quantities into the Euler-Lagrangian equations for θ_3 and x_2 given in Eq. (11.19) and (11.20) leads to the non-dimensional equations of motion as,

$$\begin{aligned} \beta^2 R^2_{\xi_3} \partial^2_{\overline{t}} \overline{x}_2 - \partial^2_{\overline{\xi}_1} \overline{x}_2 + \partial_{\overline{\xi}_1} \theta_3 &= \overline{N}_2; \\ \left[(\theta_3 - \partial_{\overline{\xi}_1} \overline{x}_2).\delta\overline{x}_2\right]^1_0 &= 0; \end{aligned} \tag{11.60}$$

and,

$$\begin{aligned} \beta^2 R^4_{\xi_3} \partial^2_{\overline{t}} \theta_3 - \beta^2 R^2_{\xi_3} \partial^2_{\overline{\xi}_1} \theta_3 + \theta_3 - \partial_{\overline{\xi}_1} \overline{x}_2 &= \overline{M}_3; \\ \left[\partial_{\overline{\xi}_1} \theta_3.\delta\theta_3\right]^1_0 &= 0. \end{aligned} \tag{11.61}$$

The non-dimensional equation of motions obtained in Eq. (11.60) and (11.61) are similar in the form to the equations (11.42) and (11.42) (for the quantities θ_2 and x_3). We omit the modal analysis for θ_3 and x_2 because the results are identical to the modal analysis for θ_2 and x_3 carried out in section 11.3.2.

11.3.4 Mode shape for x_1

To obtain the non-dimensional governing equation of motion, we define the following,

$$\overline{\xi}_1 = \frac{\xi_1}{L};\ \overline{t} = t\sqrt{\frac{E}{\rho L^2}};\ \overline{x}_1 = \frac{x_1}{L};\ \eta^2 = \frac{I_{11}\nu^2}{AL^2};\ \zeta^2 = \frac{\beta^2}{1+\nu}. \tag{11.62}$$

Substituting the above definitions into Eq. (11.14), we obtain the non-dimensionalized equation of motion as,

$$\begin{gathered}\zeta^2\eta^2\partial^4_{\overline{\xi}_1}\overline{x}_1 - \partial^2_{\overline{\xi}_1}\overline{x}_1 - \eta^2\partial^2_{\overline{t}}\partial^2_{\overline{\xi}_1}\overline{x}_1 + \partial^2_{\overline{t}}\overline{x}_1 = \overline{N}_1;\\ \left[\left(-\partial_{\overline{\xi}_1}\overline{x}_1 - \eta^2\partial^2_{\overline{t}}\partial_{\overline{\xi}_1}\overline{x}_1 + \eta^2\zeta^2\partial^3_{\overline{\xi}_1}\overline{x}_1\right).\delta\overline{x}_1\right]^l_0 = 0;\\ \left[\partial^2_{\overline{\xi}_1}\overline{x}_1.\delta\partial_{\overline{\xi}_1}\overline{x}_1\right]^l_0 = 0.\end{gathered} \tag{11.63}$$

We consider a solution to free vibration problem of form $\overline{x}_1 = e^{\lambda\overline{\xi}_1}\cos\overline{\omega}\overline{t}$ and substitute it in Eq. (11.63) yielding the characteristic equation as,

$$\zeta^2\eta^2\lambda^4 + \eta^2\lambda^2\overline{\omega}^2 - \lambda^2 - \overline{\omega}^2 = 0; \tag{11.64}$$

The characteristic equation leads to four roots (two complex and two real):

$$\lambda_1 = \pm i\sqrt{\frac{\sqrt{\eta^2\overline{\omega}^2\left(4\zeta^2 + \eta^2\overline{\omega}^2 - 2\right) + 1} + \eta^2\overline{\omega}^2 - 1}{2\zeta^2\eta^2}} = \pm i\mathfrak{s}_1; \tag{11.65}$$

$$\lambda_3 = \pm\sqrt{\frac{\sqrt{\eta^2\overline{\omega}^2\left(4\zeta^2 + \eta^2\overline{\omega}^2 - 2\right) + 1} - \eta^2\overline{\omega}^2 + 1}{2\zeta^2\eta^2}} = \pm\mathfrak{s}_2. \tag{11.66}$$

Here, $\mathfrak{s}_1, \mathfrak{s}_2 \in \mathbb{R}$. Therefore, the mode shapes can be written as:

$$\overline{x}_1 = \left(\mathfrak{c}_1 \cos\left(\mathfrak{s}_1 \overline{\xi}_1\right) + \mathfrak{c}_2 \sin\left(\mathfrak{s}_1 \overline{\xi}_1\right) + \mathfrak{c}_3 \cosh\left(\mathfrak{s}_2 \overline{\xi}_1\right) + \mathfrak{c}_4 \sinh\left(\mathfrak{s}_2 \overline{\xi}_1\right)\right) \cos\left(\overline{\omega}\overline{t}\right) \tag{11.67}$$

There are five unknowns: four $\mathfrak{c}_i$ and the natural frequency $\overline{\omega}$ that is embedded in $\mathfrak{s}_1$ and $\mathfrak{s}_2$. Four constants can be specified by applying four boundary conditions. The fifth constant is obtained by normalizing the mode shape. We consider the four boundary conditions with $\zeta = 0.544$ and $\eta = 0.1$.

11.3.4.1 Pinned-pinned boundary condition

We enforce the following boundary conditions:

$$\overline{x}_1(0,\overline{t}) = 0;\ \partial^2_{\overline{\xi}_1} \overline{x}_1(0,\overline{t}) = 0;\ \overline{x}_1(1,\overline{t}) = 0;\ \partial^2_{\overline{\xi}_1} \overline{x}_1(1,\overline{t}) = 0. \tag{11.68}$$

We obtain four simultaneous equations in $\mathfrak{c}_i$ by enforcing the boundary conditions that can be written in the form $\boldsymbol{Z}.\boldsymbol{c} = \boldsymbol{0}$, such that:

$$\overbrace{\begin{bmatrix} 0 & 1 & 0 & 1 \\ s_{\mathfrak{s}_1} & c_{\mathfrak{s}_1} & \mathrm{sh}_{\mathfrak{s}_2} & \mathrm{ch}_{\mathfrak{s}_2} \\ 0 & -\mathfrak{s}_1^2 & 0 & \mathfrak{s}_2^2 \\ -\mathfrak{s}_1^2 s_{\mathfrak{s}_1} & -c_{\mathfrak{s}_1}\mathfrak{s}_1^2 & \mathfrak{s}_2^2 \mathrm{sh}_{\mathfrak{s}_2} & \mathrm{ch}_{\mathfrak{s}_2}\mathfrak{s}_2^2 \end{bmatrix}}^{\boldsymbol{Z}} \cdot \overbrace{\begin{bmatrix} \mathfrak{c}_1 \\ \mathfrak{c}_2 \\ \mathfrak{c}_3 \\ \mathfrak{c}_4 \end{bmatrix}}^{\boldsymbol{c}} = \overbrace{\begin{bmatrix} 0 \\ 0 \\ 0 \\ 0 \end{bmatrix}}^{\boldsymbol{0}}. \tag{11.69}$$

For Eq. (11.69) to be true and solvable (ignoring the trivial solution $\boldsymbol{c} = \boldsymbol{0}$), we require:

$$\det(\boldsymbol{Z}) = s_{\mathfrak{s}_1} \mathrm{sh}_{\mathfrak{s}_2} (\mathfrak{s}_1^2 + \mathfrak{s}_2^2)^2 = 0. \tag{11.70}$$

The solution for the equation above is $\mathfrak{s}_1 = n\pi$, where $n \in \mathbb{Z}^+ - \{0\}$ and $\mathfrak{s}_1 = 0$. The latter solution is trivial for the considered boundary. The natural frequency $\overline{\omega}$ can be solved by solving for $\mathfrak{s}_1(\overline{\omega}) = n\pi$, that yields a positive and a negative solution. Since, the natural frequency $\overline{\omega} > 0$, we

ignore the negative solution and obtain,

$$\overline{\omega}_n = \frac{\pi\sqrt{\pi^2\zeta^2\eta^2 n^4 + n^2}}{\sqrt{\pi^2\eta^2 n^2 + 1}}. \tag{11.71}$$

The mode shape can be obtained by solving for any three $\mathfrak{c}_i$ in the system of Eq. (11.69), yielding

$$\tilde{x}_{1n} = \mathfrak{c}_1 \sin(n\pi\overline{\xi}_1). \tag{11.72}$$

The normalized mode shape is obtained as:

$$\tilde{x}_{1n} = \sqrt{2}\sin(\pi n\overline{\xi}_1). \tag{11.73}$$

Figure 11.8 illustrates the first five mode shapes.

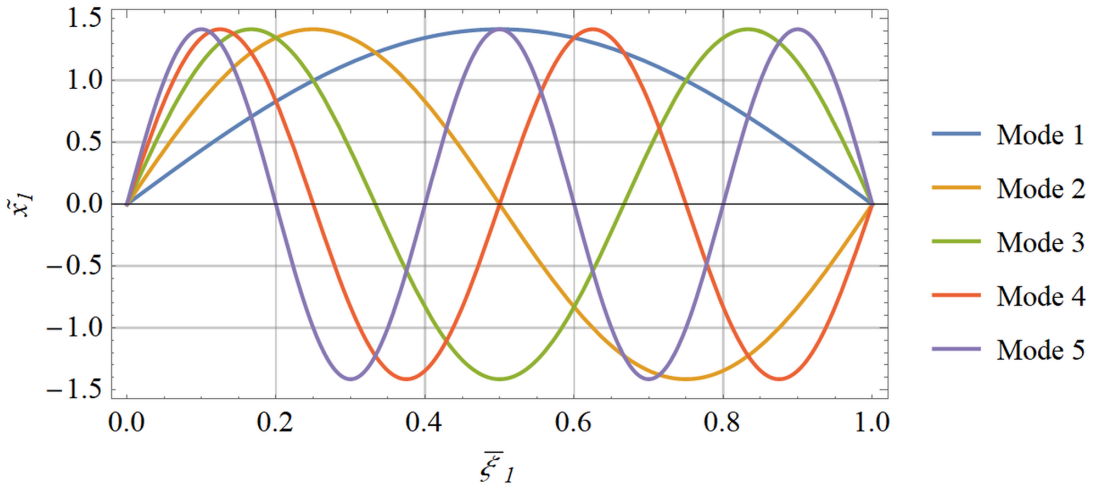

Figure 11.8: Mode shapes $\tilde{x}_{1n}$ for $1 \leq n \leq 5$ for the pinned-pinned support.

11.3.4.2 Fixed-fixed boundary condition

We enforce the following boundary conditions:

$$\overline{x}_1(0,\overline{t}) = 0;\ \partial_{\overline{\xi}_1}\overline{x}_1(0,\overline{t}) = 0;\ \overline{x}_1(1,\overline{t}) = 0;\ \partial_{\overline{\xi}_1}\overline{x}_1(1,\overline{t}) = 0. \tag{11.74}$$

We obtain four simultaneous equations in $\mathfrak{c}_i$ by enforcing the boundary conditions as:

$$\begin{bmatrix} 0 & 1 & 0 & 1 \\ s_{s_1} & c_{s_1} & \mathrm{sh}_{s_2} & \mathrm{ch}_{s_2} \\ s_1 & 0 & s_2 & 0 \\ c_{s_1} s_1 & -s_1 s_{s_1} & \mathrm{ch}_{s_2} s_2 & s_2 \mathrm{sh}_{s_2} \end{bmatrix} . \begin{bmatrix} \mathfrak{c}_1 \\ \mathfrak{c}_2 \\ \mathfrak{c}_3 \\ \mathfrak{c}_4 \end{bmatrix} = \begin{bmatrix} 0 \\ 0 \\ 0 \\ 0 \end{bmatrix} . \tag{11.75}$$

The zero determinant condition can then be obtained as:

$$\det(\boldsymbol{Z}) = 2\mathfrak{s}_1 \mathfrak{s}_2 c_{\mathfrak{s}_1} \mathrm{ch}_{\mathfrak{s}_2} + \left(\mathfrak{s}_1^2 - \mathfrak{s}_2^2\right) s_{\mathfrak{s}_1} \mathrm{sh}_{\mathfrak{s}_2} - 2\mathfrak{s}_1 \mathfrak{s}_2 = 0. \tag{11.76}$$

Unlike the pinned-pinned case, there is no closed form solution of Eq. (11.76). For the assumed ζ and η, the first five natural frequencies are obtained as $\overline{\omega} = \{3.182, 6.354, 9.507, 12.630, 15.715\}$. Figure 11.9 illustrates the first five mode shapes.

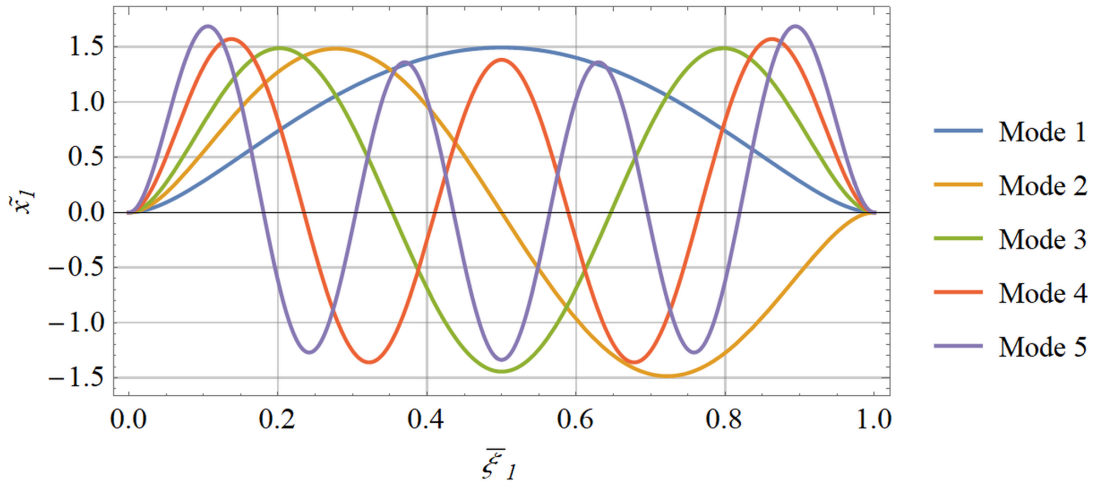

Figure 11.9: Mode shapes $\tilde{x}_{1n}$ for $1 \leq n \leq 5$ for the fixed-fixed support.

11.3.4.3 Fixed-free boundary condition

We enforce the following boundary conditions:

$$\begin{gathered}\overline{x}_1(0,\bar{t}) = 0;\ \partial_{\bar{\xi}_1}\overline{x}_1(0,\bar{t}) = 0;\\ -\partial_{\bar{\xi}_1}\overline{x}_1(1,\bar{t}) - \eta^2\partial_{\bar{t}}^2\partial_{\bar{\xi}_1}\overline{x}_1(1,\bar{t}) + \eta^2\zeta^2\partial_{\bar{\xi}_1}^3\overline{x}_1(1,\bar{t}) = 0;\ \partial_{\bar{\xi}_1}^2\overline{x}_1(1,\bar{t}) = 0.\end{gathered} \tag{11.77}$$

The zero determinant condition is,

$$\begin{aligned}\det(\mathbf{Z}) =& s_1\mathfrak{s}_2\Big(s_1^2\left(c_{s_1}\mathrm{ch}_{\mathfrak{s}_2}\left(\eta^2\overline{\omega}^2 + 2\zeta^2\eta^2\mathfrak{s}_2^2 - 1\right) - \eta^2\overline{\omega}^2 + 1\right) - \mathfrak{s}_2^2\left(\eta^2\overline{\omega}^2 - 1\right)\left(c_{s_1}\mathrm{ch}_{\mathfrak{s}_2} - 1\right)\\ &+ \zeta^2\eta^2 s_1^4 + \zeta^2\eta^2\mathfrak{s}_2^4 - \mathfrak{s}_2 s_{s_1} s_1 \mathrm{sh}_{\mathfrak{s}_2}\left(2\eta^2\overline{\omega}^2 + \zeta^2\eta^2\mathfrak{s}_2^2 - 2\right) + \zeta^2\eta^2\mathfrak{s}_2 s_{s_1} s_1^3 \mathrm{sh}_{\mathfrak{s}_2}\Big) = 0.\end{aligned} \tag{11.78}$$

The first five natural frequencies are obtained as $\overline{\omega} = \{1.645\,, 4.611,\ 6.939,\ 10.273,\ 11.755\}$.

Figure 11.10 illustrates the first five mode shapes.

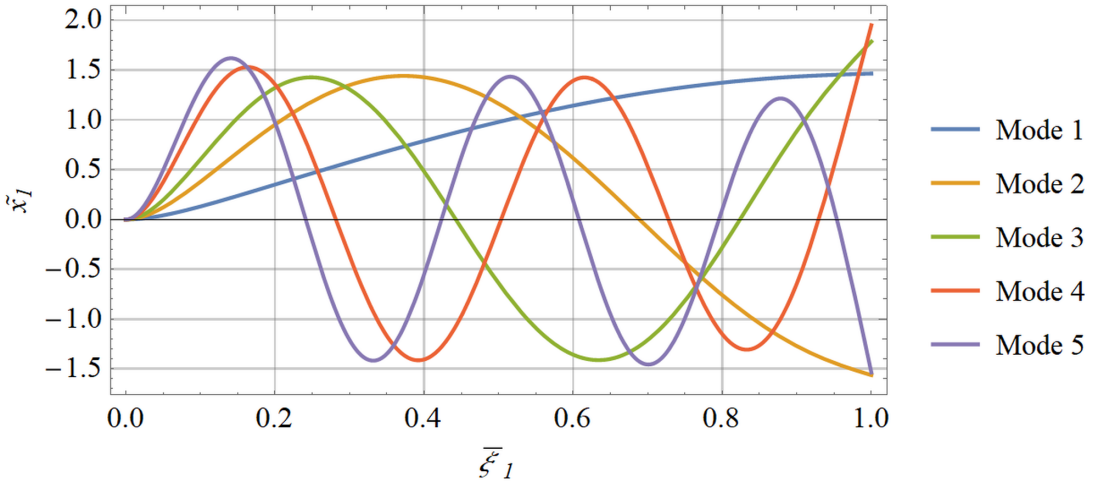

Figure 11.10: Mode shapes $\tilde{x}_{1n}$ for $1 \leq n \leq 5$ for the fixed-free support.

11.3.4.4 Free-free boundary condition

We enforce the following boundary conditions:

$$\begin{aligned}
&-\partial_{\bar{\xi}_1}\overline{x}_1(0,\bar{t}) - \eta^2\partial_{\bar{t}}^2\partial_{\bar{\xi}_1}\overline{x}_1(0,\bar{t}) + \eta^2\zeta^2\partial_{\bar{\xi}_1}^3\overline{x}_1(0,\bar{t}) = 0;\ \partial_{\bar{\xi}_1}^2\overline{x}_1(0,\bar{t}) = 0;\\
&-\partial_{\bar{\xi}_1}\overline{x}_1(1,\bar{t}) - \eta^2\partial_{\bar{t}}^2\partial_{\bar{\xi}_1}\overline{x}_1(1,\bar{t}) + \eta^2\zeta^2\partial_{\bar{\xi}_1}^3\overline{x}_1(1,\bar{t}) = 0;\ \partial_{\bar{\xi}_1}^2\overline{x}_1(1,\bar{t}) = 0.
\end{aligned} \tag{11.79}$$

The zero determinant condition yields,

$$\begin{aligned}
\det(\mathbf{Z}) =& 2\zeta^2\eta^2\mathfrak{s}_2\mathfrak{s}_1^3\left(c_{\mathfrak{s}_1}\mathrm{ch}_{\mathfrak{s}_2}-1\right)\left(\eta^2\overline{\omega}^2+\zeta^2\eta^2\mathfrak{s}_2^2-1\right)\\
&-2\mathfrak{s}_2\mathfrak{s}_1\left(\eta^2\overline{\omega}^2-1\right)\left(c_{\mathfrak{s}_1}\mathrm{ch}_{\mathfrak{s}_2}-1\right)\left(\eta^2\overline{\omega}^2+\zeta^2\eta^2\mathfrak{s}_2^2-1\right)+\zeta^4\eta^4\mathfrak{s}_2^2 s_{\mathfrak{s}_1}\mathfrak{s}_1^4\mathrm{sh}_{\mathfrak{s}_2}\\
&-s_{\mathfrak{s}_1}\mathfrak{s}_1^2\mathrm{sh}_{\mathfrak{s}_2}\left(\left(\eta^2\overline{\omega}^2-1\right)^2+\zeta^4\eta^4\mathfrak{s}_2^4+4\zeta^2\eta^2\mathfrak{s}_2^2\left(\eta^2\overline{\omega}^2-1\right)\right)\\
&+\mathfrak{s}_2^2 s_{\mathfrak{s}_1}\left(\eta^2\overline{\omega}^2-1\right)^2\mathrm{sh}_{\mathfrak{s}_2}=0.
\end{aligned} \tag{11.80}$$

The first five natural frequencies are obtained as $\overline{\omega} = \{1.645,\ 4.611,\ 6.939,\ 10.273,\ 11.755\}$.

Figure 11.11 illustrates the first five mode shapes.

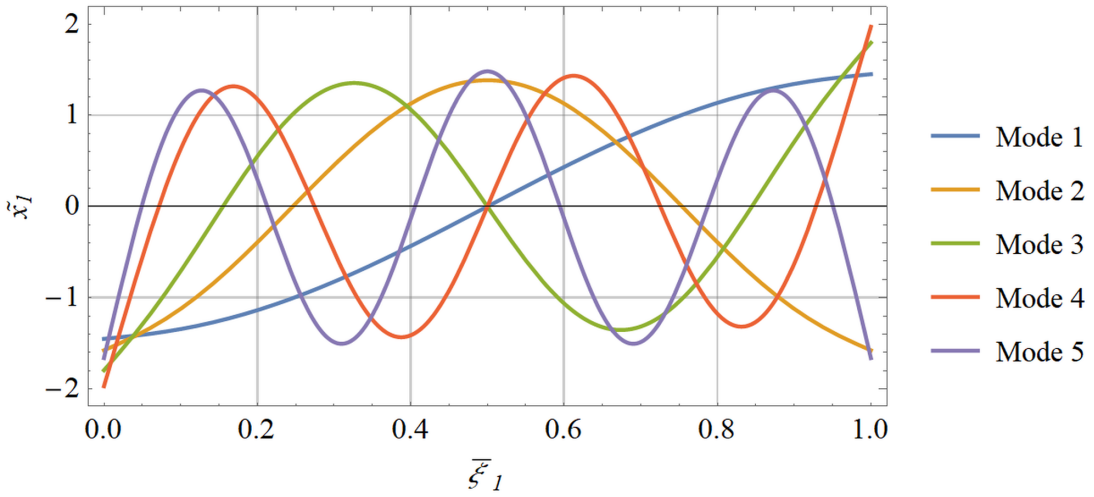

Figure 11.11: Mode shapes $\tilde{x}_{1n}$ for $1 \leq n \leq 5$ for the free-free support.

11.4 Conclusion

This chapter deals with the modal analysis of the beam theory detailed in this dissertation in the domain of small strain and small deformations considering St. Venant's and Kirchhoff linearly elastic material model. The governing equations of motion obtained in chapter 7 and 8 are non-linear and coupled. Small strain and small deformation assumption simplify the beam kinematics and yields seven linear uncoupled Euler-Lagrange equation of motion for each primary degree of freedom. The mode shapes and natural frequencies for each deformation variable are obtained.

Chapter 12

Conclusions and Future Work

In this chapter, we summarize the concepts discussed and the results obtained in this dissertation. We dedicate a section to elaborate on the new line of research that can potentially branch out of this work.

12.1 Conclusions

The goal of this work is to investigate the differential geometry of framed space curves and explore its engineering applications. This research, therefore, utilizes the application of differential geometry and mechanics to define the configuration of single-manifold characterized systems and eventually helps obtain the governing differential equations to investigate the evolution of these systems. Most importantly, this work leads to the development of an advanced non-linear beam theory, shape reconstruction of slender structures, path-estimation, and computational graphics.

Chapter 1 details various curve framing techniques. There are multiple ways to frame a space curve, ranging from intrinsic Frenet-Serret and relatively parallel adapted frames (RPAF) to the system-dependent material-adapted frame (MAF) and even more general material frame (MF). Unlike the Frenet-Serret and RPAF, the material frame is conveniently defined in terms of the parameters associated with the system configuration and is free of singularities. Hence,

various curve framing approaches and the relationship between these frames and the curvatures associated with them are studied in chapter 1. The concepts of proper orthogonal Lie group, finite rotations, tangent space, and exponential maps are also discussed.

In chapter 2, we exploit the theoretical discussions and mathematical constructions explored in chapter 1 to develop path-estimation techniques and applications in computer graphics. The evolution of the system can be mathematically defined by a state space. An approach to approximate the state space of a single-manifold characterized system (like drone or swarm of drones) using a limited number of the material linear and angular velocity vector is proposed. The relationships are applied to generate some complicated structures like double helix intertwined about a space curve, a leaf, and an entire plant.

Chapter 1 and 2 deals with the material and spatial forms of curvature of a framed space curve. Chapter 3 is a theoretical extension to chapter 1 as it details higher-order derivatives, variations, and co-rotational derivatives of curvature tensor. Parameterizing the rotation tensor using the Gibbs vector yields a suitable formula of rotation tensor that helps in deriving a closed form formula to obtain any order derivative of the curvature tensor as the summation of functions of the parameterizing quantity and its derivatives. A linearized updating algorithm for curvature and its derivatives when the configuration of the curve acquires a small increment is obtained. The results presented in this chapter can be readily used in numerical implementation of higher-order geometrically-exact beam/rod theory that requires obtaining and updating higher order derivatives of curvatures (discussed in chapter 10).

Chapter 4 and 5 elucidates the enhanced kinematics of higher-order non-linear geometrically-exact beams that incorporates bending curvatures, torsional curvatures, shear, axial strains, and fully-coupled Poisson's wand warping effects. The primary reason to investigate the coupling between Poisson's and warping effect (along with the contribution to warping due to torsional and bending induced shear) and develop a fully-coupled Poisson's transformation is to further refine the kinematics of the Cosserat beam model. This is beneficial for both forward modeling analyses

and solving inverse problems like shape reconstruction from strain measurements. Chapter 5 is dedicated to investigating the inconsistencies in the differential equation for warping obtained in chapter 4 and arriving at a simplified warping function.

The kinematics developed in chapter 4 is used to establish a measurement model of discrete and finite-length strain gauges attached to the surface of the beam (or embedded into the beam). The discrete strain gauge measurement model is then used to develop a global shape reconstruction algorithm of the Cosserat beam subjected to large deformation. The idea is to obtain the global shape of the rod using a countable number of strain gauge measurements. The finite strain parameters on to which the strain gauge reading depends (like mid-curve axial strain, curvatures and their derivatives) at a given cross-section can be evaluated from the strain gauges reading by inverting the set of scalar strain measurements. Once the material mid-curve strain vector and the curvature vector at discrete cross-section locations are obtained, the mid-curve position vector and the director triads can be estimated using similar techniques used in path-estimation (like SPEG) described in chapter 2. Preliminary noise tolerance study and boundary condition uncertainty studies show that the RMS error trends with the extraneous noise due to environmental or measurement noise and with error in specifying the one boundary condition vector required for inertial reference. The suggested reconstruction strategy is convergent and non-singular even if the mid-curve has multiple points or segments of degeneracy.

Chapter 7 details the variational formulation of geometrically-exact Cosserat beams with deforming cross-sections. The attempt to capture fully coupled Poisson's and warping effect (including bending induced non-uniform shear) results in the dependence of deformation map on derivatives of curvature fields (up to second-order). This makes the calculation of variations rather demanding. Detailed calculations of variations of kinematic quantities required to obtain the weak form are performed. The strong and weak form of governing equations is obtained. Finally, the variational formulation of the beam with a rigid cross-section (a special case) is discussed in detail. Chapter 8 further extends the variational mechanics of the geometrically-exact beam

by investigating the Poisson's bracket formulation and Hamiltonian structure of the concerned beam model. Various mathematical constructions like co-tangent space, co-tangent bundle, phase space and the associated duality (or metric) are discussed. The Hamiltonian is obtained via the Legendre transformation of the Lagrangian.

Chapter 9 details the time- and rate-independent, multi-axial linear constitutive relations restricted to large deformation, but small strain assumption is considered for isotropic Saint-Venant/Kirchhoff material. Chapter 10 delineates consistent linearization of the weak form and details finite element formulation of the geometrically-exact non-linear beam with enhanced kinematics. The matrix form of equilibrium equations is derived and solved using Newton Raphson's iterative algorithm using uniformly reduced Gauss quadrature. The numerical simulations compare and discuss the results obtained using the current beam model (referred to as Chadha-Todd beam or CT beam) with co-rotational formulation (CF), Simo-Reissener beam (SR), and Simo Vu-Quoc beam (SV). Finally, chapter 11, tackles the modal analysis of the beam model developed in previous chapters. The small strain and small deformation assumption simplify the beam kinematics and yields seven linear uncoupled Euler-Lagrange equation of motion for each primary degree of freedom. The mode shapes and natural frequencies for each deformation variable are obtained.

12.2 Future Work

1. **Numerical solutions using other approaches**: The comprehensive kinematics that was developed for Cosserat rods gives a simple but accurate description of deformation. However, the governing differential equations have higher regularity requirements. Numerical solutions were developed using standard FEM. Other approaches to numerical implementation like isogeometric and mesh-free finite element analysis using Reproducing Kernel Particle Method (RKPM) might be more suitable to solve the problem numerically. The prime

motivation to implement these numerical methods is their suitability to solve problems with higher regularity requirements. The finite element formulation presented here leads to displacement-based elements and can be extended to force-based element formulation.

2. **Material non-linearity**: The variational mechanics of the beam derived here is general, geometrically-exact, and is capable of defining beam subjected to large deformations and finite strains. Except for the reduced modeling of the beam using a framed curve (or as a single manifold structure) and prior knowledge of warping functions, no kinematic assumptions are made. However, limitations are introduced when a linear Saint Venant's/Kirchhoff material model for the isotropic case is assumed. The linear constitutive law is valid for small strain case. Further efforts could be directed to expand the current beam theory for non-linear material with composite cross-sections (like a reinforced concrete beam) that can capture damage and collapse of the structure.

3. **Numerical implementation for dynamic effects and stability analysis**: The numerical implementation described in this thesis is limited to the static case using Newton-Raphson's iteration technique. A straightforward extension to the current work is to include the dynamic effects and investigate the non-linear dynamic behavior of the beam. Secondly, problems related to stability like lateral bifurcation can be numerically modeled using arch-length control and other advanced non-linear solvers.

4. **Analysis of non-conventional structures like DNA and bio-polymers**: DNA (deoxyribonucleic acid) molecules are stress-responsive, and in the case that they are mutated, compressed or stretched, they can lead to serious deformities and illnesses in the body. Thus, the investigation of DNA elasticity and stability is necessary. The mechanics of a DNA molecule under mechanical stress can be studied within the framework of geometrically-exact Cosserat rods.

5. **Estimation of higher-order Riemannian manifold from the material curvature data**:

The path-estimation and shape sensing of slender rods using material strains and curvatures (equivalently linear and angular velocity) can be further extended to higher-order manifold problems like shape sensing of composite panels, membranes, motion of swarm of drones, space-time fabric in general relativity, etc. The sensors like strain gauges or Inertial Measurement Units (IMU) are attached to the structure; therefore, the sensor data are obtained with respect to the deformed frame of reference and are local. Local curvatures and strains associated with finite deformation can be used to obtain the state space of the system using the idea of parallel-transport and nature of manifold under consideration.

6. **Investigating errors in the problem of shape sensing and path-estimation**: The issue of dead-reckoning is observed in the problem of shape-sensing and path-estimation. Understanding the relationship between the error structure of the sensors and the estimated configuration is extremely useful to mitigate or minimize the errors and can be potentially explored.

Bibliography

[1] J. Coolidge, "The story of tangents," The American Mathematical Monthly, vol. 58, no. 7, pp. 449–462, 1951.

[2] R. Descartes, La géométrie. Leiden, 1637.

[3] L. Euler, Introductio in analysin infinitorum. MM Bousquet, 1748.

[4] F. Frenet, "Sur les courbes a double courbure.," Journal de mathématiques pures et appliquées, pp. 437–447, 1852.

[5] J. A. Serret, "Sur quelques formules relatives à la théorie des courbes à double courbure.," Journal de mathématiques pures et appliquées, pp. 193–207, 1851.

[6] G. Darboux, Leçons sur la théorie générale des surfaces. 1894.

[7] T. A. Ivey and J. M. Landsberg, Cartan for beginners: differential geometry via moving frames and exterior differential systems, vol. 61. American Mathematical Society Providence, RI, 2003.

[8] É. Cartan, "La géométrie des espaces de riemann," 1925.

[9] E. J. Cartan, On manifolds with an affine connection and the theory of general relativity. Bibliopolis, 1986.

[10] R. L. Bishop, "There is more than one way to frame a curve," The American Mathematical Monthly, vol. 82, no. 3, pp. 246–251, 1975.

[11] A. J. Hanson and H. Ma, "Parallel transport approach to curve framing," Indiana University, Techreports-TR425, vol. 11, pp. 3–7, 1995.

[12] E. Xargay, I. Kaminer, A. Pascoal, N. Hovakimyan, V. Dobrokhodov, V. Cichella, A. Aguiar, and R. Ghabcheloo, "Time-critical cooperative path following of multiple unmanned aerial vehicles over time-varying networks," Journal of Guidance, Control, and Dynamics, vol. 36, no. 2, pp. 499–516, 2013.

[13] K. Zahradová, Frame defined by parallel transport for curves in any dimension,. Bachelor Thesis, Czech Technical University, Prague., 2016.

[14] E. Kreyszig, Introduction to differential geometry and Riemannian geometry. University of Toronto Press, 1968.

[15] M. P. Do Carmo, Riemannian geometry. Cambridge University Press, 1992.

[16] M. D. Todd, C. J. Stull, and M. Dickerson, "A local material basis solution approach to reconstructing the three-dimensional displacement of rod-like structures from strain measurements," Journal of Applied Mechanics, vol. 80, no. 4, p. 041028, 2013.

[17] M. Chadha and M. D. Todd, "A generalized approach for reconstructing the three-dimensional shape of slender structures including the effects of curvature, shear, torsion, and elongation," Journal of Applied Mechanics, vol. 84, no. 4, p. 041003, 2017.

[18] M. Chadha and M. D. Todd, "An improved shape reconstruction methodology for long rod like structures using cosserat kinematics-including the poisson's effect," in Nonlinear Dynamics, Volume 1, Proceedings of the 34th IMAC, A Conference and Exposition on Structural Dynamics 2016, pp. 237–246, Springer, 2019.

[19] J. Argyris, "An excursion into large rotations," Computer methods in applied mechanics and engineering, vol. 32, no. 1-3, pp. 85–155, 1982.

[20] A. Ibrahimbegović, F. Frey, and I. Kožar, "Computational aspects of vector-like parametrization of three-dimensional finite rotations," International Journal for Numerical Methods in Engineering, vol. 38, no. 21, pp. 3653–3673, 1995.

[21] J. Diebel, "Representing attitude: Euler angles, unit quaternions, and rotation vectors," Matrix, vol. 58, no. 15-16, pp. 1–35, 2006.

[22] D. R. Wilkins, "William rowan hamilton: mathematical genius," Physics World, vol. 18, no. 8, p. 33, 2005.

[23] A. R. Klumpp, "Singularity-free extraction of a quaternion from a direction-cosine matrix," Journal of spacecraft and rockets, vol. 13, no. 12, pp. 754–755, 1976.

[24] R. A. Spurrier, "Comment on" singularity-free extraction of a quaternion from a direction-cosine matrix"," Journal of spacecraft and rockets, vol. 15, no. 4, pp. 255–255, 1978.

[25] M. Ben-Ari, "A tutorial on euler angles and quaternions," Weizmann Institute of Science, Israel., 2014.

[26] M. Chadha and M. D. Todd, "On the material and material-adapted approaches to curve framing with applications in path estimation, shape reconstruction, and computer graphics," Computers & Structures, vol. 218, pp. 60–81, 2019.

[27] F. C. Park, "Distance metrics on the rigid-body motions with applications to mechanism design," Journal of Mechanical Design, vol. 117, no. 1, pp. 48–54, 1995.

[28] D. Q. Huynh, "Metrics for 3d rotations: Comparison and analysis," Journal of Mathematical Imaging and Vision, vol. 35, no. 2, pp. 155–164, 2009.

[29] R. H. Bartels, J. C. Beatty, and B. A. Barsky, An introduction to splines for use in computer graphics and geometric modeling. Morgan Kaufmann, 1995.

[30] P. Lancaster and K. Salkauskas, "Surfaces generated by moving least squares methods," Mathematics of computation, vol. 37, no. 155, pp. 141–158, 1981.

[31] D. Levin, "The approximation power of moving least-squares," Mathematics of Computation of the American Mathematical Society, vol. 67, no. 224, pp. 1517–1531, 1998.

[32] T. Belytschko, Y. Krongauz, D. Organ, M. Fleming, and P. Krysl, "Meshless methods: an overview and recent developments," Computer methods in applied mechanics and engineering, vol. 139, no. 1-4, pp. 3–47, 1996.

[33] J.-S. Chen, M. Hillman, and S.-W. Chi, "Meshfree methods: progress made after 20 years," Journal of Engineering Mechanics, vol. 143, no. 4, p. 04017001, 2017.

[34] M. Chadha and M. D. Todd, "A comprehensive kinematic model of single-manifold cosserat beam structures with application to a finite strain measurement model for strain gauges," International Journal of Solids and Structures, vol. 159, pp. 58–76, 2019.

[35] M. Chadha and M. D. Todd, "On the derivatives of curvature of framed space curve and their time-updating scheme," Applied Mathematics Letters, 2019.

[36] M. Chadha and M. D. Todd, "On the derivatives of curvature of framed space curve and their time-updating scheme: Extended version with matlab code," arXiv of Differential Geometry:1907.11271, 2019.

[37] F. Yiu, A geometrically exact thin-walled beam theory considering in-plane cross-section distortion. PhD thesis, Cornell University, 2005.

[38] I. S. Sokolnikoff, R. D. Specht, et al., Mathematical theory of elasticity, vol. 83. McGraw-Hill New York, 1956.

[39] E. Trefftz, "Die bestimmung der knicklast gedrückter, rechteckiger platten," ZAMM-Journal of Applied Mathematics and Mechanics/Zeitschrift für Angewandte Mathematik und Mechanik, vol. 15, no. 6, pp. 339–344, 1935.

[40] E. Elter, "Two formuli of the shear center," Periodica Polytechnica Mechanical Engineering, vol. 28, no. 2-3, pp. 179–193, 1984.

[41] C. Burgoyne and E. Brown, "Nonuniform elastic torsion," International journal of mechanical sciences, vol. 36, no. 1, pp. 23–38, 1994.

[42] E. Brown and C. Burgoyne, "Nonuniform elastic torsion and flexure of members with asymmetric cross-section," International journal of mechanical sciences, vol. 36, no. 1, pp. 39–48, 1994.

[43] J. C. Simo and L. Vu-Quoc, "A geometrically-exact rod model incorporating shear and torsion-warping deformation," International Journal of Solids and Structures, vol. 27, no. 3, pp. 371–393, 1991.

[44] V. V. Z, Thin walled elastic beams. English translation published for US Science Foundation by Israel Program for Scientific Translation., 1961.

[45] J. N. Goodier, The buckling of compressed bars by torsion and flexure. Cornell University Engineering Experiment Station, 1941.

[46] A. Gjelsvik, The theory of thin walled bars. Wiley New York, 1981.

[47] W. Y. Lin and K. M. Hsiao, "More general expression for the torsional warping of a thin-walled open-section beam," International journal of mechanical sciences, vol. 45, no. 5, pp. 831–849, 2003.

[48] J. C. Simo, "A finite strain beam formulation. the three-dimensional dynamic problem. part i," Computer methods in applied mechanics and engineering, vol. 49, no. 1, pp. 55–70, 1985.

[49] M. Iura and S. Atluri, "On a consistent theory, and variational formulation of finitely stretched and rotated 3-d space-curved beams," Computational Mechanics, vol. 4, no. 2, pp. 73–88, 1988.

[50] R. Kapania and J. Li, "A formulation and implementation of geometrically exact curved beam elements incorporating finite strains and finite rotations," Computational Mechanics, vol. 30, no. 5-6, pp. 444–459, 2003.

[51] A. Cardona and M. Géradin, "A beam finite element non-linear theory with finite rotations," International journal for numerical methods in engineering, vol. 26, no. 11, pp. 2403–2438, 1988.

[52] A. Ibrahimbegović, "On finite element implementation of geometrically nonlinear reissner's beam theory: three-dimensional curved beam elements," Computer methods in applied mechanics and engineering, vol. 122, no. 1-2, pp. 11–26, 1995.

[53] M. Chadha and M. D. Todd, "An introductory treatise on reduced balance laws of cosserat beams," International Journal of Solids and Structures, vol. 126, pp. 54–73, 2017.

[54] B. Schutz, A first course in general relativity. Cambridge university press, 2009.

[55] M. Chadha and M. D. Todd, "A displacement reconstruction strategy for long, slender structures from limited strain measurements and its application to underground pipeline monitoring," in International Conference on Experimental Vibration Analysis for Civil Engineering Structures, pp. 317–327, Springer, 2017.

[56] K. S. Miller, "On the inverse of the sum of matrices," Mathematics magazine, vol. 54, no. 2, pp. 67–72, 1981.

[57] A. Friedman, M. Todd, K. Kirkendall, A. Tveten, and A. Dandridge, "Rayleigh backscatter-based fiber optic distributed strain sensor with tunable gage length," SPIE Smart Structures/NDE 5050 Proceedings, San Diego, CA, March, pp. 2–6, 2003.

[58] R. G. Duncan, M. E. Froggatt, S. T. Kreger, R. J. Seeley, D. K. Gifford, A. K. Sang, and M. S. Wolfe, "High-accuracy fiber-optic shape sensing," in Sensor Systems and Networks: Phenomena, Technology, and Applications for NDE and Health Monitoring 2007, vol. 6530, p. 65301S, International Society for Optics and Photonics, 2007.

[59] M. Todd, D. Mascarenas, L. Overbey, T. Salter, C. Baldwin, and J. Kiddy, "Towards deployment of a fiber optic smart tether for relative localization of towed bodies," in Proceedings of the SEM Annual Conference on Experimental Mechanics, Portland, OR, June, pp. 6–9, 2005.

[60] J. E. Marsden and T. J. Hughes, Mathematical foundations of elasticity. Courier Corporation, 1994.

[61] R. Asaro and V. Lubarda, Mechanics of solids and materials. Cambridge University Press, 2006.

[62] E. Reissner, "On finite deformations of space-curved beams," Zeitschrift für angewandte Mathematik und Physik ZAMP, vol. 32, no. 6, pp. 734–744, 1981.

[63] L. Euler and C. A. Truesdell, The rational mechanics of flexible or elastic bodies, 1638-1788. Verlag nicht ermittelbar, 1960.

[64] J. Ericksen and C. Truesdell, "Exact theory of stress and strain in rods and shells," Archive for Rational Mechanics and Analysis, vol. 1, no. 1, pp. 295–323, 1957.

[65] Y.-B. Yang, J.-D. Yau, and L.-J. Leu, "Recent developments in geometrically nonlinear and postbuckling analysis of framed structures," Applied Mechanics Reviews, vol. 56, no. 4, pp. 431–449, 2003.

[66] A. Travers and J. Thompson, "An introduction to the mechanics of dna," Philosophical Transactions of the Royal Society of London A: Mathematical, Physical and Engineering Sciences, vol. 362, no. 1820, pp. 1265–1279, 2004.

[67] R. S. Manning, J. H. Maddocks, and J. D. Kahn, "A continuum rod model of sequence-dependent dna structure," The Journal of chemical physics, vol. 105, no. 13, pp. 5626–5646, 1996.

[68] I. Klapper, "Biological applications of the dynamics of twisted elastic rods," Journal of Computational Physics, vol. 125, no. 2, pp. 325–337, 1996.

[69] H. Lang, J. Linn, and M. Arnold, "Multi-body dynamics simulation of geometrically exact cosserat rods," Multibody System Dynamics, vol. 25, no. 3, pp. 285–312, 2011.

[70] D. H. Hodges, Nonlinear composite beam theory. American Institute of Aeronautics and Astronautics, 2006.

[71] C. Meier, M. J. Grill, W. A. Wall, and A. Popp, "Geometrically exact beam elements and smooth contact schemes for the modeling of fiber-based materials and structures," International Journal of Solids and Structures, vol. 154, pp. 124–146, 2018.

[72] A. Green and P. Naghdi, "On thermal effects in the theory of rods," International Journal of Solids and Structures, vol. 15, no. 11, pp. 829–853, 1979.

[73] H. Altenbach, M. Bîrsan, and V. A. Eremeyev, "On a thermodynamic theory of rods with two temperature fields," Acta Mechanica, vol. 223, no. 8, pp. 1583–1596, 2012.

[74] P. Duhem, "Le potentiel thermodynamique et la pression hydrostatique," in Annales scientifiques de l'École Normale Supérieure, vol. 10, pp. 183–230, 1893.

[75] E. Cosserat and F. Cosserat, Théorie des corps déformables. A. Hermann et fils,, 1909.

[76] A. Trautman, "Einstein-cartan theory," arXiv preprint gr-qc/0606062, 2006.

[77] J. C. Simo and D. D. Fox, "On a stress resultant geometrically exact shell model. part i: Formulation and optimal parametrization," Computer Methods in Applied Mechanics and Engineering, vol. 72, no. 3, pp. 267–304, 1989.

[78] A. C. Eringen, Microcontinuum field theories: I. Foundations and solids. Springer Science & Business Media, 2012.

[79] H. Altenbach and V. A. Eremeyev, Generalized Continua-from the Theory to Engineering Applications, vol. 541. Springer, 2012.

[80] G. Hay, "The finite displacement of thin rods," Transactions of the American Mathematical Society, vol. 51, no. 1, pp. 65–102, 1942.

[81] H. Cohen, "A non-linear theory of elastic directed curves," International Journal of Engineering Science, vol. 4, no. 5, pp. 511–524, 1966.

[82] A. B. Whitman and C. N. DeSilva, "A dynamical theory of elastic directed curves," Zeitschrift für angewandte Mathematik und Physik ZAMP, vol. 20, no. 2, pp. 200–212, 1969.

[83] A. E. Green, P. Naghdi, and M. Wenner, "On the theory of rods. i. derivations from the three-dimensional equations," Proc. R. Soc. Lond. A, vol. 337, no. 1611, pp. 451–483, 1974.

[84] A. Green, P. Naghdi, and M. Wenner, "On theory of rods ii: Derivations by direct approach," Proceedings of Royal Society, London A, vol. 337, pp. 485–507, 1974.

[85] S. S. Antman, "The theory of rods," in Linear Theories of Elasticity and Thermoelasticity, pp. 641–703, Springer, 1973.

[86] S. S. Antman, "Kirchhoff's problem for nonlinearly elastic rods," Quarterly of applied mathematics, vol. 32, no. 3, pp. 221–240, 1974.

[87] S. S. Antman and K. B. Jordan, "Qualitative aspects of the spatial deformation of non-linearly elastic rods.," Proceedings of the Royal Society of Edinburgh: Section A Mathematics, vol. 73, p. 85–105, 1975.

[88] J. Argyris and S. Symeonidis, "Nonlinear finite element analysis of elastic systems under nonconservative loading-natural formulation. part i. quasistatic problems," Computer methods in applied mechanics and engineering, vol. 26, no. 1, pp. 75–123, 1980.

[89] J. Argyris and S. Symeonidis, "Nonlinear finite element analysis of elastic systems under nonconservative loading—natural formulation part ii. dynamic problems," Computer methods in applied mechanics and engineering, vol. 28, no. 2, pp. 241–258, 1980.

[90] E. Reissner, "On one-dimensional finite-strain beam theory: the plane problem," Zeitschrift für angewandte Mathematik und Physik ZAMP, vol. 23, no. 5, pp. 795–804, 1972.

[91] E. Reissner, "On one-dimensional large-displacement finite-strain beam theory," Studies in applied mathematics, vol. 52, no. 2, pp. 87–95, 1973.

[92] A. E. H. Love, A treatise on the mathematical theory of elasticity. Cambridge university press, 2013.

[93] J. Simo and T. Hughes, "On the variational foundations of assumed strain methods," Journal of applied mechanics, vol. 53, no. 1, pp. 51–54, 1986.

[94] J. C. Simo and L. Vu-Quoc, "On the dynamics in space of rods undergoing large motions — a geometrically exact approach," Computer Methods in Applied Mechanics and Engineering, vol. 66, no. 2, pp. 125–161, 1988.

[95] J. C. Simo and L. Vu-Quoc, "A three-dimensional finite-strain rod model. part ii: Computational aspects," Computer methods in applied mechanics and engineering, vol. 58, no. 1, pp. 79–116, 1986.

[96] M. Iura and S. Atluri, "Dynamic analysis of finitely stretched and rotated three-dimensional space-curved beams," Computers and Structures, vol. 29, no. 5, pp. 875 – 889, 1988.

[97] J. Mäkinen, "Total lagrangian reissner's geometrically exact beam element without singularities," International Journal for Numerical Methods in Engineering, vol. 70, no. 9, pp. 1009–1048, 2007.

[98] D. Zupan and M. Saje, "Finite-element formulation of geometrically exact three-dimensional beam theories based on interpolation of strain measures," Computer Methods in Applied Mechanics and Engineering, vol. 192, no. 49-50, pp. 5209–5248, 2003.

[99] E. Zupan and D. Zupan, "On conservation of energy and kinematic compatibility in dynamics of nonlinear velocity-based three-dimensional beams," Nonlinear Dynamics, pp. 1–16, 2018.

[100] M. A. Crisfield and G. Jelenić;, "Objectivity of strain measures in the geometrically exact three-dimensional beam theory and its finite-element implementation," Proceedings of the Royal Society of London. Series A: Mathematical, Physical and Engineering Sciences, vol. 455, no. 1983, pp. 1125–1147, 1999.

[101] C. Meier, A. Popp, and W. A. Wal, "An objective 3d large deformation finite element formulation for geometrically exact curved kirchhoff rods," Computer Methods in Applied Mechanics and Engineering, vol. 278, pp. 445 – 478, 2014.

[102] A. Borković, S. Kovačević, G. Radenković, S. Milovanović, and M. Guzijan-Dilber, "Rotation-free isogeometric analysis of an arbitrarily curved plane bernoulli–euler beam," Computer Methods in Applied Mechanics and Engineering, vol. 334, pp. 238 – 267, 2018.

[103] W. Li, H. Ma, and W. Gao, "Geometrically exact curved beam element using internal force field defined in deformed configuration," International Journal of Non-Linear Mechanics, vol. 89, pp. 116 —126, 2017.

[104] P. Mata, S. Oller, and A. Barbat, "Static analysis of beam structures under nonlinear geometric and constitutive behavior," Computer methods in applied mechanics and engineering, vol. 196, no. 45-48, pp. 4458–4478, 2007.

[105] P. Mata, S. Oller, and A. Barbat, "Dynamic analysis of beam structures considering geometric and constitutive nonlinearity," Computer Methods in Applied Mechanics and Engineering, vol. 197, no. 6-8, pp. 857–878, 2008.

[106] A. Arora, A. Kumar, and P. Steinmann, "A computational approach to obtain nonlinearly elastic constitutive relations of special cosserat rods," Computer Methods in Applied Mechanics and Engineering, 2019.

[107] P. M. Pimenta, E. M. B. Campello, and P. Wriggers, "An exact conserving algorithm for nonlinear dynamics with rotational dofs and general hyperelasticity. part 1: Rods," Computational Mechanics, vol. 42, 2008.

[108] J. C. Simo, N. Tarnow, and M. Doblare, "Non-linear dynamics of three-dimensional rods: Exact energy and momentum conserving algorithms," International Journal for Numerical Methods in Engineering, vol. 38, no. 9, pp. 1431–1473, 1995.

[109] F. Demoures, F. Gay-Balmaz, M. Kobilarov, and T. S. Ratiu, "Multisymplectic lie group variational integrator for a geometrically exact beam in r^3," Communications in Nonlinear Science and Numerical Simulation, vol. 19, no. 10, pp. 3492 – 3512, 2014.

[110] I. Romero and F. Armero, "An objective finite element approximation of the kinematics of geometrically exact rods and its use in the formulation of an energy–momentum conserving scheme in dynamics," International Journal for Numerical Methods in Engineering, vol. 54, no. 12, pp. 1683–1716, 2002.

[111] I. Sokolov, S. Krylov, and I. Harari, "Extension of non-linear beam models with deformable cross sections," Computational Mechanics, vol. 56, no. 6, pp. 999–1021, 2015.

[112] E. Carrera, G. Giunta, and M. Petrolo, Beam structures: classical and advanced theories. John Wiley & Sons, 2011.

[113] A. Pagani and E. Carrera, "Unified formulation of geometrically nonlinear refined beam theories," Mechanics of Advanced Materials and Structures, vol. 25, no. 1, pp. 15–31, 2018.

[114] E. Carrera and V. V. Zozulya, "Carrera unified formulation (cuf) for the micropolar beams: Analytical solutions," Mechanics of Advanced Materials and Structures, vol. 0, no. 0, pp. 1–25, 2019.

[115] J. N. Clelland, From Frenet to Cartan: the method of moving frames, vol. 178. American Mathematical Soc., 2017.

[116] J. C. Simo, J. E. Marsden, and P. S. Krishnaprasad, "The hamiltonian structure of nonlinear elasticity: the material and convective representations of solids, rods, and plates," Archive for Rational Mechanics and Analysis, vol. 104, no. 2, pp. 125–183, 1988.

[117] T. Lee, M. Leok, and N. H. McClamroch, Global Formulations of Lagrangian and Hamiltonian Dynamics on Manifolds. Springer, 2017.

[118] W. M. Lai, D. H. Rubin, E. Krempl, and D. Rubin, Introduction to continuum mechanics. Butterworth-Heinemann, 2009.

[119] T. J. Hughes, The finite element method: linear static and dynamic finite element analysis. Courier Corporation, 2012.

[120] S. S. Rao, Vibration of continuous systems. John Wiley & Sons, 2007.

[121] C. Lanczos, The variational principles of mechanics. Courier Corporation, 2012.

[122] E. Engel and R. M. Dreizler, Density functional theory. Springer.

[123] H. Goldstein, C. Poole, and J. Safko, "Classical mechanics," 2002.

[124] M. A. Crisfield, "A consistent co-rotational formulation for non-linear, three-dimensional, beam-elements," Computer methods in applied mechanics and engineering, vol. 81, no. 2, pp. 131–150, 1990.